# Investigating the effect of chronic activation of AMP-activated protein kinase in the liver

Dr Jennet Ruth Williams
Chain-Florey Clinical Research Fellowship

A thesis submitted to Imperial College London for the degree of Doctor of Philosophy October 2017

Cellular Stress Group
London Institute of Medical Sciences
Imperial College London

**Declarations**

I declare that the work presented in this thesis is my own work and information derived from published or unpublished work of others has been acknowledged in the text and in the list of references. This work has not been submitted in any form for another degree or diploma at any university or other institute of tertiary education.

Signed: Jennet Williams 24th October 2017



Much of the data from the first results chapter of this thesis (Section 3) has been published in the following reference (included in Appendix B):

A. Woods, J. R. Williams, P. J. Muckett, F. V. Mayer, M. Liljevald, Y. M. Bohlooly, and D. Carling. 2017. 'Liver-Specific Activation of AMPK Prevents Steatosis on a High-Fructose Diet', Cell Rep, 18: 3043-51

**Abstract**

Obesity and its associated complications, are an increasing global problem. Non-alcoholic fatty liver disease (NAFLD), the hepatic component of the Metabolic Syndrome currently affects an estimated 25% of the world's population, with 2% of those affected dying from a NAFLD liver related cause, such as hepatocellular cancer (HCC). AMP-activated protein kinase (AMPK), a master regulator of energy homeostasis that regulates anabolic and catabolic pathways in response to ATP depletion has received substantial attention as a therapeutic target in treatment of the Metabolic Syndrome. More recently, a growing number of studies have focussed on the role of AMPK in cancer.

This study has characterised a novel, activating mutation in the γ1 subunit of AMPK (D316A). Mice which express this mutation specifically in the liver (D316-Tg) have been used to investigate the effects of chronic hepatic AMPK activation under basal conditions and in response to the metabolic stresses of hypercaloric, high fat and lipogenic, high fructose diets. D316A-Tg mice have also been crossed with mice with liver specific Phospatase and tensin homologue (Pten) loss to evaluate the role of AMPK in NAFLD related HCC.

Fatty acid synthesis was reduced in hepatocytes isolated from D316A-Tg mice and these mice were protected from hepatic steatosis under lipogenic conditions. Fatty acid oxidation in hepatocytes was unaffected by increased AMPK activity and correspondingly D316A-Tg mice were not protected from hepatic lipid accumulation, following high fat feeding. Increased hepatic AMPK activity also attenuated steatohepatitis and had a marked inhibitory effect on tumourgenesis in mice with liver specific Pten loss.

Further work is required to elucidate the precise role of AMPK in tumour development. However, the findings of this study suggest that activation of AMPK in the liver may inhibit NAFLD progression and tumourgenesis and support the development of pharmacological, specific AMPK activators for use in these settings.

**Acknowledgements**

An enormous thank you to my supervisors David Carling and Angela Woods. Ang has been unbelievably patient and supportive and both have made my PhD experience exciting and incredibly valuable. I have learned so much, not just about AMPK but also about the whole process of basic scientific research. I even know which bin to use now!

I'm also hugely grateful to Phil Muckett for all his training and help with the animal studies. I have benefited enormously from his vast experience and wisdom.

I have loved and felt really privileged to be part of the Cellular Stress group. I have some great memories and have always felt supported by a number of good friends. It meant a lot that some of them were able to help us celebrate at our wedding, and I loved introducing our daughter Zoë to them when she was just a few weeks old. I will never go to a better Christmas party (and am hoping to gatecrash in future years!) and I am sure, in turn, they will miss the noise of my Sodastream (!)

Thanks to the Microscope facility – Dirk Dorman and Chad Wilding for all their help with image acquisition and analysis and to the Animal Physiology facility for their assistance with some of the animal work.

Thanks to the Chain-Florey Clinical Fellowship scheme that funded my degree. Not only has this research allowed progress to be made in the understanding of the role of AMPK, but it has also enabled me to develop my skills as a basic scientist. It is difficult, therefore, to overstate how vital and much appreciated this kind of funding is.

And finally but perhaps most of all, thank you to my family without whose love this would not have been possible. Thank you to my husband Paul, who has developed a fuller understanding of the word 'harvest'; has heard so much about genotyping he could almost certainly do it himself; and understands that 10pm is a perfectly acceptable interpretation of 9pm. I would like to attribute this last point to the workload of the PhD, but I might not get away with that for much longer! His support, encouragement and understanding have been so important, as has his help with Excel. Thank you also to my babysitters, chefs, advisors or in other words parents (Roger and Rae Williams); my sister Becca for being generally marvellous; and to my daughter Zoë, for sleeping every once in a while and for making everything, however difficult, seem not so bad after all.

## Abbreviations

| | |
|---|---|
| **ACC** | Acetyl-CoA carboxylase |
| **ACL** | ATP citrate lyase |
| **AFP** | Alpha fetoprotein |
| **AICAR** | 5-aminoimidazole-4-carboxamide ribonucleotide |
| **ALT** | Alanine transaminase |
| **ALP** | Alkaline phosphatase |
| **AST** | Aspartate transaminase |
| **AMPK** | AMP-activated protein kinase |
| **AUC** | Area under curve |
| **BAT** | Brown adipose tissue |
| **BMI** | Body mass index |
| **4E-BP** | 4E-binding protein |
| **CaMKKβ** | Calcium/calmodulin-dependent protein kinase kinase β |
| **ChREBP** | Carbohydrate responsive element-binding protein |
| **CBM** | Carbohydrate-binding module |
| **CBS** | Cystathionine-β-synthase |
| **CLAMS** | Comprehensive lab animal monitoring system |
| **CPT1** | Carnitine palmitoyl transferase 1 |
| **CREB** | cAMP response element-binding protein |
| **CRTC2** | cAMP-regulated transcriptional coactivator 2 |
| **DEN** | Diethylnitrosamine |
| **DGAT** | Diacylglcerol transferase 2 |
| **DR** | Ductular reaction |
| **DRP** | Dynamin-related protein |
| **Elovl** | Elongase |
| **ECM** | Extracellular matrix |
| **EIF4E** | Elongation factor 4E |
| **ER** | Endoplasmic reticulum |
| **FAS** | Fatty acid synthase |
| **FBP** | Fructose 1,6-bisphosphate |
| **FGF** | Fibroblast growth factor |
| **FIP200** | Focal adhesion kinase family-interacting protein of 200kDa |

| | |
|---|---|
| **FXR** | Farnesoid X receptor |
| **GAP** | GTPase-activating protein |
| **GGT** | Gamma glutamyl transpeptidase |
| **Glu-6-P** | Glucose-6-phosphate |
| **G-6-Pase** | Glucose-6-phosphatase |
| **GPAT** | glycerol 3 phosphate acyltransferase |
| **GLUT4** | Glucose transporter 4 |
| **GWAS** | Genome wide association study |
| **Het** | Heterozygous |
| **Hom** | Homozygous |
| **HCC** | Hepatocellular cancer |
| **HDL** | High density lipoprotein |
| **H&E** | Haematoxylin and eosin |
| **HFCS** | High fructose corn syrup |
| **HMG CoA** | 3-hydroxy-3-methyl-glutaryl-coenzyme A |
| **HNE** | Hydroxy-2-nonenal |
| **HOMA-IR** | Homeostasis model assessment of insulin resistance |
| **HPC** | Hepatic progenitor cell |
| **HSC** | Hepatic stellate cell |
| **IKKβ** | Inhibitor of NF-κB kinase subunit β |
| **IL** | Interleukin |
| **INSIG2** | Insulin induced gene 2 |
| **IP** | Immunoprecipitate |
| **IRS** | Insulin receptor substrate |
| **JNK** | c-Jun N-terminal kinase |
| **LDLb** | Low density lipoprotein |
| **LFTs** | Liver function tests |
| **LIRKO** | Liver-specific insulin receptor knockout |
| **LKB1** | Liver kinase B1 |
| **LPS** | Lipopolysaccharide |
| **MAGE** | Melanoma associated antigens |
| **MARK4** | Microtubule affinity-regulating kinase 4 |
| **MEF** | Mouse embryonic fibroblast |
| **MFF** | Mitochondrial fision factor |

| | |
|---|---|
| **MUFA** | Mono-unsaturated fatty acid |
| **NAS** | NAFLD activity score |
| **NAFL** | Non-alcoholic fatty liver |
| **NAFLD** | Non-alcoholic fatty liver disease |
| **NASH** | Non-alcoholic steatohepatitis |
| **NF-κB** | Nuclear factor kappa-light-chain-enhancer of activated B cells |
| **OCT** | Organic cation transporter |
| **PCA** | Principle component analysis |
| **PDK** | Phosphoinositide-dependent kinase |
| **PEPCK** | Phosphoenolpyruvate carboxykinase |
| **PFK1** | Phosphofructokinase 1 |
| **PGC** | PPARγ coactivator |
| **PPAR** | Peroxisome proliferator activated receptor |
| **PFKFB** | Phosphofructokinase 2/fructose 2,6-bisphosphate |
| **PI3K** | Phosphoinositide 3-kinase |
| **$PIP_2$** | Phosphatidylinositol bisphosphate |
| **$PIP_3$** | Phosphatidylinositol-3,4,5-triphosphate |
| **PKA/B/C** | Protein kinase A/B/C |
| **PP** | Protein phosphatase |
| **PTEN** | Phospatase and tensin homologue |
| **PUFA** | Poly-unsaturated fatty acid |
| **QALY** | Quality-adjusted life year |
| **RER** | Respiratory exchange ratio |
| **RHEB** | RAS homologue enriched in brain |
| **ROS** | Reactive oxygen species |
| **SCAP** | SREBP cleavage activating protein |
| **SCD** | Stearoyl-CoA desaturase |
| **SOCS** | Suppressor of cytokine signalling |
| **SREBP1c** | Sterol regulatory element-binding protein 1c |
| **STRAD** | Ste20-related adaptor protein |
| **TACE** | Transarterial chemoembolisation |
| **TBC1D4** | TBC domain family member 4 |
| **T2DM** | Type 2 diabetes mellitus |
| **TGF** | Transforming growth factor |

| | |
|---|---|
| **TGR5** | Transmembrane G protein-coupled receptor 5 |
| **TLC** | Thin layer chromotography |
| **TM6SF2** | Transmembrane 6 duperfamily 2 |
| **TNF** | Tumour necrosis factor |
| **mTORC** | Mammalian target of rapamycin complex |
| **Triose-P** | Triose-phosphate |
| **TSC** | Tuberous sclerosis protein |
| **ULK** | Unc-51-like kinase |
| **UPR** | Unfolded protein response |
| **USS** | Ultrasound scan |
| **VLDL** | Very low density lipoprotein |
| **WAT** | White adipose tissue |
| **WPW** | Wolff-Parkinson-White |
| **XBP** | X-box binding protein |
| **X-5-P** | Xylulose-5-phosphate |

**Table of Contents**

**Table of Figures**

**Table of Tables**

# 1 Introduction

There is a growing obesity epidemic affecting countries across the globe (Non-Communicable Disease Risk Factor Collaboration, 2016) . Currently, more than a quarter of adults in England are obese and this is set to rise to half the adult population by 2050 (https://www.noo.org.uk). Obesity is associated with complications such as dyslipidaemia, type 2 diabetes (T2DM) and cardiovascular disease, features of the metabolic syndrome (Alberti et al. 2009), as well as predisposing to cancer (Calle et al. 2003). It therefore imposes a massive medical and socioeconomic burden.

Non-alcoholic fatty liver disease (NAFLD) is regarded as the hepatic component of the metabolic syndrome and is a spectrum of pathologies ranging from simple steatosis, through non-alcoholic steatohepatitis (NASH) to fibrosis/cirrhosis (Chalasani et al. 2012). Only a small proportion of individuals with NAFLD will progress to cirrhosis and so develop liver failure and/or hepatocellular cancer (Younossi et al. 2016). However the increasing burden of NAFLD, which currently affects ~25% of the world's adult population, is such that an estimated 0.5% of people will die from a NAFLD liver related cause (Rinella and Charlton 2016).

Like NAFLD, incidence of NAFLD related hepatocellular cancer (HCC) is on the increase (Wong, Cheung, and Ahmed 2014). There is currently a lack of effective treatments for advanced HCC (EASL-EORTC 2012). However, as with NAFLD related liver cancer, the vast majority of HCCs arise on a background of chronic liver disease, other common aetiologies including hepatitis B or C infection, and alcoholic steatosis (El-Serag 2012). There is therefore potential to screen for and target this pre-cancerous lesion, slowing or even preventing its progression and/or detecting cancers at an earlier stage when treatment is more likely to be successful.

AMP-activated protein kinase (AMPK) is a highly conserved enzyme which plays a key role in energy homeostasis by down-regulating anabolic pathways such as gluconeogenesis, fatty acid synthesis and protein synthesis and up-regulating catabolic processes including fatty acid oxidation and autophagy (Merrill et al. 1997; Inoki, Zhu, and Guan 2003; Cheng et al. 2004; Koo et al. 2005; Gwinn et al. 2008; Davies et al. 1992). Correspondingly, over recent years

AMPK has received significant interest as a potential therapeutic target for treatment of obesity and its associated problems. Furthermore AMPK appears to have anti-inflammatory effects and is likely to be of importance in tumourgenesis, although the evidence as to whether AMPK protects against or promotes cancer is conflicting (Huang et al. 2008; Faubert et al. 2013; Laderoute et al. 2006; Sag et al. 2008).

The current study uses a genetically modified mouse model to investigate the effects of increased hepatic AMPK activity. The model has been phenotyped under basal conditions and then used to examine the role of hepatic AMPK in response to metabolic stresses such as hypercaloric, high fat and lipogenic, high fructose feeding. Mice with increased hepatic AMPK activity have then been crossed with mice with liver specific Phospatase and tensin homologue (Pten) loss, to allow evaluation of the function of hepatic AMPK in a NAFLD related HCC model (Stiles et al. 2004; Horie et al. 2004).

## 1.1 AMP-activated protein kinase (AMPK)

AMPK is a highly conserved protein kinase, essential to cellular energy homeostasis. Activated in response to reduced ATP levels, AMPK upregulates catabolic and downregulates anabolic processes (Carling et al. 2012; Merrill et al. 1997; Cheng et al. 2004; Koo et al. 2005; Egan et al. 2011; Xiao et al. 2013; Hardie, Ross, and Hawley 2012)

***Structure***

AMPK is a heterotrimer consisting of a catalytic α subunit and regulatory β and γ subunits (Xiao et al. 2007). In mammals seven subunit isoforms exist (two α, two β and three γ), each encoded by a different gene (**Table 1.1**). Different isoforms are expressed in different tissues and they can combine in up to 12 different combinations (Ross, MacKintosh, and Hardie 2016). Rodent liver contains approximately equal amounts of α1 and α2, combined with β1 and either γ1 or γ2. The predominant complexes in human liver are α1β2γ1 and α1β2γ2, although β1 is present (Stephenne et al. 2011).

| Subunit | Domains |
|---|---|
| α1 & α2 | Ser/Thr protein kinase<br>Regulatory domain |
| β1 & β2 | CBM<br>C terminal domain – interacts with α and ϒ |
| ϒ1, ϒ2 & ϒ3 | 4 CBS motifs<br>4 nucleotide binding regions |

***Table 1.1 - Features of the AMPK subunits*** *(Carling et al. 2012) CBM = carbohydrate binding module, CBS = cystathionine-β-synthase*

The α subunit contains an amino terminal serine/threonine protein kinase, and a carboxy terminal regulatory domain (Carling et al. 2012). Within the kinase domain is an activation loop containing threonine residue 172 (Thr172), which is phosphorylated by upstream kinases (Hawley et al. 1996). The β subunit has a carbohydrate-binding module (CBM) and its N terminal is myristoylated (Hudson et al. 2003). It interacts via its C terminal with the α and γ subunits providing a scaffold for the heterotrimeric complex (Woods et al. 1996). The γ

subunit has 4 cystathionine-β-synthase (CBS) motifs between which nucleotide binding occurs (Xiao et al. 2011; Xiao et al. 2007; Xiao et al. 2013).

Crystallographic studies of the structure of AMPK revealed that the γ1 subunit has 4 potential adenine nucleotide binding sites (sites 1-4), 3 of which are occupied (Xiao et al. 2013; Xiao et al. 2007; Xiao et al. 2011; Gu et al. 2017)(and unpublished data Sanders, Carling and Gamblin). The properties of the 4 sites are summarised in **Table 1.2**. Sites 1 and 3 are the exchangeable binding sites and site 3 has the greater binding affinity. It is thought that AMP or ADP binding at site 3 protects AMPK from dephosphorylation and results in its allosteric activation. Site 2 does not bind nucleotides and at site 4 there is non-exchangeable AMP binding.

| Site | Nucleotide binding | Affinity |
|---|---|---|
| 1 | AMP/ADP/ATP | Weak |
| 2 | | Empty |
| 3 | AMP/ADP/ATP/NADH | Tight |
| 4 | AMP | Non-exchangable |

***Table 1.2 - The AMPK γ1 binding sites*** *(Xiao et al. 2013; Xiao et al. 2011; Xiao et al. 2007; Gu et al. 2017) (and unpublished data Sanders, Carling and Gamblin).*

***Activation of AMPK***

AMPK activation is dependent upon phosphorylation at Thr172 by an upstream kinase, either liver kinase B1 (LKB1) or calcium/calmodulin-dependent protein kinase kinase β (CaMKKβ) (Carling et al. 2012; Woods et al. 2003; Hawley et al. 2005). Whilst CaMKKβ is stimulated by calcium, LKB1 is believed to be constitutively active. Changes in AMPK phosphorylation are therefore determined by the activity of CaMKKβ and/or phosphatases acting upon AMPK. AMP and ADP protect AMPK from dephosphorylation and there is also modest (2 fold) allosteric activation of AMPK by AMP (**Figure 1.1**) (Xiao et al. 2011).

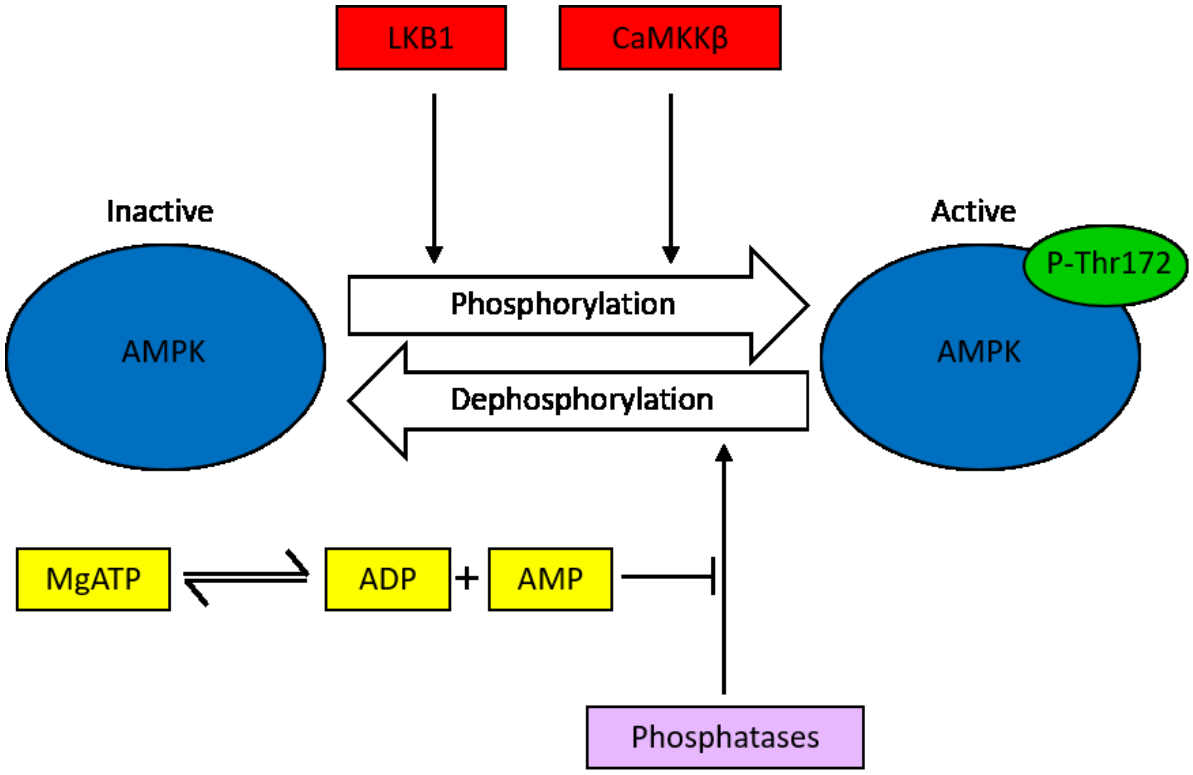


***Figure 1.1 - Regulation of AMPK.*** *CaMKKβ = calcium/calmodulin dependent protein kinase kinase β, LKB1 = liver kinase B1.*

Activation of AMPK therefore occurs in response to a rise in AMP and ADP concentrations and corresponding fall in ATP concentration or due to increased intracellular calcium levels. Nutrient deprivation and ischaemia inhibit ATP production and exercise promotes its consumption, so these metabolic stresses activate AMPK (Corton, Gillespie, and Hardie 1994; Marsin et al. 2000; Salt et al. 1998; Winder and Hardie 1996). Pharmacological compounds can activate AMPK by one of three methods (Hardie 2015a). They can behave as metabolic poisons, lowering ATP production and so increasing AMP concentration which stimulates AMPK; they can mimic AMP; or they can bind AMPK in a cleft between the α and β subunits, resulting in allosteric activation. Commonly used AMPK activators are listed in **Table 1.3**. Metabolic poisons and AMP analogues inevitably have more off target effects. With the exception of salicylate, the allosteric activators are synthetic compounds identified by high throughput screening. Compound library screening also identified Compound C, a potent

reversible AMPK inhibitor, which competes with ATP in the absence of AMP, but it is non-specific (Zhou et al. 2001).

| Metabolic poisons | AMP analogues | Allosteric activators |
|---|---|---|
| Metformin and phenformin | AICAR | Salicylate |
| Resveratrol | C13 | 991 |
| Berberine | | A-769662 |
| | | MT63-78 |
| | | MK-8722 |
| | | PF-739 |

***Table 1.3 – Pharmacological AMPK activators*** *(Hardie 2015a; Gomez-Galeno et al. 2010; Hawley et al. 2012; Xiao et al. 2013; Cool et al. 2006; Zadra et al. 2014; Myers et al. 2017; Cokorinos et al. 2017). AICAR = 5-aminoimidazole-4-carboxamide ribonucleotide*

### 1.1.1 AMPK & Metabolism

AMPK has a diverse range of roles in metabolism (**Figure 1.2**).

***Carbohydrate metabolism***

AMPK is heavily involved in glucose metabolism through regulation of glucose uptake, gluconeogenesis, glycolysis and glycogen (Pehmoller et al. 2009; Koo et al. 2005; Marsin et al. 2000; Jorgensen et al. 2004). Under basal conditions AKT substrate of 160kDa (AS160, also called TBC domain family member 4 – TBC1D4) associates with intracellular vesicles containing glucose transporter 4 (GLUT 4) (Pehmoller et al. 2009). TBC1D4 is a GTPase activating protein and hydrolyses GTP bound to Rab GTPases which are also associated with GLUT 4 vesicles. Rabs are therefore held in their GDP bound inactive state by TBC1D4. Phosphorylation of TBC1D4 by AMPK (or AKT secondary to insulin signalling) causes TBC1D4 to bind 14-3-3 proteins and dissociate from GLUT 4 vesicles. This, in turn, allows Rabs associated with GLUT 4 containing vesicles to convert to their active GTP bound forms and so translocation of the vesicles to the plasma membrane, promoting glucose uptake. This mechanism is important for increased glucose uptake in muscles following exercise stimulated activation of AMPK. Consequently mice with muscle specific total AMPK β knockout have markedly reduced muscle glucose uptake following exercise (O'Neill et al. 2011). Increased activity of GLUT 1 at the surface of cells, in response to metabolic stress, may also be AMPK dependent (Barnes et al. 2002).

Phosphofructokinase 2/fructose 2,6-bisphosphatase (PFKFB) is the bifunctional enzyme responsible for converting fructose 6-phosphate (F-6-P) to fructose 2,6-bisphosphate (F-2,6-$P_2$) and vice versa. AMPK, like AKT (downstream of insulin signalling), phosphorylates PFKFB, up-regulating its phosphofructokinase 2 activity, resulting in increased F-2,6-$P_2$ (Marsin et al. 2000; Marsin et al. 2002). F-2,6-$P_2$ allosterically activates the glycolysis enzyme phosphofructokinase 1 (PFK1), increasing its affinity for F-6-P and so increased AMPK activity up-regulates glycolysis. However, of note, AMPK only activates the PFKFB2 and PFKFB3 isoforms of PFKFB, present in cardiac myocytes and monocytes/macrophages respectively.

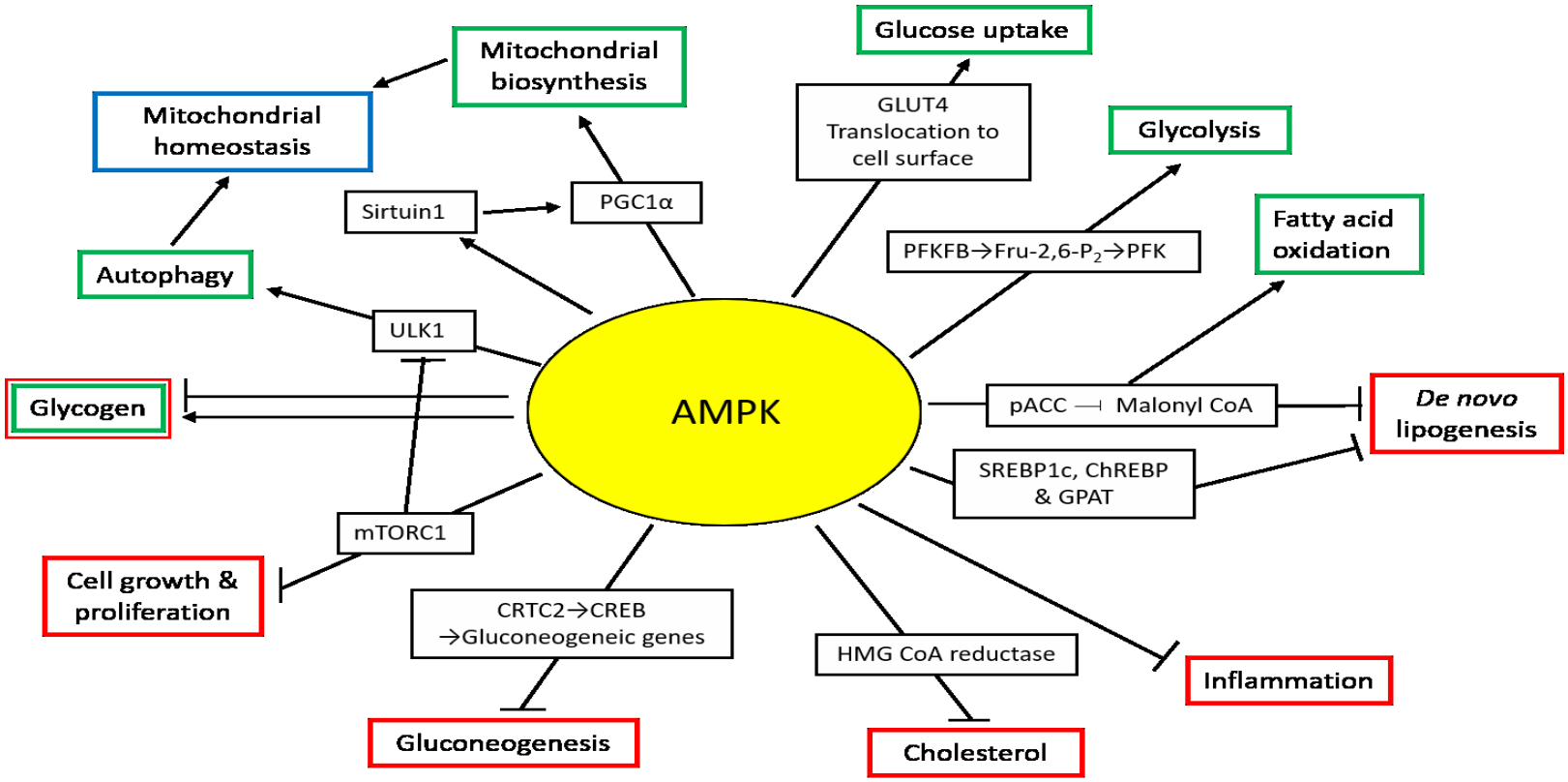


***Figure 1.2*** *- **The actions of AMPK.** Up-regulated pathways outlined in green and down-regulated pathways outlined in red. ChREBP = Carbohydrate-responsive element-binding protein, CREB = cAMP response element-binding protein, CRTC2 = cAMP regulated transcriptional co-activator 2, Fru-2,6-$P_2$ = Fructose 2,6—*bisphosphate, GLUT4 = glucose transporter 4, GPAT = *glycerol 3 phosphate acyltransferase, HMG CoA reductase = 3-hydroxy-3-methyl-glutaryl-coenzyme A reductase, mTORC1 = mammalian target of rapamycin 1, PGC1α = Peroxisome proliferator-activated receptor gamma coactivator 1-alpha, SREBP1c = sterol regulatory element-binding protein 1c, ULK1 = Unc-51-like kinase (ULK) 1.*

AMPK may also inhibit gluconeogenesis by down-regulating gluconeogenic gene expression (Koo et al. 2005). cAMP response element-binding protein (CREB) is a key transcription factor involved in gluconeogenic gene expression. cAMP-regulated transcriptional coactivator 2 (CRTC2) binds CREB and is important for its activity. Indeed mice with systemic CRTC2 deletion have reduced phosphoenolpyruvate carboxykinase (PEPCK), Glucose-6-phosphatase (G-6-Pase) and peroxisome proliferator activated receptor γ (PPARγ) coactivator 1α (PGC1α) expression although they do not develop hypoglycaemia (Le Lay et al. 2009). AMPK is believed to phosphorylate and inhibit the activity of CRTC2 by preventing its translocation to the nucleus in turn limiting gluconeogenic gene expression (Koo et al. 2005).

AMPK's role in glycogen metabolism is less clear. It appears to phosphorylate and inactivate glycogen synthase (Jorgensen et al. 2004), however mutations in human AMPK γ2 which cause Wolff-Parkinson-White (WPW) syndrome (Arad, Seidman, and Seidman 2007) and in the AMPK γ3 subunit of Hampshire Rendement Napole pigs (Milan et al. 2000), are associated with both increased AMPK activity and excessive glycogen storage.

***Lipid metabolism***

AMPK plays a central role in lipid metabolism through its phosphorylation and inactivation of acetyl-CoA carboxylase (ACC)(Davies et al. 1992; Corton, Gillespie, and Hardie 1994). ACC converts acetyl CoA to malonyl CoA, required for fatty acid synthesis and so AMPK inhibits lipogenesis. Malonyl CoA is also an allosteric inhibitor of carnitine palmitoyl transferase I (CPT1) which is required for transfer of acyl CoA from the cytosol, into the mitochondria (McGarry, Leatherman, and Foster 1978; Merrill et al. 1997). Therefore, through phosphorylation of ACC, AMPK also promotes carriage of acyl CoA into mitochondria where it undergoes fatty acid oxidation. AMPK may also lower malonyl CoA levels further through phosphorylation and activation of malonyl CoA decarboxylase (Saha et al. 2000).

AMPK is also thought to negatively regulate expression of lipogenic genes through inhibition of Sterol regulatory element-binding protein 1c (SREBP1c – **Figure 1.3**) and Carbohydrate-responsive element-binding protein (ChREBP - **Figure 1.4**) (Li et al. 2011; Foretz et al. 2005; Kawaguchi et al. 2002). Furthermore it inhibits glycerol phosphate acyl-transferase activity and so triglyceride formation (Muoio et al. 1999); and limits cholesterol synthesis through

phosphorylation and inactivation of 3-hydroxy-3-methyl-glutaryl-coenzyme A (HMG CoA) reductase (Clarke and Hardie 1990).

***Protein metabolism***

Another major cell growth and synthesis pathway inhibited by AMPK is the PTEN/AKT/mammalian target of rapamycin complex 1 (mTORC1) cascade, summarised in **Figure 1.5** (Carling et al. 2012; Gwinn et al. 2008; Inoki, Zhu, and Guan 2003; Cheng et al. 2004). AMPK inhibits mTORC1 activity via three mechanisms. Firstly, it phosphorylates tuberous sclerosis protein 2 (TSC2) (Thr1227 and Ser1345) so activating the TSC1/TSC2 complex (Inoki, Zhu, and Guan 2003); secondly, it directly phosphorylates mTOR (Thr2446), preventing its phosphorylation (Ser2448) and activation by AKT (Cheng et al. 2004); and finally, it phosphorylates mTOR's binding partner RAPTOR (Ser792), causing RAPTOR to bind 14-3-3 instead of mTOR (Gwinn et al. 2008). Thus mTORC1's kinase activity is blocked, resulting in down-regulation of cell growth and proliferation.

***Autophagy***

Autophagy, type II cell death, is an evolutionary conserved and tightly controlled process whereby cellular organelles and contents of the cytosol are encased by autophagosomes and delivered to lysosomes for degradation (Klionsky 2007). Autophagy is important for recycling or disposing of damaged cellular components and for supplying metabolites in response to nutrient deprivation. Autophagosome formation is initiated by a complex containing Unc-51-like kinase (ULK) 1, ATG13 and focal adhesion kinase family-interacting protein of 200kDa (FIP200)(Hosokawa et al. 2009). Under basal conditions ULK1 is phosphorylated and inactivated by mTORC1. In contrast, following nutrient deprivation it is phosphorylated (at alternative sites) and activated by AMPK (Egan et al. 2011; Kim et al. 2011). Furthermore, AMPK inhibits mTORC1 activity through phosphorylation of TSC2, mTOR and Raptor, so relieving mTORC1's inhibitory effect on ULK1 (Inoki, Zhu, and Guan 2003; Gwinn et al. 2008; Cheng et al. 2004; Hosokawa et al. 2009).

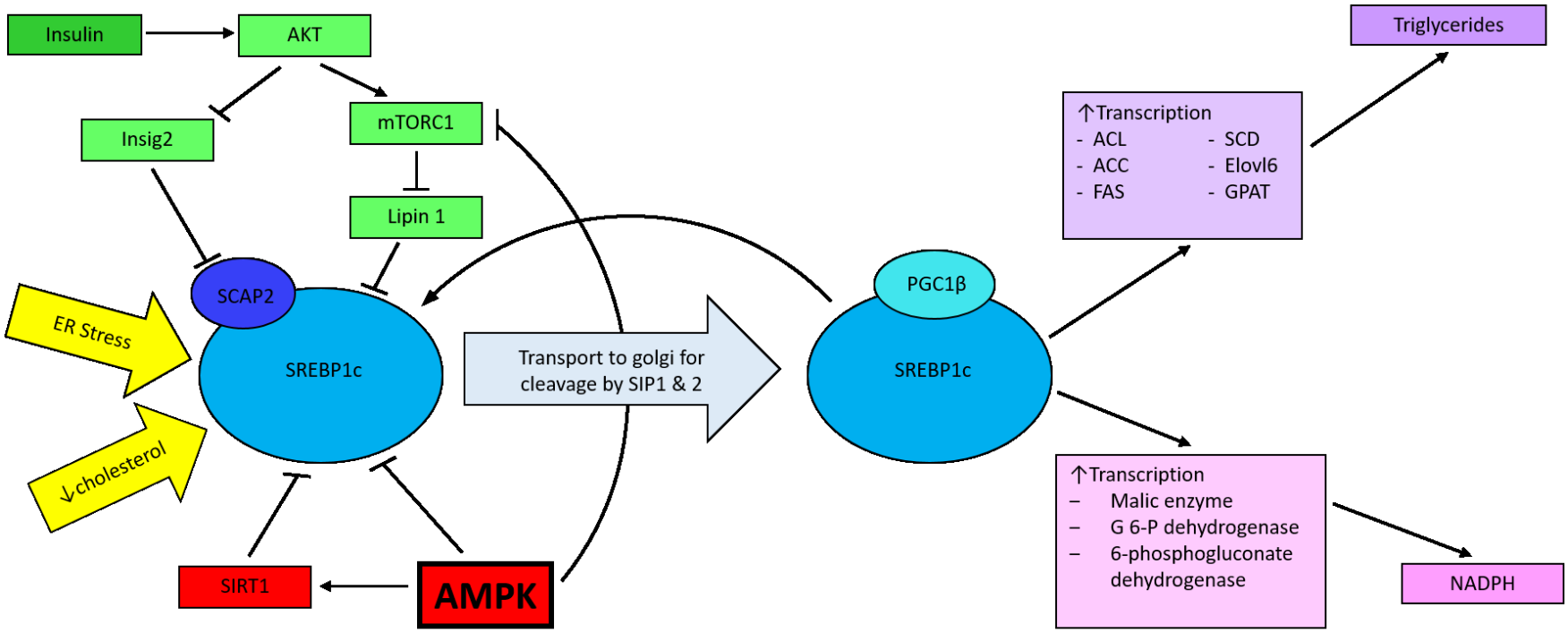


***Figure 1.3 – Negative regulation of sterol regulatory-binding protein 1c (SREBP1c) by AMPK resulting in reduced lipogenic gene transcription.*** *To become transcriptionally active, SREBPs, present in the endoplasmic reticulum (ER), require transport to the golgi apparatus (escorted by SREBP cleavage activating protein - SCAP) where they are cleaved by SIP1 and 2 proteases. AKT/mTORC1 pathway activation by insulin phosphorylates lipin-1, preventing it from translocating to the nucleus, where it constrains SREBP1c. AKT also inhibits insulin induced gene 2 (INSIG2), which binds SCAP2 preventing it from escorting SREBP to the golgi. SREBP1c cleavage is also promoted by reduced intracellular cholesterol and phosphatidylcholine levels and ER stress and SREBP1c binds its own promotor resulting in feed forward activation. Conversely the actions of SREBP1c are restricted by AMPK both directly and via SIRT1, which phosphorylate (Ser372) and acetylate it respectively. Peroxisome proliferator-activated receptor gamma coactivator-1 β (PGC-1β) is a co-activator, required for optimal SREBP1 activity. SREBP1c activation results*

*in increased expression of lipogenic genes (ATP citrate lyase (ACL), Acetyl Co-A Carboxylase (ACC), fatty acid synthase (FAS), stearoyl-CoA desaturase (SCD), fatty acyl-CoA elongase 6 (Elovl6) and glycerol 3 phosphate acyltransferase (GPAT)) as well as malic enzyme (which converts malate to pyruvate) and glucose 6-phosphate dehydrogenase and 6-phosphogluconate dehydrogenase (both pentose phosphate pathway enzymes), all 3 of which catalyse reactions producing NADPH, needed for lipid synthesis.*

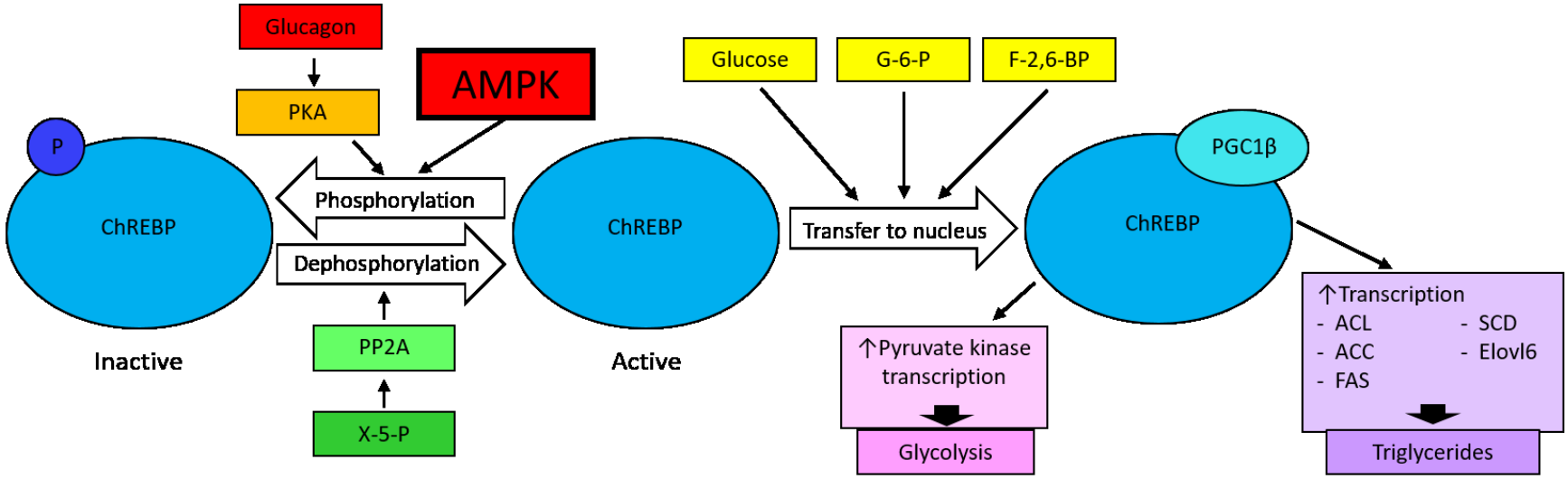


***Figure 1.4 – Negative regulation of carbohydrate-responsive element-binding protein (ChREBP) by AMPK resulting in reduced lipogenic gene expression.*** *The transcription factor ChREBP is phosphorylated and inactivated by glucagon, via protein kinase A (PKA – Ser196) and AMPK (Ser568). Conversely, xylulose-5-phosphate (X-5-P – a pentose pathway intermediate), activates protein phosphatase 2A (PP2A), resulting in ChREBP dephosphorylation and activation. Phosphorylated ChREBP binds to the cytoplasmic protein 14-3-3, preventing its transport to the nucleus. Glucose (through acetylation), glucose-6-phosphate (Glu-6-P) and fructose-2,6-bisphosphate (F-2,6-BP) all promote nuclear translocation of ChREBP and so its activity. ChREBP requires the co-activator PGC1β to operate optimally and is responsible for increased transcription of the gene encoding pyruvate kinase, as well as the lipogenic genes ACL, ACC, FAS, SCD1 and Elovl6.*

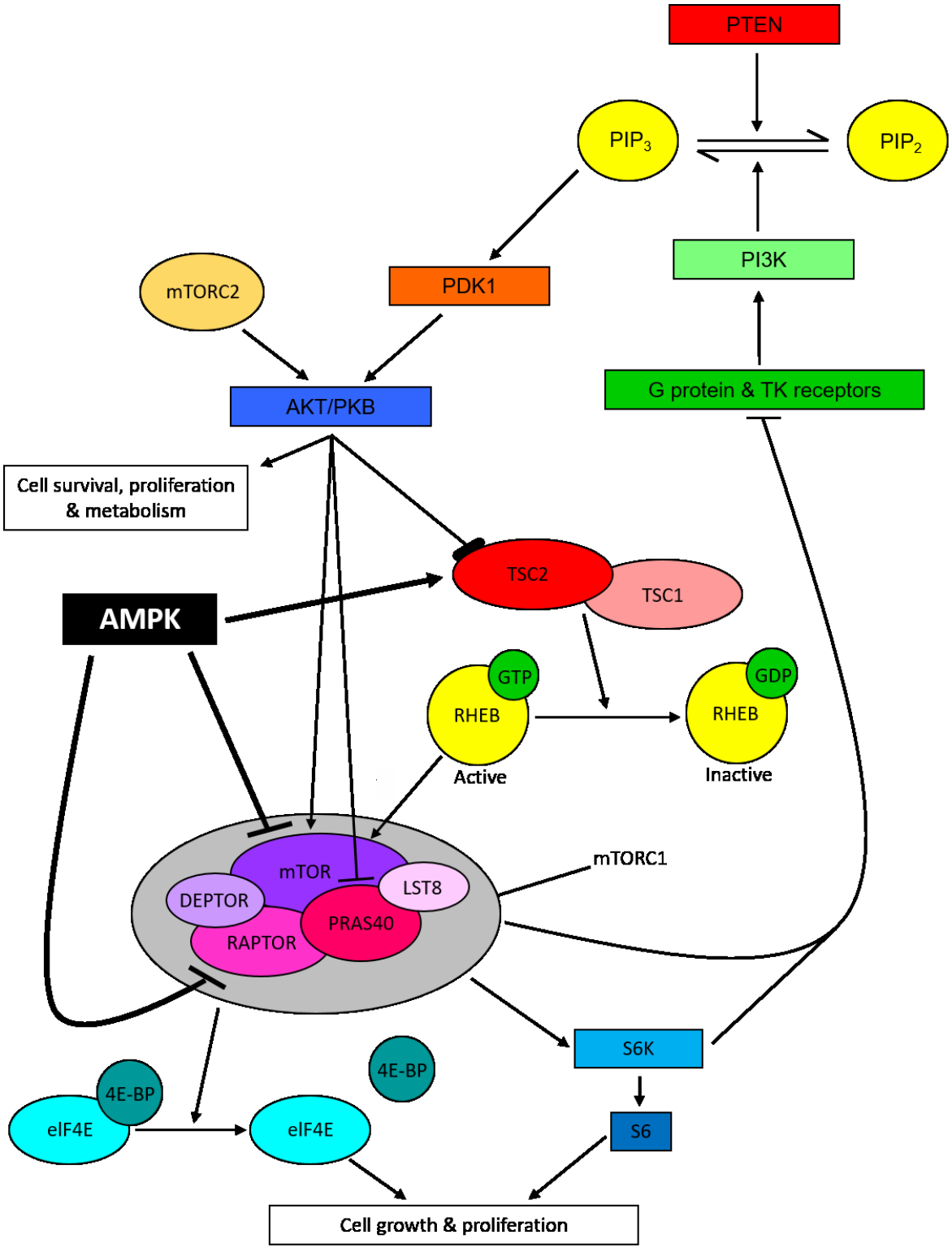


***Figure 1.5 - The PTEN/AKT/mTORC1 pathway and inhibition by AMPK.*** *PTEN dephosphorylates phosphatidylinositol-3,4,5-triphosphate ($PIP_3$) to phosphatidylinositol bisphosphate ($PIP_2$), thereby reversing the action of phosphoinositide 3-kinase (PI3K). $PIP_3$ activates 3-phosphoinositide-dependent kinase (PDK). AKT (also known as protein kinase B – PKB) binds to $PIP_3$ but for full activation requires phosphorylation at Thr308 and Ser473 by*

*complex 2 (mTORC2) respectively. Phosphorylated AKT in turn phosphorylates a number of signalling proteins including tuberous sclerosis protein 2 (TSC2). mTORC1 is activated by the GTP-bound form of the GTPase RAS homologue enriched in brain (RHEB). Hydrolysis of the GTP bound to RHEB and so inactivation of mTORC1 is promoted by the GTPase-activating protein (GAP) complex tuberous sclerosis 1 (TSC1/hamartin)-TSC2 (tuberin). Phosphorylation of TSC2 (at Ser939, Ser981 and Thr1462) by AKT releases this inhibition, resulting in activation of mTOR within mTORC1. AKT also activates mTORC1 by inactivating PRAS40, a negative regulator within the complex and through direct phosphorylation of mTOR (at Ser2448). Active mTORC1 phosphorylates 4E-binding protein (4E-BP) which releases elongation factor 4E (elF4E); and phosphorylates ribosomal protein S6 kinase which in turn phosphorylates and activates S6 (part of the 40S ribosomal subunit). Ribosomal protein S6 and elF4E both promote translation resulting in increased expression of genes involved in cell growth and proliferation. Active mTORC1 and S6K also reduce PI3K stimulation, so creating a negative feedback loop. AMPK inhibits mTORC1 activity through activation of the TCS1/TSC2 complex and phosphorylation of mTOR and RAPTOR within the mTORC1 complex.*

In addition to AMPK and mTORC1 controlling autophagy, there is evidence that activation of both AMPK and mTORC1 occurs at the lysosomal membrane (Zhang, Jiang, et al. 2014). AXIN is a scaffold protein which mediates phosphorylation of AMPK by LKB1 by bringing them into close proximity and it also interacts with Ragulator, a complex of proteins on the surface of lysosomes (Zhang, Guo, et al. 2013; Zhang, Jiang, et al. 2014). AXIN's binding to AMPK, LKB1 and Ragulator has been shown to be enhanced following glucose starvation or exposure to AMP. Recent work by Zhang et al. suggests that glucose deprivation activates AMPK independently of adenine nucleotide concentrations, by lowering fructose-1,6-bisphosphate (FBP) levels. This reduction in FBP is sensed by aldolase which promotes AMPK/LKB1/AXIN/Ragulator complex formation (Zhang et al. 2017). Conversely, when activated, Rag GTPases on the surface of lysosomes sequester mTORC1, so promoting activation of mTORC1 by Rheb (Sancak et al. 2010; Sancak et al. 2008; Kim et al. 2008). RagGTPases are up-regulated by the Ragulator following exposure to increased amino acid or glucose concentrations (Efeyan et al. 2013; Carroll and Dunlop 2017). Furthermore, in response to energy (but not low protein) stress, AXIN inhibits Ragulator mediated RagGTPase activation of mTORC1 (Zhang, Jiang, et al. 2014).

***Mitochondrial homeostasis***

Functioning mitochondria are essential for oxidative catabolism of glucose and fatty acids for ATP production and AMPK is likely a key player in their homeostasis (Mihaylova and Shaw 2011). Defective mitochondria are broken down by a specific form of autophagy called mitophagy and the mitochondria of mice with defective ULK1 have altered morphology and reduced membrane potential (Egan et al. 2011). In addition, Toyama et al. demonstrated that activation of AMPK promotes mitochondrial fragmentation (Toyama et al. 2016). Mitochondrial fision factor (MFF) is a mitochondrial membrane receptor for dynamin-related protein 1 (DRP1), a key catalyst of mitochondrial fision. AMPK phosphorylates MMF, which enhances localisation of DRP from the cytoplasm to the mitochondria and this can occur in the absence of mitochondrial stress. AMPK may also be involved in triggering mitochondrial biosynthesis, through activation of peroxisome proliferator-activated receptor gamma coactivator 1-alpha (PGC-1α)(Canto et al. 2009; Jager et al. 2007). PGC1α, which co-activates a number of transcription factors required for mitochondrial gene expression, is phosphorylated and upregulated directly by AMPK (Jager et al. 2007). PGC1α may also be deacetylated and activated by sirtuin 1 (SIRT1), which is in turn stimulated in the presence of AMPK (due to increased availability of its co-substrate NAD) (Canto et al. 2009). In-keeping with these findings, mitochondrial gene expression was increased following AICAR treatment (Winder et al. 2000).

Brown adipose tissue (BAT) is rich in mitochondria which catabolise glucose and lipid for thermogenesis and following stimulation of sympathetic innervation white adipose tissue (WAT) can increase its mitochondrial content for the same purpose (Bartelt and Heeren 2014). This so called ‘browning’ produces ‘beige’ or ‘brite’ adipose. Mottillo et al. recently found that mice with inducible, adipocyte specific AMPK β1 and β2 deletion had impaired BAT mitochondrial function and WAT browning, re-enforcing the importance of AMPK in mitochondrial homeostasis (Mottillo et al. 2016).

### 1.1.2 AMPK & Cancer

Normal cells, under aerobic conditions, convert glucose to pyruvate, via glycolysis in the cytosol (Yeluri et al. 2009). Pyruvate is transported into mitochondria where it is oxidised to acetyl CoA which then enters the Krebs cycle and produces NADH. In turn, NADH is used by the electron transport chain for oxidative phosphorylation. Under anaerobic conditions, glycolysis proceeds as above, but pyruvate remains in the cytosol, where it is converted to lactate by lactate dehydrogenase. Anaerobic respiration generates much less energy than aerobic respiration, producing only two molecules of ATP per molecule of glucose in contrast to 38.

Nobel Laureate, Otto Warburg, first identified altered energy metabolism in tumours in the 1920s (Vander Heiden, Cantley, and Thompson 2009). Even in the presence of adequate oxygen, cancer cells predominantly generate energy through an increased rate of glycolysis with conversion of pyruvate to lactate as opposed to glycolysis and mitochondrial respiration. This is termed aerobic glycolysis (or the Warburg effect) and its significance was acknowledged by Hanahan and Weinberg in 2011, when they added 'reprogrammed energy metabolism' as an emerging hallmark, to their original six hallmarks of cancer **Figure 1.6** (Hanahan and Weinberg 2011). Although aerobic glycolysis is energetically inefficient, cancer cells appear able to compensate by increasing their glucose uptake. The enhanced availability of glycolytic intermediates that results from augmented glycolytic flux provides substrates for biosynthesis of amino acids, lipids, nucleic acids and other molecules essential to cell growth and proliferation.

Given this 'reprogrammed energy metabolism' that occurs in tumour cells and the key role of AMPK in metabolism, it is likely that AMPK is of significance in cancer. However, evidence regarding AMPK's role in tumourgenesis, specifically whether it promotes or suppresses cancer development, is somewhat conflicting.

LKB1 is the major upstream kinase of AMPK. Encoded for by *STK11* on chromosome 19p13, LKB1 is a serine/threonine protein kinase and requires MO25 and Ste20-related adaptor protein (STRAD) binding for its activity (Hawley et al. 2003; Alessi, Sakamoto, and Bayascas 2006). It is a tumour suppressor and germline mutations resulting in impaired LKB1 activity

are the cause of Peutz-Jeghers syndrome, an autosomal dominant cancer predisposition syndrome associated with benign intestinal hamartomas and characteristic hyperpigmented macules on the lips and oral mucosa (Hemminki et al. 1998; Jenne et al. 1998). Furthermore, mutations in the gene encoding LKB1 are detected in up to 35% of non-small cell lung cancers and 20 % of cervical cancers (Ji et al. 2007; Wingo et al. 2009). AMPK is activated by LKB1 and

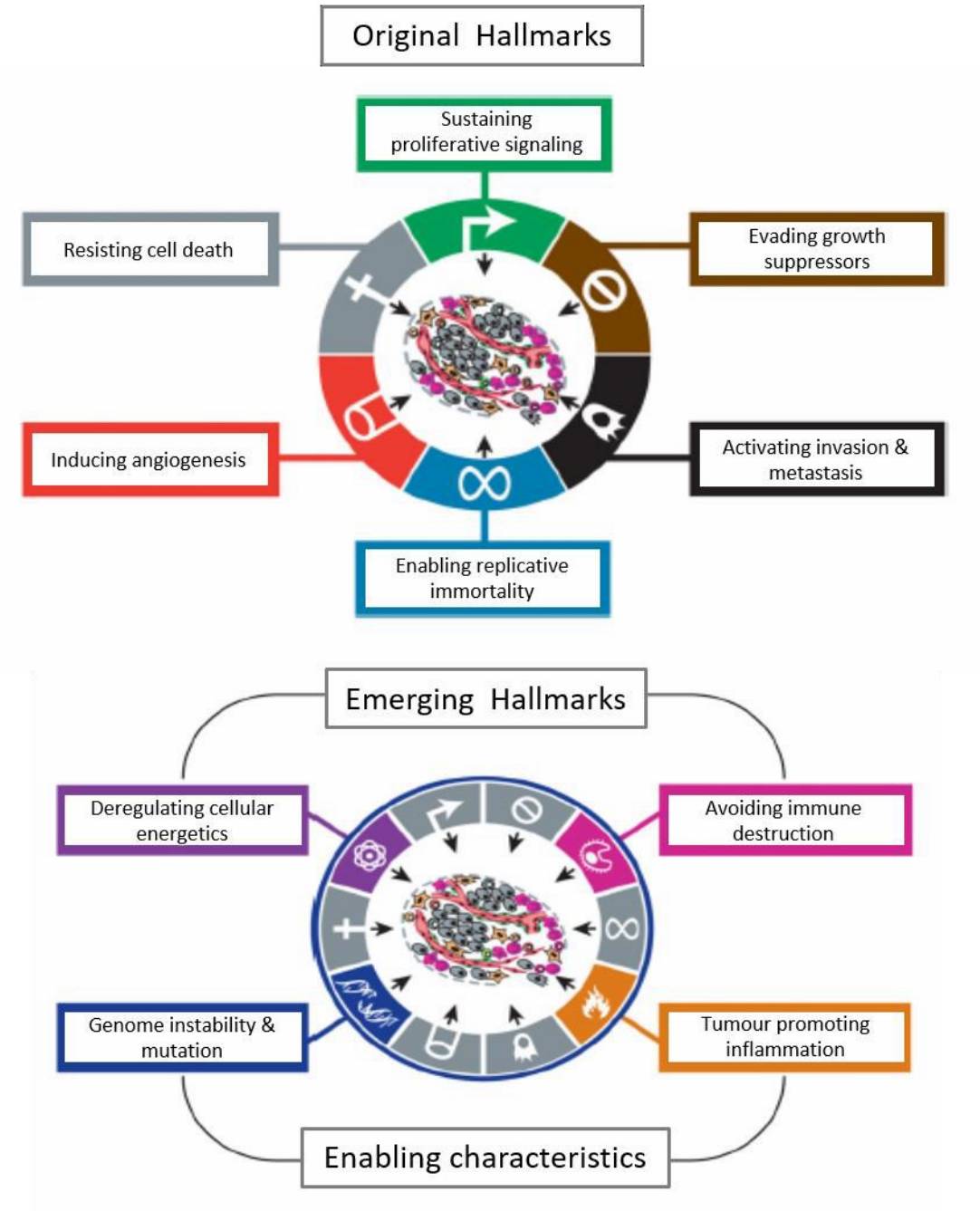


***Figure 1.6 – Original hallmarks, emerging hallmarks & enabling characteristics of cancer*** *(Hanahan and Weinberg 2011).*

so plays a key role in the execution of many of its tumour suppressor functions. However, in addition to AMPK, LKB1 phosphorylates a number of other AMPK-related kinases (such as microtubule affinity-regulating kinase 4 – MARK4) and AMPK can be activated by other molecules (such as CaMKKβ), therefore LKB1 and AMPK can operate independently (Bright, Thornton, and Carling 2009).

Peutz-Jeghers syndrome is one of four familial cancer syndromes associated with unusual pigmentation and which share related molecular aetiology. Loss of *STK11* in Peutz-Jeghers, *PTEN* in Cowdens syndrome, *TSC1/2* in Tuberous sclerosis complex and *NF1* in Neurofibromatosis type 1 all ultimately lead to increased mTORC1 activity. (Lodish and Stratakis 2010). Since, like these tumour suppressors, AMPK plays a key role in down-regulating mTORC1, it seems likely that it might have tumour suppressor like qualities (Gwinn et al. 2008; Cheng et al. 2004; Inoki, Zhu, and Guan 2003). Furthermore, the PTEN/AKT/mTORC1 pathway is not the only anabolic pathway inhibited by AMPK. AMPK also inhibits lipid synthesis, which is commonly up-regulated in tumour cells and may prevent cell cycle progression so has predominantly inhibitory effects in terms of cell growth and proliferation (Davies et al. 1992; Thoreen and Sabatini 2005; Menendez and Lupu 2007; Mounier, Bouraoui, and Rassart 2014; Zadra et al. 2014).

A growing number of studies have linked the observation that nutrient deprivation induces cell cycle arrest, with the actions of AMPK (Thoreen and Sabatini 2005). It has been suggested that AMPK activity increases phosphorylation of the cell cycle regulators tumour suppressor p53 and cyclin dependent kinase inhibitor $p27^{kip1}$, resulting in their accumulation and so limiting cell cycle progression (Jones et al. 2005; Liang et al. 2007). However, the proposed phosphorylation sites on p53 and p27 do not conform well to AMPK target sequences in other substrates. More recently it has been proposed that AMPK is indirectly involved in p53 acetylation and accumulation (Lee et al. 2012).

The yeast orthologue of AMPK is SNF1. In the presence of sufficient glucose, yeast generate ATP through fermentation which closely resembles aerobic glycolysis seen in cancer cells. However, following SNF1 activation (in response to a fall in glucose concentration), yeast switch from fermentation to mitochondrial oxidative metabolism, suggesting that AMPK

might have an 'anti-Warburg' effect (Dandapani and Hardie 2013). This suggestion was supported by a study by Faubert et al. (Faubert et al. 2013). They demonstrated up- regulated aldolase A, lactate dehydrogenase A and pyruvate dehydrogenase kinase mRNA expression, enhanced aerobic glycolysis and increased biosynthesis in cells in the absence of AMPK. They also identified that these effects were dependent upon increased hypoxia inducible factor 1α (HIF1α) expression despite normoxia and confirmed their results *in vivo,* showing that AMPK α1 deficiency promoted tumourigenesis in mice with Myc-induced B cell lymphoma.

Whilst AMPK loss alone does not appear to be sufficient to initiate tumourgenesis, there is growing evidence that in the presence of other oncogenic drivers it can facilitate cancer progression and conversely that AMPK up-regulation can inhibit tumour development (Huang et al. 2008). For example, crossing mice that are heterozygous for *Pten* and spontaneously develop tumours in a range of tissues from around 7 months of age, with mice expressing reduced levels of LKB1, accelerated oncogenesis. In contrast, tumour onset in mice treated with biguanide or A-769662 was delayed.

Somatic AMPK mutations in cancers are rare (<3% for any subunit), however AMPK activity is often reduced in tumours (Hardie 2015b; Liang and Mills 2013). Mutations in LKB1 can impair its ability to up-regulate AMPK, but a number of other mechanisms by which AMPK function is inhibited either directly or through LKB1 have also been identified.

AKT phosphorylates AMPK α1 at Ser 485 which limits Thr 172 phosphorylation (Hawley et al. 2014). AMPK activity may therefore be reduced in tumour cells with over-activation of AKT. Indeed, enhanced AMPKα1$^{Ser487}$ (the human equivalent of Ser 485) phosphorylation is seen in PTEN deficient cancer cell lines. Melanoma associated antigens (MAGEs) which are normally only found in the testis, are aberrantly expressed in some cancers and associated with increased tumour viability (Pineda et al. 2015). MAGE-A3 has been shown to interact with AMPK and promote its degradation (as a result of polyubiquitination by TRIM28) and MAGE expression in tumours inversely correlates with total and Thr172 phosphorylated AMPK levels. Phosphorylation and down-regulation of LKB1 due to enhanced B-RAF signalling was demonstrated in BRAF$^{V600E}$ mutant melanoma cells and relief of this inhibitory effect on LKB1 slowed proliferation (Zheng et al. 2009). Finally, the microRNA miR-451 which is often over-

expressed in gliomas, has been shown to inhibit MO25 expression and so LKB1 signalling (Godlewski et al. 2010).

Metformin is a biguanide drug, currently prescribed to >100 million patients worldwide and is known to activate AMPK by inhibiting complex 1 of the respiratory chain, resulting in a fall in intracellular ATP concentration (Shackelford and Shaw 2009; Zhou et al. 2001). Another biguanide, phenformin, was withdrawn from clinical use in the 1970s due to incidence of often fatal lactic acidosis. However, it is a more potent complex 1 inhibitor and distributes throughout tissues more widely than metformin, as metformin requires organic cation transporter 1 (OCT1) for its uptake into cells (Shackelford et al. 2013). A retrospective case control study by Evans et al., over an eight year period, demonstrated that T2DM patients who had been treated with metformin had significantly reduced risk (>20%) of developing cancer (Evans et al. 2005). Furthermore, the protection offered by metformin appeared dose dependent. They concluded that the reduced cancer incidence following metformin exposure could be due to increased AMPK activity.

Hardie subsequently proposed 2 alternative modes by which metformin might impose its anti-neoplastic effects (Hardie 2013). Firstly, given that metformin is known to lower blood glucose, through inhibition of gluconeogenesis and increased glucose uptake, it may reduce cancer risk in patients with T2DM by attenuating the potentially pro-tumourgenic effects of hyperglycaemia and hyperinsulinaemia. Secondly Metformin may trigger apoptosis through depletion of ATP resulting in metabolic stress. This cytotoxic effect would be enhanced in cells with defective energy homeostasis (e.g. due to LKB1 loss and so impaired AMPK activity). The latter mechanism stems from the observations by Shackelton et al. that when Kras mutant; Kras mutant and LKB1 null; and Kras mutant and p53 null mice were treated with metformin, AMPK was only activated in mice with functioning LKB1 and tumour growth and glucose uptake were only reduced in mice without functioning LKB1 (Shackelford et al. 2013).

Other studies support the hypothesis that AMPK promotes cell survival under conditions of metabolic stress. Pentose phosphate pathway NADPH generation is impaired in the absence of glucose and AMPK compensates for this by inhibiting fatty acid synthesis (reducing NADPH consumption) and promoting fatty acid oxidation (increasing NADPH production) through

phosphorylation of ACC. Jeon et al. observed that this adaptation was impaired in LKB1 deficient cells resulting in accelerated NADPH depletion, accumulation of reactive oxygen species (ROS) and cell death (Jeon, Chandel, and Hay 2012). Furthermore, the suggestion that a small amount of AMPK activity is required for tumour cell survival but that normal or increased AMPK levels have an inhibitory effect, would explain the finding that mouse embryonic fibroblasts (MEFs) deficient in AMPK α2 are more susceptible to mutant KRAS transformation than normal MEFs, whilst those lacking any AMPK α are resistant (Laderoute et al. 2006; Phoenix et al. 2012).

It is increasingly being recognised that the actions of AMPK may vary not only with context, but also subunit composition (Ross, MacKintosh, and Hardie 2016). Analysis of cBioPortal cancer genome and cancer cell line encyclopedia data revealed that changes in *PRKAA1* (encoding AMPK α1) and *PRKAB2* (encoding AMPK β2) are more frequent and are usually amplifications, whereas *PRKAA2* (encoding AMPK α2) and *PRKAB1* (encoding AMPK β1) gene changes are much less common and are mostly mutations. These findings imply that AMPK α1 and β2 are more often up-regulated in cancers whereas AMPK α2 and β1 function are lost, suggesting that AMPK α1 and β2 and AMPK α2 and β1 may have divergent roles in cancer, the former acting as oncogenes and the latter tumour suppressors.

### 1.1.3 AMPK & Inflammation

AMPK's involvement in inflammation has emerged relatively recently. A number of studies have demonstrated that when immune cells, such as phagocytic and T cells, are stimulated by lipopolysaccharide (LPS), antigen presentation, inflammatory cytokines etc, AMPK activity within them falls. This, in turn, is associated with a switch from oxidative metabolism to aerobic glycolysis, similar to that seen in cancer cells (Dandapani and Hardie 2013).

M2 'repair' macrophages resident in tissue and involved in wound healing can be activated by pro-inflammatory cytokines to become M1 'killer' macrophages and this transformation is associated with reduced AMPK activity (Sag et al. 2008). Indeed macrophages treated with (LPS – an endotoxin from gram negative bacteria) have decreased AMPK activity and in contrast, AMPK activity in cells exposed to the anti-inflammatory cytokines interleukin 10 (IL-10) and transforming growth factor β (TGF-β) is enhanced. Furthermore inhibition of AMPK in macrophages results in increased release of pro-inflammatory cytokines whereas nuclear factor kappa-light-chain-enhancer of activated B cells (NF-κB) signalling is inhibited in sensitised marcophages with constitutively active AMPK. Reduced AMPK activity and so increased aerobic glycolysis in M1 macrophages may facilitate the mitochondria to switch from ATP to ROS production, the latter required for phagocytosis (West et al. 2011). In T-cells increased aerobic glycolysis permits biosynthesis and so proliferation.

Given that AMPK can potentially contribute to reducing inflammation, it is possible that some drugs with anti-inflammatory properties operate by activating AMPK. Following absorption, aspirin is rapidly broken down to salicylate (Hawley et al. 2012). Salicylate (but not aspirin) is an allosteric AMPK activator. Unlike aspirin, salicylate is a poor inhibitor of cyclo-oxygenases and so prostanoid synthesis and it has therefore been hypothesised that salicylate, abundant following administration of aspirin, exerts an anti-inflammatory effect by activating AMPK in immune cells (Grahame Hardie 2014).

## 1.2 The metabolic syndrome

### 1.2.1 Definition, Epidemiology & Pathogenesis

Currently, a diagnosis of metabolic syndrome requires the presence of at least 3 of the 5 metabolic abnormalities listed in **Table 1.4**, all of which are risk factors for T2DM and cardiovascular disease (Alberti et al. 2009).

| Criteria | Parameters |
|---|---|
| Increased waist circumference | Population specific. Some definitions use BMI>30 kg/m$^2$ instead |
| Hypertriglyceridaemia* | ≥100 mg/dl (5.5mmol/L) |
| Reduced HDL-C* | ≤50 mg/dl (1.3mml/L) |
| Glucose intolerance* | Fasting glucose ≥100 mg/dL (5.5mmol/L) |
| Blood pressure* | ≥130/85 mm Hg |

***Table 1.4 - Metabolic syndrome diagnostic criteria*** *(Alberti et al. 2009). *Or receiving treatment for this condition, HDL-C = high density lipoprotein cholesterol.*

Obesity occurs as a result of excess energy intake over energy expenditure, in combination with genetic susceptibility factors. Surplus energy is stored in adipocytes, resulting in weight gain. Overweight (Body mass index – BMI ≥ 25 kg/m$^2$) and obesity (BMI ≥ 30 kg/m$^2$) are on the increase (Ogden et al. 2007). Data from Public Health England show that between 1993 and 2015 the prevalence of obesity among adults in England almost doubled from 14.9% to 26.9% and that in 2015 62.9% of adults in England were overweight or obese (https://www.noo.org.uk). Furthermore, it is anticipated that by 2050 obesity will affect more than 50% of the adult and 25% of the child population.

White adipose tissue in obese individuals with the metabolic syndrome is abnormal in a number of ways: It is chronically inflamed, associated with increased inflammatory cell (especially macrophage) infiltration and cytokine (such as tumour necrosis factor α - TNFα

and IL-6) release; leptin secretion is enhanced whilst that of adiponectin is reduced; its distribution tends to be more visceral as opposed to subcutaneous; and when insulin resistance develops, inhibition of adipose tissue lipolysis is impaired (Nolan, Damm, and Prentki 2011).

Free fatty acids absorbed from the diet and released from an increased adipocyte mass are converted to triglycerides in the liver and then released into the circulation in very low density lipoproteins (VLDLs). Dietary carbohydrates also contribute to liver triglyceride production through *de novo* lipogenesis. Therefore high fat and carbohydrate diets and obesity promote hypertriglyceridemia. When present, insulin resistance enhances adipocyte lipolysis, providing substrate for triglyceride synthesis and relieves VLDL secretion inhibition (Eckel, Grundy, and Zimmet 2005). Therefore, it too contributes to increased serum triglyceride concentrations. Raised VLDL levels trigger lipoprotein remodelling which in turn results in increased high density lipoprotein (HDL) clearance. Excess lipid and impaired adipose tissue function together result in ectopic lipid deposition in muscle and liver which promotes insulin resistance (Stumvoll, Goldstein, and van Haeften 2005).

In susceptible individuals, chronic energy excess causes insulin resistance and reduced pancreatic islet β cell function resulting in impaired glucose tolerance and T2DM (**Figure 1.7**) (Stumvoll, Goldstein, and van Haeften 2005; Nolan, Damm, and Prentki 2011). The number of people in the UK diagnosed with diabetes rose from 1.4 million in 1996 to 3.5 million in 2014 and the estimated prevalence is currently 4.5 million (7% of the population - https://www.diabetes.org.uk/Professionals/Position-statements-reports/Statistics).
Complications of the disease, which are mostly vascular, impose a huge medical and socioeconomic burden: In the USA diabetes is the commonest cause of blindness in adults and is responsible for 60% of non-traumatic lower-limb amputations and 44% of end-stage renal failure (www.cdc.gov/diabetes/pubs/pdf/ndfs_2011.pdf).

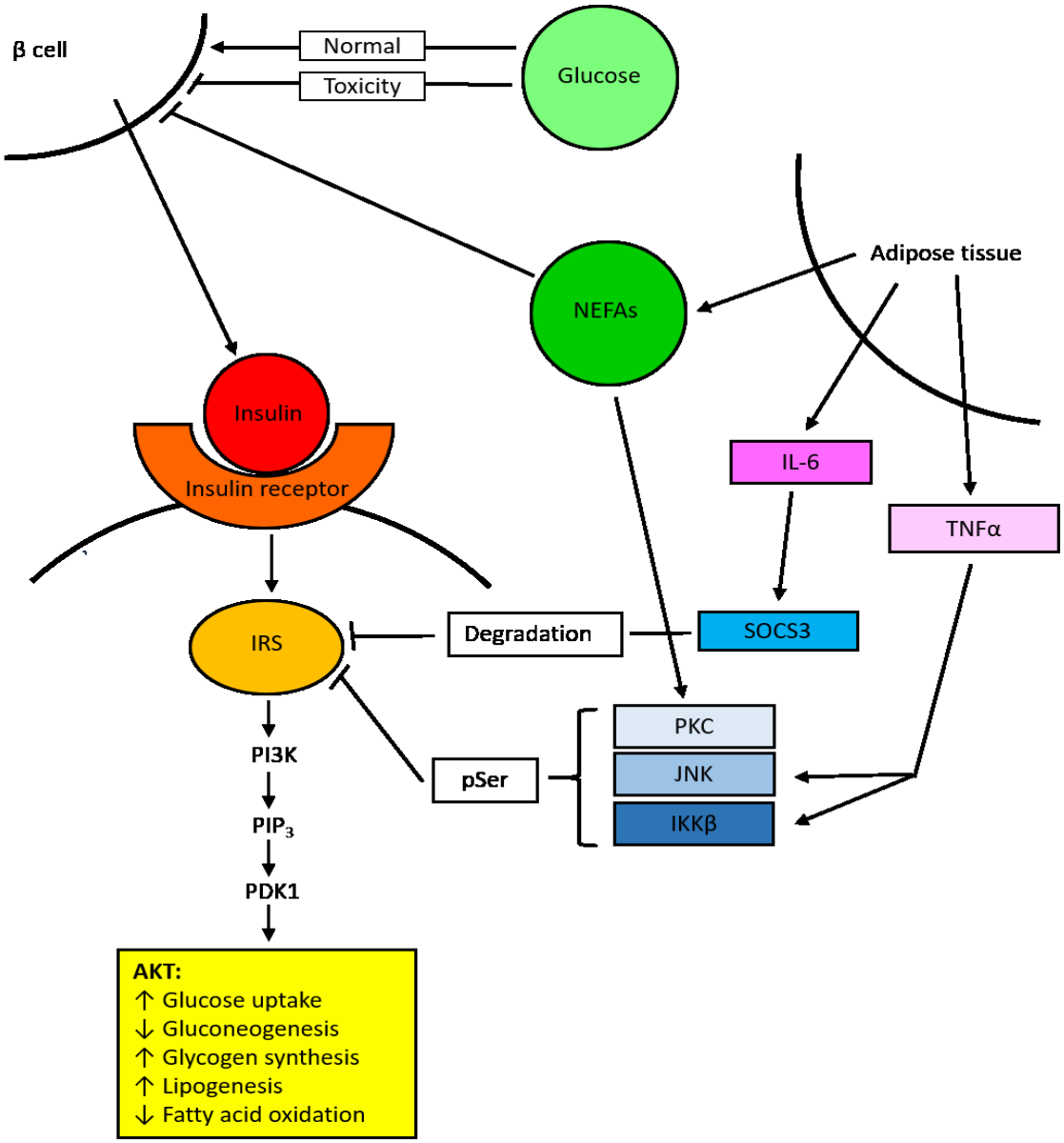


***Figure 1.7 – Insulin signalling in health and T2DM.*** *Normally, insulin release results in insulin receptor tyrosine phosphorylation, which causes insulin receptor substrate (IRS) tyrosine phosphorylation, which activates the phosphoinositide 3-kinase (PI3K)/AKT pathway. Protein kinase C (PKC), upregulated by non-esterified fatty acids (NEFAs) and c-Jun N-terminal kinase (JNK) and inhibitor of nuclear factor kappa-B kinase subunit β (IKKβ), activated by adipose tissue tumour necrosis factor α (TNFα) all cause IRS serine phosphorylation resulting in reduced tyrosine phosphorylation. IL-6 secreted by adipose tissue upregulates suppressor of cytokines signalling (SOCS) protein expression leading to IRS degradation. Glucose normally triggers β cell insulin secretion, however persistent hyperglycaemia and NEFA exposure can cause β cell glucotoxicity and lipotoxicity respectively.*

### 1.2.2 AMPK and the metabolic syndrome

Given AMPK's key role in the regulation of various aspects of metabolism and its potential function in inflammation, it is likely to be of importance in development of the metabolic syndrome. AMPK has been shown to be down-regulated in adipose tissue from obese individuals with insulin resistance, relative to those who are insulin sensitive (Xu et al. 2012). Furthermore, a number of factors which offer varying degrees of protection with regards the metabolic syndrome, such as exercise, metformin, salicylate and adiponectin, have also been shown to activate AMPK (Winder et al. 2000; Zhou et al. 2001; Zhou et al. 2009; Hawley et al. 2012). However it is unlikely that their effects are entirely AMPK dependent. Therefore, over recent years, AMPK has received substantial attention as a therapeutic target.

By inhibiting *de novo* lipogenesis and promoting fatty acid oxidation, AMPK helps to constrain ectopic lipid accumulation in liver and skeletal muscle and in so doing limit dyslipidaemia, insulin resistance and NAFLD (Davies et al. 1992; Merrill et al. 1997). AMPK also enhances glucose uptake and down-regulates gluconeogenesis and so improves glucose tolerance through direct effects on glucose handling, which, in turn reduces ectopic lipid accumulation (Koo et al. 2005; Pehmoller et al. 2009).

Adipose tissue thermogenesis, which has anti-obesity and so anti-diabetic effects, requires adequate numbers of functioning mitochondria and AMPK appears to be key in maintaining mitochondrial homeostasis (Jager et al. 2007; Egan et al. 2011). Indeed thermogenesis in mice lacking adipocyte AMPK β1 and β2 was impaired resulting in hepatic steatosis and insulin resistance (Mottillo et al. 2016).

Finally, given that obesity is considered a state of chronic inflammation which in turn is believed to contribute to the development of both NAFLD and insulin resistance, it is likely that AMPK's anti-inflammatory properties are also important to its role in protection from the metabolic syndrome (Ruderman et al. 2013; Sag et al. 2008). In line with this, Galic and colleagues recently demonstrated that mice with AMPK deficient macrophages, fed a high fat diet, had more M1 and bone marrow derived macrophages in their adipose tissue; raised levels of inflammatory cytokines in their serum and increased insulin resistance (Galic et al. 2011).

A number of studies, using pharmacological agents to examine the effects of whole body increased AMPK activity, support the idea that AMPK might be a good target for preventing and treating the metabolic syndrome. Cool et al. identified the thienopyridone A-769662 as a direct activator of AMPK and showed that it reduced fatty acid synthesis in primary hepatocytes and lowered liver malonyl CoA levels and the respiratory exchange ratio (indicative of increased use of fat as a respiratory substrate) when administered as a bolus to rats (Cool et al. 2006). Chronic treatment of diabetic ob/ob mice with A-769662 resulted in lower body, epididymal fat pad and liver weights and reduced serum triglyceride levels. Fed serum glucose concentrations were also reduced and this was associated with reduced hepatic PEPCK and G6Pase mRNA expression, but insulin levels were unaffected.

Various studies have used AICAR to activate AMPK in genetic and diet induced rodent models of obesity and demonstrated increased glucose uptake; decreased gluconeogenesis; lowered serum glucose concentrations; and improved glucose tolerance in response to treatment (Bergeron et al. 2001; Pold et al. 2005; Song et al. 2002; Iglesias et al. 2002; Buhl et al. 2002). In some cases, particularly those where AICAR was administered long-term insulin resistance and serum concentrations were also reduced. Henriksen et al. also documented decreased high fat diet induced liver triglyceride accumulation in rats treated with AICAR. Treatment was associated with reduced levels of SREBP1c, but not differences in markers of fatty acid oxidation.

Many genetic models of AMPK activation are based on naturally occurring mutations in AMPK γ2 and γ3, associated with WPW syndrome and the distinct phenotype of Hampshire pigs respectively (Arad, Seidman, and Seidman 2007; Milan et al. 2000). Most recently Yavari et al. studied the effects of an activating *Prkag2* R299Q mutation (equivalent to human R302Q) in mice (Yavari et al. 2016). Although initially presence of the mutation had some mild beneficial effects, such as increased insulin sensitivity, the most striking finding in mice with systemic increased AMPK activity was development of adult onset obesity. Yavari et al. concluded that this was due to increased gherelin dependent orexigenic signalling from the hypothalamus and so hyperphagia. They also demonstrated that γ2R299Q mutant mice had impaired pancreatic islet insulin secretion.

Global AMPK knockout models have also been studied and their findings suggest a protective role for AMPK with regards the metabolic syndrome. Mice with global AMPK α2 knockout, fed a high fat diet, gained weight more quickly; had greater adipose tissue mass due to adipocyte hypertrophy and had higher serum but not liver triglyceride levels than wild-type animals exposed to the same conditions (Villena et al. 2004). Reduced insulin sensitivity and impaired glucose tolerance was also seen in mice with AMPK α2 knockout relative to wild-type controls, but only following normal chow feeding. The effect was lost following high fat diet exposure.

Most deductions regarding the effects of AMPK in the liver stem from these studies of systemic increased or decreased AMPK activation, especially the pharmacological studies where drugs reach their highest concentrations in the liver (Cool et al. 2006). However, Foretz et al. used adenovirus-mediated transfer of a gene encoding constitutively active mutant AMPKα2 (AMPKα2-CA) to study the effects of acute liver specific AMPK activation (Foretz et al. 2005). Infected primary hepatocytes showed reduced glucose production and gluconeogenic gene (PEPCK and G6Pase) expression. Mice expressing AMPKα2-CA had reduced fasted and fed serum glucose levels, associated with increased glucagon and decreased insulin concentrations in the serum. This effect was also seen in insulin resistant *ob/ob* and streptozotocin induced type 1 diabetic mice infected with the adenovirus. Surprisingly, liver specific increased AMPK activity also led to accumulation of triglycerides in the liver, with an associated fall in adipose tissue mass and serum triglycerides and rise in ketone production (plasma β-hydroxybutyrate levels). Foretz et al. therefore concluded that acute AMPK activation in hepatocytes resulted in a switch from glucose to fatty acid metabolism, with subsequent redistribution of fatty acids from peripheral stores to the liver. Andreelli et al. demonstrated that liver specific AMPK α2 knock out resulted in impaired glucose tolerance; elevated fasting serum insulin levels (although insulin sensitivity was unaffected); and increased serum triglyceride and reduced serum ketone concentrations, without affecting body weight or composition.

### 1.2.3 Free sugars, fructose and the metabolic syndrome

It has been suggested that certain dietary components may be of particular significance in the pathogenesis of the metabolic syndrome, over and above their contribution to increased calorific intake. Free sugars, especially fructose, have received considerable attention in this context. Free sugars are monosaccharides (glucose, fructose and galactose) and disaccharides (sucrose, maltose, lactose and trehalose) either added to, or naturally present, in foods (Te Morenga, Mallard, and Mann 2012). Data from the US Department of Agriculture (USDA) suggest that in the US, between 1970 and 2007, there was a 15% increase in calories from sugar (http://www.ers.usda.gov). Indeed the rise in caloric consumption that was seen over this period was primarily due to increased carbohydrate intake (Chanmugam et al. 2003). This increase in sugar consumption parallels the global rise in prevalence of the metabolic syndrome that has occurred over recent decades (Ogden et al. 2007). There is therefore epidemiological evidence linking dietary free sugar with the metabolic syndrome.

Carbohydrate enriched diets, both iso and hypercaloric, have been shown to promote *de novo* lipogenesis compared to normal or high fat diets (Schwarz et al. 1995; Hudgins et al. 2000). Hudgins et al. demonstrated that after consumption of a high carbohydrate diet (10% fat and 75% carbohydrate – sugar to starch ratio 60:40) for 2 weeks, rates of *de novo* lipogenesis following fasting and feeding were 27 and 4 times higher respectively than those after normal carbohydrate (30% fat and 55% carbohydrate) feeding (Hudgins et al. 2000). This is the principle behind the French delicacy 'foie gras' which translated means 'fat liver' and is produced by feeding ducks or geese a high carbohydrate, low fat diet.

In addition to the increase in total free sugar consumption that has occurred over recent decades, the types of sugar being consumed, have changed. During the first half of the 20$^{th}$ century sucrose was the main dietary sugar, however in 1967 techniques were developed to produce fructose, particularly high fructose corn syrup (HFCS – commonly 55% fructose and 45% glucose), from corn (Tappy and Le 2010). In addition to sweetening foods at low cost, fructose enhances the shelf-life of baked products and these factors have led to a rapid rise in its use. USDA data indicate that between 1970 and 2007 sucrose consumption fell from 90 to 45% of sugar intake, mirrored by an increase in HFCS use from 0 to 41% of sugar ingested (http://www.ers.usda.gov). Based upon this epidemiological data, it has been suggested that

fructose plays a specific role in development of the metabolic syndrome. However, it is important to note that although total fructose consumption has increased, because the composition of HFCS is very similar to that of sucrose (50% fructose and 50% glucose), proportion of fructose in the diet is unlikely to have changed markedly. Furthermore, agricultural policies in the European Union limit HFCS production, so products such as soft drinks, outside of the USA, are still largely sweetened with sucrose (Moore, Gunn, and Fielding 2014).

A number of studies have evaluated rates of *de novo* lipogenesis after fructose feeding and some have compared these rates to those following glucose consumption (Faeh et al. 2005; Parks et al. 2008; Stanhope et al. 2009; McDevitt et al. 2001; Schwarz et al. 2015). There is considerable heterogeneity amongst investigations in terms of subject and sugar dose and although in all but one case sugar was given in addition to normal feeding, the extent of hypercaloric intake varied. However, they do demonstrate that fructose intake upregulates *de novo* lipogenesis and promotes hepatic steatosis and hyperlipidaemia. There is also some evidence that these effects are more marked following fructose as opposed to glucose consumption.

Mc Devitt et al. measured rates of *de novo* lipogenesis in lean and obese participants during 96 hours of energy balanced feeding (with control diet) and sucrose or glucose overfeeding (in both cases 50% extra calories) (McDevitt et al. 2001). *De novo* lipogenesis was significantly raised in obese relative to lean subjects following control feeding and increased with overfeeding in all subjects. However, no significant differences in *de novo* lipogenesis were seen between sucrose and glucose overfeeding. Schwarz et al. demonstrated increased *de novo* lipogenesis following consumption of a fructose enriched diet compared to an isocaloric diet in which fructose was replaced by complex carbohydrate (Schwarz et al. 2015). In Park et al.'s experiment *de novo* lipogenesis was significantly higher in healthy volunteers following a 50:50 or 25:75 compared to a 100:0 glucose:fructose bolus, indicating that the presence of fructose promoted *de novo* lipogenesis, but without a dose effect (Parks et al. 2008). In their study, following a subsequent meal, serum triglycerides were higher in those subjects that had initially been exposed to a sugar bolus, suggesting that as well as acutely increasing *de novo* lipogenesis, sugar consumption promotes metabolic processes that yield

hyperlipidaemia. Following 6 days of overfeeding (25% extra calories) with fructose in healthy men, Faeh et al. measured *de novo* lipogenesis and found that it was increased almost 6 fold relative to that in controls, however, their study lacked a non-fructose comparator (Faeh et al. 2005). Finally, Stanhope et al. documented a differential effect of fructose on *de novo* lipogenesis and hyperlipidaemia in overweight and obese subjects who consumed glucose or fructose beverages containing 25% of their usual calorific intake, in addition to their normal diet, for 10 weeks (Stanhope et al. 2009). *De novo* lipogenesis (relative to baseline) was unchanged in subjects who consumed glucose but postprandial *de novo* lipogenesis was significantly raised in those who consumed fructose. In addition, plasma lipid and lipoprotein measurements generally increased in subjects from the fructose but not the glucose group.

The stages of fructose metabolism are summarised in **Figure 1.8**. Fructokinase is only expressed in the liver and has a low Km, high Vmax and is very specific for fructose, so the vast majority of fructose entering the portal circulation undergoes first pass metabolism (Adelman, Ballard, and Weinhouse 1967). Indeed, following ingestion of 1g/kg of fructose, systemic blood levels remain in the micromolar range, unlike the 10mM increase seen with an equivalent dose of glucose (Havel 2005). Fructose which is not metabolised in the liver, undergoes minimal metabolism elsewhere and so is excreted in the urine (Hommes 1993). Hence, individuals with fructokinase deficiency suffer from the benign condition hereditary fructosuria.

Fructose metabolism differs from that of glucose in three key ways (Tappy and Le 2012, 2010):

1) Following uptake into hepatocytes glucose is converted to glucose-6-phosphate (G-6-P) by glucokinase and then via glycolysis enzymes to triose-phosphates (triose-Ps). Fructokinase has a much lower Km for fructose than glucokinase has for glucose. Therefore, unlike entry of glucose into the glycolysis pathway, which is dependent upon glucose concentration, entry of fructose into fructolysis is concentration independent.

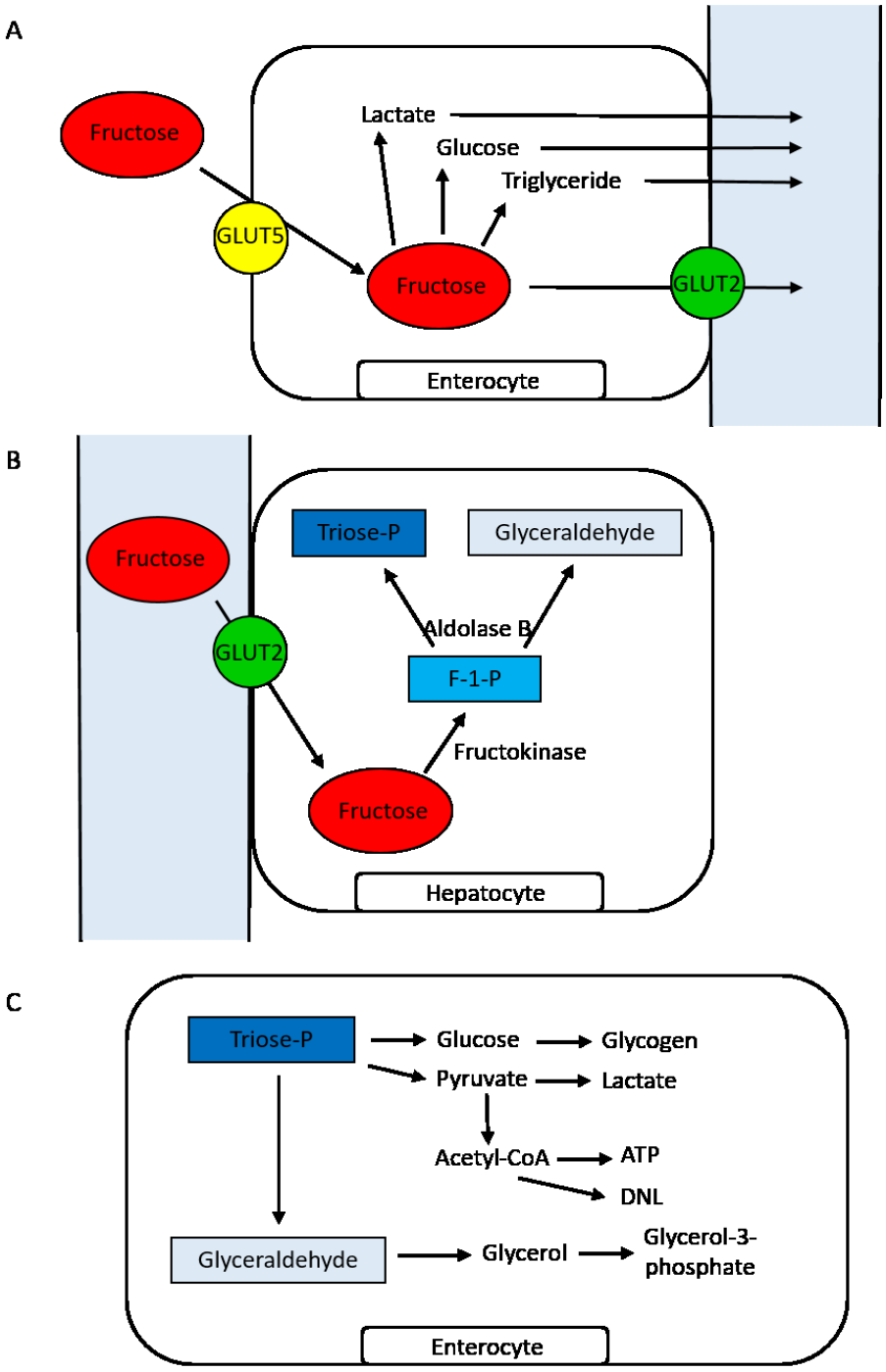


***Figure 1.8 - Fructose metabolism**. **(A)** Fructose enters enterocytes via a concentration gradient assisted by GLUT5 and the majority is transported into the portal circulation by GLUT2**. (B)** Fructose is taken up into hepatocytes by GLUT2 and converted to fructose-1-phospate (F-1-P) by fructokinase and triose-phosphates (triose-Ps) and glyceraldehyde by aldolase B. **(C)** Triose-Ps are mostly used for gluconeogenesis. Some complete glycolysis forming pyruvate, which is metabolised to lactate or converted to Acetyl-CoA. Acetyl-CoA can enter the Krebs cycle or be used in de novo lipogenesis (DNL). Conversion of glyceraldehyde to glyceraldehyde-3-phosphate occurs via glycerol, which can also be used in triglyceride synthesis.*

2) Phosphofructokinase, a key enzyme in the glycolysis pathway, is inhibited by ATP and citrate, so glycolysis is regulated by energy status. Conversion of F-1-P to triose-Ps however, is not under any such restriction.

3) Finally, Insulin is required for glucokinase gene expression, glycolytic enzyme activation and so glucose metabolism, whereas fructose metabolism is independent of insulin.

As a result of these differences more than 70% of portal fructose is converted to triose-Ps, in stark contrast to glucose, only 15-30% of which is metabolised in the liver (Tappy and Le 2012). Therefore availability of triose-Ps for *de novo* lipogenesis and glycerol synthesis is greater following fructose compared to glucose consumption and this might promote lipid synthesis. This hypothesis is not however supported by studies examining the fate of oral fructose. Chong et al. tracked the handling of a [U$^{13}$C]D-fructose labelled meal over 6 hours and found that 35% of fructose was oxidised; 0.05% was converted to FFA and secreted in VLDL; and 0.15% was used to generate glycerol which was then incorporated in triglycerides in VLDLs (Chong, Fielding, and Frayn 2007). The balance was unaccounted for, but presumably contributed to lactate and glycogen formation. Given that in Chong et al.'s study only a relatively small amount of carbon in triglycerides synthesised through *de novo* lipogenesis, derived from fructose, their findings indicate a more complex role for fructose in promotion of *de novo* lipogenesis, for instance upregulation of lipogenic gene expression and enzyme activity.

SREBP1c and ChREBP are activated and inhibited by insulin and glucagon signalling respectively and ChREBP is also directly activated by glucose (Rui 2014)(**Figure 1.3** & **Figure 1.4**). These transcription factors, key to lipogenic gene expression, are also activated by fructose and there is evidence to suggest that fructose has an enhanced effect on SREBP1c and ChREBP activity relative to glucose (Koo et al. 2009; Herman and Samuel 2016). Although attenuated relative to wild-type mice, following fructose feeding, liver-specific insulin receptor knockout (LIRKO) mice do experience up-regulation of SREBP1c, suggesting that some activation of SREBP1c by fructose occurs via insulin independent pathways (Haas et al. 2012). Mechanisms for induction of ChREBP by fructose are undetermined but may relate to increased levels of carbohydrate metabolites (Filhoulaud et al. 2013). 'Catalytic' doses of

fructose have been shown to increase glucokinase activity, and so G-6-P levels, by aiding release of glucokinase from its regulatory protein (Van Schaftingen, Detheux, and Veiga da Cunha 1994). ChREBP function appears particularly important in fructose metabolism. Reduced hepatic ChREBP expression in fructose fed mice resulted in reduced lipogenic gene expression in the liver, lower serum triglyceride levels and increased peripheral insulin sensitivity, but had much less impact in high fat diet fed mice (Erion et al. 2013). Furthermore whole body ChREBP knockout resulted in fructose but not glucose intolerance (Iizuka et al. 2004). A further transcription factor which is upregulated by carbohydrates and involved in lipogenic gene expression is X-box binding protein 1 (XBP1)(Lee et al. 2008). Conditional XBP1 knockout in fructose fed mice resulted in reduced lipogenic gene expression, hepatic steatosis and insulin resistance.

In addition to promoting *de novo* lipogenesis, there are a number of other mechanisms by which fructose consumption may predispose to features of the metabolic syndrome (Lim et al. 2010). Within the central nervous system fructose may have orexic effects by increasing AMPK activity (as a result of reduced ATP concentrations) (Cha et al. 2008). Fructose promotes the first step of fatty acid synthesis, the conversion of acetyl-CoA to malonyl-CoA by ACC. As well as being a key intermediate in *de novo* lipogenesis, malonly-CoA inhibits CPT-1 and therefore negatively regulates fatty acid oxidation. Finally excess fructose stimulates JNK signalling and lipid accumulation due to *de novo* lipogenesis up-regulates PKC. JNK and PKC have both been shown to serine phosphorylate IRS1 and therefore promote insulin resistance (**Figure 1.7**) (Wei et al. 2007; Li et al. 2004).

There is some evidence for a differential effect of fructose on *de novo* lipogenesis and other mechanisms involved in development of the metabolic syndrome. However, the effects of high fructose consumption on metabolic parameters in humans are not well defined. A number of meta-analyses have recently been performed in an attempt to address this issue and their key findings are summarised in **Table 1.5**. These studies do not provide conclusive evidence that fructose consumption plays a particular role in the metabolic syndrome, aside from providing an excess of calories. However, of note, in the isocaloric studies, fructose replaced carbohydrate, therefore these meta-analyses do not evaluate the effects of high carbohydrate feeding.

| | Isocaloric | | Hypercaloric | |
|---|---|---|---|---|
| | **Studies Participants** | **Outcome** | **Studies Participants** | **Outcome** |
| **Body weight** | 31<br>637 | → | 10<br>119 | ↑ |
| **Dyslipidaemia** (LDL-C, ApoB, non-HDL-C, TG and HDL-C) | 51<br>943 | → | 8<br>125 | ↑<br>ApoB & TG |
| **High dose & Dyslipidaemia** (TC, LDL-C and HDL-C) | 24<br>474 | ↑<br>TC & LDL | -<br>- | |
| **NAFLD** | 7<br>184 | → | 6<br>76 | ↑ |
| **Insulin sensitivity** (non-DM) | 32<br>837 | ↑ Hepatic IR<br>→ Fasting insulin & HOMA-IR | 14<br>168 | ↑ Hepatic IR & Fasting insulin<br>→ HOMA-IR |
| **Insulin sensitivity** (DM) | 18<br>209 | → Fasting glucose & insulin<br>↓ HbA1c | -<br>- | |
| **'Catalytic' dose & insulin sensitivity** | 6<br>118 | ↓HbA1c & fasting glucose | -<br>- | |

***Table 1.5 – Meta-analyses of controlled feeding trials examining the effects of long term (>7 days) fructose feeding on metabolic parameters****. (Sievenpiper et al. 2012; Chiavaroli et al. 2015; Cozma et al. 2012; Chiu et al. 2014; Zhang, An, et al. 2013; Ter Horst et al. 2016).* LDL-C = low density lipoprotein cholesterol, ApoB = apolipoprotein B, HDL-C = high density lipoprotein cholesterol, TG= triglycerides, TC = total cholesterol, DM – diabetes mellitus and HOMA-IR = homeostasis model assessment of insulin resistance. HbA1c is a measure of glycated haemoglobin.

## 1.3 Non-alcoholic fatty liver disease

Non-alcoholic fatty liver disease (NAFLD) is a spectrum of pathologies (**Figure 1.9**) ranging from simple steatosis (non-alcoholic fatty liver – NAFL), through non-alcoholic steatohepatitis (NASH) to fibrosis and cirrhosis with the associated increased risk of hepatocellular cancer (HCC) (Chalasani et al. 2012). It is regarded as the hepatic component of the metabolic syndrome. Patients with NAFLD have increased cardiovascular risk and those with other features of the metabolic syndrome are prone to more advanced disease (NASH/fibrosis) (Fotbolcu and Zorlu 2016; Younossi et al. 2016).

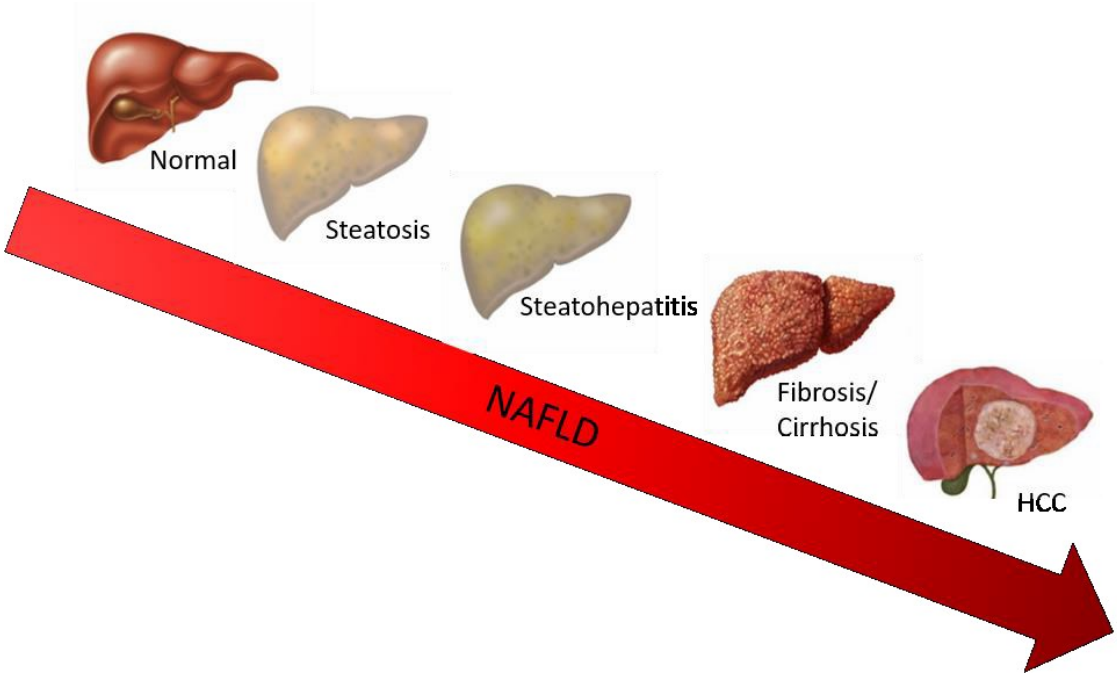


***Figure 1.9 – The spectrum of non-alcoholic fatty liver disease.***

NAFLD is common and its incidence and prevalence are increasing. NASH related cirrhosis is currently the second most common cause for liver transplantation in the USA and it is set to become the leading indication by 2020 (Younossi et al. 2016; Wree et al. 2013). Prevalence and incidence are difficult to evaluate and estimates vary, in particular depending on population studied and criteria used for diagnosis. Lazo and Clark combined the findings of 16 studies involving 2956 patients undergoing bariatric surgery and found prevalence of simple steatosis, NASH, fibrosis and cirrhosis to be 76, 37, 23 and 5.8% respectively (Lazo and Clark 2008). More recently, Younossi et al. performed a meta-analysis to evaluate the global

burden of NAFLD (Younossi et al. 2016). They showed a global prevalence of NAFLD, diagnosed on imaging of 25%. Furthermore, they calculated a liver specific mortality incidence rate among people with NAFLD of 0.77 per 1000 person-years, which translates to approximately 2% of NAFLD patients dying from a NAFLD liver related cause (Rinella and Charlton 2016). Although the latter demonstrates that liver specific complications of NAFLD are rare, taken together these findings equate to 0.5% of the world's population dying from NAFLD related cirrhosis or HCC. Interestingly regional NAFLD prevalence in Younossi et al.'s study, which was highest in South America and the Middle East, did not correlate closely with global energy intake (Younossi et al. 2016; Rinella and Charlton 2016). This finding highlights that although prevalence of obesity in patients with NAFLD and NASH is high (around 51 and 82% respectively), other environmental factors such as dietary composition and exercise, as well as genetics, are also important in NAFLD pathogenesis.

***NAFL***

Diagnosis of NAFL requires the presence of steatosis on imaging or histology in the absence of other causes such as excess alcohol consumption, hepatitis C virus (HCV) infection, Wilson's disease or drug induced steatosis (Chalasani et al. 2012). NAFL is most commonly diagnosed following investigation of abnormal serum liver function tests (LFTs) or an incidental finding of steatosis on imaging performed for another reason. Screening for NAFL in individuals with other features of the metabolic syndrome is not recommended at present. Aspartate and alanine transaminase (AST and ALT), liver alkaline phosphatase (ALP) and gamma glutamyl transpeptidase (GGT) can be, but are not always raised in NAFLD. Liver ultrasound scan (USS) is usually used to diagnose steatosis: Fatty liver appears hyperechoic as opposed to hypoechoic relative to the kidneys or spleen (Townsend and Newsome 2016). Histology is the most reliable method for diagnosing NAFL (Chalasani et al. 2012), however, given the limitations of liver biopsy, including morbidity and mortality risk, cost, and sampling error, it is not recommended currently, except in individuals at high risk of NASH and fibrosis, or where differential diagnoses causing steatosis cannot be excluded.

***NASH***

NASH is defined as steatosis with evidence of lobular inflammation and hepatocellular injury in the form of ballooning hepatocytes and is therefore a histological diagnosis (Chalasani et al. 2012; Takahashi and Fukusato 2014). More than 5% of hepatocytes must be steatotic and the steatosis is usually macrovesicular, where a small number of large lipid droplets push the nucleus to the periphery of the cell, as opposed to microvesicular, where the nucleus remains central surrounded by multiple tiny droplets of fat. Steatosis generally begins in zone 3 and becomes panacinar (**Figure 1.10**) and this extension has been shown to correlate with disease progression. Inflammation is predominantly lobular and consists of a mixed infiltrate of lymphocytes, neutrophils, eosinophils and kupffer cells (liver macrophages). Portal inflammation is usually only seen in advanced disease. Ballooned hepatocytes are enlarged

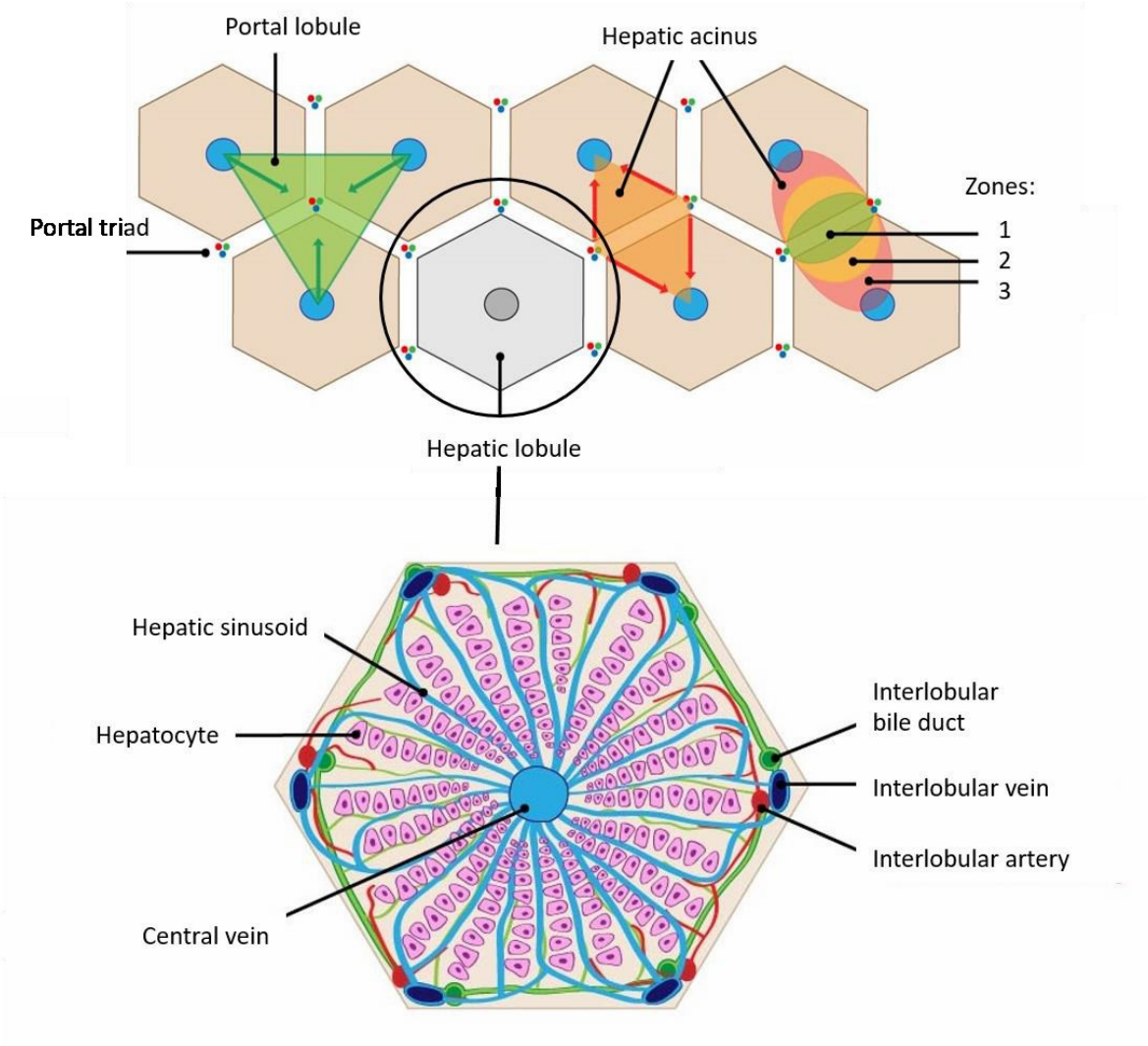


***Figure 1.10 – Histological anatomy of the liver*** *(http://fblt.cz/en/skripta/ix-travici-soustava).*

with rarefied cytoplasm. They are a sign of hepatocellular injury and occur as a result of disruption of the intermediate filament proteins cytokeratin 8 and 18. Mallory-Denk bodies, eosinophilic aggregates of cytokeratins 8 and 18, ubiquitin and p62 are often seen in NASH, especially within ballooned hepatocytes. Their significance is uncertain and they are not specific to NAFLD.

In 2005, the NASH Clinical Research Network incorporated steatosis, lobular inflammation and hepatocellular ballooning into a novel histological scoring system, the NAFLD activity score (NAS - **Figure 1.11**)(Kleiner et al. 2005). This was developed to monitor disease in clinical trials and subsequent analysis has shown that when used to diagnose, NAS ≥ 5 has sensitivity and specificity of only 75% and 83% respectively (Brunt et al. 2011).

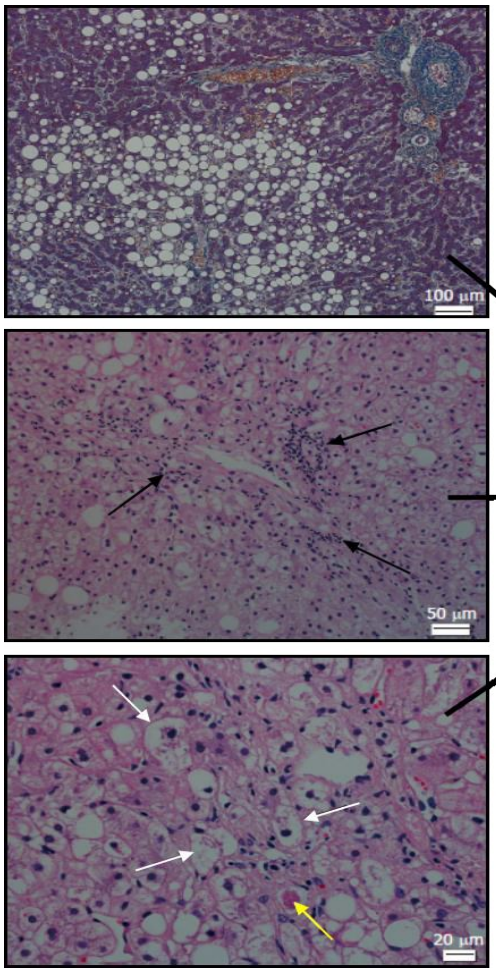


| Item | Definition | Score |
|---|---|---|
| **Steatosis**<br>Macrovesicular and zone 3 (centrilobular) | <5%<br>5%-33%<br>>33%-66%<br>>66% | 0<br>1<br>2<br>3 |
| **Lobular inflammation**<br>Mixed cell | No foci<br>>2 foci per 200 x field<br>2-4 foci per 200 x field<br>>4 foci per 200 x field | 0<br>1<br>2<br>3 |
| **Ballooned hepatocytes**<br>Disrupted cytokeratins 8 & 18 | None<br>Few balloon cells<br>Many cells/prominent ballooning | 0<br>1<br>2 |

***Figure 1.11*** *-* ***NAFLD activity score (NAS)****(Kleiner et al. 2005; Takahashi and Fukusato 2014). Arrow heads: black = necro-inflammatory foci, white = ballooned hepatocytes and yellow = Mallory-denk body.*

***Fibrosis and cirrhosis***

NAFLD related fibrosis usually starts in zone 3 and is pericellular and perisinusoidal, giving it a chicken wire appearance (Takahashi and Fukusato 2014) **Figure 1.12**. As disease progresses the fibrosis tends to expand to the portal region and bridging fibrosis and cirrhosis develop. The NAFLD activity score has a fourth component which is a measure of fibrosis (Kleiner et al. 2005).

A

| Fibrosis type | Score |
|---|---|
| None | 0 |
| Zone 3 perisinusoidal OR portal / periportal | 1 |
| Perisinusoidal AND portal / periportal | 2 |
| Bridging | 3 |
| Cirrhosis | 4 |

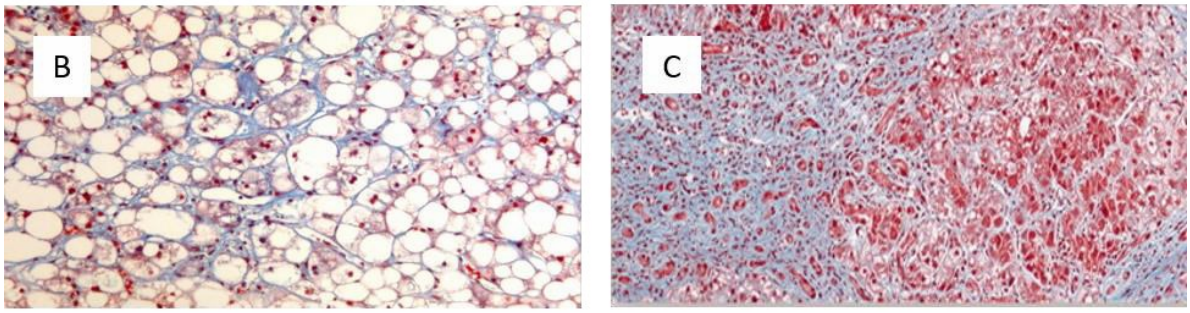


***Figure 1.12 – NAFLD fibrosis*** *(Kleiner et al. 2005; Cohen, Horton, and Hobbs 2011) https://www.intechopen.com.* ***(A)*** *NAFLD activity score (NAS) fibrosis score.* ***(B)*** *Pericellular/perisinusoidal 'chicken wire' fibrosis and* ***(C)*** *Cirrhosis on Masson trichrome staining.*

As numbers of patients requiring diagnosis and monitoring of NAFLD are rapidly increasing, there is a growing need for non-invasive tools that assess inflammation and fibrosis. Although a number of methods have been developed (**Table 1.6**) to date, none have been widely adopted (Alkhouri and Feldstein 2016).

| Tool | Method | Accuracy - AUROC curve |
|---|---|---|
| **NASH** | | |
| M30 antigen-monoclonal antibody ELISA – CK18 fragments in serum | Caspase 3 cleaves intermediate filament protein CK18 during apoptosis | 0.82 (0.76-.88) |
| MS – Serum levels of:<br>- Thiobarbituric acid<br>- Oxidised LDLs<br>- 9- & 13- HODEs<br>- 9- & 13- oxoODEs | Lipid peroxidation products contribute to hepatocyte injury | oxNASH (13-HODE:linoleic acid, age, BMI and AST) 0.73 (0.64 – 0.82) |
| Volatile organic compounds in exhaled breath | Markers of oxidative stress and lipid peroxidation | 0.77 (0.64 – 0.89) (n-tridecane, 3-methyl-butanonitrile & 1-propanol) |
| - TNFα, IL6 or IL1B<br>- Adipokines*<br>- Neutrophil:lymphocyte ratio<br>- Ferritin | Inflammatory markers increase with progression to NASH | Mixed results – no measure sufficiently accurate to use individually |
| **NAFLD Fibrosis** | | |
| Raised transaminases with AST:ALT ratio > 0.8 = Fibrosis | AST & ALT raised in NAFLD but ALT falls with fibrosis | 0.83 (0.74 – 0.91) |
| NASH: HAIR score, NPI, NASHTest and NASH score<br>Fibrosis: NAFLD fibrosis score (NFS), BARD score and FIB4 index | Simple predictive models combining clinical variables and biomarkers | NFS most validated (age, impaired GT, BMI, platelets, albumin and AST:ALT ratio) 0.85 (0.81 – 0.9) |
| European liver fibrosis (ELF): Hyaluronic acid, TIMP 1 & PIIINP | Complex predictive panel: markers of extra-cellular matrix turnover | 0.8 (0.84 – 0.96) (FibroTest also validated) |
| FibroScan (VCTE)<br>Acoustic radiation force impulse (ARFI) | Liver stiffness measurement (elastography) – Velocity of elastic shear wave proportional to tissue stiffness | Fibroscan: 0.93 (0.89 – 0.96) (ARFI similar) |

***Table 1.6 - Non-invasive tools for diagnosing and monitoring NASH and NAFLD fibrosis (Alkhouri and Feldstein 2016; McPherson et al. 2010).*** *AUROC = area under relative operating characteristic (with 95% confidence interval), CK18 = cytokeratin 18, MS = mass spectrometry, LDL = low density lipoproteins, HODEs = hydroxyoctadecadienoic acids, ODEs octadecadienoic acids, TNFα = Tumour necrosis factor α, IL = interleukin, AST and ALT = aspartate and alanine transaminase, HAIR = hypertension/AST/insulin resistance, NPI = NASH predictive index, BARD = BMI/AST:ALT ratio/diabetes, GT = glucose tolerance, TIMP1 = tissue inhibitor of metalloproteinase 1, PIIINP = procollagen III aminoterminal peptide, VCTE = vibration controlled transient elastography. *Adipokines include resistin, visfatin and retinol binding protein-4.*

### 1.3.1 Pathogenesis

***Steatosis***

Accumulation of triglycerides in the liver (steatosis) occurs as a result of imbalance between lipids in, through fatty acid uptake and *de novo* lipogenesis and lipids out via fatty acid oxidation and secretion of very low density lipoproteins (VLDLs - **Figure 1.13**) (Tuyama and Chang 2012).

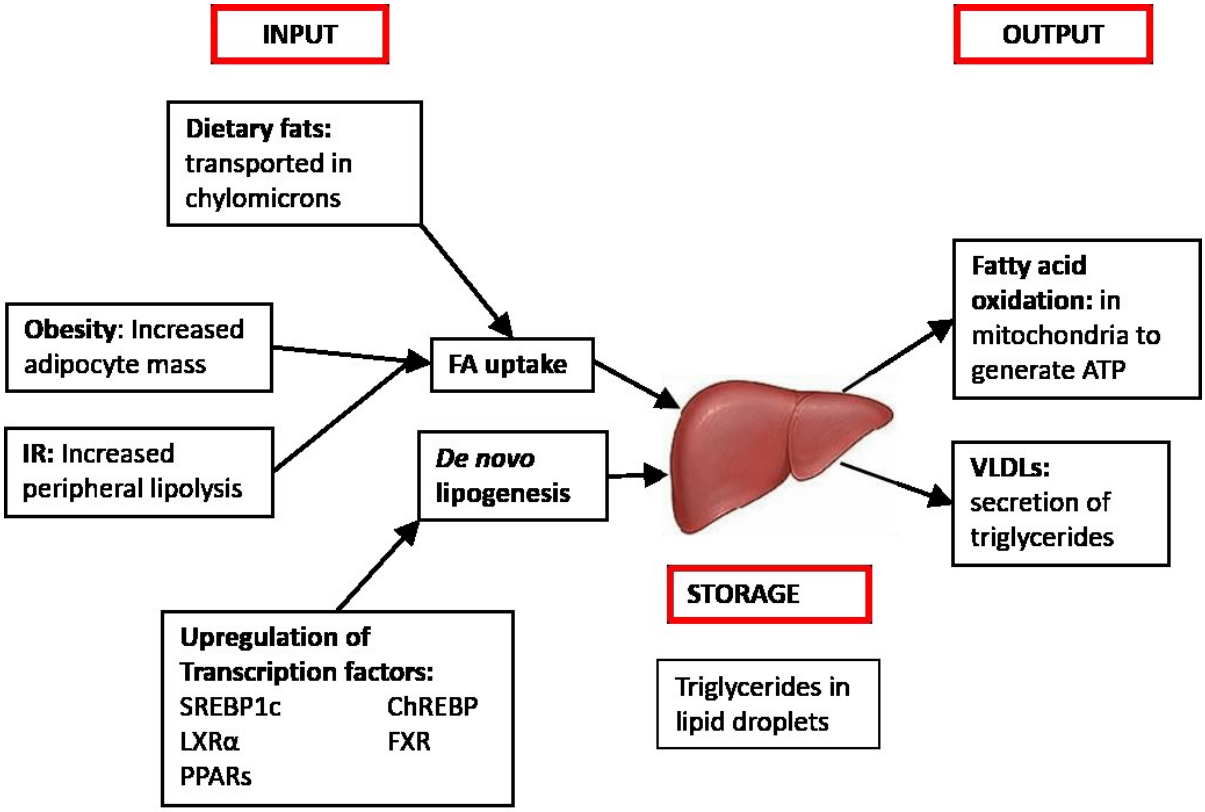


***Figure 1.13 - Lipid inputs to and outputs from the liver.*** *IR = insulin resistance, SREPB1c = Sterol regulatory element-binding protein 1c, ChREBP = carbohydrate responsive element-binding protein; LXRα = liver X receptor α; FXR = farsenoid X receptor, PPARs = peroxisome proliferator-activated receptors, FA = fatty acid, VLDL = very low density lipoproteins.*

Rate of uptake of free fatty acids into the liver is unlimited and therefore directly proportional to serum levels (Wahren et al. 1984). In order to determine the origins of lipid accumulated in the liver in NAFLD, Donnelly et al. and Lambert et al. administered stable isotopes to patients with the disease and then analysed liver tissue and/or serum VLDLs respectively (Donnelly et al. 2005; Lambert et al. 2014). Donnelly et al. demonstrated that VLDL fatty acid

composition is a good proxy for that of liver and both studies highlighted that patients with NAFLD have increased rates of *de novo* lipogenesis (**Table 1.7**). Although hepatic fatty acid oxidation and VLDL secretion are also upregulated in NAFLD patients, they do not appear to be able to increase sufficiently to compensate for the excess of fatty acids directed at the liver and so lipid accumulates (Choi and Ginsberg 2011).

| | **Donnelly et al. 2005 (FA)** | | **Lambert et al. 2014 (TG)** | |
|---|---|---|---|---|
| | NAFLD Liver | NAFLD VLDL | NAFLD VLDL | Normal VLDL |
| **Adipose tissue** | 59.0 | 62.4 | 57 | 77 |
| **Diet** | 14.9 | 14.7 | 8 | 8 |
| **DNL** | 26.1 | 22.9 | 35 | 15 |

***Table 1.7*** *-* ***Sources of lipid in liver or VLDLs of NAFLD patients or healthy subjects*** *(Donnelly et al. 2005; Lambert et al. 2014).* *Numbers are all percentages, FA = fatty acid and TG = triglyceride.*

Within hepatocytes lipid is stored in lipid droplets which have a predominantly triglyceride and cholesterol ester core, surrounded by a phospholipid monolayer, which is coated with perilipin family proteins that regulate lipid storage (Greenberg et al. 2011). These intracellular organelles are crucial to cellular energy homeostasis.

Esterification of fatty acids and their subsequent storage as triglycerides is likely to be a protective adaptation by hepatocytes to limit free fatty acid toxicity. Studies suggest that saturated fatty acids are significantly more lipotoxic than their unsaturated or esterified counterparts (Malhi and Gores 2008; Listenberger et al. 2003; Yamaguchi et al. 2007). Treatment of cells with the saturated fatty acid palmitic acid (16:0) resulted in apoptosis, but this was not seen with oleic acid (18:1), a mono-unsaturated fatty acid (MUFA) (Listenberger et al. 2003). Indeed co-treatment of palmitic acid treated cells with oleic acid resulted in reduced apoptosis due to channelling of palmitic acid into triglyceride synthesis. Furthermore, increased expression of stearoyl-CoA desaturase-1 (SCD1), the enzyme that converts saturated stearic acid (18:0) into the MUFA oleic acid, resulted in increased

triglyceride synthesis but decreased lipotoxicity. And knockout of the gene encoding diacylglycerol transferase 2 (DGAT2) which catalyses the final step of triglyceride synthesis, whereby triglyceride is formed from diacylglycerol and acyl-CoA, reduced triglyceride synthesis and rendered cells susceptible to lipotoxicity (Yamaguchi et al. 2007). In keeping with these findings, lipid composition was altered in liver tissue from patients with NASH relative to that from patients with NAFLD, which was in turn different from that of normal liver (Puri et al. 2007).

***Steatohepatitis***

An estimated 25% of patients with NAFL will develop NASH (Rinella and Charlton 2016; Younossi et al. 2016), however the pathogenesis of this progression is complex and currently incompletely understood. In 1998, Day and James proposed the 'two hit' hypothesis whereby development of NASH requires both steatosis (the 1$^{st}$ hit) and increased lipid peroxidation (the 2$^{nd}$ hit) (Day and James 1998). Subsequently, it has been demonstrated that some NAFLD patients develop hepatocyte inflammation in the absence of steatosis and that accumulation of triglycerides in the liver is likely a protective mechanism, lending support to the 'multi-hit' model of NAFLD pathogenesis proposed by Tilg and Moschen in 2010 (Tilg and Moschen 2010). Some of these potential 'hits' are described below and summarised in **Figure 1.14**.

Hepatocyte apoptosis which is a key feature of NASH, occurs via 2 pathways, the extrinsic pathway, mediated by death ligand-receptor interactions and the intrinsic pathway initiated by intracellular organelles such as the mitochondria, lysosomes and the endoplasmic reticulum (ER). It has been demonstrated that free fatty acids can elicit both (Malhi and Gores 2008; Alkhouri, Dixon, and Feldstein 2009; Feldstein et al. 2004; Malhi et al. 2007). The saturated fatty acids palmitic and stearic acid can elicit apoptosis through mitochondrial permeabilisation and lysosomal cathepsin B release (Feldstein et al. 2004; Malhi et al. 2006; Barreyro et al. 2007). Death receptors, which when bound can trigger the extrinsic apoptosis pathway, and their respective ligands are listed in **Table 1.8**. Fas receptor and DR5 are upregulated by free fatty acids and their expression in the liver is increased in patients with NASH (Feldstein, Canbay, Angulo, et al. 2003; Feldstein, Canbay, Guicciardi, et al. 2003; Malhi et al. 2007).

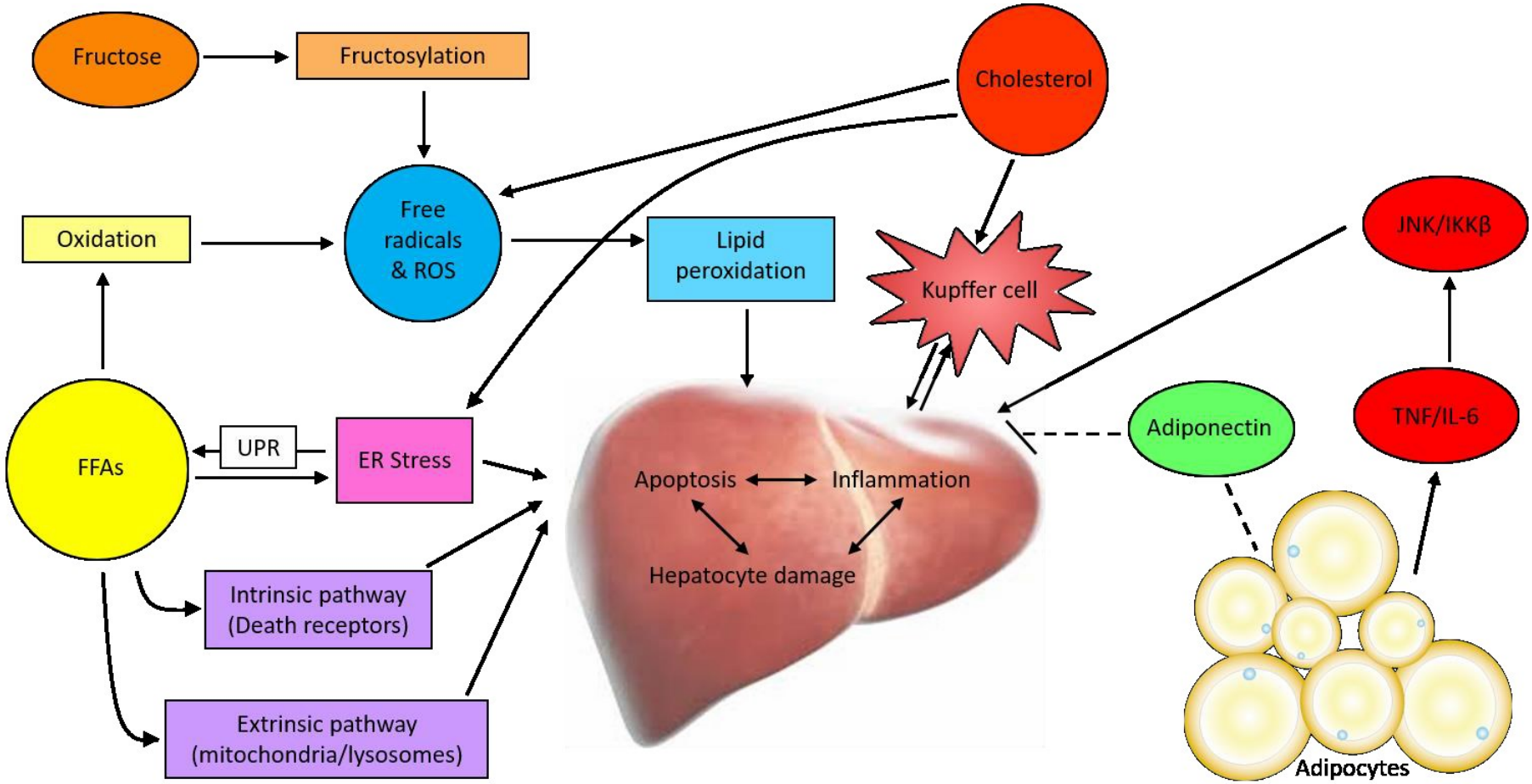


***Figure 1.14 - The pathogenesis of NASH.*** *FFAs = free fatty acids, UPR = unfolded protein response, ROS = reactive oxygen species, ER = endoplasmic reticulum, JNK = c-Jun N-terminal kinase, IKKβ = inhibitor of nuclear factor kappa-B kinase subunit, TNF = tumour necrosis factor and IL-6 = interleukin 6.*

| Death receptor | Ligand |
|---|---|
| Tumour necrosis factor receptor 1 (TNFR-1 or CD120a) | TNFα |
| Fas receptor (CD95) | Fas ligand |
| TRAIL receptor 1/death receptor 4 (DR4 or CD261) TRAIL receptor 5/DR5 (CD262) | Tumour necrosis factor related apoptosis inducing ligand (TRAIL) |

***Table 1.8 - Death receptors and their ligands***

Accumulation of saturated fatty acids can lead to increased demand upon and reduced capability of the endoplasmic reticulum (ER) causing ER stress (Puri et al. 2008; Wang, Wei, and Pagliassotti 2006; Ozcan et al. 2004). This in turn results in accumulation of unfolded proteins which trigger the unfolded protein response (UPR), mediated through IRE1, activating transcription factor 6 (ATF6) and pancreatic ER kinase (PERK)(Tilg and Moschen 2010; Bettigole and Glimcher 2015). The aim of the UPR is to resolve ER stress through various mechanisms such as reduced protein synthesis and cell cycle arrest. Failure of the UPR to restore ER homeostasis can initiate apoptosis. Furthermore, the UPR can impact upon lipid metabolism by increasing lipogenesis and decreasing VLDL synthesis as well as exacerbating insulin resistance and inflammation (Zhang, Xu, et al. 2014; Ozcan et al. 2004; Fang et al. 2013). Analysis of liver biopsies from NAFLD patients and control patients with the metabolic syndrome but normal liver, demonstrated that components of the UPR were upregulated in NAFLD but a consistent pattern was not demonstrated (Puri et al. 2008). A full understanding of the role of ER stress in NAFLD is still evolving.

In Day and James' 'two hit' hypothesis, the second hit, following steatosis, was proposed to be oxidative stress and lipid peroxidation (Day and James 1998). Fatty acid oxidation in hepatocytes occurs via three metabolic pathways, the mitochondria, peroxisomes and ER cytochrome p450 enzymes (Neuschwander-Tetri 2010). Under normal conditions, Fatty acid oxidation is reduced following feeding as free fatty acids are converted to triglycerides for secretion or storage. However in the presence of excess free fatty acids this switch is likely to be less distinct resulting in increased fatty acid oxidation and so free radical and reactive oxygen species (ROS) production and risk of lipid peroxidation and cell damage. Supporting

this mechanism of liver injury in NAFLD are the findings that hepatic CYP2E1 is induced in the disease and that markers of oxidative stress, including malondialdehyde (MDA), 4-hydroxy-2-nonenal (4-HNE – both products of lipid peroxidation), 3-nitrotyrosine and 8-hydroxydeoxyguanosine (a product of oxidative DNA damage) are raised – the latter 3 more so in patients with NASH than those with simple steatosis (Malhi and Gores 2008; Sanyal et al. 2001; Seki, Kitada, and Sakaguchi 2005; Yesilova et al. 2005; Chalasani et al. 2003). However, research has not been able to establish oxidative stress and lipid peroxidation as key to NAFLD progression (Neuschwander-Tetri 2010). The liver has an abundance of antioxidants, such as glutathione and there is no evidence that these are depleted or impaired in NAFLD, suggesting that the liver is able to process the excess free radicals and ROS produced as a result of increased fatty acid oxidation. Furthermore, upregulation of mitochondrial (through deletion of ACC2) and peroxisomal fatty acid oxidation appear to be protective in NAFLD (Choi et al. 2007; Ip et al. 2003).

As with triglycerides, accumulation of cholesterol in the liver occurs as a result of an imbalance between input (uptake from diet and peripheral sources and synthesis) and output (secretion in lipoproteins and the bile)(Ioannou 2016). Epidemiological studies have demonstrated an association between cholesterol (but not total lipid) consumption and severity of NAFLD and hepatic free cholesterol levels are elevated in patients with NASH but not simple steatosis (Ioannou et al. 2009; Puri et al. 2007; Min et al. 2012). Furthermore, in high fat diet fed mice, addition of cholesterol to their diet resulted in progression from NAFL to NASH (Savard et al. 2013).

The mechanisms by which cholesterol might promote NASH development have not been defined. Cholesterol increases membrane rigidity which may alter membrane protein function. Elevated mitochondrial membrane cholesterol reduces glutathione uptake leading to increased ROS levels; increased ER membrane cholesterol can promote ER stress and the UPR; and altered cholesterol levels within lipid droplet membranes could impact upon their function (Ioannou 2016; Mari et al. 2006; Arguello et al. 2015). Alternatively, accumulation of cholesterol within the lysosomes of Kupffer cells has been shown to trigger an inflammatory response in experimental NASH models, analogous to cholesterol induced macrophage activation in atherosclerosis (Bieghs et al. 2013).

Obese adipose tissue can produce a number of adipokines, such as TNFα and IL6, with significant roles in the development of hepatic inflammation and insulin resistance (Hotamisligil, Shargill, and Spiegelman 1993; Mohamed-Ali et al. 1997). TNFα activates the stress related protein kinases JNK and Ikkβ. JNK can promote hepatocyte apoptosis and its activity is increased in liver tissue from patients with NASH, but near normal in that from individuals with simple steatosis (Yamamoto, Ichijo, and Korsmeyer 1999; Kim, Ryu, and Song 2006; Puri et al. 2008; Musso, Gambino, and Cassader 2010). Activation of IKKβ up-regulates NF-κB, so enhancing pro-inflammatory and cell survival signals within the liver (Hacker and Karin 2006). In-keeping with these findings anti-TNF treatments have been shown to limit NASH (Van Wagner et al. 2011; Koca et al. 2008). In contrast to TNFα, adipocyte secretion of the anti-inflammatory, anti-diabetic adipokine adiponectin is reduced in individuals who are obese or insulin resistant and correspondingly serum levels are lower in patients with NASH, compared to matched controls or those with NAFL (Musso et al. 2009).

***Fibrosis and cirrhosis***

Regardless of aetiology, chronic liver injury and inflammation commonly lead to fibrosis and cirrhosis, which can be complicated by portal hypertension (causing ascites and variceal bleeding), liver failure and increased risk of HCC (Dowman, Tomlinson, and Newsome 2010). Hepatic stellate cells are pericytes, located in the space of Disse between hepatocytes and the sinusoids. They are normally quiescent and a site of storage of vitamin A, as retinol esters in perinuclear lipid droplets. However, hepatocyte damage and death and the ensuing inflammation result in hepatic stellate cell (HSC) migration and activation (Friedman et al. 1985; Wallace, Burt, and Wright 2008; Brunt 2010). Activated, HSCs, which reside in sinusoids, operate as myofibroblasts which are contractile and produce extracellular matrix (ECM), particularly collagen; matrix degrading proteins such as matrix metalloproteinases; and other cytokines and chemokines which perpetuate the inflammation-repair process. This HSC response is a normal wound healing mechanism and is reversible, however chronic activation results in progressive fibrosis and ultimately cirrhosis (Hernandez-Gea and Friedman 2011). With advanced fibrosis, features of NASH (steatosis, inflammation, ballooning etc) can disappear – so called ‘burn out NASH’ and this is a recognised cause of cryptogenic cirrhosis (Takahashi and Fukusato 2014; Caldwell et al. 1999; El-Serag and Rudolph 2007).

Normally, necrotic or apoptotic hepatocytes are replaced by adjacent mature hepatocyte proliferation, however impairment of this mechanism results in hepatic progenitor cell (HPC) activation (Richardson et al. 2007). HPCs, which are periportal and can differentiate into hepatocytes or cholangiocytes, may be important in the development of the ductular reaction (DR). In turn, the DR, an accumulation of ductules and associated ECM and inflammatory cells at the hepatocyte-biliary tree interface, is thought to be involved in expansion of fibrosis from zone 3 to the portal region, a significant step in NAFLD progression.

***Genetics***

Interethnic differences in susceptibility, familial aggregation and twin studies together suggest there is a genetic component to NAFLD (Anstee and Day 2013). It is likely that multiple relatively common genetic polymorphisms act simultaneously to increase individuals' risk of developing disease and disease progression.

In the first NAFLD genome wide association study (GWAS) in 2008 Romeo et al. discovered two such polymorphism, rs738409 encoding Ile148Met and rs6006460 encoding Ser453Ile, in the patatin-like phospholipase domain-containing 3 gene (*PNPLA3* on chromosome 22), which were associated with increased and decreased steatosis respectively (Romeo et al. 2008). Multiple candidate gene and GWAS have replicated and validated *PNPLA3* as a potential modifier of steatosis and NAFLD progression, as well as probably HCC risk (Anstee and Day 2013). Furthermore, these associations are independent of features of the metabolic syndrome such as insulin resistance and BMI. However, despite this, the physiological functions of adiponutrin, the protein encoded for by *PNPLA3*, are less clearly established. Adiponutrin is a transmembrane polypeptide, mainly found in the liver and adipose tissue and expression increases in response to insulin and certain fatty acids. Hepatic PNPLA3 Ile148Met overexpression studies suggest that adiponutrin remodels triglycerides through acylglycerol hydrolysis and FFA and triglyceride synthesis (Li et al. 2012). These findings are in-keeping with observations that the PNPLA3 Ile148Met variant is associated with reduced VLDL secretion (Pirazzi et al. 2012). However, *PNPLA3* knockout does not result in steatosis, even in the presence of a high carbohydrate diet, implying that PNPLA3 Ile148Met is not a simple loss of function polymorphism (Chen et al. 2010).

More recently, in an exome wide association study, Kozlitina et al. identified a non-synonymous polymorphism within *TM6SF2* (Glu167Lys) associated with increased hepatic triglyceride content (Kozlitina et al. 2014). This result has since been extensively validated and much attention has focused on the role of the protein it encodes, transmembrane 6 superfamily 2 (TM6SF2)(Anstee and Day 2015). TM6SF2 is a multi-pass membrane protein, which has been shown to localise to the endoplasmic reticulum and is predicted to have lipid transporter function. Knockdown studies have demonstrated that decreased TM6SF2 expression results in reduced triglyceride rich lipoprotein and apolipoprotein B (ApoB) secretion and so a fall in serum triglyceride, LDL and VLDL levels associated with increased hepatic triglyceride accumulation (Anstee and Day 2015; Holmen et al. 2014). TM6SF2 overexpression leads to dyslipidaemia and reduced number and size of lipid droplets within hepatocytes. These findings are also supported by other studies implicating TM6SF2 in both cardiovascular and NAFLD risk (Anstee and Day 2015; Liu et al. 2014; Dongiovanni et al. 2015) The more common rs58542926 major allele encoding wildtype TM6SF2 was associated with increased serum lipid levels and carotid plaques but lower hepatic lipid accumulation, whereas the rarer minor allele variant TM6SF2 Glu167Lys was protective against cardiovascular risk but increased hepatic steatosis (Anstee and Day 2015).

Only a small number of other genes identified by GWAS have been thoroughly validated (Anstee and Day 2013). These and their relative functions are listed in **Table 1.9**.

***The gut microbiota***

The advent of next generation sequencing has enabled taxonomy of the whole gut microbiota, resulting in an increased appreciation of its significance in health and disease. Changes in the gut microbiota, secondary to diet, bile acid composition, obesity and liver disease itself, may play a role in the pathogenesis of NAFLD (Yu et al. 2016; Turnbaugh et al. 2006; Schwiertz et al. 2010)

Gut microbes can alter bile acid composition and in addition to emulsifying and so promoting absorption of dietary lipids, bile acids function as ligands for farnesoid x receptor (FXR) and

| Gene & protein<br>SNP & molecular effect | Functional effect of SNP |
|---|---|
| ***GCKR* encoding glucokinase regulatory protein (GKRP)**<br>rs780094 in LD with rs1260326 = nonsynonymous Pro446Leu SNP | Unregulated glycolysis with subsequent up and down regulation of FAS and FAO respectively |
| ***PEMT* encoding phosphatidylethanolamine N-methyltransferase**<br>rs7946 = nonsynonymous Val175Met mutation | Reduced *de novo* phosphatidylcholine synthesis and therefore VLDL production |
| ***SOD2* encoding superoxide dismutase 2**<br>rs4880 = nonsynonymous Ala16Val SNP | Impaired entry of SOD2 into mitochondria resulting in reduced antioxidant activity |
| ***KLF6* encoding kruppel-like factor 6 transcription factor**<br>rs3750861 SNP promotes alternative splicing of KLF6 giving antagonistic truncated isoforms | Reduced fibrogenic gene expression by hepatic stellate cells and so less fibrosis<br>Reduced hepatic IR (?secondary to decreased GCKR activity) |
| ***ATGR1* encoding angiotensin II receptor 1**<br>rs3772622 (and other SNPs in LD) favours ATGR1 production | Increased hepatic myofibroblast survival |
| ***FADS1* encoding fatty acid desaturase 1**<br>Multiple SNPs | Increased ratio of more saturated over less saturated lipids in liver |

***Table 1.9 – Validated genetic modifiers of NAFLD*** *(Anstee and Day 2013; Wang et al. 2015).*

*SNP = single nucleotide polymorphism, LD = linkage disequilibrium, FAS = fatty acid synthesis, FAO = fatty acid oxidation, VLDL = Very low density lipoprotein and IR = insulin resistance.*

transmembrane G protein-coupled receptor TGR5 (Schaap, Trauner, and Jansen 2014; Ridlon et al. 2014). FXR and TGR5 are involved in regulation of inflammation and carbohydrate and lipid metabolism and their activation results in reduced hepatic triglyceride levels and inflammation (Li, Jadhav, and Zhang 2013). This was the rationale behind a recent phase II study using the FXR agonist obeticholic acid (Mudaliar et al. 2013): Treatment of patients

with T2DM and NAFLD resulted in reduced insulin resistance and markers of hepatic inflammation and fibrosis.

Modifications to the gut microbiota, can result in increased intestinal epithelium permeability, allowing LPS to enter the circulation (endotoxaemia)(Yoon and Cha 2014; Brun et al. 2007). High fat feeding may also promote LPS uptake due to increased chylomicron transport (Laugerette et al. 2011). LPS endotoxaemia has been shown to induce hepatic steatosis and inflammation (Cani et al. 2007). Altering the composition of microbes in the gut can also affect the rate of conversion of choline to methylamine (Dumas et al. 2006). Dietary choline is required for VLDL synthesis and deficiency therefore results in reduced hepatic lipid export and so steatosis (Buchman et al. 1995). Increased choline conversion can therefore exacerbate NAFLD due to choline depletion and inflammatory response to methylamine, which is a toxic metabolite (Dumas et al. 2006). Finally, some microbiota may be obesogenic. When microbiomes from leptin deficient mice were transplanted into wild-type microbe free mice their weight gain was increased relative to mice transplanted with microbiomes from lean mice (Turnbaugh et al. 2006).

### 1.3.2 Treatment

Recognised treatments for NAFLD and the American Association for the Study of Liver Diseases' (AASLD's) guidance regarding their use are summarised in **Table 1.10**. Systemic therapy for NAFLD should be considered in conjunction with treatment of other aspects of the metabolic syndrome (obesity, dyslipidaemia, T2DM etc) and limited to those with NASH.

| Treatment<br>Mechanism of action | Evidence & AASLD/ACG/AGA Guidance |
|---|---|
| **Weight loss (calorie restricted diet +/- exercise)** | Loss of ≈3-5% and ≈10% of bodyweight required for steatosis and NASH improvement respectively |
| **Exercise (independent of weight loss)**<br>Increased Glut4 and reduced IR | Only proven to improve steatosis |
| **Metformin**<br>Mitochondrial complex I inhibition/ AMPK activation<br>Reduced lipolysis and adipokine secretion | No significant effect on NASH histology<br>Not currently recommended specifically for NAFLD |
| **Pioglitazone***<br>PPAR activation (especially PPARγ) | Improved NASH histology<br>Can be used to treat patients with biopsy proven NASH |
| **Vitamin E (α-tocopherol – 800 IU/day)**<br>Anti-oxidant | Improved NASH histology<br>1st line pharmacotherapy for biopsy proven, non-DM, non-cirrhotic NASH |
| **Ursodeoxycholic acid**<br>May be less hepatotoxic than the more hydrophilic bile acids it replaces | No significant effect on NASH histology<br>Not recommended for the treatment of NAFLD |
| **Omega-3 fatty acids**<br>Reduced ω6:ω3 PUFA ratio - ω3 less lipotoxic | Currently no evidence of effect on NAFLD<br>Approved for hypertriglyceridaemia but not specifically for NAFLD |
| **Bariatric surgery**<br>Weight loss | Improved NASH histology when performed for obesity<br>Not recommended specifically for NAFLD |
| **Statins** | Limited evidence regarding effects in NAFLD<br>Safe to treat dyslipidaemia in NASH but not currently recommended specifically for NAFLD |

***Table 1.10 – Treatment of NAFLD.*** *AASLD = American Society for the study of liver diseases, ACG = American College of Gastroenterology, AGA = American Gastroenterological Association, IR = insulin resistance, and PPAR = peroxisome proliferator activated receptor.* ***Rosiglitazone associated with increased cardiovascular events - no longer marketed in Europe and restricted use in USA.***

## 1.4 Hepatocellular carcinoma

Globally, liver cancer is the 2nd commonest cause of cancer mortality and its incidence is rising (Global Burden of Disease Study, 2013). HCC, which accounts for around 90% of liver cancers, usually arises in patients with cirrhosis due to hepatitis virus B or C (HBV or HCV) infection; alcoholic or non-alcoholic steatosis; or genetic disorders such as haemochromatosis (Bosch et al. 2005). Differing aetiologies mean there is considerable global variation in incidence (Knudsen, Gopal, and Singal 2014). Highest incidence areas are Asia and Africa where 70% of patients with HCC have underlying HBV infection (Beasley 1988). Individuals in Africa are at further increased risk due to the synergistic effects of Aflatoxin exposure and HBV in the development of *TP53* mutations (Qian et al. 1994). Incidence in these highest risk areas may be stabilising or even falling (El-Serag 2012), however, in contrast, incidence in lower risk areas such as Europe and the USA, where HCV and NAFLD are the commonest causes of cirrhosis (responsible for approximately 60% of cases), is on the increase (Altekruse, McGlynn, and Reichman 2009). Indeed, in the USA, HCC saw the greatest rise in incidence of all solid tumours between 1995 and 2004. Furthermore, whereas prognosis for most malignancies improved over this period mortality from HCC almost doubled (El-Serag 2004).

### 1.4.1 Pathology, pathogenesis & treatment

***Pathology***

HCCs that develop on a background of cirrhosis evolve from regenerative nodules which become dysplastic (**Figure 1.15**)(Schlageter et al. 2014). Malignant lesions are also categorised as either early (well differentiated, <2cm diameter and vaguely nodular/poorly defined margins) or progressed (moderately or poorly differentiated and distinctly nodular).

The histomorphological appearance of HCC can vary widely even within the same tumour (Schlageter et al. 2014). Common growth patterns include trabecular (visually similar to normal liver), acinar (berry-like), pseudoglandular and solid (**Figure 1.16**). Progressive neovascularisation results in unpaired arteries which are not associated with portal tracts

and hypervascularisation. Bile production is also frequently seen, especially with acinar and pseudoglandular growth.

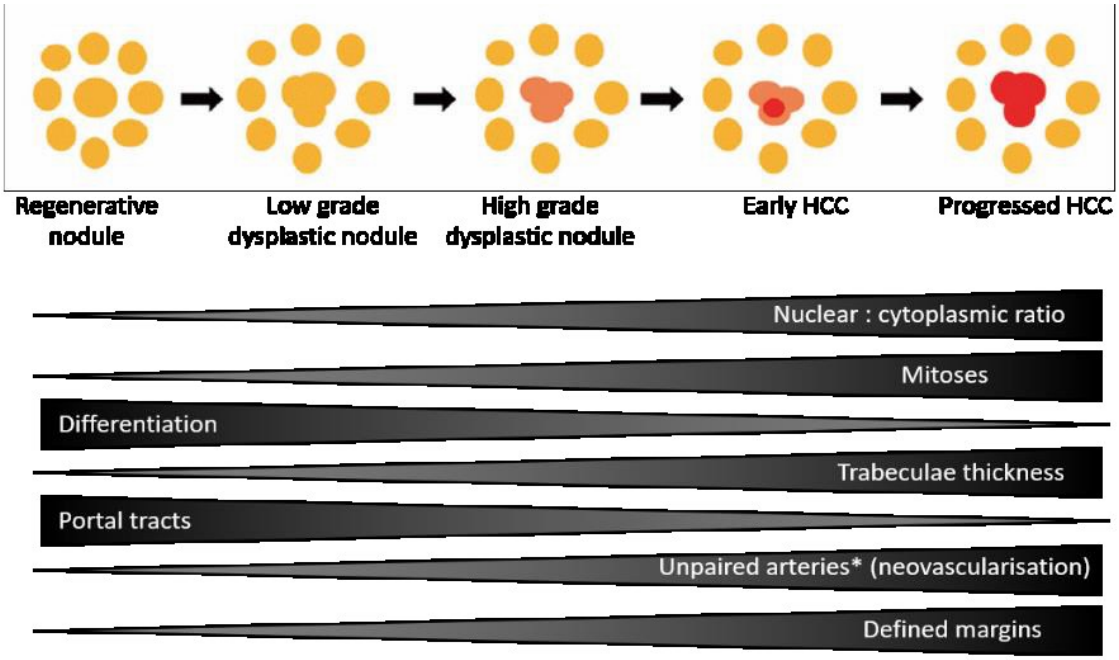


***Figure 1.15 - Stages and histopathological changes in HCC development*** *(Huh et al. 2015).*

Recently a steatohepatitic variant of HCC has been described in up to 36% of patients who develop the disease on a background of NAFLD (Salomao et al. 2012). In this variant malignant cells have steatohepatitis like features (steatosis, inflammation, ballooning and loss of cytokeratin 8/18 on immunohistochemical staining) and there is evidence of HSC activation and pericellular fibrosis within the tumours.

The differential diagnosis for HCC includes benign lesions of hepatocellular origin such as hepatocellular adenoma (HCA) and dysplastic nodules as well as cholangiocarcinoma and metastases from other carcinomas. Benign hepatocellular lesions have lower nuclear to cytoplasmic ratios and do not have nuclear pleomorphism, visable nucleoli and mitosis or vascular invasion, all of which can be present in HCCs (Goodman 2007). Immunohistochemical (IHC) stains which can be helpful in distinguishing HCCs from dysplastic nodules are listed in

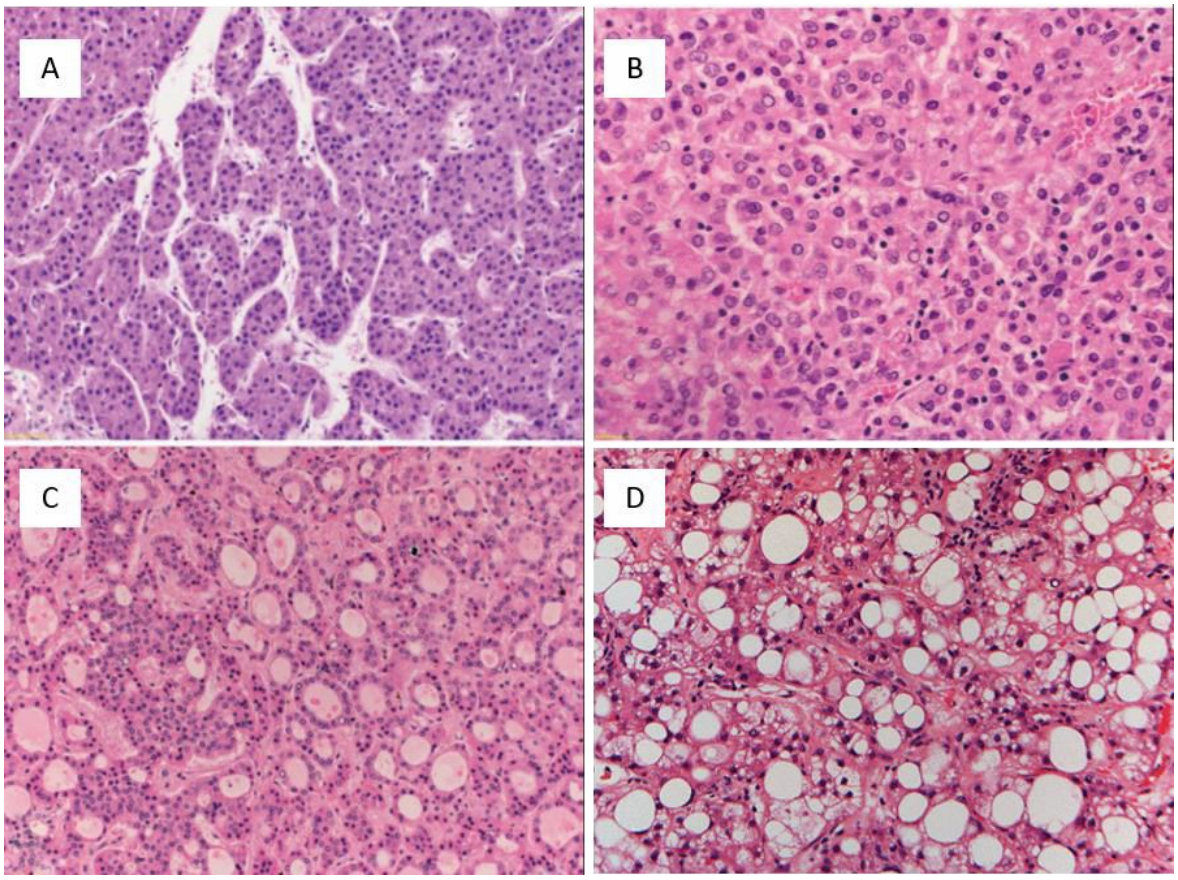


***Figure 1.16 - Hepatocellular cancer histological growth patterns*** *(Schlageter et al. 2014; Klein et al. 2014). (A) Trabecular (B) Solid (C) Pseudoglandular and (D) Steatohepatitic.*

**Table 1.11**. HCAs usually occur in women of reproductive age and are associated with contraceptive steroid use, whereas dyplastic nodules occur on a background of cirrhosis. The presence of canaliculi, bile, fat or Mallory bodies indicate that a lesion is HCC as opposed to adenocarcinoma, however the absence of these features is inconclusive. Converseley, mucin production is only seen with adenocarcinomas. IHC stains which can be useful in distinguishing HCCs from cholangiocarcinomas are detailed in **Table 1.12**.

The Barcelona Clinic Liver Cancer staging system, which is widely accepted internationally, classifies patients with HCC into 5 groups based upon their tumour burden, performance status and underlying liver dysfunction and links each group to specific therapeutic strategies (EASL-EORTC 2012).

| Antigen | Details | Distinction |
|---|---|---|
| **CD34** | Endothelial marker but absent from normal sinusoidal endothelium | Sinusoidal capillarisation (and so CD34 staining) develops with progression from dyplastic nodule to HCC |
| **Glypican 3 (GPC3)*** | Oncofetal proteoglycan | Expressed in HCC but not normal or cirrhotic liver |
| **Heat shock protein 70 (HSP70)*** | Anti-apoptotic regulator – may be involved in tumourgenesis | Expression increases with progression from benign to malignant tumour |
| **Glutamine synthetase (GS)*** | Catalyses conversion of glutamate and ammonia to glutamine. Upregulated with β-catenin activation** | Homogenous, diffuse expression in HCC |

***Table 1.11*** *- **Immunohistochemical stains for distinguishing HCCs from dysplastic nodules** (Goodman 2007; Koehne de Gonzalez, Salomao, and Lagana 2015)**.** *GPC3, HSP70 and GS tend to be performed as a panel to improve sensitivity and specificity. **See 'Pathogenesis' section below.*

| Antibody | Details | Distinction |
|---|---|---|
| **Polyclonal antiserum to carcinoembryonic antigen (CEA)** | Cross reacts with biliary glycoprotein 1 on bile canaliculi | Branching canalicular staining in HCCs v diffuse staining in CCs |
| **Hepatocyte Paraffin1 (HepPar1)** | Epitope is a urea cycle enzyme in liver mitochondria | Stains most HCCs but not CCs |
| **Anti-GPC3** | See Table 1.11 | Increased staining in HCCs with reduced differentiation. Doesn't stain CCs |
| **Anti-Arginase-1 (Arg-1)** | Urea cycle enzyme | Stains most HCCs but not CCs |
| **Anti-Bile salt export pump (BSEP)** | -Transports bile out of hepatocytes | Stains most HCCs but not CCs |

***Table 1.12 - Immunohistochemical stains for distinguishing HCCs from cholangiocarcinomas (CCs)*** *(Goodman 2007; Koehne de Gonzalez, Salomao, and Lagana 2015).*

***Pathogenesis***

The majority of HCCs arise on a background of chronic inflammation and cirrhosis (Bosch et al. 2005). Recurring cycles of hepatocyte necrosis and regeneration promote the propagation and accumulation of mutations (Farazi and DePinho 2006). Furthermore, it is now recognised that the inflammatory process is itself pro-oncogenic (Grivennikov, Greten, and Karin 2010). Indeed in 2011 Hanahan and Weinberg classified tumour-promoting inflammation as an enabling characteristic of cancer (**Figure 1.6**), recognising the capacity of immune cells, particularly those of the innate system, involved in wound healing, to secrete growth and angiogenesis promoting factors; anti-apoptotic signals; and extracellular matrix degrading enzymes which enable angiogenesis, invasion and metastasis (Hanahan and Weinberg 2011).

Several unbiased molecular analyses of HCC have been performed recently (Guichard et al. 2012; Huang et al. 2012; Fujimoto et al. 2012; Kan et al. 2013; Schulze et al. 2015; Totoki et al. 2014). These studies have demonstrated that most HCCs have 30-40 mutations, a small number of which are drivers and detected a number of mutations (some novel), likely to be key to HCC pathogenesis (Villanueva and Llovet 2014). They have also highlighted the heterogeneity of HCC and complexity of its pathogenesis.

Independent studies have identified Wnt/β-Catenin pathway upregulation in HCC, mainly due to activating mutations in *CTNNB1* (the gene encoding β-catenin)(de La Coste et al. 1998) but also due to inactivating mutations in *AXIN, APC and ZNRF3* (encoding axin, adenomatous polyposis coli and zinc and ring 3 proteins respectively)(Schulze et al. 2015; Totoki et al. 2014). Sequencing studies have also re-emphasised the importance of the tumour suppressor p53 in HCC development (Farazi and DePinho 2006). Aflatoxin B1 related *TP53* mutations may be more important in tumour initiation whereas those associated with chronic liver damage may be more significant to tumour progression. Other changes resulting in defective cell cycling, such as cyclin-dependent kinase inhibitor 2A (*CDKN2A*) deletions have also been detected (Schulze et al. 2015). Mutations in the telomerase reverse transcriptase (TERT) gene promotor are present in 6% of low grade dysplastic nodules, 20% of high grade dysplastic nodules and 60-90% (depending on stage) of HCCs (Nault et al. 2013; Llovet et al. 2016). This suggests that re-expression of TERT, which is important in telomere maintenance, is an early change in HCC development and is required to overcome the replicative senescence of

cirrhotic hepatocytes. Finally, numerous studies have identified mutations in AT-rich interaction domain proteins (ARID1A, 1B and/or 2), components of the SWI/SNF chromatin remodelling complex, a recognised tumour suppressor (Zucman-Rossi et al. 2015).

Using gene expression profiling HCCs can be classified into 2 groups, proliferative and non-proliferative, each representing approximately half of all tumours (Zucman-Rossi et al. 2015). This distinction was initially made by Thorgeirsson's group, but has subsequently been recapitulated in various independent studies (Lee and Thorgeirsson 2004; Knudsen, Gopal, and Singal 2014). Proliferative HCCs are more commonly related to HBV infection, carry a poorer prognosis and involve activation of cell proliferation and survival pathways (Zucman-Rossi et al. 2015). Non-proliferative HCCs are more frequently seen in patients with alcoholic or HCV cirrhosis, have a more favourable prognosis and are particularly associated with upregulated Wnt/β-catenin signalling.

It is becoming increasingly recognised that the stromal cells and extracellular matrix that comprise the tumour microenvironment are at least as critical to tumourgenesis as changes within tumour cells themselves (Hernandez-Gea et al. 2013). This is particularly true in HCCs, where hepatocytes interact with macrophages, lymphocytes, HSCs and endothelial cells. Indeed, Hoshida et al. demonstrated that in HCC, whilst gene expression profiles from tumorous tissue were not prognostic, those from adjacent non-tumorous tissue closely correlated with survival: NF-κB, IL-6 and epidermal growth factor up-regulation in the liver parenchyma were predictive of worse prognosis (Hoshida et al. 2008). Immune cells can generate both pro and anti-tumourgenic environments (Grivennikov, Greten, and Karin 2010) and HSC gene expression is associated with poor prognosis in HCC (Zhang et al. 2016), although the mechanisms by which activated stellate cells promote tumour development are not established.

***Treatment***

Currently approved curative treatments for patients with solitary HCC nodules (or 3 nodules <3cm) and good liver function include resection, transplantation or percutaneous radiofrequency ablation (EASL-EORTC 2012). Palliative transarterial chemoembolisation

(TACE) is appropriate for asymptomatic patients with multi-nodular disease but no vascular invasion or extrahepatic spread.

Until very recently Sorafenib (co-marketed as Nexavar by Bayer, Germany and Onyx Pharmaceuticals, USA) was the only approved treatment for advanced HCC. It is a multi-tyrosine kinase inhibitor and its targets include vascular endothelial growth factor receptor, platelet derived growth factor receptor and the Raf cascade (Scudellari 2014). However, even Sorafenib is not recommended for use in patients with advance HCC by the National Institute for Health and Care Excellence (NICE - https://www.nice.org.uk/guidance/ta189). Its high cost and limited benefit mean it has an incremental cost effectiveness ratio of at least £51900 per quality-adjusted life year (QALY) and so is not considered a cost effective use of NHS resources.

Since 2007, when Sorafenib was approved for HCC, numerous other targeted therapies have failed, many at the phase III trial stage (Scudellari 2014). However, the phase III RESOURCE trial, published early in 2017, which compared the multikinase inhibitor Regorafenib with placebo in HCC patients that had tolerated but progressed on Sorafenib, met its primary endpoint of improved overall survival (OS)(Bruix et al. 2017) . As a result, the US Food and Drug Administration (FDA) approved Regorafenib for second line treatment of HCC in April 2017. However, NICE recommendations in March 2018 did not find Regorafenib use in HCC patients cost effective (NICE - https://www.nice.org.uk/guidance/TA514). Results of the REFLECT trial comparing Lenvatinib, another mulitkinase inhibitor, with Sorafenib in the first line treatment of advanced HCC, were published early in 2018. The REFLECT trial met its primary endpoint of non-inferior OS in Lenvatinib relative to Sorfenib treated patients (Kudo et al. 2018). Furthermore Lenvatinib demonstrated superiority relative to sorafenib in terms of progression free survival and time to progression. Lenvatinib is already FDA approved for the treatment of thyroid cancer and an indication expansion is expected imminently. NICE are expected to publish their recommendations regarding Lenvatinib towards the end of 2018.

Over recent years, immune checkpoint inhibitors have garnered significant interest in the treatment of cancer, including HCC (Kudo 2017). The results of a number of early phase trials in HCC look very promising. Correspondingly, in September 2017 the FDA approved the anti-

PD1 antibody Nivolumab as a second line treatment for HCC. NICE assessment of Nivolumab is ongoing.

Work on other kinase inhibitors and immunotherapeutics as well as RNAi and miRNA based drugs for advanced HCC is ongoing. However, given that the majority of HCCs develop on a background of liver disease, particularly cirrhosis, there is potential to target this precancerous lesion and treat HCC much sooner, thereby either delaying its onset or slowing its progression at an early stage.

### 1.4.2 NAFLD related HCC

HCC resulting from NAFLD related cirrhosis was first reported in 1990 (Powell et al. 1990). Corresponding to the rapid increase in global incidence of NAFLD that has occurred since then, NAFLD associated HCC has also proven to be a growing problem, likely accounting for much of the increase in HCC incidence seen in industrialised countries (Wree et al. 2013). In a North American study of patients undergoing liver transplant for HCC between 2002 and 2012, the number of patients receiving a transplant for NAFLD related HCC rose by over 60% compared with only a 15% rise in HCV related HCC cases (Wong, Cheung, and Ahmed 2014).

There is also a growing body of evidence suggesting that a large proportion of cases of cryptogenic cirrhosis, the cause of up to 40% of HCCs in developed countries, are secondary to NAFLD (Starley, Calcagno, and Harrison 2010; El-Serag and Rudolph 2007). Indeed features of steatohepatitis are often absent in NAFLD cirrhosis, therefore NAFLD related HCC incidence may be underestimated. HCC risk in patients with NAFLD cirrhosis is probably lower than that in patients with cirrhosis from other aetiologies, such as HCV. Highest estimates suggest an incidence of 2-3% per year (Ascha et al. 2010). However HCC can also occur in non-cirrhotic NAFLD (Baffy, Brunt, and Caldwell 2012). In a Japanese cross-sectional study of patients with NASH and HCC, an alarming 49% of patients did not have cirrhosis (Yasui et al. 2011).

The increasing incidence of NAFLD and so NAFLD related HCC and the discovery that a broader spectrum of NAFLD patients are at risk of developing cancer than previously appreciated mean it is essential that there is a better understanding of the pathogenesis of NAFLD HCC, so that preventative, surveillance and treatment measures can be developed.

As with HCC stemming from other aetiologies, NAFLD related HCC largely develops on a background of repeated cycles of necrosis, inflammation and regeneration. Therefore pathogenic mechanisms involved in the development of NASH are also relevant to HCC tumourgenesis. There are also a number of potentially contributory factors in NAFLD HCC pathogenesis specific to the aetiology. This conclusion stems from evidence that obesity and diabetes are not only associated with NAFLD but also contribute independently to HCC risk (Marengo, Rosso, and Bugianesi 2016; Stickel and Hellerbrand 2010).

Obesity is a significant risk factor for a range of malignancies, including liver cancer. In a prospective, North American study involving over 900,000 individuals, the relative risk of death from liver cancer in obese males was 4.52, the highest seen in the study (Calle et al. 2003). This finding was supported by a subsequent meta-analysis (Larsson and Wolk 2007). Obesity is a state of chronic, low grade inflammation which promotes insulin resistance and carcinogenesis. Changes in adipokine secretion (such as increased TNF, IL-6, and leptin and decreased adiponectin) from rapidly expanding adipocytes enhance HCC development.

Park et al. demonstrated that in diethylnitrosamine (DEN) treated mice (that develop HCC secondary to DNA damage), diet and genetically induced obesity promoted HCC onset and progression (Park et al. 2010). They subsequently showed that this effect was almost completely reversed in mice lacking TNF receptor 1 or IL-6. Supporting the oncogenic role of TNF in HCC, Pikarsky et al. found that in multi drug resistant 2 (MDR2) transporter knockout mice (that develop cholestatic hepatitis and ultimately HCC), inhibition of NF-κB in hepatocytes (through anti-TNFα treatment or induction of IκB-super-repressor – a degradation resistant form of IκB) blocked tumour development and resulted in apoptosis of transformed hepatocytes (Pikarsky et al. 2004). Similarly hepatocarcinogenesis following DEN administration was reduced in mice lacking IKKβ in their hepatocytes and kupffer cells (Maeda et al. 2005). Of note although in the scenarios described the absence NF-κB inhibited tumourgenesis, under different circumstances, inhibition of apoptosis by NF-κB can regulate reactive cell proliferation and so cancer development (Karin 2006). IL6 activates STAT3, a transcription factor which has been shown to be upregulated in HCCs, especially those with a poorer prognosis (Calvisi et al. 2006). Furthermore studies of mice with liver specific STAT3 knockout have shown that it is required for HCC tumourgenesis (Park et al. 2010).

As well as having anorexic and pro-inflammatory effects, leptin, levels of which are increased in obesity, has been implicated in promotion of fibrosis, HCC cell proliferation, angiogenesis and inhibition of apoptosis (Wang, Lee, and Ker 2010; Chen et al. 2007). Other studies have implicated leptin in STAT3 dependent increased TERT expression (Stefanou et al. 2010). Conversely, the anti-inflammatory adipokine adiponectin, secretion of which is reduced in obesity, has been shown to antagonise the oncogenic effects of leptin though inhibition of angiogenesis and modulation of intracellular signalling including AMPK and the

PTEN/AKT/mTORC1 pathways (Dalamaga, Diakopoulos, and Mantzoros 2012; Brakenhielm et al. 2004). Correspondingly, following exposure to a NASH inducing diet, adiponectin knockout mice experienced enhanced steatosis and tumourgenesis (Kamada et al. 2007).

Analysis of Surveillance Epidemiology and End-Results Program (SEER) data from the USA found a 3 fold risk of HCC in patients with diabetes relative to non-diabetic controls (Davila et al. 2005). This result has subsequently been validated in other populations and a recent meta-analysis of 49 studies demonstrated a relative risk of HCC of 2.31 in patients with diabetes (Wang et al. 2012). Hyperinsulinaemia associated with Type II Diabetes, is believed to promote oncogenesis through stimulation of proliferative signalling pathways, such as PTEN/AKT/mTORC1 and MAPK (Reeves, Zaki, and Day 2016). Furthermore, insulin-like growth factor 1 (IGF-1) has been shown to promote proliferation and angiogenesis and inhibit apoptosis. IGF-1 levels are raised in diabetes because synthesis of insulin-like growth factor binding proteins, which bind and inhibit IGF-1, is reduced, by insulin.

Excess free fatty acids present in NAFLD may also be important to HCC development. PTEN expression was reduced in steatotic liver from rats fed a high fat diet and in liver biopsies from obese patients with steatosis (Vinciguerra et al. 2008). Vinciguerra et al. observed that PTEN mRNA levels in hepatic cells fell significantly following exposure to unsaturated fatty acids, but not glucose or insulin. They went on to propose a model whereby free fatty acids activate an mTORC/NF-κB complex which in turns triggers miRNA21 synthesis and so PTEN mRNA degradation (Vinciguerra et al. 2008; Vinciguerra, Sgroi, et al. 2009; Vinciguerra, Carrozzino, et al. 2009; Peyrou, Bourgoin, and Foti 2010).

As well as causing cell damage and inflammation, ROS, levels of which are thought to be increased in NAFLD, can induce cancer directly by mutating DNA (Hu et al. 2002). For instance the lipid peroxidation product trans-4HNE has been shown to cause p53 mutations. Furthermore, ROS, free fatty acids and cytokines all activate JNK, which may in turn be associated with altered histone methylation, resulting in up-regulation of genes responsible for cell proliferation and down-regulation of those involved in cell differentiation (Chang et al. 2009). In keeping with JNK being oncogenic, it has been found to be over-active in more than 50% of HCCs (Starley, Calcagno, and Harrison 2010).

Autophagy may play independent roles in both NAFLD progression and tumourgenesis. There is evidence to suggest that autophagy is down-regulated in obesity. Nutrient excess up-regulates mTORC1, which inhibits autophagosome formation through phosphorylation of ULK1 (Hosokawa et al. 2009). Excess lipid may accumulate in autophagosomal membranes impairing autophagosome-lysosome fusion (Koga, Kaushik, and Cuervo 2010). And, although the mechanism is unclear, cathepsin levels are reduced in ob/ob mice and liver from patients with NAFLD (Inami et al. 2011; Fukuo et al. 2014). Degradation of hepatic lipid droplets by autophagy is called lipophagy and a reduction in this process can result in steatosis (Singh et al. 2009). Loss of the autophagy related gene 5 (Atg5) in hepatocytes resulted in raised triglyceride and cholesterol levels and conversely over-expression of Atg7 in ob/ob mice or mice fed a high fat diet, limited hepatic steatosis (Yang et al. 2010). Furthermore, epidemiological studies have suggested that caffeine consumption is protective in NAFLD and Sinha et al. demonstrated that this could be due to increased autophagy and fatty acid oxidation (Sinha et al. 2014; Molloy et al. 2012).

It is not clear whether autophagy influences progression of NAFL to NASH. However, ubiquitin-binding protein p62, which is an autophagosome cargo protein and accumulates when autophagy is impaired, is a major component of Mallory-Denk bodies which are seen in NASH (Stumptner et al. 2002). In contrast to an inhibitory role of autophagy in steatosis progression, autophagy may promote hepatic fibrosis. When autophagic flux within HSCs is enhanced, they lose their retinol ester containing perinuclear lipid droplets and become activated (Hernandez-Gea et al. 2012; Thoen et al. 2011). Finally, the role of autophagy in tumour development may vary with context. Defective autophagy results in accumulation of abnormal proteins and damaged organelles including mitochondria, this causes ER stress, ROS accumulation and inflammation which promote tumourgenesis (Aghajan, Li, and Karin 2012). Correspondingly mice that are haploinsufficient for Beclin 1, a key protein in autophagosome formation, as well as mice with hepatic Atg 5 or Atg7 loss develop liver tumours (Qu et al. 2003; Komatsu et al. 2005; Takamura et al. 2011). However, under conditions of energetic stress autophagy may also promote tumour cell survival by maintaining energy homeostasis (Lavallard and Gual 2014).

### 1.4.3 HCC & AMPK

Metformin treatment in patients with T2DM significantly reduces HCC risk (Donadon et al. 2010) and evidence from a small number of studies that have investigated the role of AMPK in HCC largely suggests that AMPK has an inhibitory effect on HCC. Cheng et al. and Zheng et al. demonstrated reduced AMPK phosphorylation in HCCs relative to surrounding non-cancerous tissue, and a negative correlation between AMPK phosphorylation and aggressive clinical and pathological HCC features including high expression of the cell proliferation marker Ki67 (Zheng et al. 2013). Lee et al. also used clinical samples to investigate the significance of AMPK subunit expression, specifically AMPK α2 in HCC and found reduced AMPK α2 mRNA in HCCs relative to corresponding normal liver (Lee et al. 2012). They went on to demonstrate that in HCC cells AMPK phosphorylated the NAD dependent deacetylase sirtuin 1 (SIRT1 at Thr344), so suppressing its activity. This in turn resulted in increased acetylation (at Lys382) and accumulation of the tumour suppressor p53, enhanced expression of its target genes ($p21^{CIP}$ and Bcl-2 associated X protein – Bax) and reduced cell growth. Furthermore, Lee et al. observed that whilst p53 phosphorylation was associated with increased AMPK activity, AMPK did not directly phosphorylate p53. Yi et al. concluded that low dose metformin induced HCC cell senescence via the same mechanism (Yi et al. 2013) and other groups have also described increased expression of the cyclin dependent kinase inhibitors $p21^{CIP}$ and $p27^{KIP}$; decreased cyclin D1 expression; G1-S cell cycle arrest and reduced proliferation; in Hep G2 and PLC/PRF/5 HCC cell lines and PLC/PRF/5 xenografts treated with Metformin and AICAR (Cai et al. 2013; Cheng et al. 2014; Imamura et al. 2001).

Yu et al. used the second generation tyrosine kinase inhibitor Nilotinib to reduce human HCC cell viability and xenograft growth in an AMPK dependent manner (Yu et al. 2013). They demonstrated that the drug inhibited protein phosphatase 2A (PP2A) thereby limiting its ability to dephosphorylate AMPK, resulting in increased AMPK activation and so up-regulation of autophagy. In addition, Hu et al showed increased Hep3B and Huh7 cell death, associated with evidence of autophagy, following treatment with the mTORC1 inhibitor AZ8055 and found this effect to be attenuated by AMPK inhibition (Hu et al. 2014).

Of particular relevance to our study, Piguet et al. found that regular exercise limited tumour development in mice with liver specific Pten knockout, without affecting steatosis (liver

triglyceride content), hepatocyte injury (NAS score) or autophagy (Piguet et al. 2015). They demonstrated increased phosphorylation of AMPK (Thr172) and Raptor (Ser792) and decreased phosphorylation of S6 (Ser240/244) in the liver immediately following exercise and concluded that exercise activated AMPK leading to reduced mTORC1 signalling and so tumour growth. Although the triglyceride content of liver from exercised mice did not differ from that of sedentary animals, ACC phosphorylation (Ser79) in liver tissue was increased following exercise. Furthermore, RNA sequencing of liver tissue from exercised mice identified 6 pathways that were significantly altered, all, to some extent, involved in fatty acid metabolism. The lack of impact of exercise on steatosis could be due to the fact that animals did not begin exercising until 7-9 weeks of age, by which time steatosis is established (Horie et al. 2004; Stiles et al. 2004). It is also interesting to note that although NAS scores did not differ between exercised and sedentary mice, there was a non-significant reduction in lobular inflammation in the exercised cohort (Piguet et al. 2015).

### 1.4.4 HCC and PTEN

First identified in 1997, PTEN is a tumour suppressor, the gene for which is located at locus 10q23 (Song, Salmena, and Pandolfi 2012; Li et al. 1997; Steck et al. 1997). After *p53*, *PTEN* is the second most frequently deleted/mutated tumour suppressor gene in human cancers and its expression is reduced or absent in over 40% of HCCs (Hu et al. 2003). In contrast to Knudson's original 'two hit model' based on the retinoblastoma tumour suppressor (Knudson 1971), PTEN appears to follow a 'continuum model for tumour suppression' whereby its tumour suppressor activity is dose (expression level) dependent (Berger, Knudson, and Pandolfi 2011). This model incorporates the observations that haplo-insufficiency of *PTEN*, as well as more subtle changes in its expression or activity impact upon its role as a tumour suppressor.

The domain structure of PTEN is summarised in **Figure 1.17**. Around 40% of *PTEN* mutations in patients with Cowden's disease are in exon 5, which encodes the phosphatase domain (Eng 2003), however, somatic mutations occur throughout the gene and mutants with dysfunctional PTEN can have normal catalytic activity (Song, Salmena, and Pandolfi 2012).


***Figure 1.17 – Domain structure of PTEN*** *PTEN has 5 domains: 1) A short phosphatidylinositol bisphosphate (PIP2) binding domain (PBD) located at its N-terminus, 2) the catalytic phosphatase domain which forms a binding pocket for both polypeptide and phosphoinositide substrates, 3) a C2 domain which enables it to bind phospholipid membranes, 4) a C-terminal tail containing PEST (proline, glutamate-serine-threonine) rich sequences which promote protein stability and 5) a C-terminus PDZ binding domain, important for its interaction with scaffolding proteins.*

PTEN dephosphorylates $PIP_3$, reversing the actions of PI3K and so inactivating the AKT/mTORC1 pathway (**Figure 1.5**). PTEN loss therefore results in increased mTORC1 stimulated cell growth and proliferation as well as up-regulation of AKT. Activation of AKT

results in increased glucose uptake, glycolysis and *de novo* lipogenesis and down-regulation of gluconeogenesis and fatty acid oxidation.

Vinciguerra et al. demonstrated that overexpression of PTEN in HepG2 cells decreased triglyceride accumulation following exposure to oleic acid enriched media, whereas under the same conditions, PTEN depletion using specific siRNAs lead to increased intracellular triglyceride content (Vinciguerra et al. 2008). They also showed that lipid accumulation in PTEN deficient cells was associated with increased expression of genes involved in FA uptake (fatty acid translocase/CD36) and esterification (PEPCK and GPAT), but they did not see increased SREBP1c or FAS gene expression, or changes in mitochondrial fatty acid oxidation, in siRNA treated cells.

Global PTEN deficiency is embryonically lethal (Di Cristofano et al. 1998; Suzuki et al. 1998), however mice with global heterozygous deletion of *PTEN* exons 3-5 develop atypical adenomatous hyperplasia in their livers (Suzuki et al. 1998). Horie et al. and Stiles et al. used albumin Cre-Lox recombination to achieve liver specific Pten knockout in mice. There was considerable overlap in the results of these 2 studies with mice progressing through hepatic steatosis and steatohepatitis and developing liver tumours around 40 weeks of age (**Table 4.1**). Horie and colleagues described a milder phenotype in mice heterozygous for *Pten* and in female mice. The latter is in-keeping with evidence that oestrogens may be protective in NAFLD (Anezaki et al. 2009) and that marked differences in gene expression exist between male and female livers (Humphries 2014). Given the marked similarities between features of NAFLD and changes seen in mice with liver specific Pten loss, the latter has become accepted as a model for NAFLD (Wu 2016).

## 1.5 Aims & objectives

1) **To characterise a novel, activating AMPK γ1 mutation in mouse primary hepatocytes**

Previous cell based work has demonstrated that substitution of aspartic acid by an alanine residue at position 316 in AMPK γ1 (D316A) results in constitutive AMPK activation (Woods et al. 2017). Mice carrying a D316A mutant AMPK γ1 transgene have been crossed with mice expressing cre driven by the Albumin promotor to generate D316-Tg mice. AMPK activation in D316A-Tg mice is liver specific and because the activation is due to genetic modification, off-target effects, as can occur with pharmacological activators, are avoided. Given the central role of AMPK in energy metabolism, through up-regulation of catabolic and down-regulation of anabolic pathways, constitutive activation of AMPK within hepatocytes is likely to impact upon their metabolic processes. Work characterising the expression of transgenic AMPK γ1 and effects of increased AMPK activity within primary hepatocytes from D316A-Tg mice is presented in the first section of Chapter 3.

2) **To determine the effects of chronic activation of AMPK in the liver under basal conditions and in response to the metabolic stresses of a hypercaloric, high fat and lipogenic, high fructose diet.**

Other studies have investigated (genetically or pharmacologically induced) systemic AMPK activation and its acute activation within the liver. However, this study has used the D316A-Tg mice to examine chronic and specific hepatic AMPK activation. The effects of AMPK on metabolism and potentially inflammation have led to it receiving substantial attention as a therapeutic target in treatment of the metabolic syndrome. It is therefore important to understand the role of AMPK in the liver not only under normal conditions but also in response to metabolic stress. Work determining the effects of chronic activation of AMPK in the liver, *in vivo* and comparison of these findings with those in primary hepatocytes are detailed in the latter two sections of chapter 3.

3) **To study the effects of chronically increased hepatic AMPK activity in a mouse model of NAFLD related HCC.**

Mice with liver specific Pten loss and so AKT and mTORC1 activation, show features of steatosis and steatohepatitis and progress to develop HCC. This is therefore a good model to study not only the importance of AMPK in NAFLD, the hepatic component of the metabolic syndrome, but also the effects of chronic activation of AMPK in the liver on tumourgenesis. Whilst AMPK's function in metabolism is relatively well established, its role in cancer is less clear and evidence with regards to whether it promotes or suppresses tumour development is somewhat conflicting. Work studying the effects of increased hepatic AMPK activity on NAFLD progression and tumour development in mice with liver specific Pten loss is presented in Chapter 4.

# 2 Materials and Methods

## 2.1 Materials

### 2.1.1 General reagents

| **Sigma® (Poole,UK)** | |
|---|---|
| Adenosine triphosphate (ATP) | Methyl-tert butyl ether (MTBE) |
| Agarose | Normal goat serum |
| Ammonium heptamolybdate tetrahdrate | 4-(2-hydroxyethyl)-1-piperazineethanesulfonic acid (HEPES) |
| Benzamidine | Hydrogen peroxide |
| Bovine serum albumin (BSA) | Magnesium chloride ($MgCl_2$) |
| Bromophenol blue | β-Mercaptoethanol |
| Calcium chloride ($CaCl_2$) | Mixed dNTP (10mM) |
| Cerium sulfate hydrate complex with sulphuric acid | Oil Red O |
| Cholesterol | Oleic acid |
| Cholesterol oleate | Palmitate |
| Deoxynucleotides (dNTPs) | Petroleum ether |
| Dexamethasone | Phenylmethylsulfonyl fluoride (PMSF) |
| Dimethyl sulfoxide (DMSO) | Picric acid - 1.3% saturated aqueous solution |
| Direct red 80 (Sirius red stain) | Potassium phosphate |
| Dithiothreitol (DTT) | Protein A/G sepharose |
| Dnase 1 from bovine pancreas | Sorbitol |
| DPX mountant | Sodium acetate |
| Ethylene glycol tetraacetic acid (EGTA) | Sodium fluoride (NaF) |
| Heat inactivated foetal bovine serum (FBS) | Sodium pyrophosphate ($NaP_2O_7$) |
| Gill's haematoxylin | Triiodothyronine ($T_3$) |
| Glyceryl trilinoleate | Tris(hydroxymethyl) aminomethane (Tris) |
| Glycine | Triton X-100 |
| Lactate | |
| **VWR® (West Sussex, UK)** | |
| Chloroform | Monopotassium phosphate ($KH_2PO_4$) |
| Disodium phosphate ($Na_2HPO_4$ – anhydrous) | Potassium chloride (KCl) |
| Diethyl ether | Potassium hydroxide |
| Ethanol | Propylene glycol |
| Ethylenediaminetetraacetic acid (EDTA) | Sodium bicarbonate ($NaHCO_3$) |
| Ethylene glycol-bis(β-aminoethyl ether)-N,N,N',N'-tetraacetic acid (EGTA) | Sodium chloride (NaCl) |
| Glucose | Sodium citrate |
| Glycerol | Sodium dodecyl sulfate (SDS) |
| Hydrochloric acid | Sodium hydroxide (NaOH) |
| Lithium chloride (LiCl) | Sulphuric acid |
| Methanol | Tween 20 |
| **Gibco® (Paisley, UK)** | |
| Collagen type I (rat tail) | Insulin |
| Dulbecco's modified eagles media (DMEM) – glucose free and no phenol red | M199 media |
| | Penicillin streptomycin (Pen/Strep) |
| **Perkin Elmer® (Seer Green, UK)** | |
| $^3$H-acetate | [γ-32P] Adenosine triphosphate (ATP) |
| [1-14C] Acetic acid sodium salt | [1-14C] palmitic acid |
| **Thermo Fisher Scientific (Waltham, MA, USA)** | |

| | |
|---|---|
| Acetic acid | Orthophosphoric acid |
| NuPAGE™ Bis-Tris pre-cast protein gels (Novex) | Skimmed milk powder (Oxoid) |
| x20 MOPS running buffer (Invitrogen) | Sucrose |
| OCT compound | TRIzol® |
| **Vector Laboratories (Peterborough, UK)** | |
| Biotinylated goat secondary antibody | VectaMount ™ |
| DAB Peroxidase HRP Substrate kit | VECTASTAIN Elite ABC kit |
| **Supplier** | **Reagent** |
| StatLab (McKinney, TX, USA) | CitraClear |
| Sarstedt (Leicester, UK) | Heparinised microvettes |
| Merck Millipore (Billerica, MA, USA) | Immobilon-FL PDF membrane |
| Whatman® (Maidstone, UK) | P81 phosphocellulose paper |
| Promega (Madison, WI, USA) | Random primers |
| Lonza® (Slough, UK) | Tripsin neutraliser solution (inhibitor) |

***Table 2.1 – General reagents used in thesis and their suppliers***

### 2.1.2 Buffers

| Buffer | Contents |
|---|---|
| **Collagenase buffer** | HBSS and 1mM $CaCl_2$ |
| **HBA** | 50mM Hepes pH7.4, 50mM NaF, 50mM $NaP_2O_7$, 1mM EDTA, 10% (v/v) Glycerol, 1mM DTT, 4µg/ml Trypsin inhibitor, 0.1mM PMSF, 1mM Benzamidine |
| **HBSS** | 138mM Sodium chloride (NaCl), 50mM Hepes pH7.4, 5.56mM Glucose, 5.4mM Potassium chloride (KCl), 0.338mM $Na_2HPO_4$, 0.44mM, $KH_2PO_4$ 4.17mM $NaHCO_3$ |
| **Hepes lysis buffer** | HBA and 1% Triton X-100 |
| **HE** | 50mM Hepes pH7.4, 1mM EDTA, 10% (v/v) Glycerol, 1% (v/v) Triton X-100, 1mM DTT, 4µg/ml Trypsin inhibitor, 0.1mM PMSF, 1mM Benzamidine |
| **High salt buffer (HST)** | 20mM Tris pH7.4, 500mM NaCl, 0.5% (v/v) Tween 20 |
| **Homogenisation buffer** | 50mM Tris pH7.4, 50mM NaF, 5mM $NaP_2O_7$, 1mM EDTA, 250mM sucrose, 1mM DTT, 4µg/ml trypsin neutraliser solution, 0.1mM PMSF, 1mM benzamidine |
| **Perfusion buffer** | HBSS and 0.5mM ethylene glycol-bis(β-aminoethyl ether)-N,N,N',N'-tetraacetic acid (EGTA) |
| **Phosphate buffered saline (PBS)** | 137mM NaCl, 2.7mM KCl, 4.3mM $Na_2HPO_4$, 1.4mM $KH_2PO_4$, pH7.4 |
| **Sample buffer** | 50mM Tris-HCl pH7.4, 2.5% (w/v) SDS, 1% (v/v) β-mercaptoethanol, 10% glycerol, 0.05% (w/v) bromophenol blue |
| **Transfer buffer** | 25mM Tris, 192mM Glycine, 20% Methanol |

***Table 2.2 - Composition of buffers used in thesis***

### 2.1.3 Primers

Primers used for genotyping are listed in **Table 2.3** and those for qPCR in **Table 2.4**. DNA and RNA primers were ordered from Sigma-Genosys (Havrehill, UK) unless otherwise stated.

| Product | Product size | Sequence 5'-3' |
|---|---|---|
| **AMPK γ1** | Non-transgenic 365bp<br>Transgenic (Flag tagged) 498bp | F1:CACGTTTCCGACTTGAGTTG<br>F2:GGACGACGATGACAAGTGAG<br>R:TAAGCCTGCCCAGAAGACTC |
| **Albumin Cre** | 178bp | F:CGTACTGACGGTGGGAGAAT<br>R:CCCGGCAAAACAGGTAGTTA |
| **IL (positive control for Albumin Cre)** | 324bp | F:CTAGGCCACAGAATTGAAAGATCT<br>R:GTAGGTGGAAATTCTAGCATCATCC |
| **PTEN** | WT 156bp<br>Mutant 328bp | F:CAAGCACTCTGCGAACTGAG<br>R:AGGTTTTTGAAGGCAAGATGC |

***Table 2.3 – Genotyping primers***

| Product (Mouse) | Sequence 5'-3' |
|---|---|
| **ACC1** | F:ATGGGCGGAATGGTCTCTTTC<br>R:TGGGGACCTTGTCTTCATCAT |
| **FAS** | F:TGCTCCCAGCTGCAGGC<br>R:GCCCGGTAGCTCTGGGTGTA |
| **G6Pase** | F:CGACTCGCTATCTCCAAGTGA<br>R:GTTGAACCAGTCTCCGACCA |
| **PEPCK** | F:CCCCTTGTCTATGAAGCCCTCA<br>R:GCCCTTGTGTTCTGCAGCAG |
| **SPOT14** | Primers from Qiagen – no sequence information provided |
| **SREBP1C** | F:GGAGCCATGGATTGCACATT<br>R:GCTTCCAGAGAGGAGGCCAG |

***Table 2.4 – qPCR primers*** *(specific to mouse RNA).*

### 2.1.4 Antibodies

Primary antibodies used throughout this thesis are listed in **Table 2.5** and secondary antibodies in **Table 2.6**.

| Antibody | Raised in | Dilution | Size kDa | Supplier | Product no. | Application |
|---|---|---|---|---|---|---|
| **pACC$^{Ser79}$** | R | 1/1000 | 280 | CS | #3661 | WB |
| **Total ACC** | M | 1/1000 | 280 | Millipore | 05-1098 | WB |
| **Total ACC** | R | 1/1000 | 280 | CS | 3676 | WB |
| **Actin** | M | 1/1000 | 45 | Sigma | A3853 | WB |
| **Actin** | R | 1/1000 | 45 | CS | #4968 | WB |
| **AMPK α1 & α2** | M | 1/1000 | 62 | CS | #2793 | WB |
| **pAMPK α$^{Ser485}$** | R | 1/1000 | 62 | CS | #4184 | WB |
| **pAMPK α$^{Thr172}$** | R | 1/1000 | 62 | CS | #2535 | WB |
| **AMPK β1/β2 (Sip2)** | R | 1/5000 WB<br>1/1000 IP | 62 | In-house | N/A | WB/IP |
| **AMPK β1/β2** | | 1/1000 | 38/30 | CS | | WB |
| **AMPK Υ1** | R | 1/1000 | 37 | AbCam | Ab32508 | WB |
| **AMPK Υ1** | R | 1/1000 | 37 | Novus | NBP2-15382 | WB |
| **pAKT$^{Ser473}$** | R | 1/1000 | 60 | CS | #3787 | WB |
| **FAS** | M | 1/1000 | 265 | BD Biosciences | 610962 | WB |
| **FGF21** | | 1/1000 | 20 | Sigma | | WB |
| **Flag** | R | 1/1000 | * | CS | #2368 | WB |

| | | | | | | |
|---|---|---|---|---|---|---|
| **PTEN** | R | 1/1000 | 54 | CS | #9559 | WB |
| **pS6$^{Ser240/244}$** | R | 1/1000 | 32 | CS | #2215 | WB |
| **SCD1** | | 1/1000 | 38 | LifeTech** | | WB |
| **α Tubulin** | M | 1/1000 | 50-55 | Sigma | T5168 | WB |
| **Vinculin** | M | 1/1000 | 116 | Sigma | V9131 | WB |

***Table 2.5 - Primary antibodies used in thesis.*** *ACC = acetyl-coA carboxylase, R= rabbit, CS = Cell signalling, WB = western blot, M = mouse, IP = immunoprecipitation, FAS = fatty acid synthase, FGF-21 = fibroblast growth factor-21, SCD1 = stearoyl-CoA desaturase 1. *Weight dependent on tagged protein. **Thermo Fisher Scientific, previously Life Technology.*

| | |
|---|---|
| **Western blotting – LI-COR imaging system (LI-COR Biotechnology, Cambridge, UK)** | IRDye 800CW Goat anti-rabbit<br>IRDye 680LT Goat anti-rabbit<br>IRDye 800CW Goat anti-mouse<br>IRDye 680LT Goat anti-Rabbit<br>(All 1/20000 dilution) |
| **Immunohistochemistry** | Biotinylated Goat anti-rabbit (Vector Laboratories, Peterborough, UK – 1/200 dilution) |

***Table 2.6 – Secondary antibodies used in thesis.***

### 2.1.5 Mouse Lines

| Label | Genotype | Details |
|---|---|---|
| **WT-Tg** (*Fig 3.6* onwards) | Non-Tg | No AMPK transgenes expressed* |
| | Het WT-Tg | Single copy of WT AMPK transgene expressed in liver |
| | Hom WT-Tg | Two copies of WT AMPK transgene expressed in liver |
| **D316A-Tg** (*Fig 3.6* onwards) | Het D316A-Tg | Single copy of D316A AMPK transgene expressed in liver |
| | Hom D316A-Tg | Two copies of D316A AMPK transgene expressed in liver |
| ***Pten*$^{-/-}$** (Throughout chapter 4) | *Pten*$^{-/-}$+Non-Tg | Pten absent from liver and no AMPK transgenes expressed |
| | *Pten*$^{-/-}$+WT-Tg | Pten absent and 1 or 2 copies of WT AMPK transgene expressed in liver |
| ***Pten*$^{-/-}$*+D316A*** (Throughout chapter 4) | *Pten*$^{-/-}$+D316A-Tg | Pten absent and 1 or 2 copies of D316A AMPK transgene expressed in liver |

***Table 2.7 – Summary of mouse lines used in thesis***. **Transgene / Cre recombinase or both absent*

## 2.2 Methods

All experiments involved in the generation of transgenic animals were approved by Gothenburg Ethics Committee. All *in vivo* work was carried out in accordance with the United Kingdom Animals (Scientific Procedures) Act (1986) and approved by the Animal Welfare and Ethical Review Board at Imperial College London. Mice were housed in a specific-pathogen free barriered facility. Unless otherwise stated, mice were maintained on a 12h light/dark cycle with free access to food and water and weighed weekly.

### 2.2.1 Genotyping

DNA from ear clip or tail snip biopsies was extracted by boiling at 100$^{o}$C with 100mM NaoH for 10 minutes, followed by addition of 1M Tris pH 8 to adjust the pH to 8. DNA was amplified by polymerase chain reaction (PCR) using 2x Biomix™ Red (containing Taq DNA polymerase, Cat# BIO-25006; Bioline, London, UK) and the appropriate primers. Following amplification, DNA was analysed by agarose gel electrophoresis at 120V for 30mins on a 2% agarose gel. Bands were visualised by ultra-violet light exposure using Gene Genius (Syngene, Cambridge, UK).

### 2.2.2 Primary hepatocyte isolation

***Preparing collagen coated plates***

Collagen type I was diluted in 0.02N acetic acid to a final concentration of 0.5mg/ml. Collagen solution was then used to coat plates with 12.5µg collagen per cm$^2$ (e.g. 250µl of solution per 35mm diameter well with a surface area of approximately 10cm). Plates were then left to dry for ≥2h.

***Isolation***

Primary hepatocyte isolation was performed by the animal physiology team. Mice were anaesthetised with 2µl/g of a 3:1:3 ketamine (100mg/ml) : xylazine (20mg/ml) : water mix. The inferior vena cava was isolated and perfused with warmed perfusion buffer and the hepatic portal vein was then cut, resulting in rapid creamy discolouration of the liver. Perfusion with perfusion buffer was continued for 10-15mins and then changed to warmed collagenase buffer until the liver was well digested. Perfusion was stopped and the liver

dissected out. Hepatocytes were released by cutting the liver whilst suspended in warmed Hepes buffer. Cells were filtered through a cell sieve, re-suspended in 50ml of HBSS without EGTA and placed on ice until plating.

***Plating***

Isolated cells in HBSS were centrifuged for 5mins at 300rpm and buffer was then aspirated off to leave a cell pellet. This resuspension, centrifuge and aspiration step was repeated once. The cell pellet was then re-suspended in 10ml of cold adherence media (M199 + Earles salts media with 1% (v/v) Pen/Strep, 100nM insulin, 0.1% (w/v) BSA, 100nM triiodothyronine, 100nM dexamethasone and 2% (v/v) Ultroser™ G (Cat# 15950-017; Pall, Portsmouth, UK). A 50µl aliquot of cells was removed, 950µl of trypan blue added and a cell count acquired using a haemocytometer. This step was performed in duplicate and the average of the two cell counts taken. Viability >80% was required to proceed. Cells were diluted to a density of ≈0.3 x $10^6$ cells/ml and then plated onto collagen coated plates, ensuring even dispersion. After 3-4h, once cells had adhered, they were changed to basal medium (M199 with 1% (v/v) pen/strep, 1nM insulin and 100nM dexamethasone) and left for at least 16h before experimental manipulation.

### 2.2.3 Rapid cell lysis

Cells were washed with PBS then lysed into Hepes lysis buffer. This was done as rapidly as possible to avoid AMPK activation, so that lysates could be used for AMPK activity assays and to assess AMPK activity using Western blots. Cell lysates were centrifuged at 13000rpm for 10 mins and the lysate, containing mainly cytosolic proteins, retained.

### 2.2.4 Pierce™ BCA protein assay

Protein concentrations in cell lysates were determined using the Pierce™ BCA Protein Assay Kit (Cat# 23225; Thermo Fisher Scientific, Waltham, MA, USA), which has a range of 0-2mg/ml. BSA standards were used and the assay was run according to the manufacturer's protocol. A SpectraMax 340 (Molecular Devices, Sunnyvale, CA, USA) microplate reader was used to measure absorbance at 562nM.

### 2.2.5 Western blotting

50-100ug of total protein lysate was boiled in sample buffer. Protein was resolved by Sodium Dodecyl Sulfate Poly-Acrylamide Gel Electrophoresis (SDS-PAGE) using pre-cast NuPAGE™ (4-12% or 10%) Bis-Tris Protein Gels in MOPS running buffer at 200V for 1h. Proteins were transferred to Immobilon®-FL PDF membrane in transfer buffer at 100V for 90mins. Protein membrane was blocked in 4% (w/v) BSA /HST for 1 hour at room temperature. Primary antibodies were diluted in 4% (w/v) BSA/HST. Membrane was incubated with primary antibody either for 3h at room temperature or overnight at 4$^{o}$C. Membrane was washed in HST and probed with secondary antibody for 1h at room temperature. Secondary antibodies were diluted in 4% (w/v) skimmed milk powder/HST. Membrane was washed in HST before visualisation using an Odyssey Imaging System (LI-COR Biosciences, Cambridge, UK). Quantification was performed using LI-COR Image Studio Version 4.0.21 software.

### 2.2.6 AMPK activity assays

***AMPK immunoprecipitation***

AMPK was immunoprecipitated from cell lysates before assaying for activity. Lysate of 100µg total protein was added to 10µl of 50% protein-A sepharose and 2µl of 1/10 dilution of Sip2 antibody (against AMPKβ) and made up to a volume of 200µl with Hepes lysis buffer. Samples were vortexed at 4$^{o}$C for 1.5hr and then centrifuged at 13000rpm for 1min to pellet the immune complexes. The resulting pellet was washed once with hepes lysis buffer and once with HGE. All remaining buffer was removed using a Hamilton pipette before use in an AMPK activity assay.

***SAMS AMPK activity assay***

The activity of AMPK in the immune complexes was measured by the phosphorylation of the synthetic peptide (HMR**SAMS**GLVLKRR – Pepceuticals Ltd, Nottingham, UK), by the incorporation of [γ-$^{32}$P] ATP (specific radioactivity approximately 200cpm/pmol). The SAMS peptide is based on a sequence derived from the AMPK phosphorylation site in ACC. Immune complexes were added to 50µl SAMS assay mix before incubating for 25min at 37$^{o}$C. Final concentrations in the assay were 0.2mM ATP, 0.2mM SAMS peptide and 5mM $MgCl_2$. Immune complexes were centrifuged at 13000rpm and 20µl supernatant spotted onto P81 paper. P81 paper was washed in 1% (v/v) orthophosphoric acid. The paper was air-dried and placed in a

Tric-Carb 2800TR liquid scintillation analyser (PerkinElmer®, Seer Green, UK), which determined the counts per minute (CPM).

### 2.2.7 Hepatocyte glucose output assay

Primary hepatocytes were plated onto 6 well plates and left overnight in basal media and used the day after isolation for the hepatic glucose output assay. Glucose free DMEM media with no phenol red (plus 1% v/v pen/strep) supplemented with sodium pyruvate and lactate to final concentrations of 2mM and 20mM respectively was used for the assay. Hepatocytes were washed twice in PBS then transferred to pyruvate and lactate supplemented media (e.g. 1ml media per well on 6 well plate). After 18 hours 5µl of media was removed from each well and transferred to the 96 well plate. 20µl of water was then added to dilute each sample to within the range of the assay's standard curve. A standard curve spanning 0.025 – 2mM glucose was made up in unsupplemented media and 25µl of each standard was transferred to a 96 well plate. 100µl of glucose oxidase reagent (from a glucose oxidase assay kit, Cat# GAGO20-1KT, Sigma, Poole, UK) was added to each standard or sample in the 96 well plate and left for 10mins. 100µl of 12N sulphuric acid was then added to each well which turned the assay different shades of pink. A SpectraMax 340 (Molecular Devices, Sunnyvale, CA, USA) microplate reader was then used to measure absorbance at 540nM, allowing the glucose concentration of the media to be calculated. Cells were rapidly lysed and a protein assay performed as described above. Protein concentrations were used to normalise media glucose concentrations.

### 2.2.8 Hepatocyte lipogenesis assay

Rate of lipogenesis in hepatocytes was measured by incorporation of $^{14}C$ acetate into lipid. M199 media (plus 1% v/v pen/strep) was supplemented with sodium acetate to a final concentration of 2mM. [1-14C] acetic acid sodium salt (50.5mCi/mmol) was made up in ethanol to give $^{14}C$ sodium acetate (1mCi/ml). This was then used to spike the acetate supplemented M199 media to give $^{14}C$ acetate labelled media (3uCi/ml). Primary hepatocytes were plated onto 6 well plates, left overnight in basal media and used the day after isolation for the lipogenesis assay. Plates were washed twice with PBS and the hepatocytes were then left in $^{14}C$ acetate labelled media for 4h. Plates were washed x3 in PBS, all residual liquid was removed and cells were quenched in ice-cold methanol. Methanol samples were evaporated

to dryness and the residual pellet was extracted using methyl-tert butyl ether : methanol. Samples were centrifuged and the insoluble fraction removed. The soluble fraction was evaporated to dryness and these were then placed in a Tric-Carb 2800TR liquid scintillation analyser (PerkinElmer®, Seer Green, UK), to determine $^{14}C$ incorporation and hence *de novo* lipogenesis. Instead of quenching in methanol, cells from 2 wells of each 6 well plate were rapidly lysed and protein concentrations measured (as described above). These protein concentrations were then used to normalise lipogenesis rates.

### 2.2.9 Hepatocyte fatty acid oxidation assay

Fatty acid oxidation was assessed by measuring products of $^{14}C$ palmitate oxidation. M199 media was supplemented with 0.5mM palmitate conjugated to 2% (w/v) BSA and spiked with [1-14C] palmitic acid to give $^{14}C$ labelled media 1µCi/ml. Primary hepatocytes were plated onto 6 well plates, left overnight in basal media and used the day after isolation for the fatty acid oxidation assay. Plates were washed twice with PBS and hepatocytes were left in 1ml/well of $^{14}C$ palmitate labelled media for 6h. All media from each well was then removed, acidified with 0.1 x volume of 17N acetic acid in an air-tight vial and the $CO_2$ released captured in filter paper soaked in 1M NaOH. The plates were washed x3 in PBS, all residual liquid was removed and the cells were extracted with chloroform : methanol. The aqueous soluble fraction containing $^{14}C$ labelled palmitate oxidation products and the filter paper containing $^{14}C$ labelled $CO_2$ were placed in a Tric-Carb 2800TR liquid scintillation analyser (PerkinElmer®, Seer Green, UK). Fatty acid oxidation was calculated as the sum of $^{14}CO_2$ released and $^{14}C$ incorporated into oxidation products. Instead of adding chloroform : methanol, cells from 2 wells of each 6 well plate were rapidly lysed and protein concentrations measured (as described above). These protein concentrations were then used to normalise fatty acid oxidation rates.

### 2.2.10 Quantitative Real-Time PCR (qPCR)

***Primer design***

Primers for each target mRNA were designed using www.ncbi.nlm.nih.gov/tools/primer-blast and are shown in **Table 2.4**. All qPCR primers were designed to cover an exon-exon junction to ensure results were not skewed by genomic DNA contamination.

***RNA extraction***

Primary hepatocytes were lysed in TRIzol® (1ml per 10cm dish) or snap frozen liver tissue was homogenised in TRIzol (1ml per 50mg tissue) and chloroform was then added (200µl chloroform per 1ml TRIzol). Sample were inverted for 15 sections and then left for 3 minutes at room temperature before being centrifuged (12000rpm for 15 minutes at 4$^{o}$C), to separate the RNA fraction in the upper aqueous phase. RNA was purified using an RNeasy® Mini kit (Cat# 74106; Qiagen, Manchetser, UK) according to the manufacturer's protocol. The concentration and purity of RNA was determined using the NanoDrop ND-1000 (Thermo Scientific, Waltham, MA, USA) spectrometer for an absorbance of 260nm. A minimum absorbance ratio of 1.8 measured at 260/280nm and 260/230nm was set for all samples.

***Reverse transcription***

Synthesis of cDNA was carried out with equal amounts of total RNA (3-4µg) for each sample using Invitrogen™ Superscript II Reverse Transcriptase (Cat# 18064014; Thermo Scientific, Waltham, MA, USA), according to the manufacturer's protocol and in the presence of 200ng of random primers and 500µM mixed dNTP.

***Quantitative real-time PCR (qPCR)***

To check primer linearity, 5µl cDNA from each sample was pooled and serially diluted to give a standard curve for each target mRNA primer set. Satisfactory melting curves were obtained for all primers used. To quantify gene expression, cDNA (5µl of a 1/20 dilution) was added to 10µl 2x SensiMix™ SYBR® HiROX (Bioline, London, UK) 1.6µl forward and reverse primer mix (5µM) and dd$H_2O$ to a total reaction volume of 20µl. The qPCR plate was analysed using an Opticon thermal cycler (BioRad, Hertfordshire, UK) with OpticonMonitor Analysis Version 3.1 software to generate C(t) values for each reaction. All samples were analysed in duplicate with C(t) values measured in the exponential phase of the PCR reaction and relative expressions calculated using the $2^{-\Delta\Delta Ct}$ method (Schmittgen and Livak 2008).

### 2.2.11 Mouse diets

Chow, high fat and high fructose diets used are detailed in **Table 2.8**.

| | Chow | High fat | High fructose |
|---|---|---|---|
| **Energy (kcal/g)** | **3.64** | **4.6** | **3.99** |
| **Energy from fat (%)** | 11.5 | 46.1 | 22.6 |
| **Energy from carbohydrate (%)** | 61.57 | 35.8 | 60.8 |
| **Energy from protein (%)** | 26.93 | 18.1 | 16.7 |
| **Description** | Rat and mouse No.3 breeding diet (catalogue #801066; Special Diet Services) | DIO rodent purified diet with 45% energy from fat, dyed red (catalogue #58V8; TestDiet®) | Modification of TestDiet® 60% fructose semi-purified diet 58SH with 10% fat (reduced protein and fiber), dyed green (catalogue #5BN7; TestDiet®) |

***Table 2.8 - Mouse diets.*** *(DIO = diet induced obesity)*

### 2.2.12 Echo MRI

Body composition was assessed using EchoMRI-100® (Echo Medical Systems, New York, NY, USA) at baseline and 4 weekly intervals following the start of experimental diet (or maintenance on chow). Body fat was then determined from these measurements.

### 2.2.13 Glucose tolerance testing

Glucose tolerance testing (GTT) was performed at approximately 4 weekly intervals following the start of experimental diet (or maintenance on chow). Animals were starved for 16 hours overnight. Blood was obtained at baseline and all subsequent time-points by tail vein prick and blood glucose levels were determined using an Accu-Chek® glucometer (Roche, Mannheim, Germany). Following a baseline blood glucose reading glucose was administered to mice via intraperitoneal injection at a dose of 2g/kg or 1.5g/kg for mice on a high fat diet.

### 2.2.14 Pyruvate tolerance testing

Pyruvate tolerance testing (PTT) was performed on 10 week old chow fed animals. Mice were starved for 16 hours overnight. Blood was obtained at baseline and all subsequent time-points by tail vein prick and blood glucose levels were determined using an Accu-Chek® glucometer (Roche, Mannheim, Germany). Following a baseline blood glucose reading pyruvate was administered to mice via intraperitoneal injection at a dose of 2g/kg.

### 2.2.15 Food intake, $VO_2$ consumption and respiratory exchange ratio

Approximately 22 week old mice were housed in Comprehensive Lab Animal Monitoring System (CLAMS) metabolic cages (Columbus Instruments, Columbus, OH, USA) for 4 days, maintained on a 12 hour light/dark cycle with free access to food and water. Food intake, $O_2$ consumption ($VO_2$) and $CO_2$ production ($VCO_2$) measurements were taken after 24 hours of acclimatisation and respiratory exchange ratio (RER) was calculated ($VCO_2 \div VO_2$). The animal physiology team assisted with housing and maintainence of mice in the the CLAMS.

### 2.2.16 Tissue collection

Mice that had been fed *ad libitum* were killed by cervical dislocation and organs were rapidly harvested. Livers were weighed and some photographed, then tissues were either snap frozen in liquid nitrogen or fixed in 4% formaldehyde.

### 2.2.17 Liver triglyceride content

Snap frozen liver tissue was homogenised in 0.03x (w/v) ethanol and left for 72 hours to extract lipid. 1ml of homogenate was then centrifuged at 13000rpm for 10 minutes. Triglyceride content of the supernatant was then measured using Triglycerides liquid (Cat# 17624H; Sentinel Diagnostics, Milan, Italy) and triglyceride content as percentage of liver weight calculated.

### 2.2.18 Liver cholesterol content

Snap frozen liver tissue was homogenised in 0.03x (w/v) ethanol and left for 72 hours to extract lipid. Free and total cholesterol content were then measured using Amplex® Red Cholesterol Assay kit (Cat# A12216, Invitrogen, Carlsbad, CA, USA) according to the manufacturer's protocol.

### 2.2.19 Blood collection & sampling

Blood was acquired by either tail bleed or pre-terminal cardiac puncture under inhaled (isoflurane) anaesthesia from mice that had been fed *ad libitum* and was collected in heparinised microvettes. Whole blood was then either analysed immediately using a VetScan VS2® (Abaxis, Union City, CA, USA) or spun for 10 minutes at 5000rpm and the plasma aspirated off and stored at -80$^{o}$C.

Plasma alanine transaminase (ALT) levels in high fat diet fed mice were measured using the VetScan VS2®. Plasma cholesterol, high density lipoprotein, low density lipoprotein, triglyceride, 3-hydroxybutyrate and alkaline phosphatase levels were determined by Mouse Biochemistry Laboratories (Cambridge, UK), as were serum ALT and aspartate transaminase levels in fructose fed animals and mice with liver specific Pten knockout. The Quantikine® ELISA mouse α-fetoprotein (AFP) kit (Cat# MAFP00; R&D Systems, Oxford, UK) was used according to the manufacturer's protocol, to measure plasma AFP levels.

### 2.2.20 De novo lipogenesis in vivo

*De novo* lipogenesis was measured by incorporation of $^{3}$H-acetate into lipid. Mice were fasted overnight for 16h and then refed for 1.5h, before intraperitoneal injection of 40µCi $^{3}$H-acetate. Mice were killed after 1h and their livers snap frozen in liquid nitrogen. Lipid was subsequently extracted from liver using the Folch method (Folch, Lees, and Sloane Stanley 1957) and incorporation of radioactive acetate into lipid was determined by scintillation counting using a Tric-Carb 2800TR liquid scintillation analyser (PerkinElmer®, Seer Green, UK).

### 2.2.21 Thin layer chromatography (TLC)

All method apart from the final incubation step conducted in a fume cupboard. 3M paper was used to line an air tight Chromatography chamber. Solvent was prepared from 60ml petroleum ether, 40ml diethyl ether and 1ml acetic acid and then poured into the chromatography chamber to a depth of approximately 1cm. Standards were made up from Cholesterol (0.5 mg/ml chloroform), cholesterol oleate (1mg/ml chloroform), oleic acid (5µl in 2500µl hexane) and glyceryl trilinoleate (5µl in 2500µl hexane). Liver samples were homogenised in ETOH (see **Section 2.2.17**). 100µl aliquots were evaporated to dryness and then re-suspended in 100µl chloroform. 10x10cm TLC plates were cut from TLC Silica Gel 60

F254 plates (Cat# 1055540001, Merck Milipore, Billerica, MA, USA) and cerium-ammonium-molybdate (CAM) stain was prepared from 2.5g ammonium heptamolybdate tetrahydrate, 1g cerium (IV) sulfate hydrate complex with sulphuric acid, 90ml ultrapure water and 10ml concentrated sulphuric acid. 1µl aliquots of standards and samples were loaded onto a TLC plate (approximately 1.5cm from the bottom – so as not to be submerged in solvent when TLC plate placed in chromatography chamber) and left to dry. Standards were all loaded at the same site allowing drying in between. The TLC plate was then placed in the chromatography chamber for 10-12mins. Upon removal from the chamber, the TLC plate was allowed to dry and then placed face down in CAM stain (avoiding contact between the aluminium back of the TLC plate and the CAM stain). The TLC plate was then incubated in a hybridisation oven for 1h at 80$^{o}$C. During this time dark blue spots appeared on a white background. The plate was then scanned and the blue spots quantitated using Image J software.

### 2.2.22 Histology

***Slide preparation***

Upon dissection, the left lobe of the liver was cut into pieces <5mm diameter. These pieces were placed in 4% formaldehyde for 24-48h at 4$^{o}$C and then transferred to either 70% ethanol, in which they were stored at 4$^{o}$C prior to further processing; or 20% sucrose and frozen. Tissue processing, embedding and sectioning of samples stored in ethanol, were outsourced to Lorraine Lawrence (Leucocyte Biology Histology Unit, Imperial College, London). Frozen samples were sectioned in OCT compound using a Leicar cryostat (Wetzlar, Germany)

***Staining and immunohistochemistry***

**Haematoxylin and eosin (H&E) staining** was outsourced to Lorraine Lawrence (Leucocyte Biology Histology Unit, Imperial College, London). For **picro-sirius red staining** sections were first rehydrated by immersion for 15 minutes in each of the following solutions: Citra-Clear x2 (Xylene substitute), 100% ethanol x2, 70% ethanol x2 and d$H_2O$. Cell nuclei were stained with Gill's haematoxylin for 8 minutes and then washed in running tap water for 10 minutes. Slides were stained for 1h in picro-sirius red solution (0.5g Sirius red in 500ml saturated aqueous solution of picric acid) then washed twice in acidified water (5ml acetic acid in 1l $H_2O$).

Sections were then dehydrated in the following solutions for 15 minutes each: 70% ethanol, 100% ethanol x2 and CitraClear x2. Slides were then mounted using DPX mountant. **Frozen sections** were stained with 0.5% Oil Red O in propylene glycol warmed to 60$^{o}$C and counterstained with Gill's haematoxylin. Cover slips were then applied to sections with aqueous mounting media (VectaMount).

For immunohistochemical staining tissue sections were first rehydrated by immersion for 15 minutes in each of the following solutions: Citra-Clear x2 (Xylene substitute), 100% ethanol x2, 70% ethanol x2 and $dH_2O$. Antigen retrieval was achieved using the 2100 Antigen Retriever (Aptum, Southampton, UK) on a standard 40 minute retrieval cycle with sodium citrate buffer (10mM sodium citrate, 0.05% Tween 20, pH6.0). Sections were washed with PBS and incubated for 20 minutes with 0.3% $H_2O_2$ diluted in methanol, washed and then blocked with 10% normal goat serum in PBS. Primary antibodies (**Table 2.5**) were diluted in 1% normal goat serum and incubated with tissue sections overnight at 4$^{o}$C in a humidified chamber. The following day, sections were washed with PBS-Tween (PBT – PBS and 0.1% Tween20) and incubated with 1/200 biotinylated goat secondary antibody (**Table 2.6**) diluted in PBS for 1h at room temperature in a humidified chamber. Samples were then washed with PBT and incubated for 30 minutes with avidin-biotin complex (VECTASTAIN Elite ABC kit) according to manufacturer's protocol. Slides were washed with PBS and then stained using DAB Peroxidase HRP Substrate kit according to the manufacturer's instructions. Slides were then left in running tap water for 10 minutes and counterstained with Gill's haematoxylin. Sections were then dehydrated in the following solutions for 15 minutes each: 70% ethanol, 100% ethanol x2 and CitraClear x2. Finally slides were mounted using DPX mountant.

***Imaging & analysis***

Olympus IX70 Inverted (Tokyo, Japan) and Zeiss Axiophot Upright microscopes were used to image histology slides and Image J and QuPath software was used for analysis. H&E stained liver sections were reviewed and non-alcoholic fatty liver disease activity scoring (NAS) was performed by Dr G Bottcher, an external expert pathologist (AstraZeneca, Sweden).

### 2.2.23 Liver glycogen content

Snap frozen liver tissue was homogenised in 30% KOH and incubated at 100$^{o}$C for 1h. Samples were cooled and glycogen was precipitated by addition of 10x volume of ethanol and 7µM LiCl. Samples were centrifuged to collect precipitated glycogen which was then dissolved in 4M HCl for 1h at 100$^{o}$C. Samples were then neutralised by addition of an equal volume of $K_2CO_3$. Glycogen converted to glucose was measured using a glucose oxidase assay kit (Cat# GAGO20-1KT; Sigma, Poole, UK).

### 2.2.24 Tissue lysate preparation

Snap frozen liver was homogenised in x10 (v/w) homogenisation buffer at 30Hz for 2 minutes using the TissueLyser II (Qiagen, Manchester, UK). Supernatant was collected following centrifugation at 13000rpm for 10mins at 4$^{o}$C.

### 2.2.25 RNA Sequencing

RNA was extracted and purified as described for qPCR in section 2.2.10. RNA sequencing was performed by AstraZeneca (Cambridge, UK). Bioinformatics support was provided by the London Institute of Medical Sciences' Computing and Bioinformatics facility.

### 2.2.26 Mass spectrometry

Samples for mass spectrometry were prepared from snap frozen liver tissue. Mass spectrometry was conducted by Dr A. Kerimi, Dr L. Abranko and Prof. G. Williamson (University of Leeds, UK). The peak area of each analyte was expressed relative C17-CoA.

### 2.2.27 Ultrasound imaging

Abdominal ultrasound scanning was performed on mice with liver specific Pten loss at regular (approximately 4 week) intervals between 25 and 45 weeks of age. Mice were anaesthetised using inhaled isoflurane and their abdomens shaved prior to liver ultrasound scanning. All areas of the liver were viewed using the Vevo 770™ Imaging System (VisualSonics Inc., Toronto, ON, USA). Standard views and views incorporating tumours were captured and the latter used to measure tumour diameter. The number of tumours seen on each scan was also recorded.

# 3 Results: The effects of chronic AMPK activation in the liver in response to metabolic stress

## 3.1 Introduction

AMPK's diverse effects in upregulating catabolic and downregulating anabolic pathways as well its potential roles in autophagy, mitochondrial homeostasis and inflammation (**Figure 1.2**) mean it has garnered significant interest as a therapeutic target in the treatment of various aspects of the metabolic syndrome. However, much of the evidence regarding its effects derives from investigations using whole body AMPK activation or inhibition and studies using pharmacological AMPK activators, with potential off-target effects. We therefore developed a transgenic model with liver specific AMPK activation to more thoroughly and specifically examine the role of AMPK in the liver.

Three key aspartic acid residues have been identified within the AMPK γ1 subunit, one in each of the adenine nucleotide binding sites with the exception of the empty site (**Figure 3.1** & **Table 1.2**) (Xiao et al. 2007). They co-ordinate to the ribose of binding nucleotides and in cell-based studies, point mutation of these residues has been shown to result in both up and down regulation of basal AMPK activity. Indeed substitution of aspartic acid by an alanine residue at position 316 (residue 317 in human γ1), which lies within the non-exchangeable binding site 4, results in constitutive activation of AMPK (Woods et al. 2017). This γ1D316A mutation abolishes the previously non-exchangeable binding of AMP and leaves AMPK less sensitive to dephosphorylation by protein phosphatase 2C (PP2C).

Transgenic mice have been generated (on a C57Bl6 J background) by inserting a D316A mutant AMPK γ1 transgene into the long arm of chromosome 6, using the ROSA26 locus (**Figure 3.2**). This was done by AstraZeneca, Cambridge, UK. Control mice with wild type (WT) AMPK γ1 inserted at the same locus have also been produced. Upstream of the AMPK γ1 cDNA is a CAG promoter followed by a floxed stop cassette. The CAG promoter is a synthetically constructed promoter and is used to attain high gene expression.

It consists of a **C**ytomegalovirus early enhancer element, the chicken beta **A**ctin promoter (the first exon and intron of the gene) and the rabbit β **G**lobulin splice acceptor (Miyazaki et al. 1989). In the absence of Cre recombinase, the upstream stop cassette prevents expression of the AMPK γ1 construct. However, in the presence of Cre, the cassette is deleted, allowing the promotor to initiate expression of the transgene, which has been engineered with a C-terminal FLAG tag (DYKDDDDK) to enable it to be discriminated from endogenous AMPK γ1.

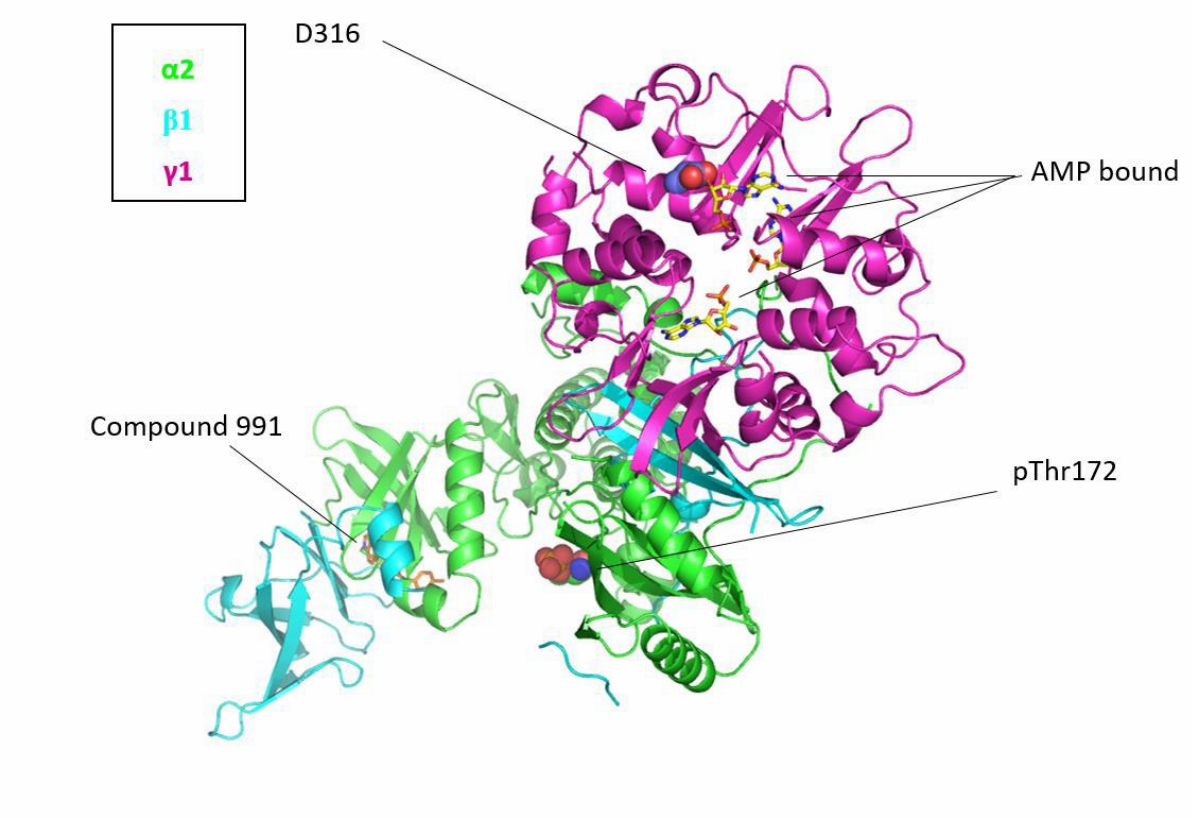


***Figure 3.1 - Crystal structure of AMPK****. AMP bound to nucleotide binding sites 1, 3 and 4, D316 residue in binding site 4 labelled, $\alpha^{Thr172}$ phosphorylated and the allosteric activator 991 present in the cleft between α and β.*

The AMPK γ1 (WT and D316A mutant) mice have been crossed with mice expressing Cre-recombinase under control of the albumin promotor (Postic et al. 1999)(Jackson Laboratory, ME, USA #B6.Cg-Tg(Alb-Cre)21Mgn/J) , to produce mice with liver specific transgenic AMPK γ1 expression. These mice are hereafter referred to as WT-Tg and D316A-Tg respectively (see **Table 2.7**).

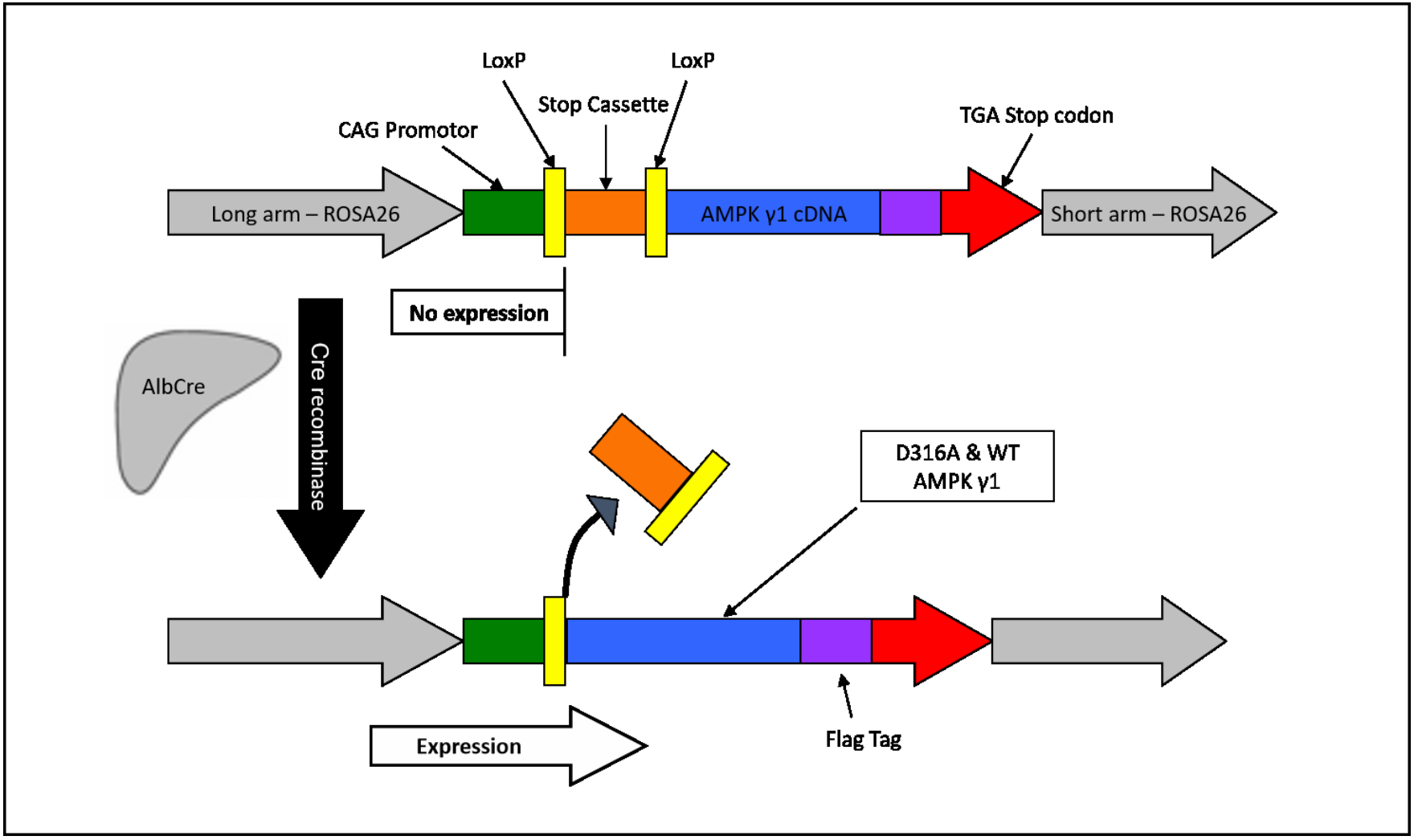


***Figure 3.2 The AMPK γ1 transgene.*** *Schematic representation of the construct used to generate transgenic mice expressing either wild-type or D316A mutant AMPK γ1.*

## 3.2 Characterisation of transgenic AMPK γ1 expression in hepatocytes

Rapid changes in adenine nucleotide levels occur upon tissue dissection and the associated fall in ATP can activate AMPK, confounding measurement of AMPK activity *in vivo* (Davies et al. 1992). To circumvent this issue, isolated primary hepatocytes from the transgenic mice were studied.

Commercial antibodies which recognise AMPK γ1 were characterised (**Table 3.1**). The Abcam antibody has been raised against the C terminal region of γ1 and does not cross-react with transgenic γ1, presumably due to interference from the flag tag. The combination of antibodies available therefore allowed distinction of endogenous, from transginc, from total AMPK γ1.

| Antibody | Specificity |
|---|---|
| Abcam γ1 – Rabbit (ab32508) | Endogenous γ1 only |
| Cell signalling Flag – Rabbit (#2368) | Transgenic γ1 only |
| Novus γ1 – Rabbit (NBP2-15382) | Both endogenous and transgenic γ1 |

***Table 3.1 – AMPK γ1 antibodies***

Flag tagged, transgenic AMPK γ1 was expressed equally in hepatocytes from all the transgenic mice, but was absent in hepatocytes from Non-Tg mice (**Figure 3.3 A** & **B**). Endogenous AMPK was barely detectable in hepatocytes from WT-Tg mice. In contrast, although endogenous AMPK was significantly reduced in hepatocytes from D316A-Tg mice, it was still present (**Figure 3.3 A** & **C**). Total AMPK γ1 levels appeared higher in hepatocytes from the transgenic, compared to the non-transgenic mice (**Figure 3.3 A** & **D**). However, there was no difference in total γ1 levels between the transgenic lines. Furthermore, there was no significant difference in total AMPK complex levels, measured as total AMPK β, between any of the mouse lines, including non-transgenic versus transgenic (**Figure 3.3 A** & **E**).

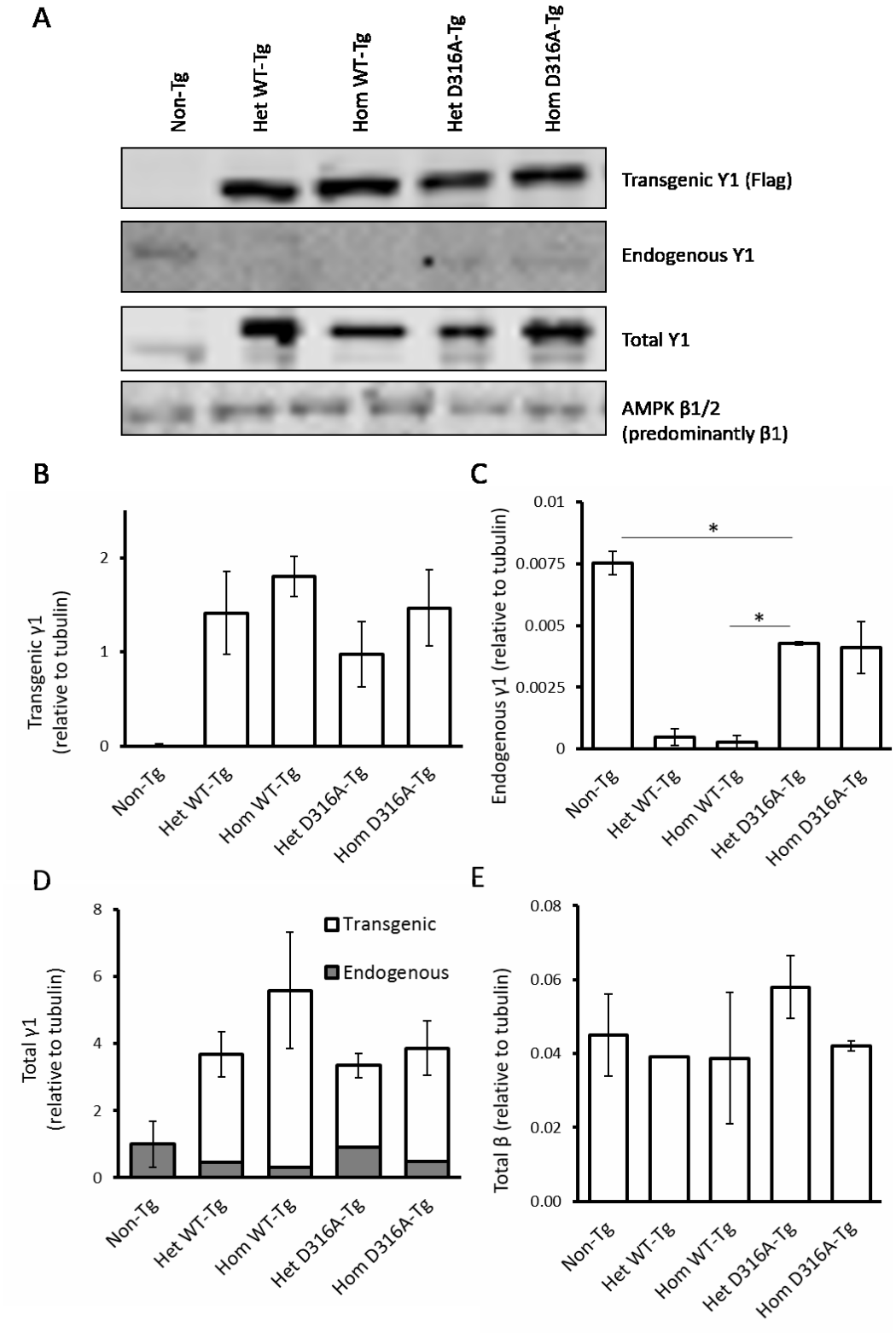


***Figure 3.3*** *- **AMPK expression in mouse hepatocytes.** **(A)** Western blots of hepatocyte lysates probed with the indicated AMPK subunit antibodies.* ***(B-E)*** *Quantification of blots, normalised to tubulin expression. Methods – see* ***section 2.2.5****. Results shown are mean ± S.E.M., from n = 2-3 independent mice in each case (except Het WT-Tg total β where n=1), *p<0.05; t-test. Het = heterozygous and Hom = homozygous.*

AMPK $\alpha^{Thr172}$ phosphorylation (pThr172), a measure of AMPK activity, was assessed using phospho-specific antibodies and found to be significantly higher in hepatocytes from D316A-Tg mice compared to those from WT-Tg mice (**Figure 3.4 A** & **B**). There were no significant differences in pThr172 levels between hepatocytes from WT-Tg and Non-Tg mice. A similar pattern was seen for the downstream target of AMPK activity phosphorylated acetyl-CoA carboxylase ($pACC^{Ser79}$ – **Figure 3.4 A** & **C**).

AMPK activity was also measured in AMPK pan-β immunoprecipitates (IPs) from primary hepatocyte lysates, using SAMS peptide assay. AMPK activity in hepatocytes from WT-Tg mice was the same as that in hepatocytes from Non-Tg mice and activity in hepatocytes from D316A-Tg mice was 2-3 fold (2.53 ± 0.158) that in hepatocytes from Non-Tg mice (**Figure 3.5 A**). This was a similar increase in AMPK activity as was seen in hepatocytes from Non-Tg mice, following pharmacological activation with the direct AMPK activator 991 (3.02 ± .0196 - **Figure 3.5 B**). The fold change in AMPK activity seen following incubation with 991 was the same in hepatocytes from all mouse lines. AMPK activity in hepatocytes from Heterozygous (Het) WT-Tg and D316A-Tg mice was not significantly different from that in Homozygous (Hom) WT-Tg and D316A-Tg mice respectively (**Figure 3.5 A**).

As no significant differences in AMPK protein levels (**Figure 3.3**) or activity (**Figure 3.5**) were seen between hepatocytes isolated from mice expressing a single copy of the AMPK γ1 transgene (heterozygous – Het) and those with homozygous (Hom) transgene expression (WT or D316A), for all further experiments, data from Hets and Homs were combined. Similarly, as no significant differences in AMPK activity were seen between Non-Tg and WT-Tg mice they were regarded as equivalent in subsequent studies (hereafter referred to as WT-Tg – see **Table 2.7**).

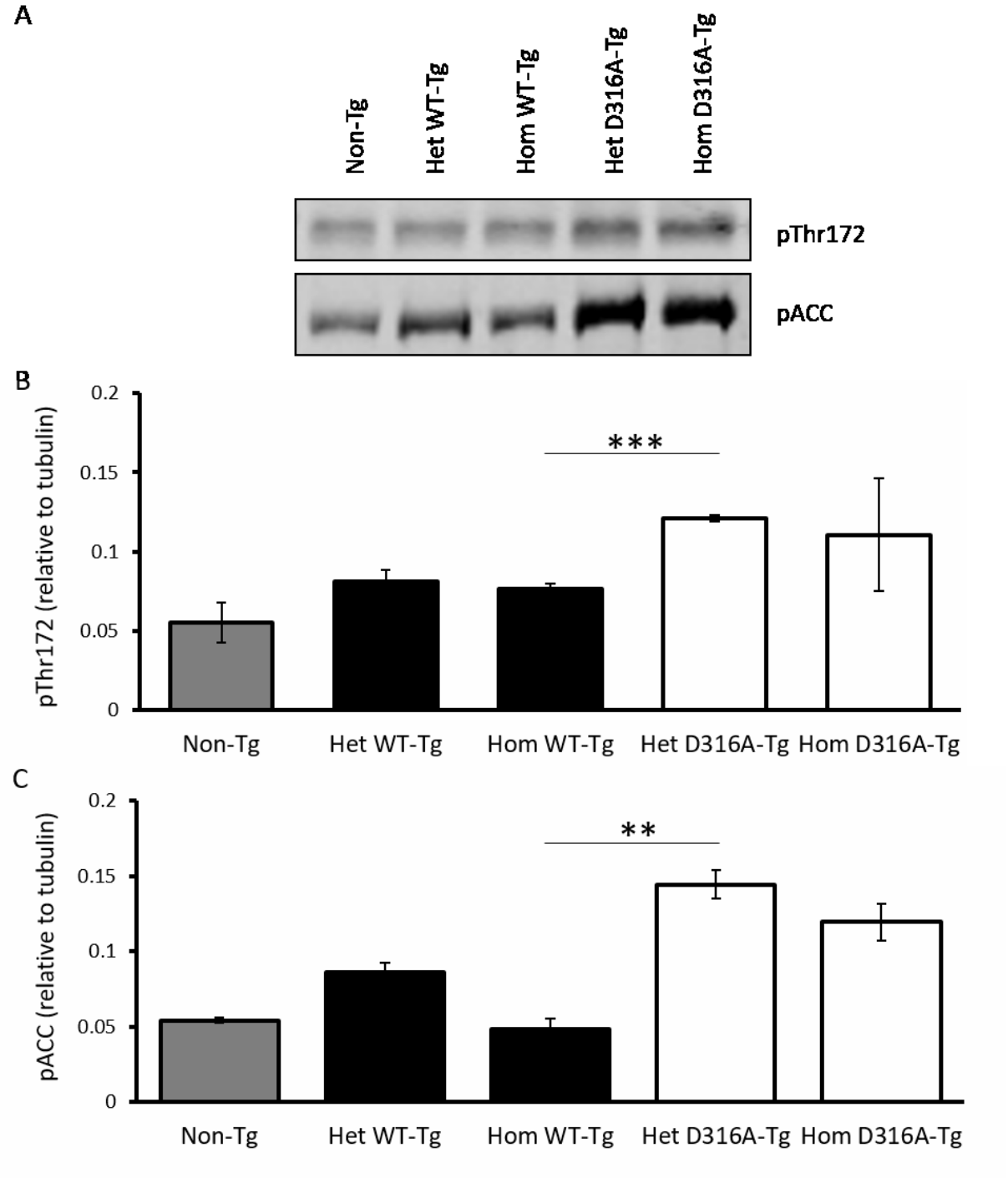


***Figure 3.4 - AMPK $\alpha^{Thr172}$ and $ACC^{Ser79}$ phosphorylation in mouse hepatocytes. (A)*** *Western blots of hepatocyte lysates probed with the indicated antibodies (pThr172 = AMPK $\alpha^{Thr172}$, pACC = $ACC^{Ser79}$).* ***(B and C)*** *Quantification of blots, normalised to tubulin expression. Methods – see* ***section 2.2.5****. Results shown are mean ± S.E.M., from n=2-3 independent mice in each case, **p<0.01 and ***p<0.001; t-test.*

-

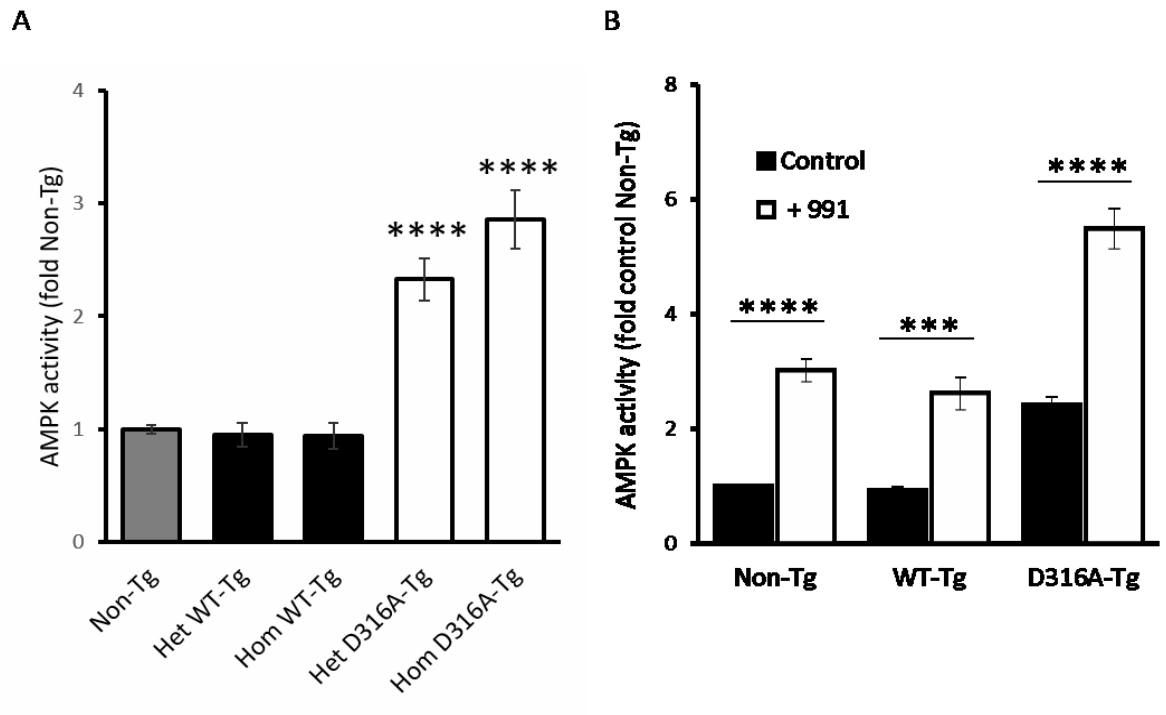


***Figure 3.5 – AMPK activity in mouse hepatocytes under basal conditions and following treatment with the direct AMPK activator 991.*** *(A) AMPK activity measured in immune complexes isolated with an AMPK pan-β antibody. Results shown are mean ± S.E.M. from n ≥ 3 independent mice of each genotype and are plotted as fold activity relative to Non-Tg. Statistically significant differences relative to Non-Tg are shown,****p<0.001; t-test. (B) Hepatocytes treated with vehicle or 10μM 991 for 30 mins before harvest and AMPK activity measured in immune complexes isolated with an AMPK pan-β antibody. Methods – see* ***section 2.2.6****. Results shown are mean ± S.E.M. from n ≥ 6 independent mice for each genotype and are plotted as fold activity relative to control Non-Tg cells. ***p<0.005 and ****p<0.001; t-test.*

AMPK has been implicated in glucose homeostasis in the liver (**Figure 1.2**). Therefore, in order to examine the role of hepatic AMPK in gluconeogenesis, glucose output from hepatocytes isolated from control and D316A-Tg mice was measured over 18 hours, in the presence and absence of glucagon stimulation (10nM - **Figure 3.6 A**). Under both conditions, glucose output was approximately 50% lower from D316A-Tg mouse hepatocytes compared to WT-Tg cells (under basal conditions WT-Tg = 0.79 ± 0.072 and D316A-Tg = 0.398 ± 0.039μmol glucose/mg protein; with glucagon stimulation WT-Tg = 1.11 ± 0.088 and D316A-Tg = 0.656 ± 0.089μmol glucose/mg protein).

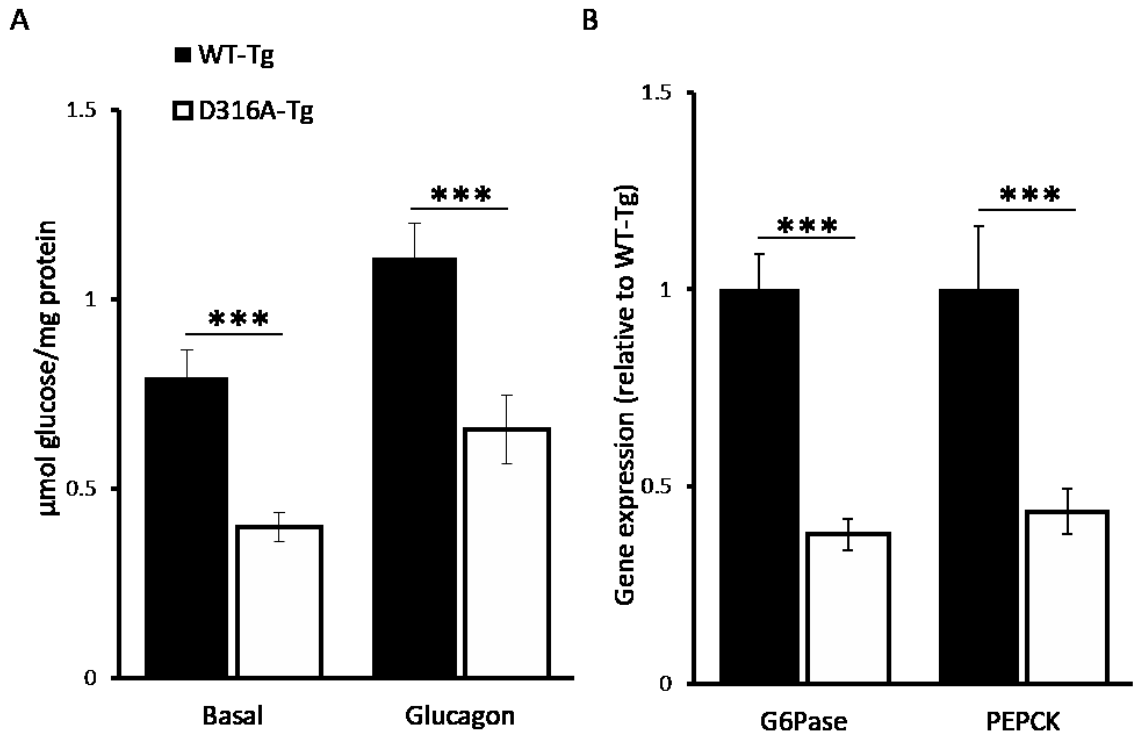


***Figure 3.6 – Glucose output and gluconeogenic gene expression in hepatocytes (A)*** *Hepatocytes from transgenic mice incubated in the presence or absence of 10nM glucagon and hepatic glucose output over 18h measured and normalised to total cellular protein. Results shown are mean ± S.E.M., from n=7-12 independent mice for each genotype, ***p<0.005; t-test.* ***(B)*** *Gluconeogenic gene expression. Methods – see* ***sections 2.2.7 and 2.2.10****. Results, shown are mean ± S.E.M. from n=6 independent mice for each genotype and are plotted relative to WT-Tg. ***p<0.005; t-test. G6Pase = glucose-6-phosphatase and PEPCK = phosphoenolpyruvate.*

In keeping with this finding, transcription of the genes encoding two key gluconeogenic enzymes, glucose-6-phosphatase and phosphoenolpyruvate carboxykinase, was significantly reduced in hepatocytes from D316A-Tg mice (**Figure 3.6 B**).

AMPK is also thought to play a key role in lipid metabolism in the liver. To assess the effects of hepatic AMPK activity on *de novo* lipogenesis, the rate of lipogenesis in hepatocytes from WT-Tg and D316A-Tg mice was measured by incorporation of $^{14}C$ sodium acetate into lipid.

Significantly less acetate was incorporated into lipid in hepatocytes isolated from D316A-Tg mice (0.74 ± 0.044) compared to cells from control mice (1 ± 0.07 - **Figure 3.7 A**). However, no differences in mRNA expression for a number of lipogenic genes, including, ACC, fatty acid synthase (FAS), sterol regulatory element-binding protein 1c and Spot 14, were seen between hepatocytes from control and D316A-Tg mice (**Figure 3.7 B**).

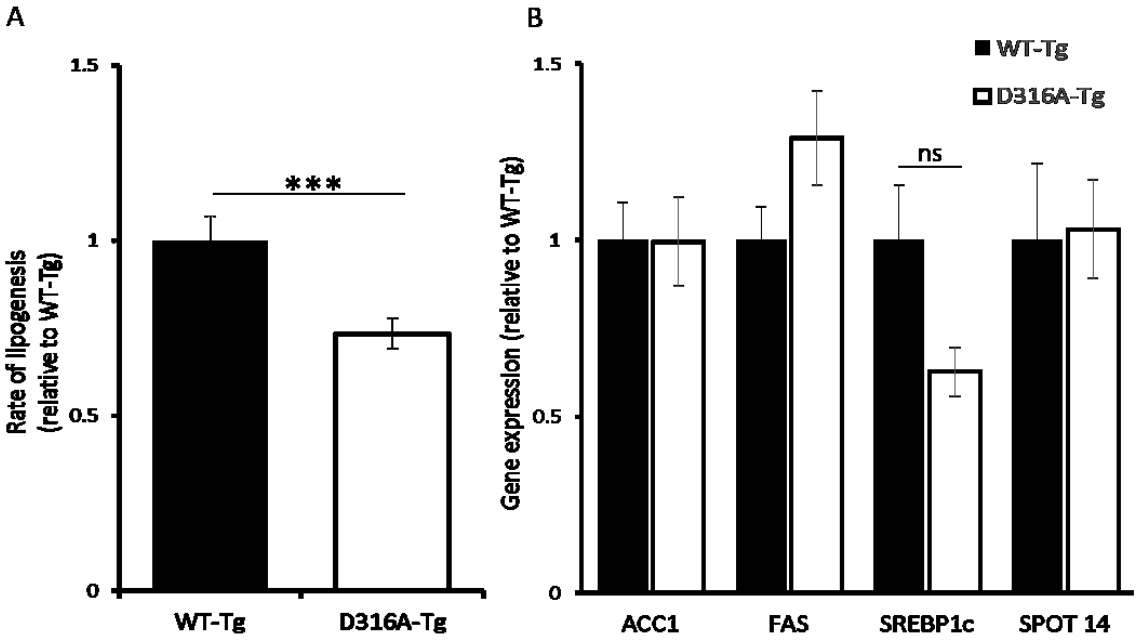


***Figure 3.7 – Rates of lipogenesis and lipogenic gene expression in hepatocytes. (A)*** *De novo lipogenesis in hepatocytes from transgenic mice measured by incorporation of $^{14}$C-acetate into lipid. Results shown are mean ± S.E.M. from n=6 independent mice for each genotype and are plotted relative to WT-Tg. ***p<0.00; t-test.* ***(B)*** *Lipogenic gene expression. Methods – see* ***sections 2.2.8 and 2.2.10****. Results shown are mean ± S.E.M. from n=6 independent mice for each genotype and are plotted relative to WT-Tg.*

Oxidation of $^{14}$C labelled palmitate and the subsequent incorporation of $^{14}$C into oxidation products or its release as $^{14}CO_2$, were used to assess the role of hepatic AMPK in fatty acid oxidation. Oxidation of palmitate was similar in hepatocytes from D316A-Tg and WT-Tg mice and was unaffected by incubation with 991 (**Figure 3.8**), suggesting that fatty acid oxidation in hepatocytes is not altered by AMPK activation. Palmitate oxidation in WT-Tg and D316A-Tg hepatocytes significantly increased in response to carnitine and decreased with the

addition of etomoxir (a carnitine palmitoyl transferase 1 inhibitor), demonstrating that primary hepatocytes can alter their rate of fatty acid oxidation.

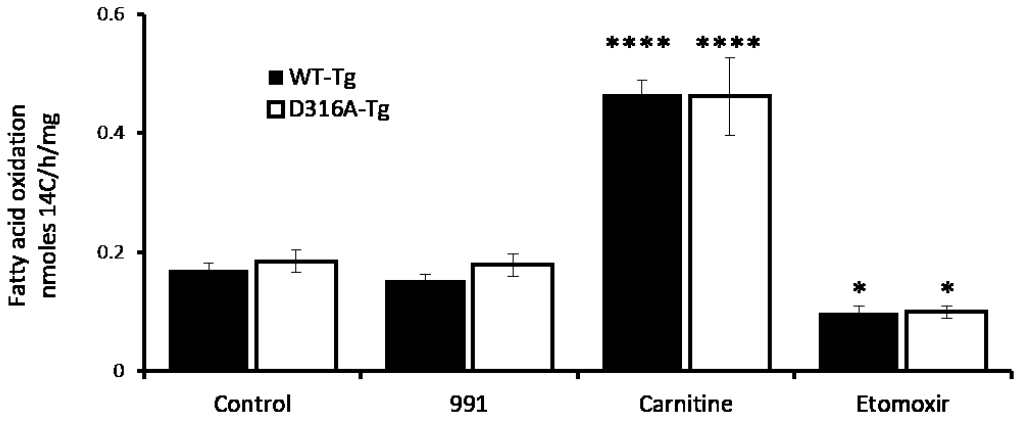


***Figure 3.8 - Fatty acid oxidation in mouse hepatocytes.*** *Oxidation of $^{14}$C-palmitate to $^{14}$C labelled oxidation products and $^{14}CO_2$ measured over 6hr in hepatocytes from WT-Tg and D316A-Tg mice, in the presence or absence of 10µM 991, 1mM carnitine or 0.1mM etomoxir. Methods – see* ***section 2.2.9****. Results shown are mean ± S.E.M. from n=6 independent mice for each genotype. Statistically significant differences in fatty acid oxidation rates relative to untreated WT-Tg cells are shown *p<0.05, ****p<0.001; ANOVA.*

### 3.3 The effects of liver specific increased AMPK activity in mice fed chow & high fat diets

To study the *in vivo* effects of liver specific constitutive AMPK activation, various metabolic parameters were evaluated in WT-Tg and D316A-Tg mice maintained on a standard chow diet. Similar measurements were also made in WT-Tg and D316A-Tg mice exposed to the metabolic stress of a high fat diet for up to 12 weeks. The high fat diet was hypercaloric relative to the chow diet (26% additional calories) and provided 46% compared to 11.5% calories from fat (diet details summarised in **Table 2.8**). This diet has previously been shown to be obesogenic in C57BL/6 mice and is derived from high fat diets which have been used to induce hyperinsulinaemia and hyperglycaemia in mice (West, Waguespack, and McCollister 1995; Surwit et al. 1995; Van Heek et al. 1997).

No differences in body weight or total body fat, assessed on Echo MRI, were seen between genotypes (WT-Tg and D316A-Tg) on a chow diet and although mice on a high fat diet gained more weight and had higher total body fat, than those receiving standard chow, again no differences were seen between WT-Tg and D316A-Tg animals (**Figure 3.9**).

All mice (both chow and high fat diet fed) underwent glucose tolerance testing at 4 weekly intervals. Mice on a chow diet also underwent a pyruvate tolerance test at 10 weeks of age. Glucose handling was not significantly different between mice with and without liver specific AMPK activation (D316A-Tg v WT-Tg respectively – **Figure 3.10**).

Comprehensive Lab Animal Monitoring System (CLAMS) metabolic cages were also used to measure a number of parameters, including food intake, oxygen consumption ($VO_2$) and carbon dioxide production ($VCO_2$) in WT-Tg and D316A-Tg mice fed chow or high fat diets. Mice were housed in the CLAMS cages for 4 days at around 22 weeks of age and metabolic parameters were monitored after 24 hours of acclimatisation.

Food intake did not differ between WT-Tg and D316A-Tg mice on a chow diet (**Figure 3.12**). Oxygen consumption ($VO_2$ in ml/kg/h) or $VCO_2$ can be used as proxies for respiratory rate. As

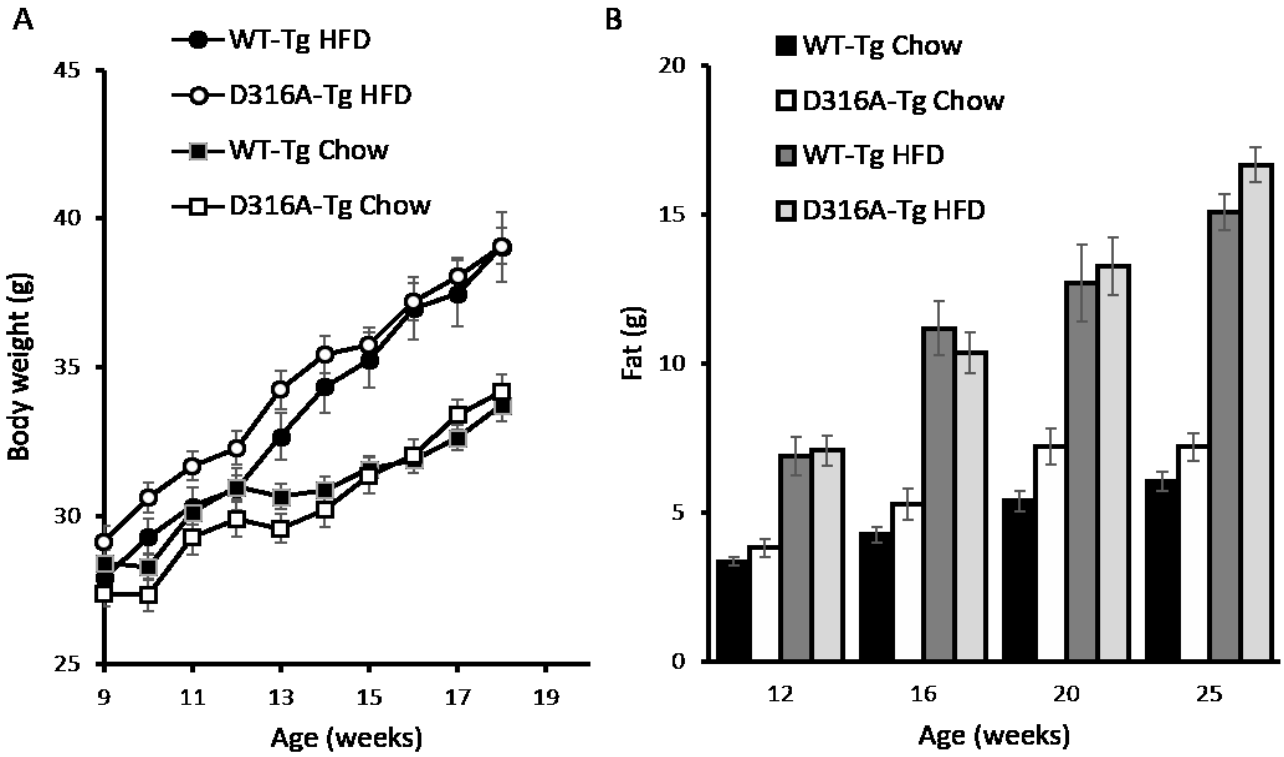


***Figure 3.9 - Body weight and composition of mice fed a chow or high fat diet.*** *(A) Bodyweights and (B) Total body fat as assessed by Echo MRI, of mice fed a chow or high fat diet (HFD) from 8 weeks of age. Methods – see* ***section 2.2.12****. Results shown are mean ± S.E.M., from n ≥ 12 for each group.*

anticipated, respiratory rates cycled over 24 hours in line with exposure to light or dark, however, there were no differences in $VO_2$ between WT-Tg and D316A-Tg mice (**Figure 3.11 A** & **B**). The RER is the ratio between $CO_2$ production and $O_2$ consumption (RER = $VCO_2 \div VO_2$) and is a measure of respiratory substrate. If $O_2$ consumed is used entirely in carbohydrate metabolism the RER is 1, whereas if $O_2$ is used exclusively for oxidation of fat the RER is 0.707. As expected, RER cycled over 24 hours in line with whether it was light or dark and the RER for mice receiving a high fat diet was lower than that for animals maintained on chow, indicating that the high fat feeding mice were using more fat for respiration. However, the RER did not differ between genotypes (WT-Tg v D316A-Tg) and this was the case for both chow and high fat diet fed mice (**Figure 3.11 C** & **D**).

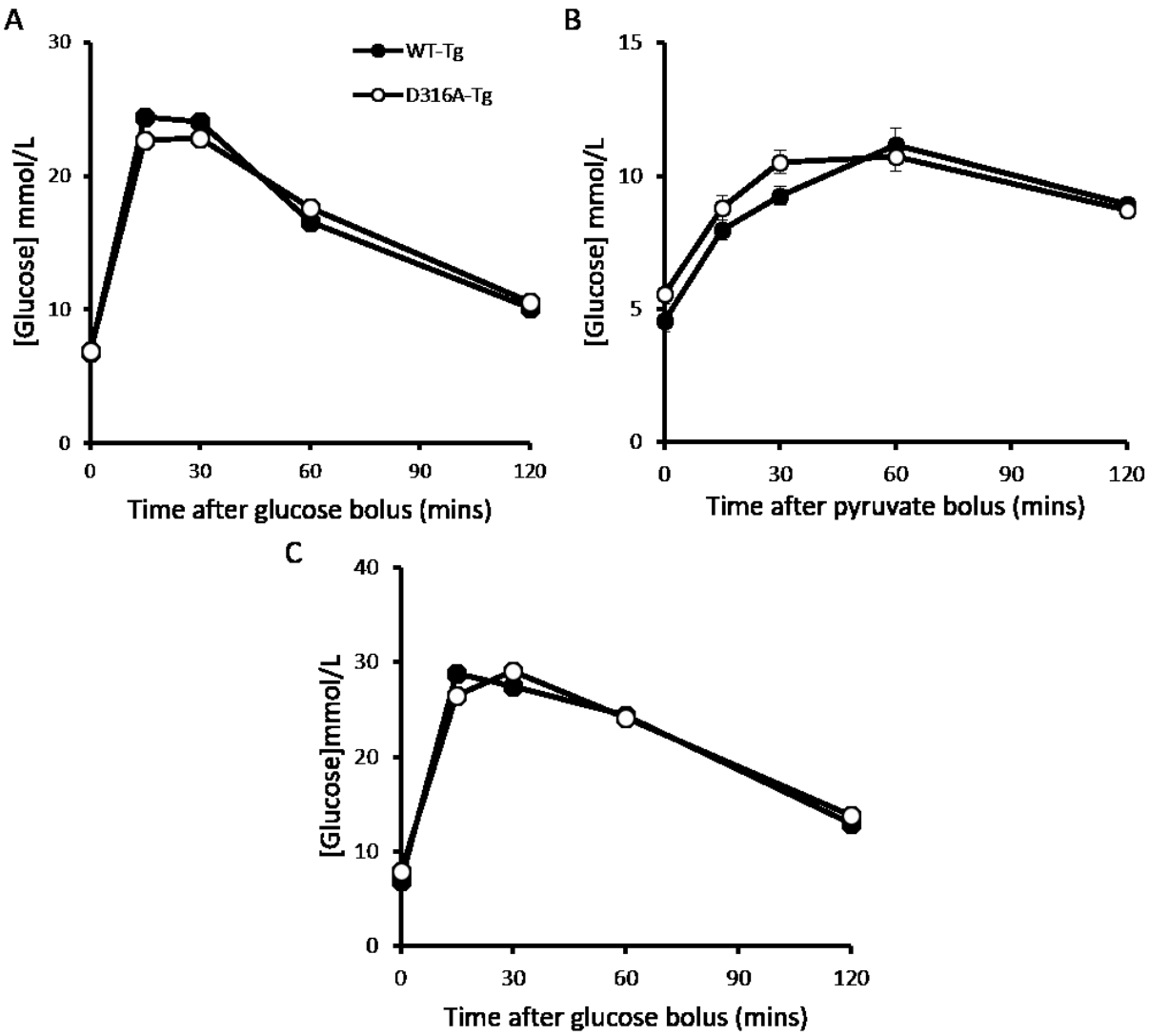


***Figure 3.10 – Glucose tolerance and gluconeogenesis in mice fed a chow or high fat diet. (A)*** *Glucose tolerance test of 16 week old mice maintained on a chow diet.* ***(B)*** *Pyruvate tolerance test of 10 week old chow fed mice.* ***(C)*** *Glucose tolerance test of 19 week old mice fed a high fat diet from 7 weeks of age. Methods – see* ***sections 2.2.13 and 2.2.14****. Results shown are mean ± S.E.M., n≥7 per group for all.*

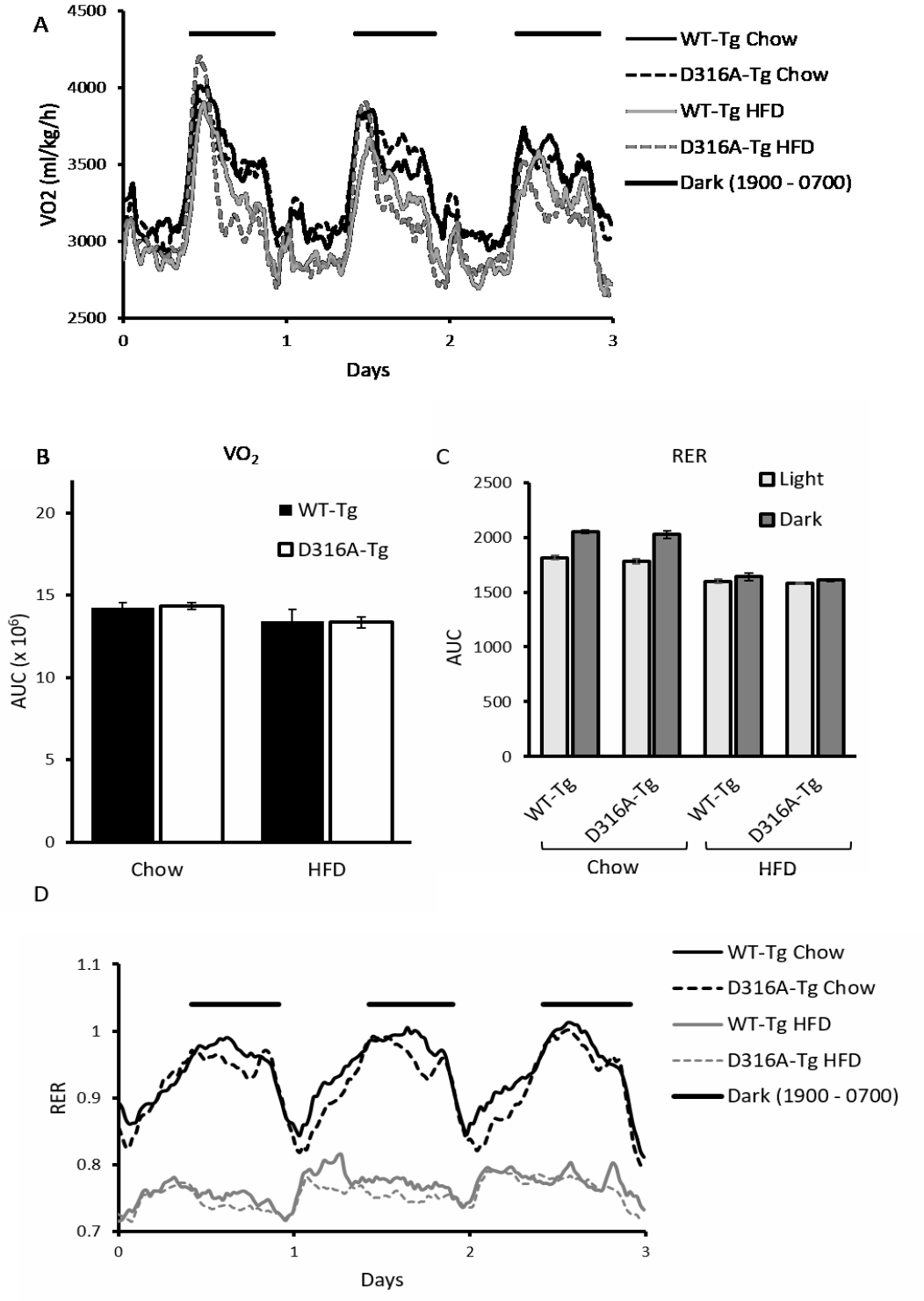


***Figure 3.11 - Respiratory rates and respiratory exchange ratios (RER) in mice fed a chow or high fat diet. (A & B)*** *Oxygen consumption ($VO_2$ – a proxy for respiratory rate) curve and area under the curve (AUC) over 3 days. Results shown are means (with S.E.M. for AUC) from n ≥ 5 per group.* ***(C & D) Respiratory exchange ratio (RER - a measure of respiratory substrate)*** *curve and AUC over 3 days. Methods – see* ***section 2.2.15****. Results shown are means (with S.E.M. for AUC) from n ≥ 6 per group.*

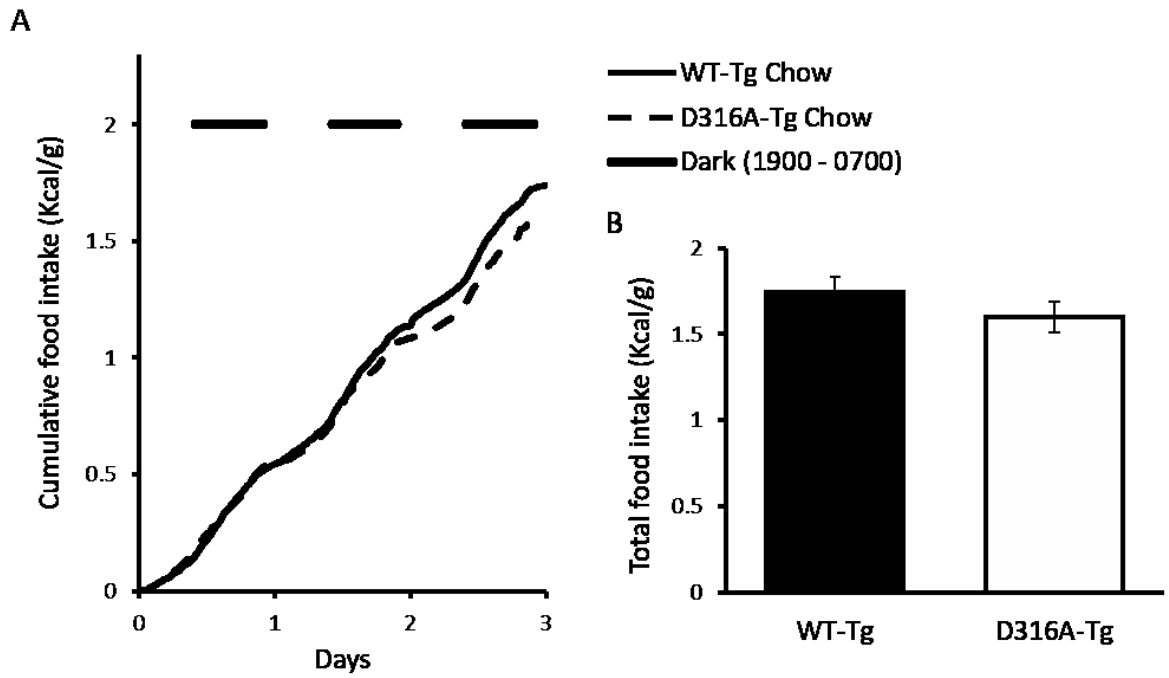


***Figure 3.12 - Food intake in mice fed a chow diet.*** ***(A)*** *Cumulative food intake over 3 days. Results shown are means from n ≥ 6 per genotype.* ***(B)*** *Total food intake over 3 days. Methods see* ***section 2.2.15****. Results shown are means ± S.E.M. for n ≥ 6 per condition.*

To assess for hepatic steatosis, total liver triglyceride content was measured in WT-Tg and D316A-Tg mice following chow and high fat feeding. Hepatic triglyceride levels were higher in mice on a high fat diet than in those receiving standard chow, however, they did not differ between D316A-Tg and WT-Tg mice on the same diet (chow or high fat - **Figure 3.13 A**). Total cholesterol content of the liver was unaffected by diet or genotype (**Figure 3.13 B**)

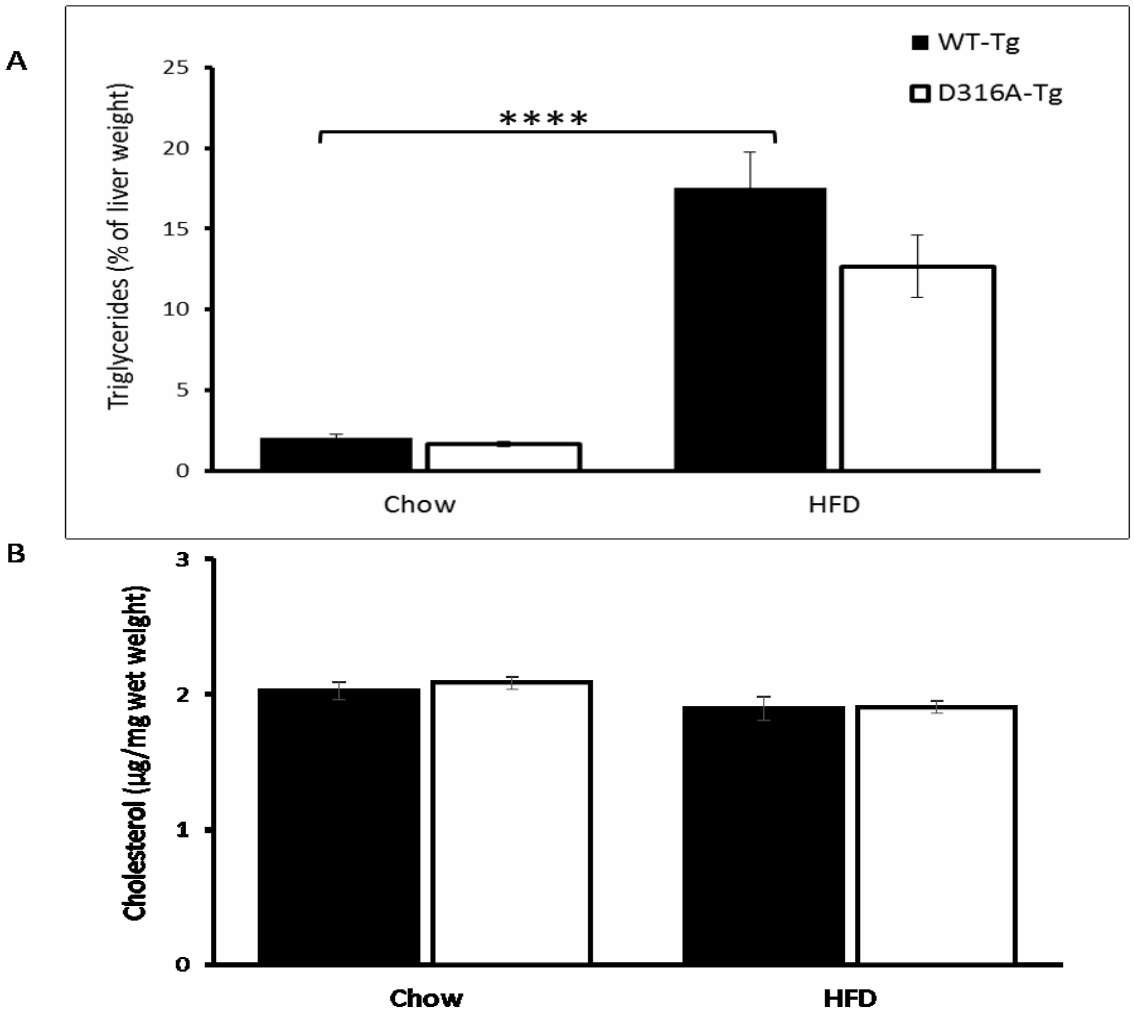


***Figure 3.13*** *-* ***Liver triglyceride and total cholesterol content in mice fed a chow or high fat diet (HFD).*** *Liver* ***(A)*** *triglyceride and* ***(B)*** *total cholesterol content in mice continued on chow or fed a high fat diet from 8 weeks of age. Methods – see* ***sections 2.2.17 and 2.2.18****. Results shown are mean ± S.E.M., from n ≥ 9 per group.*

In keeping with the observation that liver composition did not differ between WT-Tg and D316A-Tg mice, liver weight at harvest (mean age 26 weeks) was also unaffected by the presence of increased hepatic AMPK activity. There was a trend towards mice undergoing high fat feeding having heavier livers than those on a chow diet, but this was not significant (**Figure 3.14 A**). Because bodyweight was significantly elevated in high fat diet fed mice, liver to bodyweight ratio was significantly lower in these mice relative to their chow fed counterparts (**Figure 3.14 B**).

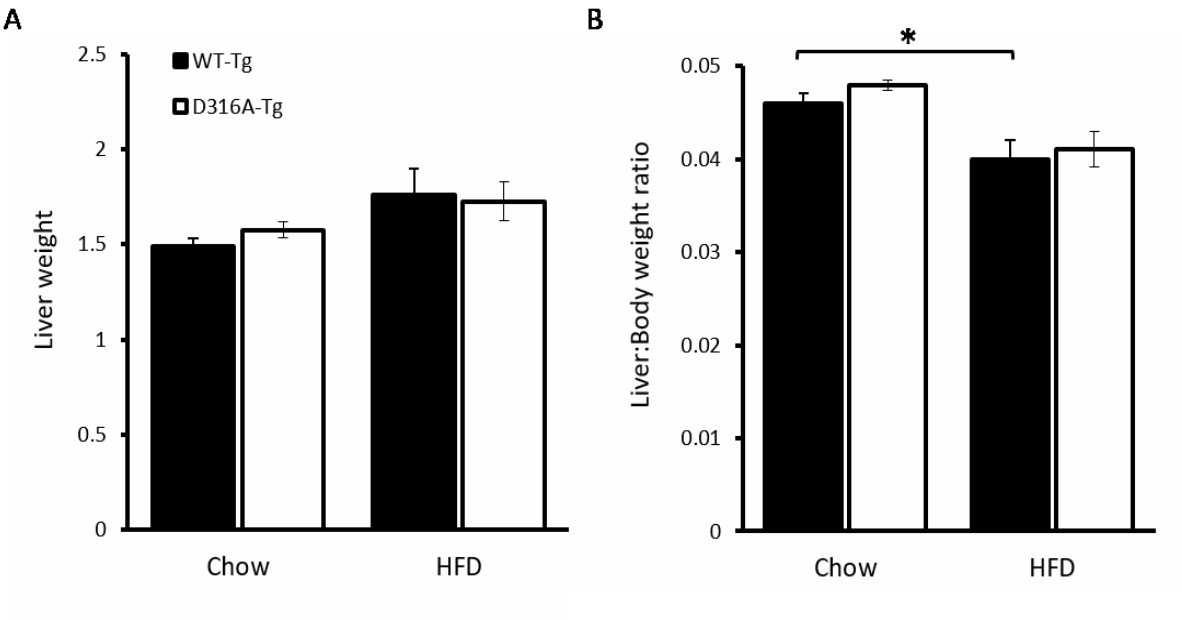


***Figure 3.14 - Liver weights and liver to body weight ratios of mice fed a chow or high fat diet (HFD).*** *(A) Liver weight and (B) Liver to bodyweight ratio at harvest (mean age 26 weeks) in mice maintained on chow or undergoing high fat feeding from 8 weeks of age. Results shown are mean ± S.E.M. from n ≥ 12 per condition, *p ≤ 0.05; t-test.*

Liver alanine transaminase (ALT) levels in the serum of high fat diet fed WT-Tg and D316A-Tg mice, were measured at harvest (33 weeks of age), to determine if the hepatic triglyceride

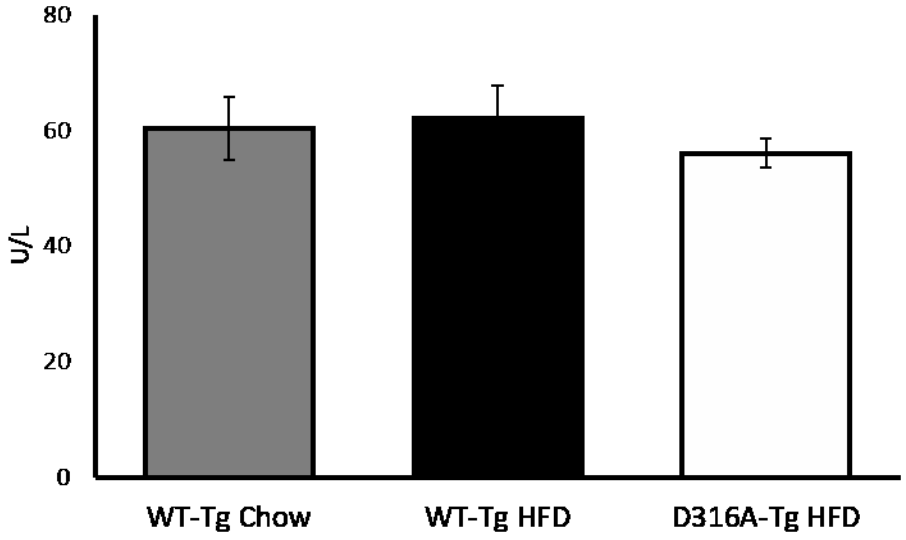


***Figure 3.15*** *-* ***Serum markers of hepatocyte inflammation in mice on a high fat diet.*** *Serum ALT levels in mice after 18 weeks of high fat feeding (26 weeks of age). Levels in chow fed mice of a similar age are shown for comparison. Methods – see* ***section 2.2.19****. Results shown are mean ± S.E.M. from n ≥ 7 per condition*

accumulation seen in these animals had precipitated an inflammatory response. Serum ALT levels did not differ between WT-Tg mice fed either chow or high fat diet, or between WT-Tg and D316A-Tg mice fed a high fat diet (**Figure 3.15**). Therefore, although high fat feeding induced steatosis, after 26 weeks of diet, it had not caused significant hepatic inflammation.

## 3.4 The effects of liver specific increased AMPK activity in mice fed a lipogenic, high fructose diet

One of the most marked differences between genotypes (WT-Tg v D316A-Tg) in the primary hepatocyte studies, was the lower rate of *de novo* lipogenesis in cells with constitutive AMPK activation (D316A-Tg). The *in* vivo effects of liver specific AMPK activation were therefore examined in mice fed a lipogenic diet. High carbohydrate diets promote *de novo* lipogenesis and there is evidence that fructose may be more potent than glucose in this respect, hence a high fructose diet was used (Hudgins et al. 2000; Stanhope et al. 2009; Parks et al. 2008). The high fructose diet was mildly hypercaloric relative to chow (10% additional calories) and the proportion of calories from carbohydrate was similar (61% and 62% for high fructose and chow respectively), however, carbohydrate in the high fructose diet consisted entirely of fructose, whereas free sugar made up only 8% of carbohydrate in the chow diet (diet details summarised in **Table 2.8**).

No significant differences were seen between WT-Tg and D316A-Tg mice fed a high fructose diet, in terms of body weight or total body fat, the latter assessed using Echo MRI (**Figure 3.16**). Glucose tolerance was tested at 4 weekly intervals in mice on a high fructose diet and again no differences were seen between WT-Tg and D316A-Tg mice at any time-point (**Figure 3.17**).

Serum cholesterol, high density lipoprotein (HDL), low density lipoprotein (LDL), and triglyceride levels were measured in WT-Tg mice on a chow diet and in WT-Tg and D316A-Tg mice undergoing high fructose feeding. Cholesterol, HDL and LDL levels were all significantly elevated in mice on a high fructose diet, relative to those receiving standard chow, but there were no differences between genotypes (WT-Tg v D316A-Tg) on a fructose diet (**Figure 3.18**).

Mice that had been maintained on high fructose diet for approximately 6 weeks (14 weeks of age) were housed in the CLAMS metabolic cages for 4 days. After a 24 hour period to allow acclimatisation, food intake, $VO_2$ and $VCO_2$ were measured and used to calculate RER. Oxygen consumption and RER varied appropriately over 24 hours in line with the dark/light cycle but

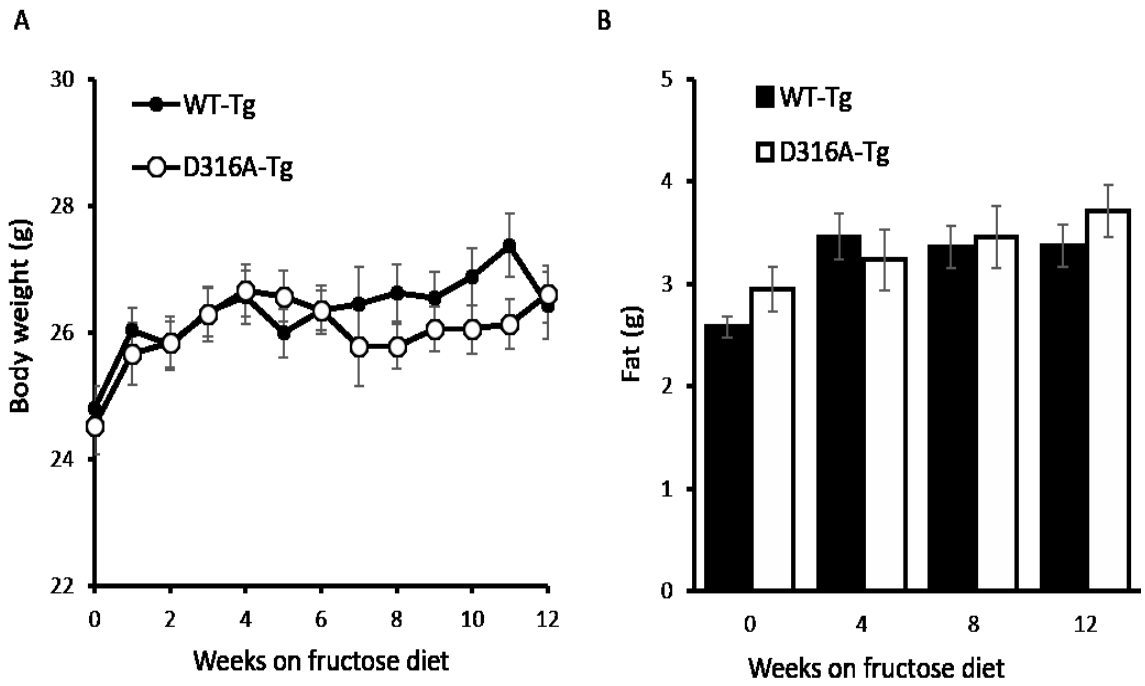


***Figure 3.16 - Body weight and composition of mice fed a high fructose diet.*** ***(A)*** *Bodyweight of mice fed a high fructose diet from 8 weeks of age. Results shown are mean ± S.E.M., from n=20 for each genotype.* ***(B)*** *Total body mass of mice fed a high fructose diet measured by Echo MRI. Methods – see* ***section 2.2.12****. Results shown are mean ± S.E.M., from n=8-13 for each genotype.*

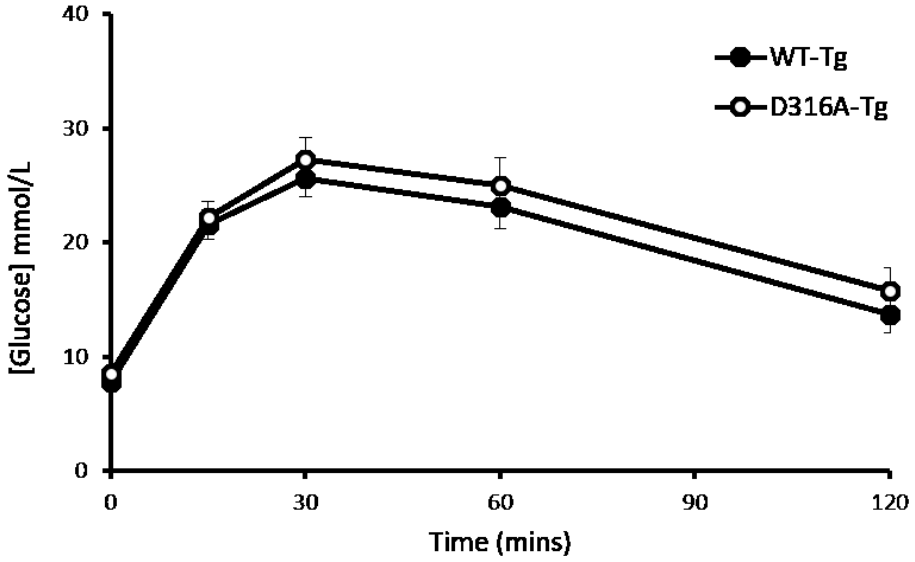


***Figure 3.17 – Glucose tolerance in mice fed a high fructose diet.*** *Glucose tolerance testing performed after 12 weeks of high fructose feeding. Methods – see section 2.2.13. Results shown are mean ± S.E.M., from n=9-13 for each genotype.*

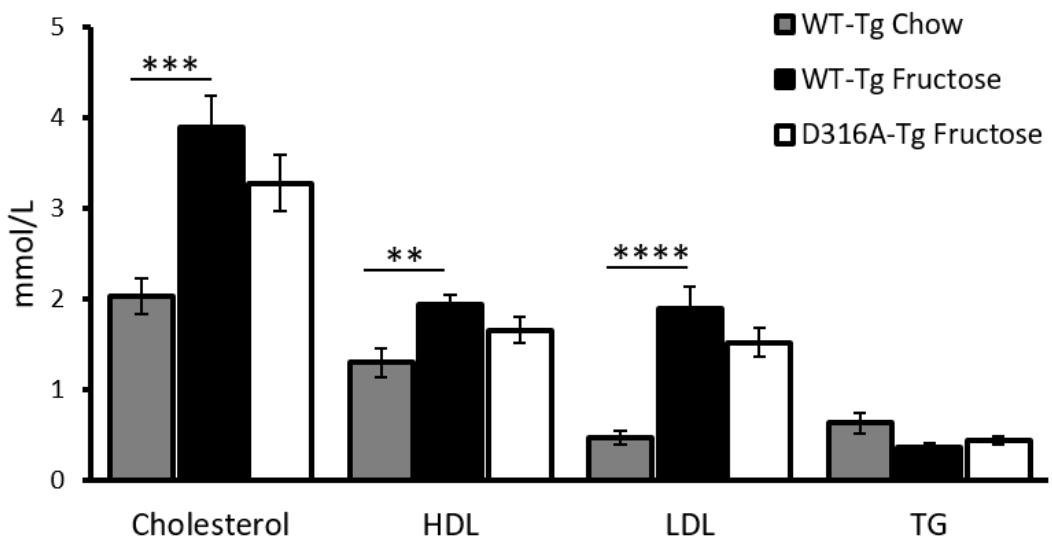


***Figure 3.18 - Serum lipids in mice fed a high fructose diet.*** *Serum cholesterol, high density lipoprotein (HDL), low density lipoprotein (LDL), and triglyceride (TG) levels in mice fed a high fructose diet for 12 weeks and compared to levels in WT-Tg mice fed standard chow. Methods – see* ***section 2.2.19****. Results shown are mean ± S.E.M. from n=9-12 per group, **=p<0.01, ***=p<0.001, and ****=p<0.0001.*

no differences were seen for either parameter between WT-Tg mice and those with liver specific AMPK activation (D316-Tg - **Figure 3.19**).

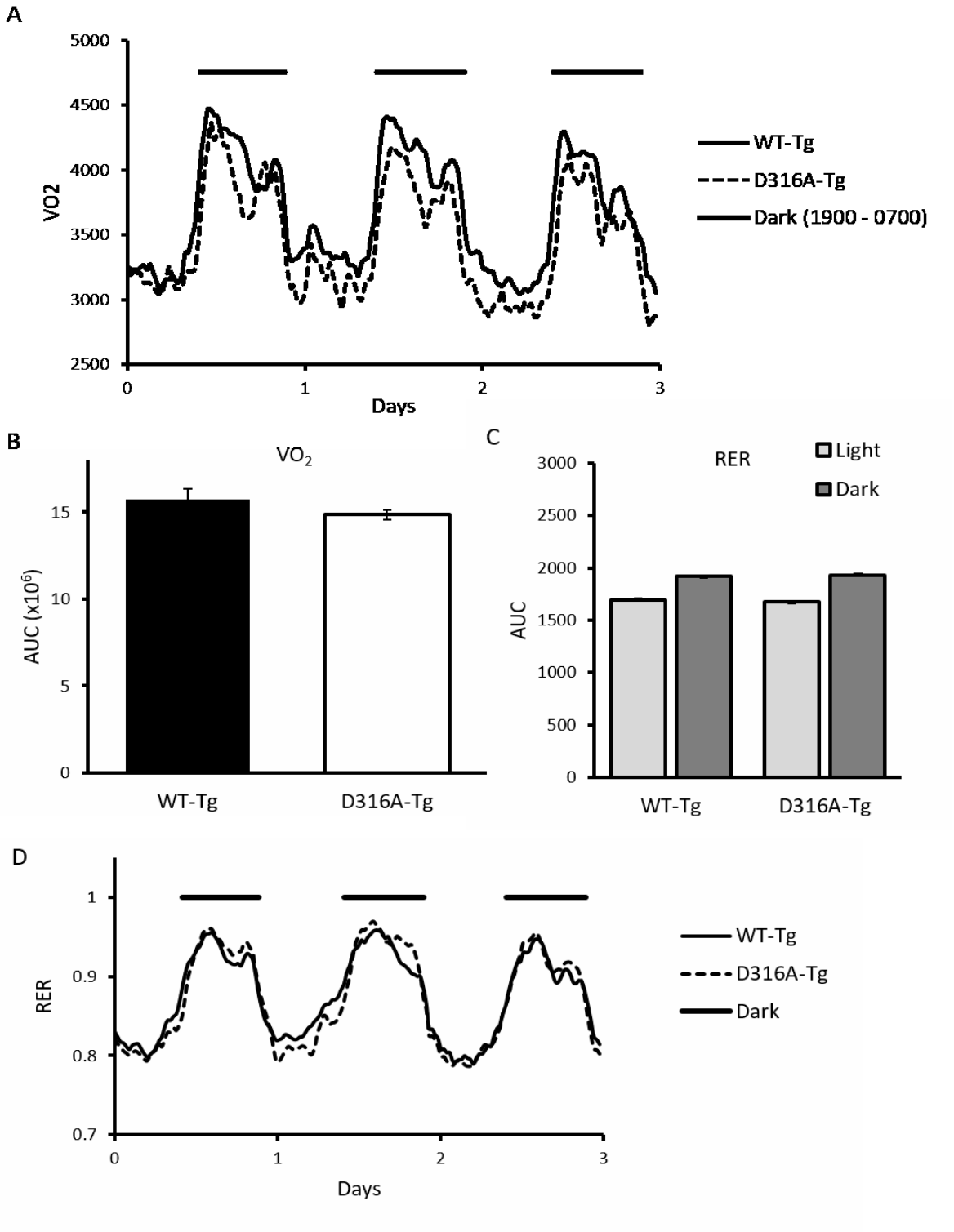


***Figure 3.19 - Respiratory rates and respiratory exchange ratios (RER) in mice fed a high fructose diet. (A & B)*** *Oxygen consumption ($VO_2$ – a proxy for respiratory rate) curve and area under the curve (AUC) over 3 days.* ***(C & D)*** *Respiratory exchange ratio (RER - a measure of respiratory substrate) curve and AUC over 3 days. Methods – see* ***section 2.2.15****. Results shown are means (with S.E.M. for AUC) from n ≥ 10 per genotype.*

The lack of a difference in RER between WT-Tg and D316A-Tg mice on a fructose diet, implied that the 2 genotypes were metabolising fat equally. This suggestion was further supported by the finding that serum levels of the ketone 3-hydroxybutyrate, a product of fatty acid oxidation, in mice fed a high fructose diet were unaffected by increased hepatic AMPK activity (**Figure 3.20**).

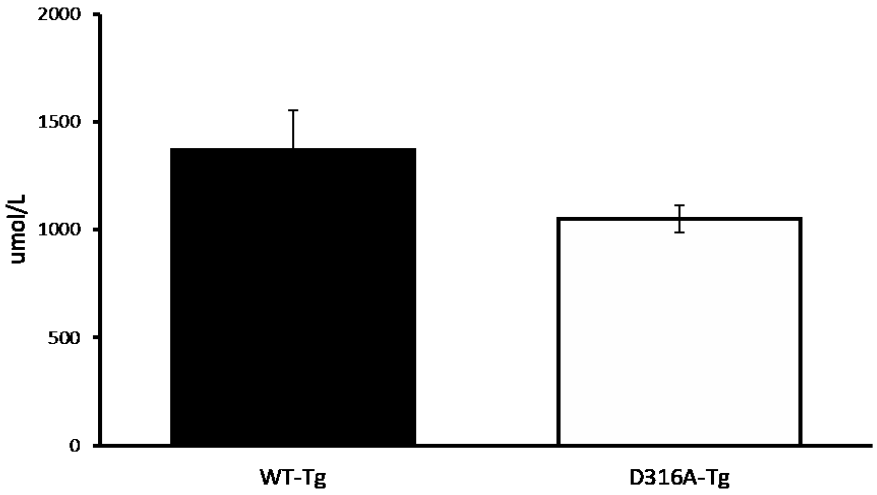


***Figure 3.20 - Fasting serum 3-hydroxybutyrate levels in mice on a high fructose diet*** *(8 weeks of diet / 17weeks of age). Methods – see* ***section 2.2.19****. Results shown are mean ± S.E.M.*

Hepatocyte studies showed a marked reduction in fatty acid synthesis in cells from D316A-Tg relative WT-Tg mice. To determine if this finding was translatable, incorporation of radio-

-

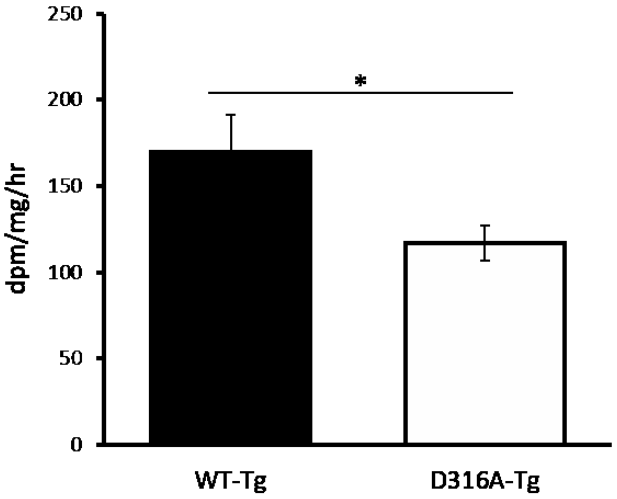


***Figure 3.21 – De novo lipogenesis in the livers of WT-Tg and D316A-Tg mice.*** *Incorporation of [$^3$H]-acetate into liver lipid. Methods – see* ***section 2.2.20.*** *Results shown are mean ± S.E.M. from n=8 per genotype, *p<0.05; t-test.*

labelled acetate into hepatic lipid was used to measure *in vivo* hepatic *de novo* lipogenesis. In keeping with the primary hepatocyte findings, *de novo* lipogenesis in the liver was reduced in D316A-Tg relative to WT-Tg mice (**Figure 3.21**).

Despite a lack of effect of liver specific AMPK activation on systemic parameters, but in-keeping with evidence of reduced hepatic *de novo* lipogenesis in D316A-Tg relative to WT-Tg mice, analysis of the livers of transgenic mice fed a high fructose diet found reduced triglyceride accumulation in mice with increased hepatic AMPK activation (**Figure 3.22**). This effect was so marked that despite a more than 3 fold increase in liver triglyceride levels in WT-Tg mice fed a high fructose diet relative to WT-Tg animals fed chow (7.10 ± 0.860 percent of liver weight v 2.07 ± 0.211%), triglyceride levels in the livers of D316A-Tg mice fed the high fructose diet were equivalent to those of mice fed a chow diet (2.08 ± 0.181% v 2.07 ± 0.211%).

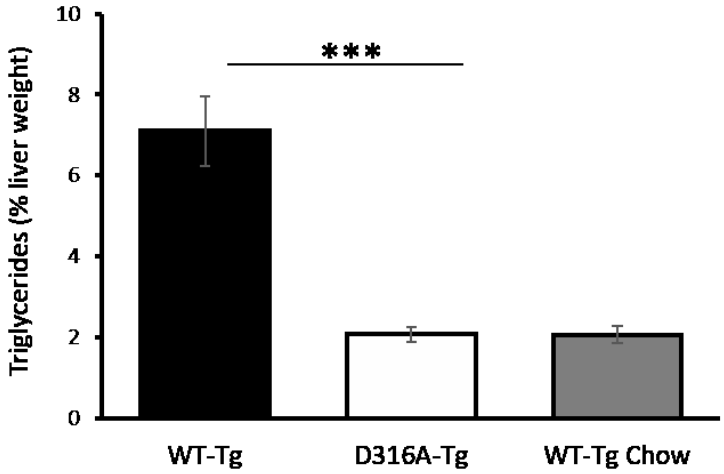


***Figure 3.22 - Liver triglyceride content in mice on a high fructose diet*** *(20 weeks of age / 12 weeks of diet). Triglyceride levels in WT-Tg mice maintained on chow included for comparison. Methods – see* ***section 2.2.17.*** *Results shown are mean ± S.E.M., from n=12, ***p<0.005; t-test.*

Thin layer chromatography (TLC) was also used to measure liver lipid composition (including total cholesterol, cholesterol esters, triglycerides and fatty acids) of WT-Tg and D316A-Tg mice on a lipogenic, high fructose diet (**Figure 3.23**). This analysis confirmed that high fructose fed WT-Tg mice had significantly higher liver triglyceride levels than their D316A-Tg counterparts. Cholesterol ester content was also significantly lower in mice with increased

hepatic AMPK activity (D316A-Tg v WT-Tg 63.5 ± 5.35 v 121.5 ± 9.36). Free cholesterol levels in the liver did not vary between WT-Tg and D316A-Tg mice. TLC plate analysis suggested that fatty acid levels might be slightly, but significantly elevated in D316A-Tg relative to WT-Tg mice (20.8 ± 1.16 v 17.7 ± 0.68). However fatty acid spots on the TLC plate were much more faint than those for other lipids, limiting the accuracy of spot area measurement in this instance and so the validity of this result.

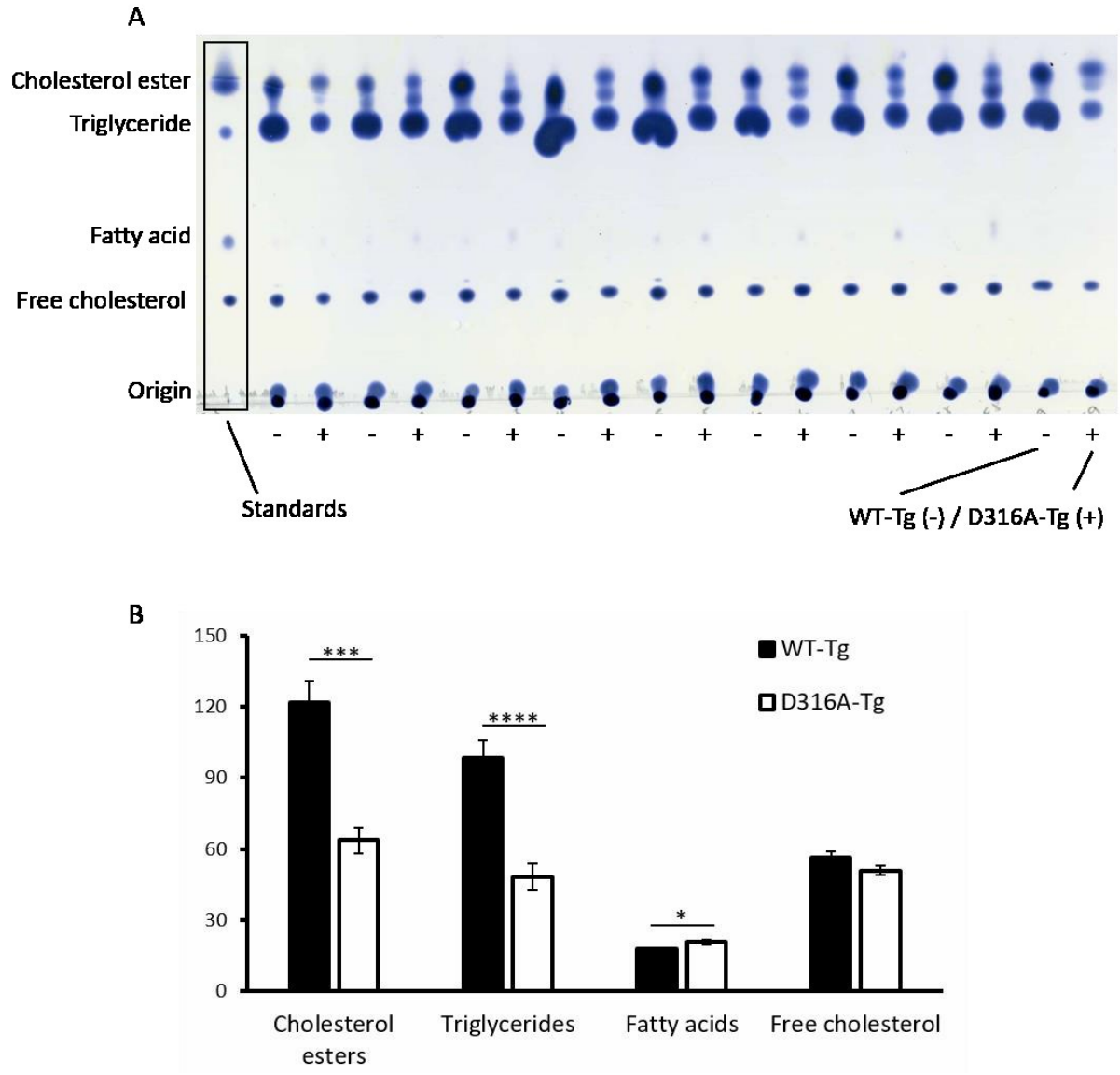


***Figure 3.23 – Liver lipid levels in mice on a high fructose diet. (A)*** *Thin layer chromatography (TLC) plate demonstrating cholesterol ester, triglyceride, fatty acid and free cholesterol content of liver homogenate from 9 mice of each genotype.* ***(B)*** *TLC plate spot area analysis. Methods – see* ***section 2.2.21.*** *Results shown are mean ± S.E.M. from n = 9, *p<0.05, ***p<0.001 and ****p<0.0001; t-test.*

Lipid accumulation in WT-Tg mice fed a high fructose diet and its absence from mice with liver specific AMPK activation (D316A-Tg) could also be clearly visualised on histology with haematoxylin and eosin (H&E) and oil red O staining (**Figure 3.25**).

Assay measurements of hepatic free cholesterol and glycogen content were also made. These confirmed that free cholesterol levels were not different between WT-Tg and D316A-Tg mice and that glycogen content too was unaffected by either diet (chow v fructose) or increased hepatic AMPK activity (WT-Tg v D316A-Tg - **Figure 3.24**).

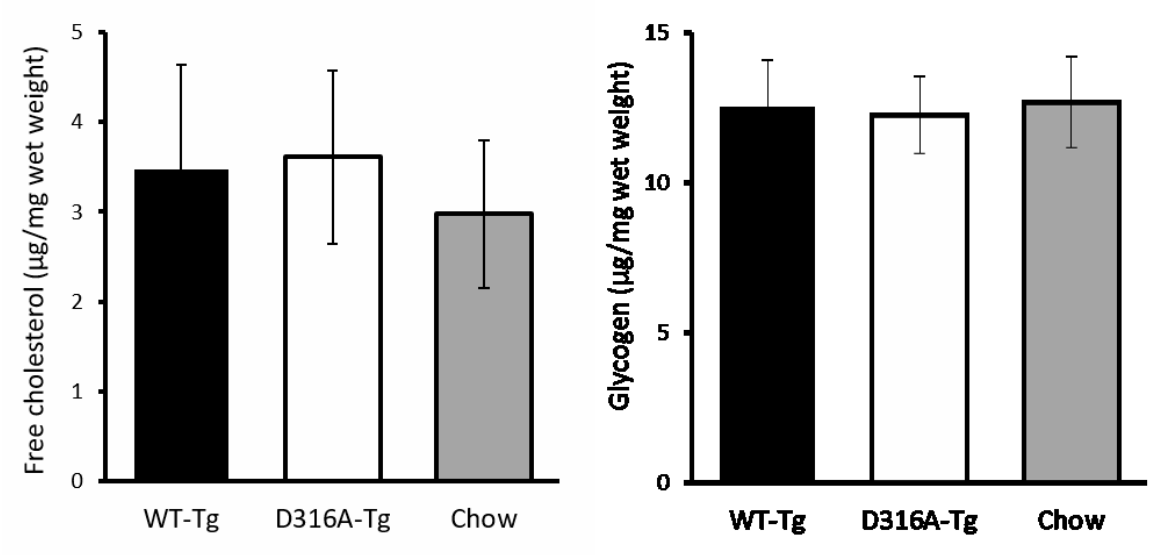


***Figure 3.24*** *-* ***Liver free cholesterol and glycogen content in mice on a high fructose diet.*** *Mouse liver* ***(A)*** *free cholesterol and* ***(B)*** *glycogen levels at 20 weeks of age after 12 weeks of high fructose diet. Levels in WT-Tg mice maintained on a chow diet are included for comparison. Methods – see* ***sections 2.2.18*** *and* ***2.2.23****. Results shown are mean ± S.E.M., from n=12 per group*

As might be anticipated, livers from D316A-Tg mice which contained less triglyceride than livers from WT-Tg mice, were also significantly lighter (1.18 ± 0.092 v 1.46 ± 0.041 – **Figure 3.26)**.

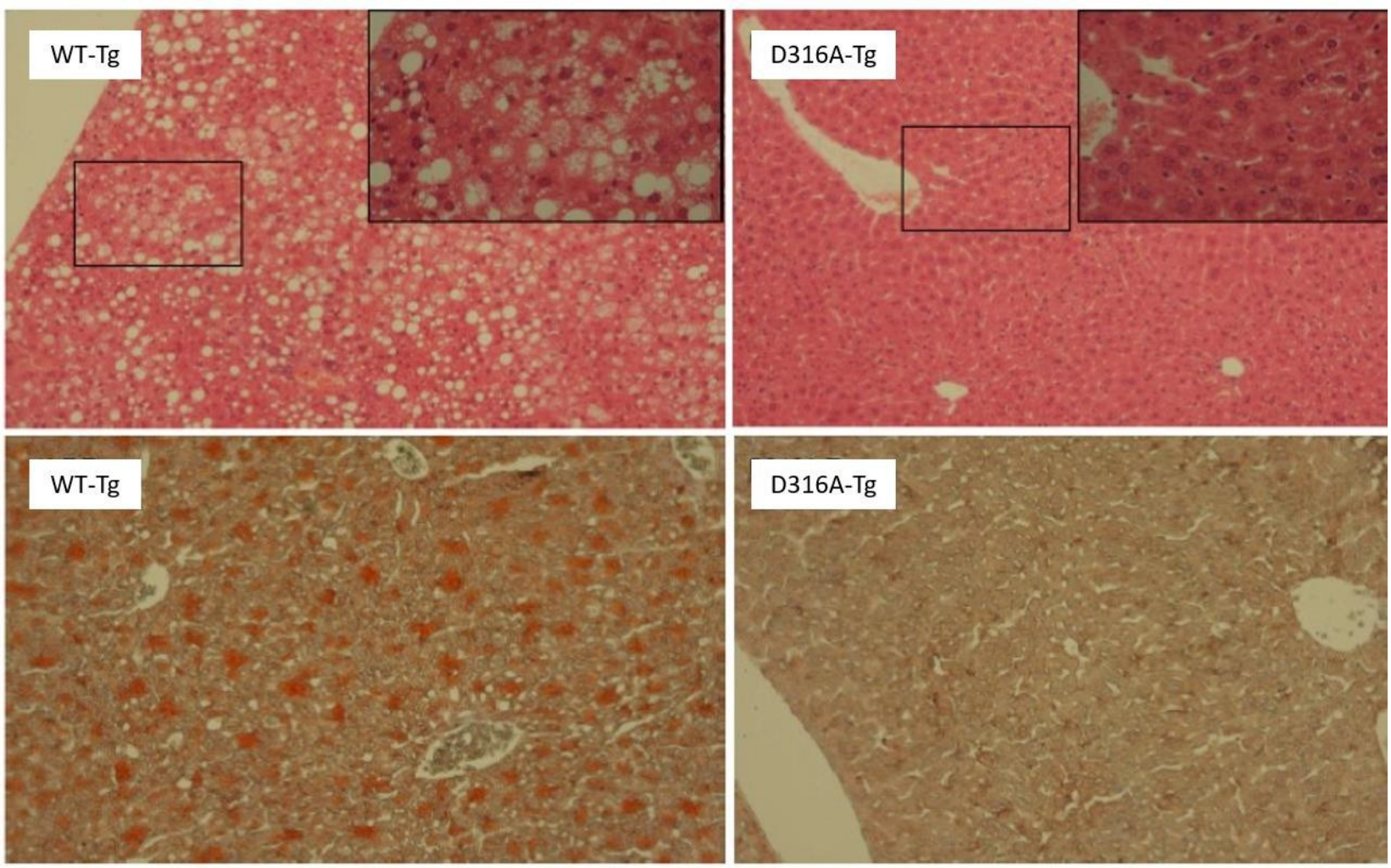


***Figure 3.25*** - ***Histological assessment of liver from mice fed a high fructose diet.*** *Liver sections taken from mice at 20 weeks of age, after 12 weeks of high fructose diet and stained with haematoxylin and eosin (H&E - top panel) or oil red O (bottom panel). For the H&E stained images, the boxed area is shown magnified in the top right hand corner inset.*

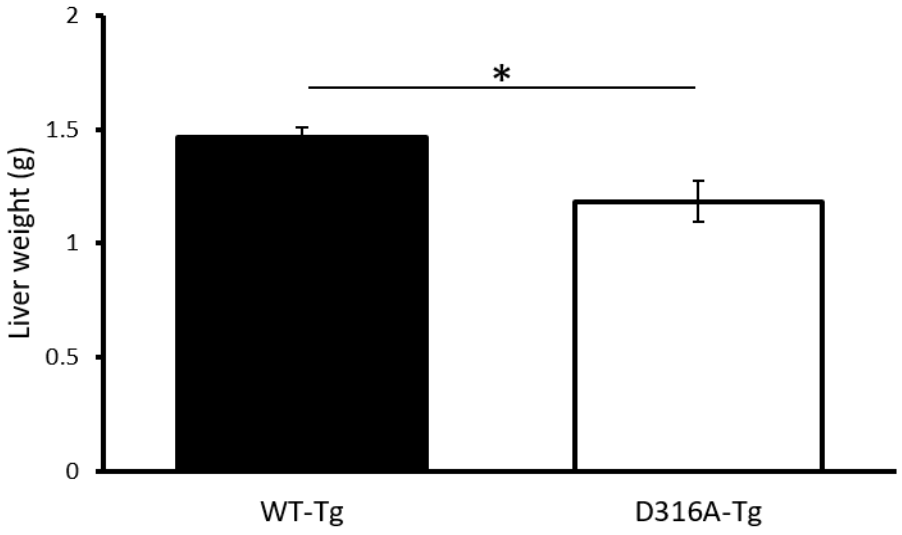


***Figure 3.26*** *- **Liver weights in mice with increased hepatic AMPK activity on a high fructose diet.** Liver weight at harvest (mean age 23 weeks). Results shown are mean ± S.E.M. from n ≥ 17 per genotype, *p ≤ 0.05; t-test.*

To determine if the steatosis seen in high fructose diet fed WT-Tg mice had instigated an inflammatory response, from which D316-Tg mice without steatosis were spared, serum liver

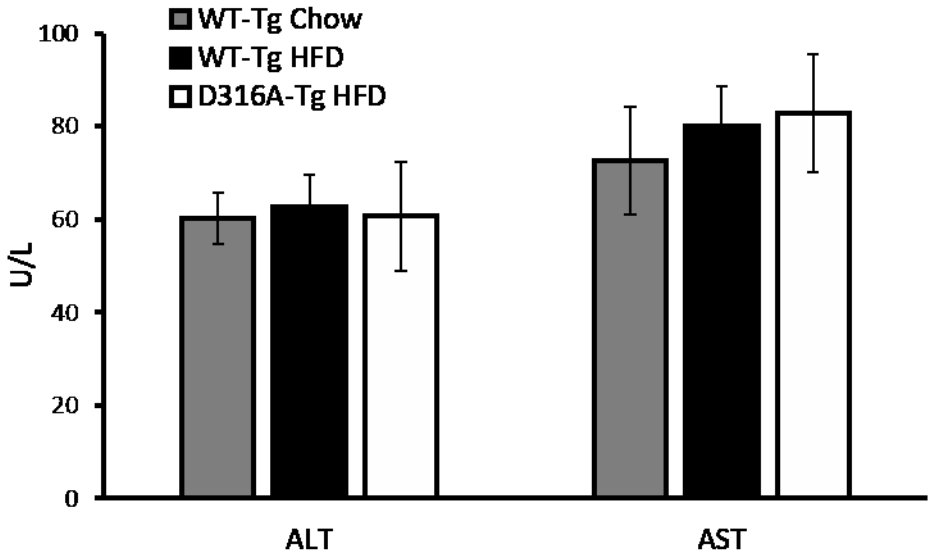


***Figure 3.27 – Serum markers of hepatocyte inflammation in mice on a high fructose diet.*** *Serum alanine and aspartate transaminase (ALT and AST) levels in mice after 14 weeks of high fructose feeding (23 weeks of age). Levels in chow fed mice of a similar age are shown for comparison. Methods – see **section 2.2.19.** Results shown are mean ± S.E.M. from n ≥ 10 per condition.*

transaminase levels were measured at harvest after 14 weeks of high fructose feeding (23 weeks of age). Serum transaminases did not differ between WT-Tg mice fed either chow or high fructose diet, indicating that although high fructose feeding induced steatosis, this had not, after 14 weeks of diet, precipitated an inflammatory response. Therefore, there was also no difference in transaminase levels seen between the genotypes on a fructose diet (WT-Tg v D316A-Tg - **Figure 3.27**).

Given the reduced hepatic *de novo* lipogenesis seen in D316A-Tg relative to WT-Tg mice, Western blotting was used to measure hepatic expression at harvest (following 14 weeks of a high fructose diet) of a number of lipogenic enzymes including ACC, FAS and stearoyl-CoA desaturase-1 (SCD-1) as well as fibroblast growth factor 21 (FGF21). The latter is a hormone, expression of which is up-regulated by increased carbohydrate-responsive element-binding protein (ChREBP) activity and therefore high fructose and sucrose feeding (Dushay et al. 2015). ACC, FAS, SCD-1 and FGF21 expression were all enhanced by high fructose relative to chow feeding in WT-Tg and D316A-Tg mice, however, there was no difference in their expression between the two genotypes on a high fructose diet (**Figure 3.28**). Together these findings indicate that fructose was entering hepatocytes and stimulating lipogenic protein expression and that this process was not affected by increased hepatic AMPK activity.

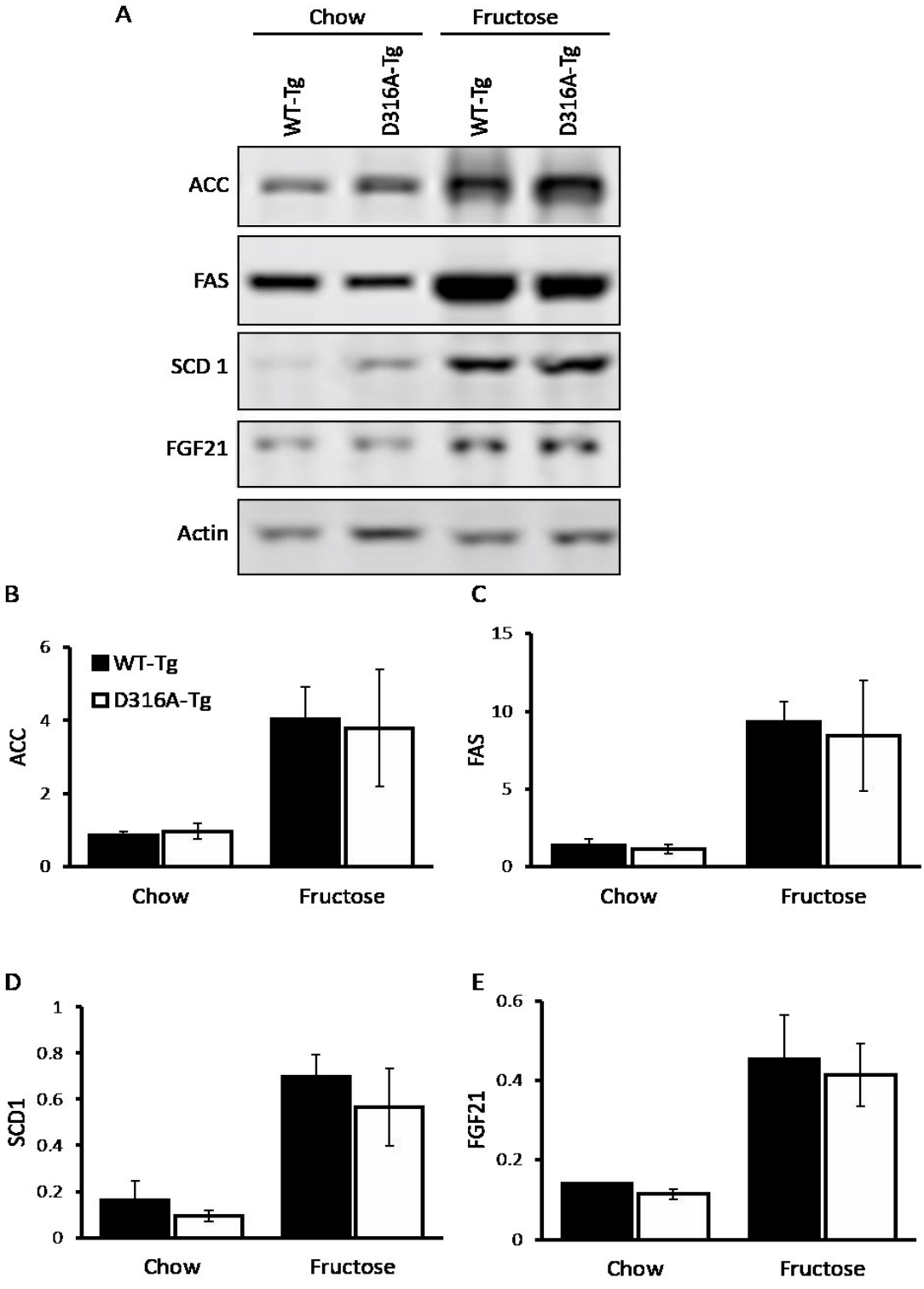


***Figure 3.28 - Lipogenic protein expression in liver from chow and high fructose diet fed mice. (A)*** *Western blot of liver homogenates from mice, probed with the indicated antibodies.* ***(B-E)*** *Quantification of blots, normalised to actin expression. Methods - see* ***section 2.2.5.*** *Results shown are mean ± S.E.M., from n=4 in each case.*

To determine if differences seen in D316A-Tg relative to WT-Tg mice resulted from altered gene expression, RNA from the livers of WT-Tg and D316A-Tg mice that had been fed either a chow or high fructose diet, was sequenced. **Figure 3.29** is the principle component analysis (PCA) plot for these samples. This demonstrates that diet had a greater impact on gene expression in the liver than increased hepatic AMPK activity (presence of the D316A

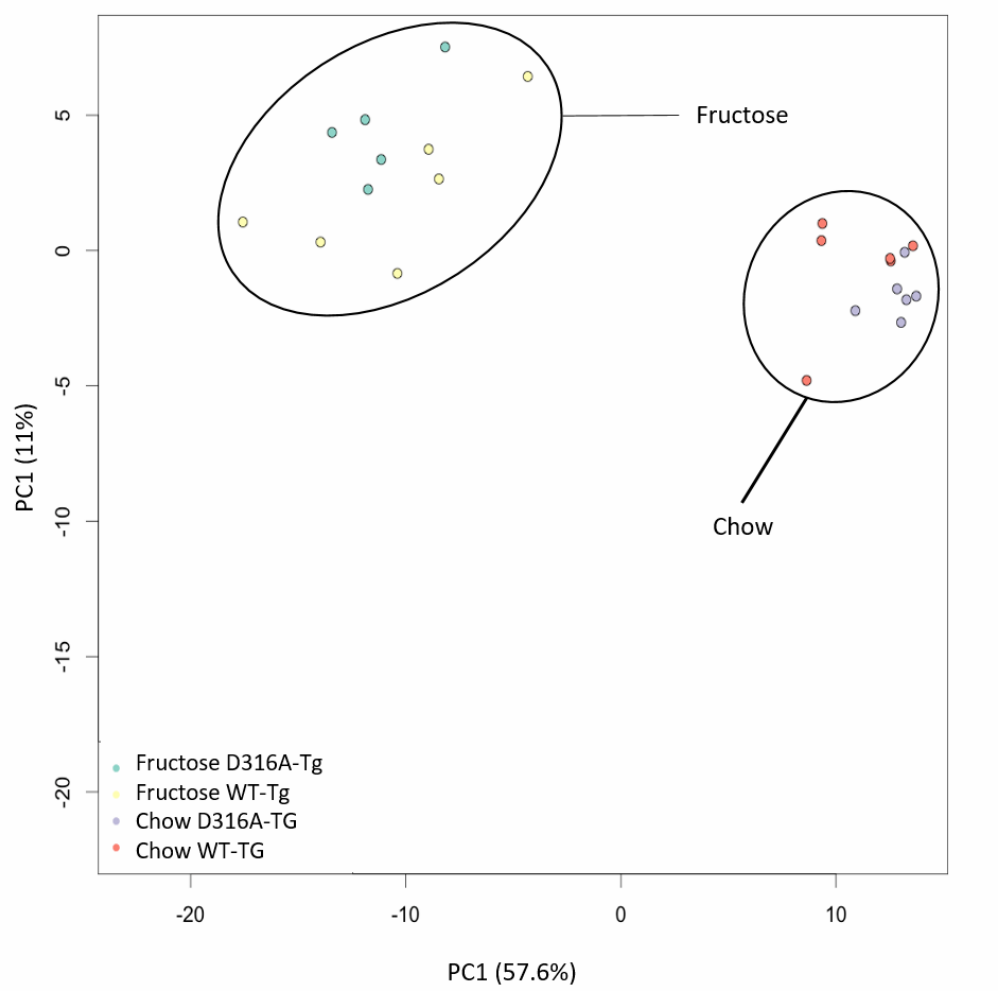


***Figure 3.29 - Principle component analysis for WT-Tg and D316A-Tg mice following chow or high fructose feeding.*** *Sequencing was performed on RNA from 5-6 mice for each of the 4 groups listed in the legend.*

transgene). Analysis of the sequencing data identified 326 genes which were altered in chow fed D316A-Tg relative WT-Tg mice (**Appendix A** - **Table 7.2**) and 241 genes which were changed in fructose fed D316A-Tg compared to WT-Tg mice (**Appendix A** - **Table 7.3**). Forty-six of these genes were common to both comparisons **(Appendix A** - **Table 7.1**). Given the inhibitory effect of AMPK on *de novo* lipogenesis seen in both the hepatocyte studies and *in*

*vivo,* expression of 8 common lipogenic genes was assessed (**Table 4.4**). With the exception of Acacβ which was up-regulated in chow fed D316A-Tg relative to WT-Tg mice and Elovl 7 and 2 which were up and down-regulated respectively in fructose fed D316A-Tg compared to WT-Tg animals, expression of the 8 genes in the liver did not differ in the presence or absence of increased hepatic AMPK activity. This data is disucsssed further in **section 4.8**.

## 3.5 Discussion

Insertion of a mutant (D316A) AMPK γ1 transgene which is only expressed in the presence of Cre recombinase, in mice expressing Cre under the albumin promoter, results in mice with liver specific constitutively active AMPK (D316A-Tg). An advantage of expressing mutant, constitutively active AMPK in the liver is that its effects can be evaluated at a cellular level using primary hepatocytes. This is particularly important given that the rapid fall in ATP levels that occurs upon tissue dissection can activate AMPK, confounding measurement of AMPK activity *in vivo* (Davies et al. 1992).

AMPK activity in primary hepatocytes from D316A-Tg mice is 2-3 fold that in hepatocytes from analogous mice with a wild-type transgene (WT-Tg – **Figures 3.4** and **3.5**). This increase is similar to that seen following treatment of Non-Tg hepatocytes with the specific AMPK activator 991 and is associated with increased AMPK $\alpha^{Thr172}$ and ACC phosphorylation in D316A-Tg hepatocytes. D316A-Tg mice are therefore a good model for examining the role of chronically increased AMPK activity in the liver.

AMPK γ1 levels appear higher in transgenic (both WT-Tg and D316A-Tg) compared to Non-Tg mice, presumably due to the strong CAG promoter upstream of the AMPK γ1 transgene (**Figure 3.3)**. However, total AMPK levels (measured as total AMPK β) were not different. This is in-keeping with previous work which has shown that when AMPK α or γ subunits are over-expressed in isolation and therefore do not combine to form the heterotrimeric AMPK complex, they are rapidly degraded (Carling et al. unpublished data).

Endogenous AMPK γ1 is virtually entirely replaced by transgenic protein in WT-Tg mice but is only reduced in D316A-Tg mice. A possible explanation for this is that AMPK heterotrimers incorporating the mutant AMPK γ1 subunit are more prone to degradation than those containing wild-type γ1. Alternatively AMPK α and β subunits may bind wild-type γ1 preferentially over mutant.

As might be anticipated on the basis of previous studies examining the effects of both systemic and hepatic increased AMPK activity (Bergeron et al. 2001; Buhl et al. 2002; Iglesias

et al. 2002; Song et al. 2002; Pold et al. 2005; Foretz et al. 2005), glucose production and gluconeogenic gene (G-6-P and PEPCK) expression were reduced in primary hepatocytes isolated from D316A-Tg relative to WT-Tg mice (**Figure 3.6**). However, *in vivo* there were no differences in glucose handling between the two genotypes on chow, high fat or high fructose diets (**Figures 3.10** and **3.17)**. This discrepancy between *in vitro* and *in vivo* findings could be explained by compensatory extrahepatic mechanisms operating *in vivo* and is not without precedent. For example mice lacking hepatic PEPCK expression have dramatically reduced hepatic glucose production but near-normal blood glucose levels due to increased extrahepatic gluconeogenesis and reduced whole-body glucose utilisation (She et al. 2003). These results emphasise the problems of using isolated cells to try to recapitulate *in vivo* conditions and in this respect highlight the advantages of our mouse model which allows evaluation of the effects of chronic AMPK activation in a tissue specific manner.

One of the main differences seen between D316A-Tg and WT-Tg hepatocytes was decreased fatty acid synthesis in hepatocytes with increased AMPK activity (D316A-Tg – **Figure 3.7**). Similarly, incorporation of radiolabelled acetate into hepatic lipid was reduced in D316A-Tg relative to WT-Tg mice (**Figure 3.21**). In keeping with these findings of reduced *de novo* lipogenesis in the presence of increased hepatocyte AMPK activity, D316A-Tg mice were protected from hepatic steatosis on a lipogenic high fructose diet (**Figures 3.22** and **3.23**). Their liver triglyceride levels were equivalent to those in mice on a chow diet and markedly lower than those in high fructose fed WT-Tg mice. Of note, D316A-Tg mice developed hepatic steatosis to a similar degree as WT-Tg mice following high fat feeding (**Figure 3.13**).

Previous studies have shown that high fructose feeding can induce hepatic steatosis. Pagliassotti et al. found that after just 1 week of a high sucrose diet (68% of calories from sucrose instead of corn starch) rats had raised blood and liver triglyceride content and as in the current study, these changes were not associated with increased body weight or altered body composition (Pagliassotti et al. 1996; Bizeau and Pagliassotti 2005). Huang et al. compared isocaloric standard (10% sucrose and 47% corn starch), high (60%) glucose and high (60%) fructose diets fed to athymic Nu/Nu mice for 12 weeks (Huang et al. 2011). Again neither glucose nor fructose feeding impacted on bodyweight, but high fructose diet fed mice had higher hepatic triglyceride levels, compared to glucose or standard diet fed mice. In

contrast to high carbohydrate and particularly high fructose diets which promote *de novo* lipogenesis, high lipid diets do not induce and may even suppress this process (Duarte et al. 2014). This would explain the diet specific effects of increased hepatic AMPK activity with regards the development of fatty liver**.**

Given that ACC phosphorylation (and therefore inhibition) was greater in D316A-Tg than in WT-Tg hepatocytes, it is likely that attenuated ACC activity was key to the reduced fatty acid synthesis seen in livers of mice with increased hepatic AMPK activity. In addition, RNA sequencing was used to evaluate whether differences in lipogenic gene expression were also contributing to the reduced triglyceride accumulation seen in fructose fed D316A-Tg relative to WT-Tg mice (**Table 4.4**). However expression of a number of common lipogenic genes was unaffected by presence of the AMPK γ1 D316A transgene. Together these results suggest that the effects of increased hepatic AMPK on *de novo* lipogenesis in the liver were due to post-translational changes.

Liver cholesterol ester levels following lipogenic high fructose feeding also appeared lower in mice with increased hepatic AMPK activity (**Figure 3.23**). This difference may be due to increased phosphorylation and inactivation of HMG CoA-reductase by AMPK and so reduced cholesterol synthesis within the liver (Clarke and Hardie 1990).

Although WT-Tg and D316A-Tg mice on a high fat diet and WT-Tg mice on a high fructose diet developed hepatic steatosis, in the time-frames examined, neither of these diets caused hepatic inflammation (**Figures 3.15** and **3.27**). It was therefore not possible to evaluate the effects of hepatic AMPK activity on the development of steatohepatitis. This is consistent with previous studies using diet induced NAFLD models. Whilst high fat feeding can cause hepatic inflammation, high fat and high fructose diets are commonly combined either with each other or with other dietary component such as cholesterol, in order to more rapidly and robustly mimic the histological changes seen in NAFLD (Xu et al. 2010; Dowman et al. 2014; Hebbard and George 2011; Asgharpour et al. 2016). It is also important to note that the impact of diets can vary with the strain of mouse under investigation (Nagata et al. 2004).

Importantly, hepatic expression of a number of lipogenic proteins (ACC, FAS and SCD-1) was increased in response to high fructose feeding, however, concentrations of these enzymes did not differ between WT-Tg and D316A-Tg mice (**Figure 3.28**). This implies that uptake of fructose into hepatocytes and so its stimulatory effects on lipogenic protein expression were unaffected by increased hepatic AMPK activity. These findings also provide further support for the idea that activation of AMPK in the liver inhibited *de novo* lipogenesis through post-translational effects as opposed to altering lipogenic gene expression.

All fructose fed mice (WT-Tg and D316A-Tg) had significantly higher serum cholesterol, HDL and LDL levels than chow fed animals (**Figure 3.18**). Despite reduced hepatic fatty acid synthesis and steatosis in D316A-Tg relative to WT-Tg mice fed a high fructose diet, serum lipid levels did not vary between the two genotypes. This observation was perhaps unexpected, but could be due to a secondary effect of fructose metabolism in the liver which was not affected by increased hepatic AMPK activity.

Despite increased ACC phosphorylation in D316A-Tg relative to WT-Tg mouse hepatocytes, rates of fatty acid oxidation did not differ between the two genotypes (**Figure 3.8**). Neither were fatty acid oxidation rates in hepatocytes altered by treatment with the direct AMPK activator 991. Furthermore, *in vivo,* WT-Tg and D316A-Tg mice had similar RERs (indicative of equal use of fat as a respiratory substrate) and serum ketone (5-hydroxybutyrate) levels (**Figures 3.11, 3.19** and **3.20**).

These findings are perhaps somewhat surprising and do not entirely correspond with previous studies examining the effects of ACC phosphorylation by AMPK. Fullerton et al. examined the effects of AMPK activation (using the direct activator A769662) on fatty acid oxidation in wild-type mice and mice harbouring mutations in the AMPK phosphorylation sites of ACC1 (serine 79 to alanine) and ACC2 (serine 212 to alanine), which rendered them independent of AMPK regulation (Fullerton et al. 2013). Whilst treatment of wild-type hepatocytes with A769662 resulted in a modest increase in fatty acid oxidation, A769662 treatment had no effect in ACC mutant cells. It is unclear why the findings of this current study with regards hepatic fatty acid oxidation, differ from those of Fullerton et al. However, it is evident that the relationship between AMPK, ACC and fatty acid oxidation is complex. Hawley et al. recently showed that

Canagliflozin which activates AMPK, reduced RER in ACC1 and ACC2 double knockout mice (Hawley et al. 2016) and Zordoky et al. previously demonstrated that cardiac ischaemia, which activates AMPK, enhanced fatty acid oxidation in the heart equally in wild-type mice and mice carrying the ACC mutations described above (which remove ACC from regulation by AMPK) (Zordoky et al. 2014). A recent study of two novel direct AMPK activators provides further support for the suggestion that AMPK does not promote fatty acid oxidation in the liver. PF-739, which activates all AMPK complexes and PF-249 which is β1 subunit specific and therefore activates hepatic AMPK but has limited effect in skeletal muscle, were administered to mice with diet induced obesity. Serum ketone levels were only increased in PF-739 (not PF-249) treated mice implying that fatty acid oxidation was only affected when AMPK was activated in skeletal muscle (Cokorinos et al. 2017).

Cool et al. used the direct AMPK activator A769662 to evaluate the effects of systemic AMPK activation (Cool et al. 2006). In their study, in keeping with the findings of this current study, fatty acid synthesis was reduced in A769662 treated hepatocytes. However, Cool et al. also demonstrated an effect of increased AMPK activity on glucose handling *in vivo*, with reduced serum glucose concentrations and hepatic gluconeogenic gene transcription in *ob/ob* mice receiving A769662. Furthermore, they observed lower RERs (indicative of increased fatty acid oxidation) and reduced serum and hepatic triglyceride levels in A769662 treated rats and obese mice respectively. Although A769662 is a direct AMPK activator, subsequent work by Benziane et al. has shown that in skeletal muscle cells it inhibits active sodium ion transport independently of AMPK. Taking the latter observation and the findings of this current study into consideration, it seems likely that at least some of the metabolic effects of A769662 *in vivo* are mediated independently of AMPK activation in the liver.

Henriksen et al. treated rats on a chow or high fat diet with 5-aminoimidazole-4-carboxamide ribonucleotide (AICAR), an indirect AMPK activator (Henriksen et al. 2013). Treated rats had reduced SREBP1c expression and hepatic triglyceride levels relative to untreated mice, irrespective of diet. It is not possible, based upon Henriksen et al.'s findings, to determine the role of hepatic AMPK activity, as, like A769662, AICAR has both systemic and AMPK independent effects.

Yavari et al. used mice, homozygous for an AMPK γ2 mutation (R299Q) equivalent to that seen in patients with Wolff-Parkinson-White syndrome (R302Q) to examine the effects of systemic increased AMPK activity (Yavari et al. 2016). Somewhat surprisingly, the mutant mice developed adult onset obesity and impaired pancreatic insulin secretion: The former due to hyperphagia, likely as a result of increased hypothalamic signalling. Thus, the main effects of AMPK in Yavari et al.'s investigation were extrahepatic and so one would not anticipate that they would be replicated in this study. It is also not clear whether outcomes as a result of increased AMPK activity are subunit specific. Therefore, the phenotype of global carriers of the AMPK γ1 D316A transgene might differ from that of AMPK α2 R299Q mice.

Villena et al. showed that following exposure to a high fat diet, mice with global AMPK α2 knockout gained fat weight more quickly and had higher serum triglyceride levels than equivalent wild-type mice (Villena et al. 2004). These knockout mice also had relatively impaired glucose tolerance on a chow diet. Andreelli et al. demonstrated that the effects of liver specific AMPK α2 knockout were similar, although bodyweight in these animals was not altered (Andreelli et al. 2006). Whilst knockout studies can be useful when evaluating the role of AMPK in the liver, their findings can only be used to infer the effects of increased hepatic AMPK activity. It is therefore unsurprising that the findings of this current study are not the exact opposite of those of Villena et al. and Andreelli et al.

Finally, Foretz et al. used adenoviral delivery of truncated, constitutively active, AMPK α2 to the liver (Foretz et al. 2005). In keeping with the findings of this current study, glucose output and gluconeogenic gene expression were reduced in hepatocytes with acute hepatic AMPK activation. However, serum glucose and insulin concentrations in the infected mice were also lower, as were adipocyte mass and serum triglyceride levels with unexpected triglyceride accumulation in hepatocytes, possibly as a result of mobilisation of fatty acids from adipose tissue to the liver. It is perhaps unsurprising that the effects of acute AMPK activation seen in Foretz et al.'s study differ from those of chronic activation seen in this current study. Also, importantly, the mutant, constitutively active, AMPK α2 subunit used in Foretz et al.'s study is truncated meaning it does not bind with the β and γ subunits, which could confound its effects.

### 3.6 Summary of key findings

- AMPK activity was increased 2-3 fold in primary hepatocytes from D316A-Tg relative to WT-Tg mice without a change in total levels of the AMPK complex. D316A-Tg mice are therefore a valuable tool for evaluating the effects of chronic and specific hepatic AMPK activation.
- Gluconeogenesis was reduced in primary hepatocytes from D316A-Tg compared to WT-Tg mice but systemic glucose handling was unaffected. The latter finding could be due compensatory extrahepatic mechanisms.
- *De novo* lipogenesis both in primary hepatocytes and *in vivo* was reduced in the presence of the AMPK γ1 D316A transgene. In-keeping with these findings, D316A-Tg mice were protected from hepatic steatosis on a lipogenic, high fructose diet. However they were not protected from accumulation of triglycerides in the liver following high fat feeding (when *de novo* lipogenesis rates are either normal or suppressed).
- Based on both primary hepatocyte and *in vivo* data, fatty acid oxidation was unaffected by presence of the AMPK γ1 D316A transgene. This corresponds with some but conflicts with other previous studies evaluating the effects of AMPK on fatty acid oxidation in the liver.

# 4 Results: AMPK activation in a liver specific PTEN knockout model of NAFLD and HCC

## 4.1 Introduction

Given that liver specific AMPK activation prevented the development of steatosis caused by high fructose feeding, it was decided to assess its role in another, more aggressive, NAFLD model. To do this, albumin cre D316A-Tg or WT-Tg mice were crossed with *Pten*$^{flox}$ mice (Prof. J. Downward, Cancer Research UK, Clare Hall Laboratories, UK #B6.129S4Ptentm1Hwu) to give mice with liver specific knockout of the tumour suppressor phosphatase and tensin homologue (Pten), with or without liver specific AMPK activation, hereafter referred to as *Pten*$^{-/-}$*+D316A* or *Pten*$^{-/-}$ respectively. As previously described by Horie et al. and Stiles et al., mice with defective hepatic Pten rapidly progress through the stages of NAFLD and develop tumours by around 40 weeks of age (**Table 4.1**). This model therefore allowed the effects of AMPK activation on tumour development to be assessed, in addition to evaluating their impact on the precancerous NAFLD like lesion.

Horie and colleagues described a milder phenotype in mice heterozygous for *Pten* and in female mice. Given these findings, only male homozygous mice were used for *in vivo* experiments in the current study, although primary hepatocytes were isolated from both male and female homozygous mice. AMPK activity did not differ between Non-Tg and Tg-WT mice or between mice that were Het or Hom for the same AMPK γ1 transgene. Therefore, as previously, we combined mice with liver specific Pten loss crossed with either WT-Tg or Non-Tg mice (*Pten*$^{-/-}$) and also Het and Hom transgenic mice in order to maximise animal usage (see **Table 2.7**).

| Horie et al. 2004 | Stiles et al. 2004 |
|---|---|
| • Pale livers and hepatomegaly at 10 and 40 weeks<br>• Microvesicular steatosis in zone 3 at 10 weeks, progressing to widespread macrovesicular steatosis at 40 weeks<br>• Increased total liver cell number at 40 weeks (1.5 fold)<br>• Raised liver TG (>7 fold) and cholesterol ester (2 and 7 fold) content at 10 and 40 weeks respectively. (Normal free FA, free cholesterol and phospholipid content).<br>• Serum TG and cholesterol levels normal throughout<br>• Raised serum AST,ALT and ALP at 40 weeks (elevated but not significantly at 10 weeks)<br>• Lobular inflammatory infiltrate at 40 weeks<br>• Mild sinusoidal fibrosis at 40 weeks<br>• Macroscopic tumours (66% at 40 weeks, 100% at ≈75 weeks). Adenomas at 40 weeks progressing to HCC (83%) at ≈75 weeks<br>• Raised hepatic $H_2O_2$ at 10 weeks (7 fold)<br>• Increased insulin sensitivity and reduced serum glucose and insulin levels at 12 weeks<br>• Increased PPARϒ (and adipsin, adiponectin and aP2) but not PPARα expression<br>• Upregulated SREBP1c, FAS, ACC and SCD1 expression<br>• Increased AKT, FOXO1 and MAPK phosphorylation<br>• Positive adiponectin (adipocyte marker) staining on IHC<br>• Enhanced BrdU incorporation into hepatocytes (proliferation) at 10 weeks<br>• No differences on TUNEL assay (apoptosis) at 10 or 40 weeks | • Pale livers and hepatomegaly<br>• Microvesicular steatosis in zone 3 at 1 month, progressing to widespread macrovesicular steatosis at 6 months<br>• Raised liver triglyceride content (3 fold)<br>• Increased glycogen storage in livers (assessed by PAS staining)<br>• No difference in rate of FA uptake in hepatocytes (measured using FACS) or FA transporter expression (FATP2 or FATP5) at 3 months<br>• Raised DNL in liver at 1 month (2.5 fold – assessed using $D_2O$ incorporation into FAs)<br>• Increased FA secretion into plasma at 1 month (higher plasma TG levels after triton injection)<br>• Normal TG levels but reduced free FA levels (30%) in serum at 1 month<br>• Inflammatory infiltrate and mild fibrosis in some livers at 6 months<br>• Decreased body fat content at 1 month (50%)<br>• Reduced stimulated lipolysis at 1 month<br>• Lower serum insulin levels and increased insulin sensitivity at all ages<br>• Lower serum glucose levels at 1 and 3 months<br>• Increased GSKβ phosphorylation in liver<br>• Higher FAS levels in liver<br>• Reduced gluconeogenic enzyme (G6Pase and PEPCK) levels in liver |

***Table 4.1 - Effects of liver specific Pten loss*** *(Horie et al. 2004; Stiles et al. 2004). Horie et al. deleted Pten exons 4 and 5 and evaluated mice at 10 and 40 weeks of age. Stiles et al excised exon 5 and assessed animals at 1,3 and 6 months. TG = triglyceride, FA = fatty acid, AST and ALT = aspartate and alanine transaminase, ALP = alkaline phosphatase, HCC = hepatocellular carcinoma, PPAR = peroxisome proliferator activated receptor, aP2 = adipocyte protein 2, SREBP1c = sterol regulatory element-binding protein 1c, SCD = stearoyl-CoA desaturase-1, FOXO1 = forkhead box protein O1, MAPK = mitogen activated protein kinase, IHC = immunohistochemistry, TUNEL = Terminal deoxynucleotidyl transferase dUTP nick end labelling, PAS = periodic acid Schiff, FACS = fluorescence-activated cell sorter analysis, DNL = de novo lipogenesis, GSK-β = glycogen synthase kinase β, FAS = fatty acid synthase, G6Pase = glucose 6-phosphatase, PEPCK = phosphoenolpyruvate carboxykinase.*

## 4.2 Hepatic AMPK activity reduced in mice with liver specific Pten loss but increased in the presence of the AMPK γ1 D316A transgene

As previously discussed, AMPK is activated during tissue dissection due to the rapid rise in ATP concentration (Davies et al. 1992). Primary hepatocyte experiments avoid this complication and therefore offer a much more accurate means of measuring AMPK activity and its downstream effects.

Western blotting demonstrated reduced phosphorylation of AMPK $\alpha^{Thr172}$ (**Figure 4.1 A** & **B**) and its downstream target $ACC^{Ser79}$ (**Figure 4.1 A** & **C**) in hepatocyte lysates from *Pten*$^{-/-}$ relative to WT-Tg mice. There was also a trend towards reduced AMPK activity in immune complexes isolated from the lysates (using a pan AMPKβ antibody) of mice with hepatic Pten loss (0.84 ± 0.125, **Figure 4.1 D**). This latter change corresponded with those seen on Western blotting and it is probable that it did not reach significance due to insufficient n numbers. AMPK $\alpha^{Thr172}$ (**Figure 4.1 A** & **B**) and $ACC^{Ser79}$ (**Figure 4.1 A** & **C**) phosphorylation were increased in hepatocyte lysates from *Pten*$^{-/-}$*+D316A* relative to *Pten*$^{-/-}$ or WT-Tg mice. AMPK activity, in immune complexes isolated from hepatocyte lysates with a pan AMPKβ antibody, was at least 3 fold higher in complexes from *Pten*$^{-/-}$*+D316A* compared to *Pten*$^{-/-}$ or WT-Tg mice (*Pten*$^{-/-}$*+D316A*:WT-Tg = 3.0 ± 0.538) (**Figure 4.1 D**).

Hawley et al. previously showed that increased phosphorylation and activation of AKT in the absence of Pten, resulted in increased Ser485 (equivalent to Ser487 in human) phosphorylation of APMK α1 and that this in turn led to decreased AMPK $\alpha^{Thr172}$ phosphorylation and so inactivation of AMPK (Hawley et al. 2014). This result was supported by findings from our *Pten*$^{-/-}$ mouse hepatocyte experiments. AMPK $\alpha1^{Ser485}$ phosphorylation was greater in AMPK α1 immune complexes isolated from *Pten*$^{-/-}$ hepatocyte lysates, than in those from WT-Tg hepatocytes (**Figure 4.2 A**). Correspondingly, AMPK activity was lower (0.45 ± 0.061) in AMPK α1 immuno-precipitates from *Pten*$^{-/-}$ relative to WT-Tg hepatocytes (**Figure 4.2 C**)**.** However, AMPK α1 activity was still higher (1.9 ± 0.185) in *Pten*$^{-/-}$*+D316A* compared to WT-Tg hepatocytes. Of note, phosphorylation of the equivalent site to Ser485

on AMPK α2 (Ser491) and α2 activity were not altered in the absence of Pten, consistent with Hawley et al.'s findings (**Figure 4.2 B** & **D**) (Hawley et al. 2014).

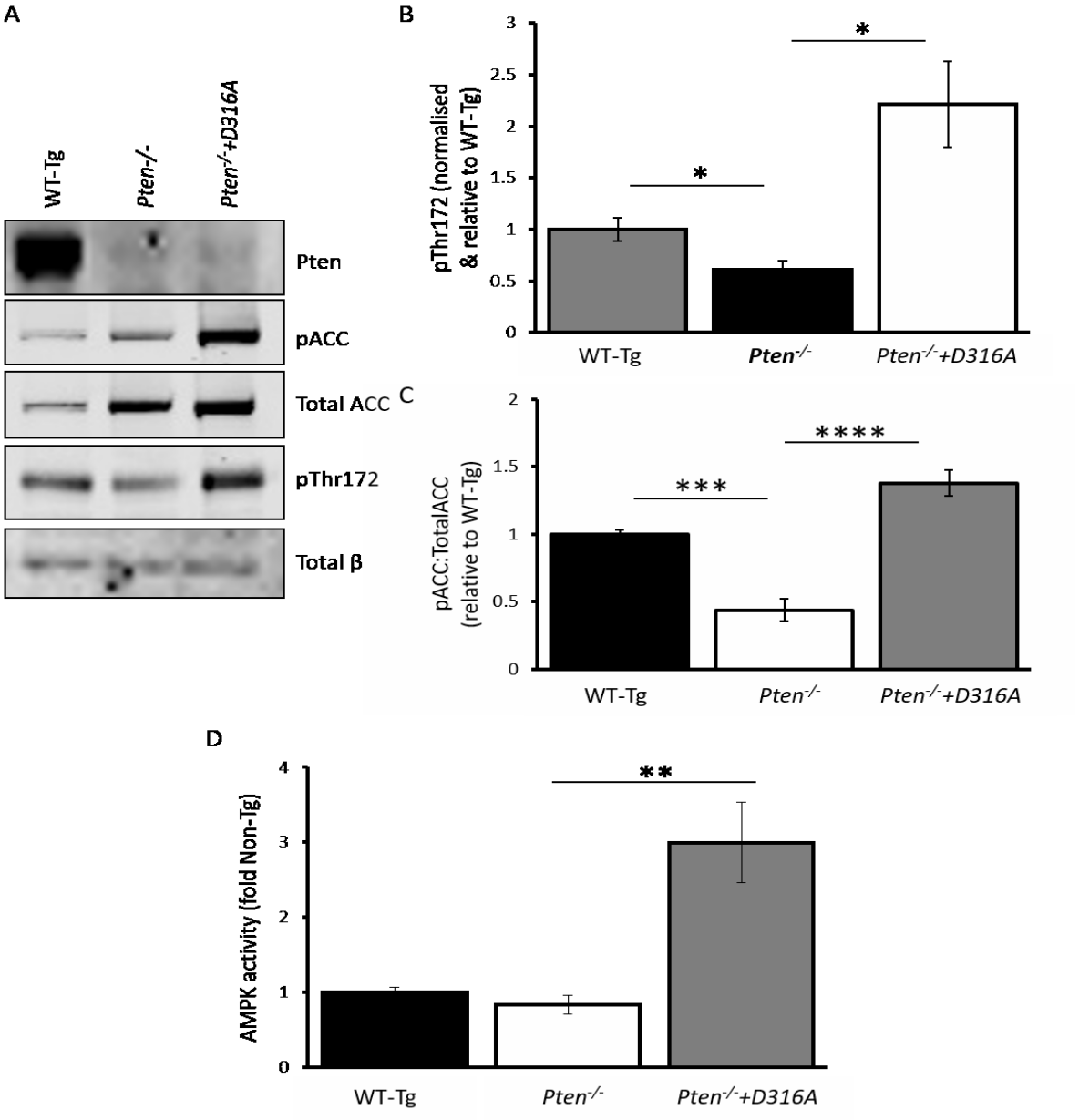


***Figure 4.1*** *- **AMPK activity in hepatocytes from WT-Tg, Pten$^{-/-}$ and Pten$^{-/-}$+D316A mice. (A)** An example of hepatocyte lysates, probed with the indicated antibodies. pACC = pACC$^{Ser79}$, pThr172 = pAMPK α$^{Thr172}$ and Total β = total AMPK β. **(B and C)** Quantification of the blots. Methods – see section **2.2.5.** Results shown are mean ± S.E.M. from n≥3 independent mice for each genotype, *p<0.05, ***p<0.001 and ****p<0.0001; t-test. **(D)** AMPK activity measured in immune complexes isolated with an AMPK pan-β antibody. Methods – see **section 2.2.6.** Results shown are relative to WT-Tg and are mean ± S.E.M from n=7-10 independent mice for each genotype, **p<0.01; t-test.*

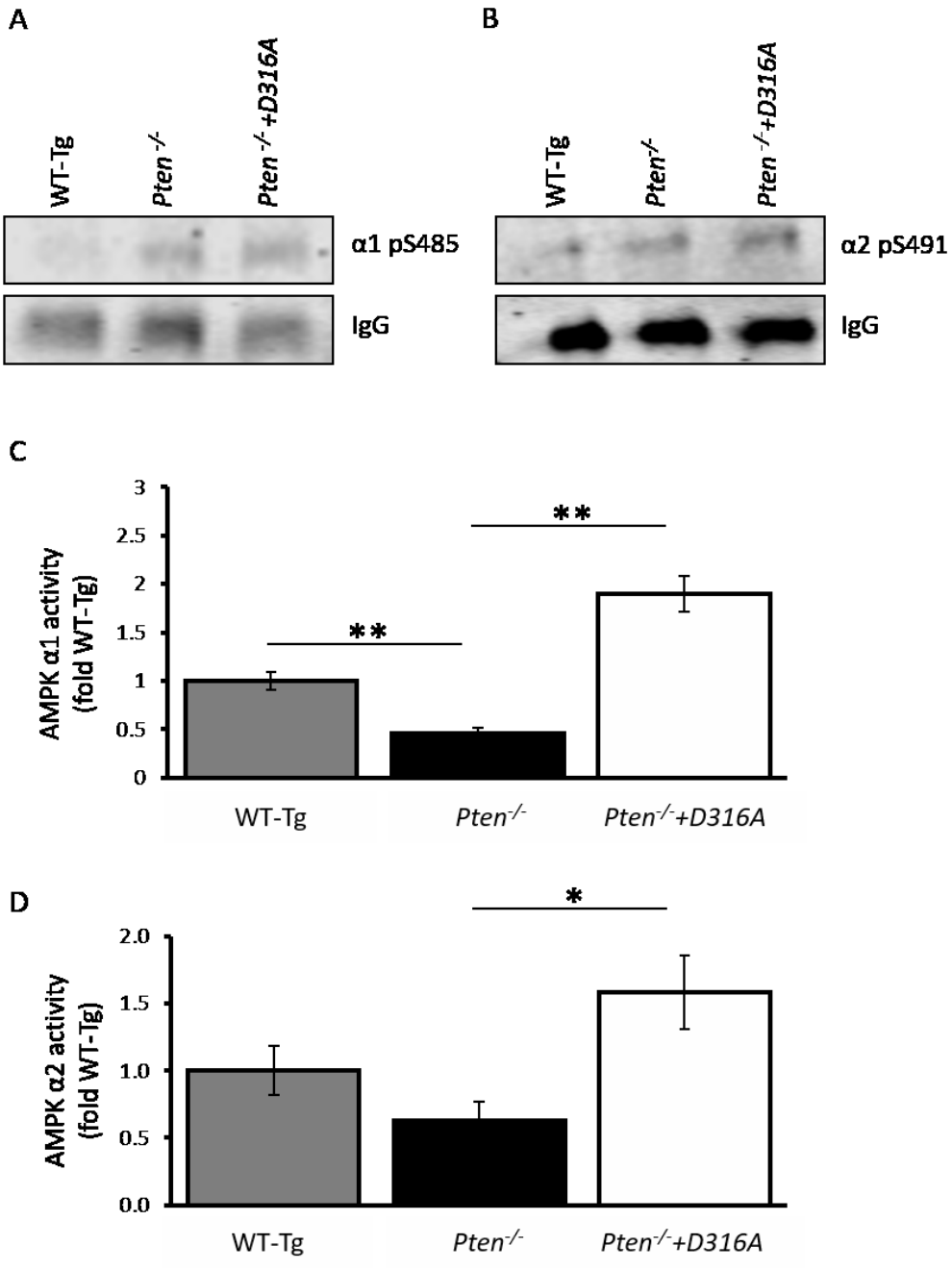


***Figure 4.2 - AMPK α1$^{Ser485}$ and α2$^{Ser491}$ phosphorylation and α1 and α2 activity in hepatocytes from WT-Tg, Pten$^{-/-}$ and Pten$^{-/-}$+D316A mice. (A & B)*** *Examples of immune complexes isolated from hepatocyte lysates using an AMPK α1 or α2 antibody, then probed for AMPK α1$^{Ser485}$ or α2$^{Ser491}$.* ***(C & D)*** *AMPK activity measured in immune complexes isolated from hepatocyte lysates using an AMPK α1 or α2 antibody. Methods – see* ***sections 2.2.5*** *and* ***2.2.6****. Results shown relative to WT-Tg and are mean ± S.E.M. from n=5-8 mice for each genotype *p<0.05 and **p<0.01; t-test.*

## 4.3 Hepatic steatosis in mice with liver specific Pten loss attenuated in the presence of increased hepatic AMPK activity

Given that increased AMPK activity was shown to reduce fatty acid synthesis in hepatocytes from D316A-Tg mice and that Stiles et al. observed enhanced *de novo* lipogenesis in mice with liver specific Pten loss, we anticipated that *Pten*$^{-/-}$*+D316A* mice might develop less steatosis than their *Pten*$^{-/-}$ counterparts (Stiles et al. 2004).

The triglyceride content of liver from *Pten*$^{-/-}$ and *Pten*$^{-/-}$*+D316A* mice, at various ages, was measured and compared to levels in WT-Tg mice (**Figure 4.3 A**). Liver triglyceride content was increased in *Pten*$^{-/-}$ and *Pten*$^{-/-}$*+D316A* mice from 6 weeks of age. However, at all time points except 45 weeks, liver triglyceride levels in *Pten*$^{-/-}$*+D316A* mice were significantly lower than those in *Pten*$^{-/-}$ mice. A similar pattern was seen with liver cholesterol content (**Figure 4.3 B**). Cholesterol was raised in *Pten*$^{-/-}$ and *Pten*$^{-/-}$*+D316A* mice from 25 weeks of age, but rose more slowly and so by 35 weeks was significantly lower in mice with increased hepatic AMPK activity. By 45 weeks of age a relatively high proportion of liver tissue was occupied by tumours, especially in *Pten*$^{-/-}$ mice, therefore complicating assessment of lipid content in background, non-tumourous tissue.

Liver sections from WT-Tg, *Pten*$^{-/-}$and *Pten*$^{-/-}$*+D316A* mice were stained with haematoxylin and eosin (H&E). Reduced zone 3 (peri-venular) steatosis could be clearly visualised at 6 weeks of age in *Pten*$^{-/-}$*+D316A* relative to *Pten*$^{-/-}$ liver (**Figure 4.4**). Although liver triglyceride and cholesterol levels continued to be lower in *Pten*$^{-/-}$*+D316A* compared to *Pten*$^{-/-}$ mice, the visual difference in steatosis became less apparent over time. This was reflected in the histological hepatic steatosis scores which were calculated by an external, expert pathologist (Dr G Böttcher, Astrazeneca, Sweden - **Figure 4.5**). *Pten*$^{-/-}$ mice had higher hepatic steatosis scores than WT-Tg animals and this difference was significant at all time points except 45 weeks of age. *Pten*$^{-/-}$*+D316A* mice had lower mean steatosis scores than *Pten*$^{-/-}$ mice at all time points except 45 weeks, however this difference was only significant at 6 weeks of age. As previously discussed, by 45 weeks of age a relatively high proportion of liver tissue was occupied by tumours, especially in *Pten*$^{-/-}$ mice, complicating the assessment of background, non-

tumourous tissue, which could account for the somewhat inconsistent findings at this time-point.

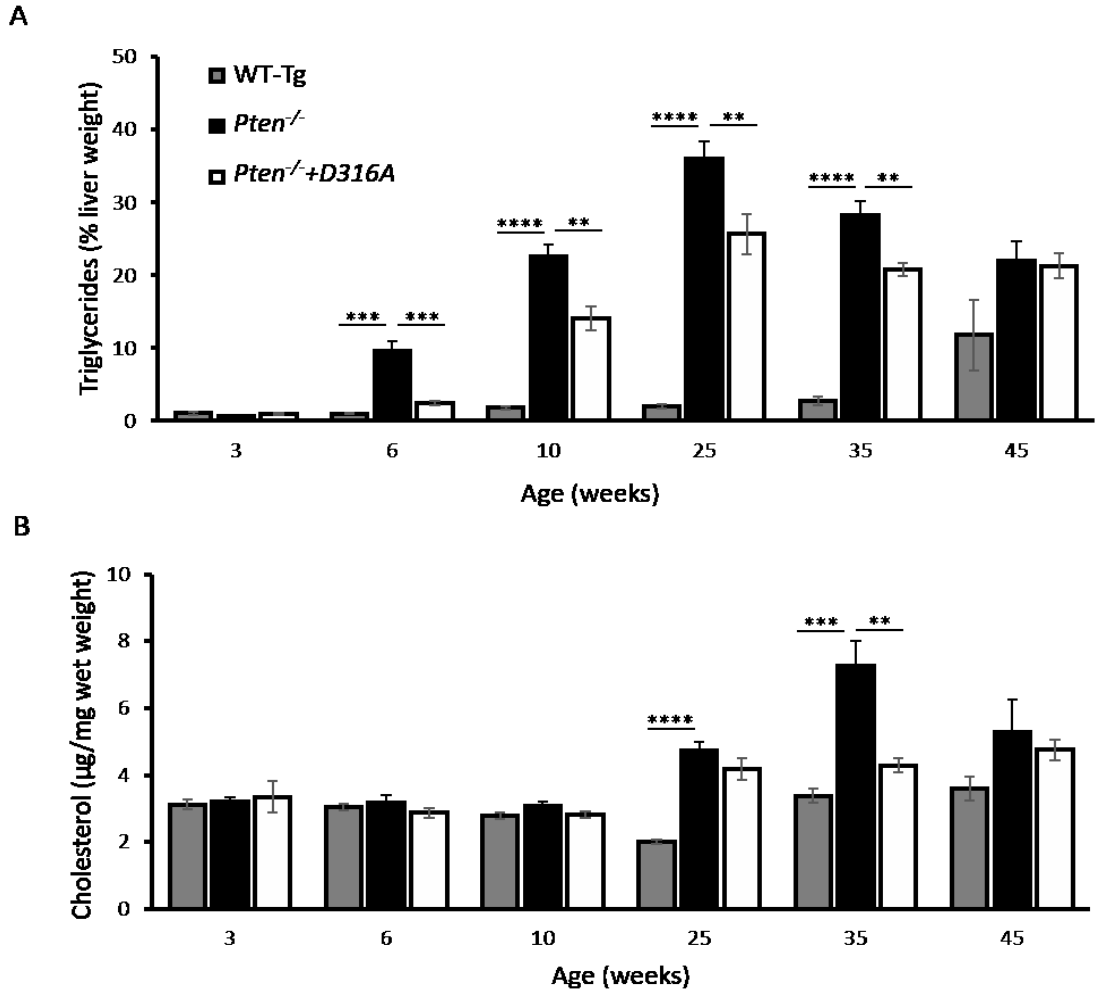


***Figure 4.3 - Hepatic lipid levels in WT-Tg, Pten$^{-/-}$ and Pten$^{-/-}$+D316A mice. (A)*** *Triglyceride and* ***(B)*** *cholesterol content of liver. Methods - see sections* ***2.2.17*** *and* ***2.2.18****. Results shown are mean ± S.E.M. from n≥8, **p<0.01, ***p<0.001 and ****p<0.0001; t-test.*

Previous studies describe a change over time in the character of steatosis seen in the livers of mice with liver specific Pten loss, with microvesicular steatosis early on (when lipid accumulation is relatively confined to zone 3) progressing to macrovesicular steatosis later (associated with more panacinar involvement) (Stiles et al. 2004; Horie et al. 2004). By 25 weeks of age there was extensive steatosis visible in H&E stained liver sections from *Pten$^{-/-}$* and *Pten$^{-/-}$+D316A* mice, however, qualitatively, steatosis in liver from *Pten$^{-/-}$+ D316A* mice was more microvesicular compared to that in liver from *Pten$^{-/-}$* animals which was

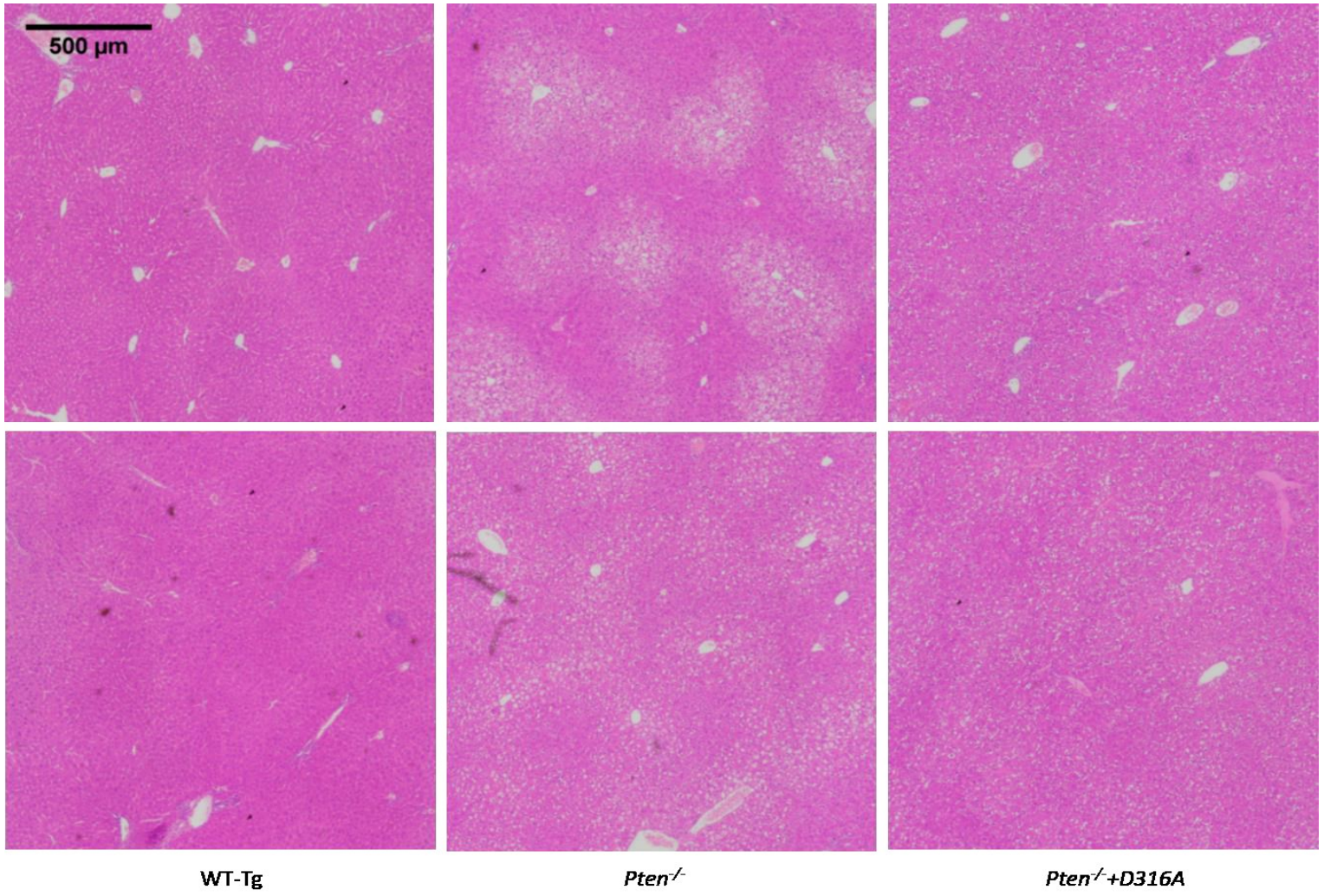


***Figure 4.4 - Haematoxylin and eosin stained liver sections, from 6 week old WT-Tg, Pten$^{-/-}$ and Pten$^{-/-}$+D316A mice.*** *Two examples from each genotype.*

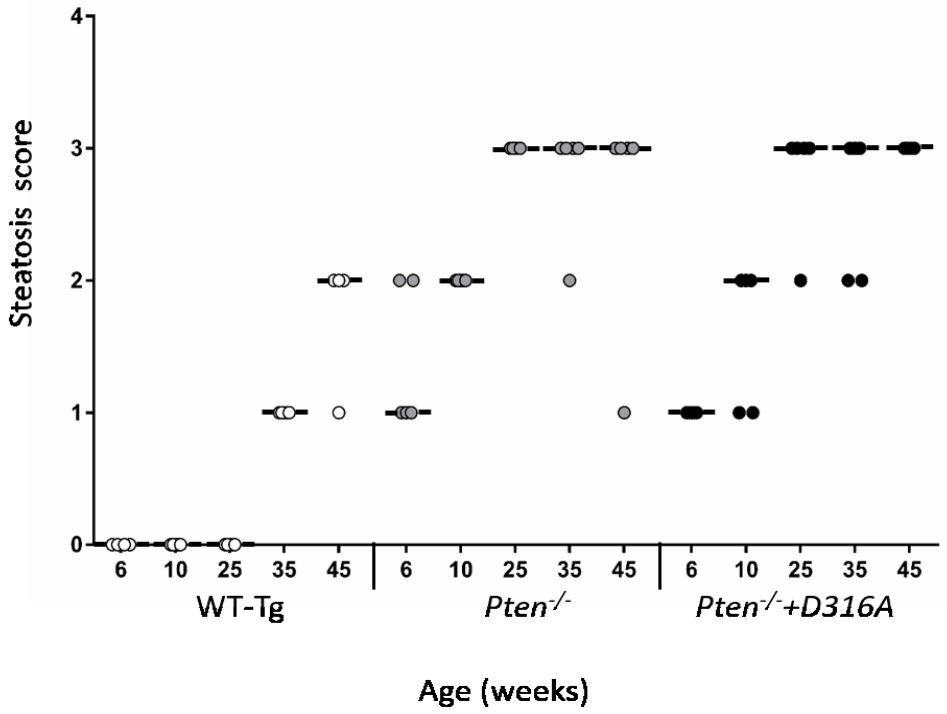


***Figure 4.5 – Histopathological hepatic steatosis scores for WT-Tg, Pten$^{-/-}$ and Pten$^{-/-}$+D316A mice.*** *Scores at different time-points, calculated by an external expert pathologist (Dr G.Bottcher, Astrazeneca, Sweden). Results shown are from 4-5 different mice of each genotype at each time point, with the median for each group shown as a horizontal black line.*

more macrovesicular (**Figure 4.6**). This is in-keeping with the findings of reduced triglyceride and cholesterol accumulation in liver from *Pten$^{-/-}$+D316A* relative to *Pten$^{-/-}$* mice. Together these results suggest that progression of steatosis in mice with liver specific Pten loss is slowed in the presence of increased hepatic AMPK activity.

*Pten$^{-/-}$* and *Pten$^{-/-}$+D316A* mice both developed hepatomegaly and had significantly higher liver weights and liver to bodyweight ratios from 6 weeks of age compared to non-steatotic WT-Tg mice (**Figure 4.7**). However, despite the lipid content of *Pten$^{-/-}$+D316A* liver being significantly lower than that of *Pten$^{-/-}$* liver from 6 weeks of age onwards, no differences in liver weights or liver to body weight ratios were observed between these two genotypes until 45 weeks of age. Liver weights and liver to bodyweight ratios at 45 weeks were lower in *Pten$^{-/-}$+D316A* than *Pten$^{-/-}$* mice (5.57 ± 0.276 v 6.77 ± 0.307 and 0.16 ± 0.007 v 0.2 ± 0.0095 respectively). This difference was likely due to reduced tumour burden in *Pten$^{-/-}$+D316A* liver (discussed further below).

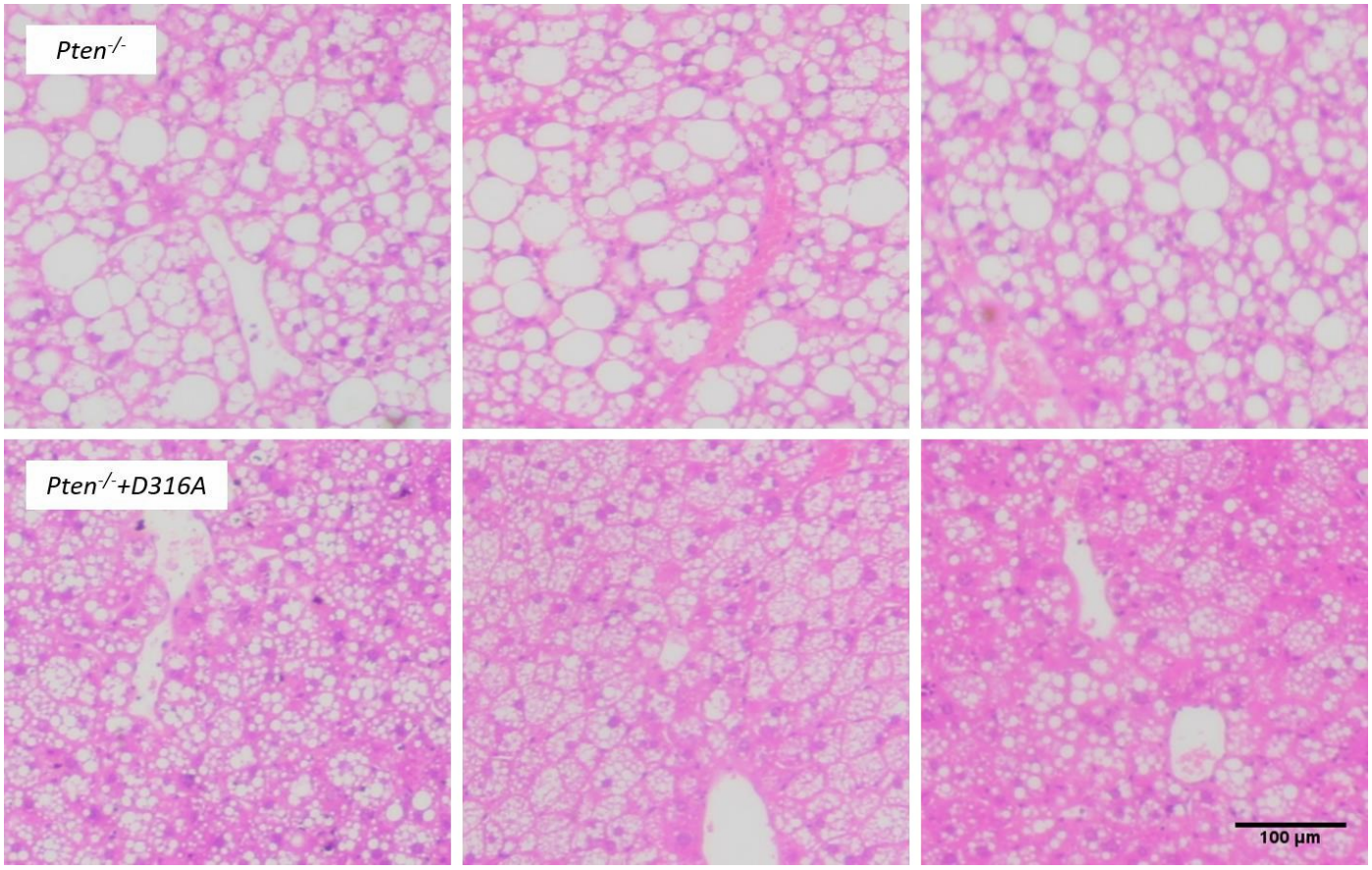


***Figure 4.6 - Haematoxylin and eosin stained liver sections from 25 week old Pten$^{-/-}$ and Pten$^{-/-}$+D316A mice.*** *Three examples from each genotype.*

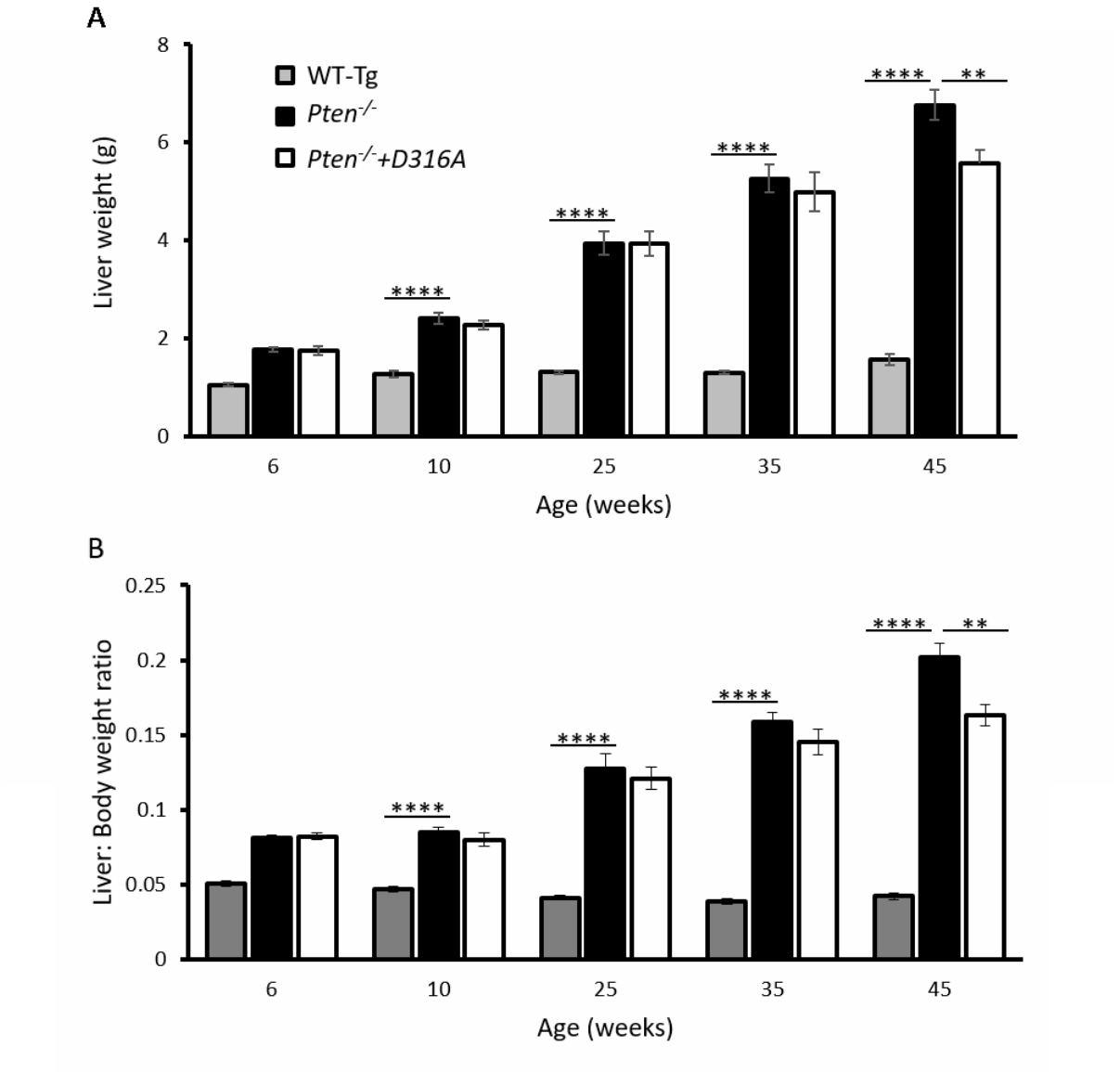


***Figure 4.7 – Liver weight measurements in WT-Tg, Pten$^{-/-}$ and Pten$^{-/-}$+D316A mice of different ages.*** ***(A)*** *Liver weights and* ***(B)*** *liver to bodyweight ratios. Results shown are mean +/- S.E.M. from n = 4-11 for WT-Tg, n = 7-19 for Pten$^{-/-}$ and n = 8-24 for Pten$^{-/-}$+D316A respectively, **p<0.01 and ****p<0.0001; t-test.*

To determine if the differences in steatosis between *Pten$^{-/-}$* and WT-Tg and *Pten$^{-/-}$+D316A* and *Pten$^{-/-}$* mice were due to variations in *de novo* lipogenesis, fatty acid synthesis rates in primary hepatocytes from WT-Tg, *Pten$^{-/-}$* and *Pten$^{-/-}$+D316A* mice were assessed. This was achieved by measuring incorporation of radiolabelled sodium acetate into lipid and for each genotype lipogenesis was assessed in the presence and absence of the direct AMPK activator 991. Fatty acid synthesis was increased more than 3 fold (3.34 ± 0.364) in hepatocytes from *Pten$^{-/-}$*

relative to WT-Tg mice (**Figure 4.8**). However, lipogenesis rates were attenuated in *Pten*$^{-/-}$ *+D316A* relative to *Pten*$^{-/-}$ hepatocytes and in 991 treated *Pten*$^{-/-}$ and *Pten*$^{-/-}$*+D316A* cells relative to their untreated counterparts. Together these results indicate that liver specific Pten knockout upregulates hepatic lipogenesis but that this effect is reduced in the presence of increased hepatic AMPK activity.

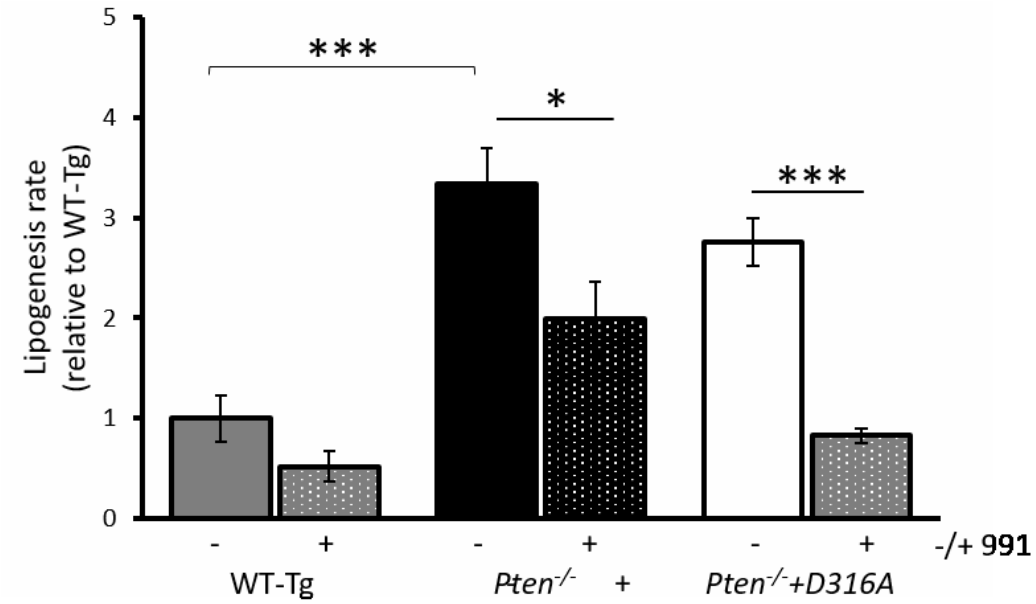


***Figure 4.8 – Rates of fatty acid synthesis in hepatocytes from WT-Tg, Pten$^{-/-}$ and Pten$^{-/-}$ +D316A mice, under basal conditions and following treatment with 10µl of the direct AMPK activator 991.*** *Incorporation of 14C acetate into lipid. Methods – see* ***section 2.2.8.*** *Results shown are relative to WT-Tg and are mean ± S.E.M. from at least 4 independent experiments, **p<0.01 and ***p<0.001; t-test.*

## 4.4 Steatohepatitis in mice with liver specific Pten loss attenuated in the presence of increased hepatic AMPK activity

There is a lack of non-invasive measures for assessing liver damage and inflammation in NAFLD, however serum levels of liver alkaline phosphatase (ALP) and transaminases are often elevated in patients with the disease (Alkhouri and Feldstein 2016). We therefore measured serum ALP and alanine and aspartate aminotransferase (ALT and AST) levels in *Pten*$^{-/-}$ and *Pten*$^{-/-}$*+D316A* mice at different stages of disease progression and compared them to levels in 45 week old WT-Tg mice. From 25 weeks of age, serum ALP, ALT and AST levels in *Pten*$^{-/-}$ and *Pten*$^{-/-}$*+D316A* mice were raised relative to those in WT-Tg controls (**Figure 4.9**). However, as with steatosis, elevation of serum ALP, ALT and AST levels was attenuated in mice with increased hepatic AMPK activity (*Pten*$^{-/-}$*+D316A*) implying their livers were less damaged and inflamed.

NASH is a histological diagnosis and it was therefore important to assess histologically the liver injury and inflammation seen in this model. An external expert pathologist graded steatosis, hepatocyte ballooning and lobular inflammation seen in H&E stained liver sections from WT-Tg, *Pten*$^{-/-}$ and *Pten*$^{-/-}$*+D316A* mice of different ages (**Figure 4.10**). These grades were then adapted and combined to give a NAFLD activity score (NAS - **Figure 1.11**) for each sample. Mean NASs for *Pten*$^{-/-}$ liver were higher than those for WT-Tg sections and this difference was significant at all time points except 45 weeks of age. There was also a trend towards lower NASs for *Pten*$^{-/-}$*+D316A* relative to *Pten*$^{-/-}$ liver, however this difference was not significant.

Given that serum markers of liver damage and inflammation (ALP, ALT and AST) were markedly reduced in *Pten*$^{-/-}$*+D316* relative to *Pten*$^{-/-}$ mice, it is likely that the trend towards a reduced NAS score seen in mice with increased hepatic AMPK activity was real. Although it was possible, from the small numbers of slides examined for each age/genotype, to distinguish presence/absence of steatohepatitis, the numbers were insufficient to determine differences in NASH severity. As previously described, accurate assessment of background liver tissue at 45 weeks of age, was complicated by tumour burden, particularly in *Pten*$^{-/-}$ mice.

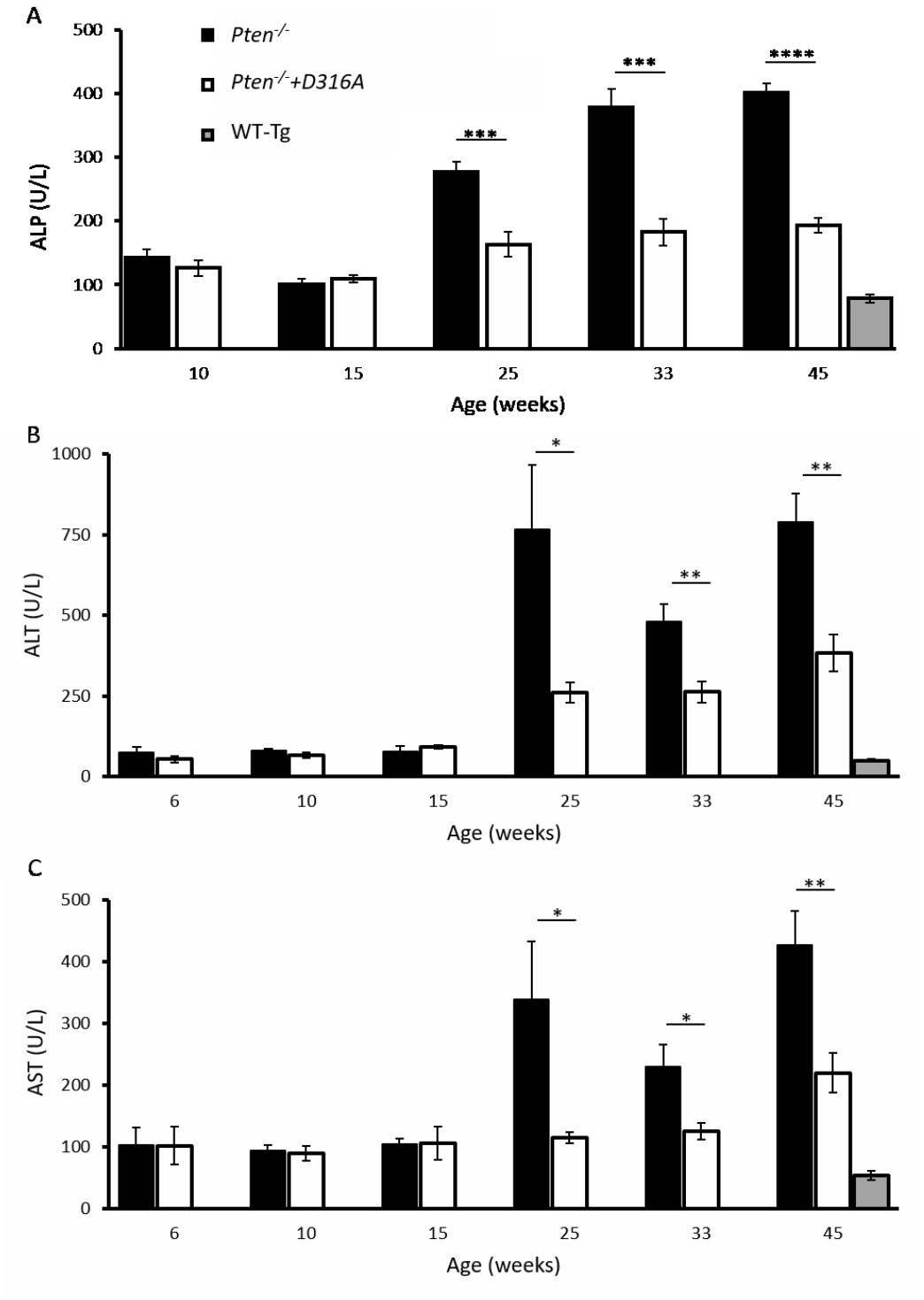


***Figure 4.9 – Serum liver damage and inflammation markers in Pten$^{-/-}$ and Pten$^{-/-}$ +D316A mice of different ages and 45 week old WT-Tg mice.*** *Serum levels of* ***(A)*** *liver alkaline phosphatase (ALP),* ***(B)*** *alananine aminotransferase (ALT) and* ***(C)*** *aspartate aminotransferase (AST). Methods see* ***section 2.2.19.*** *Results shown are mean ± S.E.M, from n≥6 for each genotype/time-point, *p<0.05, **p<0.01, ***p<0.001, and ****p<0.0001; t-test.*

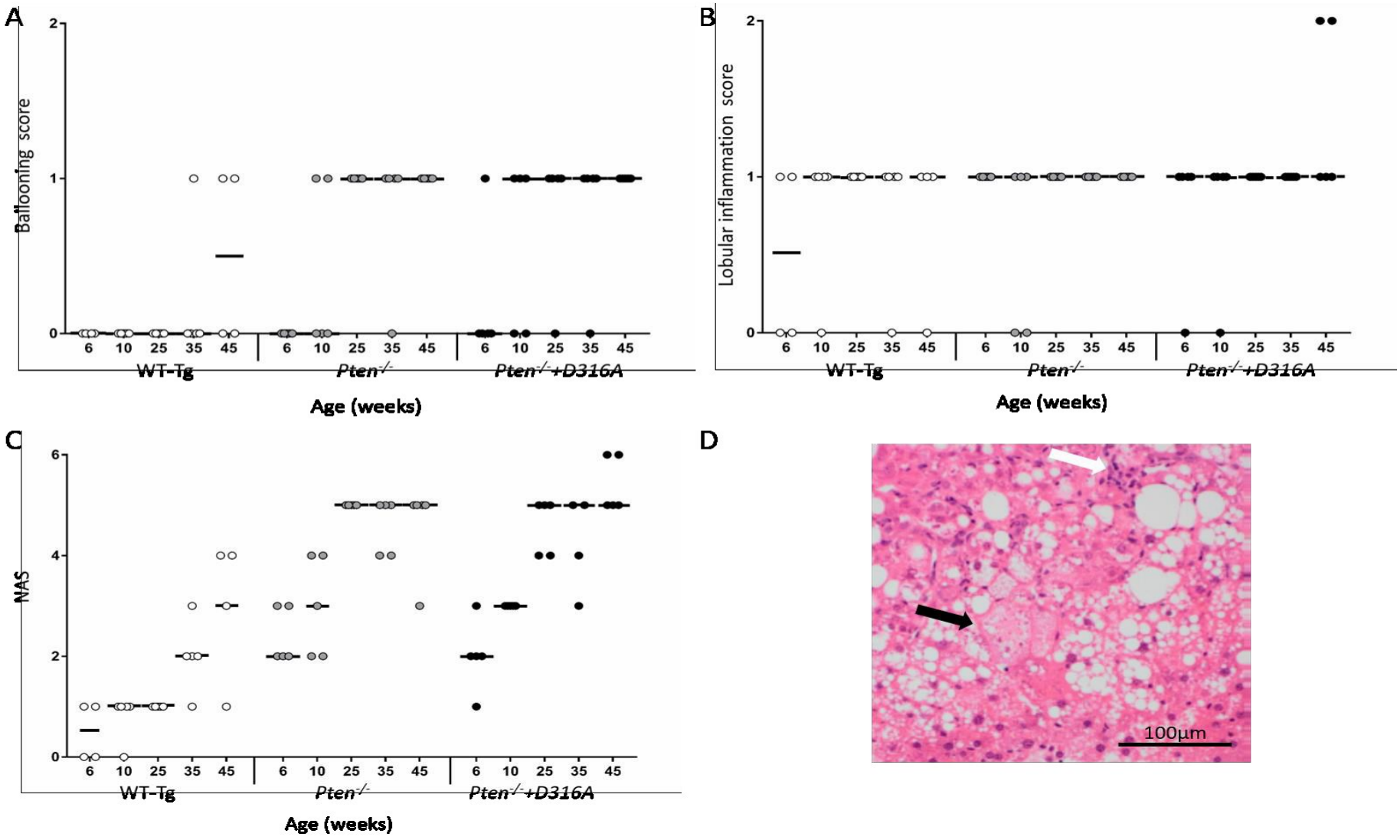


***Figure 4.10 - Histological assessment of NAFLD activity in WT-Tg, Pten$^{-/-}$ and Pten$^{-/-}$+D316A mice.***

***Figure 4.10 - Continued (A)*** *Hepatocyte ballooning scores,* ***(B)*** *lobular inflammation scores and* ***(C)*** *total NAFLD activity scores (NAS – which incorporate evaluation of steatosis, hepatocyte ballooning and lobular inflammation) at different time points, calculated by an external expert pathologist (Dr G.Bottcher, Astrazeneca, Sweden). Results shown are from 4-5 different mice of each genotype at each time point, with the median for each group shown as a horizontal line.* ***(D)*** *Examples of ballooned hepatocytes (black arrowhead) and inflammatory infiltrate (white arrowhead).*

Some lipid species may be more lipotoxic than others (Listenberger et al. 2003), indeed accumulation of triglycerides in NAFLD is likely to be a protective mechanism which limits exposure to more damaging free fatty acids (Malhi and Gores 2008). To determine if differences in fatty acid composition were responsible for the reduced liver injury and inflammation seen in mice with increased hepatic AMPK activity, mass spectrometry was performed by Dr A. Kerimi, Dr L. Abranko and Prof. G. Williamson (University of Leeds, UK) on normal WT-Tg, steatotic Pten$^{-/-}$ and Pten$^{-/-}$+D316A mouse liver (**Table 4.2**).

Saturated and mono-unsaturated fatty acids (MUFAs – except 10:1) were increased whilst poly-unsaturated fatty acids (PUFAs – C10:2, C16:2 and C18:2) were mostly decreased in liver from 6 week old *Pten*$^{-/-}$ relative to WT-Tg mice (**Table 4.2**). Saturated (except C2 and C14) and mono-unsaturated (except C12:1) fatty acids continued to be elevated in liver from 10 week old *Pten*$^{-/-}$ relative to WT-Tg mice, but by this time only one PUFA (C16:2) was lower in *Pten*$^{-/-}$ compared to WT-Tg liver.

Saturated (except C2) and mono-unsaturated fatty acids (MUFAs) were significantly less raised in liver from 6 week old *Pten*$^{-/-}$*+D316A* relative to *Pten*$^{-/-}$ mice (**Table 4.2**). Interestingly, those PUFAs that were decreased in liver from 6 week old *Pten*$^{-/-}$ relative to WT-Tg mice (and C12:2) were further reduced in *Pten*$^{-/-}$*+D316A* liver (C12:2 and C16:2 significantly so). However, these effects of increased hepatic AMPK activity were essentially lost by 10 weeks of age. By this time point fatty acid composition of *Pten*$^{-/-}$ and *Pten*$^{-/-}$*+D316A* mouse liver was very similar, apart from the unsaturated fatty acids C18 and C20 which remained lower in *Pten*$^{-/-}$*+D316A*, relative to *Pten*$^{-/-}$ liver.

Based upon these findings it appears that absence of Pten in the liver promotes unsaturated fatty acid and MUFA over PUFA synthesis and presence of increased hepatic AMPK activity delays accumulation of fatty acids across the board. However, the benefit of the latter is largely lost by 10 weeks of age.

| Saturated fatty acids | 6 weeks | | 10 weeks | |
|---|---|---|---|---|
| | *Pten*$^{-/-}$ v WT-Tg | *Pten*$^{-/-}$*+D316A* v *Pten*$^{-/-}$ | *Pten*$^{-/-}$ v WT-Tg | *Pten*$^{-/-}$*+D316A* v *Pten*$^{-/-}$ |
| C2 | ↑ | → | → | → |
| C4 | ↑ | ↓ | ↑ | → |
| C6 | ↑ | ↓ | ↑ | → |
| C8 | ↑ | ↓ | ↑ | → |
| C10 | ↑ | ↓ | ↑ | → |
| C12 | ↑ | ↓ | ↑ | → |
| C14 | ↑ | ↓ | → | → |
| C16 | ↑ | ↓ | ↑ | → |
| C18 | ↑ | ↓ | ↑ | ↓ |
| C20 | ↑ | ↓ | ↑ | ↓ |

| MUFAs | 6 weeks | | 10 weeks | |
|---|---|---|---|---|
| | *Pten*$^{-/-}$ v WT-Tg | *Pten*$^{-/-}$*+D316A* v *Pten*$^{-/-}$ | *Pten*$^{-/-}$ v WT-Tg | *Pten*$^{-/-}$*+D316A* v *Pten*$^{-/-}$ |
| C10:1 | → | → | ↑ | → |
| C12:1 | ↑ | ↓ | → | → |
| C14:1 | ↑ | ↓ | ↑ | → |
| C16:1 | ↑ | ↓ | ↑ | → |
| C18:1 | ↑ | ↓ | ↑ | ↓ |

| PUFAs | 6 weeks | | 10 weeks | |
|---|---|---|---|---|
| | *Pten*$^{-/-}$ v WT-Tg | *Pten*$^{-/-}$*+D316A* v *Pten*$^{-/-}$ | *Pten*$^{-/-}$ v WT-Tg | *Pten*$^{-/-}$*+D316A* v *Pten*$^{-/-}$ |
| C10:2 | ↓ | → | → | → |
| C12:2 | → | ↓ | → | → |
| C14:2 | → | → | → | → |
| C16:2 | ↓ | ↓ | ↓ | → |
| C18:2 | ↓ | → | → | → |

| ↑Increased | ↓Decreased |
|---|---|

***Table 4.2 - Summary of differences in fatty acid composition of liver WT-Tg v Pten$^{-/-}$ and Pten$^{-/-}$+D316 v Pten$^{-/-}$ mice at 6 and 10 weeks of age***. *Mass-spectrometry analysis performed by Dr A. Kerimi, Dr L. Abranko, & Prof. G. Williamson (University of Leeds, UK). MUFA = monounsaturated fatty acid and PUFA = polyunsaturated fatty acid.*

## 4.5 Hepatic fibrosis in mice with liver specific Pten loss unaffected by increased hepatic AMPK activity

To evaluate fibrosis, sections of liver from 25, 35 and 45 week old *Pten*$^{-/-}$ and *Pten*$^{-/-}$*+D316A* and 25 week old WT-Tg mice were stained using picrosirius red (**Figure 4.11 A**). Sections were then imaged under polarised light to allow quantification of staining (**Figure 4.11 B** & **C**). Periductal and pericellular staining were seen on all samples, regardless of age or genotype. Whereas staining of *Pten*$^{-/-}$ liver sections was similar to that of WT-Tg ones at 25 weeks of age, it was significantly increased in *Pten*$^{-/-}$ liver by 35 weeks of age. However, although staining in 35 week *Pten*$^{-/-}$ liver was increased (relative to WT-Tg) it was not extensive, suggesting that fibrosis is not a key feature of the hepatic Pten loss model of NAFLD.

No differences in picrosirius red staining were seen between *Pten*$^{-/-}$ and *Pten*$^{-/-}$*+D316A* liver sections at 35 weeks, implying that fibrosis development was not influenced by increased hepatic AMPK activity. By 45 weeks of age large portions of liver sections were occupied by tumour, especially those from *Pten*$^{-/-}$ mice and some of the tumours were fibrous (**Figure 4.11 A** – Black arrow). It was therefore not possible to assess fibrosis in background non-tumourous tissue at this time-point, using this method.

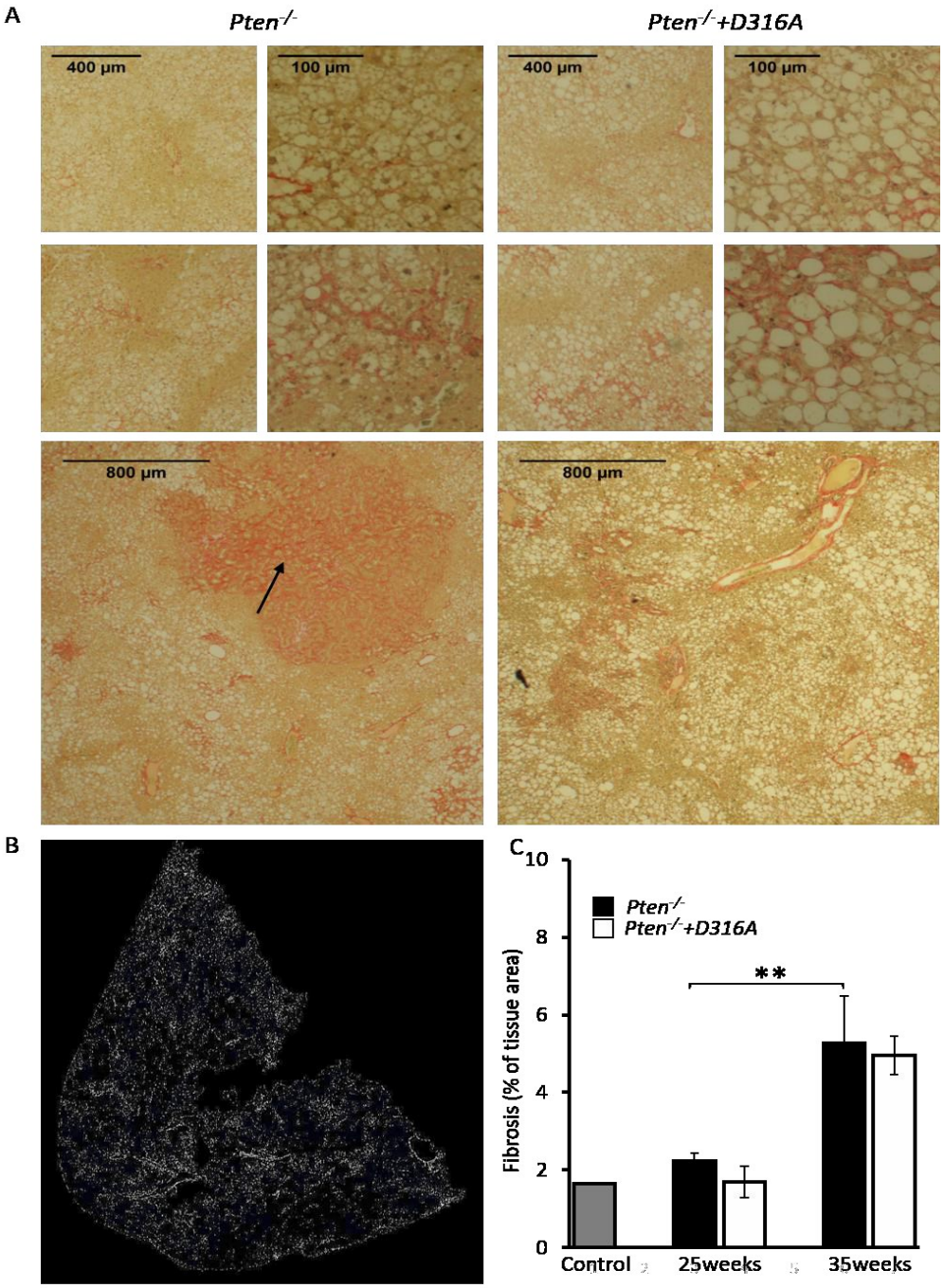


***Figure 4.11 – Picrosirius red staining of liver sections from WT-Tg, Pten$^{-/-}$ and Pten$^{-/-}$+D316A mice, to assess fibrosis.*** ***(A)*** *Liver sections from Pten$^{-/-}$ (left) and Pten$^{-/-}$+D316A (right) mice at 25 (top 4 images) 35 (middle 4 images) and 45 (bottom 2 images) weeks of age stained with picrosirius red. Black arrow indicating tumour.* ***(B)*** *Example of picrosirius red stained liver under polarised light.* ***(C)*** *Quantification of collagen fibre picrosirius red staining using polarised light imaging. Methods – see* ***section 2.2.22.*** *Results shown are mean +/- S.E.M. from n = 3-4 per genotype, **p<0.01; t-test. Control = WT-Tg at 25 weeks.*

## 4.6 Tumour development in mice with liver specific Pten loss, slowed in the presence of increased hepatic AMPK activity

Liver ultrasound scanning (USS) was used to evaluate the effects of liver specific AMPK activation on liver tumour development. Pilot USS studies demonstrated that hepatic steatosis could be clearly visualised in all *Pten*$^{-/-}$ mice from 10 weeks of age (**Figure 4.12**). Few mice developed liver tumours before 25 weeks of age and all had evidence of tumours by 45 weeks. Subsequently, a cohort of 13 *Pten*$^{-/-}$ and 13 *Pten*$^{-/-}$*+D316A* mice was established and their livers were scanned regularly from 25 weeks of age until 45 weeks, at which time surviving animals were culled and their livers assessed for tumours.

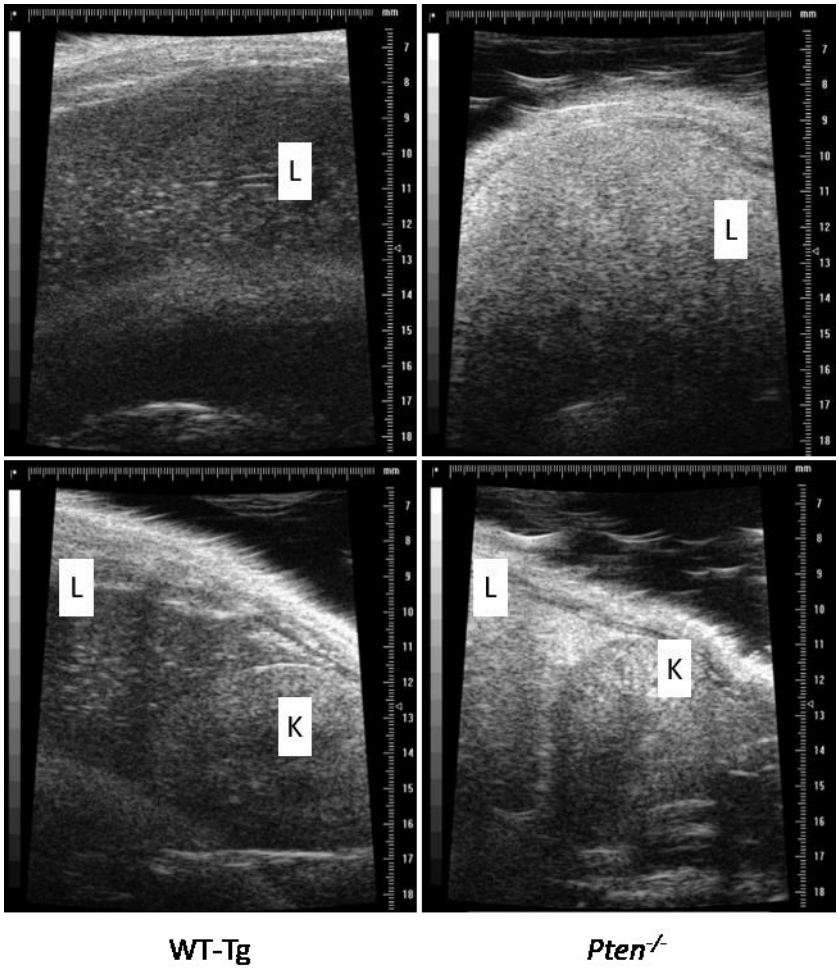


***Figure 4.12 – Ultrasound images of 10 week old normal WT-Tg (left) and steatotic Pten$^{-/-}$ (right) mouse livers.*** *Normal liver has similar echogenicity to kidney. Steatotic liver is hyperechoic (white) relative to normal liver and kidney. L=Liver, K=Kidney.*

Ninety-two percent of *Pten*$^{-/-}$ and 100% of *Pten* $^{-/-}$*+D316A* mice were tumour free at the start of scanning and all mice had developed tumours by 45 weeks of age. However, tumour onset was delayed in *Pten*$^{-/-}$*+D316A* relative to *Pten*$^{-/-}$ mice. At 37 and 41 weeks significantly fewer *Pten*$^{-/-}$*+D316A* mice had developed tumours than *Pten*$^{-/-}$ animals (p=0.015 and p=0.036 respectively). These differences in tumour free survival are illustrated in **Figure 4.13**.

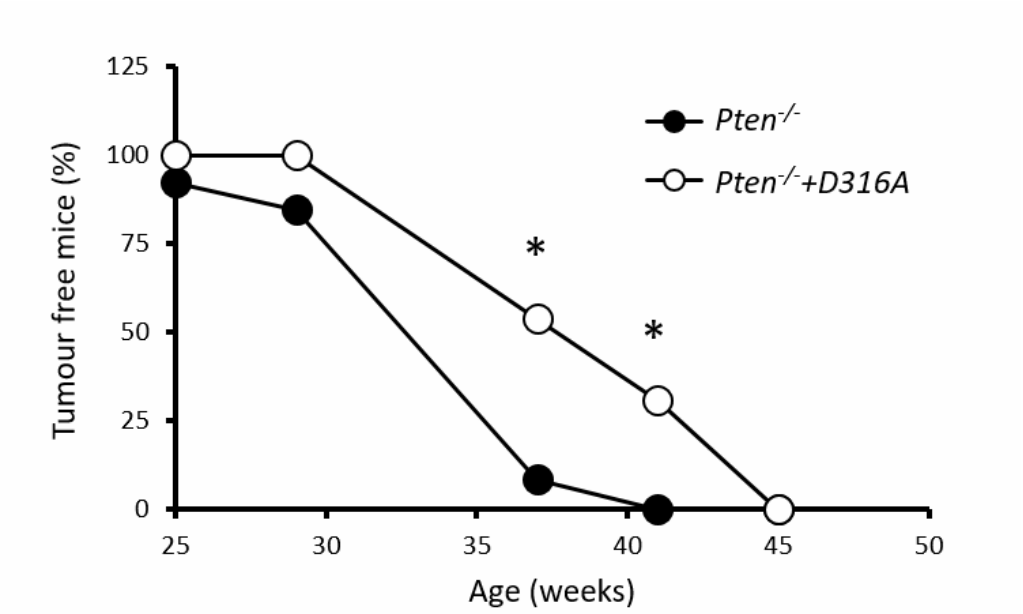


***Figure 4.13 - Tumour free survival in Pten*$^{-/-}$ *and Pten*$^{-/-}$*+D316A mice.*** *Presence of tumour assessed using liver ultrasound scanning from 25 weeks of age. Results from n=13 per genotype, *p<0.05, chi-squared test.*

Each time a mouse liver was scanned, in addition to determining whether tumours were present, the number and diameter of tumours seen was recorded. For welfare reasons, 5 of the 13 *Pten*$^{-/-}$ mice in the USS cohort were culled or harvested before their 45 week scan. Furthermore, in 4 instances it was not possible to identify and measure individual tumours on ultrasound as tumours had coalesced and/or the architecture of the liver was too distorted. Hence, tumour number and diameter data were from only 10, 9 and 7 *Pten*$^{-/-}$ mice at 37, 41, and 45 weeks respectively and so it is likely that means for this genotype were underestimated. Despite this, at all time points *Pten*$^{-/-}$*+D316A* mice had fewer tumours and this difference was significant from 37 weeks of age onwards (**Figure 4.14 A**). Furthermore, in order to give an indication of total tumour volume, the sum of the diameters of all the tumours seen on each USS was calculated and this figure too was lower in *Pten*$^{-/-}$*+D316A*

relative to *Pten*$^{-/-}$ mice, from 33 weeks of age onwards (**Figure 4.14 B**). **Figure 4.15** illustrates the difference in tumour development, seen on USS, between *Pten*$^{-/-}$ and *Pten*$^{-/-}$*+D316A* mice.

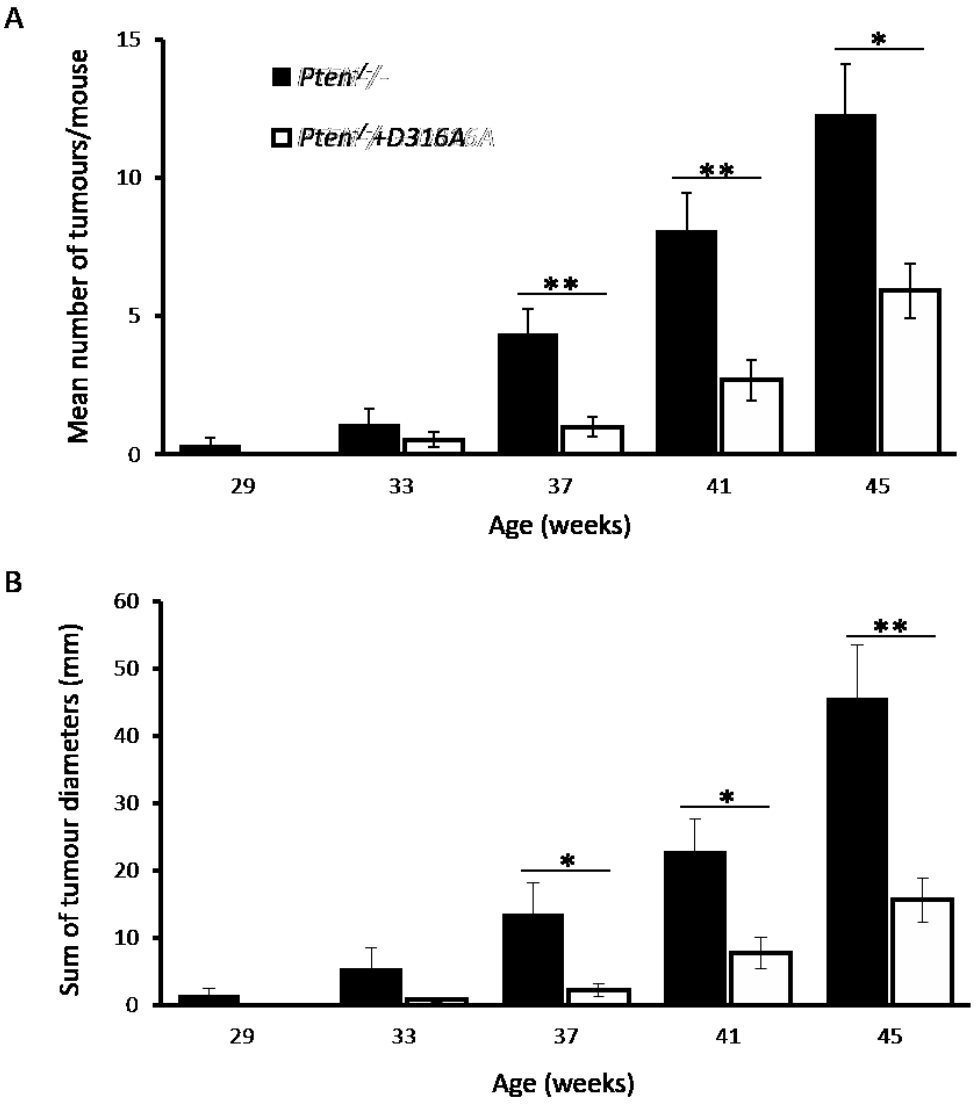


***Figure 4.14 – Tumour number and sum of tumour diameters in Pten$^{-/-}$ and Pten$^{-/-}$+D316A mice.*** *Ultrasound scanning used to count and measure diameters of tumours. Results shown are mean ± S.E.M. from n=7-13, *p<0.05, **p<0.01; t-test.*

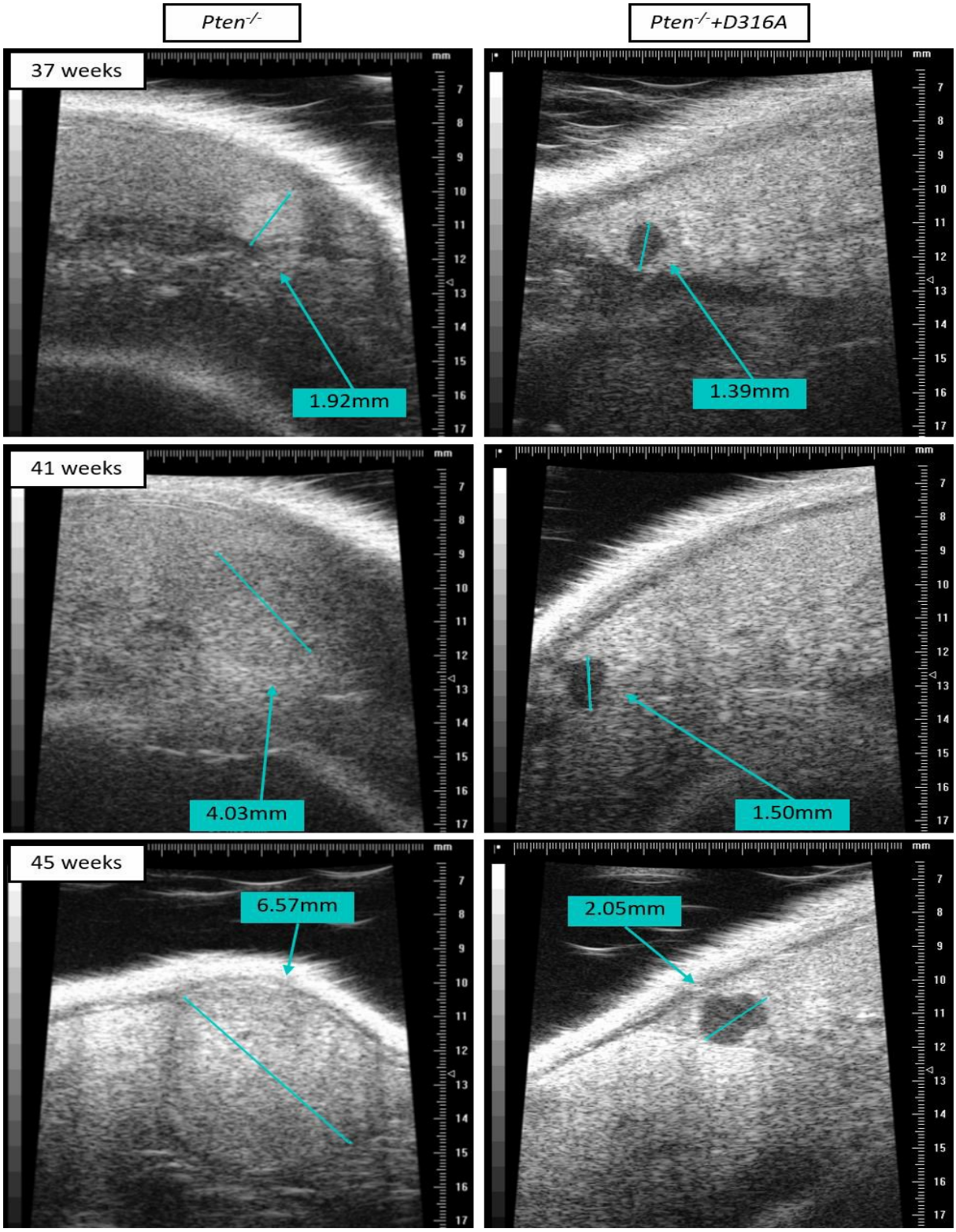


***Figure 4.15 - Ultrasound images following progression of 2 tumours, one in the liver of a Pten$^{-/-}$ mouse (left) and the other in the liver of a Pten$^{-/-}$+D316A mouse (right).*** *One example from each geotype. Images taken at 37, 41 and 45 weeks of age.*

Surviving mice were harvested after their 45 week USS and this provided further evidence that tumour development in mice with liver specific Pten loss was slowed in the presence of increased hepatic AMPK activity. There was a marked difference in the appearance of livers from 45 week old *Pten*$^{-/-}$ and *Pten*$^{-/-}$*+D316A mice*. As **Figure 4.17** clearly illustrates, *Pten*$^{-/-}$ mice had a higher tumour burden than *Pten*$^{-/-}$*+D316A* animals. This difference was also reflected in the liver and liver to bodyweight ratios which were both significantly higher in *Pten*$^{-/-}$ relative to *Pten*$^{-/-}$*+D316A* mice at 45 weeks of age (**Figure 4.7**).

Serum alpha fetoprotein (AFP) levels are monitored as part of HCC screening and are elevated in some but not all hepatocellular cancer models including chemically and genetically induced models as well as xenografts (Sell et al. 1991; Yao et al. 2003; Ambade et al. 2016; Chalasani et al. 2012). AFP levels were measured in serum from mice of all ages to determine if they could provide further quantitative evaluation of tumour burden (**Figure 4.16**). However, serum AFP levels remained within normal range in all mice despite tumour development, suggesting that AFP production is not a feature of tumours in the hepatic Pten loss model.

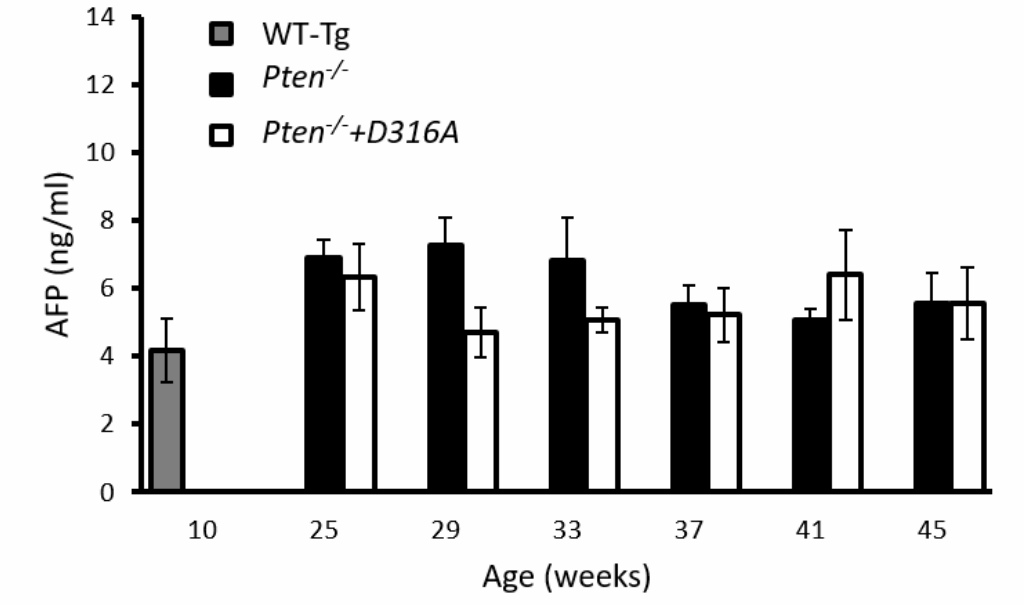


***Figure 4.16 – Serum alpha fetoprotein (AFP) levels in Pten$^{-/-}$ and Pten$^{-/-}$+D316A mice of different ages.*** *Methods – see* ***section 2.2.19****. Results are mean +/- S.E.M. from n= 4 -13.*

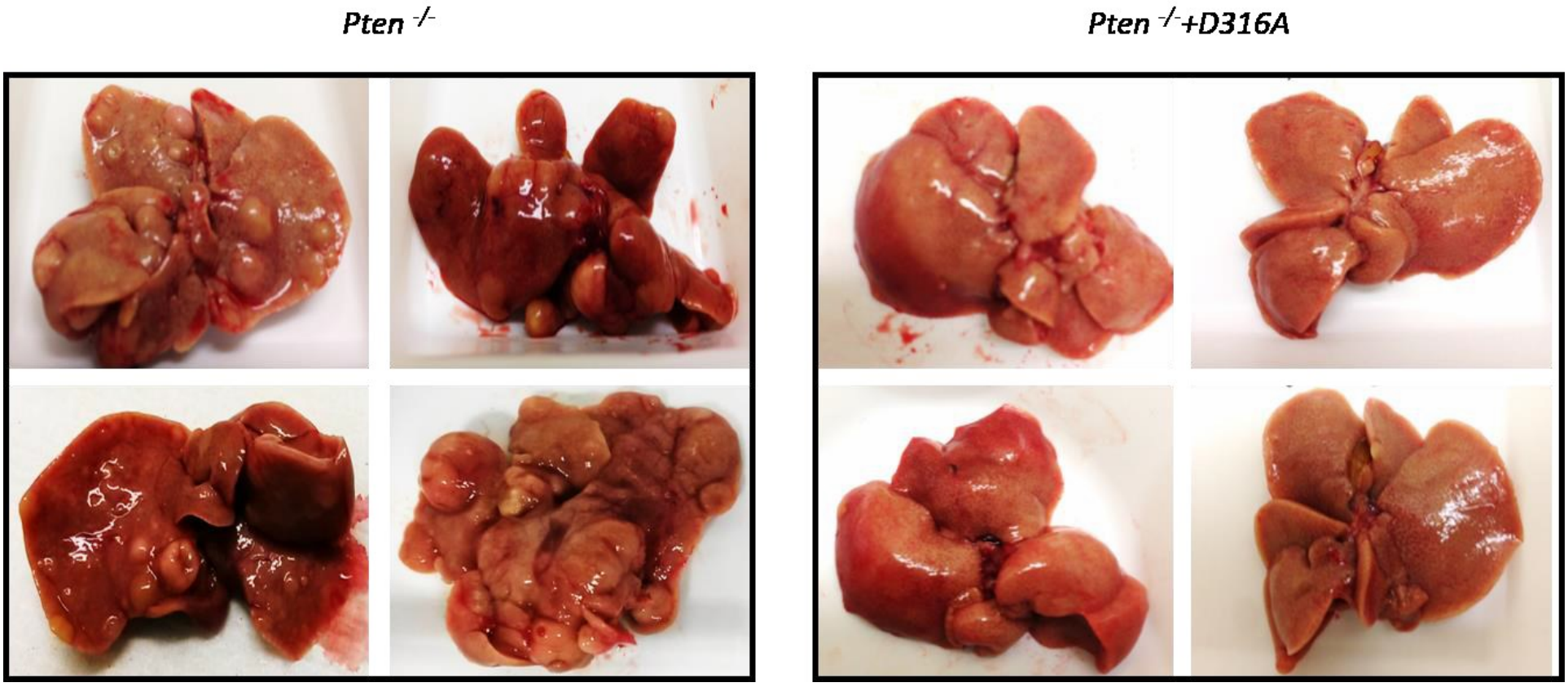


***Figure 4.17 - Livers from Pten$^{-/-}$ and Pten$^{-/-}$+D316A mice at 45 weeks of age.*** *Four examples of each genotype.*

In order to characterise the tumours associated with liver specific Pten loss, H&E stained liver sections from *Pten*$^{-/-}$ and *Pten*$^{-/-}$*+D316A* mice with signs of tumour development were inspected by an external expert pathologist (Dr G Bottcher, AstraZeneca, Sweden). Areas of ductular reaction (**Figure 4.18 A** - proliferation of bile ductules with associated inflammatory cells and stroma) were present in both phenotypes and tumours appeared to derive from these lesions (Richardson et al. 2007). There was significant heterogeneity between tumours both within and between genotypes, with some showing growth patterns resembling cholangiocarcinoma (**Figure 4.18 B**) and others appearances more typical of hepatocellular carcinoma (**Figure 4.18 C**). Immunohistochemical staining (for instance of GPC3, HSP70 and GP and with HepPar-1 and anti-BSEP - see **Table 1.11** and **1.12**) would be helpful in determining whether the tumours seen were malignant and whether they show both

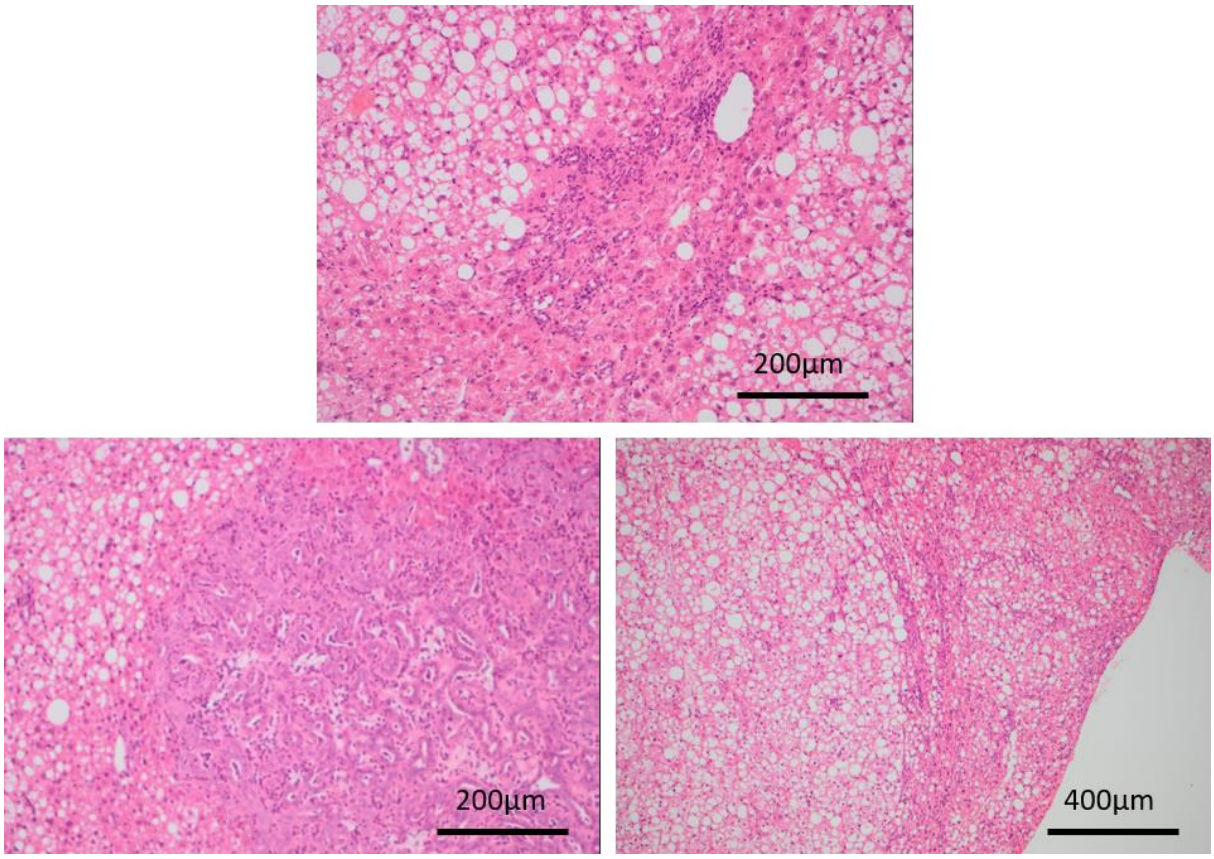


***Figure 4.18 - H&E stained sections of liver, demonstrating tumour development in mice with liver specific Pten loss.*** *Examples of* ***(A)*** *ductular reaction, and tumours with* ***(B)*** *cholangio and* ***(C)*** *hepatocellular carcinoma growth patterns.*

cholangio and hepatoceullar carcinoma differentiation. The observations that tumours tend to occur within areas of ductular reaction and that some tumours have features more typical of cholangioncarcinoma, together suggest that hepatic tumours in mice with liver specific Pten loss may arise from hepatic progenitor cells. From the tumours examined, there was no evidence of a difference in tumour phenotype between *Pten*$^{-/-}$ and *Pten*$^{-/-}$*+D316A* mice, however numbers were small. Also, given the large numbers of lesions within some livers, tumours studied in one histological section may not have been representative of the whole liver.

Given the reduction in tumourgenesis seen in the presence of increased hepatic AMPK activity in mice with liver specific Pten loss and the observation that AMPK inhibits mTORC1 activity through phosphorylation of TSC2, mTOR and RAPTOR (Cheng et al. 2004; Gwinn et al. 2008; Inoki, Zhu, and Guan 2003) one might anticipate that mTORC1 activity, which is enhanced in the absence of Pten (*Pten*$^{-/-}$ mice) would be less so when AMPK is up-regulated (*Pten*$^{-/-}$*+D316A* mice). Pten pathway activity was therefore assessed in WT-Tg, *Pten*$^{-/-}$ and *Pten*$^{-/-}$*+D316A* mice. Reduced Pten protein levels (**Figure 4.19 A** & **B**) and increased phosphorylation of Akt (**Figure 4.19 A** & **C**) were confirmed in liver homogenates from *Pten*$^{-/-}$ and *Pten*$^{-/-}$*+D316A* mice. Pten protein present in liver lysates from *Pten*$^{-/-}$ and *Pten*$^{-/-}$*+D316A* mice likely originates from non-hepatocyte cells (kupffer cells, stellate cells, cholangiocytes etc). S6 is phosphorylated by S6K in response to increased mTORC1 activity. It would therefore be expected that S6 phosphorylation would be increased in mice with defective Pten. In keeping with this, we showed that S6 phosphorylation was increased in *Pten*$^{-/-}$ relative to WT-Tg mouse liver (**Figure 4.19 A** & **D**), although this did not reach significance (probably due to small n numbers). However, there was no difference in S6 phosphorylation between *Pten*$^{-/-}$ and *Pten*$^{-/-}$*+D316A* mice, suggesting that mTORC1 activity was not altered by up- regulation of AMPK.

To determine if the reduced tumour development seen in *Pten*$^{-/-}$*+D316A* relative to *Pten*$^{-/-}$ mice was due to differences in proliferation within the liver, tissue sections were taken from mice at 35 weeks of age and immunohistochemical staining for Ki67 was performed. QuPath software (https://qupath.github.io) was used to count total (DAB stained) and proliferating

(Ki67 stained) cells and the percentage of Ki67 stained cells was then calculated (**Figure 4.20 A**). The percentages of positive cells within sections (total), tumours and background, non-tumourous liver tissue (total minus tumour) were all determined (**Figure 4.20 B** & **C**).

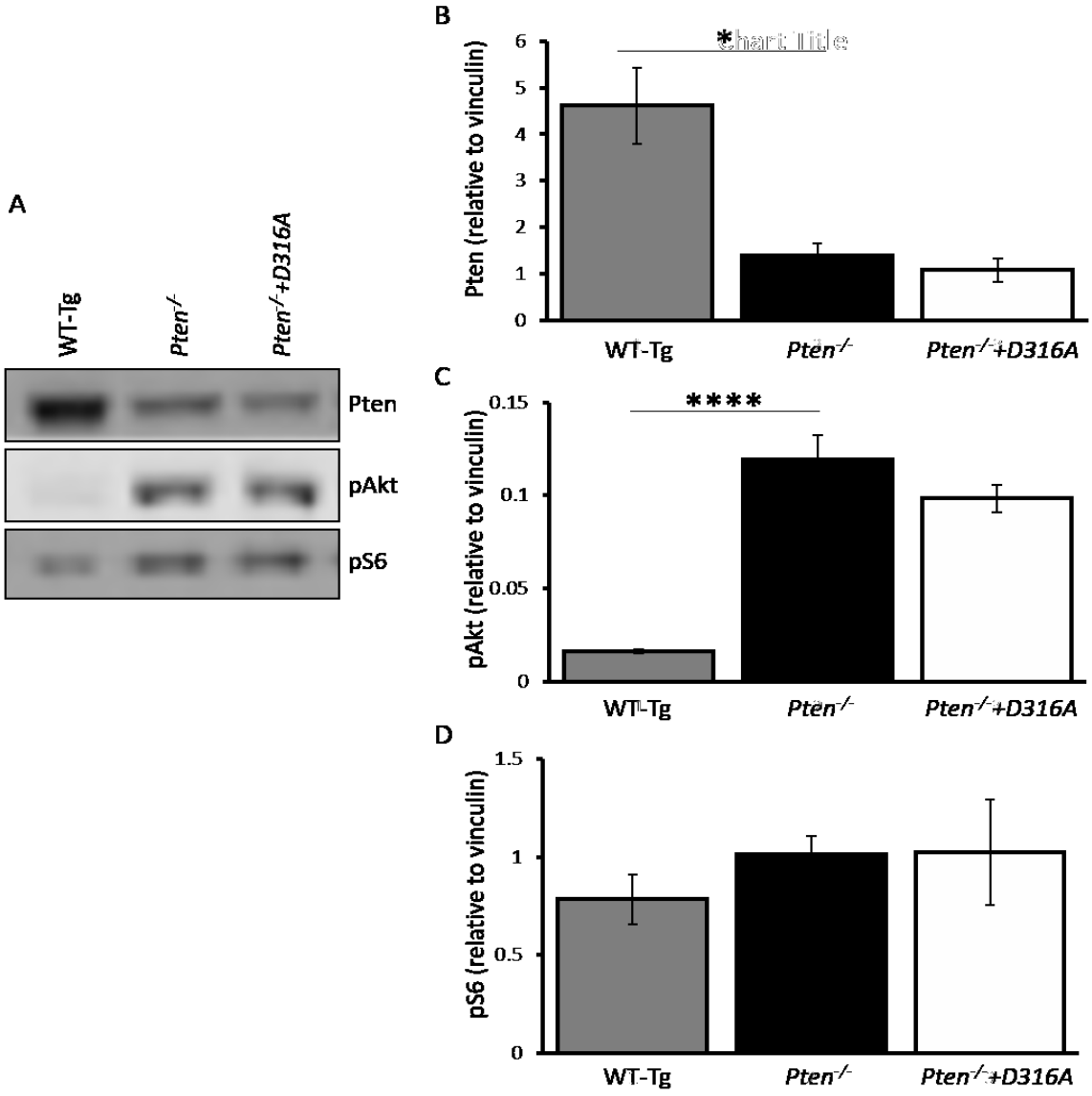


***Figure 4.19 - Pten protein expression and Akt and S6 phosphorylation in WT-Tg, Pten$^{-/-}$ and Pten$^{-/-}$+D316A mouse liver.*** *(A) Examples of liver homogenates probed with the indicated antibodies. pAkt = pAkt$^{Ser473}$, pS6 = pS6$^{Ser240/244}$. (B-D) Quantification of blots, normalised to vinculin expression. Methods – see* ***section 2.2.5****. Results shown are mean ± S/.E.M. from n=4 in each case, *p<0.05 and ****p<0.0001; t-test.*

Unsurprisingly, the number of Ki67 stained cells per section was heavily influenced by the presence or absence of tumour. However, histological sections were not representative of

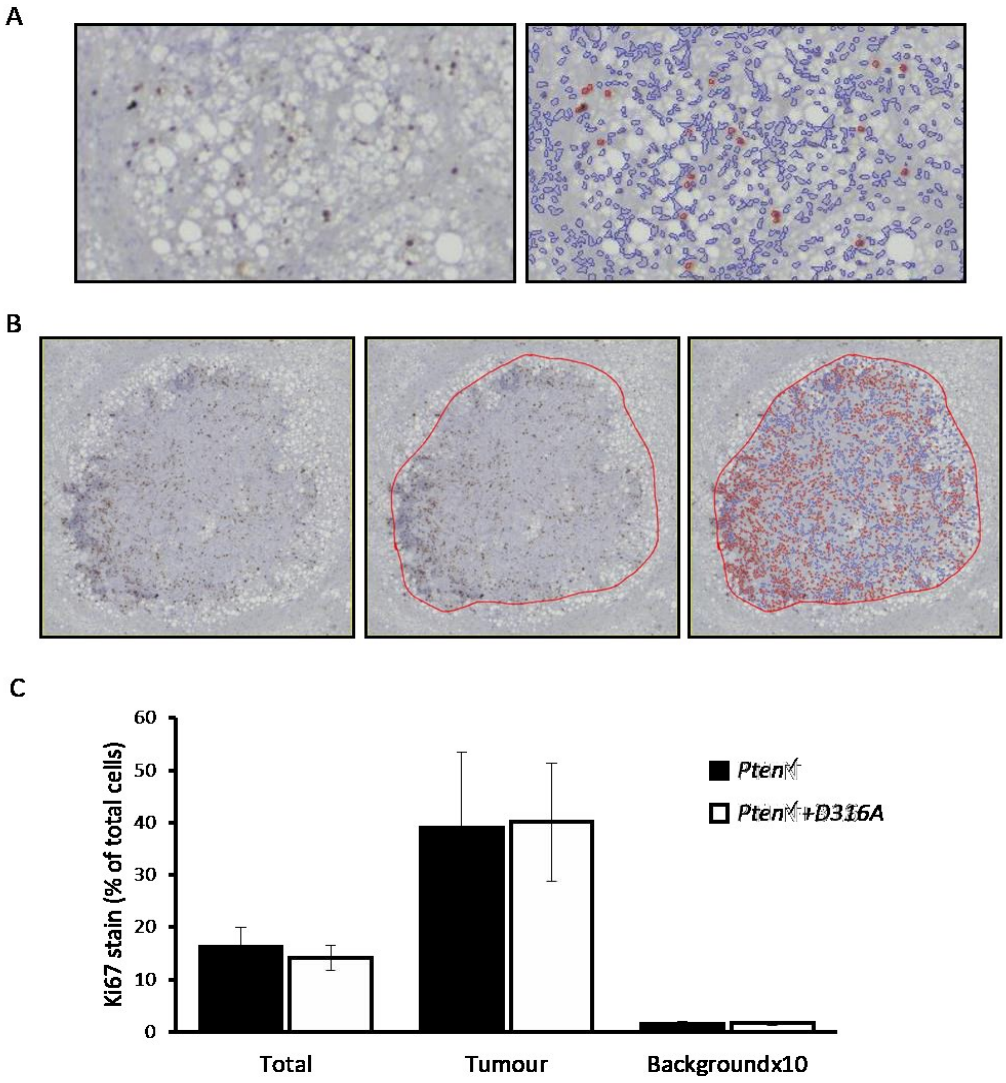


***Figure 4.20 - Ki67 proliferation staining within tumours and background liver tissue of Pten$^{-/-}$ and Pten$^{-/-}$+D316A mice.*** *Immunohistochemical Ki67 staining was performed on liver sections from 35 week old mice.* ***(A)*** *QuPath software (https://qupath.github.io/) was used to count total DAB stained cells (circled in blue on right hand image) and proliferating Ki67 stained cells (circled in red) and the percentage of Ki67 stained cells was calculated.* ***(B)*** *Tumours areas within sections were identified and the percentage of positive cells within these defined regions calculated.* ***(C)*** *Percentages of positive cells within total sections, defined tumour areas and background tissue (calculated after tumour counts subtracted from total counts for each section). Results shown are mean ± S.E.M. from n=5 sections per genotype and each section from a different mouse.*

whole liver so could not be used to verify USS findings in terms of tumour number. There was minimal staining of background non-tumourous liver tissue and this did not differ between *Pten*$^{-/-}$ and *Pten*$^{-/-}$*+D316A* mice. There was marked variation in Ki67 staining between liver tumours from the same mouse or mice of the same genotype, explaining the large error bars seen in **Figure 4.20 C** but mean values for *Pten*$^{-/-}$ and *Pten*$^{-/-}$*+D316A* mice were very similar.

## 4.7 Hepatic gene expression changes in mice with liver specific Pten loss in the presence and absence of increased hepatic AMPK activity

In order to investigate mechanisms by which increased AMPK activity slows NAFLD development in mice with liver specific Pten loss, RNA from the livers of *Pten*$^{-/-}$ and *Pten*$^{-/-}$ *+D316A* mice at 6 and 25 weeks of age and WT-Tg mice at 25 weeks of age, was sequenced. The resulting analysis was compared with mRNA expression data derived from normal or steatotic human liver samples (Ahrens et al. 2013).

Analysis of RNA from human liver identified 446 genes expression of which differed between normal and steatotic tissue. Of these 446 genes, 67 (15%) were also altered, in the same direction (58 up and 9 down-regulated), in 6 week old Pten$^{-/-}$ relative to WT-Tg mouse liver. Expression of these 67 genes, in the human and mouse samples, is illustrated in **Figure 4.21.**

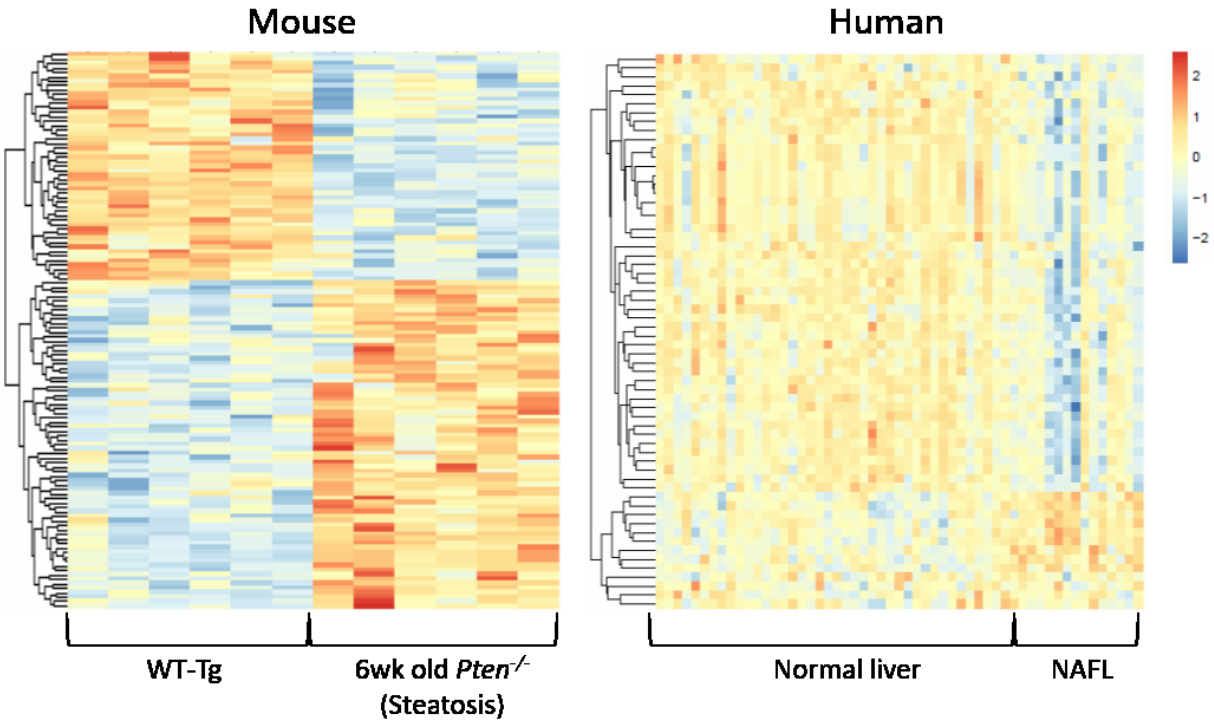


***Figure 4.21 - Heat maps illustrating RNA expression in mouse and human liver samples, for those genes which were altered in the same direction in Pten$^{-/-}$ (relative to WT-Tg) mouse and steatotic (relative to normal) human liver****. Analysis of 6 WT-Tg and 6 Pten$^{-/-}$ mouse and 41 normal and 14 steatotic (human) samples.*

There is some similarity between the expression patterns for mouse and human liver with and without steatosis. Allowing for the difference in species and the fact that human steatosis is induced by both genetic and environmental factors, whereas the mouse model is purely genetic, these findings suggest that from a gene expression perspective mouse liver specific Pten loss is a reasonable model of human NAFLD.

**Figure 4.22** is the principle component analysis (PCA) plot for the RNA sequencing samples from WT-Tg mice and mice with liver specific Pten loss. Analysis identified 3656 named genes at 6 weeks of age and 6614 genes at 25 weeks, expression of which was significantly ($p<0.05$) altered in liver from *Pten*$^{-/-}$ relative to WT-Tg mice (**Table 4.3**). These comparisons evaluate the effects of Pten loss. Similarly, 271 genes at 6 weeks and 256 genes at 25 weeks were changed in *Pten*$^{-/-}$*+D316A* relative to *Pten*$^{-/-}$ mouse liver. These changes (listed in **Appendix A**) reflect the effects of increased AMPK activity and 14 of the altered genes from each age group overlapped. These results demonstrate that absence of PTEN and age impact more upon hepatic gene expression than increased hepatic AMPK activity.

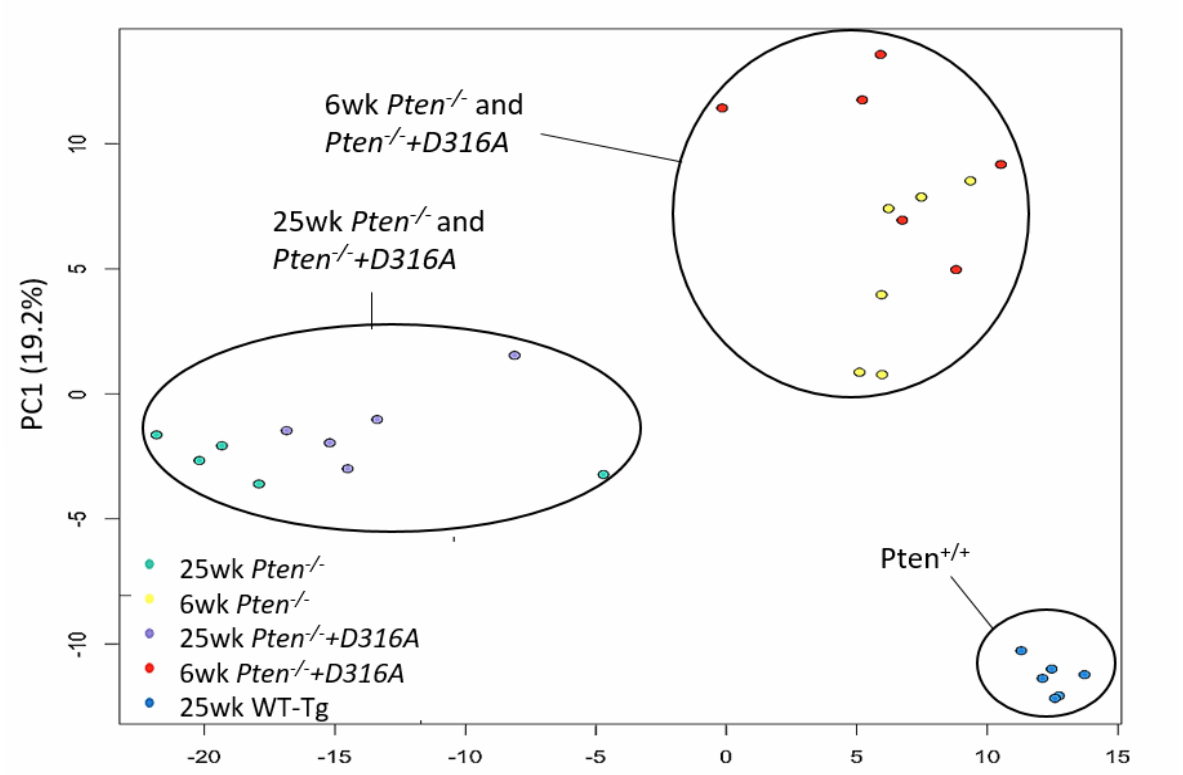


***Figure 4.22 - Principle component analysis for WT-Tg, Pten$^{-/-}$ and Pten$^{-/-}$+D316A mice at 6 and 25 weeks of age.*** *Sequencing was performed on RNA from 5-6 mice for each of the ages/genotypes listed in the legend.*

| Comparison | Age | |
|---|---|---|
| | 6 weeks | 25 weeks |
| ***Pten*$^{-/-}$ v WT-Tg** | 3656 | 6614 |
| ***Pten*$^{-/-}$*+D316A* v *Pten*$^{-/-}$** | 271 | 256 |

***Table 4.3 - Numbers of genes expression of which was significantly altered between genotypes****. Two comparisons repeated at 2 different ages.*

Liver RNA was examined early on (6 weeks of age) to separate the direct effects of Pten loss and AMPK activation on gene expression from their indirect effects, mediated through their impact on steatosis.

Given the exacerbating and relieving effects of Pten loss and increased hepatic AMPK activity respectively on the development of steatosis, expression of 8 common lipogenic genes (listed in **Table 4.4**) was compared in liver from *Pten*$^{-/-}$ v WT-Tg and *Pten*$^{-/-}$*+D316A* v *Pten*$^{-/-}$ mice. Expression of 5 of these genes (Acacβ, Elovl1, mitochondrial Gpa, Thrsp and Scd1) was up-regulated in liver from *Pten*$^{-/-}$ relative to WT-Tg mice. However, expression of all 8 genes was unaltered by increased hepatic AMPK activity.

Gene ontology enrichment analysis was performed on the 271 genes, expression of which was modified by increased AMPK activity at 6 weeks of age and this identified 109 altered pathways. Fourteen of these 109 pathways (12.8% - containing 22 genes) and 40% of the 10 most significantly changed pathways, contained the terms catabolic, metabolic or biosynthesis (**Table 4.5**). Although these pathways are all involved in metabolic processes, the types of metabolism with which they are associated are diverse, making their significance hard to evaluate. Furthermore, only 4 of the 109 pathways significantly altered by increased AMPK activity were involved in lipid metabolism (glycolipid catabolism, ceramide catabolism retinoic acid catabolism and regulation of ceramide biosynthesis) and none of these were directly associated with triglyceride or cholesterol metabolism. Taken together, these results

from 6 week old mice suggest that increased hepatic AMPK activity does not reduce the impact of liver specific Pten loss on steatosis through changes in gene expression.

| Gene (& symbol) | Chow | Fructose | 6 week Pten |
|---|---|---|---|
| **Acetyl-CoA carboxylase (*Acac*)** | ↑Acacβ | → | → |
| **ATP citrate lyase (*Acly*)** | → | → | → |
| **ELOVL protein (*Elovl*)** | → | ↑Elovl7<br>↓Elovl2 | → |
| **Fatty acid synthase (*Fasn*)** | → | → | → |
| **Glycerol-3-phosphate acyltransferase (*Gpa*)** | → | → | → |
| **SPOT14 (*Thrsp)*** | → | → | → |
| **SREBP (*Srebf*)** | → | → | → |
| **Stearoyl-CoA desaturase (*Scd*)** | → | → | → |

***Table 4.4 - Lipogenic gene expression in liver from D316A-Tg relative to WT-Tg mice on a chow or fructose diet and 6 week old Pten$^{-/-}$+D316A compared to Pten$^{-/-}$ mice.*** *SREBP = Sterol regulatory element-binding protein and ELOVL = elongation of very long chain fatty acids.*

| Pathway | Genes in Term | Term Depth | Significance (Elim) |
|---|---|---|---|
| **Glycolipid catabolism** | Galc;Hexb;Naga;Neu1 | 8 | 3.20E-05 |
| **Ceramide catabolism** | Galc;Hexb;Neu1 | 9 | 0.00085 |
| **Retinoic acid catabolism** | Cyp26a1;Cyp26b1 | 11 | 0.00113 |
| **AMP biosynthesis** | Adss;Prps2 | 12 | 0.00186 |
| **Oligosaccharide catabolism** | Hexb;Neu1 | 7 | 0.00507 |
| **Regulation of ceramide biosynthesis** | Pla2g6;Ormdl3 | 10 | 0.00507 |
| **Mannose metabolism** | Man2b1;Man2b2 | 8 | 0.00645 |
| **Nucleotide-sugar biosynthesis** | Cmas;Uap1l1 | 7 | 0.01151 |
| **Carnitine metabolism** | Crat;Slc22a5 | 6 | 0.01151 |
| **N-acetylglucosamine metabolism** | Hexb;Renbp | 7 | 0.01559 |
| **Purine ribonucleoside diphosphate metabolism** | Entpd2;Entpd5;Guk1; Gale | 10 | 0.03348 |
| **5-phosphoribose 1-diphosphate biosynthesis** | Prps2 | 8 | 0.04099 |
| **Heparan sulfate proteoglycan catabolism** | Gpc1 | 9 | 0.04099 |
| **dGDP metabolism** | Guk1 | 12 | 0.04099 |

***Table 4.5 – Metabolic pathways containing genes differentially expressed in Pten$^{-/-}$+D316A v Pten$^{-/-}$ mouse liver.*** *Lipid metabolism pathways highlighted in yellow.*

Given that *Pten* $^{-/-}$ mice develop tumours from 25 weeks of age, RNA was examined at this time point, in order to capture early oncogenic changes in gene expression. A disadvantage of studying liver at this age is the presence of steatohepatitis: Deciphering which gene expression changes in *Pten$^{-/-}$+D316A* relative to the *Pten$^{-/-}$* mice are directly due to increased hepatic AMPK activity and which are due to reduced steatohepatitis (an indirect result of increased hepatic AMPK activity) is challenging.

Gene ontology enrichment analysis, conducted on the 276 genes, hepatic expression of which was modified in *Pten*$^{-/-}$*+D316A* relative to the *Pten*$^{-/-}$ mice at 25 weeks of age, identified 187 altered pathways. More than 20% (39/187) of all these pathways and 60% of the 10 most significantly changed, contained the terms immune or inflammation; the name of an immune cell (leukocyte, macrophage etc); or terms related to cytokine signalling (chemokine, interleukin etc). Pathways with a term depth ≤ 3 were considered too non-specific and therefore excluded from further analysis. The 49 genes involved in the remaining 38 pathways are listed in **Table 4.6**. Expression of the majority of these genes (43/49) was up-regulated in *Pten*$^{-/-}$ relative WT-Tg liver and down-regulated in *Pten*$^{-/-}$*+D316A* compared to *Pten*$^{-/-}$ liver, suggesting that in this context, Pten loss and AMPK activation were having opposing effects on inflammatory and immune gene expression.

Given the marked changes in inflammatory and immune gene expression observed in liver in the absence of Pten and presence of increased AMPK activity, we proceeded to determine the effects of these modifications on fibrotic gene expression. Hepatocellular damage and hepatic stellate cell (HSC) activation are associated with increased collagen (*COL*), smooth muscle actin (*ACTA*), desmin (*DES*) and tissue inhibitor of metalloproteinase (*TIMP*) gene expression (He et al. 2016). We therefore sought to determine whether these genes were among the 6614 significantly altered as a result of Pten loss. Expression of *Sma*, *Des*, 4 *Timp* and 20 *Col* genes was indeed up-regulated in *Pten*$^{-/-}$ relative to WT-Tg liver (**Table 4.7**). However, only 4 of these genes were differentially expressed in *Pten*$^{-/-}$*+D316A* compared to *Pten*$^{-/-}$ liver. *Col 1a2, 6a1* and *6a5* and *Timp 2* expression were all lower in mice with increased hepatic AMPK activity. Together these results suggest that in this context, increased hepatic AMPK activity may have to some extent limited the pro-fibrotic effects of liver specific Pten loss, but, if present, this opposition was small.

| Gene name | Gene symbol | *Pten*$^{-/-}$ v WT-Tg | *Pten*$^{-/-}$*+D316A-Tg* v *Pten*$^{-/-}$ |
|---|---|---|---|
| ATP-binding cassette, sub-family G (WHITE), member 1 | Abcg1 | ↑ | ↓ |
| A disintegrin and metallopeptidase domain 8 | Adam8 | ↑ | ↓ |
| AXL receptor tyrosine kinase | Axl | ↑ | ↓ |
| Complement component 3a receptor 1 | C3ar1 | ↑ | ↓ |
| Cell adhesion molecule 1 | Cadm1 | → | ↓ |
| Chemokine (C-C motif) ligand 5 | Ccl5 | ↑ | ↓ |
| Chemokine (C-C motif) ligand 6 | Ccl6 | ↑ | ↓ |
| CD180 antigen | Cd180 | ↑ | ↓ |
| CD300C molecule 2 | Cd300c2 | ↑ | ↓ |
| CD74 antigen (invariant polypeptide of MHC, class II) | Cd74 | ↑ | ↓ |
| CD79A antigen (immunoglobulin-associated alpha) | Cd79a | ↑ | ↓ |
| CD84 antigen | Cd84 | ↑ | ↓ |
| Coronin actin binding protein 1A | Coro1a | ↑ | ↓ |
| C-reactive protein, pentraxin-related | Crp | ↓ | ↑ |
| Cathepsin S | Ctss | ↑ | ↓ |
| Chemokine (C-X-C motif) ligand 16 | Cxcl16 | ↑ | ↓ |
| Dedicator of cyto-kinesis 2 | Dock2 | ↑ | ↓ |
| Ephrin B1 | Efnb1 | → | ↓ |
| Fc receptor, IgE, high affinity I, gamma polypeptide | Fcer1g | ↑ | ↓ |
| Histocompatibility 2, class II antigen A, alpha | H2-Aa | ↑ | ↓ |
| Histocompatibility 2, class II, locus DMa | H2-DMa | ↑ | ↓ |
| Insulin-like growth factor binding protein 2 | Igfbp2 | → | ↓ |
| Jagged 2 | Jag2 | ↑ | ↓ |
| Kruppel-like factor 2 (lung) | Klf2 | → | ↓ |
| Linker for activation of T cells family, member 2 | Lat2 | ↑ | ↓ |
| Lipoprotein lipase | Lpl | ↑ | ↓ |
| Leupaxin | Lpxn | ↑ | ↓ |

| | | | |
|---|---|---|---|
| Macrophage scavenger receptor 1 | Msr1 | ↑ | ↓ |
| NCK associated protein 1 like | Nckap1l | ↑ | ↓ |
| Nuclear factor of activated T cells 4 | Nfatc4 | ↑ | ↓ |
| NLR family, CARD domain containing 4 | Nlrc4 | ↑ | ↓ |
| Negative regulator of reactive oxygen species | Nrros | ↑ | ↓ |
| Pannexin 1 | Panx1 | ↑ | ↓ |
| Phosphatidylinositol 3-kinase catalytic delta polypeptide | Pik3cd | ↑ | ↓ |
| Phospholipase D2 | Pld2 | ↑ | ↓ |
| Phosphatidylinositol-3,4,5-trisphosphate-dependent Rac | Prex1 | ↑ | ↓ |
| Prostaglandin E receptor 1 (subtype EP1) | Ptger1 | ↑ | ↓ |
| Protein tyrosine phosphatase, receptor type, C | Ptprc | ↑ | ↓ |
| Protein tyrosine phosphatase, receptor type, E | Ptpre | ↑ | ↓ |
| Retinoic acid receptor, gamma | Rarg | ↑ | ↓ |
| Raftlin lipid raft linker 1 | Rftn1 | ↑ | ↓ |
| Spleen focus forming virus (SFFV) proviral integration oncogene | Spi1 | ↑ | ↓ |
| Toll-like receptor 1 | Tlr1 | ↑ | ↓ |
| Toll-like receptor 4 | Tlr4 | ↑ | ↓ |
| Toll interacting protein | Tollip | → | ↑ |
| Triggering receptor expressed on myeloid cells 2 | Trem2 | ↑ | ↓ |
| Ubiquitin associated and SH3 domain containing, B | Ubash3b | ↑ | ↓ |
| Unc-13 homolog D (C. elegans) | Unc13d | ↑ | ↓ |
| V-set immune-regulatory receptor | Vsir | ↑ | ↓ |

***Table 4.6 – Genes from inflammatory and immune pathways differentially expressed in Pten$^{-/-}$+D316A v Pten$^{-/-}$ mouse liver.*** *Direction of change Pten$^{-/-}$ v WT-Tg and Pten$^{-/-}$+D316A v Pten$^{-/-}$ indicated by arrows. MHC = major histocompatibility complex.*

| Gene name | Gene symbol | *Pten*$^{-/-}$ v WT-Tg | | *Pten*$^{-/-}$*+ D316A v Pten*$^{-/-}$ | |
|---|---|---|---|---|---|
| | | Fold change | p Adj | Fold change | p Adj |
| Collage, Type | | | | | |
| **1α1** | Col1a1 | 11.69 | 1.7E-26 | | |
| **1α2** | Col1a2 | 9.74 | 7.5E-32 | 0.522693016 | 0.0427 |
| **3α1** | Col3a1 | 8.26 | 1.7E-23 | | |
| **4α1** | Col4a1 | 3.67 | 2.7E-16 | | |
| **4α2** | Col4a2 | 2.63 | 5.3E-16 | | |
| **4α5** | Col4a5 | 2.73 | 8.9E-06 | | |
| **4α6** | Col4a6 | 2.68 | 4.5E-04 | | |
| **5α1** | Col5a1 | 2.84 | 2.7E-10 | | |
| **5α2** | Col5a2 | 3.83 | 8.5E-10 | | |
| **6α1** | Col6a1 | 3.51 | 4.8E-17 | 0.569771208 | 0.01964 |
| **6α2** | Col6a2 | 4.10 | 6.0E-17 | | |
| **6α3** | Col6a3 | 4.13 | 2.0E-14 | | |
| **6α5** | Col6a5 | 5.83 | 4.8E-11 | 0.415683112 | 0.03948 |
| **6α6** | Col6a6 | 2.24 | 2.0E-03 | | |
| **8α1** | Col8a1 | 2.81 | 5.4E-05 | | |
| **12α1** | Col12a1 | 3.28 | 1.9E-23 | | |
| **14α1** | Col14a1 | 2.48 | 1.0E-11 | | |
| **15α1** | Col15a1 | 2.11 | 2.9E-06 | | |
| **16α1** | Col16a1 | 2.64 | 3.9E-11 | | |
| **18α1** | Col18a1 | 0.71 | 9.3E-07 | | |
| **25a1** | Col25a1 | 0.31 | 2.2E-05 | | |
| **27α1** | Col27a1 | 1.57 | 1.8E-02 | | |
| **Smooth muscle actin** | Acta2 | 2.07 | 1.2E-02 | | |
| **Desmin** | Des | 1.46 | 2.4E-02 | | |
| **Tissue inhibitor of metalloproteinase** | | | | | |
| **1** | Timp1 | 6.24 | 8.6E-12 | | |
| **2** | Timp2 | 2.32 | 1.6E-11 | 0.669352258 | 0.04876 |
| **3** | Timp3 | 3.12 | 7.2E-11 | | |

***Table 4.7 - Fibrotic genes differentially expressed in Pten$^{-/-}$ v WT-Tg and where indicated, Pten$^{-/-}$+D316A v Pten$^{-/-}$ mouse liver.*** *Up-regulated genes highlighted in red and down-regulated genes highlighted in green. p.Adj = adjusted p value.*

## 4.8 Hepatic gene expression changes, under basal conditions and following diet or genetically induced metabolic stress, in the presence of increased hepatic AMPK activity

As well as looking at differential hepatic gene expression in $Pten^{-/-}$+D316A compared to $Pten^{-/-}$ mice at 2 different ages, gene expression changes in D316A-Tg relative to WT-Tg liver from mice on a chow and high fructose diet were also examined (discussed in **section 3.4**). The results of each of these analyses (listed in **Table 4.8**) were then compared (**Figure 4.23**). This identified 5 genes which were up-regulated in the livers of mice with increased hepatic AMPK activity under all conditions (chow diet, high fructose diet and hepatic Pten loss at 6 and 25 weeks of age) and 21 other genes that were up-regulated in 3 of these 4 conditions. These 26 (5 + 21) genes are listed in **Table 4.9** with a brief description of their function. Eight of the 26 genes listed in **Table 4.9** are involved in lysosomal metabolism. They are Ctsa a, l and z, Galc, Hexb, Plin3, Scpep1 and Neu1 . The other genes listed have diverse roles and do not appear to relate to any particular pathway or process.

| Comparison | Number of genes |
|---|---|
| D316A-Tg v WT-Tg on a chow diet | 326 |
| D316A-Tg v WT-Tg on a fructose diet | 241 |
| *$Pten^{-/-}$+D316A v $Pten^{-/-}$* at 6 weeks | 271 |
| *$Pten^{-/-}$+D316A v $Pten^{-/-}$* at 25 weeks | 256 |

***Table 4.8 – Numbers of genes expression of which was significantly altered in the presence of the D316A transgene.***

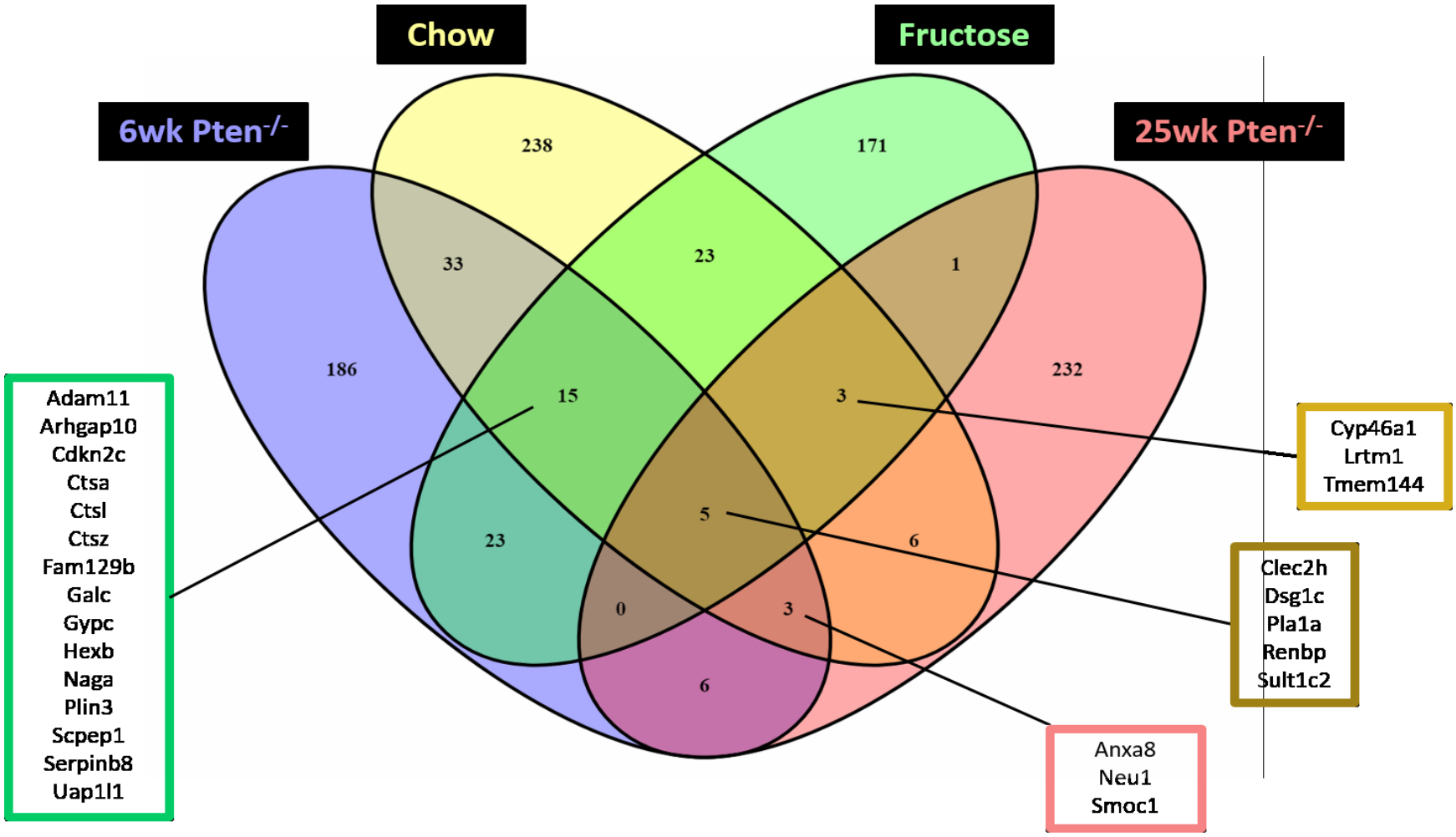


***Figure 4.23 - Four way Venn illustrating the numbers of genes, hepatic expression of which was altered in D316A-Tg relative to WT-Tg mice on chow and high fructose diets and Pten$^{-/-}$+D316A compared to Pten$^{-/-}$ mice at 6 and 25 weeks of age.*** *Listed, are those genes that were up-regulated in the liver in the presence of increased hepatic AMPK activity under 3 or more conditions (see* ***Table 4:9****).*

| Gene Symbol | Protein | Function |
|---|---|---|
| **Up-regulated with increased AMPK activity under all conditions** | | |
| **Clec2h** | C-type lectin domain family 2 member H | Lectin like receptor found on the surface of natural killer cells |
| Dsg1c | Desmoglein 1c | Cadherin like glycoprotein. Component of desmosomes (cell-cell junctions) |
| Pla1a | Phospholipase A1 Member A | Phospholipase that hydrolyses phosphatidylserine in liposomes |
| Renbp | Renin binding protein | Binds renin and inhibits its activity |
| Sult1c2 | Sulfotransferase 1C2 | Catalyses sulphate conjugation of endogenous and exogenous substances |
| **Up-regulated with increased AMPK activity in chow, fructose and 6wk *Pten*$^{-/-}$ cohorts** | | |
| Adam11 | Disintegrin and metalloproteinase domain-containing protein 11 | Membrane anchored protein involved in cell-cell and cell-matrix interactions. Candidate TS |
| Arhgap10 | Rho GTPase-activating protein 10 | RhoGAP protein - inactivates Cdc42 by converting it from GTP to GDP-bound form |
| Cdkn2c | Cyclin dependent kinase inhibitor 2C | Inhibits CDK4 & CDK6 - controls G1/S cell cycle progression. (Cdkn2a = TS) |
| Ctsa, Ctsl & Ctsz | Cathepsin A, L & Z | Lysosomal cysteine proteinases |
| Fam129b | Family with sequence similarity 129 member B | Adherans junction associated protein. May inhibit apoptosis |
| Galc | Galactosylceramidase | Lysosomal protein that hydrolyses galactose ester bonds |
| Gypc | Glycophorin C | Integral erythrocyte membrane glycoprotein |
| Hexb | Hexosaminidase B | β subunit of the lysosomal enzyme hexosaminidase that catalyses degradation of terminal N-acetyl hexosamine containing molecules |

| | | |
|---|---|---|
| Naga | N-acetyl-galactosaminidase α | Removes terminal alpha-N-acetylgalactosamine residues from glycolipids and glycopeptides |
| Plin3 | Perilipin-3 | Coat protein for lipid droplets. Interacts with mannose 6-phosphate receptors that transport lysosomal hydrolase between golgi and endosomes. |
| Scpep1 | Serine carboxypeptidase | Similar to the Cathepsins (see above) |
| Serpinb8 | Serine proteinase inhibitor B8 | Regulates complement activation, fibrinolysis & coagulation |
| Uap1l1 | UDP-N-Acetylglucosamine Pyrophosphorylase 1 Like 1 | Involved in amino sugar and nucleotide sugar metabolism |
| **Up-regulated with increased AMPK activity in chow, fructose and 25wk Pten$^{-/-}$ cohorts** | | |
| Cyp46a1 | Cholesterol 24-hydroxylase | Converts cholesterol into 24S-hydroxycholesterol |
| Lrtm1 | Leucine-rich repeat and transmembrane domain-containing protein 1 | |
| Tmem 144 | Transmembrane protein 44 | |
| **Up-regulated with increased AMPK activity in chow, 6wk and 25wk Pten$^{-/-}$ cohorts** | | |
| Anxa8 | Annexin A8 | Anticoagulant protein - indirect inhibitor of the thromboplastin-specific complex |
| Neu1 | Neuraminidase 1 | Lysosomal enzyme that cleaves terminal sialic acid residues. Forms heterotrimer with β-galactosidase and Cathepsin A |
| Smoc1 | **SPARC related modular calcium binding protein 1** | Critical role in ocular and limb development |

***Table 4.9 – Summary of genes that were up-regulated in the liver in the presence of increased hepatic AMPK activity under 3 or more conditions*** *(see* ***Figure 4.23****). Liposomal genes highlighted in yellow. (http://www.genecards.org, http://www.ensembl.org and http://www.ncbi.nlm.nih.gov/gen ). TS = tumour suppressor.*

## 4.9 Discussion

Given the marked benefits of increased hepatic AMPK activity seen in the lipogenic, high fructose model of hepatic steatosis, we went on to evaluate the effects of enhanced hepatic AMPK activity in a more severe model of NAFLD. Mice with liver specific Pten loss (*Pten*$^{-/-}$) progress rapidly from steatosis, through NASH and fibrosis and develop HCC (Horie et al. 2004; Stiles et al. 2004). D316A-Tg and WT-Tg mice were therefore crossed with *Pten*$^{-/-}$ mice to create animals with liver specific Pten loss with and without increased hepatic AMPK activity (*Pten*$^{-/-}$*+D316A* and *Pten*$^{-/-}$ respectively). *Pten*$^{-/-}$*+D316A* mice had reduced hepatic steatosis; less hepatocyte damage and inflammation; and delayed tumour development relative to their *Pten*$^{-/-}$ counterparts. AMPK may have protected against NAFLD progression and HCC in this model through a number of mechanisms, summarised in **Figure 4.24**.

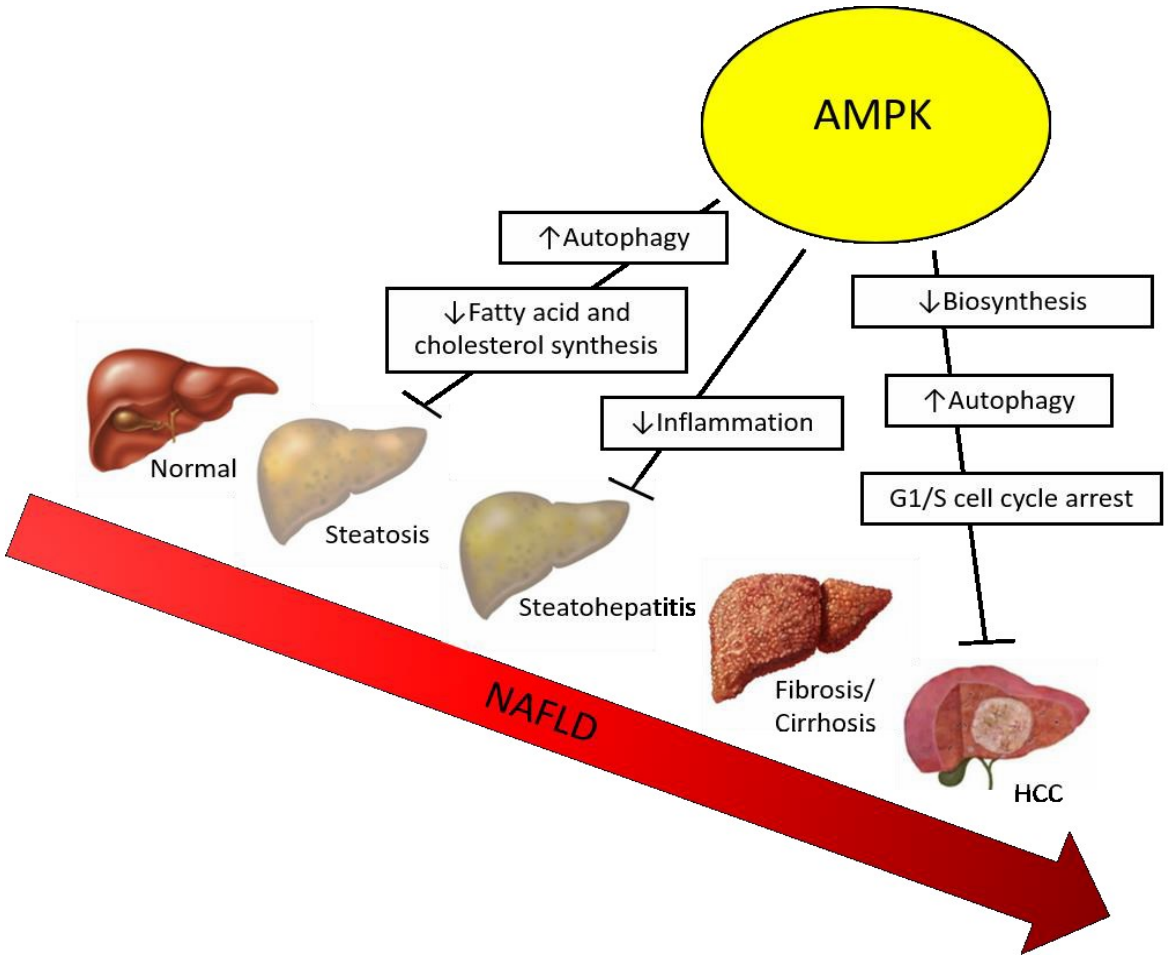


***Figure 4.24 - Potential mechanisms of action of hepatic AMPK in reducing NAFLD progression and HCC development in mice with liver specific Pten loss.***

Comparison of RNA sequencing data from WT-Tg and *Pten*$^{-/-}$ mice with similar data derived from liver tissue of patients with normal liver and steatosis, identified almost 70 genes, expression of which was altered in the same direction in *Pten*$^{-/-}$ mouse and steatotic human liver. This is in contrast to a similar study by Teufel et al. which compared hepatic RNA expression in 9 mouse models of NAFLD (including liver specific Pten loss) with that in patients with normal liver and NAFLD (Teufel et al. 2016). Somewhat surprisingly, they identified only 3 genes which were significantly altered in the same direction in both NAFLD and Pten loss. Furthermore, of these 3 apparently unrelated genes, which included Hal (encoding histidine ammonia-lyase), Stmn2 (encoding stathmin 2, involved in microtubule dynamics and cell signalling) and Nit2 (encoding nitrilase family member 2 that cleaves carbon-nitrogen bonds), only Hal expression followed the same pattern in liver from our *Pten*$^{-/-}$ mice relative to that in WT-Tg mice. Of note Teufel et al. examined RNA expression in liver tissue from 10 week old females, whereas we used 6 week old males. Anezaki et al. previously determined that the NAFLD phenotype associated with liver specific Pten loss is milder in female mice (Anezaki et al. 2009) and this may to some extent explain the differences between our and Teufel et al.'s findings. No mouse model can perfectly recapitulate human disease. However, in the current study, comparison of RNA sequencing data from mice with that from patients suggests that liver specific Pten loss is a reasonable model of NAFLD.

It has previously been shown that increased AKT activity due to PTEN loss results in phosphorylation of AMPK α1 at Ser485 by AKT which, in turn, inhibits AMPK activity (Hawley et al. 2014). Increased AMPK α1 Ser485 phosphorylation was seen in hepatocytes isolated from *Pten*$^{-/-}$ and *Pten*$^{-/-}$*+D316A* mice in this study (**Figure 4.2**). However, whilst this was associated with reduced AMPK activity in *Pten*$^{-/-}$ relative to WT-Tg mice, AMPK activity in hepatocytes from *Pten*$^{-/-}$*+D316A* mice was still more than 2 fold that in WT-Tg animals (**Figure 4.1**). ACC phosphorylation was also increased in *Pten*$^{-/-}$*+D316A* hepatocytes.

Stiles et al. demonstrated that accumulation of lipid in livers of *Pten*$^{-/-}$ mice was due to increased fatty acid synthesis as opposed to reduced fatty acid oxidation (Stiles et al. 2004). We too saw increased fatty acid synthesis in hepatocytes from *Pten*$^{-/-}$ mice, but this effect was attenuated in the presence of increased hepatic AMPK activity (**Figure 4.8**). In-keeping with decreased fatty acid synthesis in hepatocytes from *Pten*$^{-/-}$*+D316A* mice, triglyceride levels in

the livers of these animals were also lower relative to those in *Pten*$^{-/-}$ mice (**Figure 4.3**). In addition to reducing triglyceride accumulation, increased hepatic AMPK activity appeared to delay progression from micro to macrovesicular steatosis in *Pten*$^{-/-}$*+D316A* mice (**Figure 4.6**).

Increased hepatic AMPK activity reduced fatty acid synthesis in D316A-Tg mice on a lipogenic, high fructose diet through increased phosphorylation and inhibition of ACC and it is likely that this same mechanism was responsible for limiting *de novo* lipogenesis and delaying steatosis in *Pten*$^{-/-}$*+D316A* mice (Davies et al. 1992). The idea that post-translational effects as opposed to transcriptional events were responsible for reduced lipid accumulation in mice with increased hepatic AMPK activity, is supported by the RNA sequencing data, from Pten$^{-/-}$ and *Pten*$^{-/-}$*+D316A* mice (**Table 4.4**). Expression of a number of common lipogenic genes was unaffected by increased hepatic AMPK activity. Furthermore, <4% of pathways altered in *Pten*$^{-/-}$*+D316A* relative to *Pten*$^{-/-}$ mice were involved in lipid metabolism and of these only 1 pathway (regulation of ceramide biosynthesis) related to lipogenesis (**Table 4.5**). Together these findings imply that effects of AMPK were post-translational. Liver cholesterol accumulation was also attenuated in *Pten*$^{-/-}$*+D316A* relative to *Pten*$^{-/-}$ mice (**Figure 4.3**). Given that AMPK has been shown to phosphorylate and inhibit HMG CoA-reductase, the lower hepatic cholesterol levels seen in *Pten*$^{-/-}$*+D316A* mice are most likely due to reduced cholesterol synthesis (Clarke and Hardie 1990). However, good antibodies to phospho-HMG CoA-reductase are not available, limiting further investigation of this potential mechanism.

Serum markers of hepatocyte damage and inflammation (ALP, ALT and AST) were less elevated and histological NAS tended to be lower in *Pten*$^{-/-}$*+D316A* compared to *Pten*$^{-/-}$ mice (**Figures 4.9** and **4.10**). In-keeping with this finding, RNA sequencing demonstrated that although expression of a number of genes involved in inflammatory and immune pathways was up-regulated in *Pten*$^{-/-}$ mice, this effect was attenuated in the presence of increased hepatic AMPK activity (*Pten*$^{-/-}$*+D316A* – ***Table 4.6***).

*Pten*$^{-/-}$*+D316A* mice may have had less hepatocyte damage and inflammation as a result of reduced hepatic triglyceride accumulation and hence lower levels of lipotoxicity (Malhi and Gores 2008; Alkhouri, Dixon, and Feldstein 2009). There is also evidence to suggest that cholesterol may be of particular importance in the progression of NAFLD to NASH and given

that *Pten*$^{-/-}$*+D316A* mice had significantly lower liver cholesterol levels than *Pten*$^{-/-}$ mice, it is possible that AMPK limited hepatocyte damage and inflammation in this study by reducing cholesterol synthesis (Ioannou 2016; Clarke and Hardie 1990; Min et al. 2012).

Saturated fatty acids may be more lipotoxic than their unsaturated or esterified counterparts (Malhi and Gores 2008). The fatty acid composition of liver from *Pten*$^{-/-}$ and *Pten*$^{-/-}$*+D316A* mice was therefore assessed using mass spectrometry, to determine if mice with increased hepatic AMPK activity had a different and relatively less toxic distribution of fatty acids which was contributing to the reduced liver damage and inflammation seen in this genotype (**Table 4.2**). Hepatic concentrations of saturated fatty acids and MUFAs were elevated at 6 and 10 weeks of age and PUFA levels were reduced at 6 weeks in *Pten*$^{-/-}$ relative to WT-Tg mice. Saturated fatty acids, MUFA and PUFA levels were all lower in *Pten*$^{-/-}$*+D316A* compared to *Pten*$^{-/-}$ mice at 6 weeks of age, however fatty acid distribution was not different. There were no differences between *Pten*$^{-/-}$ and *Pten*$^{-/-}$*+D316A* mice by 10 weeks of age.

Muir and colleagues also performed lipidomic profiling on liver tissue from mice with liver specific Pten loss and their results are summarised in **Table 4.10** (Muir et al. 2013). In-keeping with the findings of this study and opposing the idea that MUFAs may be less lipotoxic, Mui et al. showed that proportionally, hepatic MUFA levels were raised in *Pten*$^{-/-}$ relative to wild-type mice. In contrast to the current study, SFA concentrations in Muir et al.'s study were reduced. This variation in results could be accounted for by the fact that Muir et al. studied year old as opposed to ≤ 10 week old mice and it is likely that fatty acid distribution in mouse livers changes as the animals develop steatohepatitis and tumours. Muir et al.'s PUFA analysis was broader than that in the current study which enabled them to also detect an increased n6 to n3-PUFA ratio in mice with hepatic Pten loss.

Another potential explanation for the differences seen in markers of hepatocyte damage and inflammation between *Pten*$^{-/-}$ and *Pten*$^{-/-}$*+D316A* mice is AMPK's potential role in inflammation. It has been suggested that AMPK has anti-inflammatory properties and promotes polarisation of macrophages from an M1 ('killer') to an M2 ('repair') phenotype (Sag et al. 2008). These functions may have been important in limiting kupffer cell activation

| Increased | Decreased |
|---|---|
| **MUFAs** | **SFAs** |
| **16:1n9** | 15:0 |
| **18:1n7 (vaccenic)** | 16:0 |
| **18:1n9 (oleic)** | 17:0 (margaric) |
| **20:1n9** | 22:0 |
| **22:1n9 (erucic)** | 24:0 (lignoceric) |
| **24:1n9** | |
| **n6-PUFAs** | **n6-PUFAs** |
| **20:3n6** | 18:2n6 (linoleic) |
| **22:4n6 (adrenic)** | 18:3n6 |
| **22:5n6 (osbond)** | |
| | **n3-PUFAs** |
| | 18:3n3 |
| | 20:5n3 (eicosapentaenoic) |
| | 22:6n3 (cervonic) |

***Table 4.10 – Fatty acid composition changes in 12 month old Pten$^{-/-}$ relative to wild-type mouse liver.*** *Relative composition in % of phospholipid fraction. Levels of the fatty acids highlighted in red correlated with tumour size or burden and plasma levels of the species in serum from patients with NASH ± HCC.*

and so steatohepatitis, in this study. However, further investigation of these pathways is necessary in order to determine whether they are influenced by AMPK.

Hepatic fibrosis was not marked in either *Pten$^{-/-}$* or *Pten$^{-/-}$+D316A* mice with evidence of tumour development (**Figure 4.11**). This is in-keeping with previous studies examining fibrosis in mice with liver specific Pten loss and suggests that fibrosis is not a key feature of this NAFLD related HCC model (He et al. 2016). Interestingly, He et al. also demonstrated that stellate cell activation in mice with liver specific Pten loss was dependent upon hepatic injury as opposed to AKT activation and so would be alleviated if steatosis and subsequent hepatocyte damage and inflammation were reduced.

Whether increased hepatic AMPK activity has a beneficial effect with regards hepatic fibrosis and cirrhosis in mice with liver specific Pten loss was not clear from this study. No differences were seen in the extent or distribution of collagen staining between *Pten*$^{-/-}$ and *Pten*$^{-/-}$*+D316A* mice (**Figure 4.11**). Furthermore, although RNA sequencing demonstrated that expression of a large number of fibrotic genes was up-regulated in *Pten*$^{-/-}$ relative to WT-Tg mice, expression of only a few of these genes was down-regulated in the presence of increased hepatic AMPK activity (**Table 4.7**).

Increased hepatic AMPK activity showed a marked benefit with regards tumour development in mice with liver specific Pten loss (**Figures 4.13, 4.14** and **4.17**). *Pten*$^{-/-}$*+D316A* mice developed tumours later (assessed on USS) and had a much lower tumour burden (assessed on USS and evident macroscopically at harvest) than their age matched *Pten*$^{-/-}$ counterparts.

Irrespective of aetiology, most HCCs arise on a background of chronic inflammation and cirrhosis (Bosch et al. 2005). Recurring cycles of hepatocyte death and regeneration lead to an accumulation of mutations and the associated inflammatory reaction also promotes tumourgenesis (Farazi and DePinho 2006; Grivennikov, Greten, and Karin 2010; Hanahan and Weinberg 2011). Tumour development in *Pten*$^{-/-}$*+D316A* mice may therefore have been delayed due to attenuated steatohepatitis in these animals, as a result of reduced *lipid* accumulation and/or the potential anti-inflammatory effects of AMPK. AMPK may also have played a more direct role in limiting tumourgenesis in *Pten*$^{-/-}$*+D316A* mice. The lack of a clear difference in fibrosis between *Pten*$^{-/-}$ and *Pten*$^{-/-}$*+D316A* mice and the observation that tumours appear in mice with liver specific Pten loss before extensive fibrosis has developed lend support to the latter.

Gallicia et al. studied double knockout mice with liver specific loss of both Pten and Akt (Galicia et al. 2010). Steatosis and hepatocellular damage were markedly reduced and tumour development was significantly delayed in these animals relative to single knockout mice with only Pten loss. However, following treatment with 3,5-dietoxycarbonyl-1,4 dihydrocollidine (DDC – which induces liver injury) progenitor cell proliferation and formation of pre-malignant lesions in single and double knockout mice was identical. Gallicia et al. therefore concluded that hepatic Pten loss leads to hepatic progenitor cell transformation

and liver injury (the latter via activation of AKT which causes steatohepatitis) and that both processes are required for liver tumour development. It is therefore possible that the inhibitory role of AMPK on tumourgenesis in the current study was due to either its impact on steatohepatitis, or its effects on progenitor cell transformation.

*De novo* lipogenesis is increased in cancers, irrespective of free fatty acid availability or homeostatic regulation (Mounier, Bouraoui, and Rassart 2014; Menendez and Lupu 2007). Furthermore ACC and FAS are often up-regulated in tumour cells and inhibition of either results in decreased growth and increased apoptosis (Pizer et al. 1998; Chajes et al. 2006; Milgraum et al. 1997; Svensson et al. 2016). In the current study hepatic ACC phosphorylation was increased and fatty acid synthesis reduced in mice with up-regulated AMPK activity in the liver. Therefore, AMPK may have slowed tumour development in mice with hepatic Pten loss by limiting lipid synthesis required for tumour cell growth and proliferation. In line with this effect of AMPK, Zadra et al. described reduced lipogenesis and prostate cancer growth in mice treated with the direct AMPK activator MT 63-78 and Guo et al. demonstrated that AICAR induced AMPK activation blocked glioblastoma cell proliferation by inhibiting cholesterol and fatty acid synthesis (Zadra et al. 2014; Guo et al. 2009).

AMPK has also been shown to slow tumourgenesis through down-regulation of other anabolic processes, in particular, inhibition of mTORC1 signalling through activation of tuberous sclerosis complex 2 (TSC2) and inhibition of Raptor and mTOR (Inoki, Zhu, and Guan 2003; Cheng et al. 2014; Gwinn et al. 2008). Absence of PTEN results in increased downstream AKT and mTORC1 signalling and it could therefore be that increased hepatic AMPK activity in the current study attenuated up-regulation of mTORC1 signalling and so tumour development. In keeping with this suggestion, Huang and colleagues described delayed tumour onset as a result of reduced mTORC signalling, in Pten deficient mice treated with the direct AMPK activator A-769662, or a biguanide and conversely showed that LKB1 loss accelerated tumourgenesis in the same model (Huang et al. 2008). Similarly, in a study reported by Rosillo et al. AICAR or Metformin treatment increased AMPK and inhibited mTORC activity resulting in reduced growth of Pten deficient lymphoma cell xenografts (Rosilio et al. 2013). However, in the current study, although phosphorylation of S6, a key downstream target of mTORC1, was increased in liver from *Pten*$^{-/-}$ relative to WT-Tg mice, it was not different in *Pten*$^{-/-}$*+D316A*

compared to *Pten*$^{-/-}$ mice, suggesting that in this instance mTORC1 signalling was not affected by AMPK activity (**Figure 4.19**).

Piguet et al. demonstrated reduced tumour development in mice with liver specific Pten loss following regular exercise (Piguet et al. 2015) and proposed that these findings were due to exercise induced AMPK activation and so reduced mTORC1 activity. Importantly, Piguet and colleagues did not see a difference in hepatic triglyceride levels or NAS between exercised and sedentary mice implying that differences in tumourgenesis between the two groups were not due to reduced steatohepatitis in exercised animals. Piguet et al. also conducted RNA sequencing to determine the effects of exercise on hepatic gene expression and identified 6 pathways, mainly involved in fatty acid metabolism, that were significantly altered in exercised relative to sedentary mice (**Table 4.11**). With the exception of Cpt1a, which was down-regulated in fructose fed D316A-Tg compared to WT-Tg mice and Lpl, which was down-regulated in *Pten*$^{-/-}$*+D316A* relative to *Pten*$^{-/-}$ mice, none of the genes in these pathways were altered in the presence of the AMPK γ1 D316A transgene in chow or fructose fed mice or 6 week old mice with liver specific Pten loss. This suggests that the changes in hepatic fatty acid gene expression following exercise in Piguet et al's study were not due to activation of AMPK.

It should also be noted that whilst most evidence implicates mTORC1 in carcinogenesis, through up-regulation of biosynthetic pathways, in a recent study reduced mTORC1 activity promoted tumour development (Umemura et al. 2014). Umemura and colleagues showed that treatment of high fat diet fed mice with the mTOR inhibitor Rapamycin reduced hepatic steatosis but also stimulated inflammation with increased IL-6 production and so oncogenic STAT3 activation. Correspondingly tumour development following diethylnitrosamine (DEN) exposure was greater in hepatocyte-specific raptor-deficient mice with reduced mTORC1 activity than in control animals.

Mice with thyroid specific Pten loss develop thyroid hyperplasia which progresses to follicular carcinoma. Antico Arciuch et al. concluded that thyrocyte proliferation in the absence of Pten occurs as a result of AMPK inhibition (due to $\alpha1^{Ser485}$ phosphorylation by AKT) which in turn promotes a switch from oxidative to glycolytic respiration (Antico Arciuch et al. 2013). This

| Gene Symbol | Gene name | Regulation |
|---|---|---|
| **Fatty acid, triacyl glycerol & ketone body metabolism** | | |
| Ugt1a1 | UDP Glucuronosyltransferase Family 1 Member A1 | ↓ |
| Crebbp | CREB binding protein | ↑ |
| Cyp7a1 | Cytochrome P450 Family 7 Subfamily A Member 1 | ↓ |
| Cpt1a/Cpt1b | Carnitine Palmitoyltransferase 1B | ↑ |
| **Fatty acid β oxidation** | | |
| Cpt1a | Carnitine Palmitoyltransferase 1A | ↓ |
| Lpl | Lipoprotein lipase | ↑ |
| **PPAR signalling** | | |
| Aqp7 | Aquaporin 7 | ↓ |
| Ppard | Peroxisome proliferator-activated receptor delta | ↑ |
| **NAFLD** | | |
| Ddit3 | DNA Damage Inducible Transcript 3 | ↑ |
| Mlxipl | MLX Interacting Protein Like | ↑ |
| Akt3 | AKT Serine/Threonine Kinase 3 | ↑ |
| Cox6a2 | Cytochrome C Oxidase Subunit 6A2 | ↑ |

***Table 4.11 - Fatty acid metabolism pathways and genes significantly altered following exercise*** *(Piguet et al. 2015). Far right column (regulation) indicates direction in which gene expression changed. CREB = cAMP response element binding protein.*

same process could be promoting hepatocyte or hepatic progenitor cell proliferation in mice with liver specific Pten loss. However, based on RNA sequencing data from the current study, none of the 7 Kreb's cycle genes (succinate dehydrogenase, isocitrate dehydrogenase, malate dehydrogenase, aconitase, dihydrolipoamide dehydrogenase, pyruvate dehydrogenase and citrate synthase) expression of which was reduced in Pten deficient thyroid cells, were down-regulated in liver from mice with liver specific Pten loss and correspondingly their expression did not differ between *Pten*$^{-/-}$ and *Pten*$^{-/-}$*+D316A* mice. It is therefore unlikely that AMPK inhibited tumour development in the current study by reversing the switch to aerobic glycolysis described by Antico Arciuch et al.

Two studies have demonstrated the importance of AMPK activity in inhibiting hepatocellular cancer cell viability through increased autophagy (Yu et al. 2013; Hu et al. 2014). Yu et al. used Nilotinib, which activated AMPK and increased autophagy, whereas Hu et al. demonstrated that up-regulation of autophagy following mTORC inhibition was AMPK dependent. This corresponds with other evidence suggesting that lipophagy may limit hepatic lipid accumulation and that impaired autophagy is important in HCC development (Aghajan, Li, and Karin 2012; Singh et al. 2009). It is therefore possible that in the current study increased hepatic AMPK activity in mice with liver specific Pten loss, promoted autophagy resulting in reduced hepatic lipid accumulation and attenuated tumour development.

Autophagy was not directly measured in *Pten*$^{-/-}$ and *Pten*$^{-/-}$*+D316A* mice, however, interrogation of the mRNA sequencing data identified 8 (from a total of 26) lysosomal genes which were up-regulated in mice with the AMPK γ1 D316A transgene under 3 or more conditions (**Table 4.12**). This is in-keeping with Young et al.'s findings (Young et al. 2016). They demonstrated impaired lysosomal function in AMPK knock-out mouse embryonic fibroblasts due to reduced transcription factor EB (Tfeb) phosphorylation and so lysosomal gene expression, particularly lysosomal associated membrane protein 1 (Lamp 1), Cd63 (Lamp3), Hexa and Rab7 (a member of the RAS oncogene family). In the current study, Hexa, Cd63 and lysosomal protein transmembrane 4b (Laptm4b) mRNA expression were increased in fructose fed D316A-Tg relative to WT-Tg mice and Cd63 and glycosylated lysosomal membrane protein (Glmp) were up-regulated in *Pten*$^{-/-}$*+D316A* compared to *Pten*$^{-/-}$ mice at 6 weeks of age. Further evaluation of autophagy and its impact on NAFLD progression and

tumourgenesis in mice with liver specific Pten loss with and without increased hepatic AMPK activity, is therefore warranted.

| Gene Symbol | Protein | Function |
|---|---|---|
| Ctsa, Ctsl & Ctsz | Cathepsin A, L & Z | Lysosomal cysteine proteinases |
| Galc | Galactosylceramidase | Lysosomal protein that hydrolyses galactose ester bonds |
| Hexb | Hexosaminidase B | β subunit of the lysosomal enzyme hexosaminidase that catalyses degradation of terminal N-acetyl hexosamine containing molecules |
| Plin3 | Perilipin-3 | Coat protein for lipid droplets. Interacts with mannose 6-phosphate receptors that transport lysosomal hydrolase between golgi and endosomes. |
| Scpep1 | Serine carboxypeptidase 1 | Similar to the Cathepsins (see above) |
| Neu1 | Neuraminidase 1 | Lysosomal enzyme that cleaves terminal sialic acid residues. Forms heterotrimer with β-galactosidase and Cathepsin A |

***Table 4.12 - Lysosomal genes expression of which was up-regulated in the liver in the presence of increased hepatic AMPK activity, under 3 or more conditions.***

Finally, a number of studies have shown that in the presence of increased AMPK activity p53 and p27 accumulate leading to G1/S cell cycle arrest (Jones et al. 2005; Liang et al. 2007; Lee et al. 2012). It has been suggested that p53 and p27 accumulate due to direct phosphorylation or in the case of p53 as a result of increased acetylation secondary to inhibition of the deacetylase SIRT1. Much of this evidence derives from studies of HCC and so may be particularly pertinent when considering mechanisms involved in the current study (Lee et al. 2012; Yi et al. 2013). Whilst Ki67 staining did not differ within tumours from *Pten*$^{-/-}$ and *Pten*$^{-/-}$*+D316A* mice, it would be important to assess more robustly the effects of increased hepatic AMPK activity on the cell cycle, in particular p53/p27 levels, in this model (**Fig 4.20**).

### 4.10 Summary of key findings

- Fatty acid synthesis was reduced in hepatocytes from *Pten*$^{-/-}$*+D316A* relative to *Pten*$^{-/-}$ mice and hepatic triglyceride and cholesterol accumulation were attenuated in mice with liver specific Pten loss in the presence of increased AMPK activity.
- Reduced fatty acid synthesis was likely due to phosphorylation and so inactivation of ACC by AMPK as opposed to altered lipogenic gene expression.
- Steatohepatitis was reduced in *Pten*$^{-/-}$*+D316A* relative to *Pten*$^{-/-}$ mice. This may have been the result of less lipotoxicity or due to anti-inflammatory effects of AMPK.
- Tumour development was markedly reduced, resulting in increased tumour free survival and decreased tumour burden in *Pten*$^{-/-}$*+D316A* relative to *Pten*$^{-/-}$ mice. This may have been due to less steatohepatitis in animals with the AMPK γ1 D316A transgene, or more direct effects of AMPK on tumourgenesis. Further work is required to clarify the role of AMPK in tumour development.

# 5 Future perspectives

There is a growing, global obesity epidemic (Non-communicable Disease Risk Factor Collaboration 2016). Obesity is associated with features of the Metabolic Syndrome and increased cancer risk (Eckel, Grundy, and Zimmet 2005; Calle et al. 2003). Current estimates suggest that NAFLD, the hepatic component of the metabolic syndrome affects 25% of the global population with 2% of those affected dying from NAFLD liver related causes (liver failure and HCC). There is therefore an urgent need for strategies that will either prevent or limit obesity and its consequences. In this context, AMPK, which up-regulates catabolic and down-regulates anabolic processes and is essential to energy homeostasis, has recently received significant interest as a potential therapeutic target. There is also increasing evidence that AMPK may play important roles in carcinogenesis and possibly inflammation (Huang et al. 2008; Faubert et al. 2013; Lee et al. 2012; Sag et al. 2008).

This study describes a novel AMPK γ1 mutation (D316A) which results in constitutively active AMPK. The degree of activation seen in hepatocytes isolated from mice carrying an AMPK γ1 D316A mutant transgene, expressed in the liver (D316A-Tg), was similar to that following treatment with direct AMPK activators such as 991. D316A-Tg mice had reduced hepatic *de novo* lipogenesis and so were protected from steatosis under lipogenic conditions (high fructose feeding or liver specific Pten loss). Increased hepatic AMPK activity also limited steatohepatitis and had a profound inhibitory effect on tumour development in mice with liver specific Pten loss. Interestingly, fatty acid oxidation in the liver was unaffected by increased hepatic AMPK activity and correspondingly D316A-Tg mice were not protected from liver steatosis following high fat feeding.

Previous studies examining the effects of increased AMPK activity have largely focussed on pharmacological or genetic models in which AMPK is globally activated (Cool et al. 2006; Yavari et al. 2016; Bergeron et al. 2001). AMPK γ1 D316A transgenic mice are an extremely useful and specific model for examining the effects of chronically increased AMPK activity in individual tissues. This study used transgenic mice to investigate the effects of increased AMPK activity in the liver, however, mice carrying the transgene could also be crossed with mice expressing Cre-recombinase under promotors other than albumin, to examine the role

of AMPK in other tissues. Mice carrying the D316A transgene have already been crossed with adiponectin-Cre mice, to study the effects of AMPK in adipose tissue and actin-Cre mice to evaluate global AMPK activation. These studies are ongoing. In direct relation to this study, given the perhaps somewhat surprising finding that hepatic fatty acid oxidation was unaltered in D316A-Tg mice, it would be particularly interesting to determine if AMPK activity affects this process in other tissues such as skeletal muscle.

Mice with increased hepatic AMPK activity did not accumulate lipid in their livers following high fructose feeding. However, their calorific intake, body fat and fatty acid oxidation and respiratory rates did not differ from those of wild-type animals. It is therefore not clear to where the calories that were not stored as lipid in the liver were redirected. Given that following high fructose feeding lipogenic and FGF21 gene expression are equally increased in livers of D316A-Tg and wild-type mice, fructose is presumably entering hepatocytes in the presence of increased hepatic AMPK activity. However, its destination beyond this is unresolved. It would therefore be interesting to perform metabolomics studies using $^{13}C$ labelled high fructose feed *in vivo* and measure labelled metabolites in tissue, serum, urine and stool, to determine to where carbon from fructose that does not accumulate in the liver as lipid, is re-directed.

It is not clear from this study whether AMPK inhibited tumourgenesis by reducing toxic lipid accumulation; limiting steatohepatitis due to its anti-inflammatory properties; or more direct effects on tumour cells. To elucidate the role of AMPK in tumour development it would be helpful to examine the effects of the AMPK γ1 D316A transgene in other mouse HCC models. Administration of the genotoxic carbon tetrachloride ($CCl_4$) causes hepatocyte damage, stimulates an inflammatory reaction from kuppfer cells and ultimately leads to HCC development (Weber, Boll, and Stampfl 2003). This model could be used to evaluate the effects of increased AMPK activity on liver injury and inflammation, independently from steatosis. Diethylnitrosamine (DEN – another genotoxic) treated mice and mice over-expressing oncogenes such as the transcription factor Myc, develop HCCs without marked inflammation or regeneration, so these models could be used to assess whether enhanced AMPK activity plays a more direct role in tumourgenesis (Thorgeirsson and Santoni-Rugiu 1996; Vesselinovitch et al. 1984).

Tumours arise in mice with liver specific Pten loss before extensive fibrosis/cirrhosis is present. The finding that AMPK limited the development of these tumours suggests that it plays a direct inhibitory role in tumourgenesis. It is possible that AMPK slowed tumour development by reducing biosynthesis (through inhibition of the mTORC1 pathway and/or lipogenesis), increasing autophagy, or inhibiting G1/S cell cycle progression (Zadra et al. 2014; Lee et al. 2012; Yu et al. 2013; Shaw et al. 2004) and it would be important to more thoroughly assess these potential mechanisms. Examining the effects of an ACC inhibitor, given to *Pten*$^{-/-}$ mice after hepatosteatosis has developed but whilst their tumour burden is still minimal, would allow the importance of reduced *de novo* lipogenesis with regards tumourgenesis in this model, to be evaluated. Similarly the effects of increased hepatic AMPK activity on autophagy deserve further investigation. For example, liver tissue could be stained for markers of autophagic flux, such as p62 and TFEB phosphorylation and liposomal function in hepatocytes from transgenic mice could be analysed with the use of a DQ-BSA assay. Finally, hepatic p53 (Ser15) and p27$^{kip1}$ (Thr197) phosphorylation, p53 (Lys382) acetylation and p53, p21 and p27 levels could be measured by western blotting.

Tumour burden was reduced in mice with increased hepatic AMPK activity, however, because tumour onset was delayed in *Pten*$^{-/-}$*+D316A* relative to *Pten*$^{-/-}$ mice tumour growth in the 2 genotypes was not comparable. It was therefore not possible, using this model, to evaluate the effects of increased AMPK activity on tumour progression. However, if AMPK does slow tumourgenesis directly by one of the mechanisms discussed, it is likely that it would also have an inhibitory effect on progression of established tumours. To examine the effects of increased hepatic AMPK on tumour progression using the D316A-Tg mice, they could be crossed with mice expressing Cre recombinase under an inducible promotor. This model could then be combined with an HCC model (that doesn't involve Cre recombinase) and AMPK induced after tumour onset.

There has been much investment in the development of compounds which both activate AMPK and are bioavailable and this work is ongoing. Cokorinos et al. recently described a novel direct AMPK activator and showed that it altered glucose handling when administered orally to primates. It is therefore feasible that pharmacological AMPK activators for use in humans will be available in the not too distant future. The findings of the current study

support the investigation of such compounds not only in patients with features of the metabolic syndrome, especially NAFLD, but also in a broader Oncology setting.

This study has furthered understanding of the effects of chronically increased hepatic AMPK activity and shown that AMPK protects against liver steatosis under lipogenic conditions and limits tumourgenesis in a NAFLD related HCC model. Further work is required to determine whether AMPK plays a wider role in tumour onset and progression and might therefore inhibit hepatocellular and other cancer development irrespective of aetiology. Given the growing prevalence of NAFLD and its complications such as liver failure and HCC and the current lack of effective treatments to slow or prevent NAFLD progression and HCC development, the findings of this study are acutely relevant (Younossi et al. 2016; El-Serag and Kanwal 2014; Townsend and Newsome 2016; Chalasani et al. 2012). Development of specific pharmacological activators of AMPK for use in this setting could be extremely valuable.

# 6 References


Adelman, R. C., F. J. Ballard, and S. Weinhouse. 1967. 'Purification and properties of rat liver fructokinase', *J Biol Chem*, 242: 3360-5.

Aghajan, M., N. Li, and M. Karin. 2012. 'Obesity, autophagy and the pathogenesis of liver and pancreatic cancers', *J Gastroenterol Hepatol*, 27 Suppl 2: 10-4.

Ahrens, M., O. Ammerpohl, W. von Schonfels, J. Kolarova, S. Bens, T. Itzel, A. Teufel, A. Herrmann, M. Brosch, H. Hinrichsen, W. Erhart, J. Egberts, B. Sipos, S. Schreiber, R. Hasler, F. Stickel, T. Becker, M. Krawczak, C. Rocken, R. Siebert, C. Schafmayer, and J. Hampe. 2013. 'DNA methylation analysis in nonalcoholic fatty liver disease suggests distinct disease-specific and remodeling signatures after bariatric surgery', *Cell Metab*, 18: 296-302.

Alberti, K. G., R. H. Eckel, S. M. Grundy, P. Z. Zimmet, J. I. Cleeman, K. A. Donato, J. C. Fruchart, W. P. James, C. M. Loria, and S. C. Smith, Jr. 2009. 'Harmonizing the metabolic syndrome: a joint interim statement of the International Diabetes Federation Task Force on Epidemiology and Prevention; National Heart, Lung, and Blood Institute; American Heart Association; World Heart Federation; International Atherosclerosis Society; and International Association for the Study of Obesity', *Circulation*, 120: 1640-5.

Alessi, D. R., K. Sakamoto, and J. R. Bayascas. 2006. 'LKB1-dependent signaling pathways', *Annu Rev Biochem*, 75: 137-63.

Alkhouri, N., L. J. Dixon, and A. E. Feldstein. 2009. 'Lipotoxicity in nonalcoholic fatty liver disease: not all lipids are created equal', *Expert Rev Gastroenterol Hepatol*, 3: 445-51.

Alkhouri, N., and A. E. Feldstein. 2016. 'Noninvasive diagnosis of nonalcoholic fatty liver disease: Are we there yet?', *Metabolism*, 65: 1087-95.

Altekruse, S. F., K. A. McGlynn, and M. E. Reichman. 2009. 'Hepatocellular carcinoma incidence, mortality, and survival trends in the United States from 1975 to 2005', *J Clin Oncol*, 27: 1485-91.

Ambade, A., A. Satishchandran, B. Gyongyosi, P. Lowe, and G. Szabo. 2016. 'Adult mouse model of early hepatocellular carcinoma promoted by alcoholic liver disease', *World J Gastroenterol*, 22: 4091-108.

Andreelli, F., M. Foretz, C. Knauf, P. D. Cani, C. Perrin, M. A. Iglesias, B. Pillot, A. Bado, F. Tronche, G. Mithieux, S. Vaulont, R. Burcelin, and B. Viollet. 2006. 'Liver adenosine monophosphate-activated kinase-alpha2 catalytic subunit is a key target for the control of hepatic glucose production by adiponectin and leptin but not insulin', *Endocrinology*, 147: 2432-41.

Anezaki, Y., S. Ohshima, H. Ishii, N. Kinoshita, T. Dohmen, E. Kataoka, W. Sato, M. Iizuka, T. Goto, J. Sasaki, T. Sasaki, A. Suzuki, H. Ohnishi, and Y. Horie. 2009. 'Sex difference in the liver of hepatocyte-specific Pten-deficient mice: A model of nonalcoholic steatohepatitis', *Hepatol Res*, 39: 609-18.

Anstee, Q. M., and C. P. Day. 2013. 'The genetics of NAFLD', *Nat Rev Gastroenterol Hepatol*, 10: 645-55.

———. 2015. 'The Genetics of Nonalcoholic Fatty Liver Disease: Spotlight on PNPLA3 and TM6SF2', *Semin Liver Dis*, 35: 270-90.

Antico Arciuch, V. G., M. A. Russo, K. S. Kang, and A. Di Cristofano. 2013. 'Inhibition of AMPK and Krebs cycle gene expression drives metabolic remodeling of Pten-deficient preneoplastic thyroid cells', *Cancer Res*, 73: 5459-72.

Arad, M., C. E. Seidman, and J. G. Seidman. 2007. 'AMP-activated protein kinase in the heart: role during health and disease', *Circ Res*, 100: 474-88.

Arguello, G., E. Balboa, M. Arrese, and S. Zanlungo. 2015. 'Recent insights on the role of cholesterol in non-alcoholic fatty liver disease', *Biochim Biophys Acta*, 1852: 1765-78.

Ascha, M. S., I. A. Hanouneh, R. Lopez, T. A. Tamimi, A. F. Feldstein, and N. N. Zein. 2010. 'The incidence and risk factors of hepatocellular carcinoma in patients with nonalcoholic steatohepatitis', *Hepatology*, 51: 1972-8.

Asgharpour, A., S. C. Cazanave, T. Pacana, M. Seneshaw, R. Vincent, B. A. Banini, D. P. Kumar, K. Daita, H. K. Min, F. Mirshahi, P. Bedossa, X. Sun, Y. Hoshida, S. V. Koduru, D. Contaifer, Jr., U. O. Warncke, D. S. Wijesinghe, and A. J. Sanyal. 2016. 'A diet-induced animal model of non-alcoholic fatty liver disease and hepatocellular cancer', *J Hepatol*, 65: 579-88.

Baffy, G., E. M. Brunt, and S. H. Caldwell. 2012. 'Hepatocellular carcinoma in non-alcoholic fatty liver disease: an emerging menace', *J Hepatol*, 56: 1384-91.

Barnes, K., J. C. Ingram, O. H. Porras, L. F. Barros, E. R. Hudson, L. G. Fryer, F. Foufelle, D. Carling, D. G. Hardie, and S. A. Baldwin. 2002. 'Activation of GLUT1 by metabolic and osmotic stress: potential involvement of AMP-activated protein kinase (AMPK)', *J Cell Sci*, 115: 2433-42.

Barreyro, F. J., S. Kobayashi, S. F. Bronk, N. W. Werneburg, H. Malhi, and G. J. Gores. 2007. 'Transcriptional regulation of Bim by FoxO3A mediates hepatocyte lipoapoptosis', *J Biol Chem*, 282: 27141-54.

Bartelt, A., and J. Heeren. 2014. 'Adipose tissue browning and metabolic health', *Nat Rev Endocrinol*, 10: 24-36.

Beasley, R. P. 1988. 'Hepatitis B virus. The major etiology of hepatocellular carcinoma', *Cancer*, 61: 1942-56.

Berger, A. H., A. G. Knudson, and P. P. Pandolfi. 2011. 'A continuum model for tumour suppression', *Nature*, 476: 163-9.

Bergeron, R., S. F. Previs, G. W. Cline, P. Perret, R. R. Russell, 3rd, L. H. Young, and G. I. Shulman. 2001. 'Effect of 5-aminoimidazole-4-carboxamide-1-beta-D-ribofuranoside infusion on in vivo glucose and lipid metabolism in lean and obese Zucker rats', *Diabetes*, 50: 1076-82.

Bettigole, S. E., and L. H. Glimcher. 2015. 'Endoplasmic reticulum stress in immunity', *Annu Rev Immunol*, 33: 107-38.

Bieghs, V., S. M. Walenbergh, T. Hendrikx, P. J. van Gorp, F. Verheyen, S. W. Olde Damink, A. A. Masclee, G. H. Koek, M. H. Hofker, C. J. Binder, and R. Shiri-Sverdlov. 2013. 'Trapping of oxidized LDL in lysosomes of Kupffer cells is a trigger for hepatic inflammation', *Liver Int*, 33: 1056-61.

Bizeau, M. E., and M. J. Pagliassotti. 2005. 'Hepatic adaptations to sucrose and fructose', *Metabolism*, 54: 1189-201.

Bosch, F. X., J. Ribes, R. Cleries, and M. Diaz. 2005. 'Epidemiology of hepatocellular carcinoma', *Clin Liver Dis*, 9: 191-211, v.

Brakenhielm, E., N. Veitonmaki, R. Cao, S. Kihara, Y. Matsuzawa, B. Zhivotovsky, T. Funahashi, and Y. Cao. 2004. 'Adiponectin-induced antiangiogenesis and antitumor activity involve caspase-mediated endothelial cell apoptosis', *Proc Natl Acad Sci U S A*, 101: 2476-81.

Bright, N. J., C. Thornton, and D. Carling. 2009. 'The regulation and function of mammalian AMPK-related kinases', *Acta Physiol (Oxf)*, 196: 15-26.

Bruix, J., S. Qin, P. Merle, A. Granito, Y. H. Huang, G. Bodoky, M. Pracht, O. Yokosuka, O. Rosmorduc, V. Breder, R. Gerolami, G. Masi, P. J. Ross, T. Song, J. P. Bronowicki, I. Ollivier-Hourmand, M. Kudo, A. L. Cheng, J. M. Llovet, R. S. Finn, M. A. LeBerre, A. Baumhauer, G. Meinhardt, and G. Han. 2017. 'Regorafenib for patients with hepatocellular carcinoma who progressed on sorafenib treatment (RESORCE): a randomised, double-blind, placebo-controlled, phase 3 trial', *Lancet*, 389: 56-66.

Brun, P., I. Castagliuolo, V. Di Leo, A. Buda, M. Pinzani, G. Palu, and D. Martines. 2007. 'Increased intestinal permeability in obese mice: new evidence in the pathogenesis of nonalcoholic steatohepatitis', *Am J Physiol Gastrointest Liver Physiol*, 292: G518-25.

Brunt, E. M. 2010. 'Pathology of nonalcoholic fatty liver disease', *Nat Rev Gastroenterol Hepatol*, 7: 195-203.

Brunt, E. M., D. E. Kleiner, L. A. Wilson, P. Belt, and B. A. Neuschwander-Tetri. 2011. 'Nonalcoholic fatty liver disease (NAFLD) activity score and the histopathologic diagnosis in NAFLD: distinct clinicopathologic meanings', *Hepatology*, 53: 810-20.

Buchman, A. L., M. D. Dubin, A. A. Moukarzel, D. J. Jenden, M. Roch, K. M. Rice, J. Gornbein, and M. E. Ament. 1995. 'Choline deficiency: a cause of hepatic steatosis during parenteral nutrition that can be reversed with intravenous choline supplementation', *Hepatology*, 22: 1399-403.

Buhl, E. S., N. Jessen, R. Pold, T. Ledet, A. Flyvbjerg, S. B. Pedersen, O. Pedersen, O. Schmitz, and S. Lund. 2002. 'Long-term AICAR administration reduces metabolic disturbances and lowers blood pressure in rats displaying features of the insulin resistance syndrome', *Diabetes*, 51: 2199-206.

Cai, X., X. Hu, B. Cai, Q. Wang, Y. Li, X. Tan, H. Hu, X. Chen, J. Huang, J. Cheng, and X. Jing. 2013. 'Metformin suppresses hepatocellular carcinoma cell growth through induction of cell cycle G1/G0 phase arrest and p21CIP and p27KIP expression and downregulation of cyclin D1 in vitro and in vivo', *Oncol Rep*, 30: 2449-57.

Caldwell, S. H., D. H. Oelsner, J. C. Iezzoni, E. E. Hespenheide, E. H. Battle, and C. J. Driscoll. 1999. 'Cryptogenic cirrhosis: clinical characterization and risk factors for underlying disease', *Hepatology*, 29: 664-9.

Calle, E. E., C. Rodriguez, K. Walker-Thurmond, and M. J. Thun. 2003. 'Overweight, obesity, and mortality from cancer in a prospectively studied cohort of U.S. adults', *N Engl J Med*, 348: 1625-38.

Calvisi, D. F., S. Ladu, A. Gorden, M. Farina, E. A. Conner, J. S. Lee, V. M. Factor, and S. S. Thorgeirsson. 2006. 'Ubiquitous activation of Ras and Jak/Stat pathways in human HCC', *Gastroenterology*, 130: 1117-28.

Cani, P. D., J. Amar, M. A. Iglesias, M. Poggi, C. Knauf, D. Bastelica, A. M. Neyrinck, F. Fava, K. M. Tuohy, C. Chabo, A. Waget, E. Delmee, B. Cousin, T. Sulpice, B. Chamontin, J. Ferrieres, J. F. Tanti, G. R. Gibson, L. Casteilla, N. M. Delzenne, M. C. Alessi, and R. Burcelin. 2007. 'Metabolic endotoxemia initiates obesity and insulin resistance', *Diabetes*, 56: 1761-72.

Canto, C., Z. Gerhart-Hines, J. N. Feige, M. Lagouge, L. Noriega, J. C. Milne, P. J. Elliott, P. Puigserver, and J. Auwerx. 2009. 'AMPK regulates energy expenditure by modulating NAD+ metabolism and SIRT1 activity', *Nature*, 458: 1056-60.

Carling, D., C. Thornton, A. Woods, and M. J. Sanders. 2012. 'AMP-activated protein kinase: new regulation, new roles?', *Biochem J*, 445: 11-27.

Carroll, B., and E. A. Dunlop. 2017. 'The lysosome: a crucial hub for AMPK and mTORC1 signalling', *Biochem J*, 474: 1453-66.

Cha, S. H., M. Wolfgang, Y. Tokutake, S. Chohnan, and M. D. Lane. 2008. 'Differential effects of central fructose and glucose on hypothalamic malonyl-CoA and food intake', *Proc Natl Acad Sci U S A*, 105: 16871-5.

Chajes, V., M. Cambot, K. Moreau, G. M. Lenoir, and V. Joulin. 2006. 'Acetyl-CoA carboxylase alpha is essential to breast cancer cell survival', *Cancer Res*, 66: 5287-94.

Chalasani, N., J. C. Gorski, M. S. Asghar, A. Asghar, B. Foresman, S. D. Hall, and D. W. Crabb. 2003. 'Hepatic cytochrome P450 2E1 activity in nondiabetic patients with nonalcoholic steatohepatitis', *Hepatology*, 37: 544-50.

Chalasani, N., Z. Younossi, J. E. Lavine, A. M. Diehl, E. M. Brunt, K. Cusi, M. Charlton, and A. J. Sanyal. 2012. 'The diagnosis and management of non-alcoholic fatty liver disease: practice Guideline by the American Association for the Study of Liver Diseases, American College of Gastroenterology, and the American Gastroenterological Association', *Hepatology*, 55: 2005-23.

Chang, Q., Y. Zhang, K. J. Beezhold, D. Bhatia, H. Zhao, J. Chen, V. Castranova, X. Shi, and F. Chen. 2009. 'Sustained JNK1 activation is associated with altered histone H3 methylations in human liver cancer', *J Hepatol*, 50: 323-33.

Chanmugam, P., J. F. Guthrie, S. Cecilio, J. F. Morton, P. P. Basiotis, and R. Anand. 2003. 'Did fat intake in the United States really decline between 1989-1991 and 1994-1996?', *J Am Diet Assoc*, 103: 867-72.

Chen, C., Y. C. Chang, C. L. Liu, T. P. Liu, K. J. Chang, and I. C. Guo. 2007. 'Leptin induces proliferation and anti-apoptosis in human hepatocarcinoma cells by up-regulating cyclin D1 and down-regulating Bax via a Janus kinase 2-linked pathway', *Endocr Relat Cancer*, 14: 513-29.

Chen, W., B. Chang, L. Li, and L. Chan. 2010. 'Patatin-like phospholipase domain-containing 3/adiponutrin deficiency in mice is not associated with fatty liver disease', *Hepatology*, 52: 1134-42.

Cheng, J., T. Huang, Y. Li, Y. Guo, Y. Zhu, Q. Wang, X. Tan, W. Chen, Y. Zhang, W. Cheng, T. Yamamoto, X. Jing, and J. Huang. 2014. 'AMP-activated protein kinase suppresses the in vitro and in vivo proliferation of hepatocellular carcinoma', *PLoS One*, 9: e93256.

Cheng, S. W., L. G. Fryer, D. Carling, and P. R. Shepherd. 2004. 'Thr2446 is a novel mammalian target of rapamycin (mTOR) phosphorylation site regulated by nutrient status', *J Biol Chem*, 279: 15719-22.

Chiavaroli, L., R. J. de Souza, V. Ha, A. I. Cozma, A. Mirrahimi, D. D. Wang, M. Yu, A. J. Carleton, M. Di Buono, A. L. Jenkins, L. A. Leiter, T. M. Wolever, J. Beyene, C. W. Kendall, D. J. Jenkins, and J. L. Sievenpiper. 2015. 'Effect of Fructose on Established Lipid Targets: A Systematic Review and Meta-Analysis of Controlled Feeding Trials', *J Am Heart Assoc*, 4: e001700.

Chiu, S., J. L. Sievenpiper, R. J. de Souza, A. I. Cozma, A. Mirrahimi, A. J. Carleton, V. Ha, M. Di Buono, A. L. Jenkins, L. A. Leiter, T. M. Wolever, A. C. Don-

Wauchope, J. Beyene, C. W. Kendall, and D. J. Jenkins. 2014. 'Effect of fructose on markers of non-alcoholic fatty liver disease (NAFLD): a systematic review and meta-analysis of controlled feeding trials', *Eur J Clin Nutr*, 68: 416-23.

Choi, C. S., D. B. Savage, L. Abu-Elheiga, Z. X. Liu, S. Kim, A. Kulkarni, A. Distefano, Y. J. Hwang, R. M. Reznick, R. Codella, D. Zhang, G. W. Cline, S. J. Wakil, and G. I. Shulman. 2007. 'Continuous fat oxidation in acetyl-CoA carboxylase 2 knockout mice increases total energy expenditure, reduces fat mass, and improves insulin sensitivity', *Proc Natl Acad Sci U S A*, 104: 16480-5.

Choi, S. H., and H. N. Ginsberg. 2011. 'Increased very low density lipoprotein (VLDL) secretion, hepatic steatosis, and insulin resistance', *Trends Endocrinol Metab*, 22: 353-63.

Chong, M. F., B. A. Fielding, and K. N. Frayn. 2007. 'Mechanisms for the acute effect of fructose on postprandial lipemia', *Am J Clin Nutr*, 85: 1511-20.

Clarke, P. R., and D. G. Hardie. 1990. 'Regulation of HMG-CoA reductase: identification of the site phosphorylated by the AMP-activated protein kinase in vitro and in intact rat liver', *Embo j*, 9: 2439-46.

Cohen, J. C., J. D. Horton, and H. H. Hobbs. 2011. 'Human fatty liver disease: old questions and new insights', *Science*, 332: 1519-23.

Cokorinos, E. C., J. Delmore, A. R. Reyes, B. Albuquerque, R. Kjobsted, N. O. Jorgensen, J. L. Tran, A. Jatkar, K. Cialdea, R. M. Esquejo, J. Meissen, M. F. Calabrese, J. Cordes, R. Moccia, D. Tess, C. T. Salatto, T. M. Coskran, A. C. Opsahl, D. Flynn, M. Blatnik, W. Li, E. Kindt, M. Foretz, B. Viollet, J. Ward, R. G. Kurumbail, A. S. Kalgutkar, J. F. P. Wojtaszewski, K. O. Cameron, and R. A. Miller. 2017. 'Activation of Skeletal Muscle AMPK Promotes Glucose Disposal and Glucose Lowering in Non-human Primates and Mice', *Cell Metab*, 25: 1147-59.e10.

Cool, B., B. Zinker, W. Chiou, L. Kifle, N. Cao, M. Perham, R. Dickinson, A. Adler, G. Gagne, R. Iyengar, G. Zhao, K. Marsh, P. Kym, P. Jung, H. S. Camp, and E. Frevert. 2006. 'Identification and characterization of a small molecule AMPK activator that treats key components of type 2 diabetes and the metabolic syndrome', *Cell Metab*, 3: 403-16.

Corton, J. M., J. G. Gillespie, and D. G. Hardie. 1994. 'Role of the AMP-activated protein kinase in the cellular stress response', *Curr Biol*, 4: 315-24.

Cozma, A. I., J. L. Sievenpiper, R. J. de Souza, L. Chiavaroli, V. Ha, D. D. Wang, A. Mirrahimi, M. E. Yu, A. J. Carleton, M. Di Buono, A. L. Jenkins, L. A. Leiter, T. M. Wolever, J. Beyene, C. W. Kendall, and D. J. Jenkins. 2012. 'Effect of fructose on glycemic control in diabetes: a systematic review and meta-analysis of controlled feeding trials', *Diabetes Care*, 35: 1611-20.

Dalamaga, M., K. N. Diakopoulos, and C. S. Mantzoros. 2012. 'The role of adiponectin in cancer: a review of current evidence', *Endocr Rev*, 33: 547-94.

Dandapani, M., and D. G. Hardie. 2013. 'AMPK: opposing the metabolic changes in both tumour cells and inflammatory cells?', *Biochem Soc Trans*, 41: 687-93.

Davies, S. P., D. Carling, M. R. Munday, and D. G. Hardie. 1992. 'Diurnal rhythm of phosphorylation of rat liver acetyl-CoA carboxylase by the AMP-activated protein kinase, demonstrated using freeze-clamping. Effects of high fat diets', *Eur J Biochem*, 203: 615-23.

Davila, J. A., R. O. Morgan, Y. Shaib, K. A. McGlynn, and H. B. El-Serag. 2005. 'Diabetes increases the risk of hepatocellular carcinoma in the United States: a population based case control study', *Gut*, 54: 533-9.

Day, C. P., and O. F. James. 1998. 'Steatohepatitis: a tale of two "hits"?', *Gastroenterology*, 114: 842-5.

de La Coste, A., B. Romagnolo, P. Billuart, C. A. Renard, M. A. Buendia, O. Soubrane, M. Fabre, J. Chelly, C. Beldjord, A. Kahn, and C. Perret. 1998. 'Somatic mutations of the beta-catenin gene are frequent in mouse and human hepatocellular carcinomas', *Proc Natl Acad Sci U S A*, 95: 8847-51.

Di Cristofano, A., B. Pesce, C. Cordon-Cardo, and P. P. Pandolfi. 1998. 'Pten is essential for embryonic development and tumour suppression', *Nat Genet*, 19: 348-55.

Donadon, V., M. Balbi, M. D. Mas, P. Casarin, and G. Zanette. 2010. 'Metformin and reduced risk of hepatocellular carcinoma in diabetic patients with chronic liver disease', *Liver Int*, 30: 750-8.

Dongiovanni, P., S. Petta, C. Maglio, A. L. Fracanzani, R. Pipitone, E. Mozzi, B. M. Motta, D. Kaminska, R. Rametta, S. Grimaudo, S. Pelusi, T. Montalcini, A. Alisi, M. Maggioni, V. Karja, J. Boren, P. Kakela, V. Di Marco, C. Xing, V. Nobili, B. Dallapiccola, A. Craxi, J. Pihlajamaki, S. Fargion, L. Sjostrom, L. M. Carlsson, S. Romeo, and L. Valenti. 2015. 'Transmembrane 6 superfamily member 2 gene variant disentangles nonalcoholic steatohepatitis from cardiovascular disease', *Hepatology*, 61: 506-14.

Donnelly, K. L., C. I. Smith, S. J. Schwarzenberg, J. Jessurun, M. D. Boldt, and E. J. Parks. 2005. 'Sources of fatty acids stored in liver and secreted via lipoproteins in patients with nonalcoholic fatty liver disease', *J Clin Invest*, 115: 1343-51.

Dowman, J. K., L. J. Hopkins, G. M. Reynolds, N. Nikolaou, M. J. Armstrong, J. C. Shaw, D. D. Houlihan, P. F. Lalor, J. W. Tomlinson, S. G. Hubscher, and P. N. Newsome. 2014. 'Development of hepatocellular carcinoma in a

murine model of nonalcoholic steatohepatitis induced by use of a high-fat/fructose diet and sedentary lifestyle', *Am J Pathol*, 184: 1550-61.
Dowman, J. K., J. W. Tomlinson, and P. N. Newsome. 2010. 'Pathogenesis of non-alcoholic fatty liver disease', *Qjm*, 103: 71-83.
Duarte, J. A., F. Carvalho, M. Pearson, J. D. Horton, J. D. Browning, J. G. Jones, and S. C. Burgess. 2014. 'A high-fat diet suppresses de novo lipogenesis and desaturation but not elongation and triglyceride synthesis in mice', *J Lipid Res*, 55: 2541-53.
Dumas, M. E., R. H. Barton, A. Toye, O. Cloarec, C. Blancher, A. Rothwell, J. Fearnside, R. Tatoud, V. Blanc, J. C. Lindon, S. C. Mitchell, E. Holmes, M. I. McCarthy, J. Scott, D. Gauguier, and J. K. Nicholson. 2006. 'Metabolic profiling reveals a contribution of gut microbiota to fatty liver phenotype in insulin-resistant mice', *Proc Natl Acad Sci U S A*, 103: 12511-6.
Dushay, J. R., E. Toschi, E. K. Mitten, F. M. Fisher, M. A. Herman, and E. Maratos-Flier. 2015. 'Fructose ingestion acutely stimulates circulating FGF21 levels in humans', *Mol Metab*, 4: 51-7.
EASL-EORTC. 2012. 'EASL-EORTC clinical practice guidelines: management of hepatocellular carcinoma', *J Hepatol*, 56: 908-43.
Eckel, R. H., S. M. Grundy, and P. Z. Zimmet. 2005. 'The metabolic syndrome', *Lancet*, 365: 1415-28.
Efeyan, A., R. Zoncu, S. Chang, I. Gumper, H. Snitkin, R. L. Wolfson, O. Kirak, D. D. Sabatini, and D. M. Sabatini. 2013. 'Regulation of mTORC1 by the Rag GTPases is necessary for neonatal autophagy and survival', *Nature*, 493: 679-83.
Egan, D. F., D. B. Shackelford, M. M. Mihaylova, S. Gelino, R. A. Kohnz, W. Mair, D. S. Vasquez, A. Joshi, D. M. Gwinn, R. Taylor, J. M. Asara, J. Fitzpatrick, A. Dillin, B. Viollet, M. Kundu, M. Hansen, and R. J. Shaw. 2011. 'Phosphorylation of ULK1 (hATG1) by AMP-activated protein kinase connects energy sensing to mitophagy', *Science*, 331: 456-61.
El-Serag, H. B. 2004. 'Hepatocellular carcinoma: recent trends in the United States', *Gastroenterology*, 127: S27-34.
———. 2012. 'Epidemiology of viral hepatitis and hepatocellular carcinoma', *Gastroenterology*, 142: 1264-73.e1.
El-Serag, H. B., and F. Kanwal. 2014. 'Epidemiology of hepatocellular carcinoma in the United States: where are we? Where do we go?', *Hepatology*, 60: 1767-75.
El-Serag, H. B., and K. L. Rudolph. 2007. 'Hepatocellular carcinoma: epidemiology and molecular carcinogenesis', *Gastroenterology*, 132: 2557-76.
Eng, C. 2003. 'PTEN: one gene, many syndromes', *Hum Mutat*, 22: 183-98.

Erion, D. M., V. Popov, J. J. Hsiao, D. Vatner, K. Mitchell, S. Yonemitsu, Y. Nagai, M. Kahn, M. P. Gillum, J. Dong, S. F. Murray, V. P. Manchem, S. Bhanot, G. W. Cline, G. I. Shulman, and V. T. Samuel. 2013. 'The role of the carbohydrate response element-binding protein in male fructose-fed rats', *Endocrinology*, 154: 36-44.

Evans, J. M., L. A. Donnelly, A. M. Emslie-Smith, D. R. Alessi, and A. D. Morris. 2005. 'Metformin and reduced risk of cancer in diabetic patients', *Bmj*, 330: 1304-5.

Faeh, D., K. Minehira, J. M. Schwarz, R. Periasamy, S. Park, and L. Tappy. 2005. 'Effect of fructose overfeeding and fish oil administration on hepatic de novo lipogenesis and insulin sensitivity in healthy men', *Diabetes*, 54: 1907-13.

Fang, D. L., Y. Wan, W. Shen, J. Cao, Z. X. Sun, H. H. Yu, Q. Zhang, W. H. Cheng, J. Chen, and B. Ning. 2013. 'Endoplasmic reticulum stress leads to lipid accumulation through upregulation of SREBP-1c in normal hepatic and hepatoma cells', *Mol Cell Biochem*, 381: 127-37.

Farazi, P. A., and R. A. DePinho. 2006. 'Hepatocellular carcinoma pathogenesis: from genes to environment', *Nat Rev Cancer*, 6: 674-87.

Faubert, B., G. Boily, S. Izreig, T. Griss, B. Samborska, Z. Dong, F. Dupuy, C. Chambers, B. J. Fuerth, B. Viollet, O. A. Mamer, D. Avizonis, R. J. DeBerardinis, P. M. Siegel, and R. G. Jones. 2013. 'AMPK is a negative regulator of the Warburg effect and suppresses tumor growth in vivo', *Cell Metab*, 17: 113-24.

Feldstein, A. E., A. Canbay, P. Angulo, M. Taniai, L. J. Burgart, K. D. Lindor, and G. J. Gores. 2003. 'Hepatocyte apoptosis and fas expression are prominent features of human nonalcoholic steatohepatitis', *Gastroenterology*, 125: 437-43.

Feldstein, A. E., A. Canbay, M. E. Guicciardi, H. Higuchi, S. F. Bronk, and G. J. Gores. 2003. 'Diet associated hepatic steatosis sensitizes to Fas mediated liver injury in mice', *J Hepatol*, 39: 978-83.

Feldstein, A. E., N. W. Werneburg, A. Canbay, M. E. Guicciardi, S. F. Bronk, R. Rydzewski, L. J. Burgart, and G. J. Gores. 2004. 'Free fatty acids promote hepatic lipotoxicity by stimulating TNF-alpha expression via a lysosomal pathway', *Hepatology*, 40: 185-94.

Filhoulaud, G., S. Guilmeau, R. Dentin, J. Girard, and C. Postic. 2013. 'Novel insights into ChREBP regulation and function', *Trends Endocrinol Metab*, 24: 257-68.

Folch, J., M. Lees, and G. H. Sloane Stanley. 1957. 'A simple method for the isolation and purification of total lipides from animal tissues', *J Biol Chem*, 226: 497-509.

Foretz, M., N. Ancellin, F. Andreelli, Y. Saintillan, P. Grondin, A. Kahn, B. Thorens, S. Vaulont, and B. Viollet. 2005. 'Short-term overexpression of a constitutively active form of AMP-activated protein kinase in the liver leads to mild hypoglycemia and fatty liver', *Diabetes*, 54: 1331-9.

Fotbolcu, H., and E. Zorlu. 2016. 'Nonalcoholic fatty liver disease as a multi-systemic disease', *World J Gastroenterol*, 22: 4079-90.

Friedman, S. L., F. J. Roll, J. Boyles, and D. M. Bissell. 1985. 'Hepatic lipocytes: the principal collagen-producing cells of normal rat liver', *Proc Natl Acad Sci U S A*, 82: 8681-5.

Fujimoto, A., Y. Totoki, T. Abe, K. A. Boroevich, F. Hosoda, H. H. Nguyen, M. Aoki, N. Hosono, M. Kubo, F. Miya, Y. Arai, H. Takahashi, T. Shirakihara, M. Nagasaki, T. Shibuya, K. Nakano, K. Watanabe-Makino, H. Tanaka, H. Nakamura, J. Kusuda, H. Ojima, K. Shimada, T. Okusaka, M. Ueno, Y. Shigekawa, Y. Kawakami, K. Arihiro, H. Ohdan, K. Gotoh, O. Ishikawa, S. Ariizumi, M. Yamamoto, T. Yamada, K. Chayama, T. Kosuge, H. Yamaue, N. Kamatani, S. Miyano, H. Nakagama, Y. Nakamura, T. Tsunoda, T. Shibata, and H. Nakagawa. 2012. 'Whole-genome sequencing of liver cancers identifies etiological influences on mutation patterns and recurrent mutations in chromatin regulators', *Nat Genet*, 44: 760-4.

Fukuo, Y., S. Yamashina, H. Sonoue, A. Arakawa, E. Nakadera, T. Aoyama, A. Uchiyama, K. Kon, K. Ikejima, and S. Watanabe. 2014. 'Abnormality of autophagic function and cathepsin expression in the liver from patients with non-alcoholic fatty liver disease', *Hepatol Res*, 44: 1026-36.

Fullerton, M. D., S. Galic, K. Marcinko, S. Sikkema, T. Pulinilkunnil, Z. P. Chen, H. M. O'Neill, R. J. Ford, R. Palanivel, M. O'Brien, D. G. Hardie, S. L. Macaulay, J. D. Schertzer, J. R. Dyck, B. J. van Denderen, B. E. Kemp, and G. R. Steinberg. 2013. 'Single phosphorylation sites in Acc1 and Acc2 regulate lipid homeostasis and the insulin-sensitizing effects of metformin', *Nat Med*, 19: 1649-54.

Galic, S., M. D. Fullerton, J. D. Schertzer, S. Sikkema, K. Marcinko, C. R. Walkley, D. Izon, J. Honeyman, Z. P. Chen, B. J. van Denderen, B. E. Kemp, and G. R. Steinberg. 2011. 'Hematopoietic AMPK beta1 reduces mouse adipose tissue macrophage inflammation and insulin resistance in obesity', *J Clin Invest*, 121: 4903-15.

Galicia, V. A., L. He, H. Dang, G. Kanel, C. Vendryes, B. A. French, N. Zeng, J. A. Bayan, W. Ding, K. S. Wang, S. French, M. J. Birnbaum, C. B. Rountree, and B. L. Stiles. 2010. 'Expansion of hepatic tumor progenitor cells in Pten-null mice requires liver injury and is reversed by loss of AKT2', *Gastroenterology*, 139: 2170-82.

'Global, regional, and national age-sex specific all-cause and cause-specific mortality for 240 causes of death, 1990-2013: a systematic analysis for the Global Burden of Disease Study 2013'. 2015. *Lancet*, 385: 117-71.

Godlewski, J., M. O. Nowicki, A. Bronisz, G. Nuovo, J. Palatini, M. De Lay, J. Van Brocklyn, M. C. Ostrowski, E. A. Chiocca, and S. E. Lawler. 2010. 'MicroRNA-451 regulates LKB1/AMPK signaling and allows adaptation to metabolic stress in glioma cells', *Mol Cell*, 37: 620-32.

Gomez-Galeno, J. E., Q. Dang, T. H. Nguyen, S. H. Boyer, M. P. Grote, Z. Sun, M. Chen, W. A. Craigo, P. D. van Poelje, D. A. MacKenna, E. E. Cable, P. A. Rolzin, P. D. Finn, B. Chi, D. L. Linemeyer, S. J. Hecker, and M. D. Erion. 2010. 'A Potent and Selective AMPK Activator That Inhibits de Novo Lipogenesis', *ACS Med Chem Lett*, 1: 478-82.

Goodman, Z. D. 2007. 'Neoplasms of the liver', *Mod Pathol*, 20 Suppl 1: S49-60.

Grahame Hardie, D. 2014. 'AMP-activated protein kinase: a key regulator of energy balance with many roles in human disease', *J Intern Med*, 276: 543-59.

Greenberg, A. S., R. A. Coleman, F. B. Kraemer, J. L. McManaman, M. S. Obin, V. Puri, Q. W. Yan, H. Miyoshi, and D. G. Mashek. 2011. 'The role of lipid droplets in metabolic disease in rodents and humans', *J Clin Invest*, 121: 2102-10.

Grivennikov, S. I., F. R. Greten, and M. Karin. 2010. 'Immunity, inflammation, and cancer', *Cell*, 140: 883-99.

Gu, X., Y. Yan, S. J. Novick, A. Kovich, D. Goswami, J. Ke, M. H. E. Tan, L. Wang, X. Li, P. de Waal, M. R. Webb, P. R. Griffin, H. E. Xu, and K. Melcher. 2017. 'Deconvoluting AMP-dependent kinase (AMPK) adenine nucleotide binding and sensing', *J Biol Chem*.

Guichard, C., G. Amaddeo, S. Imbeaud, Y. Ladeiro, L. Pelletier, I. B. Maad, J. Calderaro, P. Bioulac-Sage, M. Letexier, F. Degos, B. Clement, C. Balabaud, E. Chevet, A. Laurent, G. Couchy, E. Letouze, F. Calvo, and J. Zucman-Rossi. 2012. 'Integrated analysis of somatic mutations and focal copy-number changes identifies key genes and pathways in hepatocellular carcinoma', *Nat Genet*, 44: 694-8.

Guo, D., I. J. Hildebrandt, R. M. Prins, H. Soto, M. M. Mazzotta, J. Dang, J. Czernin, J. Y. Shyy, A. D. Watson, M. Phelps, C. G. Radu, T. F. Cloughesy, and P. S. Mischel. 2009. 'The AMPK agonist AICAR inhibits the growth of EGFRvIII-expressing glioblastomas by inhibiting lipogenesis', *Proc Natl Acad Sci U S A*, 106: 12932-7.

Gwinn, D. M., D. B. Shackelford, D. F. Egan, M. M. Mihaylova, A. Mery, D. S. Vasquez, B. E. Turk, and R. J. Shaw. 2008. 'AMPK phosphorylation of raptor mediates a metabolic checkpoint', *Mol Cell*, 30: 214-26.

Haas, J. T., J. Miao, D. Chanda, Y. Wang, E. Zhao, M. E. Haas, M. Hirschey, B. Vaitheesvaran, R. V. Farese, Jr., I. J. Kurland, M. Graham, R. Crooke, F. Foufelle, and S. B. Biddinger. 2012. 'Hepatic insulin signaling is required for obesity-dependent expression of SREBP-1c mRNA but not for feeding-dependent expression', *Cell Metab*, 15: 873-84.

Hacker, H., and M. Karin. 2006. 'Regulation and function of IKK and IKK-related kinases', *Sci STKE*, 2006: re13.

Hanahan, D., and R. A. Weinberg. 2011. 'Hallmarks of cancer: the next generation', *Cell*, 144: 646-74.

Hardie, D. G. 2013. 'The LKB1-AMPK pathway-friend or foe in cancer?', *Cancer Cell*, 23: 131-2.

———. 2015a. 'AMPK: positive and negative regulation, and its role in whole-body energy homeostasis', *Curr Opin Cell Biol*, 33: 1-7.

———. 2015b. 'Molecular Pathways: Is AMPK a Friend or a Foe in Cancer?', *Clin Cancer Res*, 21: 3836-40.

Hardie, D. G., F. A. Ross, and S. A. Hawley. 2012. 'AMPK: a nutrient and energy sensor that maintains energy homeostasis', *Nat Rev Mol Cell Biol*, 13: 251-62.

Havel, P. J. 2005. 'Dietary fructose: implications for dysregulation of energy homeostasis and lipid/carbohydrate metabolism', *Nutr Rev*, 63: 133-57.

Hawley, S. A., J. Boudeau, J. L. Reid, K. J. Mustard, L. Udd, T. P. Makela, D. R. Alessi, and D. G. Hardie. 2003. 'Complexes between the LKB1 tumor suppressor, STRAD alpha/beta and MO25 alpha/beta are upstream kinases in the AMP-activated protein kinase cascade', *J Biol*, 2: 28.

Hawley, S. A., M. Davison, A. Woods, S. P. Davies, R. K. Beri, D. Carling, and D. G. Hardie. 1996. 'Characterization of the AMP-activated protein kinase kinase from rat liver and identification of threonine 172 as the major site at which it phosphorylates AMP-activated protein kinase', *J Biol Chem*, 271: 27879-87.

Hawley, S. A., R. J. Ford, B. K. Smith, G. J. Gowans, S. J. Mancini, R. D. Pitt, E. A. Day, I. P. Salt, G. R. Steinberg, and D. G. Hardie. 2016. 'The Na+/Glucose Cotransporter Inhibitor Canagliflozin Activates AMPK by Inhibiting Mitochondrial Function and Increasing Cellular AMP Levels', *Diabetes*, 65: 2784-94.

Hawley, S. A., M. D. Fullerton, F. A. Ross, J. D. Schertzer, C. Chevtzoff, K. J. Walker, M. W. Peggie, D. Zibrova, K. A. Green, K. J. Mustard, B. E. Kemp, K. Sakamoto, G. R. Steinberg, and D. G. Hardie. 2012. 'The ancient drug salicylate directly activates AMP-activated protein kinase', *Science*, 336: 918-22.

Hawley, S. A., D. A. Pan, K. J. Mustard, L. Ross, J. Bain, A. M. Edelman, B. G. Frenguelli, and D. G. Hardie. 2005. 'Calmodulin-dependent protein kinase kinase-beta is an alternative upstream kinase for AMP-activated protein kinase', *Cell Metab*, 2: 9-19.

Hawley, S. A., F. A. Ross, G. J. Gowans, P. Tibarewal, N. R. Leslie, and D. G. Hardie. 2014. 'Phosphorylation by Akt within the ST loop of AMPK-alpha1 down-regulates its activation in tumour cells', *Biochem J*, 459: 275-87.

He, L., J. Gubbins, Z. Peng, V. Medina, F. Fei, K. Asahina, J. Wang, M. Kahn, C. B. Rountree, and B. L. Stiles. 2016. 'Activation of hepatic stellate cell in Pten null liver injury model', *Fibrogenesis Tissue Repair*, 9: 8.

Hebbard, L., and J. George. 2011. 'Animal models of nonalcoholic fatty liver disease', *Nat Rev Gastroenterol Hepatol*, 8: 35-44.

Hemminki, A., D. Markie, I. Tomlinson, E. Avizienyte, S. Roth, A. Loukola, G. Bignell, W. Warren, M. Aminoff, P. Hoglund, H. Jarvinen, P. Kristo, K. Pelin, M. Ridanpaa, R. Salovaara, T. Toro, W. Bodmer, S. Olschwang, A. S. Olsen, M. R. Stratton, A. de la Chapelle, and L. A. Aaltonen. 1998. 'A serine/threonine kinase gene defective in Peutz-Jeghers syndrome', *Nature*, 391: 184-7.

Henriksen, B. S., M. E. Curtis, N. Fillmore, B. R. Cardon, D. M. Thomson, and C. R. Hancock. 2013. 'The effects of chronic AMPK activation on hepatic triglyceride accumulation and glycerol 3-phosphate acyltransferase activity with high fat feeding', *Diabetol Metab Syndr*, 5: 29.

Herman, M. A., and V. T. Samuel. 2016. 'The Sweet Path to Metabolic Demise: Fructose and Lipid Synthesis', *Trends Endocrinol Metab*, 27: 719-30.

Hernandez-Gea, V., and S. L. Friedman. 2011. 'Pathogenesis of liver fibrosis', *Annu Rev Pathol*, 6: 425-56.

Hernandez-Gea, V., Z. Ghiassi-Nejad, R. Rozenfeld, R. Gordon, M. I. Fiel, Z. Yue, M. J. Czaja, and S. L. Friedman. 2012. 'Autophagy releases lipid that promotes fibrogenesis by activated hepatic stellate cells in mice and in human tissues', *Gastroenterology*, 142: 938-46.

Hernandez-Gea, V., S. Toffanin, S. L. Friedman, and J. M. Llovet. 2013. 'Role of the microenvironment in the pathogenesis and treatment of hepatocellular carcinoma', *Gastroenterology*, 144: 512-27.

Holmen, O. L., H. Zhang, Y. Fan, D. H. Hovelson, E. M. Schmidt, W. Zhou, Y. Guo, J. Zhang, A. Langhammer, M. L. Lochen, S. K. Ganesh, L. Vatten, F. Skorpen, H. Dalen, J. Zhang, S. Pennathur, J. Chen, C. Platou, E. B. Mathiesen, T. Wilsgaard, I. Njolstad, M. Boehnke, Y. E. Chen, G. R. Abecasis, K. Hveem, and C. J. Willer. 2014. 'Systematic evaluation of coding variation identifies a candidate causal variant in TM6SF2

influencing total cholesterol and myocardial infarction risk', *Nat Genet*, 46: 345-51.

Hommes, F. A. 1993. 'Inborn errors of fructose metabolism', *Am J Clin Nutr*, 58: 788s-95s.

Horie, Y., A. Suzuki, E. Kataoka, T. Sasaki, K. Hamada, J. Sasaki, K. Mizuno, G. Hasegawa, H. Kishimoto, M. Iizuka, M. Naito, K. Enomoto, S. Watanabe, T. W. Mak, and T. Nakano. 2004. 'Hepatocyte-specific Pten deficiency results in steatohepatitis and hepatocellular carcinomas', *J Clin Invest*, 113: 1774-83.

Hoshida, Y., A. Villanueva, M. Kobayashi, J. Peix, D. Y. Chiang, A. Camargo, S. Gupta, J. Moore, M. J. Wrobel, J. Lerner, M. Reich, J. A. Chan, J. N. Glickman, K. Ikeda, M. Hashimoto, G. Watanabe, M. G. Daidone, S. Roayaie, M. Schwartz, S. Thung, H. B. Salvesen, S. Gabriel, V. Mazzaferro, J. Bruix, S. L. Friedman, H. Kumada, J. M. Llovet, and T. R. Golub. 2008. 'Gene expression in fixed tissues and outcome in hepatocellular carcinoma', *N Engl J Med*, 359: 1995-2004.

Hosokawa, N., T. Hara, T. Kaizuka, C. Kishi, A. Takamura, Y. Miura, S. Iemura, T. Natsume, K. Takehana, N. Yamada, J. L. Guan, N. Oshiro, and N. Mizushima. 2009. 'Nutrient-dependent mTORC1 association with the ULK1-Atg13-FIP200 complex required for autophagy', *Mol Biol Cell*, 20: 1981-91.

Hotamisligil, G. S., N. S. Shargill, and B. M. Spiegelman. 1993. 'Adipose expression of tumor necrosis factor-alpha: direct role in obesity-linked insulin resistance', *Science*, 259: 87-91.

Hu, M., H. Huang, R. Zhao, P. Li, M. Li, H. Miao, N. Chen, and M. Chen. 2014. 'AZD8055 induces cell death associated with autophagy and activation of AMPK in hepatocellular carcinoma', *Oncol Rep*, 31: 649-56.

Hu, T. H., C. C. Huang, P. R. Lin, H. W. Chang, L. P. Ger, Y. W. Lin, C. S. Changchien, C. M. Lee, and M. H. Tai. 2003. 'Expression and prognostic role of tumor suppressor gene PTEN/MMAC1/TEP1 in hepatocellular carcinoma', *Cancer*, 97: 1929-40.

Hu, W., Z. Feng, J. Eveleigh, G. Iyer, J. Pan, S. Amin, F. L. Chung, and M. S. Tang. 2002. 'The major lipid peroxidation product, trans-4-hydroxy-2-nonenal, preferentially forms DNA adducts at codon 249 of human p53 gene, a unique mutational hotspot in hepatocellular carcinoma', *Carcinogenesis*, 23: 1781-9.

Huang, D., T. Dhawan, S. Young, W. H. Yong, L. G. Boros, and A. P. Heaney. 2011. 'Fructose impairs glucose-induced hepatic triglyceride synthesis', *Lipids Health Dis*, 10: 20.

Huang, J., Q. Deng, Q. Wang, K. Y. Li, J. H. Dai, N. Li, Z. D. Zhu, B. Zhou, X. Y. Liu, R. F. Liu, Q. L. Fei, H. Chen, B. Cai, B. Zhou, H. S. Xiao, L. X. Qin, and Z. G. Han. 2012. 'Exome sequencing of hepatitis B virus-associated hepatocellular carcinoma', *Nat Genet*, 44: 1117-21.

Huang, X., S. Wullschleger, N. Shpiro, V. A. McGuire, K. Sakamoto, Y. L. Woods, W. McBurnie, S. Fleming, and D. R. Alessi. 2008. 'Important role of the LKB1-AMPK pathway in suppressing tumorigenesis in PTEN-deficient mice', *Biochem J*, 412: 211-21.

Hudgins, L. C., M. K. Hellerstein, C. E. Seidman, R. A. Neese, J. D. Tremaroli, and J. Hirsch. 2000. 'Relationship between carbohydrate-induced hypertriglyceridemia and fatty acid synthesis in lean and obese subjects', *J Lipid Res*, 41: 595-604.

Hudson, E. R., D. A. Pan, J. James, J. M. Lucocq, S. A. Hawley, K. A. Green, O. Baba, T. Terashima, and D. G. Hardie. 2003. 'A novel domain in AMP-activated protein kinase causes glycogen storage bodies similar to those seen in hereditary cardiac arrhythmias', *Curr Biol*, 13: 861-6.

Huh, J., K. W. Kim, J. Kim, and E. Yu. 2015. 'Pathology-MRI Correlation of Hepatocarcinogenesis: Recent Update', *J Pathol Transl Med*, 49: 218-29.

Humphries, C. 2014. 'Sex differences: Luck of the chromosomes', *Nature*, 516: S10-1.

Iglesias, M. A., J. M. Ye, G. Frangioudakis, A. K. Saha, E. Tomas, N. B. Ruderman, G. J. Cooney, and E. W. Kraegen. 2002. 'AICAR administration causes an apparent enhancement of muscle and liver insulin action in insulin-resistant high-fat-fed rats', *Diabetes*, 51: 2886-94.

Iizuka, K., R. K. Bruick, G. Liang, J. D. Horton, and K. Uyeda. 2004. 'Deficiency of carbohydrate response element-binding protein (ChREBP) reduces lipogenesis as well as glycolysis', *Proc Natl Acad Sci U S A*, 101: 7281-6.

Imamura, K., T. Ogura, A. Kishimoto, M. Kaminishi, and H. Esumi. 2001. 'Cell cycle regulation via p53 phosphorylation by a 5'-AMP activated protein kinase activator, 5-aminoimidazole- 4-carboxamide-1-beta-D-ribofuranoside, in a human hepatocellular carcinoma cell line', *Biochem Biophys Res Commun*, 287: 562-7.

Inami, Y., S. Yamashina, K. Izumi, T. Ueno, I. Tanida, K. Ikejima, and S. Watanabe. 2011. 'Hepatic steatosis inhibits autophagic proteolysis via impairment of autophagosomal acidification and cathepsin expression', *Biochem Biophys Res Commun*, 412: 618-25.

Inoki, K., T. Zhu, and K. L. Guan. 2003. 'TSC2 mediates cellular energy response to control cell growth and survival', *Cell*, 115: 577-90.

Ioannou, G. N. 2016. 'The Role of Cholesterol in the Pathogenesis of NASH', *Trends Endocrinol Metab*, 27: 84-95.

Ioannou, G. N., O. B. Morrow, M. L. Connole, and S. P. Lee. 2009. 'Association between dietary nutrient composition and the incidence of cirrhosis or liver cancer in the United States population', *Hepatology*, 50: 175-84.

Ip, E., G. C. Farrell, G. Robertson, P. Hall, R. Kirsch, and I. Leclercq. 2003. 'Central role of PPARalpha-dependent hepatic lipid turnover in dietary steatohepatitis in mice', *Hepatology*, 38: 123-32.

Jager, S., C. Handschin, J. St-Pierre, and B. M. Spiegelman. 2007. 'AMP-activated protein kinase (AMPK) action in skeletal muscle via direct phosphorylation of PGC-1alpha', *Proc Natl Acad Sci U S A*, 104: 12017-22.

Jenne, D. E., H. Reimann, J. Nezu, W. Friedel, S. Loff, R. Jeschke, O. Muller, W. Back, and M. Zimmer. 1998. 'Peutz-Jeghers syndrome is caused by mutations in a novel serine threonine kinase', *Nat Genet*, 18: 38-43.

Jeon, S. M., N. S. Chandel, and N. Hay. 2012. 'AMPK regulates NADPH homeostasis to promote tumour cell survival during energy stress', *Nature*, 485: 661-5.

Ji, H., M. R. Ramsey, D. N. Hayes, C. Fan, K. McNamara, P. Kozlowski, C. Torrice, M. C. Wu, T. Shimamura, S. A. Perera, M. C. Liang, D. Cai, G. N. Naumov, L. Bao, C. M. Contreras, D. Li, L. Chen, J. Krishnamurthy, J. Koivunen, L. R. Chirieac, R. F. Padera, R. T. Bronson, N. I. Lindeman, D. C. Christiani, X. Lin, G. I. Shapiro, P. A. Janne, B. E. Johnson, M. Meyerson, D. J. Kwiatkowski, D. H. Castrillon, N. Bardeesy, N. E. Sharpless, and K. K. Wong. 2007. 'LKB1 modulates lung cancer differentiation and metastasis', *Nature*, 448: 807-10.

Jones, R. G., D. R. Plas, S. Kubek, M. Buzzai, J. Mu, Y. Xu, M. J. Birnbaum, and C. B. Thompson. 2005. 'AMP-activated protein kinase induces a p53-dependent metabolic checkpoint', *Mol Cell*, 18: 283-93.

Jorgensen, S. B., J. N. Nielsen, J. B. Birk, G. S. Olsen, B. Viollet, F. Andreelli, P. Schjerling, S. Vaulont, D. G. Hardie, B. F. Hansen, E. A. Richter, and J. F. Wojtaszewski. 2004. 'The alpha2-5'AMP-activated protein kinase is a site 2 glycogen synthase kinase in skeletal muscle and is responsive to glucose loading', *Diabetes*, 53: 3074-81.

Kamada, Y., H. Matsumoto, S. Tamura, J. Fukushima, S. Kiso, K. Fukui, T. Igura, N. Maeda, S. Kihara, T. Funahashi, Y. Matsuzawa, I. Shimomura, and N. Hayashi. 2007. 'Hypoadiponectinemia accelerates hepatic tumor formation in a nonalcoholic steatohepatitis mouse model', *J Hepatol*, 47: 556-64.

Kan, Z., H. Zheng, X. Liu, S. Li, T. D. Barber, Z. Gong, H. Gao, K. Hao, M. D. Willard, J. Xu, R. Hauptschein, P. A. Rejto, J. Fernandez, G. Wang, Q. Zhang, B. Wang, R. Chen, J. Wang, N. P. Lee, W. Zhou, Z. Lin, Z. Peng, K. Yi, S. Chen, L. Li, X. Fan, J. Yang, R. Ye, J. Ju, K. Wang, H. Estrella, S. Deng, P.

Wei, M. Qiu, I. H. Wulur, J. Liu, M. E. Ehsani, C. Zhang, A. Loboda, W. K. Sung, A. Aggarwal, R. T. Poon, S. T. Fan, J. Wang, J. Hardwick, C. Reinhard, H. Dai, Y. Li, J. M. Luk, and M. Mao. 2013. 'Whole-genome sequencing identifies recurrent mutations in hepatocellular carcinoma', *Genome Res*, 23: 1422-33.

Karin, M. 2006. 'Nuclear factor-kappaB in cancer development and progression', *Nature*, 441: 431-6.

Kawaguchi, T., K. Osatomi, H. Yamashita, T. Kabashima, and K. Uyeda. 2002. 'Mechanism for fatty acid "sparing" effect on glucose-induced transcription: regulation of carbohydrate-responsive element-binding protein by AMP-activated protein kinase', *J Biol Chem*, 277: 3829-35.

Kim, B. J., S. W. Ryu, and B. J. Song. 2006. 'JNK- and p38 kinase-mediated phosphorylation of Bax leads to its activation and mitochondrial translocation and to apoptosis of human hepatoma HepG2 cells', *J Biol Chem*, 281: 21256-65.

Kim, E., P. Goraksha-Hicks, L. Li, T. P. Neufeld, and K. L. Guan. 2008. 'Regulation of TORC1 by Rag GTPases in nutrient response', *Nat Cell Biol*, 10: 935-45.

Kim, J., M. Kundu, B. Viollet, and K. L. Guan. 2011. 'AMPK and mTOR regulate autophagy through direct phosphorylation of Ulk1', *Nat Cell Biol*, 13: 132-41.

Klein, J., L. A. Dawson, T. H. Tran, O. Adeyi, T. Purdie, M. Sherman, and A. Brade. 2014. 'Metabolic syndrome-related hepatocellular carcinoma treated by volumetric modulated arc therapy', *Curr Oncol*, 21: e340-4.

Kleiner, D. E., E. M. Brunt, M. Van Natta, C. Behling, M. J. Contos, O. W. Cummings, L. D. Ferrell, Y. C. Liu, M. S. Torbenson, A. Unalp-Arida, M. Yeh, A. J. McCullough, and A. J. Sanyal. 2005. 'Design and validation of a histological scoring system for nonalcoholic fatty liver disease', *Hepatology*, 41: 1313-21.

Klionsky, D. J. 2007. 'Autophagy: from phenomenology to molecular understanding in less than a decade', *Nat Rev Mol Cell Biol*, 8: 931-7.

Knudsen, E. S., P. Gopal, and A. G. Singal. 2014. 'The changing landscape of hepatocellular carcinoma: etiology, genetics, and therapy', *Am J Pathol*, 184: 574-83.

Knudson, A. G., Jr. 1971. 'Mutation and cancer: statistical study of retinoblastoma', *Proc Natl Acad Sci U S A*, 68: 820-3.

Koca, S. S., I. H. Bahcecioglu, O. K. Poyrazoglu, I. H. Ozercan, K. Sahin, and B. Ustundag. 2008. 'The treatment with antibody of TNF-alpha reduces the inflammation, necrosis and fibrosis in the non-alcoholic steatohepatitis induced by methionine- and choline-deficient diet', *Inflammation*, 31: 91-8.

Koehne de Gonzalez, A. K., M. A. Salomao, and S. M. Lagana. 2015. 'Current concepts in the immunohistochemical evaluation of liver tumors', *World J Hepatol*, 7: 1403-11.

Koga, H., S. Kaushik, and A. M. Cuervo. 2010. 'Altered lipid content inhibits autophagic vesicular fusion', *Faseb j*, 24: 3052-65.

Komatsu, M., S. Waguri, T. Ueno, J. Iwata, S. Murata, I. Tanida, J. Ezaki, N. Mizushima, Y. Ohsumi, Y. Uchiyama, E. Kominami, K. Tanaka, and T. Chiba. 2005. 'Impairment of starvation-induced and constitutive autophagy in Atg7-deficient mice', *J Cell Biol*, 169: 425-34.

Koo, H. Y., M. Miyashita, B. H. Cho, and M. T. Nakamura. 2009. 'Replacing dietary glucose with fructose increases ChREBP activity and SREBP-1 protein in rat liver nucleus', *Biochem Biophys Res Commun*, 390: 285-9.

Koo, S. H., L. Flechner, L. Qi, X. Zhang, R. A. Screaton, S. Jeffries, S. Hedrick, W. Xu, F. Boussouar, P. Brindle, H. Takemori, and M. Montminy. 2005. 'The CREB coactivator TORC2 is a key regulator of fasting glucose metabolism', *Nature*, 437: 1109-11.

Kozlitina, J., E. Smagris, S. Stender, B. G. Nordestgaard, H. H. Zhou, A. Tybjaerg-Hansen, T. F. Vogt, H. H. Hobbs, and J. C. Cohen. 2014. 'Exome-wide association study identifies a TM6SF2 variant that confers susceptibility to nonalcoholic fatty liver disease', *Nat Genet*, 46: 352-6.

Kudo, M. 2017. 'Systemic Therapy for Hepatocellular Carcinoma: 2017 Update', *Oncology*, 93 Suppl 1: 135-46.

Kudo, M., R. S. Finn, S. Qin, K. H. Han, K. Ikeda, F. Piscaglia, A. Baron, J. W. Park, G. Han, J. Jassem, J. F. Blanc, A. Vogel, D. Komov, T. R. J. Evans, C. Lopez, C. Dutcus, M. Guo, K. Saito, S. Kraljevic, T. Tamai, M. Ren, and A. L. Cheng. 2018. 'Lenvatinib versus sorafenib in first-line treatment of patients with unresectable hepatocellular carcinoma: a randomised phase 3 non-inferiority trial', *Lancet*, 391: 1163-73.

Laderoute, K. R., K. Amin, J. M. Calaoagan, M. Knapp, T. Le, J. Orduna, M. Foretz, and B. Viollet. 2006. '5'-AMP-activated protein kinase (AMPK) is induced by low-oxygen and glucose deprivation conditions found in solid-tumor microenvironments', *Mol Cell Biol*, 26: 5336-47.

Lambert, J. E., M. A. Ramos-Roman, J. D. Browning, and E. J. Parks. 2014. 'Increased de novo lipogenesis is a distinct characteristic of individuals with nonalcoholic fatty liver disease', *Gastroenterology*, 146: 726-35.

Larsson, S. C., and A. Wolk. 2007. 'Overweight, obesity and risk of liver cancer: a meta-analysis of cohort studies', *Br J Cancer*, 97: 1005-8.

Laugerette, F., C. Vors, A. Geloen, M. A. Chauvin, C. Soulage, S. Lambert-Porcheron, N. Peretti, M. Alligier, R. Burcelin, M. Laville, H. Vidal, and M.

C. Michalski. 2011. 'Emulsified lipids increase endotoxemia: possible role in early postprandial low-grade inflammation', *J Nutr Biochem*, 22: 53-9.
Lavallard, V. J., and P. Gual. 2014. 'Autophagy and non-alcoholic fatty liver disease', *Biomed Res Int*, 2014: 120179.
Lazo, M., and J. M. Clark. 2008. 'The epidemiology of nonalcoholic fatty liver disease: a global perspective', *Semin Liver Dis*, 28: 339-50.
Le Lay, J., G. Tuteja, P. White, R. Dhir, R. Ahima, and K. H. Kaestner. 2009. 'CRTC2 (TORC2) contributes to the transcriptional response to fasting in the liver but is not required for the maintenance of glucose homeostasis', *Cell Metab*, 10: 55-62.
Lee, A. H., E. F. Scapa, D. E. Cohen, and L. H. Glimcher. 2008. 'Regulation of hepatic lipogenesis by the transcription factor XBP1', *Science*, 320: 1492-6.
Lee, C. W., L. L. Wong, E. Y. Tse, H. F. Liu, V. Y. Leong, J. M. Lee, D. G. Hardie, I. O. Ng, and Y. P. Ching. 2012. 'AMPK promotes p53 acetylation via phosphorylation and inactivation of SIRT1 in liver cancer cells', *Cancer Res*, 72: 4394-404.
Lee, J. S., and S. S. Thorgeirsson. 2004. 'Genome-scale profiling of gene expression in hepatocellular carcinoma: classification, survival prediction, and identification of therapeutic targets', *Gastroenterology*, 127: S51-5.
Li, J., C. Yen, D. Liaw, K. Podsypanina, S. Bose, S. I. Wang, J. Puc, C. Miliaresis, L. Rodgers, R. McCombie, S. H. Bigner, B. C. Giovanella, M. Ittmann, B. Tycko, H. Hibshoosh, M. H. Wigler, and R. Parsons. 1997. 'PTEN, a putative protein tyrosine phosphatase gene mutated in human brain, breast, and prostate cancer', *Science*, 275: 1943-7.
Li, J. Z., Y. Huang, R. Karaman, P. T. Ivanova, H. A. Brown, T. Roddy, J. Castro-Perez, J. C. Cohen, and H. H. Hobbs. 2012. 'Chronic overexpression of PNPLA3I148M in mouse liver causes hepatic steatosis', *J Clin Invest*, 122: 4130-44.
Li, Y., K. Jadhav, and Y. Zhang. 2013. 'Bile acid receptors in non-alcoholic fatty liver disease', *Biochem Pharmacol*, 86: 1517-24.
Li, Y., T. J. Soos, X. Li, J. Wu, M. Degennaro, X. Sun, D. R. Littman, M. J. Birnbaum, and R. D. Polakiewicz. 2004. 'Protein kinase C Theta inhibits insulin signaling by phosphorylating IRS1 at Ser(1101)', *J Biol Chem*, 279: 45304-7.
Li, Y., S. Xu, M. M. Mihaylova, B. Zheng, X. Hou, B. Jiang, O. Park, Z. Luo, E. Lefai, J. Y. Shyy, B. Gao, M. Wierzbicki, T. J. Verbeuren, R. J. Shaw, R. A. Cohen, and M. Zang. 2011. 'AMPK phosphorylates and inhibits SREBP activity to attenuate hepatic steatosis and atherosclerosis in diet-induced insulin-resistant mice', *Cell Metab*, 13: 376-88.

Liang, J., and G. B. Mills. 2013. 'AMPK: a contextual oncogene or tumor suppressor?', *Cancer Res*, 73: 2929-35.

Liang, J., S. H. Shao, Z. X. Xu, B. Hennessy, Z. Ding, M. Larrea, S. Kondo, D. J. Dumont, J. U. Gutterman, C. L. Walker, J. M. Slingerland, and G. B. Mills. 2007. 'The energy sensing LKB1-AMPK pathway regulates p27(kip1) phosphorylation mediating the decision to enter autophagy or apoptosis', *Nat Cell Biol*, 9: 218-24.

Lim, J. S., M. Mietus-Snyder, A. Valente, J. M. Schwarz, and R. H. Lustig. 2010. 'The role of fructose in the pathogenesis of NAFLD and the metabolic syndrome', *Nat Rev Gastroenterol Hepatol*, 7: 251-64.

Listenberger, L. L., X. Han, S. E. Lewis, S. Cases, R. V. Farese, Jr., D. S. Ory, and J. E. Schaffer. 2003. 'Triglyceride accumulation protects against fatty acid-induced lipotoxicity', *Proc Natl Acad Sci U S A*, 100: 3077-82.

Liu, Y. L., H. L. Reeves, A. D. Burt, D. Tiniakos, S. McPherson, J. B. Leathart, M. E. Allison, G. J. Alexander, A. C. Piguet, R. Anty, P. Donaldson, G. P. Aithal, S. Francque, L. Van Gaal, K. Clement, V. Ratziu, J. F. Dufour, C. P. Day, A. K. Daly, and Q. M. Anstee. 2014. 'TM6SF2 rs58542926 influences hepatic fibrosis progression in patients with non-alcoholic fatty liver disease', *Nat Commun*, 5: 4309.

Llovet, J. M., J. Zucman-Rossi, E. Pikarsky, B. Sangro, M. Schwartz, M. Sherman, and G. Gores. 2016. 'Hepatocellular carcinoma', *Nat Rev Dis Primers*, 2: 16018.

Lodish, M. B., and C. A. Stratakis. 2010. 'Endocrine tumours in neurofibromatosis type 1, tuberous sclerosis and related syndromes', *Best Pract Res Clin Endocrinol Metab*, 24: 439-49.

Maeda, S., H. Kamata, J. L. Luo, H. Leffert, and M. Karin. 2005. 'IKKbeta couples hepatocyte death to cytokine-driven compensatory proliferation that promotes chemical hepatocarcinogenesis', *Cell*, 121: 977-90.

Malhi, H., F. J. Barreyro, H. Isomoto, S. F. Bronk, and G. J. Gores. 2007. 'Free fatty acids sensitise hepatocytes to TRAIL mediated cytotoxicity', *Gut*, 56: 1124-31.

Malhi, H., S. F. Bronk, N. W. Werneburg, and G. J. Gores. 2006. 'Free fatty acids induce JNK-dependent hepatocyte lipoapoptosis', *J Biol Chem*, 281: 12093-101.

Malhi, H., and G. J. Gores. 2008. 'Molecular mechanisms of lipotoxicity in nonalcoholic fatty liver disease', *Semin Liver Dis*, 28: 360-9.

Marengo, A., C. Rosso, and E. Bugianesi. 2016. 'Liver Cancer: Connections with Obesity, Fatty Liver, and Cirrhosis', *Annu Rev Med*, 67: 103-17.

Mari, M., F. Caballero, A. Colell, A. Morales, J. Caballeria, A. Fernandez, C. Enrich, J. C. Fernandez-Checa, and C. Garcia-Ruiz. 2006. 'Mitochondrial

free cholesterol loading sensitizes to TNF- and Fas-mediated steatohepatitis', *Cell Metab*, 4: 185-98.

Marsin, A. S., L. Bertrand, M. H. Rider, J. Deprez, C. Beauloye, M. F. Vincent, G. Van den Berghe, D. Carling, and L. Hue. 2000. 'Phosphorylation and activation of heart PFK-2 by AMPK has a role in the stimulation of glycolysis during ischaemia', *Curr Biol*, 10: 1247-55.

Marsin, A. S., C. Bouzin, L. Bertrand, and L. Hue. 2002. 'The stimulation of glycolysis by hypoxia in activated monocytes is mediated by AMP-activated protein kinase and inducible 6-phosphofructo-2-kinase', *J Biol Chem*, 277: 30778-83.

McDevitt, R. M., S. J. Bott, M. Harding, W. A. Coward, L. J. Bluck, and A. M. Prentice. 2001. 'De novo lipogenesis during controlled overfeeding with sucrose or glucose in lean and obese women', *Am J Clin Nutr*, 74: 737-46.

McGarry, J. D., G. F. Leatherman, and D. W. Foster. 1978. 'Carnitine palmitoyltransferase I. The site of inhibition of hepatic fatty acid oxidation by malonyl-CoA', *J Biol Chem*, 253: 4128-36.

McPherson, S., S. F. Stewart, E. Henderson, A. D. Burt, and C. P. Day. 2010. 'Simple non-invasive fibrosis scoring systems can reliably exclude advanced fibrosis in patients with non-alcoholic fatty liver disease', *Gut*, 59: 1265-9.

Menendez, J. A., and R. Lupu. 2007. 'Fatty acid synthase and the lipogenic phenotype in cancer pathogenesis', *Nat Rev Cancer*, 7: 763-77.

Merrill, G. F., E. J. Kurth, D. G. Hardie, and W. W. Winder. 1997. 'AICA riboside increases AMP-activated protein kinase, fatty acid oxidation, and glucose uptake in rat muscle', *Am J Physiol*, 273: E1107-12.

Mihaylova, M. M., and R. J. Shaw. 2011. 'The AMPK signalling pathway coordinates cell growth, autophagy and metabolism', *Nat Cell Biol*, 13: 1016-23.

Milan, D., J. T. Jeon, C. Looft, V. Amarger, A. Robic, M. Thelander, C. Rogel-Gaillard, S. Paul, N. Iannuccelli, L. Rask, H. Ronne, K. Lundstrom, N. Reinsch, J. Gellin, E. Kalm, P. L. Roy, P. Chardon, and L. Andersson. 2000. 'A mutation in PRKAG3 associated with excess glycogen content in pig skeletal muscle', *Science*, 288: 1248-51.

Milgraum, L. Z., L. A. Witters, G. R. Pasternack, and F. P. Kuhajda. 1997. 'Enzymes of the fatty acid synthesis pathway are highly expressed in in situ breast carcinoma', *Clin Cancer Res*, 3: 2115-20.

Min, H. K., A. Kapoor, M. Fuchs, F. Mirshahi, H. Zhou, J. Maher, J. Kellum, R. Warnick, M. J. Contos, and A. J. Sanyal. 2012. 'Increased hepatic synthesis and dysregulation of cholesterol metabolism is associated with the severity of nonalcoholic fatty liver disease', *Cell Metab*, 15: 665-74.

Miyazaki, J., S. Takaki, K. Araki, F. Tashiro, A. Tominaga, K. Takatsu, and K. Yamamura. 1989. 'Expression vector system based on the chicken beta-actin promoter directs efficient production of interleukin-5', *Gene*, 79: 269-77.

Mohamed-Ali, V., S. Goodrick, A. Rawesh, D. R. Katz, J. M. Miles, J. S. Yudkin, S. Klein, and S. W. Coppack. 1997. 'Subcutaneous adipose tissue releases interleukin-6, but not tumor necrosis factor-alpha, in vivo', *J Clin Endocrinol Metab*, 82: 4196-200.

Molloy, J. W., C. J. Calcagno, C. D. Williams, F. J. Jones, D. M. Torres, and S. A. Harrison. 2012. 'Association of coffee and caffeine consumption with fatty liver disease, nonalcoholic steatohepatitis, and degree of hepatic fibrosis', *Hepatology*, 55: 429-36.

Moore, J. B., P. J. Gunn, and B. A. Fielding. 2014. 'The role of dietary sugars and de novo lipogenesis in non-alcoholic fatty liver disease', *Nutrients*, 6: 5679-703.

Mottillo, E. P., E. M. Desjardins, J. D. Crane, B. K. Smith, A. E. Green, S. Ducommun, T. I. Henriksen, I. A. Rebalka, A. Razi, K. Sakamoto, C. Scheele, B. E. Kemp, T. J. Hawke, J. Ortega, J. G. Granneman, and G. R. Steinberg. 2016. 'Lack of Adipocyte AMPK Exacerbates Insulin Resistance and Hepatic Steatosis through Brown and Beige Adipose Tissue Function', *Cell Metab*, 24: 118-29.

Mounier, C., L. Bouraoui, and E. Rassart. 2014. 'Lipogenesis in cancer progression (review)', *Int J Oncol*, 45: 485-92.

Mudaliar, S., R. R. Henry, A. J. Sanyal, L. Morrow, H. U. Marschall, M. Kipnes, L. Adorini, C. I. Sciacca, P. Clopton, E. Castelloe, P. Dillon, M. Pruzanski, and D. Shapiro. 2013. 'Efficacy and safety of the farnesoid X receptor agonist obeticholic acid in patients with type 2 diabetes and nonalcoholic fatty liver disease', *Gastroenterology*, 145: 574-82.e1.

Muir, K., A. Hazim, Y. He, M. Peyressatre, D. Y. Kim, X. Song, and L. Beretta. 2013. 'Proteomic and lipidomic signatures of lipid metabolism in NASH-associated hepatocellular carcinoma', *Cancer Res*, 73: 4722-31.

Muoio, D. M., K. Seefeld, L. A. Witters, and R. A. Coleman. 1999. 'AMP-activated kinase reciprocally regulates triacylglycerol synthesis and fatty acid oxidation in liver and muscle: evidence that sn-glycerol-3-phosphate acyltransferase is a novel target', *Biochem J*, 338 ( Pt 3): 783-91.

Musso, G., R. Gambino, and M. Cassader. 2010. 'Non-alcoholic fatty liver disease from pathogenesis to management: an update', *Obes Rev*, 11: 430-45.

Musso, G., R. Gambino, G. Pacini, G. Pagano, M. Durazzo, and M. Cassader. 2009. 'Transcription factor 7-like 2 polymorphism modulates glucose and

lipid homeostasis, adipokine profile, and hepatocyte apoptosis in NASH', *Hepatology*, 49: 426-35.

Myers, R. W., H. P. Guan, J. Ehrhart, A. Petrov, S. Prahalada, E. Tozzo, X. Yang, M. M. Kurtz, M. Trujillo, D. Gonzalez Trotter, D. Feng, S. Xu, G. Eiermann, M. A. Holahan, D. Rubins, S. Conarello, X. Niu, S. C. Souza, C. Miller, J. Liu, K. Lu, W. Feng, Y. Li, R. E. Painter, J. A. Milligan, H. He, F. Liu, A. Ogawa, D. Wisniewski, R. J. Rohm, L. Wang, M. Bunzel, Y. Qian, W. Zhu, H. Wang, B. Bennet, L. LaFranco Scheuch, G. E. Fernandez, C. Li, M. Klimas, G. Zhou, M. van Heek, T. Biftu, A. Weber, D. E. Kelley, N. Thornberry, M. D. Erion, D. M. Kemp, and I. K. Sebhat. 2017. 'Systemic pan-AMPK activator MK-8722 improves glucose homeostasis but induces cardiac hypertrophy', *Science*, 357: 507-11.

Nagata, R., Y. Nishio, O. Sekine, Y. Nagai, Y. Maeno, S. Ugi, H. Maegawa, and A. Kashiwagi. 2004. 'Single nucleotide polymorphism (-468 Gly to A) at the promoter region of SREBP-1c associates with genetic defect of fructose-induced hepatic lipogenesis [corrected]', *J Biol Chem*, 279: 29031-42.

Nault, J. C., M. Mallet, C. Pilati, J. Calderaro, P. Bioulac-Sage, C. Laurent, A. Laurent, D. Cherqui, C. Balabaud, and J. Zucman-Rossi. 2013. 'High frequency of telomerase reverse-transcriptase promoter somatic mutations in hepatocellular carcinoma and preneoplastic lesions', *Nat Commun*, 4: 2218.

Neuschwander-Tetri, B. A. 2010. 'Hepatic lipotoxicity and the pathogenesis of nonalcoholic steatohepatitis: the central role of nontriglyceride fatty acid metabolites', *Hepatology*, 52: 774-88.

Nolan, C. J., P. Damm, and M. Prentki. 2011. 'Type 2 diabetes across generations: from pathophysiology to prevention and management', *Lancet*, 378: 169-81.

O'Neill, H. M., S. J. Maarbjerg, J. D. Crane, J. Jeppesen, S. B. Jorgensen, J. D. Schertzer, O. Shyroka, B. Kiens, B. J. van Denderen, M. A. Tarnopolsky, B. E. Kemp, E. A. Richter, and G. R. Steinberg. 2011. 'AMP-activated protein kinase (AMPK) beta1beta2 muscle null mice reveal an essential role for AMPK in maintaining mitochondrial content and glucose uptake during exercise', *Proc Natl Acad Sci U S A*, 108: 16092-7.

Ogden, C. L., S. Z. Yanovski, M. D. Carroll, and K. M. Flegal. 2007. 'The epidemiology of obesity', *Gastroenterology*, 132: 2087-102.

Ozcan, U., Q. Cao, E. Yilmaz, A. H. Lee, N. N. Iwakoshi, E. Ozdelen, G. Tuncman, C. Gorgun, L. H. Glimcher, and G. S. Hotamisligil. 2004. 'Endoplasmic reticulum stress links obesity, insulin action, and type 2 diabetes', *Science*, 306: 457-61.

Pagliassotti, M. J., P. A. Prach, T. A. Koppenhafer, and D. A. Pan. 1996. 'Changes in insulin action, triglycerides, and lipid composition during sucrose feeding in rats', *Am J Physiol*, 271: R1319-26.

Park, E. J., J. H. Lee, G. Y. Yu, G. He, S. R. Ali, R. G. Holzer, C. H. Osterreicher, H. Takahashi, and M. Karin. 2010. 'Dietary and genetic obesity promote liver inflammation and tumorigenesis by enhancing IL-6 and TNF expression', *Cell*, 140: 197-208.

Parks, E. J., L. E. Skokan, M. T. Timlin, and C. S. Dingfelder. 2008. 'Dietary sugars stimulate fatty acid synthesis in adults', *J Nutr*, 138: 1039-46.

Pehmoller, C., J. T. Treebak, J. B. Birk, S. Chen, C. Mackintosh, D. G. Hardie, E. A. Richter, and J. F. Wojtaszewski. 2009. 'Genetic disruption of AMPK signaling abolishes both contraction- and insulin-stimulated TBC1D1 phosphorylation and 14-3-3 binding in mouse skeletal muscle', *Am J Physiol Endocrinol Metab*, 297: E665-75.

Peyrou, M., L. Bourgoin, and M. Foti. 2010. 'PTEN in non-alcoholic fatty liver disease/non-alcoholic steatohepatitis and cancer', *Dig Dis*, 28: 236-46.

Phoenix, K. N., C. V. Devarakonda, M. M. Fox, L. E. Stevens, and K. P. Claffey. 2012. 'AMPKalpha2 Suppresses Murine Embryonic Fibroblast Transformation and Tumorigenesis', *Genes Cancer*, 3: 51-62.

Piguet, A. C., U. Saran, C. Simillion, I. Keller, L. Terracciano, H. L. Reeves, and J. F. Dufour. 2015. 'Regular exercise decreases liver tumors development in hepatocyte-specific PTEN-deficient mice independently of steatosis', *J Hepatol*, 62: 1296-303.

Pikarsky, Eli, Rinnat M. Porat, Ilan Stein, Rinat Abramovitch, Sharon Amit, Shafika Kasem, Elena Gutkovich-Pyest, Simcha Urieli-Shoval, Eithan Galun, and Yinon Ben-Neriah. 2004. 'NF-[kappa]B functions as a tumour promoter in inflammation-associated cancer', *Nature*, 431: 461-66.

Pineda, C. T., S. Ramanathan, K. Fon Tacer, J. L. Weon, M. B. Potts, Y. H. Ou, M. A. White, and P. R. Potts. 2015. 'Degradation of AMPK by a cancer-specific ubiquitin ligase', *Cell*, 160: 715-28.

Pirazzi, C., M. Adiels, M. A. Burza, R. M. Mancina, M. Levin, M. Stahlman, M. R. Taskinen, M. Orho-Melander, J. Perman, A. Pujia, L. Andersson, C. Maglio, T. Montalcini, O. Wiklund, J. Boren, and S. Romeo. 2012. 'Patatin-like phospholipase domain-containing 3 (PNPLA3) I148M (rs738409) affects hepatic VLDL secretion in humans and in vitro', *J Hepatol*, 57: 1276-82.

Pizer, E. S., F. J. Chrest, J. A. DiGiuseppe, and W. F. Han. 1998. 'Pharmacological inhibitors of mammalian fatty acid synthase suppress DNA replication and induce apoptosis in tumor cell lines', *Cancer Res*, 58: 4611-5.

Pold, R., L. S. Jensen, N. Jessen, E. S. Buhl, O. Schmitz, A. Flyvbjerg, N. Fujii, L. J. Goodyear, C. F. Gotfredsen, C. L. Brand, and S. Lund. 2005. 'Long-term

AICAR administration and exercise prevents diabetes in ZDF rats', *Diabetes*, 54: 928-34.

Postic, C., M. Shiota, K. D. Niswender, T. L. Jetton, Y. Chen, J. M. Moates, K. D. Shelton, J. Lindner, A. D. Cherrington, and M. A. Magnuson. 1999. 'Dual roles for glucokinase in glucose homeostasis as determined by liver and pancreatic beta cell-specific gene knock-outs using Cre recombinase', *J Biol Chem*, 274: 305-15.

Powell, E. E., W. G. Cooksley, R. Hanson, J. Searle, J. W. Halliday, and L. W. Powell. 1990. 'The natural history of nonalcoholic steatohepatitis: a follow-up study of forty-two patients for up to 21 years', *Hepatology*, 11: 74-80.

Puri, P., R. A. Baillie, M. M. Wiest, F. Mirshahi, J. Choudhury, O. Cheung, C. Sargeant, M. J. Contos, and A. J. Sanyal. 2007. 'A lipidomic analysis of nonalcoholic fatty liver disease', *Hepatology*, 46: 1081-90.

Puri, P., F. Mirshahi, O. Cheung, R. Natarajan, J. W. Maher, J. M. Kellum, and A. J. Sanyal. 2008. 'Activation and dysregulation of the unfolded protein response in nonalcoholic fatty liver disease', *Gastroenterology*, 134: 568-76.

Qian, G. S., R. K. Ross, M. C. Yu, J. M. Yuan, Y. T. Gao, B. E. Henderson, G. N. Wogan, and J. D. Groopman. 1994. 'A follow-up study of urinary markers of aflatoxin exposure and liver cancer risk in Shanghai, People's Republic of China', *Cancer Epidemiol Biomarkers Prev*, 3: 3-10.

Qu, X., J. Yu, G. Bhagat, N. Furuya, H. Hibshoosh, A. Troxel, J. Rosen, E. L. Eskelinen, N. Mizushima, Y. Ohsumi, G. Cattoretti, and B. Levine. 2003. 'Promotion of tumorigenesis by heterozygous disruption of the beclin 1 autophagy gene', *J Clin Invest*, 112: 1809-20.

Reeves, H. L., M. Y. Zaki, and C. P. Day. 2016. 'Hepatocellular Carcinoma in Obesity, Type 2 Diabetes, and NAFLD', *Dig Dis Sci*, 61: 1234-45.

Richardson, M. M., J. R. Jonsson, E. E. Powell, E. M. Brunt, B. A. Neuschwander-Tetri, P. S. Bhathal, J. B. Dixon, M. D. Weltman, H. Tilg, A. R. Moschen, D. M. Purdie, A. J. Demetris, and A. D. Clouston. 2007. 'Progressive fibrosis in nonalcoholic steatohepatitis: association with altered regeneration and a ductular reaction', *Gastroenterology*, 133: 80-90.

Ridlon, J. M., D. J. Kang, P. B. Hylemon, and J. S. Bajaj. 2014. 'Bile acids and the gut microbiome', *Curr Opin Gastroenterol*, 30: 332-8.

Rinella, M., and M. Charlton. 2016. 'The globalization of nonalcoholic fatty liver disease: Prevalence and impact on world health', *Hepatology*, 64: 19-22.

Romeo, S., J. Kozlitina, C. Xing, A. Pertsemlidis, D. Cox, L. A. Pennacchio, E. Boerwinkle, J. C. Cohen, and H. H. Hobbs. 2008. 'Genetic variation in

PNPLA3 confers susceptibility to nonalcoholic fatty liver disease', *Nat Genet*, 40: 1461-5.

Rosilio, C., N. Lounnas, M. Nebout, V. Imbert, T. Hagenbeek, H. Spits, V. Asnafi, R. Pontier-Bres, J. Reverso, J. F. Michiels, I. B. Sahra, F. Bost, and J. F. Peyron. 2013. 'The metabolic perturbators metformin, phenformin and AICAR interfere with the growth and survival of murine PTEN-deficient T cell lymphomas and human T-ALL/T-LL cancer cells', *Cancer Lett*, 336: 114-26.

Ross, F. A., C. MacKintosh, and D. G. Hardie. 2016. 'AMP-activated protein kinase: a cellular energy sensor that comes in 12 flavours', *Febs j*, 283: 2987-3001.

Ruderman, N. B., D. Carling, M. Prentki, and J. M. Cacicedo. 2013. 'AMPK, insulin resistance, and the metabolic syndrome', *J Clin Invest*, 123: 2764-72.

Rui, L. 2014. 'Energy metabolism in the liver', *Compr Physiol*, 4: 177-97.

Sag, D., D. Carling, R. D. Stout, and J. Suttles. 2008. 'Adenosine 5'-monophosphate-activated protein kinase promotes macrophage polarization to an anti-inflammatory functional phenotype', *J Immunol*, 181: 8633-41.

Saha, A. K., A. J. Schwarsin, R. Roduit, F. Masse, V. Kaushik, K. Tornheim, M. Prentki, and N. B. Ruderman. 2000. 'Activation of malonyl-CoA decarboxylase in rat skeletal muscle by contraction and the AMP-activated protein kinase activator 5-aminoimidazole-4-carboxamide-1-beta -D-ribofuranoside', *J Biol Chem*, 275: 24279-83.

Salomao, M., H. Remotti, R. Vaughan, A. B. Siegel, J. H. Lefkowitch, and R. K. Moreira. 2012. 'The steatohepatitic variant of hepatocellular carcinoma and its association with underlying steatohepatitis', *Hum Pathol*, 43: 737-46.

Salt, I. P., G. Johnson, S. J. Ashcroft, and D. G. Hardie. 1998. 'AMP-activated protein kinase is activated by low glucose in cell lines derived from pancreatic beta cells, and may regulate insulin release', *Biochem J*, 335 ( Pt 3): 533-9.

Sancak, Y., L. Bar-Peled, R. Zoncu, A. L. Markhard, S. Nada, and D. M. Sabatini. 2010. 'Ragulator-Rag complex targets mTORC1 to the lysosomal surface and is necessary for its activation by amino acids', *Cell*, 141: 290-303.

Sancak, Y., T. R. Peterson, Y. D. Shaul, R. A. Lindquist, C. C. Thoreen, L. Bar-Peled, and D. M. Sabatini. 2008. 'The Rag GTPases bind raptor and mediate amino acid signaling to mTORC1', *Science*, 320: 1496-501.

Sanyal, A. J., C. Campbell-Sargent, F. Mirshahi, W. B. Rizzo, M. J. Contos, R. K. Sterling, V. A. Luketic, M. L. Shiffman, and J. N. Clore. 2001. 'Nonalcoholic

steatohepatitis: association of insulin resistance and mitochondrial abnormalities', *Gastroenterology*, 120: 1183-92.

Savard, C., E. V. Tartaglione, R. Kuver, W. G. Haigh, G. C. Farrell, S. Subramanian, A. Chait, M. M. Yeh, L. S. Quinn, and G. N. Ioannou. 2013. 'Synergistic interaction of dietary cholesterol and dietary fat in inducing experimental steatohepatitis', *Hepatology*, 57: 81-92.

Schaap, F. G., M. Trauner, and P. L. Jansen. 2014. 'Bile acid receptors as targets for drug development', *Nat Rev Gastroenterol Hepatol*, 11: 55-67.

Schlageter, M., L. M. Terracciano, S. D'Angelo, and P. Sorrentino. 2014. 'Histopathology of hepatocellular carcinoma', *World J Gastroenterol*, 20: 15955-64.

Schmittgen, T. D., and K. J. Livak. 2008. 'Analyzing real-time PCR data by the comparative C(T) method', *Nat Protoc*, 3: 1101-8.

Schulze, K., S. Imbeaud, E. Letouze, L. B. Alexandrov, J. Calderaro, S. Rebouissou, G. Couchy, C. Meiller, J. Shinde, F. Soysouvanh, A. L. Calatayud, R. Pinyol, L. Pelletier, C. Balabaud, A. Laurent, J. F. Blanc, V. Mazzaferro, F. Calvo, A. Villanueva, J. C. Nault, P. Bioulac-Sage, M. R. Stratton, J. M. Llovet, and J. Zucman-Rossi. 2015. 'Exome sequencing of hepatocellular carcinomas identifies new mutational signatures and potential therapeutic targets', *Nat Genet*, 47: 505-11.

Schwarz, J. M., R. A. Neese, S. Turner, D. Dare, and M. K. Hellerstein. 1995. 'Short-term alterations in carbohydrate energy intake in humans. Striking effects on hepatic glucose production, de novo lipogenesis, lipolysis, and whole-body fuel selection', *J Clin Invest*, 96: 2735-43.

Schwarz, J. M., S. M. Noworolski, M. J. Wen, A. Dyachenko, J. L. Prior, M. E. Weinberg, L. A. Herraiz, V. W. Tai, N. Bergeron, T. P. Bersot, M. N. Rao, M. Schambelan, and K. Mulligan. 2015. 'Effect of a High-Fructose Weight-Maintaining Diet on Lipogenesis and Liver Fat', *J Clin Endocrinol Metab*, 100: 2434-42.

Schwiertz, A., D. Taras, K. Schafer, S. Beijer, N. A. Bos, C. Donus, and P. D. Hardt. 2010. 'Microbiota and SCFA in lean and overweight healthy subjects', *Obesity (Silver Spring)*, 18: 190-5.

Scudellari, M. 2014. 'Drug development: try and try again', *Nature*, 516: S4-6.

Seki, S., T. Kitada, and H. Sakaguchi. 2005. 'Clinicopathological significance of oxidative cellular damage in non-alcoholic fatty liver diseases', *Hepatol Res*, 33: 132-4.

Sell, S., J. M. Hunt, H. A. Dunsford, and F. V. Chisari. 1991. 'Synergy between hepatitis B virus expression and chemical hepatocarcinogens in transgenic mice', *Cancer Res*, 51: 1278-85.

Shackelford, D. B., E. Abt, L. Gerken, D. S. Vasquez, A. Seki, M. Leblanc, L. Wei, M. C. Fishbein, J. Czernin, P. S. Mischel, and R. J. Shaw. 2013. 'LKB1 inactivation dictates therapeutic response of non-small cell lung cancer to the metabolism drug phenformin', *Cancer Cell*, 23: 143-58.

Shackelford, D. B., and R. J. Shaw. 2009. 'The LKB1-AMPK pathway: metabolism and growth control in tumour suppression', *Nat Rev Cancer*, 9: 563-75.

Shaw, R. J., N. Bardeesy, B. D. Manning, L. Lopez, M. Kosmatka, R. A. DePinho, and L. C. Cantley. 2004. 'The LKB1 tumor suppressor negatively regulates mTOR signaling', *Cancer Cell*, 6: 91-9.

She, P., S. C. Burgess, M. Shiota, P. Flakoll, E. P. Donahue, C. R. Malloy, A. D. Sherry, and M. A. Magnuson. 2003. 'Mechanisms by which liver-specific PEPCK knockout mice preserve euglycemia during starvation', *Diabetes*, 52: 1649-54.

Sievenpiper, J. L., R. J. de Souza, A. Mirrahimi, M. E. Yu, A. J. Carleton, J. Beyene, L. Chiavaroli, M. Di Buono, A. L. Jenkins, L. A. Leiter, T. M. Wolever, C. W. Kendall, and D. J. Jenkins. 2012. 'Effect of fructose on body weight in controlled feeding trials: a systematic review and meta-analysis', *Ann Intern Med*, 156: 291-304.

Singh, R., S. Kaushik, Y. Wang, Y. Xiang, I. Novak, M. Komatsu, K. Tanaka, A. M. Cuervo, and M. J. Czaja. 2009. 'Autophagy regulates lipid metabolism', *Nature*, 458: 1131-5.

Sinha, R. A., B. L. Farah, B. K. Singh, M. M. Siddique, Y. Li, Y. Wu, O. R. Ilkayeva, J. Gooding, J. Ching, J. Zhou, L. Martinez, S. Xie, B. H. Bay, S. A. Summers, C. B. Newgard, and P. M. Yen. 2014. 'Caffeine stimulates hepatic lipid metabolism by the autophagy-lysosomal pathway in mice', *Hepatology*, 59: 1366-80.

Song, M. S., L. Salmena, and P. P. Pandolfi. 2012. 'The functions and regulation of the PTEN tumour suppressor', *Nat Rev Mol Cell Biol*, 13: 283-96.

Song, X. M., M. Fiedler, D. Galuska, J. W. Ryder, M. Fernstrom, A. V. Chibalin, H. Wallberg-Henriksson, and J. R. Zierath. 2002. '5-Aminoimidazole-4-carboxamide ribonucleoside treatment improves glucose homeostasis in insulin-resistant diabetic (ob/ob) mice', *Diabetologia*, 45: 56-65.

Stanhope, K. L., J. M. Schwarz, N. L. Keim, S. C. Griffen, A. A. Bremer, J. L. Graham, B. Hatcher, C. L. Cox, A. Dyachenko, W. Zhang, J. P. McGahan, A. Seibert, R. M. Krauss, S. Chiu, E. J. Schaefer, M. Ai, S. Otokozawa, K. Nakajima, T. Nakano, C. Beysen, M. K. Hellerstein, L. Berglund, and P. J. Havel. 2009. 'Consuming fructose-sweetened, not glucose-sweetened, beverages increases visceral adiposity and lipids and decreases insulin sensitivity in overweight/obese humans', *J Clin Invest*, 119: 1322-34.

Starley, B. Q., C. J. Calcagno, and S. A. Harrison. 2010. 'Nonalcoholic fatty liver disease and hepatocellular carcinoma: a weighty connection', *Hepatology*, 51: 1820-32.

Steck, P. A., M. A. Pershouse, S. A. Jasser, W. K. Yung, H. Lin, A. H. Ligon, L. A. Langford, M. L. Baumgard, T. Hattier, T. Davis, C. Frye, R. Hu, B. Swedlund, D. H. Teng, and S. V. Tavtigian. 1997. 'Identification of a candidate tumour suppressor gene, MMAC1, at chromosome 10q23.3 that is mutated in multiple advanced cancers', *Nat Genet*, 15: 356-62.

Stefanou, N., V. Papanikolaou, Y. Furukawa, Y. Nakamura, and A. Tsezou. 2010. 'Leptin as a critical regulator of hepatocellular carcinoma development through modulation of human telomerase reverse transcriptase', *BMC Cancer*, 10: 442.

Stephenne, X., M. Foretz, N. Taleux, G. C. van der Zon, E. Sokal, L. Hue, B. Viollet, and B. Guigas. 2011. 'Metformin activates AMP-activated protein kinase in primary human hepatocytes by decreasing cellular energy status', *Diabetologia*, 54: 3101-10.

Stickel, F., and C. Hellerbrand. 2010. 'Non-alcoholic fatty liver disease as a risk factor for hepatocellular carcinoma: mechanisms and implications', *Gut*, 59: 1303-7.

Stiles, B., Y. Wang, A. Stahl, S. Bassilian, W. P. Lee, Y. J. Kim, R. Sherwin, S. Devaskar, R. Lesche, M. A. Magnuson, and H. Wu. 2004. 'Liver-specific deletion of negative regulator Pten results in fatty liver and insulin hypersensitivity [corrected]', *Proc Natl Acad Sci U S A*, 101: 2082-7.

Stumptner, C., A. Fuchsbichler, H. Heid, K. Zatloukal, and H. Denk. 2002. 'Mallory body--a disease-associated type of sequestosome', *Hepatology*, 35: 1053-62.

Stumvoll, M., B. J. Goldstein, and T. W. van Haeften. 2005. 'Type 2 diabetes: principles of pathogenesis and therapy', *Lancet*, 365: 1333-46.

Surwit, R. S., M. N. Feinglos, J. Rodin, A. Sutherland, A. E. Petro, E. C. Opara, C. M. Kuhn, and M. Rebuffe-Scrive. 1995. 'Differential effects of fat and sucrose on the development of obesity and diabetes in C57BL/6J and A/J mice', *Metabolism*, 44: 645-51.

Suzuki, A., J. L. de la Pompa, V. Stambolic, A. J. Elia, T. Sasaki, I. del Barco Barrantes, A. Ho, A. Wakeham, A. Itie, W. Khoo, M. Fukumoto, and T. W. Mak. 1998. 'High cancer susceptibility and embryonic lethality associated with mutation of the PTEN tumor suppressor gene in mice', *Curr Biol*, 8: 1169-78.

Svensson, R. U., S. J. Parker, L. J. Eichner, M. J. Kolar, M. Wallace, S. N. Brun, P. S. Lombardo, J. L. Van Nostrand, A. Hutchins, L. Vera, L. Gerken, J. Greenwood, S. Bhat, G. Harriman, W. F. Westlin, H. J. Harwood, Jr., A.

Saghatelian, R. Kapeller, C. M. Metallo, and R. J. Shaw. 2016. 'Inhibition of acetyl-CoA carboxylase suppresses fatty acid synthesis and tumor growth of non-small-cell lung cancer in preclinical models', *Nat Med*, 22: 1108-19.

Takahashi, Y., and T. Fukusato. 2014. 'Histopathology of nonalcoholic fatty liver disease/nonalcoholic steatohepatitis', *World J Gastroenterol*, 20: 15539-48.

Takamura, A., M. Komatsu, T. Hara, A. Sakamoto, C. Kishi, S. Waguri, Y. Eishi, O. Hino, K. Tanaka, and N. Mizushima. 2011. 'Autophagy-deficient mice develop multiple liver tumors', *Genes Dev*, 25: 795-800.

Tappy, L., and K. A. Le. 2010. 'Metabolic effects of fructose and the worldwide increase in obesity', *Physiol Rev*, 90: 23-46.

———. 2012. 'Does fructose consumption contribute to non-alcoholic fatty liver disease?', *Clin Res Hepatol Gastroenterol*, 36: 554-60.

Te Morenga, L., S. Mallard, and J. Mann. 2012. 'Dietary sugars and body weight: systematic review and meta-analyses of randomised controlled trials and cohort studies', *Bmj*, 346: e7492.

Ter Horst, K. W., M. R. Schene, R. Holman, J. A. Romijn, and M. J. Serlie. 2016. 'Effect of fructose consumption on insulin sensitivity in nondiabetic subjects: a systematic review and meta-analysis of diet-intervention trials', *Am J Clin Nutr*, 104: 1562-76.

Teufel, A., T. Itzel, W. Erhart, M. Brosch, X. Y. Wang, Y. O. Kim, W. von Schonfels, A. Herrmann, S. Bruckner, F. Stickel, J. F. Dufour, T. Chavakis, C. Hellerbrand, R. Spang, T. Maass, T. Becker, S. Schreiber, C. Schafmayer, D. Schuppan, and J. Hampe. 2016. 'Comparison of Gene Expression Patterns Between Mouse Models of Nonalcoholic Fatty Liver Disease and Liver Tissues From Patients', *Gastroenterology*, 151: 513-25.e0.

Thoen, L. F., E. L. Guimaraes, L. Dolle, I. Mannaerts, M. Najimi, E. Sokal, and L. A. van Grunsven. 2011. 'A role for autophagy during hepatic stellate cell activation', *J Hepatol*, 55: 1353-60.

Thoreen, C. C., and D. M. Sabatini. 2005. 'AMPK and p53 help cells through lean times', *Cell Metab*, 1: 287-8.

Thorgeirsson, S. S., and E. Santoni-Rugiu. 1996. 'Transgenic mouse models in carcinogenesis: interaction of c-myc with transforming growth factor alpha and hepatocyte growth factor in hepatocarcinogenesis', *Br J Clin Pharmacol*, 42: 43-52.

Tilg, H., and A. R. Moschen. 2010. 'Evolution of inflammation in nonalcoholic fatty liver disease: the multiple parallel hits hypothesis', *Hepatology*, 52: 1836-46.

Totoki, Y., K. Tatsuno, K. R. Covington, H. Ueda, C. J. Creighton, M. Kato, S. Tsuji, L. A. Donehower, B. L. Slagle, H. Nakamura, S. Yamamoto, E. Shinbrot, N. Hama, M. Lehmkuhl, F. Hosoda, Y. Arai, K. Walker, M. Dahdouli, K. Gotoh, G. Nagae, M. C. Gingras, D. M. Muzny, H. Ojima, K. Shimada, Y. Midorikawa, J. A. Goss, R. Cotton, A. Hayashi, J. Shibahara, S. Ishikawa, J. Guiteau, M. Tanaka, T. Urushidate, S. Ohashi, N. Okada, H. Doddapaneni, M. Wang, Y. Zhu, H. Dinh, T. Okusaka, N. Kokudo, T. Kosuge, T. Takayama, M. Fukayama, R. A. Gibbs, D. A. Wheeler, H. Aburatani, and T. Shibata. 2014. 'Trans-ancestry mutational landscape of hepatocellular carcinoma genomes', *Nat Genet*, 46: 1267-73.

Townsend, S. A., and P. N. Newsome. 2016. 'Non-alcoholic fatty liver disease in 2016', *Br Med Bull*, 119: 143-56.

Toyama, E. Q., S. Herzig, J. Courchet, T. L. Lewis, Jr., O. C. Loson, K. Hellberg, N. P. Young, H. Chen, F. Polleux, D. C. Chan, and R. J. Shaw. 2016. 'Metabolism. AMP-activated protein kinase mediates mitochondrial fission in response to energy stress', *Science*, 351: 275-81.

'Trends in adult body-mass index in 200 countries from 1975 to 2014: a pooled analysis of 1698 population-based measurement studies with 19.2 million participants'. 2016. *Lancet*, 387: 1377-96.

Turnbaugh, P. J., R. E. Ley, M. A. Mahowald, V. Magrini, E. R. Mardis, and J. I. Gordon. 2006. 'An obesity-associated gut microbiome with increased capacity for energy harvest', *Nature*, 444: 1027-31.

Tuyama, A. C., and C. Y. Chang. 2012. 'Non-alcoholic fatty liver disease', *J Diabetes*, 4: 266-80.

Umemura, A., E. J. Park, K. Taniguchi, J. H. Lee, S. Shalapour, M. A. Valasek, M. Aghajan, H. Nakagawa, E. Seki, M. N. Hall, and M. Karin. 2014. 'Liver damage, inflammation, and enhanced tumorigenesis after persistent mTORC1 inhibition', *Cell Metab*, 20: 133-44.

Van Heek, M., D. S. Compton, C. F. France, R. P. Tedesco, A. B. Fawzi, M. P. Graziano, E. J. Sybertz, C. D. Strader, and H. R. Davis, Jr. 1997. 'Diet-induced obese mice develop peripheral, but not central, resistance to leptin', *J Clin Invest*, 99: 385-90.

Van Schaftingen, E., M. Detheux, and M. Veiga da Cunha. 1994. 'Short-term control of glucokinase activity: role of a regulatory protein', *Faseb j*, 8: 414-9.

Van Wagner, L. B., S. W. Koppe, E. M. Brunt, J. Gottstein, K. Gardikiotes, R. M. Green, and M. E. Rinella. 2011. 'Pentoxifylline for the treatment of non-alcoholic steatohepatitis: a randomized controlled trial', *Ann Hepatol*, 10: 277-86.

Vander Heiden, M. G., L. C. Cantley, and C. B. Thompson. 2009. 'Understanding the Warburg effect: the metabolic requirements of cell proliferation', *Science*, 324: 1029-33.

Vesselinovitch, S. D., M. Koka, N. Mihailovich, and K. V. Rao. 1984. 'Carcinogenicity of diethylnitrosamine in newborn, infant, and adult mice', *J Cancer Res Clin Oncol*, 108: 60-5.

Villanueva, A., and J. M. Llovet. 2014. 'Liver cancer in 2013: Mutational landscape of HCC--the end of the beginning', *Nat Rev Clin Oncol*, 11: 73-4.

Villena, J. A., B. Viollet, F. Andreelli, A. Kahn, S. Vaulont, and H. S. Sul. 2004. 'Induced adiposity and adipocyte hypertrophy in mice lacking the AMP-activated protein kinase-alpha2 subunit', *Diabetes*, 53: 2242-9.

Vinciguerra, M., F. Carrozzino, M. Peyrou, S. Carlone, R. Montesano, R. Benelli, and M. Foti. 2009. 'Unsaturated fatty acids promote hepatoma proliferation and progression through downregulation of the tumor suppressor PTEN', *J Hepatol*, 50: 1132-41.

Vinciguerra, M., A. Sgroi, C. Veyrat-Durebex, L. Rubbia-Brandt, L. H. Buhler, and M. Foti. 2009. 'Unsaturated fatty acids inhibit the expression of tumor suppressor phosphatase and tensin homolog (PTEN) via microRNA-21 up-regulation in hepatocytes', *Hepatology*, 49: 1176-84.

Vinciguerra, M., C. Veyrat-Durebex, M. A. Moukil, L. Rubbia-Brandt, F. Rohner-Jeanrenaud, and M. Foti. 2008. 'PTEN down-regulation by unsaturated fatty acids triggers hepatic steatosis via an NF-kappaBp65/mTOR-dependent mechanism', *Gastroenterology*, 134: 268-80.

Wahren, J., Y. Sato, J. Ostman, L. Hagenfeldt, and P. Felig. 1984. 'Turnover and splanchnic metabolism of free fatty acids and ketones in insulin-dependent diabetics at rest and in response to exercise', *J Clin Invest*, 73: 1367-76.

Wallace, K., A. D. Burt, and M. C. Wright. 2008. 'Liver fibrosis', *Biochem J*, 411: 1-18.

Wang, D., Y. Wei, and M. J. Pagliassotti. 2006. 'Saturated fatty acids promote endoplasmic reticulum stress and liver injury in rats with hepatic steatosis', *Endocrinology*, 147: 943-51.

Wang, L., S. Athinarayanan, G. Jiang, N. Chalasani, M. Zhang, and W. Liu. 2015. 'Fatty acid desaturase 1 gene polymorphisms control human hepatic lipid composition', *Hepatology*, 61: 119-28.

Wang, P., D. Kang, W. Cao, Y. Wang, and Z. Liu. 2012. 'Diabetes mellitus and risk of hepatocellular carcinoma: a systematic review and meta-analysis', *Diabetes Metab Res Rev*, 28: 109-22.

Wang, S. N., K. T. Lee, and C. G. Ker. 2010. 'Leptin in hepatocellular carcinoma', *World J Gastroenterol*, 16: 5801-9.

Weber, L. W., M. Boll, and A. Stampfl. 2003. 'Hepatotoxicity and mechanism of action of haloalkanes: carbon tetrachloride as a toxicological model', *Crit Rev Toxicol*, 33: 105-36.

Wei, Y., D. Wang, F. Topczewski, and M. J. Pagliassotti. 2007. 'Fructose-mediated stress signaling in the liver: implications for hepatic insulin resistance', *J Nutr Biochem*, 18: 1-9.

West, A. P., I. E. Brodsky, C. Rahner, D. K. Woo, H. Erdjument-Bromage, P. Tempst, M. C. Walsh, Y. Choi, G. S. Shadel, and S. Ghosh. 2011. 'TLR signalling augments macrophage bactericidal activity through mitochondrial ROS', *Nature*, 472: 476-80.

West, D. B., J. Waguespack, and S. McCollister. 1995. 'Dietary obesity in the mouse: interaction of strain with diet composition', *Am J Physiol*, 268: R658-65.

Winder, W. W., and D. G. Hardie. 1996. 'Inactivation of acetyl-CoA carboxylase and activation of AMP-activated protein kinase in muscle during exercise', *Am J Physiol*, 270: E299-304.

Winder, W. W., B. F. Holmes, D. S. Rubink, E. B. Jensen, M. Chen, and J. O. Holloszy. 2000. 'Activation of AMP-activated protein kinase increases mitochondrial enzymes in skeletal muscle', *J Appl Physiol (1985)*, 88: 2219-26.

Wingo, S. N., T. D. Gallardo, E. A. Akbay, M. C. Liang, C. M. Contreras, T. Boren, T. Shimamura, D. S. Miller, N. E. Sharpless, N. Bardeesy, D. J. Kwiatkowski, J. O. Schorge, K. K. Wong, and D. H. Castrillon. 2009. 'Somatic LKB1 mutations promote cervical cancer progression', *PLoS One*, 4: e5137.

Wong, R. J., R. Cheung, and A. Ahmed. 2014. 'Nonalcoholic steatohepatitis is the most rapidly growing indication for liver transplantation in patients with hepatocellular carcinoma in the U.S', *Hepatology*, 59: 2188-95.

Woods, A., P. C. Cheung, F. C. Smith, M. D. Davison, J. Scott, R. K. Beri, and D. Carling. 1996. 'Characterization of AMP-activated protein kinase beta and gamma subunits. Assembly of the heterotrimeric complex in vitro', *J Biol Chem*, 271: 10282-90.

Woods, A., S. R. Johnstone, K. Dickerson, F. C. Leiper, L. G. Fryer, D. Neumann, U. Schlattner, T. Wallimann, M. Carlson, and D. Carling. 2003. 'LKB1 is the upstream kinase in the AMP-activated protein kinase cascade', *Curr Biol*, 13: 2004-8.

Woods, A., J. R. Williams, P. J. Muckett, F. V. Mayer, M. Liljevald, Y. M. Bohlooly, and D. Carling. 2017. 'Liver-Specific Activation of AMPK Prevents Steatosis on a High-Fructose Diet', *Cell Rep*, 18: 3043-51.

Wree, A., L. Broderick, A. Canbay, H. M. Hoffman, and A. E. Feldstein. 2013. 'From NAFLD to NASH to cirrhosis-new insights into disease mechanisms', *Nat Rev Gastroenterol Hepatol*, 10: 627-36.

Wu, J. 2016. 'Utilization of animal models to investigate nonalcoholic steatohepatitis-associated hepatocellular carcinoma', *Oncotarget*, 7: 42762-76.

Xiao, B., R. Heath, P. Saiu, F. C. Leiper, P. Leone, C. Jing, P. A. Walker, L. Haire, J. F. Eccleston, C. T. Davis, S. R. Martin, D. Carling, and S. J. Gamblin. 2007. 'Structural basis for AMP binding to mammalian AMP-activated protein kinase', *Nature*, 449: 496-500.

Xiao, B., M. J. Sanders, D. Carmena, N. J. Bright, L. F. Haire, E. Underwood, B. R. Patel, R. B. Heath, P. A. Walker, S. Hallen, F. Giordanetto, S. R. Martin, D. Carling, and S. J. Gamblin. 2013. 'Structural basis of AMPK regulation by small molecule activators', *Nat Commun*, 4: 3017.

Xiao, B., M. J. Sanders, E. Underwood, R. Heath, F. V. Mayer, D. Carmena, C. Jing, P. A. Walker, J. F. Eccleston, L. F. Haire, P. Saiu, S. A. Howell, R. Aasland, S. R. Martin, D. Carling, and S. J. Gamblin. 2011. 'Structure of mammalian AMPK and its regulation by ADP', *Nature*, 472: 230-3.

Xu, X. J., M. S. Gauthier, D. T. Hess, C. M. Apovian, J. M. Cacicedo, N. Gokce, M. Farb, R. J. Valentine, and N. B. Ruderman. 2012. 'Insulin sensitive and resistant obesity in humans: AMPK activity, oxidative stress, and depot-specific changes in gene expression in adipose tissue', *J Lipid Res*, 53: 792-801.

Xu, Z. J., J. G. Fan, X. D. Ding, L. Qiao, and G. L. Wang. 2010. 'Characterization of high-fat, diet-induced, non-alcoholic steatohepatitis with fibrosis in rats', *Dig Dis Sci*, 55: 931-40.

Yamaguchi, K., L. Yang, S. McCall, J. Huang, X. X. Yu, S. K. Pandey, S. Bhanot, B. P. Monia, Y. X. Li, and A. M. Diehl. 2007. 'Inhibiting triglyceride synthesis improves hepatic steatosis but exacerbates liver damage and fibrosis in obese mice with nonalcoholic steatohepatitis', *Hepatology*, 45: 1366-74.

Yamamoto, K., H. Ichijo, and S. J. Korsmeyer. 1999. 'BCL-2 is phosphorylated and inactivated by an ASK1/Jun N-terminal protein kinase pathway normally activated at G(2)/M', *Mol Cell Biol*, 19: 8469-78.

Yang, L., P. Li, S. Fu, E. S. Calay, and G. S. Hotamisligil. 2010. 'Defective hepatic autophagy in obesity promotes ER stress and causes insulin resistance', *Cell Metab*, 11: 467-78.

Yao, X., J. F. Hu, M. Daniels, H. Yien, H. Lu, H. Sharan, X. Zhou, Z. Zeng, T. Li, Y. Yang, and A. R. Hoffman. 2003. 'A novel orthotopic tumor model to study growth factors and oncogenes in hepatocarcinogenesis', *Clin Cancer Res*, 9: 2719-26.

Yasui, K., E. Hashimoto, Y. Komorizono, K. Koike, S. Arii, Y. Imai, T. Shima, Y. Kanbara, T. Saibara, T. Mori, S. Kawata, H. Uto, S. Takami, Y. Sumida, T. Takamura, M. Kawanaka, and T. Okanoue. 2011. 'Characteristics of patients with nonalcoholic steatohepatitis who develop hepatocellular carcinoma', *Clin Gastroenterol Hepatol*, 9: 428-33; quiz e50.

Yavari, A., C. J. Stocker, S. Ghaffari, E. T. Wargent, V. Steeples, G. Czibik, K. Pinter, M. Bellahcene, A. Woods, P. B. Martinez de Morentin, C. Cansell, B. Y. Lam, A. Chuster, K. Petkevicius, M. S. Nguyen-Tu, A. Martinez-Sanchez, T. J. Pullen, P. L. Oliver, A. Stockenhuber, C. Nguyen, M. Lazdam, J. F. O'Dowd, P. Harikumar, M. Toth, C. Beall, T. Kyriakou, J. Parnis, D. Sarma, G. Katritsis, D. D. Wortmann, A. R. Harper, L. A. Brown, R. Willows, S. Gandra, V. Poncio, M. J. de Oliveira Figueiredo, N. R. Qi, S. N. Peirson, R. J. McCrimmon, B. Gereben, L. Tretter, C. Fekete, C. Redwood, G. S. Yeo, L. K. Heisler, G. A. Rutter, M. A. Smith, D. J. Withers, D. Carling, E. B. Sternick, J. R. Arch, M. A. Cawthorne, H. Watkins, and H. Ashrafian. 2016. 'Chronic Activation of gamma2 AMPK Induces Obesity and Reduces beta Cell Function', *Cell Metab*, 23: 821-36.

Yeluri, S., B. Madhok, K. R. Prasad, P. Quirke, and D. G. Jayne. 2009. 'Cancer's craving for sugar: an opportunity for clinical exploitation', *J Cancer Res Clin Oncol*, 135: 867-77.

Yesilova, Z., H. Yaman, C. Oktenli, A. Ozcan, A. Uygun, E. Cakir, S. Y. Sanisoglu, A. Erdil, Y. Ates, M. Aslan, U. Musabak, M. K. Erbil, N. Karaeren, and K. Dagalp. 2005. 'Systemic markers of lipid peroxidation and antioxidants in patients with nonalcoholic Fatty liver disease', *Am J Gastroenterol*, 100: 850-5.

Yi, G., Z. He, X. Zhou, L. Xian, T. Yuan, X. Jia, J. Hong, L. He, and J. Liu. 2013. 'Low concentration of metformin induces a p53-dependent senescence in hepatoma cells via activation of the AMPK pathway', *Int J Oncol*, 43: 1503-10.

Yoon, H. J., and B. S. Cha. 2014. 'Pathogenesis and therapeutic approaches for non-alcoholic fatty liver disease', *World J Hepatol*, 6: 800-11.

Young, N. P., A. Kamireddy, J. L. Van Nostrand, L. J. Eichner, M. N. Shokhirev, Y. Dayn, and R. J. Shaw. 2016. 'AMPK governs lineage specification through Tfeb-dependent regulation of lysosomes', *Genes Dev*, 30: 535-52.

Younossi, Z. M., A. B. Koenig, D. Abdelatif, Y. Fazel, L. Henry, and M. Wymer. 2016. 'Global epidemiology of nonalcoholic fatty liver disease-Meta-analytic assessment of prevalence, incidence, and outcomes', *Hepatology*, 64: 73-84.

Yu, H. C., C. S. Lin, W. T. Tai, C. Y. Liu, C. W. Shiau, and K. F. Chen. 2013. 'Nilotinib induces autophagy in hepatocellular carcinoma through AMPK activation', *J Biol Chem*, 288: 18249-59.

Yu, J., S. Marsh, J. Hu, W. Feng, and C. Wu. 2016. 'The Pathogenesis of Nonalcoholic Fatty Liver Disease: Interplay between Diet, Gut Microbiota, and Genetic Background', *Gastroenterol Res Pract*, 2016: 2862173.

Zadra, G., C. Photopoulos, S. Tyekucheva, P. Heidari, Q. P. Weng, G. Fedele, H. Liu, N. Scaglia, C. Priolo, E. Sicinska, U. Mahmood, S. Signoretti, N. Birnberg, and M. Loda. 2014. 'HAA novel direct activator of AMPK inhibits prostate cancer growth by blocking lipogenesis', *EMBO Mol Med*, 6: 519-38.

Zhang, C. S., S. A. Hawley, Y. Zong, M. Li, Z. Wang, A. Gray, T. Ma, J. Cui, J. W. Feng, M. Zhu, Y. Q. Wu, T. Y. Li, Z. Ye, S. Y. Lin, H. Yin, H. L. Piao, D. G. Hardie, and S. C. Lin. 2017. 'Fructose-1,6-bisphosphate and aldolase mediate glucose sensing by AMPK', *Nature*, 548: 112-16.

Zhang, C. S., B. Jiang, M. Li, M. Zhu, Y. Peng, Y. L. Zhang, Y. Q. Wu, T. Y. Li, Y. Liang, Z. Lu, G. Lian, Q. Liu, H. Guo, Z. Yin, Z. Ye, J. Han, J. W. Wu, H. Yin, S. Y. Lin, and S. C. Lin. 2014. 'The lysosomal v-ATPase-Ragulator complex is a common activator for AMPK and mTORC1, acting as a switch between catabolism and anabolism', *Cell Metab*, 20: 526-40.

Zhang, D. Y., N. Goossens, J. Guo, M. C. Tsai, H. I. Chou, C. Altunkaynak, A. Sangiovanni, M. Iavarone, M. Colombo, M. Kobayashi, H. Kumada, A. Villanueva, J. M. Llovet, Y. Hoshida, and S. L. Friedman. 2016. 'A hepatic stellate cell gene expression signature associated with outcomes in hepatitis C cirrhosis and hepatocellular carcinoma after curative resection', *Gut*, 65: 1754-64.

Zhang, X. Q., C. F. Xu, C. H. Yu, W. X. Chen, and Y. M. Li. 2014. 'Role of endoplasmic reticulum stress in the pathogenesis of nonalcoholic fatty liver disease', *World J Gastroenterol*, 20: 1768-76.

Zhang, Y. H., T. An, R. C. Zhang, Q. Zhou, Y. Huang, and J. Zhang. 2013. 'Very high fructose intake increases serum LDL-cholesterol and total cholesterol: a meta-analysis of controlled feeding trials', *J Nutr*, 143: 1391-8.

Zhang, Y. L., H. Guo, C. S. Zhang, S. Y. Lin, Z. Yin, Y. Peng, H. Luo, Y. Shi, G. Lian, C. Zhang, M. Li, Z. Ye, J. Ye, J. Han, P. Li, J. W. Wu, and S. C. Lin. 2013. 'AMP as a low-energy charge signal autonomously initiates assembly of AXIN-AMPK-LKB1 complex for AMPK activation', *Cell Metab*, 18: 546-55.

Zheng, B., J. H. Jeong, J. M. Asara, Y. Y. Yuan, S. R. Granter, L. Chin, and L. C. Cantley. 2009. 'Oncogenic B-RAF Negatively Regulates the Tumor Suppressor LKB1 to Promote Melanoma Cell Proliferation', *Mol Cell*, 33: 237-47.

Zheng, L., W. Yang, F. Wu, C. Wang, L. Yu, L. Tang, B. Qiu, Y. Li, L. Guo, M. Wu, G. Feng, D. Zou, and H. Wang. 2013. 'Prognostic significance of AMPK activation and therapeutic effects of metformin in hepatocellular carcinoma', *Clin Cancer Res*, 19: 5372-80.

Zhou, G., R. Myers, Y. Li, Y. Chen, X. Shen, J. Fenyk-Melody, M. Wu, J. Ventre, T. Doebber, N. Fujii, N. Musi, M. F. Hirshman, L. J. Goodyear, and D. E. Moller. 2001. 'Role of AMP-activated protein kinase in mechanism of metformin action', *J Clin Invest*, 108: 1167-74.

Zhou, L., S. S. Deepa, J. C. Etzler, J. Ryu, X. Mao, Q. Fang, D. D. Liu, J. M. Torres, W. Jia, J. D. Lechleiter, F. Liu, and L. Q. Dong. 2009. 'Adiponectin activates AMP-activated protein kinase in muscle cells via APPL1/LKB1-dependent and phospholipase C/Ca2+/Ca2+/calmodulin-dependent protein kinase kinase-dependent pathways', *J Biol Chem*, 284: 22426-35.

Zordoky, B. N., J. Nagendran, T. Pulinilkunnil, P. C. Kienesberger, G. Masson, T. J. Waller, B. E. Kemp, G. R. Steinberg, and J. R. Dyck. 2014. 'AMPK-dependent inhibitory phosphorylation of ACC is not essential for maintaining myocardial fatty acid oxidation', *Circ Res*, 115: 518-24.

Zucman-Rossi, J., A. Villanueva, J. C. Nault, and J. M. Llovet. 2015. 'Genetic Landscape and Biomarkers of Hepatocellular Carcinoma', *Gastroenterology*, 149: 1226-39.e4.

# 7 Appendices

## 7.1 Appendix A

### 7.1.1 Lists of genes, hepatic expression of which is significantly altered in D316A-Tg relative WT-Tg mice

| GeneName | Gene Symbol | Gene Number | Fold change | Adj p |
|---|---|---|---|---|
| **cytochrome P450, family 46, subfamily a, polypeptide 1** | Cyp46a1 | ENSMUSG00000021259 | 8.07 | 2.1E-32 |
| **sulfotransferase family, cytosolic, 1C, member 2** | Sult1c2 | ENSMUSG00000023122 | 3.87 | 7.5E-22 |
| **cathepsin Z** | Ctsz | ENSMUSG00000016256 | 1.71 | 4.1E-12 |
| **cathepsin A** | Ctsa | ENSMUSG00000017760 | 1.47 | 9.8E-10 |
| **ankyrin repeat and SOCS box-containing 2** | Asb2 | ENSMUSG00000021200 | 3.04 | 8.6E-08 |
| **secreted phosphoprotein 2** | Spp2 | ENSMUSG00000026295 | 1.54 | 7.4E-07 |
| **C-type lectin domain family 2, member h** | Clec2h | ENSMUSG00000030364 | 2.99 | 2.4E-06 |
| **leucine-rich repeats and transmembrane domains 1** | Lrtm1 | ENSMUSG00000045776 | 3.75 | 2.7E-06 |
| **hexosaminidase A** | Hexa | ENSMUSG00000025232 | 1.47 | 2.7E-06 |
| **hexosaminidase B** | Hexb | ENSMUSG00000021665 | 2.20 | 2.7E-06 |
| **desmoglein 1 gamma** | Dsg1c | ENSMUSG00000034774 | 2.83 | 7.2E-06 |
| **renin binding protein** | Renbp | ENSMUSG00000031387 | 2.66 | 1.6E-05 |
| **glycophorin C** | Gypc | ENSMUSG00000090523 | 2.07 | 3.0E-05 |
| **transducin-like enhancer of split 3, homolog of Drosophila E(spl)** | Tle3 | ENSMUSG00000032280 | 1.61 | 4.7E-05 |
| **folliculin interacting protein 2** | Fnip2 | ENSMUSG00000061175 | 1.69 | 5.1E-05 |
| **galactosylceramidase** | Galc | ENSMUSG00000021003 | 1.57 | 3.5E-04 |
| **CDK5 and Abl enzyme substrate 1** | Cables1 | ENSMUSG00000040957 | 2.03 | 4.3E-04 |
| **perilipin 3** | Plin3 | ENSMUSG00000024197 | 1.46 | 4.6E-04 |
| **major facilitator superfamily domain containing 6** | Mfsd6 | ENSMUSG00000041439 | 0.67 | 7.5E-04 |
| **peroxiredoxin 1** | Prdx1 | ENSMUSG00000028691 | 0.84 | 1.2E-03 |
| **unc-13 homolog B (C. elegans)** | Unc13b | ENSMUSG00000028456 | 0.58 | 1.4E-03 |
| **cyclin-dependent kinase inhibitor 2C (p18, inhibits CDK4)** | Cdkn2c | ENSMUSG00000028551 | 1.78 | 1.8E-03 |
| **OCIA domain containing 2** | Ociad2 | ENSMUSG00000029153 | 0.74 | 1.8E-03 |
| **small nucleolar RNA host gene 11** | Snhg11 | ENSMUSG00000044349 | 1.96 | 2.1E-03 |
| **PQ loop repeat containing 2** | Pqlc2 | ENSMUSG00000028744 | 1.37 | 2.2E-03 |

| | | | | |
|---|---|---|---|---|
| **KH domain containing, RNA binding, signal transduction associated 3** | Khdrbs3 | ENSMUSG00000022332 | 0.72 | 3.5E-03 |
| **coactosin-like 1 (Dictyostelium)** | Cotl1 | ENSMUSG00000031827 | 1.57 | 3.9E-03 |
| **serine carboxypeptidase 1** | Scpep1 | ENSMUSG00000000278 | 1.32 | 4.7E-03 |
| **a disintegrin and metallopeptidase domain 11** | Adam11 | ENSMUSG00000020926 | 1.89 | 4.8E-03 |
| **UDP-N-acteylglucosamine pyrophosphorylase 1-like 1** | Uap1l1 | ENSMUSG00000026956 | 1.94 | 6.0E-03 |
| **phospholipase A1 member A** | Pla1a | ENSMUSG00000002847 | 1.32 | 6.3E-03 |
| **family with sequence similarity 131, member C** | Fam131c | ENSMUSG00000006218 | 0.56 | 7.6E-03 |
| **centrosomal protein 70** | Cep70 | ENSMUSG00000056267 | 1.58 | 7.6E-03 |
| **metallothionein 1** | Mt1 | ENSMUSG00000031765 | 2.68 | 7.8E-03 |
| **serine (or cysteine) peptidase inhibitor, clade B, member 8** | Serpinb8 | ENSMUSG00000026315 | 2.09 | 8.2E-03 |
| **cytochrome P450, family 2, subfamily g, polypeptide 1** | Cyp2g1 | ENSMUSG00000049685 | 2.36 | 9.3E-03 |
| **zinc finger, FYVE domain containing 26** | Zfyve26 | ENSMUSG00000066440 | 1.32 | 1.1E-02 |
| **Rho GTPase activating protein 10** | Arhgap10 | ENSMUSG00000037148 | 1.75 | 1.2E-02 |
| **N-acetyl galactosaminidase, alpha** | Naga | ENSMUSG00000022453 | 1.19 | 1.7E-02 |
| **cathepsin L** | Ctsl | ENSMUSG00000021477 | 1.33 | 1.8E-02 |
| **family with sequence similarity 129, member B** | Fam129b | ENSMUSG00000026796 | 1.89 | 2.6E-02 |
| **zinc finger protein 750** | Zfp750 | ENSMUSG00000039238 | 0.69 | 2.8E-02 |
| **dpy-19-like 3 (C. elegans)** | Dpy19l3 | ENSMUSG00000043671 | 0.59 | 3.3E-02 |
| **transmembrane protein 144** | Tmem144 | ENSMUSG00000027956 | 1.38 | 3.7E-02 |
| **aminolevulinic acid synthase 1** | Alas1 | ENSMUSG00000032786 | 1.79 | 3.7E-02 |
| **numb gene homolog (Drosophila)** | Numb | ENSMUSG00000021224 | 0.88 | 4.8E-02 |

***Table 7.1 - Genes, hepatic expression of which is altered in D316A relative to WT-Tg mice following either chow or high fructose feeding.***

| GeneName | Gene Symbol | Gene Number | Fold change | Adj p |
|---|---|---|---|---|
| **hyperpolarization-activated, cyclic nucleotide-gated K+ 3** | Hcn3 | ENSMUSG00000028051 | 3.97 | 5.4E-10 |
| **transcription elongation factor A (SII)-like 8** | Tceal8 | ENSMUSG00000051579 | 2.15 | 6.0E-06 |
| **stabilin 2** | Stab2 | ENSMUSG00000035459 | 1.59 | 6.5E-06 |
| **neuraminidase 1** | Neu1 | ENSMUSG00000007038 | 1.45 | 7.2E-06 |

| | | | | |
|---|---|---|---|---|
| **gremlin 2 homolog, cysteine knot superfamily (Xenopus laevis)** | Grem2 | ENSMUSG00000050069 | 2.30 | 1.5E-05 |
| **transcobalamin 2** | Tcn2 | ENSMUSG00000020432 | 1.34 | 2.2E-05 |
| **Pbx/knotted 1 homeobox 2** | Pknox2 | ENSMUSG00000035934 | 0.36 | 3.3E-05 |
| **acyl-Coenzyme A oxidase 2, branched chain** | Acox2 | ENSMUSG00000021751 | 0.69 | 5.1E-05 |
| **mal, T cell differentiation protein 2** | Mal2 | ENSMUSG00000024479 | 0.67 | 6.9E-05 |
| **coenzyme Q10 homolog A (yeast)** | Coq10a | ENSMUSG00000039914 | 1.34 | 9.4E-05 |
| **protein kinase, cGMP-dependent, type II** | Prkg2 | ENSMUSG00000029334 | 2.92 | 1.1E-04 |
| **neurotrophic tyrosine kinase, receptor, type 2** | Ntrk2 | ENSMUSG00000055254 | 2.76 | 1.1E-04 |
| **zinc finger, DHHC domain containing 2** | Zdhhc2 | ENSMUSG00000039470 | 0.34 | 1.2E-04 |
| **pyruvate kinase liver and red blood cell** | Pklr | ENSMUSG00000041237 | 1.93 | 1.3E-04 |
| **carnitine O-octanoyltransferase** | Crot | ENSMUSG00000003623 | 0.65 | 2.9E-04 |
| **malectin** | Mlec | ENSMUSG00000048578 | 0.72 | 2.9E-04 |
| **Ras association (RalGDS/AF-6) domain family member 4** | Rassf4 | ENSMUSG00000042129 | 1.76 | 2.9E-04 |
| **occludin** | Ocln | ENSMUSG00000021628 | 0.64 | 3.8E-04 |
| **HEAT repeat containing 7A** | Heatr7a | ENSMUSG00000022558 | 1.29 | 3.8E-04 |
| **cadherin 18** | Cdh18 | ENSMUSG00000040420 | 2.32 | 3.8E-04 |
| **Sec24 related gene family, member D (S. cerevisiae)** | Sec24d | ENSMUSG00000039234 | 0.66 | 4.8E-04 |
| **RUN and FYVE domain containing 4** | Rufy4 | ENSMUSG00000061815 | 0.42 | 6.1E-04 |
| **family with sequence similarity 176, member A** | Fam176a | ENSMUSG00000035104 | 1.46 | 6.1E-04 |
| **peroxisomal biogenesis factor 26** | Pex26 | ENSMUSG00000067825 | 1.46 | 6.1E-04 |
| **glucosamine (N-acetyl)-6-sulfatase** | Gns | ENSMUSG00000034707 | 1.22 | 6.1E-04 |
| **interleukin-1 receptor-associated kinase 2** | Irak2 | ENSMUSG00000060477 | 0.74 | 6.8E-04 |
| **copine II** | Cpne2 | ENSMUSG00000034361 | 0.63 | 9.3E-04 |
| **reticulon 4** | Rtn4 | ENSMUSG00000020458 | 1.50 | 1.1E-03 |
| **protein disulfide isomerase associated 4** | Pdia4 | ENSMUSG00000025823 | 0.68 | 1.1E-03 |

| | | | | |
|---|---|---|---|---|
| **DEAH (Asp-Glu-Ala-His) box polypeptide 36** | Dhx36 | ENSMUSG00000027770 | 0.79 | 1.4E-03 |
| **purinergic receptor P2X, ligand-gated ion channel 4** | P2rx4 | ENSMUSG00000029470 | 1.38 | 1.5E-03 |
| **SH2B adaptor protein 3** | Sh2b3 | ENSMUSG00000042594 | 1.33 | 1.7E-03 |
| **cytochrome P450, family 21, subfamily a, polypeptide 1** | Cyp21a1 | ENSMUSG00000024365 | 2.87 | 1.7E-03 |
| **regulator of G-protein signaling 3** | Rgs3 | ENSMUSG00000059810 | 2.18 | 1.8E-03 |
| **mucolipin 1** | Mcoln1 | ENSMUSG00000004567 | 1.22 | 1.8E-03 |
| **nucleosome assembly protein 1-like 1** | Nap1l1 | ENSMUSG00000058799 | 0.76 | 1.9E-03 |
| **methionine sulfoxide reductase B3** | Msrb3 | ENSMUSG00000051236 | 0.68 | 1.9E-03 |
| **tumor necrosis factor receptor superfamily, member 25** | Tnfrsf25 | ENSMUSG00000024793 | 2.42 | 2.1E-03 |
| **dishevelled 2, dsh homolog (Drosophila)** | Dvl2 | ENSMUSG00000020888 | 1.59 | 2.1E-03 |
| **kininogen 2** | Kng2 | ENSMUSG00000060450 | 1.30 | 2.1E-03 |
| **solute carrier family 46, member 3** | Slc46a3 | ENSMUSG00000029650 | 1.95 | 2.2E-03 |
| **asparagine-linked glycosylation 2 homolog (yeast, alpha-1,3-mannosyltransferase)** | Alg2 | ENSMUSG00000039740 | 0.67 | 2.2E-03 |
| **smoothened homolog (Drosophila)** | Smo | ENSMUSG00000001761 | 0.58 | 2.2E-03 |
| **Trk-fused gene** | Tfg | ENSMUSG00000022757 | 0.80 | 2.2E-03 |
| **SEC23B (S. cerevisiae)** | Sec23b | ENSMUSG00000027429 | 0.71 | 2.4E-03 |
| **ligand of numb-protein X 2** | Lnx2 | ENSMUSG00000016520 | 0.67 | 2.5E-03 |
| **heat shock factor 2** | Hsf2 | ENSMUSG00000019878 | 0.77 | 2.6E-03 |
| **ATPase, class II, type 9A** | Atp9a | ENSMUSG00000027546 | 0.80 | 2.7E-03 |
| **inscuteable homolog (Drosophila)** | Insc | ENSMUSG00000048782 | 0.55 | 2.8E-03 |
| **abhydrolase domain containing 14b** | Abhd14b | ENSMUSG00000042073 | 1.26 | 2.8E-03 |
| **glycerol-3-phosphate dehydrogenase 1 (soluble)** | Gpd1 | ENSMUSG00000023019 | 0.66 | 2.8E-03 |
| **UBX domain protein 4** | Ubxn4 | ENSMUSG00000026353 | 0.79 | 3.0E-03 |
| **Sec1 family domain containing 1** | Scfd1 | ENSMUSG00000020952 | 0.77 | 3.1E-03 |
| **cytochrome b** | CYTB | ENSMUSG00000064370 | 1.35 | 3.1E-03 |

| | | | | |
|---|---|---|---|---|
| **aldehyde oxidase 1** | Aox1 | ENSMUSG00000063558 | 0.62 | 3.1E-03 |
| **protein kinase domain containing, cytoplasmic** | Pkdcc | ENSMUSG00000024247 | 1.40 | 3.4E-03 |
| **Rho guanine nucleotide exchange factor (GEF) 3** | Arhgef3 | ENSMUSG00000021895 | 0.63 | 3.6E-03 |
| **RIKEN cDNA 2810008M24 gene** | 2810008M24Rik | ENSMUSG00000071180 | 0.79 | 3.8E-03 |
| **transmembrane protein 167** | Tmem167 | ENSMUSG00000012422 | 0.83 | 3.9E-03 |
| **CDK5 regulatory subunit associated protein 1** | Cdk5rap1 | ENSMUSG00000027487 | 0.60 | 3.9E-03 |
| **pleckstrin homology domain containing, family G (with RhoGef domain) member 5** | Plekhg5 | ENSMUSG00000039713 | 1.79 | 3.9E-03 |
| **mannosidase 2, alpha B1** | Man2b1 | ENSMUSG00000005142 | 1.24 | 3.9E-03 |
| **mesencephalic astrocyte-derived neurotrophic factor** | Manf | ENSMUSG00000032575 | 0.57 | 3.9E-03 |
| **transmembrane protein 164** | Tmem164 | ENSMUSG00000047045 | 0.70 | 4.2E-03 |
| **eukaryotic translation initiation factor 4 gamma, 3** | Eif4g3 | ENSMUSG00000028760 | 0.79 | 4.4E-03 |
| **RIKEN cDNA 2810474O19 gene** | 2810474O19Rik | ENSMUSG00000032712 | 1.42 | 4.4E-03 |
| **ubiquitin specific peptidase 14** | Usp14 | ENSMUSG00000047879 | 0.83 | 4.4E-03 |
| **fucosidase, alpha-L- 2, plasma** | Fuca2 | ENSMUSG00000019810 | 1.50 | 4.4E-03 |
| **zinc finger protein 655** | Zfp655 | ENSMUSG00000007812 | 1.46 | 4.7E-03 |
| **coronin 7** | Coro7 | ENSMUSG00000039637 | 1.34 | 4.9E-03 |
| **BUD13 homolog (yeast)** | Bud13 | ENSMUSG00000032077 | 1.95 | 5.2E-03 |
| **glutathione reductase** | Gsr | ENSMUSG00000031584 | 0.79 | 5.2E-03 |
| **ligand of numb-protein X 1** | Lnx1 | ENSMUSG00000029228 | 2.60 | 5.3E-03 |
| **zinc finger protein 259** | Zfp259 | ENSMUSG00000032078 | 1.56 | 5.7E-03 |
| **family with sequence similarity 20, member A** | Fam20a | ENSMUSG00000020614 | 0.71 | 5.7E-03 |
| **NHS-like 1** | Nhsl1 | ENSMUSG00000039835 | 0.68 | 6.3E-03 |
| **golgi associated, gamma adaptin ear containing, ARF binding protein 2** | Gga2 | ENSMUSG00000030872 | 1.33 | 6.3E-03 |
| **retinoic acid early transcript gamma** | Raet1c | ENSMUSG00000053219 | 0.52 | 6.5E-03 |

| | | | | |
|---|---|---|---|---|
| **heat shock protein 5** | Hspa5 | ENSMUSG00000026864 | 0.63 | 6.5E-03 |
| **a disintegrin and metallopeptidase domain 23** | Adam23 | ENSMUSG00000025964 | 1.52 | 6.5E-03 |
| **TRAF3 interacting protein 1** | Traf3ip1 | ENSMUSG00000034292 | 1.31 | 6.5E-03 |
| **epoxide hydrolase 1, microsomal** | Ephx1 | ENSMUSG00000038776 | 0.62 | 6.5E-03 |
| **melatonin receptor 1A** | Mtnr1a | ENSMUSG00000054764 | 0.46 | 6.5E-03 |
| **patatin-like phospholipase domain containing 7** | Pnpla7 | ENSMUSG00000036833 | 0.74 | 6.9E-03 |
| **leucine rich repeat and fibronectin type III domain containing 3** | Lrfn3 | ENSMUSG00000036957 | 0.51 | 7.0E-03 |
| **signal peptidase complex subunit 2 homolog (S. cerevisiae)** | Spcs2 | ENSMUSG00000035227 | 0.76 | 7.0E-03 |
| **estrogen related receptor, alpha** | Esrra | ENSMUSG00000024955 | 1.29 | 7.3E-03 |
| **RIKEN cDNA 1810074P20 gene** | 1810074P20Rik | ENSMUSG00000040359 | 0.76 | 7.5E-03 |
| **dynein light chain LC8-type 1** | Dynll1 | ENSMUSG00000009013 | 0.65 | 7.6E-03 |
| **sorting nexin 8** | Snx8 | ENSMUSG00000029560 | 1.35 | 7.6E-03 |
| **microtubule associated monoxygenase, calponin and LIM domain containing 2** | Mical2 | ENSMUSG00000038244 | 0.71 | 7.6E-03 |
| **cytokine inducible SH2-containing protein** | Cish | ENSMUSG00000032578 | 2.67 | 7.6E-03 |
| **UDP-glucose pyrophosphorylase 2** | Ugp2 | ENSMUSG00000001891 | 1.36 | 7.6E-03 |
| **neuroepithelial cell transforming gene 1** | Net1 | ENSMUSG00000021215 | 0.72 | 7.6E-03 |
| **retinoic acid early transcript beta** | Raet1b | ENSMUSG00000078452 | 0.53 | 7.8E-03 |
| **crystallin, zeta** | Cryz | ENSMUSG00000028199 | 1.28 | 9.2E-03 |
| **adaptor protein, phosphotyrosine interaction, PH domain and leucine zipper containing 2** | Appl2 | ENSMUSG00000020263 | 1.36 | 9.6E-03 |
| **inhibin beta-C** | Inhbc | ENSMUSG00000025405 | 0.64 | 9.6E-03 |
| **protein phosphatase 1M** | Ppm1m | ENSMUSG00000020253 | 0.77 | 9.6E-03 |
| **protein tyrosine phosphatase, receptor type, U** | Ptpru | ENSMUSG00000028909 | 0.46 | 1.0E-02 |
| **pyridine nucleotide-disulphide oxidoreductase domain 2** | Pyroxd2 | ENSMUSG00000060224 | 1.27 | 1.0E-02 |
| **catenin, beta like 1** | Ctnnbl1 | ENSMUSG00000027649 | 0.79 | 1.0E-02 |

| | | | | |
|---|---|---|---|---|
| **trypsin domain containing 1** | Tysnd1 | ENSMUSG00000020087 | 0.81 | 1.0E-02 |
| **TRAF-interacting protein with forkhead-associated domain** | Tifa | ENSMUSG00000046688 | 1.77 | 1.1E-02 |
| **oligosaccharyltransferase complex subunit** | Ostc | ENSMUSG00000041084 | 0.77 | 1.1E-02 |
| **myeloid/lymphoid or mixed-lineage leukemia (trithorax homolog, Drosophila); translocated to, 6** | Mllt6 | ENSMUSG00000038437 | 1.29 | 1.1E-02 |
| **chondroitin sulfate proteoglycan 5** | Cspg5 | ENSMUSG00000032482 | 0.41 | 1.2E-02 |
| **carboxylesterase 1B** | Ces1b | ENSMUSG00000078964 | 0.65 | 1.2E-02 |
| **proline dehydrogenase** | Prodh | ENSMUSG00000003526 | 1.54 | 1.2E-02 |
| **interferon, alpha-inducible protein 27 like 1** | Ifi27l1 | ENSMUSG00000064215 | 0.66 | 1.2E-02 |
| **hypoxia up-regulated 1** | Hyou1 | ENSMUSG00000032115 | 0.59 | 1.3E-02 |
| **tectonic family member 2** | Tctn2 | ENSMUSG00000029386 | 1.79 | 1.3E-02 |
| **tripartite motif-containing 2** | Trim2 | ENSMUSG00000027993 | 0.70 | 1.3E-02 |
| **CCAAT/enhancer binding protein (C/EBP), epsilon** | Cebpe | ENSMUSG00000052435 | 1.51 | 1.3E-02 |
| **bridging integrator 1** | Bin1 | ENSMUSG00000024381 | 0.77 | 1.4E-02 |
| **pleckstrin homology-like domain, family A, member 1** | Phlda1 | ENSMUSG00000020205 | 2.24 | 1.4E-02 |
| **aminoacylase 1** | Acy1 | ENSMUSG00000023262 | 1.27 | 1.4E-02 |
| **poly(rC) binding protein 4** | Pcbp4 | ENSMUSG00000023495 | 1.46 | 1.4E-02 |
| **phosphodiesterase 6C, cGMP specific, cone, alpha prime** | Pde6c | ENSMUSG00000024992 | 2.44 | 1.4E-02 |
| **mortality factor 4 like 2** | Morf4l2 | ENSMUSG00000031422 | 0.79 | 1.4E-02 |
| **trichohyalin** | Tchh | ENSMUSG00000052415 | 2.41 | 1.4E-02 |
| **Kruppel-like factor 2 (lung)** | Klf2 | ENSMUSG00000055148 | 1.50 | 1.4E-02 |
| **unc-119 homolog (C. elegans)** | Unc119 | ENSMUSG00000002058 | 0.67 | 1.4E-02 |
| **farnesyl diphosphate synthetase** | Fdps | ENSMUSG00000059743 | 1.77 | 1.4E-02 |
| **solute carrier family 25 (mitochondrial carrier, adenine nucleotide translocator), member 5** | Slc25a5 | ENSMUSG00000016319 | 1.16 | 1.4E-02 |

| | | | | |
|---|---|---|---|---|
| **Eph receptor A2** | Epha2 | ENSMUSG00000006445 | 0.54 | 1.5E-02 |
| **ST6 (alpha-N-acetyl-neuraminyl-2,3-beta-galactosyl-1,3)-N-acetylgalactosaminide alpha-2,6-sialyltransferase 4** | St6galnac4 | ENSMUSG00000079442 | 1.83 | 1.5E-02 |
| **calpain 2** | Capn2 | ENSMUSG00000026509 | 0.82 | 1.5E-02 |
| **ectonucleotide pyrophosphatase/phosphodiesterase 5** | Enpp5 | ENSMUSG00000023960 | 1.42 | 1.5E-02 |
| **lysine (K)-specific demethylase 5B** | Kdm5b | ENSMUSG00000042207 | 1.26 | 1.5E-02 |
| **signal-induced proliferation-associated 1 like 1** | Sipa1l1 | ENSMUSG00000042700 | 0.78 | 1.5E-02 |
| **RAD23b homolog (S. cerevisiae)** | Rad23b | ENSMUSG00000028426 | 0.85 | 1.5E-02 |
| **STT3, subunit of the oligosaccharyltransferase complex, homolog B (S. cerevisiae)** | Stt3b | ENSMUSG00000032437 | 0.84 | 1.5E-02 |
| **syntaxin 5A** | Stx5a | ENSMUSG00000010110 | 0.80 | 1.5E-02 |
| **cleavage and polyadenylation factor subunit homolog (S. cerevisiae)** | Pcf11 | ENSMUSG00000041328 | 1.27 | 1.6E-02 |
| **glutamine fructose-6-phosphate transaminase 1** | Gfpt1 | ENSMUSG00000029992 | 0.67 | 1.6E-02 |
| **dynamin binding protein** | Dnmbp | ENSMUSG00000025195 | 0.67 | 1.6E-02 |
| **patched homolog 2** | Ptch2 | ENSMUSG00000028681 | 2.08 | 1.7E-02 |
| **trans-acting transcription factor 3** | Sp3 | ENSMUSG00000027109 | 0.82 | 1.7E-02 |
| **nephronectin** | Npnt | ENSMUSG00000040908 | 0.42 | 1.7E-02 |
| **solute carrier family 7 (cationic amino acid transporter, y+ system), member 8** | Slc7a8 | ENSMUSG00000022180 | 1.79 | 1.7E-02 |
| **Ellis van Creveld gene homolog (human)** | Evc | ENSMUSG00000029122 | 1.95 | 1.7E-02 |
| **solute carrier family 45, member 3** | Slc45a3 | ENSMUSG00000026435 | 0.52 | 1.7E-02 |
| **transmembrane protein 97** | Tmem97 | ENSMUSG00000037278 | 1.33 | 1.7E-02 |
| **paired-like homeodomain transcription factor 3** | Pitx3 | ENSMUSG00000025229 | 0.40 | 1.8E-02 |
| **blocked early in transport 1 homolog (S. cerevisiae)** | Bet1 | ENSMUSG00000032757 | 0.76 | 1.8E-02 |
| **heat shock transcription factor 4** | Hsf4 | ENSMUSG00000033249 | 1.41 | 1.8E-02 |

| | | | | |
|---|---|---|---|---|
| **ATG13 autophagy related 13 homolog (S. cerevisiae)** | Atg13 | ENSMUSG00000027244 | 0.81 | 1.8E-02 |
| **coatomer protein complex, subunit gamma** | Copg | ENSMUSG00000030058 | 0.85 | 1.8E-02 |
| **brain protein I3** | Bri3 | ENSMUSG00000047843 | 1.30 | 1.8E-02 |
| **membrane associated guanylate kinase, WW and PDZ domain containing 1** | Magi1 | ENSMUSG00000045095 | 0.81 | 1.8E-02 |
| **plakophilin 2** | Pkp2 | ENSMUSG00000041957 | 0.77 | 1.8E-02 |
| **sulfatase 2** | Sulf2 | ENSMUSG00000006800 | 1.69 | 1.9E-02 |
| **proteasome (prosome, macropain) 26S subunit, non-ATPase, 11** | Psmd11 | ENSMUSG00000017428 | 0.84 | 1.9E-02 |
| **prion protein** | Prnp | ENSMUSG00000079037 | 1.41 | 1.9E-02 |
| **caspase 6** | Casp6 | ENSMUSG00000027997 | 1.26 | 2.0E-02 |
| **talin 2** | Tln2 | ENSMUSG00000052698 | 0.72 | 2.0E-02 |
| **one cut domain, family member 1** | Onecut1 | ENSMUSG00000043013 | 2.32 | 2.0E-02 |
| **ubiquilin 1** | Ubqln1 | ENSMUSG00000005312 | 0.84 | 2.1E-02 |
| **acylphosphatase 2, muscle type** | Acyp2 | ENSMUSG00000060923 | 0.65 | 2.1E-02 |
| **tubulin, beta 2A class IIA** | Tubb2a | ENSMUSG00000058672 | 0.50 | 2.1E-02 |
| **LIM and SH3 protein 1** | Lasp1 | ENSMUSG00000038366 | 0.80 | 2.1E-02 |
| **Ras-related GTP binding C** | Rragc | ENSMUSG00000028646 | 1.24 | 2.2E-02 |
| **tubulin, beta 4B class IVB** | Tubb4b | ENSMUSG00000036752 | 0.73 | 2.2E-02 |
| **RIKEN cDNA 2810030E01 gene** | 2810030E01Rik | ENSMUSG00000054074 | 2.28 | 2.2E-02 |
| **perilipin 5** | Plin5 | ENSMUSG00000011305 | 0.63 | 2.2E-02 |
| **polymerase (DNA directed), alpha 2** | Pola2 | ENSMUSG00000024833 | 1.31 | 2.2E-02 |
| **FIC domain containing** | Ficd | ENSMUSG00000053334 | 0.65 | 2.2E-02 |
| **myotubularin related protein 4** | Mtmr4 | ENSMUSG00000018401 | 0.72 | 2.2E-02 |
| **F-box protein 4** | Fbxo4 | ENSMUSG00000022184 | 0.82 | 2.2E-02 |
| **retinoic acid induced 14** | Rai14 | ENSMUSG00000022246 | 0.81 | 2.2E-02 |

| | | | | |
|---|---|---|---|---|
| **postmeiotic segregation increased 2 (S. cerevisiae)** | Pms2 | ENSMUSG00000079109 | 1.55 | 2.3E-02 |
| **Eph receptor B6** | Ephb6 | ENSMUSG00000029869 | 0.47 | 2.4E-02 |
| **solute carrier family 44, member 1** | Slc44a1 | ENSMUSG00000028412 | 0.78 | 2.5E-02 |
| **serine incorporator 2** | Serinc2 | ENSMUSG00000023232 | 0.68 | 2.5E-02 |
| **PDZ and LIM domain 5** | Pdlim5 | ENSMUSG00000028273 | 0.83 | 2.5E-02 |
| **dual specificity phosphatase 14** | Dusp14 | ENSMUSG00000018648 | 1.99 | 2.5E-02 |
| **paternally expressed 10** | Peg10 | ENSMUSG00000092035 | 0.48 | 2.6E-02 |
| **transmembrane channel-like gene family 7** | Tmc7 | ENSMUSG00000042246 | 0.52 | 2.6E-02 |
| **RIKEN cDNA 4930452B06 gene** | 4930452B06Rik | ENSMUSG00000021747 | 1.95 | 2.6E-02 |
| **hydroxysteroid 11-beta dehydrogenase 1** | Hsd11b1 | ENSMUSG00000016194 | 1.30 | 2.6E-02 |
| **zinc finger protein 9** | Zfp9 | ENSMUSG00000072623 | 0.49 | 2.6E-02 |
| **NSFL1 (p97) cofactor (p47)** | Nsfl1c | ENSMUSG00000027455 | 0.87 | 2.6E-02 |
| **Hermansky-Pudlak syndrome 4 homolog (human)** | Hps4 | ENSMUSG00000042328 | 1.45 | 2.6E-02 |
| **transmembrane protein 98** | Tmem98 | ENSMUSG00000035413 | 0.77 | 2.6E-02 |
| **somatostatin receptor 2** | Sstr2 | ENSMUSG00000047904 | 0.46 | 2.6E-02 |
| **spindlin 1** | Spin1 | ENSMUSG00000021395 | 0.79 | 2.6E-02 |
| **lysocardiolipin acyltransferase 1** | Lclat1 | ENSMUSG00000054469 | 0.86 | 2.6E-02 |
| **cytokine receptor-like factor 2** | Crlf2 | ENSMUSG00000033467 | 0.73 | 2.6E-02 |
| **mitogen-activated protein kinase kinase 1** | Map2k1 | ENSMUSG00000004936 | 0.87 | 2.6E-02 |
| **prostaglandin D2 synthase (brain)** | Ptgds | ENSMUSG00000015090 | 2.30 | 2.7E-02 |
| **SPARC related modular calcium binding 1** | Smoc1 | ENSMUSG00000021136 | 1.20 | 2.7E-02 |
| **cystinosis, nephropathic** | Ctns | ENSMUSG00000005949 | 1.28 | 2.7E-02 |
| **interferon, alpha-inducible protein 27 like 2B** | Ifi27l2b | ENSMUSG00000021208 | 0.56 | 2.8E-02 |
| **ATPase, Ca++ transporting, cardiac muscle, slow twitch 2** | Atp2a2 | ENSMUSG00000029467 | 0.73 | 2.8E-02 |
| **fatty acid binding protein 5, epidermal** | Fabp5 | ENSMUSG00000027533 | 1.93 | 2.8E-02 |

| | | | | |
|---|---|---|---|---|
| **chaperonin containing Tcp1, subunit 3 (gamma)** | Cct3 | ENSMUSG00000001416 | 0.86 | 2.9E-02 |
| **tuberous sclerosis 1** | Tsc1 | ENSMUSG00000026812 | 1.33 | 3.0E-02 |
| **solute carrier family 2 (facilitated glucose transporter), member 5** | Slc2a5 | ENSMUSG00000028976 | 1.87 | 3.1E-02 |
| **phosphatidylinositol 4-kinase, catalytic, alpha polypeptide** | Pi4ka | ENSMUSG00000041720 | 1.20 | 3.1E-02 |
| **histidine triad nucleotide binding protein 3** | Hint3 | ENSMUSG00000019791 | 1.22 | 3.3E-02 |
| **REST corepressor 1** | Rcor1 | ENSMUSG00000037896 | 0.79 | 3.3E-02 |
| **SET domain containing 4** | Setd4 | ENSMUSG00000022948 | 0.59 | 3.3E-02 |
| **F-box protein 25** | Fbxo25 | ENSMUSG00000038365 | 0.76 | 3.4E-02 |
| **insulin induced gene 2** | Insig2 | ENSMUSG00000003721 | 0.59 | 3.5E-02 |
| **annexin A8** | Anxa8 | ENSMUSG00000021950 | 2.07 | 3.5E-02 |
| **expressed sequence AI428936** | AI428936 | ENSMUSG00000019737 | 1.92 | 3.5E-02 |
| **adenine phosphoribosyl transferase** | Aprt | ENSMUSG00000006589 | 1.42 | 3.5E-02 |
| **solute carrier family 12, member 6** | Slc12a6 | ENSMUSG00000027130 | 1.32 | 3.5E-02 |
| **tubby-like protein 2** | Tulp2 | ENSMUSG00000023467 | 1.89 | 3.6E-02 |
| **chloride channel 7** | Clcn7 | ENSMUSG00000036636 | 1.21 | 3.6E-02 |
| **solute carrier family 33 (acetyl-CoA transporter), member 1** | Slc33a1 | ENSMUSG00000027822 | 0.80 | 3.6E-02 |
| **plasma membrane proteolipid** | Pllp | ENSMUSG00000031775 | 0.70 | 3.6E-02 |
| **protein phosphatase 1F (PP2C domain containing)** | Ppm1f | ENSMUSG00000026181 | 0.80 | 3.7E-02 |
| **synovial apoptosis inhibitor 1, synoviolin** | Syvn1 | ENSMUSG00000024807 | 0.66 | 3.7E-02 |
| **G protein-coupled receptor, family C, group 5, member B** | Gprc5b | ENSMUSG00000008734 | 0.47 | 3.7E-02 |
| **glutathione S-transferase, mu 4** | Gstm4 | ENSMUSG00000027890 | 0.71 | 3.7E-02 |
| **cyclin F** | Ccnf | ENSMUSG00000072082 | 0.70 | 3.8E-02 |
| **complement factor properdin** | Cfp | ENSMUSG00000001128 | 1.52 | 3.8E-02 |
| **palladin, cytoskeletal associated protein** | Palld | ENSMUSG00000058056 | 0.67 | 3.9E-02 |
| **t-complex protein 1** | Tcp1 | ENSMUSG00000068039 | 0.89 | 3.9E-02 |

| | | | | |
|---|---|---|---|---|
| **WW, C2 and coiled-coil domain containing 1** | Wwc1 | ENSMUSG00000018849 | 0.77 | 3.9E-02 |
| **activating transcription factor 6 beta** | Atf6b | ENSMUSG00000015461 | 0.80 | 3.9E-02 |
| **carnitine acetyltransferase** | Crat | ENSMUSG00000026853 | 0.63 | 3.9E-02 |
| **transformation related protein 53 inducible nuclear protein 1** | Trp53inp1 | ENSMUSG00000028211 | 0.62 | 3.9E-02 |
| **zinc finger, DHHC domain containing 6** | Zdhhc6 | ENSMUSG00000024982 | 0.87 | 3.9E-02 |
| **ring finger protein 11** | Rnf11 | ENSMUSG00000028557 | 0.82 | 4.0E-02 |
| **platelet-derived growth factor receptor-like** | Pdgfrl | ENSMUSG00000031595 | 0.45 | 4.0E-02 |
| **methylthioadenosine phosphorylase** | Mtap | ENSMUSG00000062937 | 0.81 | 4.0E-02 |
| **nuclear factor, interleukin 3, regulated** | Nfil3 | ENSMUSG00000056749 | 0.55 | 4.0E-02 |
| **transmembrane protein 56** | Tmem56 | ENSMUSG00000028132 | 0.73 | 4.0E-02 |
| **actin binding LIM protein family, member 3** | Ablim3 | ENSMUSG00000032735 | 0.67 | 4.0E-02 |
| **hemopoietic cell kinase** | Hck | ENSMUSG00000003283 | 1.63 | 4.0E-02 |
| **testis expressed gene 2** | Tex2 | ENSMUSG00000040548 | 0.82 | 4.0E-02 |
| **ARP10 actin-related protein 10 homolog (S. cerevisiae)** | Actr10 | ENSMUSG00000021076 | 0.89 | 4.0E-02 |
| **calcium/calmodulin-dependent protein kinase IV** | Camk4 | ENSMUSG00000038128 | 1.74 | 4.0E-02 |
| **peptidylprolyl isomerase F (cyclophilin F)** | Ppif | ENSMUSG00000021868 | 1.26 | 4.0E-02 |
| **predicted gene 4477** | Gm4477 | ENSMUSG00000089694 | 2.28 | 4.1E-02 |
| **serine palmitoyltransferase, long chain base subunit 1** | Sptlc1 | ENSMUSG00000021468 | 0.86 | 4.1E-02 |
| **prostaglandin-endoperoxide synthase 1** | Ptgs1 | ENSMUSG00000047250 | 1.41 | 4.1E-02 |
| **BTB (POZ) domain containing 1** | Btbd1 | ENSMUSG00000025103 | 0.84 | 4.1E-02 |
| **proteasome (prosome, macropain) 26S subunit, non-ATPase, 7** | Psmd7 | ENSMUSG00000039067 | 0.87 | 4.1E-02 |
| **golgi phosphoprotein 3-like** | Golph3l | ENSMUSG00000046519 | 0.73 | 4.2E-02 |
| **hydroxysteroid dehydrogenase like 2** | Hsdl2 | ENSMUSG00000028383 | 0.76 | 4.2E-02 |
| **Rho GTPase activating protein 6** | Arhgap6 | ENSMUSG00000031355 | 1.52 | 4.2E-02 |
| **tight junction protein 2** | Tjp2 | ENSMUSG00000024812 | 0.79 | 4.2E-02 |

| | | | | |
|---|---|---|---|---|
| **major facilitator superfamily domain containing 8** | Mfsd8 | ENSMUSG00000025759 | 0.80 | 4.2E-02 |
| **mitogen-activated protein kinase kinase kinase 14** | Map3k14 | ENSMUSG00000020941 | 1.60 | 4.3E-02 |
| **complement component 2 (within H-2S)** | C2 | ENSMUSG00000024371 | 1.28 | 4.4E-02 |
| **UTP6, small subunit (SSU) processome component, homolog (yeast)** | Utp6 | ENSMUSG00000035575 | 0.88 | 4.4E-02 |
| **nuclear receptor subfamily 4, group A, member 2** | Nr4a2 | ENSMUSG00000026826 | 0.51 | 4.4E-02 |
| **vasorin** | Vasn | ENSMUSG00000039646 | 0.64 | 4.4E-02 |
| **zinc finger, CCHC domain containing 2** | Zcchc2 | ENSMUSG00000038866 | 1.28 | 4.4E-02 |
| **glutamyl-tRNA synthetase 2 (mitochondrial)(putative)** | Ears2 | ENSMUSG00000030871 | 0.80 | 4.4E-02 |
| **CD97 antigen** | Cd97 | ENSMUSG00000002885 | 1.40 | 4.4E-02 |
| **cell division cycle 27 homolog (S. cerevisiae)** | Cdc27 | ENSMUSG00000020687 | 0.83 | 4.4E-02 |
| **caseinolytic peptidase X (E.coli)** | Clpx | ENSMUSG00000015357 | 0.64 | 4.4E-02 |
| **small G protein signaling modulator 2** | Sgsm2 | ENSMUSG00000038351 | 0.72 | 4.4E-02 |
| **cysteine-rich with EGF-like domains 2** | Creld2 | ENSMUSG00000023272 | 0.58 | 4.4E-02 |
| **thioredoxin domain containing 11** | Txndc11 | ENSMUSG00000022498 | 0.79 | 4.4E-02 |
| **cadherin 5** | Cdh5 | ENSMUSG00000031871 | 1.41 | 4.5E-02 |
| **developmentally regulated GTP binding protein 1** | Drg1 | ENSMUSG00000020457 | 0.89 | 4.5E-02 |
| **SEC22 vesicle trafficking protein homolog B (S. cerevisiae)** | Sec22b | ENSMUSG00000027879 | 0.82 | 4.5E-02 |
| **neural precursor cell expressed, developmentally down-regulated gene 4-like** | Nedd4l | ENSMUSG00000024589 | 0.64 | 4.5E-02 |
| **target of myb1-like 2 (chicken)** | Tom1l2 | ENSMUSG00000000538 | 1.20 | 4.6E-02 |
| **Alport syndrome, mental retardation, midface hypoplasia and elliptocytosis chromosomal region gene 1 homolog (human)** | Ammecr1 | ENSMUSG00000042225 | 0.67 | 4.6E-02 |
| **phospholipase A2, group XIIB** | Pla2g12b | ENSMUSG00000009646 | 0.83 | 4.6E-02 |
| **mannoside acetylglucosaminyltransferase 2** | Mgat2 | ENSMUSG00000043998 | 0.76 | 4.7E-02 |
| **acetyl-Coenzyme A carboxylase beta** | Acacb | ENSMUSG00000042010 | 1.57 | 4.7E-02 |

| | | | | |
|---|---|---|---|---|
| **peptidyl-tRNA hydrolase 2** | Ptrh2 | ENSMUSG00000072582 | 0.82 | 4.7E-02 |
| **phosphatidylinositol glycan anchor biosynthesis, class U** | Pigu | ENSMUSG00000038383 | 0.82 | 4.8E-02 |
| **nuclear receptor binding factor 2** | Nrbf2 | ENSMUSG00000075000 | 0.82 | 4.8E-02 |
| **immunoglobulin superfamily, member 6** | Igsf6 | ENSMUSG00000035004 | 1.73 | 4.8E-02 |
| **KDEL (Lys-Asp-Glu-Leu) endoplasmic reticulum protein retention receptor 2** | Kdelr2 | ENSMUSG00000079111 | 0.83 | 4.8E-02 |
| **pleckstrin homology domain containing, family O member 2** | Plekho2 | ENSMUSG00000050721 | 1.60 | 4.8E-02 |
| **transmembrane protein 30B** | Tmem30b | ENSMUSG00000034435 | 0.84 | 4.8E-02 |
| **solute carrier family 13 (sodium-dependent dicarboxylate transporter), member 3** | Slc13a3 | ENSMUSG00000018459 | 1.48 | 4.9E-02 |
| **outer dense fiber of sperm tails 2** | Odf2 | ENSMUSG00000026790 | 1.30 | 4.9E-02 |
| **ring finger protein 19B** | Rnf19b | ENSMUSG00000028793 | 1.23 | 4.9E-02 |
| **RIKEN cDNA 6030446N20 gene** | 6030446N20Rik | ENSMUSG00000049411 | 1.37 | 4.9E-02 |

***Table 7.2** - Genes, hepatic expression of which is altered in D316A relative to WT-Tg mice following chow feeding.*

| GeneName | Symbol | Gene | Fold change | Adj p |
|---|---|---|---|---|
| **CD63 antigen** | Cd63 | ENSMUSG00000025351 | 3.39 | 2.2E-05 |
| **interferon regulatory factor 6** | Irf6 | ENSMUSG00000026638 | 1.43 | 3.3E-05 |
| **ArfGAP with GTPase domain, ankyrin repeat and PH domain 2** | Agap2 | ENSMUSG00000025422 | 0.35 | 3.3E-05 |
| **tetraspanin 31** | Tspan31 | ENSMUSG00000006736 | 0.73 | 1.5E-04 |
| **serine/arginine repetitive matrix 4** | Srrm4 | ENSMUSG00000063919 | 2.86 | 2.8E-04 |
| **pleckstrin homology domain containing, family D (with coiled-coil domains) member 1** | Plekhd1 | ENSMUSG00000066438 | 3.52 | 3.5E-04 |
| **3'-phosphoadenosine 5'-phosphosulfate synthase 1** | Papss1 | ENSMUSG00000028032 | 0.57 | 4.5E-04 |
| **deiodinase, iodothyronine, type I** | Dio1 | ENSMUSG00000034785 | 0.51 | 4.5E-04 |
| **glycerate kinase** | Glyctk | ENSMUSG00000020258 | 0.71 | 5.9E-04 |

| | | | | |
|---|---|---|---|---|
| **serine (or cysteine) peptidase inhibitor, clade E, member 2** | Serpine2 | ENSMUSG00000026249 | 0.41 | 1.5E-03 |
| **Ral GEF with PH domain and SH3 binding motif 1** | Ralgps1 | ENSMUSG00000038831 | 1.92 | 1.5E-03 |
| **microrchidia 4** | Morc4 | ENSMUSG00000031434 | 1.84 | 1.6E-03 |
| **Ras-related GTP binding D** | Rragd | ENSMUSG00000028278 | 2.52 | 1.6E-03 |
| **HCLS1 binding protein 3** | Hs1bp3 | ENSMUSG00000020605 | 1.32 | 1.6E-03 |
| **growth arrest specific 7** | Gas7 | ENSMUSG00000033066 | 1.81 | 1.7E-03 |
| **regulating synaptic membrane exocytosis 4** | Rims4 | ENSMUSG00000035226 | 2.98 | 2.3E-03 |
| **Rho GDP dissociation inhibitor (GDI) alpha** | Arhgdia | ENSMUSG00000025132 | 1.50 | 2.7E-03 |
| **glycerol kinase** | Gk | ENSMUSG00000025059 | 0.74 | 3.7E-03 |
| **pumilio RNA-binding family member 1** | Pum1 | ENSMUSG00000028580 | 0.81 | 3.7E-03 |
| **cell death-inducing DNA fragmentation factor, alpha subunit-like effector B** | Cideb | ENSMUSG00000022219 | 0.76 | 3.8E-03 |
| **ubiquitination factor E4A** | Ube4a | ENSMUSG00000059890 | 0.81 | 3.8E-03 |
| **3-hydroxybutyrate dehydrogenase, type 1** | Bdh1 | ENSMUSG00000046598 | 0.74 | 3.8E-03 |
| **aldehyde dehydrogenase 1 family, member B1** | Aldh1b1 | ENSMUSG00000035561 | 2.12 | 3.9E-03 |
| **transcription elongation factor A (SII), 3** | Tcea3 | ENSMUSG00000001604 | 0.73 | 3.9E-03 |
| **obscurin, cytoskeletal calmodulin and titin-interacting RhoGEF** | Obscn | ENSMUSG00000061462 | 2.91 | 3.9E-03 |
| **tousled-like kinase 1** | Tlk1 | ENSMUSG00000041997 | 0.72 | 4.0E-03 |
| **DNA segment, Chr 2, Wayne State University 81, expressed** | D2Wsu81e | ENSMUSG00000039660 | 0.72 | 4.1E-03 |
| **poly (ADP-ribose) polymerase family, member 3** | Parp3 | ENSMUSG00000023249 | 1.33 | 4.9E-03 |
| **monoglyceride lipase** | Mgll | ENSMUSG00000033174 | 0.71 | 5.8E-03 |
| **c-src tyrosine kinase** | Csk | ENSMUSG00000032312 | 0.80 | 6.3E-03 |
| **lymphocyte antigen 6 complex, locus D** | Ly6d | ENSMUSG00000034634 | 2.05 | 6.3E-03 |
| **agmatine ureohydrolase (agmatinase)** | Agmat | ENSMUSG00000040706 | 0.80 | 6.6E-03 |
| **phosphatidylinositol 3-kinase, C2 domain containing, alpha polypeptide** | Pik3c2a | ENSMUSG00000030660 | 0.68 | 6.6E-03 |

| | | | | |
|---|---|---|---|---|
| **amplified in osteosarcoma** | Os9 | ENSMUSG00000040462 | 0.81 | 6.6E-03 |
| **solute carrier family 37 (glycerol-3-phosphate transporter), member 1** | Slc37a1 | ENSMUSG00000024036 | 2.47 | 7.4E-03 |
| **transmembrane and ubiquitin-like domain containing 1** | Tmub1 | ENSMUSG00000028958 | 0.74 | 7.9E-03 |
| **kelch-like 8** | Klhl8 | ENSMUSG00000029312 | 1.56 | 7.9E-03 |
| **chitinase-like 1** | Chil1 | ENSMUSG00000064246 | 2.77 | 8.8E-03 |
| **Ellis van Creveld syndrome 2** | Evc2 | ENSMUSG00000050248 | 2.29 | 8.8E-03 |
| **cullin 9** | Cul9 | ENSMUSG00000040327 | 1.44 | 8.9E-03 |
| **sel-1 suppressor of lin-12-like 3 (C. elegans)** | Sel1l3 | ENSMUSG00000029189 | 0.73 | 9.6E-03 |
| **dehydrogenase/reductase (SDR family) member 1** | Dhrs1 | ENSMUSG00000002332 | 0.73 | 9.6E-03 |
| **leukocyte cell-derived chemotaxin 2** | Lect2 | ENSMUSG00000021539 | 0.71 | 9.6E-03 |
| **pyrophosphatase (inorganic) 1** | Ppa1 | ENSMUSG00000020089 | 0.77 | 1.0E-02 |
| **roundabout guidance receptor 1** | Robo1 | ENSMUSG00000022883 | 1.78 | 1.1E-02 |
| **dipeptidylpeptidase 7** | Dpp7 | ENSMUSG00000026958 | 1.30 | 1.1E-02 |
| **family with sequence similarity 206, member A** | Fam206a | ENSMUSG00000038827 | 1.48 | 1.1E-02 |
| **CD14 antigen** | Cd14 | ENSMUSG00000051439 | 2.10 | 1.2E-02 |
| **tryptophan 2,3-dioxygenase** | Tdo2 | ENSMUSG00000028011 | 0.63 | 1.2E-02 |
| **chemokine (C-C motif) ligand 2** | Ccl2 | ENSMUSG00000035385 | 2.67 | 1.2E-02 |
| **SET domain containing 3** | Setd3 | ENSMUSG00000056770 | 0.88 | 1.2E-02 |
| **forkhead box O3** | Foxo3 | ENSMUSG00000048756 | 0.69 | 1.3E-02 |
| **interleukin 1 beta** | Il1b | ENSMUSG00000027398 | 2.41 | 1.3E-02 |
| **pleckstrin homology domain containing, family G (with RhoGef domain) member 3** | Plekhg3 | ENSMUSG00000052609 | 0.76 | 1.3E-02 |
| **transmembrane emp24 protein transport domain containing 4** | Tmed4 | ENSMUSG00000004394 | 0.84 | 1.3E-02 |
| **microtubule associated serine/threonine kinase family member 4** | Mast4 | ENSMUSG00000034751 | 1.47 | 1.3E-02 |
| **galactosamine (N-acetyl)-6-sulfate sulfatase** | Galns | ENSMUSG00000015027 | 1.61 | 1.4E-02 |

| | | | | |
|---|---|---|---|---|
| **solute carrier family 39 (zinc transporter), member 4** | Slc39a4 | ENSMUSG00000063354 | 1.83 | 1.5E-02 |
| **proline dehydrogenase (oxidase) 2** | Prodh2 | ENSMUSG00000036892 | 0.76 | 1.5E-02 |
| **aspartoacylase (aminoacylase) 3** | Acy3 | ENSMUSG00000024866 | 0.74 | 1.5E-02 |
| **cysteine rich, DPF motif domain containing 1** | Cdpf1 | ENSMUSG00000064284 | 1.49 | 1.6E-02 |
| **RAB8A, member RAS oncogene family** | Rab8a | ENSMUSG00000003037 | 0.88 | 1.6E-02 |
| **coiled-coil domain containing 152** | Ccdc152 | ENSMUSG00000091119 | 0.70 | 1.7E-02 |
| **Niemann-Pick type C2** | Npc2 | ENSMUSG00000021242 | 1.28 | 1.7E-02 |
| **solute carrier family 25, member 47** | Slc25a47 | ENSMUSG00000048856 | 0.74 | 1.7E-02 |
| **histocompatibility 2, Q region locus 10** | H2-Q10 | ENSMUSG00000067235 | 0.85 | 1.7E-02 |
| **Sec24 related gene family, member A (S. cerevisiae)** | Sec24a | ENSMUSG00000036391 | 0.81 | 1.8E-02 |
| **MYB binding protein (P160) 1a** | Mybbp1a | ENSMUSG00000040463 | 1.28 | 1.8E-02 |
| **STAM binding protein like 1** | Stambpl1 | ENSMUSG00000024776 | 2.32 | 1.8E-02 |
| **glycogen synthase 2** | Gys2 | ENSMUSG00000030244 | 0.64 | 1.8E-02 |
| **nuclear receptor subfamily 1, group D, member 2** | Nr1d2 | ENSMUSG00000021775 | 0.71 | 1.8E-02 |
| **carnitine palmitoyltransferase 1a, liver** | Cpt1a | ENSMUSG00000024900 | 0.71 | 1.8E-02 |
| **exonuclease 5** | Exo5 | ENSMUSG00000028629 | 1.58 | 1.8E-02 |
| **thyrotroph embryonic factor** | Tef | ENSMUSG00000022389 | 0.60 | 1.8E-02 |
| **RIKEN cDNA 1700017B05 gene** | 1700017B05Rik | ENSMUSG00000032300 | 1.74 | 1.9E-02 |
| **cDNA sequence BC003331** | BC003331 | ENSMUSG00000006010 | 0.85 | 1.9E-02 |
| **minichromosome maintenance 10 replication initiation factor** | Mcm10 | ENSMUSG00000026669 | 0.60 | 2.0E-02 |
| **trans-acting transcription factor 5** | Sp5 | ENSMUSG00000075304 | 0.52 | 2.0E-02 |
| **NA** | NA | ENSMUSG00000085214 | 0.76 | 2.0E-02 |
| **adhesion molecule with Ig like domain 2** | Amigo2 | ENSMUSG00000048218 | 0.64 | 2.0E-02 |
| **glutaredoxin** | Glrx | ENSMUSG00000021591 | 0.70 | 2.0E-02 |
| **kielin/chordin-like protein** | Kcp | ENSMUSG00000059022 | 1.66 | 2.0E-02 |

| | | | | |
|---|---|---|---|---|
| **ectonucleoside triphosphate diphosphohydrolase 2** | Entpd2 | ENSMUSG00000015085 | 1.74 | 2.0E-02 |
| **chemokine (C-X-C motif) ligand 10** | Cxcl10 | ENSMUSG00000034855 | 2.35 | 2.0E-02 |
| **cut-like homeobox 2** | Cux2 | ENSMUSG00000042589 | 2.55 | 2.0E-02 |
| **apolipoprotein F** | Apof | ENSMUSG00000047631 | 0.80 | 2.0E-02 |
| **saccharopine dehydrogenase (putative)** | Sccpdh | ENSMUSG00000038936 | 1.66 | 2.0E-02 |
| **transmembrane protein 138** | Tmem138 | ENSMUSG00000024666 | 1.58 | 2.0E-02 |
| **BCL2-associated athanogene 2** | Bag2 | ENSMUSG00000042215 | 1.53 | 2.2E-02 |
| **phosphorylase kinase, gamma 2 (testis)** | Phkg2 | ENSMUSG00000030815 | 0.77 | 2.2E-02 |
| **RNA binding motif protein 20** | Rbm20 | ENSMUSG00000043639 | 1.66 | 2.2E-02 |
| **splicing factor 3b, subunit 1** | Sf3b1 | ENSMUSG00000025982 | 0.86 | 2.2E-02 |
| **N-acetylglutamate synthase** | Nags | ENSMUSG00000048217 | 0.81 | 2.2E-02 |
| **solute carrier family 2, (facilitated glucose transporter), member 8** | Slc2a8 | ENSMUSG00000026791 | 1.22 | 2.2E-02 |
| **spermidine/spermine N1-acetyl transferase 1** | Sat1 | ENSMUSG00000025283 | 1.47 | 2.2E-02 |
| **transmembrane protease, serine 4** | Tmprss4 | ENSMUSG00000032091 | 2.44 | 2.2E-02 |
| **ceroid-lipofuscinosis, neuronal 6** | Cln6 | ENSMUSG00000032245 | 1.79 | 2.2E-02 |
| **elongation of very long chain fatty acids (FEN1/Elo2, SUR4/Elo3, yeast)-like 2** | Elovl2 | ENSMUSG00000021364 | 0.69 | 2.2E-02 |
| **Iroquois related homeobox 1 (Drosophila)** | Irx1 | ENSMUSG00000060969 | 0.43 | 2.2E-02 |
| **tubulin tyrosine ligase-like family, member 8** | Ttll8 | ENSMUSG00000022388 | 0.44 | 2.2E-02 |
| **tripartite motif-containing 13** | Trim13 | ENSMUSG00000035235 | 1.55 | 2.3E-02 |
| **out at first homolog** | Oaf | ENSMUSG00000032014 | 0.74 | 2.3E-02 |
| **lin-52 homolog (C. elegans)** | Lin52 | ENSMUSG00000085793 | 0.76 | 2.3E-02 |
| **RAN binding protein 3-like** | Ranbp3l | ENSMUSG00000048424 | 0.44 | 2.3E-02 |
| **major urinary protein 20** | Mup20 | ENSMUSG00000078672 | 0.49 | 2.4E-02 |
| **family with sequence similarity 234, member B** | Fam234b | ENSMUSG00000030207 | 0.72 | 2.4E-02 |

| | | | | |
|---|---|---|---|---|
| **peroxisome proliferative activated receptor, gamma, coactivator 1 beta** | Ppargc1b | ENSMUSG00000033871 | 0.61 | 2.4E-02 |
| **ectonucleotide pyrophosphatase/phosphodiesterase 2** | Enpp2 | ENSMUSG00000022425 | 1.63 | 2.4E-02 |
| **death effector domain-containing DNA binding protein 2** | Dedd2 | ENSMUSG00000054499 | 0.76 | 2.5E-02 |
| **zinc finger homeobox 3** | Zfhx3 | ENSMUSG00000038872 | 0.76 | 2.5E-02 |
| **inositol hexaphosphate kinase 1** | Ip6k1 | ENSMUSG00000032594 | 0.85 | 2.5E-02 |
| **tetratricopeptide repeat domain 3** | Ttc3 | ENSMUSG00000040785 | 1.25 | 2.5E-02 |
| **SEC16 homolog B (S. cerevisiae)** | Sec16b | ENSMUSG00000026589 | 0.79 | 2.5E-02 |
| **hydroxypyruvate isomerase (putative)** | Hyi | ENSMUSG00000006395 | 1.29 | 2.5E-02 |
| **kazrin, periplakin interacting protein** | Kazn | ENSMUSG00000040606 | 2.02 | 2.7E-02 |
| **DnaJ heat shock protein family (Hsp40) member A1** | Dnaja1 | ENSMUSG00000028410 | 0.76 | 2.7E-02 |
| **mannose-binding lectin (protein C) 2** | Mbl2 | ENSMUSG00000024863 | 0.72 | 2.7E-02 |
| **adenylate kinase 2** | Ak2 | ENSMUSG00000028792 | 0.74 | 2.8E-02 |
| **low density lipoprotein receptor-related protein associated protein 1** | Lrpap1 | ENSMUSG00000029103 | 1.29 | 2.8E-02 |
| **transmembrane protein 120A** | Tmem120a | ENSMUSG00000039886 | 0.77 | 2.8E-02 |
| **tetraspanin 12** | Tspan12 | ENSMUSG00000029669 | 0.82 | 2.8E-02 |
| **caspase recruitment domain family, member 14** | Card14 | ENSMUSG00000013483 | 2.37 | 2.8E-02 |
| **RIKEN cDNA E430025E21 gene** | E430025E21Rik | ENSMUSG00000022350 | 1.24 | 2.8E-02 |
| **lipase, endothelial** | Lipg | ENSMUSG00000053846 | 0.54 | 2.8E-02 |
| **vesicle-associated membrane protein 7** | Vamp7 | ENSMUSG00000051412 | 0.77 | 2.8E-02 |
| **brain expressed X-linked 2** | Bex2 | ENSMUSG00000042750 | 2.45 | 2.9E-02 |
| **ELOVL family member 7, elongation of long chain fatty acids (yeast)** | Elovl7 | ENSMUSG00000021696 | 2.44 | 2.9E-02 |
| **syntrophin, acidic 1** | Snta1 | ENSMUSG00000027488 | 1.29 | 2.9E-02 |
| **scavenger receptor class B, member 1** | Scarb1 | ENSMUSG00000037936 | 0.81 | 3.0E-02 |

| | | | | |
|---|---|---|---|---|
| **Kruppel-like factor 15** | Klf15 | ENSMUSG00000030087 | 0.65 | 3.0E-02 |
| **aldehyde oxidase 3** | Aox3 | ENSMUSG00000064294 | 0.64 | 3.1E-02 |
| **ubiquitin specific peptidase 2** | Usp2 | ENSMUSG00000032010 | 0.44 | 3.1E-02 |
| **mitogen-activated protein kinase kinase kinase 1** | Map3k1 | ENSMUSG00000021754 | 1.36 | 3.1E-02 |
| **apolipoprotein N** | Apon | ENSMUSG00000051716 | 0.75 | 3.3E-02 |
| **Rho GTPase activating protein 42** | Arhgap42 | ENSMUSG00000050730 | 0.77 | 3.3E-02 |
| **transmembrane protein 86A** | Tmem86a | ENSMUSG00000010307 | 0.55 | 3.3E-02 |
| **CXADR-like membrane protein** | Clmp | ENSMUSG00000032024 | 1.81 | 3.3E-02 |
| **zinc finger protein 85** | Zfp85 | ENSMUSG00000058331 | 0.61 | 3.3E-02 |
| **retinoblastoma binding protein 4** | Rbbp4 | ENSMUSG00000057236 | 0.82 | 3.4E-02 |
| **mannose-6-phosphate receptor, cation dependent** | M6pr | ENSMUSG00000007458 | 1.13 | 3.4E-02 |
| **spermine oxidase** | Smox | ENSMUSG00000027333 | 1.86 | 3.4E-02 |
| **lysophosphatidic acid receptor 1** | Lpar1 | ENSMUSG00000038668 | 0.59 | 3.5E-02 |
| **Nedd4 family interacting protein 1** | Ndfip1 | ENSMUSG00000024425 | 0.84 | 3.5E-02 |
| **sosondowah ankyrin repeat domain family member B** | Sowahb | ENSMUSG00000045314 | 1.65 | 3.5E-02 |
| **zinc finger and BTB domain containing 25** | Zbtb25 | ENSMUSG00000056459 | 1.54 | 3.5E-02 |
| **SEC23 homolog A, COPII coat complex component** | Sec23a | ENSMUSG00000020986 | 0.80 | 3.6E-02 |
| **kelch domain containing 8A** | Klhdc8a | ENSMUSG00000042115 | 1.75 | 3.6E-02 |
| **golgi reassembly stacking protein 2** | Gorasp2 | ENSMUSG00000014959 | 0.76 | 3.6E-02 |
| **glucose-6-phosphate dehydrogenase X-linked** | G6pdx | ENSMUSG00000031400 | 1.72 | 3.6E-02 |
| **adenylate cyclase 1** | Adcy1 | ENSMUSG00000020431 | 2.32 | 3.7E-02 |
| **phosducin-like 3** | Pdcl3 | ENSMUSG00000026078 | 1.20 | 3.8E-02 |
| **histocompatibility 2, blastocyst** | H2-Bl | ENSMUSG00000073406 | 0.52 | 3.9E-02 |
| **serine palmitoyltransferase, long chain base subunit 2** | Sptlc2 | ENSMUSG00000021036 | 1.27 | 3.9E-02 |
| **VPS9 domain containing 1** | Vps9d1 | ENSMUSG00000001062 | 0.80 | 3.9E-02 |

| | | | | |
|---|---|---|---|---|
| **cDNA sequence BC021891** | BC021891 | ENSMUSG00000031853 | 0.70 | 3.9E-02 |
| **lysosomal-associated protein transmembrane 4B** | Laptm4b | ENSMUSG00000022257 | 1.20 | 4.0E-02 |
| **phosphofructokinase, platelet** | Pfkp | ENSMUSG00000021196 | 1.59 | 4.0E-02 |
| **AT rich interactive domain 5A (MRF1-like)** | Arid5a | ENSMUSG00000037447 | 1.94 | 4.0E-02 |
| **a disintegrin-like and metallopeptidase (reprolysin type) with thrombospondin type 1 motif, 4** | Adamts4 | ENSMUSG00000006403 | 2.36 | 4.0E-02 |
| **nicotinamide nucleotide transhydrogenase** | Nnt | ENSMUSG00000025453 | 0.65 | 4.1E-02 |
| **Rho-related BTB domain containing 3** | Rhobtb3 | ENSMUSG00000021589 | 0.68 | 4.1E-02 |
| **histone deacetylase 11** | Hdac11 | ENSMUSG00000034245 | 0.79 | 4.1E-02 |
| **intraflagellar transport 22** | Ift22 | ENSMUSG00000007987 | 1.42 | 4.2E-02 |
| **APC membrane recruitment 1** | Amer1 | ENSMUSG00000050332 | 0.69 | 4.3E-02 |
| **cysteine and glycine-rich protein 2** | Csrp2 | ENSMUSG00000020186 | 0.80 | 4.3E-02 |
| **tRNA methyltransferase 1 like** | Trmt1l | ENSMUSG00000053286 | 0.83 | 4.3E-02 |
| **SEC22 homolog C, vesicle trafficking protein** | Sec22c | ENSMUSG00000061536 | 0.70 | 4.4E-02 |
| **UDP glucuronosyltransferase 2 family, polypeptide B36** | Ugt2b36 | ENSMUSG00000070704 | 0.78 | 4.5E-02 |
| **BRCA1 associated protein** | Brap | ENSMUSG00000029458 | 0.76 | 4.5E-02 |
| **anoctamin 10** | Ano10 | ENSMUSG00000037949 | 1.26 | 4.5E-02 |
| **CDK5 regulatory subunit associated protein 1-like 1** | Cdkal1 | ENSMUSG00000006191 | 0.78 | 4.5E-02 |
| **lipid droplet associated hydrolase** | Ldah | ENSMUSG00000037669 | 0.79 | 4.5E-02 |
| **tumor necrosis factor, alpha-induced protein 8-like 1** | Tnfaip8l1 | ENSMUSG00000044469 | 0.61 | 4.5E-02 |
| **pleckstrin homology domain containing, family A member 7** | Plekha7 | ENSMUSG00000045659 | 0.73 | 4.6E-02 |
| **PX domain containing serine/threonine kinase** | Pxk | ENSMUSG00000033885 | 0.85 | 4.6E-02 |
| **Kruppel-like factor 13** | Klf13 | ENSMUSG00000052040 | 0.67 | 4.6E-02 |
| **major facilitator superfamily domain containing 12** | Mfsd12 | ENSMUSG00000034854 | 1.36 | 4.6E-02 |
| **E26 avian leukemia oncogene 2, 3' domain** | Ets2 | ENSMUSG00000022895 | 1.52 | 4.6E-02 |

| | | | | |
|---|---|---|---|---|
| **oxysterol binding protein-like 1A** | Osbpl1a | ENSMUSG00000044252 | 0.88 | 4.6E-02 |
| **a disintegrin and metallopeptidase domain 19 (meltrin beta)** | Adam19 | ENSMUSG00000011256 | 1.84 | 4.6E-02 |
| **trafficking protein, kinesin binding 1** | Trak1 | ENSMUSG00000032536 | 0.80 | 4.6E-02 |
| **STRA6-like** | Stra6l | ENSMUSG00000028327 | 1.31 | 4.6E-02 |
| **RAB GTPase activating protein 1-like** | Rabgap1l | ENSMUSG00000026721 | 0.86 | 4.6E-02 |
| **RIKEN cDNA C330021F23 gene** | C330021F23Rik | ENSMUSG00000065952 | 1.75 | 4.6E-02 |
| **olfactomedin 3** | Olfm3 | ENSMUSG00000027965 | 0.66 | 4.6E-02 |
| **aquaporin 4** | Aqp4 | ENSMUSG00000024411 | 0.54 | 4.6E-02 |
| **armadillo repeat containing, X-linked 3** | Armcx3 | ENSMUSG00000049047 | 1.55 | 4.7E-02 |
| **aldehyde dehydrogenase 18 family, member A1** | Aldh18a1 | ENSMUSG00000025007 | 1.97 | 4.7E-02 |
| **pygopus 1** | Pygo1 | ENSMUSG00000034910 | 2.11 | 4.8E-02 |
| **CUB domain containing protein 1** | Cdcp1 | ENSMUSG00000035498 | 1.66 | 4.8E-02 |
| **TBC1 domain family, member 8** | Tbc1d8 | ENSMUSG00000003134 | 0.60 | 4.8E-02 |
| **regulator of chromosome condensation 1** | Rcc1 | ENSMUSG00000028896 | 1.33 | 4.8E-02 |
| **myotubularin related protein 7** | Mtmr7 | ENSMUSG00000039431 | 0.68 | 4.8E-02 |
| **serum/glucocorticoid regulated kinase 3** | Sgk3 | ENSMUSG00000025915 | 1.28 | 4.9E-02 |
| **plakophilin 1** | Pkp1 | ENSMUSG00000026413 | 0.47 | 4.9E-02 |

***Table 7.3*** *- **Genes, hepatic expression of which is altered in D316A relative to WT-Tg mice following high fructose feeding**.*

### 7.1.2 Lists of genes, hepatic expression of which is significantly altered in *Pten$^{-/-}$+D316A* relative to *Pten$^{-/-}$* mice

| Gene Name | Gene Symbol | Gene Number | Fold change | Adj p |
|---|---|---|---|---|
| **sulfotransferase family, cytosolic, 1C, member 2** | Sult1c2 | ENSMUSG00000023122 | 2.81 | 5.1E-12 |
| **C-type lectin domain family 2, member h** | Clec2h | ENSMUSG00000030364 | 3.43 | 3.4E-08 |
| **desmoglein 1 gamma** | Dsg1c | ENSMUSG00000034774 | 3.27 | 1.8E-07 |
| **SET domain containing 5** | Setd5 | ENSMUSG00000034269 | 1.60 | 1.3E-05 |
| **neuraminidase 1** | Neu1 | ENSMUSG00000007038 | 1.35 | 1.2E-03 |

| | | | | |
|---|---|---|---|---|
| **SPARC related modular calcium binding 1** | Smoc1 | ENSMUSG00000021136 | 1.26 | 3.6E-03 |
| **matrix metallopeptidase 27** | Mmp27 | ENSMUSG00000070323 | 2.52 | 4.5E-03 |
| **renin binding protein** | Renbp | ENSMUSG00000031387 | 2.01 | 9.2E-03 |
| **neuritin 1** | Nrn1 | ENSMUSG00000039114 | 1.24 | 1.5E-02 |
| **major facilitator superfamily domain containing 1** | Mfsd1 | ENSMUSG00000027775 | 1.24 | 1.7E-02 |
| **aspartylglucosaminidase** | Aga | ENSMUSG00000031521 | 1.23 | 1.7E-02 |
| **annexin A8** | Anxa8 | ENSMUSG00000021950 | 1.95 | 2.7E-02 |
| **prostaglandin E synthase** | Ptges | ENSMUSG00000050737 | 0.50 | 3.2E-02 |
| **phospholipase A1 member A** | Pla1a | ENSMUSG00000002847 | 1.26 | 4.7E-02 |

***Table 7.4 - Genes, hepatic expression of which is altered in Pten$^{-/-}$+D316A relative to Pten$^{-/-}$ mice at 6 and 25 weeks of age.***

| Gene Name | Gene Symbol | Gene Number | Fold change | Adj p |
|---|---|---|---|---|
| **caspase 6** | Casp6 | ENSMUSG00000027997 | 1.53 | 1.9E-07 |
| **cathepsin A** | Ctsa | ENSMUSG00000017760 | 1.39 | 1.5E-06 |
| **orosomucoid 2** | Orm2 | ENSMUSG00000061540 | 4.46 | 3.0E-06 |
| **brain expressed X-linked 2** | Bex2 | ENSMUSG00000042750 | 4.41 | 3.8E-06 |
| **cathepsin Z** | Ctsz | ENSMUSG00000016256 | 1.49 | 3.8E-06 |
| **glutaredoxin** | Glrx | ENSMUSG00000021591 | 0.57 | 6.7E-06 |
| **laminin, beta 3** | Lamb3 | ENSMUSG00000026639 | 0.44 | 1.3E-05 |
| **insulin-like growth factor 2 mRNA binding protein 3** | Igf2bp3 | ENSMUSG00000029814 | 3.07 | 2.3E-05 |
| **Ellis van Creveld syndrome 2** | Evc2 | ENSMUSG00000050248 | 2.94 | 4.6E-05 |
| **N-acetyl galactosaminidase, alpha** | Naga | ENSMUSG00000022453 | 1.29 | 6.1E-05 |
| **Ellis van Creveld gene syndrome** | Evc | ENSMUSG00000029122 | 2.58 | 6.4E-05 |
| **Fas (TNFRSF6) binding factor 1** | Fbf1 | ENSMUSG00000020776 | 0.32 | 7.6E-05 |
| **cytochrome P450, family 3, subfamily a, polypeptide 44** | Cyp3a44 | ENSMUSG00000054417 | 3.67 | 1.4E-04 |
| **acetyl-Coenzyme A acyltransferase 1B** | Acaa1b | ENSMUSG00000010651 | 0.56 | 1.6E-04 |
| **MAS-related GPR, member E** | Mrgpre | ENSMUSG00000048965 | 2.48 | 2.4E-04 |
| **growth arrest specific 7** | Gas7 | ENSMUSG00000033066 | 1.94 | 3.0E-04 |
| **Bet1 golgi vesicular membrane trafficking protein** | Bet1 | ENSMUSG00000032757 | 0.68 | 3.0E-04 |
| **pyruvate carboxylase** | Pcx | ENSMUSG00000024892 | 0.79 | 5.5E-04 |
| **transmembrane protein 9** | Tmem9 | ENSMUSG00000026411 | 1.34 | 5.6E-04 |
| **USO1 vesicle docking factor** | Uso1 | ENSMUSG00000029407 | 0.77 | 6.7E-04 |
| **SWI/SNF related, matrix associated, actin dependent** | Smarca4 | ENSMUSG00000032187 | 0.80 | 8.1E-04 |

| | | | | |
|---|---|---|---|---|
| **regulator of chromatin, subfamily a, member 4** | | | | |
| **a disintegrin and metallopeptidase domain 11** | Adam11 | ENSMUSG00000020926 | 2.09 | 8.9E-04 |
| **adenylosuccinate synthetase, non muscle** | Adss | ENSMUSG00000015961 | 0.78 | 8.9E-04 |
| **HCLS1 binding protein 3** | Hs1bp3 | ENSMUSG00000020605 | 1.32 | 9.4E-04 |
| **neutrophilic granule protein** | Ngp | ENSMUSG00000032484 | 3.22 | 9.4E-04 |
| **RAB11 family interacting protein 4 (class II)** | Rab11fip4 | ENSMUSG00000017639 | 2.07 | 9.6E-04 |
| **CD63 antigen** | Cd63 | ENSMUSG00000025351 | 2.72 | 9.6E-04 |
| **family with sequence similarity 129, member B** | Fam129b | ENSMUSG00000026796 | 2.32 | 9.6E-04 |
| **Ras-related GTP binding D** | Rragd | ENSMUSG00000028278 | 2.54 | 1.2E-03 |
| **coatomer protein complex, subunit gamma 1** | Copg1 | ENSMUSG00000030058 | 0.81 | 1.2E-03 |
| **stabilin 2** | Stab2 | ENSMUSG00000035459 | 1.44 | 1.3E-03 |
| **Rab geranylgeranyl transferase, a subunit** | Rabggta | ENSMUSG00000040472 | 0.76 | 1.6E-03 |
| **SET and MYND domain containing 2** | Smyd2 | ENSMUSG00000026603 | 0.79 | 2.2E-03 |
| **sulfotransferase family 4A, member 1** | Sult4a1 | ENSMUSG00000018865 | 3.07 | 2.5E-03 |
| **ras homolog family member Q** | Rhoq | ENSMUSG00000024143 | 1.64 | 2.5E-03 |
| **six transmembrane epithelial antigen of prostate 2** | Steap2 | ENSMUSG00000015653 | 1.90 | 2.7E-03 |
| **aldehyde oxidase 1** | Aox1 | ENSMUSG00000063558 | 0.61 | 3.1E-03 |
| **RIKEN cDNA E430025E21 gene** | E430025E21Rik | ENSMUSG00000022350 | 1.30 | 3.3E-03 |
| **pyrin domain containing 3** | Pydc3 | ENSMUSG00000066677 | 0.45 | 3.3E-03 |
| **pyrophosphatase (inorganic) 1** | Ppa1 | ENSMUSG00000020089 | 0.75 | 3.3E-03 |
| **LIM domain containing 2** | Limd2 | ENSMUSG00000040699 | 1.56 | 3.5E-03 |
| **aldehyde dehydrogenase family 3, subfamily A2** | Aldh3a2 | ENSMUSG00000010025 | 0.57 | 3.5E-03 |
| **torsin family 1, member A (torsin A)** | Tor1a | ENSMUSG00000026849 | 0.81 | 3.5E-03 |
| **microrchidia 4** | Morc4 | ENSMUSG00000031434 | 1.79 | 3.6E-03 |
| **jade family PHD finger 2** | Jade2 | ENSMUSG00000020387 | 1.56 | 3.6E-03 |
| **ring finger protein 217** | Rnf217 | ENSMUSG00000063760 | 1.39 | 3.9E-03 |
| **plakophilin 2** | Pkp2 | ENSMUSG00000041957 | 0.74 | 4.1E-03 |
| **cDNA sequence BC003331** | BC003331 | ENSMUSG00000006010 | 0.83 | 4.3E-03 |
| **thiopurine methyltransferase** | Tpmt | ENSMUSG00000021376 | 0.59 | 4.6E-03 |
| **LIM-domain containing, protein kinase** | Limk1 | ENSMUSG00000029674 | 0.58 | 5.5E-03 |
| **protocadherin 1** | Pcdh1 | ENSMUSG00000051375 | 1.37 | 5.6E-03 |
| **CCCTC-binding factor (zinc finger protein)-like** | Ctcfl | ENSMUSG00000070495 | 0.44 | 5.9E-03 |
| **glycosylated lysosomal membrane protein** | Glmp | ENSMUSG00000001418 | 1.21 | 6.1E-03 |

| | | | | |
|---|---|---|---|---|
| **poly (ADP-ribose) polymerase family, member 16** | Parp16 | ENSMUSG00000032392 | 0.76 | 6.1E-03 |
| **solute carrier family 2, (facilitated glucose transporter), member 8** | Slc2a8 | ENSMUSG00000026791 | 1.24 | 6.1E-03 |
| **inter-alpha (globulin) inhibitor H5** | Itih5 | ENSMUSG00000025780 | 1.61 | 6.4E-03 |
| **phosphatidylcholine transfer protein** | Pctp | ENSMUSG00000020553 | 0.62 | 6.4E-03 |
| **mannosidase 2, alpha B2** | Man2b2 | ENSMUSG00000029119 | 1.36 | 6.4E-03 |
| **purinergic receptor P2X, ligand-gated ion channel 4** | P2rx4 | ENSMUSG00000029470 | 1.35 | 6.4E-03 |
| **intestinal cell kinase** | Ick | ENSMUSG00000009828 | 0.74 | 6.4E-03 |
| **breast cancer anti-estrogen resistance 3** | Bcar3 | ENSMUSG00000028121 | 0.70 | 6.6E-03 |
| **family with sequence similarity 3, member A** | Fam3a | ENSMUSG00000031399 | 0.82 | 6.6E-03 |
| **MAP kinase-activated protein kinase 5** | Mapkapk5 | ENSMUSG00000029454 | 0.83 | 6.7E-03 |
| **leucine rich repeat containing 59** | Lrrc59 | ENSMUSG00000020869 | 0.73 | 7.0E-03 |
| **ORM1-like 3 (S. cerevisiae)** | Ormdl3 | ENSMUSG00000038150 | 0.78 | 7.0E-03 |
| **Niemann-Pick type C2** | Npc2 | ENSMUSG00000021242 | 1.30 | 7.3E-03 |
| **protein phosphatase 1M** | Ppm1m | ENSMUSG00000020253 | 0.76 | 8.0E-03 |
| **cyclin-dependent kinase 11B** | Cdk11b | ENSMUSG00000029062 | 0.86 | 8.0E-03 |
| **RNA exonuclease 2** | Rexo2 | ENSMUSG00000032026 | 0.79 | 8.0E-03 |
| **inhibin beta-A** | Inhba | ENSMUSG00000041324 | 1.92 | 8.0E-03 |
| **PHD finger protein 8** | Phf8 | ENSMUSG00000041229 | 1.82 | 8.5E-03 |
| **alpha-N-acetylglucosaminidase (Sanfilippo disease IIIB)** | Naglu | ENSMUSG00000001751 | 1.30 | 8.8E-03 |
| **Sec1 family domain containing 1** | Scfd1 | ENSMUSG00000020952 | 0.78 | 8.8E-03 |
| **Rho GTPase activating protein 10** | Arhgap10 | ENSMUSG00000037148 | 1.75 | 8.8E-03 |
| **deleted in liver cancer 1** | Dlc1 | ENSMUSG00000031523 | 0.70 | 9.0E-03 |
| **neuropilin 2** | Nrp2 | ENSMUSG00000025969 | 0.57 | 9.1E-03 |
| **TATA-box binding protein associated factor 2** | Taf2 | ENSMUSG00000037343 | 1.57 | 9.1E-03 |
| **cathepsin L** | Ctsl | ENSMUSG00000021477 | 1.37 | 9.2E-03 |
| **major facilitator superfamily domain containing 2A** | Mfsd2a | ENSMUSG00000028655 | 0.59 | 9.2E-03 |
| **perilipin 3** | Plin3 | ENSMUSG00000024197 | 1.36 | 9.6E-03 |
| **SEC22 homolog B, vesicle trafficking protein** | Sec22b | ENSMUSG00000027879 | 0.78 | 9.6E-03 |
| **phosphoribosyl pyrophosphate synthetase 2** | Prps2 | ENSMUSG00000025742 | 1.31 | 1.0E-02 |
| **ligand of numb-protein X 2** | Lnx2 | ENSMUSG00000016520 | 0.69 | 1.1E-02 |
| **solute carrier family 25, member 47** | Slc25a47 | ENSMUSG00000048856 | 0.73 | 1.1E-02 |

| | | | | |
|---|---|---|---|---|
| **ring finger protein 2** | Rnf2 | ENSMUSG00000026484 | 1.29 | 1.1E-02 |
| **growth arrest specific 2** | Gas2 | ENSMUSG00000030498 | 1.37 | 1.1E-02 |
| **ependymin related protein 1 (zebrafish)** | Epdr1 | ENSMUSG00000002808 | 2.62 | 1.1E-02 |
| **protein kinase domain containing, cytoplasmic** | Pkdcc | ENSMUSG00000024247 | 1.36 | 1.1E-02 |
| **prolyl 4-hydroxylase, beta polypeptide** | P4hb | ENSMUSG00000025130 | 0.84 | 1.1E-02 |
| **ligand of numb-protein X 1** | Lnx1 | ENSMUSG00000029228 | 2.38 | 1.1E-02 |
| **regulator of microtubule dynamics 3** | Rmdn3 | ENSMUSG00000070730 | 0.80 | 1.1E-02 |
| **solute carrier family 17, member 9** | Slc17a9 | ENSMUSG00000023393 | 0.65 | 1.1E-02 |
| **pygopus 1** | Pygo1 | ENSMUSG00000034910 | 2.25 | 1.1E-02 |
| **zinc finger CCCH type containing 12C** | Zc3h12c | ENSMUSG00000035164 | 1.69 | 1.2E-02 |
| **inositol polyphosphate-5-phosphatase B** | Inpp5b | ENSMUSG00000028894 | 0.80 | 1.2E-02 |
| **adhesion G protein-coupled receptor V1** | Adgrv1 | ENSMUSG00000069170 | 0.45 | 1.2E-02 |
| **transmembrane protein 189** | Tmem189 | ENSMUSG00000090213 | 0.68 | 1.2E-02 |
| **Rho GTPase activating protein 6** | Arhgap6 | ENSMUSG00000031355 | 1.66 | 1.2E-02 |
| **MAX-like protein X** | Mlx | ENSMUSG00000017801 | 0.84 | 1.2E-02 |
| **SEC16 homolog B (S. cerevisiae)** | Sec16b | ENSMUSG00000026589 | 0.78 | 1.2E-02 |
| **forkhead box A2** | Foxa2 | ENSMUSG00000037025 | 1.60 | 1.2E-02 |
| **bile acid-Coenzyme A: amino acid N-acyltransferase** | Baat | ENSMUSG00000039653 | 0.80 | 1.2E-02 |
| **serum amyloid A 3** | Saa3 | ENSMUSG00000040026 | 2.25 | 1.2E-02 |
| **ataxin 1** | Atxn1 | ENSMUSG00000046876 | 0.61 | 1.2E-02 |
| **mannosidase 2, alpha B1** | Man2b1 | ENSMUSG00000005142 | 1.22 | 1.2E-02 |
| **regulator of calcineurin 3** | Rcan3 | ENSMUSG00000059713 | 1.80 | 1.3E-02 |
| **hexosaminidase B** | Hexb | ENSMUSG00000021665 | 1.64 | 1.3E-02 |
| **calmodulin 1** | Calm1 | ENSMUSG00000001175 | 0.88 | 1.3E-02 |
| **dipeptidylpeptidase 7** | Dpp7 | ENSMUSG00000026958 | 1.28 | 1.3E-02 |
| **serine carboxypeptidase 1** | Scpep1 | ENSMUSG00000000278 | 1.29 | 1.4E-02 |
| **calsyntenin 3** | Clstn3 | ENSMUSG00000008153 | 0.52 | 1.5E-02 |
| **erb-b2 receptor tyrosine kinase 4** | Erbb4 | ENSMUSG00000062209 | 1.99 | 1.5E-02 |
| **cytochrome P450, family 26, subfamily b, polypeptide 1** | Cyp26b1 | ENSMUSG00000063415 | 0.39 | 1.5E-02 |
| **mesoderm development candidate 2** | Mesdc2 | ENSMUSG00000038503 | 0.85 | 1.5E-02 |
| **interleukin-1 receptor-associated kinase 2** | Irak2 | ENSMUSG00000060477 | 0.78 | 1.5E-02 |
| **proteasome (prosome, macropain) 26S subunit, non-ATPase, 14** | Psmd14 | ENSMUSG00000026914 | 0.80 | 1.5E-02 |
| **syntrophin, acidic 1** | Snta1 | ENSMUSG00000027488 | 1.31 | 1.6E-02 |

| | | | | |
|---|---|---|---|---|
| **osteoclast stimulatory transmembrane protein** | Ocstamp | ENSMUSG00000027670 | 0.56 | 1.6E-02 |
| **post-GPI attachment to proteins 2** | Pgap2 | ENSMUSG00000030990 | 1.28 | 1.6E-02 |
| **myosin VC** | Myo5c | ENSMUSG00000033590 | 2.55 | 1.6E-02 |
| **testis-specific kinase 2** | Tesk2 | ENSMUSG00000033985 | 1.42 | 1.6E-02 |
| **membrane magnesium transporter 1** | Mmgt1 | ENSMUSG00000061273 | 0.81 | 1.6E-02 |
| **brain expressed X-linked 4** | Bex4 | ENSMUSG00000047844 | 2.23 | 1.6E-02 |
| **calcium and integrin binding family member 3** | Cib3 | ENSMUSG00000074240 | 2.34 | 1.6E-02 |
| **pleckstrin homology domain containing, family A member 7** | Plekha7 | ENSMUSG00000045659 | 0.70 | 1.6E-02 |
| **mitochondrial calcium uniporter regulator 1** | Mcur1 | ENSMUSG00000021371 | 0.84 | 1.6E-02 |
| **galactose-4-epimerase, UDP** | Gale | ENSMUSG00000028671 | 0.62 | 1.6E-02 |
| **cyclin-dependent kinase inhibitor 2C (p18, inhibits CDK4)** | Cdkn2c | ENSMUSG00000028551 | 1.58 | 1.6E-02 |
| **cell death-inducing DFFA-like effector c** | Cidec | ENSMUSG00000030278 | 0.41 | 1.6E-02 |
| **NAD synthetase 1** | Nadsyn1 | ENSMUSG00000031090 | 1.16 | 1.7E-02 |
| **glypican 1** | Gpc1 | ENSMUSG00000034220 | 0.56 | 1.7E-02 |
| **anoctamin 8** | Ano8 | ENSMUSG00000034863 | 1.50 | 1.7E-02 |
| **abhydrolase domain containing 17C** | Abhd17c | ENSMUSG00000038459 | 1.22 | 1.7E-02 |
| **potassium intermediate/small conductance calcium-activated channel, subfamily N, member 2** | Kcnn2 | ENSMUSG00000054477 | 1.43 | 1.7E-02 |
| **REV3 like, DNA directed polymerase zeta catalytic subunit** | Rev3l | ENSMUSG00000019841 | 1.28 | 1.7E-02 |
| **Rho guanine nucleotide exchange factor (GEF) 19** | Arhgef19 | ENSMUSG00000028919 | 0.69 | 1.7E-02 |
| **gremlin 2, DAN family BMP antagonist** | Grem2 | ENSMUSG00000050069 | 1.73 | 1.7E-02 |
| **sema domain, seven thrombospondin repeats (type 1 and type 1-like), transmembrane domain (TM) and short cytoplasmic domain, (semaphorin) 5B** | Sema5b | ENSMUSG00000052133 | 0.49 | 1.7E-02 |
| **solute carrier family 22 (organic cation transporter), member 26** | Slc22a26 | ENSMUSG00000053303 | 2.51 | 1.7E-02 |
| **PEST proteolytic signal containing nuclear protein** | Pcnp | ENSMUSG00000071533 | 0.82 | 1.7E-02 |
| **SPO11 meiotic protein covalently bound to DSB** | Spo11 | ENSMUSG00000005883 | 0.40 | 1.7E-02 |

| | | | | |
|---|---|---|---|---|
| **proteasome (prosome, macropain) 26S subunit, ATPase, 6** | Psmc6 | ENSMUSG00000021832 | 0.87 | 1.7E-02 |
| **solute carrier family 22 (organic cation transporter), member 5** | Slc22a5 | ENSMUSG00000018900 | 0.62 | 1.8E-02 |
| **WD repeat, SAM and U-box domain containing 1** | Wdsub1 | ENSMUSG00000026988 | 1.41 | 1.9E-02 |
| **ferric-chelate reductase 1** | Frrs1 | ENSMUSG00000033386 | 1.39 | 1.9E-02 |
| **hepcidin antimicrobial peptide 2** | Hamp2 | ENSMUSG00000056978 | 2.50 | 1.9E-02 |
| **zinc finger protein 871** | Zfp871 | ENSMUSG00000024298 | 2.23 | 1.9E-02 |
| **PTPRF interacting protein, binding protein 2 (liprin beta 2)** | Ppfibp2 | ENSMUSG00000036528 | 0.77 | 1.9E-02 |
| **solute carrier family 22 (organic cation transporter), member 3** | Slc22a3 | ENSMUSG00000023828 | 0.58 | 2.0E-02 |
| **helicase with zinc finger 2, transcriptional coactivator** | Helz2 | ENSMUSG00000027580 | 0.80 | 2.0E-02 |
| **dimethylarginine dimethylaminohydrolase 1** | Ddah1 | ENSMUSG00000028194 | 0.70 | 2.0E-02 |
| **DNA segment, Chr 2, Wayne State University 81, expressed** | D2Wsu81e | ENSMUSG00000039660 | 0.76 | 2.1E-02 |
| **hyperpolarization-activated, cyclic nucleotide-gated K+ 3** | Hcn3 | ENSMUSG00000028051 | 1.99 | 2.1E-02 |
| **myosin IE** | Myo1e | ENSMUSG00000032220 | 1.40 | 2.1E-02 |
| **fat storage-inducing transmembrane protein 1** | Fitm1 | ENSMUSG00000022215 | 0.54 | 2.2E-02 |
| **phospholipase A2, group VI** | Pla2g6 | ENSMUSG00000042632 | 0.70 | 2.2E-02 |
| **serine incorporator 5** | Serinc5 | ENSMUSG00000021703 | 1.33 | 2.2E-02 |
| **solute carrier family 25 (mitochondrial carrier, adenine nucleotide translocator), member 4** | Slc25a4 | ENSMUSG00000031633 | 1.74 | 2.2E-02 |
| **eva-1 homolog A (C. elegans)** | Eva1a | ENSMUSG00000035104 | 1.34 | 2.2E-02 |
| **pleckstrin homology domain containing, family G (with RhoGef domain) member 5** | Plekhg5 | ENSMUSG00000039713 | 1.64 | 2.2E-02 |
| **like-glycosyltransferase** | Large | ENSMUSG00000004383 | 1.46 | 2.2E-02 |
| **angiomotin** | Amot | ENSMUSG00000041688 | 1.52 | 2.2E-02 |
| **fasciculation and elongation protein zeta 2 (zygin II)** | Fez2 | ENSMUSG00000056121 | 0.83 | 2.2E-02 |
| **cytidine deaminase** | Cda | ENSMUSG00000028755 | 0.58 | 2.3E-02 |
| **galactosylceramidase** | Galc | ENSMUSG00000021003 | 1.39 | 2.3E-02 |
| **solute carrier family 25 (mitochondrial carrier, dicarboxylate transporter), member 10** | Slc25a10 | ENSMUSG00000025792 | 0.76 | 2.3E-02 |
| **GIPC PDZ domain containing family, member 2** | Gipc2 | ENSMUSG00000039131 | 2.45 | 2.3E-02 |
| **acyl-Coenzyme A oxidase 1, palmitoyl** | Acox1 | ENSMUSG00000020777 | 0.70 | 2.4E-02 |

| | | | | |
|---|---|---|---|---|
| **transmembrane protein 167** | Tmem167 | ENSMUSG00000012422 | 0.86 | 2.4E-02 |
| **cyclin-dependent kinase 12** | Cdk12 | ENSMUSG00000003119 | 1.29 | 2.4E-02 |
| **proteasome (prosome, macropain) 26S subunit, non-ATPase, 12** | Psmd12 | ENSMUSG00000020720 | 0.85 | 2.4E-02 |
| **p21 protein (Cdc42/Rac)-activated kinase 1** | Pak1 | ENSMUSG00000030774 | 1.79 | 2.5E-02 |
| **G protein-coupled receptor 180** | Gpr180 | ENSMUSG00000022131 | 0.82 | 2.5E-02 |
| **peptidyl-tRNA hydrolase 2** | Ptrh2 | ENSMUSG00000072582 | 0.81 | 2.6E-02 |
| **gamma-glutamyltransferase 6** | Ggt6 | ENSMUSG00000040471 | 0.68 | 2.6E-02 |
| **tumor suppressing subtransferable candidate 1** | Tssc1 | ENSMUSG00000036613 | 0.76 | 2.7E-02 |
| **Sec24 related gene family, member D (S. cerevisiae)** | Sec24d | ENSMUSG00000039234 | 0.74 | 2.7E-02 |
| **S100 calcium binding protein A8 (calgranulin A)** | S100a8 | ENSMUSG00000056054 | 2.43 | 2.7E-02 |
| **ventricular zone expressed PH domain-containing 1** | Veph1 | ENSMUSG00000027831 | 2.13 | 2.7E-02 |
| **collagen, type IV, alpha 5** | Col4a5 | ENSMUSG00000031274 | 1.93 | 2.7E-02 |
| **SET domain containing (lysine methyltransferase) 7** | Setd7 | ENSMUSG00000037111 | 1.60 | 2.7E-02 |
| **protein tyrosine phosphatase, receptor type, K** | Ptprk | ENSMUSG00000019889 | 1.28 | 2.7E-02 |
| **ATPase, Na+/K+ transporting, beta 1 polypeptide** | Atp1b1 | ENSMUSG00000026576 | 1.46 | 2.7E-02 |
| **SEC23 homolog B, COPII coat complex component** | Sec23b | ENSMUSG00000027429 | 0.76 | 2.7E-02 |
| **leukocyte cell derived chemotaxin 1** | Lect1 | ENSMUSG00000022025 | 0.48 | 2.8E-02 |
| **transmembrane protein 120A** | Tmem120a | ENSMUSG00000039886 | 0.78 | 2.9E-02 |
| **growth regulation by estrogen in breast cancer-like** | Greb1l | ENSMUSG00000042942 | 2.25 | 2.9E-02 |
| **glycophorin C** | Gypc | ENSMUSG00000090523 | 1.60 | 2.9E-02 |
| **leucyl/cystinyl aminopeptidase** | Lnpep | ENSMUSG00000023845 | 1.79 | 2.9E-02 |
| **ectonucleoside triphosphate diphosphohydrolase 5** | Entpd5 | ENSMUSG00000021236 | 0.76 | 2.9E-02 |
| **pre B cell leukemia transcription factor interacting protein 1** | Pbxip1 | ENSMUSG00000042613 | 1.33 | 2.9E-02 |
| **cDNA sequence BC005561** | BC005561 | ENSMUSG00000079065 | 1.68 | 3.0E-02 |
| **serine (or cysteine) peptidase inhibitor, clade A (alpha-1 antiproteinase, antitrypsin), member 7** | Serpina7 | ENSMUSG00000031271 | 0.61 | 3.0E-02 |
| **inscuteable homolog (Drosophila)** | Insc | ENSMUSG00000048782 | 0.62 | 3.0E-02 |
| **UDP-N-acteylglucosamine pyrophosphorylase 1-like 1** | Uap1l1 | ENSMUSG00000026956 | 1.76 | 3.1E-02 |
| **FtsJ RNA methyltransferase homolog 1 (E. coli)** | Ftsj1 | ENSMUSG00000031171 | 0.82 | 3.1E-02 |

| | | | | |
|---|---|---|---|---|
| **heparan sulfate 6-O-sulfotransferase 1** | Hs6st1 | ENSMUSG00000045216 | 1.26 | 3.1E-02 |
| **RAD23 homolog B, nucleotide excision repair protein** | Rad23b | ENSMUSG00000028426 | 0.86 | 3.1E-02 |
| **phospholipase A2, group XIIA** | Pla2g12a | ENSMUSG00000027999 | 1.50 | 3.1E-02 |
| **interleukin-1 receptor-associated kinase 1 binding protein 1** | Irak1bp1 | ENSMUSG00000032251 | 1.69 | 3.2E-02 |
| **milk fat globule-EGF factor 8 protein** | Mfge8 | ENSMUSG00000030605 | 1.74 | 3.3E-02 |
| **cytochrome P450, family 26, subfamily a, polypeptide 1** | Cyp26a1 | ENSMUSG00000024987 | 0.48 | 3.3E-02 |
| **uridine-cytidine kinase 1** | Uck1 | ENSMUSG00000002550 | 0.72 | 3.4E-02 |
| **family with sequence similarity 209** | Fam209 | ENSMUSG00000027505 | 0.47 | 3.4E-02 |
| **glucosaminyl (N-acetyl) transferase 4, core 2 (beta-1,6-N-acetylglucosaminyltransferase)** | Gcnt4 | ENSMUSG00000091387 | 1.66 | 3.4E-02 |
| **coiled-coil domain containing 50** | Ccdc50 | ENSMUSG00000038127 | 1.16 | 3.5E-02 |
| **carnitine acetyltransferase** | Crat | ENSMUSG00000026853 | 0.62 | 3.5E-02 |
| **cytidine monophospho-N-acetylneuraminic acid synthetase** | Cmas | ENSMUSG00000030282 | 0.79 | 3.5E-02 |
| **peroxisomal biogenesis factor 11 alpha** | Pex11a | ENSMUSG00000030545 | 0.68 | 3.5E-02 |
| **ectonucleoside triphosphate diphosphohydrolase 2** | Entpd2 | ENSMUSG00000015085 | 1.65 | 3.6E-02 |
| **dual specificity phosphatase 14** | Dusp14 | ENSMUSG00000018648 | 1.79 | 3.6E-02 |
| **cadherin 18** | Cdh18 | ENSMUSG00000040420 | 1.96 | 3.7E-02 |
| **succinyl-CoA glutarate-CoA transferase** | Sugct | ENSMUSG00000055137 | 0.74 | 3.7E-02 |
| **sarcoglycan, epsilon** | Sgce | ENSMUSG00000004631 | 1.61 | 3.7E-02 |
| **solute carrier family 6 (neurotransmitter transporter, creatine), member 8** | Slc6a8 | ENSMUSG00000019558 | 1.59 | 3.7E-02 |
| **F-box and leucine-rich repeat protein 5** | Fbxl5 | ENSMUSG00000039753 | 1.22 | 3.8E-02 |
| **SH3 binding domain protein 5 like** | Sh3bp5l | ENSMUSG00000013646 | 1.21 | 3.8E-02 |
| **ADP-ribosylation factor 4** | Arf4 | ENSMUSG00000021877 | 0.83 | 3.9E-02 |
| **proteasome (prosome, macropain) 26S subunit, ATPase 3** | Psmc3 | ENSMUSG00000002102 | 0.88 | 3.9E-02 |
| **homogentisate 1, 2-dioxygenase** | Hgd | ENSMUSG00000022821 | 0.77 | 3.9E-02 |
| **PHD finger protein 21B** | Phf21b | ENSMUSG00000016624 | 1.88 | 4.0E-02 |
| **chaperonin containing Tcp1, subunit 3 (gamma)** | Cct3 | ENSMUSG00000001416 | 0.86 | 4.0E-02 |

| | | | | |
|---|---|---|---|---|
| **zinc finger protein 704** | Zfp704 | ENSMUSG00000040209 | 1.54 | 4.1E-02 |
| **catenin, beta like 1** | Ctnnbl1 | ENSMUSG00000027649 | 0.81 | 4.1E-02 |
| **guanylate kinase 1** | Guk1 | ENSMUSG00000020444 | 0.82 | 4.2E-02 |
| **N-myristoyltransferase 1** | Nmt1 | ENSMUSG00000020936 | 0.89 | 4.2E-02 |
| **Trk-fused gene** | Tfg | ENSMUSG00000022757 | 0.84 | 4.2E-02 |
| **serine (or cysteine) peptidase inhibitor, clade B, member 8** | Serpinb8 | ENSMUSG00000026315 | 1.87 | 4.2E-02 |
| **cyclin T2** | Ccnt2 | ENSMUSG00000026349 | 1.19 | 4.2E-02 |
| **crystallin, beta B3** | Crybb3 | ENSMUSG00000029352 | 2.12 | 4.2E-02 |
| **transforming growth factor, beta receptor III** | Tgfbr3 | ENSMUSG00000029287 | 1.37 | 4.2E-02 |
| **mitochondrial elongation factor 2** | Mief2 | ENSMUSG00000018599 | 0.79 | 4.2E-02 |
| **WW domain-containing oxidoreductase** | Wwox | ENSMUSG00000004637 | 1.41 | 4.4E-02 |
| **POC1 centriolar protein B** | Poc1b | ENSMUSG00000019952 | 0.75 | 4.4E-02 |
| **thioredoxin domain containing 5** | Txndc5 | ENSMUSG00000038991 | 0.81 | 4.4E-02 |
| **cytochrome P450, family 2, subfamily d, polypeptide 40** | Cyp2d40 | ENSMUSG00000068083 | 0.63 | 4.5E-02 |
| **methyltransferase like 1** | Mettl1 | ENSMUSG00000006732 | 0.74 | 4.5E-02 |
| **transmembrane protein 109** | Tmem109 | ENSMUSG00000034659 | 0.81 | 4.5E-02 |
| **zinc finger protein 764** | Zfp764 | ENSMUSG00000045757 | 1.52 | 4.5E-02 |
| **dynamin binding protein** | Dnmbp | ENSMUSG00000025195 | 0.69 | 4.6E-02 |
| **cullin-associated and neddylation-dissociated 2 (putative)** | Cand2 | ENSMUSG00000030319 | 2.16 | 4.6E-02 |
| **glucuronidase, beta** | Gusb | ENSMUSG00000025534 | 1.22 | 4.6E-02 |
| **proprotein convertase subtilisin/kexin type 5** | Pcsk5 | ENSMUSG00000024713 | 1.32 | 4.6E-02 |
| **sema domain, immunoglobulin domain (Ig), transmembrane domain (TM) and short cytoplasmic domain, (semaphorin) 4A** | Sema4a | ENSMUSG00000028064 | 1.25 | 4.7E-02 |
| **zinc finger, FYVE domain containing 19** | Zfyve19 | ENSMUSG00000068580 | 0.83 | 4.7E-02 |
| **solute carrier family 31, member 2** | Slc31a2 | ENSMUSG00000066152 | 1.23 | 4.7E-02 |
| **monoglyceride lipase** | *Mgll* | ENSMUSG00000033174 | 0.76 | 4.8E-02 |
| **protein tyrosine phosphatase, receptor type, F** | Ptprf | ENSMUSG00000033295 | 1.29 | 4.8E-02 |
| **ISG15 ubiquitin-like modifier** | Isg15 | ENSMUSG00000035692 | 0.73 | 4.8E-02 |
| **ELMO/CED-12 domain containing 3** | Elmod3 | ENSMUSG00000056698 | 0.71 | 4.8E-02 |
| **C-type lectin domain family 4, member g** | Clec4g | ENSMUSG00000074491 | 0.71 | 4.8E-02 |

| | | | | |
|---|---|---|---|---|
| **collagen, type XVIII, alpha 1** | Col18a1 | ENSMUSG00000001435 | 1.22 | 4.9E-02 |
| **activated leukocyte cell adhesion molecule** | Alcam | ENSMUSG00000022636 | 1.35 | 5.0E-02 |
| **mitogen-activated protein kinase kinase 1** | Map2k1 | ENSMUSG00000004936 | 0.88 | 5.0E-02 |
| **phenylalanyl-tRNA synthetase, beta subunit** | Farsb | ENSMUSG00000026245 | 0.84 | 5.0E-02 |
| **oxysterol binding protein-like 3** | Osbpl3 | ENSMUSG00000029822 | 0.48 | 5.0E-02 |
| **small glutamine-rich tetratricopeptide repeat (TPR)-containing, beta** | Sgtb | ENSMUSG00000042743 | 0.62 | 5.0E-02 |

***Table 7.5 - Genes, hepatic expression of which is altered in Pten$^{-/-}$+D316A relative to Pten$^{-/-}$ mice at 6 weeks of age.***

| GeneName | Gene Symbol | Gene Number | Fold change | Adj p |
|---|---|---|---|---|
| **cytochrome P450, family 46, subfamily a, polypeptide 1** | Cyp46a1 | ENSMUSG00000021259 | 2.57 | 1.8E-04 |
| **serine palmitoyltransferase, long chain base subunit 3** | Sptlc3 | ENSMUSG00000039092 | 2.87 | 1.8E-04 |
| **laminin, alpha 5** | Lama5 | ENSMUSG00000015647 | 0.42 | 3.5E-04 |
| **very low density lipoprotein receptor** | Vldlr | ENSMUSG00000024924 | 0.41 | 5.8E-04 |
| **chemokine (C-C motif) ligand 5** | Ccl5 | ENSMUSG00000035042 | 0.40 | 6.1E-04 |
| **microfibrillar-associated protein 4** | Mfap4 | ENSMUSG00000042436 | 0.40 | 2.5E-03 |
| **hematopoietic prostaglandin D synthase** | Hpgds | ENSMUSG00000029919 | 0.41 | 3.1E-03 |
| **filamin A interacting protein 1-like** | Filip1l | ENSMUSG00000043336 | 0.49 | 3.1E-03 |
| **jagged 1** | Jag1 | ENSMUSG00000027276 | 0.59 | 4.1E-03 |
| **CD72 antigen** | Cd72 | ENSMUSG00000028459 | 0.47 | 4.2E-03 |
| **natural killer cell group 7 sequence** | Nkg7 | ENSMUSG00000004612 | 0.38 | 5.0E-03 |
| **cytohesin 4** | Cyth4 | ENSMUSG00000018008 | 0.47 | 5.0E-03 |
| **synaptotagmin VII** | Syt7 | ENSMUSG00000024743 | 0.41 | 5.0E-03 |
| **CD84 antigen** | Cd84 | ENSMUSG00000038147 | 0.55 | 5.0E-03 |
| **zinc finger, MYND-type containing 15** | Zmynd15 | ENSMUSG00000040829 | 0.57 | 5.0E-03 |
| **platelet derived growth factor, B polypeptide** | Pdgfb | ENSMUSG00000000489 | 0.43 | 6.9E-03 |

| | | | | |
|---|---|---|---|---|
| **DENN/MADD domain containing 1C** | Dennd1c | ENSMUSG00000002668 | 0.59 | 6.9E-03 |
| **CD22 antigen** | Cd22 | ENSMUSG00000030577 | 0.44 | 7.0E-03 |
| **basal cell adhesion molecule** | Bcam | ENSMUSG00000002980 | 0.58 | 8.4E-03 |
| **protein phosphatase 1, regulatory subunit 9B** | Ppp1r9b | ENSMUSG00000038976 | 0.61 | 8.4E-03 |
| **RAB3 GTPase activating protein subunit 1** | Rab3gap1 | ENSMUSG00000036104 | 1.34 | 1.0E-02 |
| **gamma-aminobutyric acid (GABA) B receptor, 1** | Gabbr1 | ENSMUSG00000024462 | 0.54 | 1.1E-02 |
| **macrophage scavenger receptor 1** | Msr1 | ENSMUSG00000025044 | 0.60 | 1.1E-02 |
| **SPEG complex locus** | Speg | ENSMUSG00000026207 | 0.47 | 1.1E-02 |
| **2'-5' oligoadenylate synthetase-like 2** | Oasl2 | ENSMUSG00000029561 | 0.57 | 1.1E-02 |
| **triggering receptor expressed on myeloid cells 2** | Trem2 | ENSMUSG00000023992 | 0.41 | 1.2E-02 |
| **histocompatibility (minor) HA-1** | Hmha1 | ENSMUSG00000035697 | 0.62 | 1.2E-02 |
| **UDP glucuronosyltransferase 2 family, polypeptide A3** | Ugt2a3 | ENSMUSG00000035780 | 1.42 | 1.3E-02 |
| **ATP-binding cassette, sub-family G (WHITE), member 1** | Abcg1 | ENSMUSG00000024030 | 0.55 | 1.4E-02 |
| **RAB3A interacting protein (rabin3)-like 1** | Rab3il1 | ENSMUSG00000024663 | 0.53 | 1.4E-02 |
| **solute carrier family 15, member 3** | Slc15a3 | ENSMUSG00000024737 | 0.54 | 1.4E-02 |
| **ring finger protein 13** | Rnf13 | ENSMUSG00000036503 | 1.19 | 1.4E-02 |
| **leucine-rich repeats and transmembrane domains 1** | Lrtm1 | ENSMUSG00000045776 | 2.61 | 1.4E-02 |
| **protein tyrosine phosphatase, receptor type, C** | Ptprc | ENSMUSG00000026395 | 0.57 | 1.5E-02 |
| **lysosomal-associated protein transmembrane 5** | Laptm5 | ENSMUSG00000028581 | 0.57 | 1.5E-02 |
| **solute carrier family 37 (glycerol-3-phosphate transporter), member 2** | Slc37a2 | ENSMUSG00000032122 | 0.51 | 1.5E-02 |
| **guanylate-binding protein 9** | Gbp9 | ENSMUSG00000029298 | 0.60 | 1.5E-02 |
| **toll-like receptor 1** | Tlr1 | ENSMUSG00000044827 | 0.42 | 1.5E-02 |
| **RALBP1 associated Eps domain containing protein 2** | Reps2 | ENSMUSG00000040855 | 1.44 | 1.6E-02 |
| **cyclin D2** | Ccnd2 | ENSMUSG00000000184 | 0.57 | 1.6E-02 |
| **limb-bud and heart** | Lbh | ENSMUSG00000024063 | 0.59 | 1.6E-02 |

| | | | | |
|---|---|---|---|---|
| **latent transforming growth factor beta binding protein 3** | Ltbp3 | ENSMUSG00000024940 | 0.53 | 1.6E-02 |
| **interaction protein for cytohesin exchange factors 1** | Ipcef1 | ENSMUSG00000064065 | 0.39 | 1.8E-02 |
| **calpain 10** | Capn10 | ENSMUSG00000026270 | 1.47 | 1.9E-02 |
| **chemokine (C-C motif) ligand 8** | Ccl8 | ENSMUSG00000009185 | 0.41 | 1.9E-02 |
| **NECAP endocytosis associated 2** | Necap2 | ENSMUSG00000028923 | 0.71 | 1.9E-02 |
| **retinoic acid receptor, gamma** | Rarg | ENSMUSG00000001288 | 0.57 | 1.9E-02 |
| **Rho guanine nucleotide exchange factor (GEF) 25** | Arhgef25 | ENSMUSG00000019467 | 0.51 | 1.9E-02 |
| **V-set immunoregulatory receptor** | Vsir | ENSMUSG00000020101 | 0.62 | 1.9E-02 |
| **fermitin family member 3** | Fermt3 | ENSMUSG00000024965 | 0.58 | 1.9E-02 |
| **dual specificity phosphatase 2** | Dusp2 | ENSMUSG00000027368 | 0.40 | 1.9E-02 |
| **growth differentiation factor 3** | Gdf3 | ENSMUSG00000030117 | 0.38 | 1.9E-02 |
| **signal-regulatory protein alpha** | Sirpa | ENSMUSG00000037902 | 0.54 | 1.9E-02 |
| **negative regulator of reactive oxygen species** | Nrros | ENSMUSG00000052384 | 0.58 | 1.9E-02 |
| **PWWP domain containing 2B** | Pwwp2b | ENSMUSG00000060260 | 0.57 | 1.9E-02 |
| **a disintegrin and metallopeptidase domain 8** | Adam8 | ENSMUSG00000025473 | 0.41 | 1.9E-02 |
| **3-hydroxyacyl-CoA dehydratase 4** | Hacd4 | ENSMUSG00000028497 | 0.51 | 1.9E-02 |
| **sterile alpha motif domain containing 14** | Samd14 | ENSMUSG00000047181 | 0.54 | 1.9E-02 |
| **Kruppel-like factor 2 (lung)** | Klf2 | ENSMUSG00000055148 | 0.62 | 1.9E-02 |
| **collagen, type VI, alpha 1** | Col6a1 | ENSMUSG00000001119 | 0.57 | 2.0E-02 |
| **zinc finger protein 710** | Zfp710 | ENSMUSG00000048897 | 0.70 | 2.1E-02 |
| **platelet derived growth factor receptor, beta polypeptide** | Pdgfrb | ENSMUSG00000024620 | 0.59 | 2.1E-02 |
| **UFM1-specific peptidase 2** | Ufsp2 | ENSMUSG00000031634 | 1.23 | 2.1E-02 |
| **potassium inwardly-rectifying channel, subfamily J, member 2** | Kcnj2 | ENSMUSG00000041695 | 0.48 | 2.1E-02 |
| **eva-1 homolog B (C. elegans)** | Eva1b | ENSMUSG00000050212 | 0.64 | 2.2E-02 |
| **leupaxin** | Lpxn | ENSMUSG00000024696 | 0.58 | 2.2E-02 |

| | | | | |
|---|---|---|---|---|
| **CD180 antigen** | Cd180 | ENSMUSG00000021624 | 0.51 | 2.3E-02 |
| **thromboxane A synthase 1, platelet** | Tbxas1 | ENSMUSG00000029925 | 0.51 | 2.3E-02 |
| **raftlin lipid raft linker 1** | Rftn1 | ENSMUSG00000039316 | 0.54 | 2.4E-02 |
| **neuron navigator 2** | Nav2 | ENSMUSG00000052512 | 0.63 | 2.4E-02 |
| **G protein-coupled receptor kinase-interactor 2** | Git2 | ENSMUSG00000041890 | 0.76 | 2.5E-02 |
| **lysyl oxidase-like 3** | Loxl3 | ENSMUSG00000000693 | 0.59 | 2.5E-02 |
| **apolipoprotein B mRNA editing enzyme, catalytic polypeptide 3** | Apobec3 | ENSMUSG00000009585 | 0.52 | 2.5E-02 |
| **coiled-coil domain containing 88C** | Ccdc88c | ENSMUSG00000021182 | 0.49 | 2.5E-02 |
| **integrin alpha X** | Itgax | ENSMUSG00000030789 | 0.44 | 2.5E-02 |
| **linker for activation of T cells family, member 2** | Lat2 | ENSMUSG00000040751 | 0.49 | 2.5E-02 |
| **kinesin family member 21B** | Kif21b | ENSMUSG00000041642 | 0.51 | 2.5E-02 |
| **C-type lectin domain family 7, member a** | Clec7a | ENSMUSG00000079293 | 0.48 | 2.5E-02 |
| **latent transforming growth factor beta binding protein 2** | Ltbp2 | ENSMUSG00000002020 | 0.49 | 2.5E-02 |
| **a disintegrin and metallopeptidase domain 33** | Adam33 | ENSMUSG00000027318 | 0.47 | 2.5E-02 |
| **unc-13 homolog D (C. elegans)** | Unc13d | ENSMUSG00000057948 | 0.51 | 2.5E-02 |
| **proteolipid protein 2** | Plp2 | ENSMUSG00000031146 | 0.53 | 2.5E-02 |
| **insulin-like growth factor binding protein 2** | Igfbp2 | ENSMUSG00000039323 | 0.54 | 2.5E-02 |
| **neuralized E3 ubiquitin protein ligase 3** | Neurl3 | ENSMUSG00000047180 | 0.59 | 2.5E-02 |
| **alkylglycerol monooxygenase** | Agmo | ENSMUSG00000050103 | 1.24 | 2.6E-02 |
| **pleckstrin homology domain containing, family O member 1** | Plekho1 | ENSMUSG00000015745 | 0.67 | 2.6E-02 |
| **microtubule associated monooxygenase, calponin and LIM domain containing 1** | Mical1 | ENSMUSG00000019823 | 0.48 | 2.6E-02 |
| **filamin, alpha** | Flna | ENSMUSG00000031328 | 0.60 | 2.6E-02 |
| **protein tyrosine phosphatase, non-receptor type 13** | Ptpn13 | ENSMUSG00000034573 | 0.51 | 2.6E-02 |
| **muscleblind-like 3 (Drosophila)** | Mbnl3 | ENSMUSG00000036109 | 2.34 | 2.6E-02 |
| **zinc finger and BTB domain containing 8b** | Zbtb8b | ENSMUSG00000048485 | 0.39 | 2.6E-02 |

| | | | | |
|---|---|---|---|---|
| **RIKEN cDNA 2700081O15 gene** | 2700081O15Rik | ENSMUSG00000053080 | 0.57 | 2.6E-02 |
| **hydroxysteroid 11-beta dehydrogenase 1** | Hsd11b1 | ENSMUSG00000016194 | 1.37 | 2.6E-02 |
| **DNA-damage regulated autophagy modulator 1** | Dram1 | ENSMUSG00000020057 | 0.51 | 2.6E-02 |
| **mannosidase, alpha, class 1C, member 1** | Man1c1 | ENSMUSG00000037306 | 0.57 | 2.6E-02 |
| **ADP-ribosylation factor-like 4C** | Arl4c | ENSMUSG00000049866 | 0.54 | 2.7E-02 |
| **kinesin family member C3** | Kifc3 | ENSMUSG00000031788 | 0.66 | 2.7E-02 |
| **START domain containing 9** | Stard9 | ENSMUSG00000033705 | 0.59 | 2.7E-02 |
| **AT-hook transcription factor** | Akna | ENSMUSG00000039158 | 0.57 | 2.7E-02 |
| **NLR family, CARD domain containing 4** | Nlrc4 | ENSMUSG00000039193 | 0.43 | 2.7E-02 |
| **cytochrome P450, family 2, subfamily c, polypeptide 29** | Cyp2c29 | ENSMUSG00000003053 | 1.76 | 2.8E-02 |
| **chemokine (C-X-C motif) ligand 16** | Cxcl16 | ENSMUSG00000018920 | 0.60 | 2.8E-02 |
| **complement component 3a receptor 1** | C3ar1 | ENSMUSG00000040552 | 0.55 | 2.8E-02 |
| **pannexin 1** | Panx1 | ENSMUSG00000031934 | 0.46 | 2.8E-02 |
| **protein-L-isoaspartate (D-aspartate) O-methyltransferase domain containing 1** | Pcmtd1 | ENSMUSG00000051285 | 1.30 | 2.8E-02 |
| **bridging integrator 2** | Bin2 | ENSMUSG00000098112 | 0.52 | 3.0E-02 |
| **filamin binding LIM protein 1** | Fblim1 | ENSMUSG00000006219 | 0.49 | 3.0E-02 |
| **sema domain, immunoglobulin domain (Ig), short basic domain, secreted, (semaphorin) 3G** | Sema3g | ENSMUSG00000021904 | 0.40 | 3.0E-02 |
| **Rho GTPase activating protein 25** | Arhgap25 | ENSMUSG00000030047 | 0.53 | 3.1E-02 |
| **creatine kinase, brain** | Ckb | ENSMUSG00000001270 | 0.58 | 3.1E-02 |
| **FXYD domain-containing ion transport regulator 5** | Fxyd5 | ENSMUSG00000009687 | 0.61 | 3.1E-02 |
| **chemokine (C-C motif) ligand 6** | Ccl6 | ENSMUSG00000018927 | 0.57 | 3.1E-02 |
| **adenylate cyclase 7** | Adcy7 | ENSMUSG00000031659 | 0.55 | 3.1E-02 |
| **inositol 1,4,5-triphosphate receptor 3** | Itpr3 | ENSMUSG00000042644 | 0.55 | 3.1E-02 |
| **Rho GTPase activating protein 30** | Arhgap30 | ENSMUSG00000048865 | 0.57 | 3.1E-02 |

| | | | | |
|---|---|---|---|---|
| **WD repeat and FYVE domain containing 4** | Wdfy4 | ENSMUSG00000051506 | 0.60 | 3.1E-02 |
| **cDNA sequence BC147527** | BC147527 | ENSMUSG00000094796 | 0.40 | 3.1E-02 |
| **talin 1** | Tln1 | ENSMUSG00000028465 | 0.84 | 3.1E-02 |
| **proline rich 12** | Prr12 | ENSMUSG00000046574 | 0.74 | 3.1E-02 |
| **transmembrane protein 144** | Tmem144 | ENSMUSG00000027956 | 1.45 | 3.2E-02 |
| **regulator of G-protein signaling 9** | Rgs9 | ENSMUSG00000020599 | 0.41 | 3.2E-02 |
| **Ena-vasodilator stimulated phosphoprotein** | Evl | ENSMUSG00000021262 | 0.54 | 3.3E-02 |
| **serine (or cysteine) peptidase inhibitor, clade A, member 3M** | Serpina3m | ENSMUSG00000079012 | 1.72 | 3.3E-02 |
| **phosphodiesterase 10A** | Pde10a | ENSMUSG00000023868 | 0.46 | 3.3E-02 |
| **leukocyte tyrosine kinase** | Ltk | ENSMUSG00000027297 | 0.41 | 3.3E-02 |
| **tweety family member 3** | Ttyh3 | ENSMUSG00000036565 | 0.72 | 3.3E-02 |
| **myoferlin** | Myof | ENSMUSG00000048612 | 0.51 | 3.3E-02 |
| **microtubule associated serine/threonine kinase 1** | Mast1 | ENSMUSG00000053693 | 0.52 | 3.3E-02 |
| **capping protein (actin filament), gelsolin-like** | Capg | ENSMUSG00000056737 | 0.53 | 3.3E-02 |
| **N-acetyltransferase 8 (GCN5-related) family member 7** | Nat8f7 | ENSMUSG00000089694 | 2.46 | 3.3E-02 |
| **matrix metallopeptidase 2** | Mmp2 | ENSMUSG00000031740 | 0.50 | 3.3E-02 |
| **cathepsin S** | Ctss | ENSMUSG00000038642 | 0.59 | 3.3E-02 |
| **pleckstrin homology domain containing, family O member 2** | Plekho2 | ENSMUSG00000050721 | 0.58 | 3.3E-02 |
| **crystallin, zeta** | Cryz | ENSMUSG00000028199 | 1.28 | 3.5E-02 |
| **GLIS family zinc finger 2** | Glis2 | ENSMUSG00000014303 | 0.55 | 3.5E-02 |
| **glycoprotein galactosyltransferase alpha 1, 3** | Ggta1 | ENSMUSG00000035778 | 0.55 | 3.5E-02 |
| **CD300C molecule 2** | Cd300c2 | ENSMUSG00000044811 | 0.58 | 3.6E-02 |
| **spleen focus forming virus (SFFV) proviral integration oncogene** | Spi1 | ENSMUSG00000002111 | 0.56 | 3.6E-02 |
| **cytochrome P450, family 4, subfamily f, polypeptide 18** | Cyp4f18 | ENSMUSG00000003484 | 0.47 | 3.6E-02 |

| | | | | |
|---|---|---|---|---|
| **epidermal growth factor-containing fibulin-like extracellular matrix protein 2** | Efemp2 | ENSMUSG00000024909 | 0.62 | 3.6E-02 |
| **dystrophia myotonica-protein kinase** | Dmpk | ENSMUSG00000030409 | 0.60 | 3.7E-02 |
| **SEC14-like lipid binding 4** | Sec14l4 | ENSMUSG00000019368 | 1.50 | 3.7E-02 |
| **PDS5 cohesin associated factor B** | Pds5b | ENSMUSG00000034021 | 1.33 | 3.7E-02 |
| **androgen receptor** | Ar | ENSMUSG00000046532 | 1.70 | 3.7E-02 |
| **solute carrier family 25, member 36** | Slc25a36 | ENSMUSG00000032449 | 0.64 | 3.7E-02 |
| **lipoprotein lipase** | Lpl | ENSMUSG00000015568 | 0.49 | 3.8E-02 |
| **SEC62 homolog (S. cerevisiae)** | Sec62 | ENSMUSG00000027706 | 1.17 | 3.9E-02 |
| **fatty acid binding protein 5, epidermal** | Fabp5 | ENSMUSG00000027533 | 2.04 | 3.9E-02 |
| **cytochrome P450, family 2, subfamily r, polypeptide 1** | Cyp2r1 | ENSMUSG00000030670 | 1.32 | 3.9E-02 |
| **activin A receptor, type II-like 1** | Acvrl1 | ENSMUSG00000000530 | 0.60 | 3.9E-02 |
| **membrane-spanning 4-domains, subfamily A, member 7** | Ms4a7 | ENSMUSG00000024672 | 0.46 | 3.9E-02 |
| **mitochondrial ribosome-associated GTPase 1** | Mtg1 | ENSMUSG00000039018 | 1.23 | 3.9E-02 |
| **family with sequence similarity 102, member B** | Fam102b | ENSMUSG00000040339 | 0.57 | 3.9E-02 |
| **plasminogen activator, tissue** | Plat | ENSMUSG00000031538 | 0.49 | 3.9E-02 |
| **collagen, type VI, alpha 5** | Col6a5 | ENSMUSG00000091345 | 0.42 | 3.9E-02 |
| **histocompatibility 2, class II, locus DMa** | H2-DMa | ENSMUSG00000037649 | 0.56 | 4.0E-02 |
| **ets variant 5** | Etv5 | ENSMUSG00000013089 | 0.63 | 4.0E-02 |
| **protein phosphatase 1J** | Ppm1j | ENSMUSG00000002228 | 0.44 | 4.0E-02 |
| **AXL receptor tyrosine kinase** | Axl | ENSMUSG00000002602 | 0.64 | 4.0E-02 |
| **heterogeneous nuclear ribonucleoprotein H1** | Hnrnph1 | ENSMUSG00000007850 | 0.78 | 4.0E-02 |
| **dedicator of cyto-kinesis 2** | Dock2 | ENSMUSG00000020143 | 0.55 | 4.0E-02 |
| **discs, large homolog 4 (Drosophila)** | Dlg4 | ENSMUSG00000020886 | 0.51 | 4.0E-02 |
| **family with sequence similarity 129, member A** | Fam129a | ENSMUSG00000026483 | 0.58 | 4.0E-02 |

| | | | | |
|---|---|---|---|---|
| **ring finger protein 39** | Rnf39 | ENSMUSG00000036492 | 0.65 | 4.0E-02 |
| **runt related transcription factor 2** | Runx2 | ENSMUSG00000039153 | 0.43 | 4.0E-02 |
| **phosphatidylinositol 3-kinase catalytic delta polypeptide** | Pik3cd | ENSMUSG00000039936 | 0.56 | 4.0E-02 |
| **Rho GTPase activating protein 9** | Arhgap9 | ENSMUSG00000040345 | 0.55 | 4.0E-02 |
| **interferon regulatory factor 8** | Irf8 | ENSMUSG00000041515 | 0.62 | 4.0E-02 |
| **RIKEN cDNA 6030498E09 gene** | 6030498E09Rik | ENSMUSG00000051361 | 2.40 | 4.0E-02 |
| **LIM and cysteine-rich domains 1** | Lmcd1 | ENSMUSG00000057604 | 0.47 | 4.0E-02 |
| **DnaJ heat shock protein family (Hsp40) member B14** | Dnajb14 | ENSMUSG00000074212 | 1.27 | 4.0E-02 |
| **Kv channel interacting protein 3, calsenilin** | Kcnip3 | ENSMUSG00000079056 | 0.49 | 4.0E-02 |
| **a disintegrin and metallopeptidase domain 19 (meltrin beta)** | Adam19 | ENSMUSG00000011256 | 0.51 | 4.0E-02 |
| **deoxyribose-phosphate aldolase (putative)** | Dera | ENSMUSG00000030225 | 1.24 | 4.0E-02 |
| **1-acylglycerol-3-phosphate O-acyltransferase 1 (lysophosphatidic acid acyltransferase, alpha)** | Agpat1 | ENSMUSG00000034254 | 0.75 | 4.0E-02 |
| **insulin-like growth factor binding protein 7** | Igfbp7 | ENSMUSG00000036256 | 0.69 | 4.0E-02 |
| **adhesion G protein-coupled receptor G3** | Adgrg3 | ENSMUSG00000060470 | 0.61 | 4.0E-02 |
| **coronin, actin binding protein 1A** | Coro1a | ENSMUSG00000030707 | 0.56 | 4.1E-02 |
| **erythrocyte membrane protein band 4.1 like 1** | Epb41l1 | ENSMUSG00000027624 | 0.52 | 4.1E-02 |
| **pogo transposable element with ZNF domain** | Pogz | ENSMUSG00000038902 | 0.81 | 4.1E-02 |
| **ral guanine nucleotide dissociation stimulator-like 2** | Rgl2 | ENSMUSG00000041354 | 0.78 | 4.1E-02 |
| **predicted gene 7120** | Gm7120 | ENSMUSG00000094114 | 1.90 | 4.1E-02 |
| **ephrin B1** | Efnb1 | ENSMUSG00000031217 | 0.71 | 4.1E-02 |
| **FK506 binding protein 10** | Fkbp10 | ENSMUSG00000001555 | 0.51 | 4.2E-02 |
| **transmembrane protein 106B** | Tmem106b | ENSMUSG00000029571 | 1.22 | 4.2E-02 |
| **Fc receptor, IgE, high affinity I, gamma polypeptide** | Fcer1g | ENSMUSG00000058715 | 0.60 | 4.2E-02 |

| | | | | |
|---|---|---|---|---|
| **nuclear factor of activated T cells, cytoplasmic, calcineurin dependent 4** | Nfatc4 | ENSMUSG00000023411 | 0.47 | 4.3E-02 |
| **sialic acid binding Ig-like lectin F** | Siglecf | ENSMUSG00000039013 | 0.42 | 4.3E-02 |
| **membrane-spanning 4-domains, subfamily A, member 4B** | Ms4a4b | ENSMUSG00000056290 | 0.50 | 4.3E-02 |
| **eosinophil-associated, ribonuclease A family, member 2** | Ear2 | ENSMUSG00000072596 | 0.53 | 4.3E-02 |
| **solute carrier family 4 (anion exchanger), member 3** | Slc4a3 | ENSMUSG00000006576 | 0.49 | 4.3E-02 |
| **pleckstrin homology like domain, family B, member 2** | Phldb2 | ENSMUSG00000033149 | 0.79 | 4.3E-02 |
| **signal peptide, CUB domain, EGF-like 1** | Scube1 | ENSMUSG00000016763 | 0.45 | 4.3E-02 |
| **collagen, type I, alpha 2** | Col1a2 | ENSMUSG00000029661 | 0.52 | 4.3E-02 |
| **COMM domain containing 3** | Commd3 | ENSMUSG00000051154 | 1.16 | 4.3E-02 |
| **CD79A antigen (immunoglobulin-associated alpha)** | Cd79a | ENSMUSG00000003379 | 0.50 | 4.3E-02 |
| **toll interacting protein** | Tollip | ENSMUSG00000025139 | 1.19 | 4.3E-02 |
| **leukocyte immunoglobulin-like receptor, subfamily B, member 4A** | Lilrb4a | ENSMUSG00000062593 | 0.56 | 4.3E-02 |
| **ubiquitin associated and SH3 domain containing, B** | Ubash3b | ENSMUSG00000032020 | 0.58 | 4.4E-02 |
| **chemokine (C-X-C motif) receptor 4** | Cxcr4 | ENSMUSG00000045382 | 0.48 | 4.4E-02 |
| **NCK associated protein 1 like** | Nckap1l | ENSMUSG00000022488 | 0.59 | 4.5E-02 |
| **CD74 antigen (invariant polypeptide of major histocompatibility complex, class II antigen-associated)** | Cd74 | ENSMUSG00000024610 | 0.54 | 4.5E-02 |
| **a disintegrin-like and metallopeptidase (reprolysin type) with thrombospondin type 1 motif, 10** | Adamts10 | ENSMUSG00000024299 | 0.62 | 4.5E-02 |
| **phosphatidylinositol-3,4,5-trisphosphate-dependent Rac exchange factor 1** | Prex1 | ENSMUSG00000039621 | 0.65 | 4.5E-02 |
| **ankyrin repeat domain 33B** | Ankrd33b | ENSMUSG00000022237 | 1.51 | 4.5E-02 |
| **lysozyme 2** | Lyz2 | ENSMUSG00000069516 | 0.58 | 4.5E-02 |

| | | | | |
|---|---|---|---|---|
| **jagged 2** | Jag2 | ENSMUSG00000002799 | 0.43 | 4.5E-02 |
| **C-reactive protein, pentraxin-related** | Crp | ENSMUSG00000037942 | 1.30 | 4.5E-02 |
| **membrane magnesium transporter 2** | Mmgt2 | ENSMUSG00000048497 | 0.51 | 4.5E-02 |
| **protein tyrosine phosphatase, receptor type, E** | Ptpre | ENSMUSG00000041836 | 0.55 | 4.6E-02 |
| **RAB6B, member RAS oncogene family** | Rab6b | ENSMUSG00000032549 | 0.54 | 4.6E-02 |
| **sorting nexin 20** | Snx20 | ENSMUSG00000031662 | 0.50 | 4.6E-02 |
| **purinergic receptor P2Y, G-protein coupled 10** | P2ry10 | ENSMUSG00000050921 | 0.44 | 4.6E-02 |
| **prolyl 3-hydroxylase 3** | P3h3 | ENSMUSG00000023191 | 0.64 | 4.6E-02 |
| **family with sequence similarity 105, member A** | Fam105a | ENSMUSG00000056069 | 0.57 | 4.6E-02 |
| **pleckstrin homology domain-containing, family A (phosphoinositide binding specific) member 2** | Plekha2 | ENSMUSG00000031557 | 0.64 | 4.7E-02 |
| **TBC1 domain family, member 9** | Tbc1d9 | ENSMUSG00000031709 | 0.57 | 4.7E-02 |
| **zinc finger E-box binding homeobox 2** | Zeb2 | ENSMUSG00000026872 | 0.66 | 4.7E-02 |
| **SH3-domain kinase binding protein 1** | Sh3kbp1 | ENSMUSG00000040990 | 0.60 | 4.7E-02 |
| **formin homology 2 domain containing 1** | Fhod1 | ENSMUSG00000014778 | 0.65 | 4.7E-02 |
| **RIKEN cDNA 4930452B06 gene** | 4930452B06Rik | ENSMUSG00000021747 | 1.79 | 4.7E-02 |
| **WD repeat domain 7** | Wdr7 | ENSMUSG00000040560 | 1.26 | 4.7E-02 |
| **cortexin 1** | Ctxn1 | ENSMUSG00000048644 | 0.49 | 4.7E-02 |
| **2'-5' oligoadenylate synthetase 1A** | Oas1a | ENSMUSG00000052776 | 0.65 | 4.7E-02 |
| **ecotropic viral integration site 2a** | Evi2a | ENSMUSG00000078771 | 0.54 | 4.7E-02 |
| **phospholipase D2** | Pld2 | ENSMUSG00000020828 | 0.75 | 4.7E-02 |
| **aldehyde dehydrogenase family 1, subfamily A2** | Aldh1a2 | ENSMUSG00000013584 | 0.44 | 4.8E-02 |
| **Fc receptor, IgG, high affinity I** | Fcgr1 | ENSMUSG00000015947 | 0.58 | 4.8E-02 |
| **cell adhesion molecule 1** | Cadm1 | ENSMUSG00000032076 | 0.78 | 4.8E-02 |
| **histocompatibility 2, class II antigen A, alpha** | H2-Aa | ENSMUSG00000036594 | 0.53 | 4.8E-02 |

| | | | | |
|---|---|---|---|---|
| **tissue inhibitor of metalloproteinase 2** | Timp2 | ENSMUSG00000017466 | 0.67 | 4.9E-02 |
| **CD53 antigen** | Cd53 | ENSMUSG00000040747 | 0.62 | 4.9E-02 |
| **GRAM domain containing 1B** | Gramd1b | ENSMUSG00000040111 | 0.62 | 4.9E-02 |
| **ATP-binding cassette, sub-family C (CFTR/MRP), member 1** | Abcc1 | ENSMUSG00000023088 | 0.58 | 5.0E-02 |
| **coagulation factor IX** | F9 | ENSMUSG00000031138 | 1.21 | 5.0E-02 |
| **suppression of tumorigenicity 14 (colon carcinoma)** | St14 | ENSMUSG00000031995 | 0.47 | 5.0E-02 |
| **toll-like receptor 4** | Tlr4 | ENSMUSG00000039005 | 0.58 | 5.0E-02 |
| **ureidoimidazoline (2-oxo-4-hydroxy-4-carboxy-5) decarboxylase** | Urad | ENSMUSG00000075543 | 1.76 | 5.0E-02 |
| **prostaglandin E receptor 1 (subtype EP1)** | Ptger1 | ENSMUSG00000019464 | 0.69 | 5.0E-02 |
| **UDP glucuronosyltransferase 2 family, polypeptide B37** | Ugt2b37 | ENSMUSG00000057425 | 2.27 | 5.0E-02 |
| **Sp110 nuclear body protein** | Sp110 | ENSMUSG00000070034 | 0.55 | 5.0E-02 |
| **PHD finger protein 12** | Phf12 | ENSMUSG00000037791 | 0.83 | 5.0E-02 |

***Table 7.6 - Genes, hepatic expression of which is altered in Pten$^{-/-}$+D316A relative to Pten$^{-/-}$ mice at 25 weeks of age.***

## 7.2 Appendix B

Please see PDF of the following reference:

A. Woods, J. R. Williams, P. J. Muckett, F. V. Mayer, M. Liljevald, Y. M. Bohlooly, and D. Carling. 2017. 'Liver-Specific Activation of AMPK Prevents Steatosis on a High-Fructose Diet', Cell Rep, 18: 3043-51

Report

Cell Reports

# Liver-Specific Activation of AMPK Prevents Steatosis on a High-Fructose Diet

## Graphical Abstract

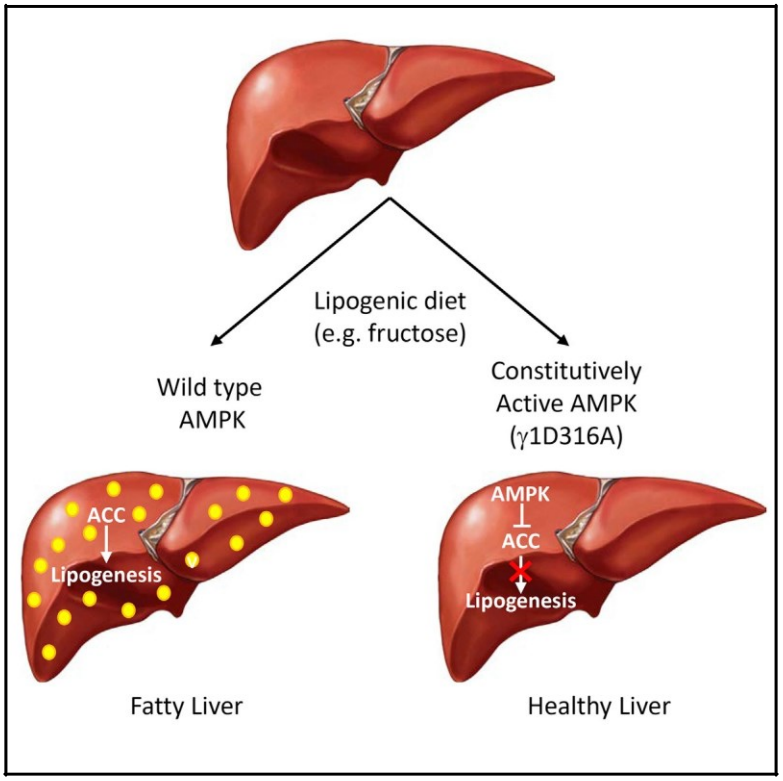


## Highlights

- A mutation in AMPK γ1 subunit leads to constitutive activation of the kinase
- AMPK activation in liver protects against steatosis on a fructose diet
- AMPK inhibits de novo lipogenesis with no effect on hepatic fatty acid oxidation
- AMPK provides an attractive pharmacological target for protection against NAFLD

## Authors

Angela Woods, Jennet R. Williams, Phillip J. Muckett, Faith V. Mayer, Maria Liljevald, Mohammad Bohlooly-Y, David Carling

## Correspondence

angela.woods@lms.mrc.ac.uk (A.W.), david.carling@lms.mrc.ac.uk (D.C.)

## In Brief

Using a gain-of-function mouse model, Woods et al. show that hepatic activation of AMPK protects against triglyceride accumulation in the liver. AMPK inhibits de novo lipogenesis but has no effect on hepatic fatty acid oxidation. These findings highlight AMPK as an attractive therapeutic target for protection against fatty liver disease.

Woods et al., 2017, Cell Reports 18, 3043–3051
March 28, 2017 
http://dx.doi.org/10.1016/j.celrep.2017.03.011

Cell Reports
Report



# Liver-Specific Activation of AMPK Prevents Steatosis on a High-Fructose Diet

Angela Woods,[1,*] Jennet R. Williams,[1] Phillip J. Muckett,[1] Faith V. Mayer,[1] Maria Liljevald,[3] Mohammad Bohlooly-Y,[4] and David Carling[1,2,5,*]
[1]MRC London Institute of Medical Sciences, Imperial College London, Hammersmith Hospital, London W12 0NN, UK
[2]Institute of Clinical Sciences, Imperial College London, Hammersmith Hospital, London W12 0NN, UK
[3]Drug Safety and Metabolism, Innovative Medicines and Early Development Biotech Unit, AstraZeneca, Pepparedsleden 1, Mölndal 431 83, Sweden
[4]Discovery Sciences, Innovative Medicines and Early Development Biotech Unit, AstraZeneca, Pepparedsleden 1, Mölndal 431 83, Sweden
[5]Lead Contact
*Correspondence: angela.woods@lms.mrc.ac.uk (A.W.), david.carling@lms.mrc.ac.uk (D.C.)
http://dx.doi.org/10.1016/j.celrep.2017.03.011

## SUMMARY

AMP-activated protein kinase (AMPK) plays a key role in integrating metabolic pathways in response to energy demand. We identified a mutation in the g1 subunit ($g1^{D316A}$) that leads to activation of AMPK. We generated mice with this mutation to study the effect of chronic liver-specific activation of AMPK in vivo. Primary hepatocytes isolated from these mice have reduced gluconeogenesis and fatty acid synthesis, but there is no effect on fatty acid oxidation compared to cells from wild-type mice. Liver-specific activation of AMPK decreases lipogenesis in vivo and completely protects against hepatic steatosis when mice are fed a high-fructose diet. Our findings demonstrate that liver-specific activation of AMPK is sufficient to protect against hepatic triglyceride accumulation, a hallmark of non-alcoholic fatty liver disease (NAFLD). These results emphasize the clinical relevance of activating AMPK in the liver to combat NAFLD and potentially other associated complications (e.g., cirrhosis and hepatocellular carcinoma).

## INTRODUCTION

The incidence of non-alcoholic fatty liver disease (NAFLD) is increasing rapidly and is now one of the most common diseases worldwide. A recent meta-analysis study concluded that the global prevalence of NAFLD is over 25% (Younossi et al., 2016). While NAFLD can be benign, approximately 25% of patients with the disease will go on to develop non-alcoholic steatohepatitis (NASH), a more serious disease characterized by hepatic inflammation (Matteoni et al., 1999; Younossi et al., 2016). Patients with NASH risk developing additional complications, and 2% of patients will die of NAFLD liver-related mortality (Younossi et al., 2016). The initial hallmark of NAFLD is excessive accumulation of liver triglycerides (Postic and Girard, 2008). Currently, there are no approved drugs available for the treatment of NAFLD or NASH, and these diseases represent a major unmet clinical need.

AMP-activated protein kinase (AMPK) plays an important role in maintaining energy homeostasis (Carling et al., 2012; Steinberg and Kemp, 2009). Activation of AMPK leads to a decrease in ATP-consuming pathways and an increase in ATP-producing pathways. Given its key role in regulating energy balance, AMPK has become an attractive target for treatments aimed at diseases caused by disruption of energy metabolism. A number of direct AMPK activators have been reported (Cool et al., 2006; Xiao et al., 2013; Zadra et al., 2014), although, to date, the poor bioavailability of the compounds has limited their use in vivo. The first direct activator to be reported, a thienopyridone, A769662, was shown to reverse some of the metabolic disorders associated with the metabolic syndrome (Cool et al., 2006). A number of compounds lead to activation of AMPK through indirect mechanisms, including the widely used antidiabetic drug, metformin (Dandapani and Hardie, 2013). A caveat with interpreting the effects of pharmacological studies is the possibility of off-target effects of drugs. Another potential weakness is that it can be difficult to determine the particular cell type(s) involved in response to the drug.

A number of studies have examined the effects of specific AMPK subunits in vivo using transgenic knockout mouse models (Viollet et al., 2009). These studies, however, do not address the effect of AMPK activation on whole-animal physiology. Naturally occurring gain-of-function mutations in the g2 subunit of AMPK have been identified in humans with heart disease (Arad et al., 2007) and in the g3 subunit in Hampshire pigs with skeletal muscle glycogen storage disease (Milan et al., 2000). However, the limited tissue distribution of g2 (predominantly expressed in heart) and g3 (predominantly expressed in skeletal muscle) limits their suitability for use as models to understand the role of AMPK in non-muscle tissues. In an attempt to overcome these limitations, we identified a gain-of-function mutation in the widely expressed g1 subunit of AMPK. Transgenic mice expressing this mutant form of g1 in a conditional manner were generated and used to investigate the effects of liver-specific activation of AMPK.

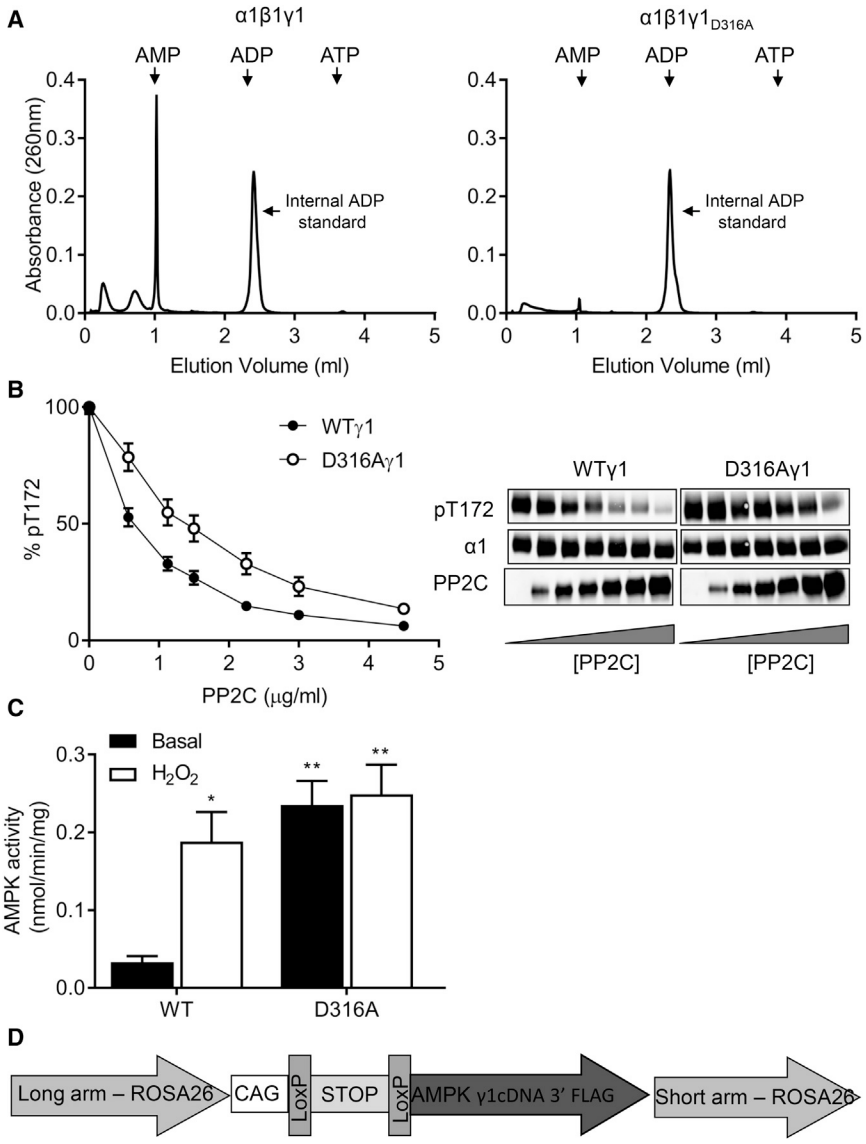


Figure 1. Characterization of g1D316A Mutation In Vitro

(A) AMP in perchloric acid extracts of bacterially expressed AMPK complexes (wild-type a1b1g1 or a1b1g1$_{D316A}$) was determined by ion-exchange chromatography. The elution positions of AMP, ADP, and ATP standards are indicated by the arrows. ADP (4 nmol) was added prior to extraction as an internal standard and is marked by an arrow.

(B) Following phosphorylation by CaMKKb, recombinant AMPK complexes were incubated in the presence of increasing concentrations of Protein phosphatase 2C (PP2C) for 20 min and then analyzed for T172 phosphorylation by western blotting. A representative blot showing the level of T172 phosphorylation, total AMPKa1, and PP2C is shown. Quantification of T172 phosphorylation relative to a control (in the absence of PP2C) is shown (n = 4).

(C) COS7 cells were co-transfected with cDNAs encoding a1, b1, and either wild-type or D316A g1, harboring a C-terminal Flag epitope tag. AMPK activity from cells treated with or without 1 mM $H_2O_2$ for 15 min was measured in immune-complexes isolated with anti-Flag antibody (n = 4, *p < 0.05, **p < 0.01).

(D) Schematic representation of the construct used to generate transgenic mice expressing either WTg1 or D316Ag1.

Here, we show that liver-specific activation of AMPK has no significant metabolic effect on mice fed a normal chow diet or a high-fat diet. Activation of hepatic AMPK decreases de novo lipogenesis, and this protects against the development of liver steatosis following a high-fructose diet. Our findings have important implications for understanding the impact of potential therapeutic targeting of AMPK. By reducing de novo lipogenesis, activation of hepatic AMPK would be anticipated to slow the progression of NAFLD, decreasing the risk of associated complications, such as NASH, cirrhosis, and hepatocellular carcinoma (Matteoni et al., 1999).

## RESULTS

During our previous analysis of adenine nucleotide binding to AMPK, we identified aspartic acid residues present within each of the three occupied sites in the g1 subunit that interact with the $2^0$ and $3^0$ hydroxyl groups of the ribose moiety (Xiao et al., 2007). The tightly bound AMP in site 4, which we found to be non-exchangeable in solution, interacts with aspartic acid residue 316 (residue 317 in human g1). Mutation of D316 to an alanine (D316A) abolished binding of this tightly bound AMP molecule (Figure 1A) and rendered the complex less sensitive to dephosphorylation by protein phosphatase 2C (PP2C) (Figure 1B). In mammalian cells, co-expression of g1 harboring the D316A mutation with a1 and b1 led to increased basal AMPK activity compared to wild-type enzyme (Figure 1C). Wild-type AMPK was activated approximately 7-fold by treatment of the cells, with hydrogen peroxide bringing its activity to a similar level as the D316A mutant. Hydrogen peroxide treatment had no significant effect on the activity of the D316A mutant AMPK complex. These results show that mutation of D316 to alanine in g1 leads to a gain of function in AMPK activity, presumably mediated by a decrease in the rate of dephosphorylation of T172.

We designed Cre/loxP conditional ROSA26 targeting vectors for expression of either wild-type or mutant g1 and used these to generate transgenic mouse lines (hereafter referred to as wild-type g1 [WT-Tg] or D316A mutant g1 [D316A-Tg] transgenic mice). We engineered a sequence encoding the Flag epitope at the C terminus to allow recognition by an anti-Flag antibody (see Figure 1D). To generate liver-specific expression of the

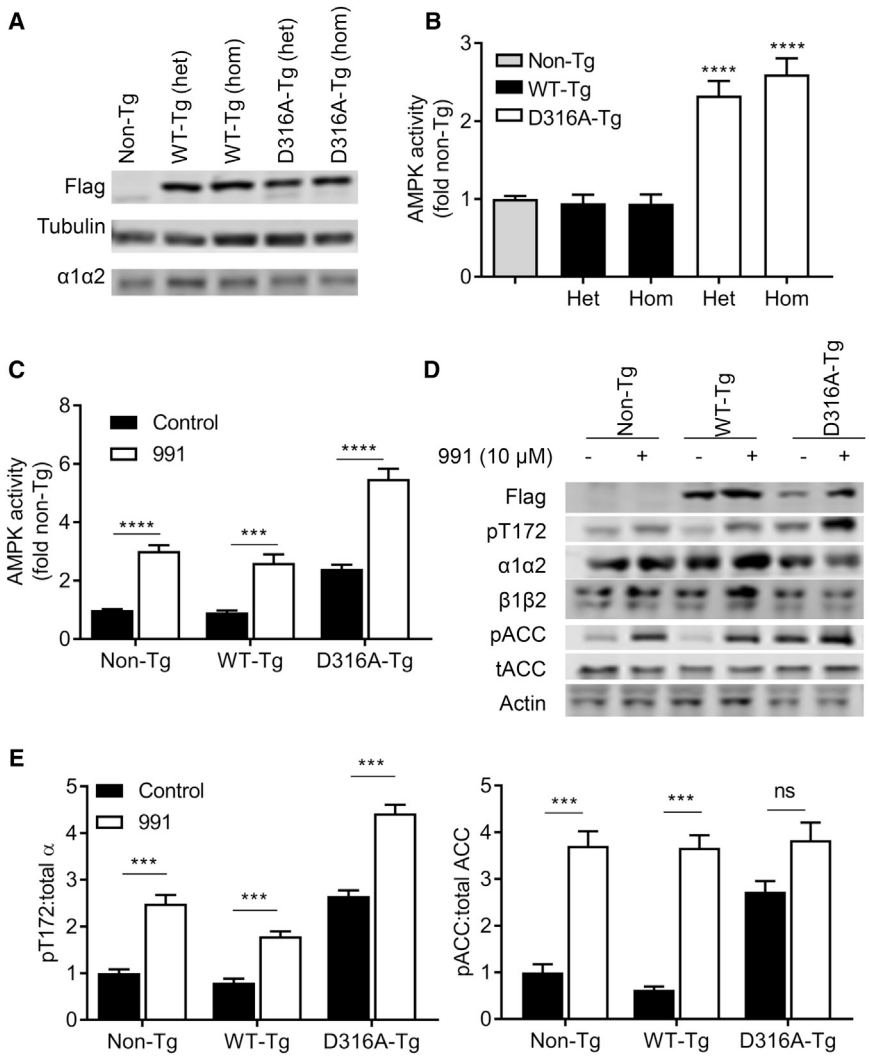


Figure 2. Expression of g1D316A in Mouse Hepatocytes

(A) Hepatocyte lysates isolated from mice either heterozygous (het) or homozygous (hom) for WT or D316A g1 transgene were blotted with the indicated antibodies.

(B) AMPK activity was measured in immune complexes isolated with a pan AMPKb antibody. Results shown are plotted as fold activity relative to hepatocytes from Non-Tg mice.

(C) Hepatocytes were treated in the presence or absence of 10 mM 991 for 30 min, and AMPK activity was measured in immune complexes isolated with a pan AMPKb antibody. Results shown are plotted relative to the activity in Non-Tg, untreated control cells, from at least six independent experiments.

(D and E) (D) A representative blot of hepatocyte lysates after treatment with or without 10 mM 991 for 30 min probed with the indicated antibodies and (E) quantification of blots for three independent experiments; ***p < 0.005, ****p < 0.001; NS, not significant.

transgenes, animals were crossed with mice expressing Cre-recombinase under the control of the albumin promoter (Postic et al., 1999). Measurement of AMPK activity in the liver can be confounded by post-mortem changes in T172 phosphorylation caused by rapid depletion of ATP during tissue isolation (Davies et al., 1992). In order to overcome this issue, we isolated primary hepatocytes to allow determination of AMPK activity in the basal state. Expression of both WT and D316A g1 protein was confirmed by western blot analysis (Figure 2A). Similar levels of expression and AMPK activity (Figure 2B) were observed in mice either heterozygous or homozygous for the transgene. Importantly, however, under basal conditions, total AMPK activity was approximately 2.5-fold higher in hepatocytes from D316A-Tg mice compared to cells from either non-Tg or WT-Tg mice (Figures 2B and 2C). Following incubation with 991, a direct activator of AMPK (Xiao et al., 2013), AMPK activity was increased 2- to 3-fold in all cases (Figure 2C). Phosphorylation of T172 and acetyl-CoA carboxylase (ACC), a downstream substrate of AMPK, increased in parallel with the increase in AMPK activity (Figures 2D and 2E). These results demonstrate that in vivo expression of D316A g1 increases basal AMPK activity to a similar level as that seen following pharmacological activation with a direct AMPK activator. No difference in total AMPK expression was detected in cells from Non-Tg, WT-Tg, or D316A-Tg mice, as assessed by blotting for either total a or b subunits (Figure 2D). We were unable to determine total g1 expression, as the anti-g1 antibody that we used was raised against the C-terminal region of g1 and did not cross-react with the transgenic g1 protein, presumably due to interference by the addition of the Flag epitope tag (data not shown). As there was no difference in AMPK activity in WT-Tg compared to Non-Tg hepatocytes, we used WT-Tg animals as controls for the remaining studies. Similarly, since we detected no difference in AMPK expression or activity between heterozygous or homozygous transgenic mice, we combined both heterozygous and homozygous mice for all further studies in order to maximize animal usage.

AMPK has been implicated in the regulation of a number of metabolic pathways in the liver, including gluconeogenesis, fatty acid synthesis, and fatty acid oxidation (FAO) (Hardie and Carling, 1997; Steinberg and Kemp, 2009). Basal and glucagon-stimulated glucose outputs were decreased by approximately 50% in hepatocytes isolated from D316A-Tg compared to WT-Tg cells (Figure 3A). Consistent with this effect, we found that expressions of glucose-6-phosphatase (G6Pase) and phosphoenolpyruvate carboxykinase (PEPCK) mRNA, genes coding for two key enzymes in gluconeogenesis, were significantly decreased in hepatocytes from the D316A-Tg mice (Figure 3B). Fatty acid synthesis, as measured by incorporation of $^{14}$C-acetate into fatty acid, was significantly decreased in hepatocytes

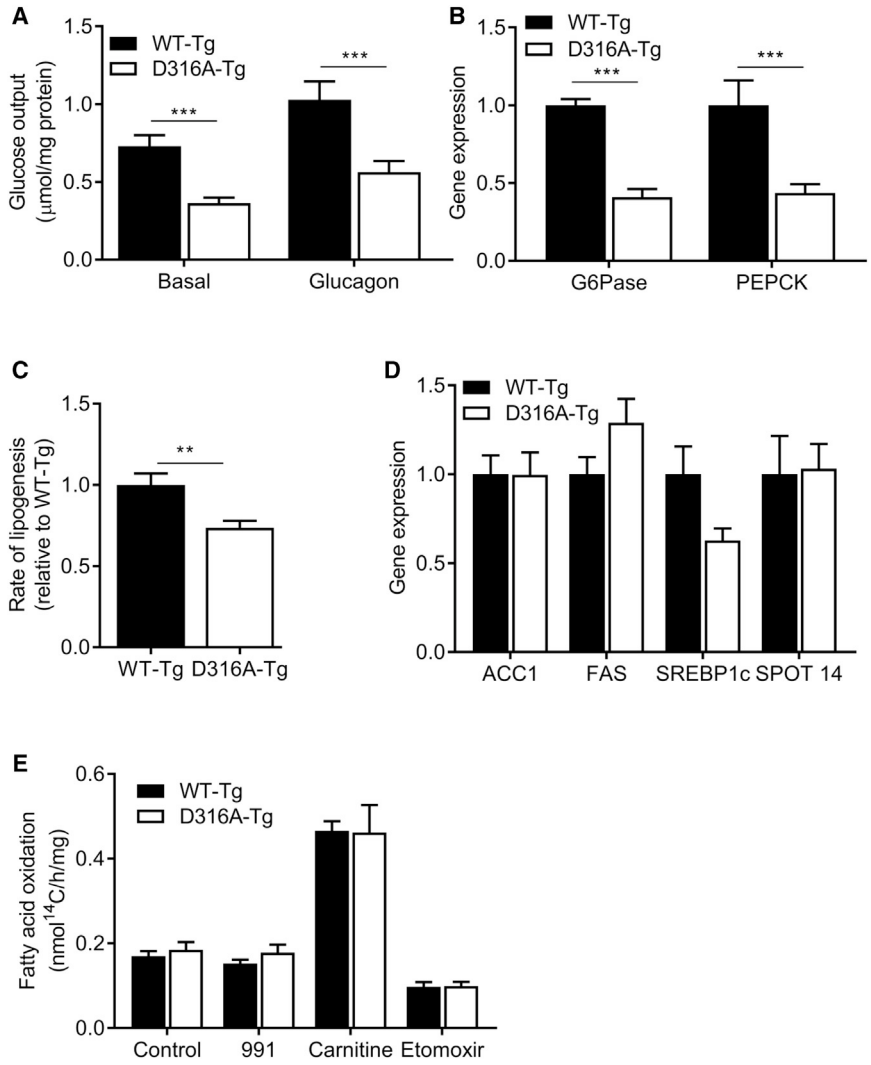


Figure 3. Metabolic Effects of Chronic Expression of g1D316A in Mouse Hepatocytes

(A) Hepatocytes from transgenic mice were incubated in the presence or absence of 10 nM glucagon, and hepatic glucose output over 18 hr was measured and normalized to total cellular protein.

(B) Relative expression of gluconeogenic genes, glucose-6-phosphatase (G6Pase), and phosphoenolpyruvate carboxykinase (PEPCK).

(C) De novo lipogenesis was measured in isolated hepatocytes by incorporation of $^{14}$C-acetate into lipids.

(D) Lipogenic gene expression plotted relative to expression in WT-Tg cells.

(E) Fatty acid oxidation was measured over 6 hr using $^{14}$C-palmitate in the presence or absence of 10 mM 991, 1 mM carnitine, or 0.1 mM etomoxir. In each case, results are from at least six independent experiments; *p < 0.05, **p < 0.01, ***p < 0.005, ****p < 0.001.

from D316A-Tg compared to WT-Tg mice (Figure 3C), although we did not detect any significant change in expression of a number of genes involved in lipogenesis (Figure 3D). A number of studies have reported that treatments that cause activation of AMPK increase FAO. AMPK phosphorylates and inactivates ACC, which leads to reduced levels of malonyl-CoA, thereby increasing mitochondrial fatty acid uptake, increasing FAO. However, most of the previous reports linking AMPK activation to increased FAO have studied skeletal muscle, and very few studies have provided direct evidence that AMPK activation increases FAO in the liver (Fullerton et al., 2013). We did not detect any significant difference in fatty acid oxidation of $^{14}$C-labeled palmitate in D316A-Tg cells relative to WT-Tg cells (Figure 3E). We also failed to detect a change in FAO following treatment with 991 (Figure 3E). Addition of carnitine increased, whereas treatment of the cells with etomoxir, an inhibitor of carnitine palmitoyl transferase I, reduced FAO, demonstrating that the hepatocytes have the capacity to respond to changes in FAO rates.

In order to determine the effect of liver-specific AMPK activation on whole-body metabolism in vivo, we measured a number of metabolic parameters in WT-Tg and D316A-Tg mice fed on a chow diet. We were unable to detect any significant differences in body weight, total body fat, liver triglycerides, liver cholesterol, glucose handling, respiratory exchange ratio (RER), or $VO_2$ consumption between the two genotypes (Figure S1). Similarly, we did not see any significant difference in these parameters when mice were fed a high-fat diet (Figure S1). No difference in RER was observed between WT-Tg and D316A-Tg mice on either a chow or high-fat diet. Consistent with previously published studies, RER values were lower in mice fed a high-fat diet, reflecting an increased reliance on FAO (Figure S1H). In light of our finding in isolated primary hepatocytes that AMPK activation had no effect on fatty acid oxidation, but did significantly reduce lipogenesis, we measured in vivo de novo lipogenesis rates. De novo lipogenesis was reduced by approximately 30% in D316A-Tg mice compared to WT-Tg mice (Figure 4A). In order to determine the physiological relevance of this effect, we fed mice a diet high in fructose (60% of calories derived from fructose), which is known to increase hepatic lipogenesis in rodents and humans (Mayes, 1993; Tappy and Lê, 2010). There was no significant difference in body weight, total fat mass, glucose tolerance, serum lipids, serum 3-hydroxybutyrate, RER, or $VO_2$ consumption between the WT-Tg and D316A-Tg mice after 12 weeks on the high-fructose diet (Figure 4). In contrast, there was a dramatic reduction in hepatic triglyceride content in liver from D316A-Tg mice compared to WT-Tg mice (Figure 5A). Remarkably, hepatic triglyceride levels in the D316A-Tg mice were similar to those in mice maintained

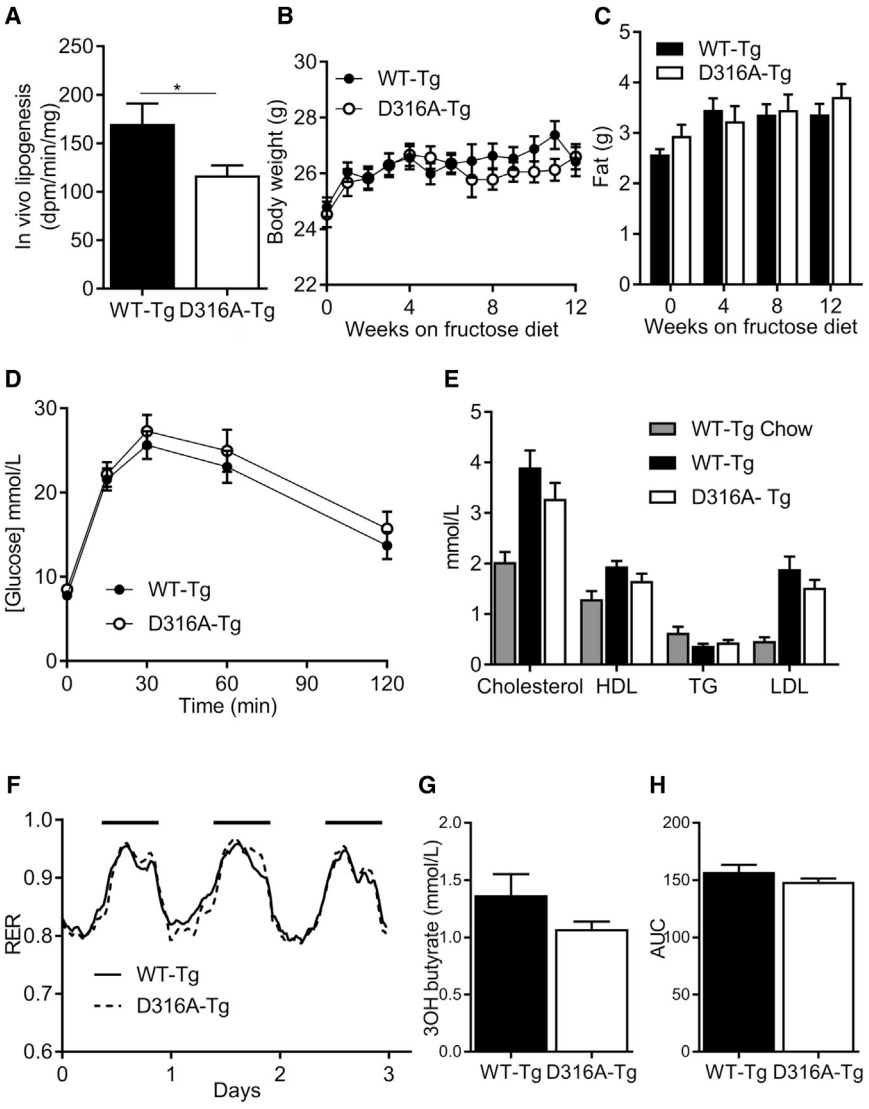


**Figure 4. Whole-Body Metabolic Effects of Chronic Hepatic Activation of AMPK on Mice Fed a High-Fructose Diet**

(A) In vivo hepatic lipogenesis was determined by measuring incorporation of $^{3}$H-acetate into lipids (n = 8 per group).

(B) Body weights of mice fed a high-fructose diet from eight weeks of age (n = 20).

(C and D) (C) Total body fat measured by EchoMRI and (D) glucose tolerance test of mice fed a high-fructose diet for 12 weeks (n = 8–13).

(E) Serum lipids of mice fed a high-fructose diet for 12 weeks and compared to WT-Tg mice fed on chow (n = 9–12).

(F) Respiratory exchange ratio (RER) measured over 3 days for WT-Tg and D316A-Tg mice fed a high-fructose diet for 4 weeks. The solid black bars indicate the dark period between 19.00 and 07.00.

(G) Serum 3-hydroxybutyrate levels in mice fed a high-fructose diet for 12 weeks (n = 9–10).

(H) Total area under the curve (AUC) for $VO_2$ consumption measured over three days for mice fed a high-fructose diet for four weeks (n = 10–12).

on a normal chow diet (Figure 5A). No significant differences in liver cholesterol (Figure 5B), glycogen (Figure 5C), or serum transaminases (Figures 5D and 5E) were detected either between the different transgenic mice or between fructose and chow diets. Similarly, we did not detect any changes in expression of a number of genes correlated with liver injury, e.g., CCL2, CCL4, IL6, and TGFb1 (data not shown). The expression of the lipogenic enzymes ACC, fatty acid synthase (FAS), and stearoyl-CoA desaturase (SCD1) were all increased in livers of mice fed a high-fructose diet relative to normal chow, and this was similar in both genotypes (Figures 5F and 5G). Expression of fibroblast growth factor 21 (FGF21) was also increased in response to the high-fructose diet in livers from both WT-Tg and D316A-Tg mice, consistent with previous studies showing increased expression in response to fructose (Dushay et al., 2014). These results indicate that the signaling pathway that leads to increased protein expression of lipogenic enzymes in response to fructose remains intact in the D316A-Tg mice. Hematoxylin and Eosin (H&E) staining of livers from WT-Tg mice fed on a high-fructose diet showed large lipid droplets, which were completely absent in livers from the D316A-Tg mice (Figure 5H).

## DISCUSSION

Here, we describe a mouse model for investigating the effects of chronic AMPK activation in vivo. We found that mutation of aspartic acid residue 316 to alanine in mouse g1 (residue 317 in human g1) makes AMPK a worse substrate for dephosphorylation, leading to increased AMPK activity when expressed in mammalian cells. Generation of transgenic mice with conditional expression of this mutant provided us with the opportunity to investigate the consequence of chronic, tissue-specific activation of AMPK.

The liver plays a key role in regulating whole-body energy metabolism (Rui, 2014), and previous studies suggest an important role for AMPK in coordinating changes in hepatic metabolism required for maintaining overall energy balance (Davies et al., 1992; Woods et al., 2000). An advantage of expressing the transgene in liver was that it allowed us to use primary hepatocytes to characterize the effect of the g1 mutation on AMPK and downstream pathways at a cellular level. Expression of the transgenic g1 protein has no effect on the total level of AMPK complex, indicating that transgenic g1 protein competes with endogenous g1. Importantly, basal AMPK activity is 2- to 3-fold higher in hepatocytes isolated from D316A-Tg mice, compared to either WT-Tg or Non-Tg mice. This degree of activation is similar to that obtained following treatment of

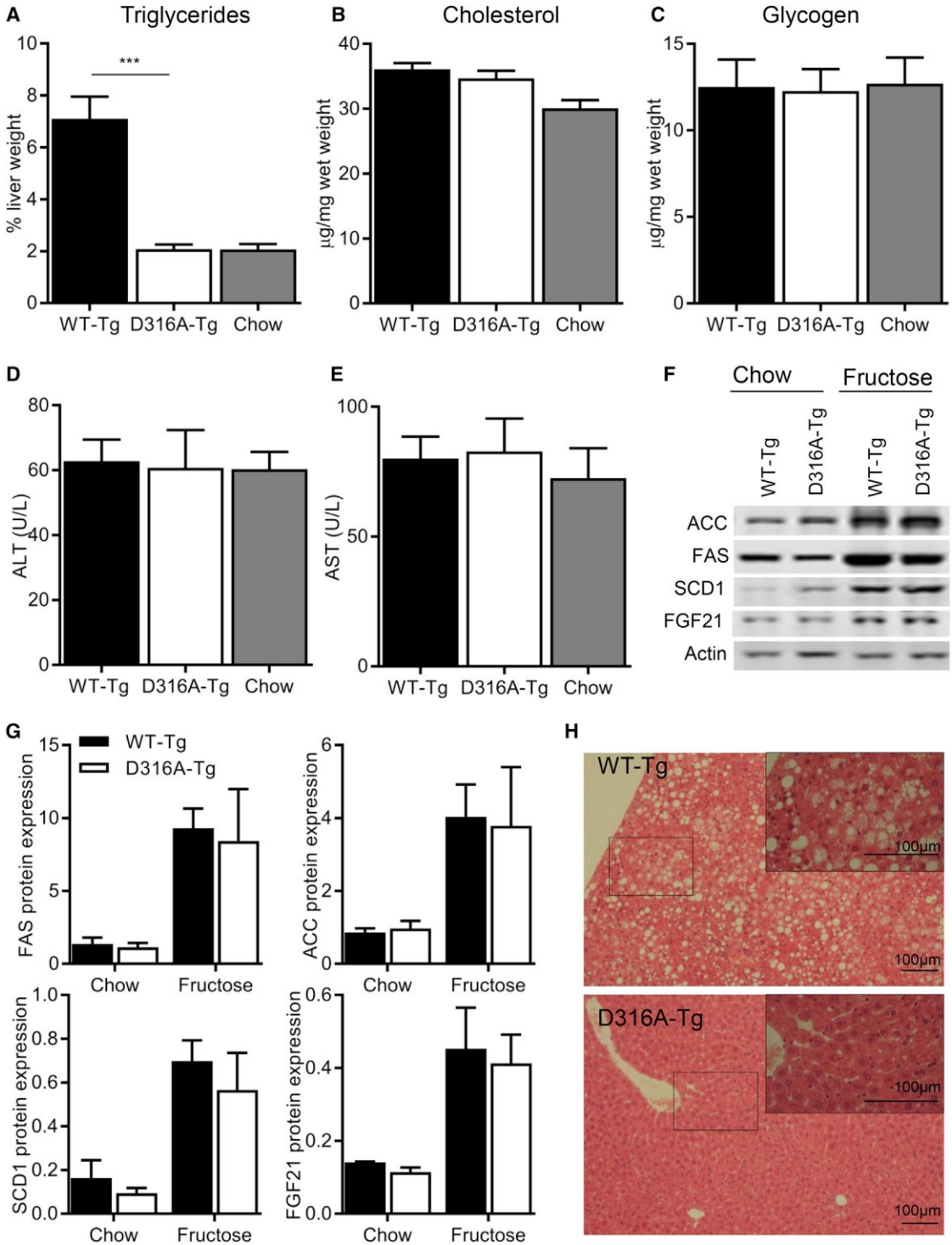


Figure 5. Effects of Liver-Specific Activation of AMPK on Hepatic Lipid Accumulation on a High-Fructose Diet

(A–C) (A) Triglyceride, (B) cholesterol, and (C) glycogen content of livers from transgenic mice fed a high-fructose diet for 12 weeks was determined (n = 12 mice, ***$p < 0.005$). Levels in livers from WT-Tg mice fed a chow diet are shown for comparison.

(D and E) Liver transaminase levels in serum (n = 10–12).

(F) A representative western blot of liver homogenates from mice fed either a chow or high-fructose diet probed with the indicated antibodies is shown.

(G) Quantification of the blots normalized to the level of actin expression (n = 4).

(H) Liver sections from transgenic mice fed a high-fructose diet for 12 weeks stained with H&E. The boxed area is shown magnified in the inset in the top right-hand corner of the image.

hepatocytes with the AMPK activator 991. This finding makes this genetic model an attractive one for understanding the likely pharmacological effects of liver-specific AMPK activation in vivo.

Previous studies have reported that pharmacological activation of AMPK inhibits hepatic gluconeogenesis (Bergeron et al., 2001; Zhou et al., 2001), although subsequent studies have shown that AMPK is not required for inhibition of gluconeogenesis by metformin (Foretz et al., 2010). Genetic activation of AMPK caused a significant reduction in glucose output in isolated hepatocytes, and this was likely mediated by decreased mRNA expression of G6Pase and PEPCK. While there are multiple pathways by which transcription of these two key gluconeogenic genes can be regulated, our results show that activation of AMPK per se has a significant effect on their expression and hepatic glucose output. However, despite the effect of AMPK activation on gluconeogenesis in isolated hepatocytes, we did not detect any change in glucose handling in vivo. This is not without precedent and could be explained by compensatory extrahepatic mechanisms. A previous study reported that mice lacking hepatic PEPCK expression, which have dramatically reduced hepatic glucose production, display near-normal blood glucose levels. This is achieved through compensatory mechanisms, including an increase in extrahepatic gluconeogenesis coupled with reduced whole-body glucose utilization (She et al., 2003).

Activation of AMPK in the liver has been reported to inhibit fatty acid synthesis and promote FAO via phosphorylation and inactivation of ACC. In parallel with increased phosphorylation of ACC, fatty acid synthesis was significantly reduced in hepatocytes expressing the D316A mutation. In contrast, there was no effect on FAO. Treatment of hepatocytes with 991 also had no effect on FAO. Fullerton et al. generated a mouse model in which the key AMPK phosphorylation sites in ACC1 (serine 79) and ACC2 (serine 212) were mutated to alanine residues (Fullerton et al., 2013). In that study, treatment of hepatocytes with A769662, a direct activator of AMPK, caused a modest increase in FAO in cells expressing wild-type ACC but had no effect in cells expressing the mutant ACC enzymes (Fullerton et al., 2013). Although we are unable to explain the difference between our results and those obtained in the previous study, it is interesting to note that, using the same ACC phosphorylation-deficient mouse model, phosphorylation of ACC by AMPK was not required for regulation of FAO in heart (Zordoky et al., 2014). In a more recent study, canagliflozin, which was shown to activate AMPK in the liver, decreased RER independently of ACC phosphorylation (Hawley et al., 2016). These findings suggest that the relationship between AMPK, ACC phosphorylation, and the regulation of FAO is not a simple one and that other mechanisms, independent of AMPK phosphorylation and inhibition of ACC, regulate FAO in vivo.

The effect of diet on hepatic fatty acid synthesis has been studied extensively in both rodents and humans. Increasing the proportion of carbohydrates in the diet leads to a marked increase in de novo lipogenesis in the liver, and this is associated with increased expression of enzymes involved in fatty acid synthesis (Girard et al., 1997). The effect of a high-fat diet is less clear, although a recent study in mice reported that a high-fat diet decreased de novo lipogenesis in the liver despite insulin resistance and obesity (Duarte et al., 2014). In healthy humans, it has been estimated that less than 5% of total triglyceride synthesis is accounted for by de novo lipogenesis on a moderate fat diet (30% fat and 55% carbohydrate), compared to over 25% on a low-fat diet (10% fat and 75% carbohydrate) (Hudgins et al., 2000). An increase in the consumption of sugars, including fructose, particularly in Western diets, has been linked to the increasing prevalence of obesity, together with associated metabolic diseases. The most striking effect of liver-specific AMPK activation that we observed is the complete protection against hepatic triglyceride accumulation in mice fed a high-fructose diet. The simplest explanation for this effect is that AMPK activation inhibits hepatic de novo fatty acid synthesis by directly inactivating ACC. Consistent with this, we found that de novo lipogenesis was reduced in isolated hepatocytes and in the liver in vivo in mice expressing the gain-of-function AMPK mutant. There was no obvious metabolic effect of AMPK activation in mice fed either a chow or a high-fat diet. Under these conditions, the rates of hepatic de novo lipogenesis will be low (relative to the rate on a high-fructose diet) and so would provide only a minor contribution toward total liver triglyceride accumulation. Importantly, activation of AMPK did not increase FAO in hepatocytes, and there was no difference in RER between WT-Tg and D316A-Tg mice on any diet. In addition, there was no change in serum 3-hydroxybutyrate levels between genotypes, indicating that FAO rates in vivo were not different. These results show that liver-specific activation of AMPK does not alter FAO rates in vivo. These findings suggest that the predominant metabolic effect of AMPK activation in the liver is suppression of de novo lipogenesis mediated by phosphorylation of ACC. We hypothesize that this occurs under all dietary conditions, and therefore a phenotype is only revealed under conditions leading to high rates of hepatic de novo lipogenesis (e.g., on a high-fructose diet).

A previous study reported beneficial effects of pharmacological activation of AMPK in animal models of the metabolic syndrome (Cool et al., 2006). In that study, acute treatment of rats in vivo with A769662 led to a transient decrease in RER, indicative of an increase in whole-body FAO. In the same study, chronic treatment of ob/ob mice with A769662 led to a small decrease in body weight, a decrease in fed plasma glucose levels, and a decrease in plasma and liver triglycerides. Although the authors speculated that these changes were likely to be mediated by activation of AMPK in the liver, other mechanisms, including AMPK activation in non-hepatic tissues, such as skeletal muscle, could not be ruled out (Cool et al., 2006). Another potentially confounding factor with the use of A769662 is that a subsequent study reported an AMPK-independent effect of A769662 in skeletal muscle cells (Benziane et al., 2009). Taking these considerations into account and in light of the results in our current study, it seems likely that at least some of the metabolic effects of A769662 treatment in vivo could be mediated independently of AMPK activation in the liver. A more recent study investigated the effect of chronic dosing with AICA (5 aminoimidazole-4-carboxamide) riboside in rats. Treatment with AICA riboside led to decreased hepatic triglyceride accumulation in rats maintained on either a chow or high-fat diet (Henriksen et al., 2013). As with the study using A769662 in vivo, it is not possible to determine the role of the liver-specific

activation of AMPK in these effects, since, as well as activating AMPK in other tissues, AICA riboside has been shown to have AMPK-independent effects.

In another study, short-term activation of AMPK in the liver was achieved by expression of a constitutively active truncated form of AMPKa2 using adenoviral delivery (Foretz et al., 2005). A number of changes were reported, including an increase in hepatic triglyceride accumulation, which the authors speculated could have been caused by increased mobilization of fatty acids from the adipose tissue. Whether this would still occur in response to chronic AMPK activation was not addressed. As well as differences in chronic versus acute activation, that study is confounded by the nature of the constitutively active AMPKa2 mutant used. Truncated a2 does not bind to the b and g regulatory subunits (Crute et al., 1998; Stein et al., 2000), and so it is possible that this might alter the function of the mutant a2 subunit.

Previous studies have employed different genetic mouse models to determine the effect of AMPK activation in skeletal muscle (Barnes et al., 2004; Barré et al., 2007; Schönke et al., 2015). A striking feature of the mouse models is increased skeletal muscle glycogen accumulation, although no major changes in lipid metabolism were reported. A chronic gain-of-function AMPK model resulting from expression of AMPKg2 with mutation of arginine 302 to glutamine (R302Q) was reported recently (Yavari et al., 2016). Mice with global homozygous expression of this mutation are hyperphagic, obese, and display impaired pancreatic insulin secretion (Yavari et al., 2016). At least some of these effects appear to be mediated by changes in AMPK activity in the hypothalamus. Whether these effects result from an overall increase in AMPK activity, or are due to a specific increase in g2-associated AMPK activity, is unclear at present. Further studies using the gain-of-function AMPKg1 mouse model should help address both the isoform- and tissue-specific effects of AMPK activation in vivo.

In summary, our study reveals that AMPK activation in liver completely prevents lipid accumulation on a high-carbohydrate diet. This finding may have implications for the therapeutic potential of targeting hepatic AMPK. The incidence of NAFLD is increasing rapidly and is associated with the increasing prevalence of obesity. Although NAFLD is classified as a benign condition, many individuals with the disease go on to develop more serious conditions, including NASH, cirrhosis, liver failure, and hepatocellular carcinoma. De novo lipogenesis is significantly increased in patients with NAFLD, and this increase is thought to contribute to the accumulation of hepatic triglycerides in NAFLD (Donnelly et al., 2005). Our findings indicate that direct activation of AMPK in the liver might provide an attractive therapeutic strategy for preventing progression of NAFLD and subsequent development of associated complications.

## EXPERIMENTAL PROCEDURES

### Animal Models

cDNA (Epoch Life Science) for the mouse Prkag1 gene and cDNA harboring the D316A mutation were specifically integrated into the Rosa26 locus. Chow-standard breeding diet number 3 was from Special Diets Services; high-fat diet (45% energy from fat) and high-fructose diet (60% fructose diet with 10% fat) were obtained from TestDiet. All experiments involved in the generation of transgenic animals were approved by Gothenburg Ethics Committee. All in vivo studies were performed in accordance with the UK Animals (Scientific Procedures) Act (1986) and approved by the Animal Welfare and Ethical Review Board at Imperial College London.

### In Vivo Lipogenesis

De novo lipogenesis was determined by incorporation of $^{3}$H-acetate into lipid. Mice were fasted overnight and refed for 1.5 hr before intraperitoneal injection with 40 mCi $^{3}$H-acetate (Perkin Elmer). After 1 hr, mice were sacrificed and livers extracted using the Folch Method. Incorporation of radioactivity in the lipid fraction was determined by scintillation counting.

### Histology

Tissue was fixed in 4% paraformaldehyde and processed to paraffin wax. Sections were stained with H&E.

### Statistical Analysis

Data are expressed as mean ± SEM unless otherwise stated. Where appropriate, results were analyzed using either Student's t test or ANOVA with Dunnet's post-test.

## SUPPLEMENTAL INFORMATION

Supplemental Information includes Supplemental Experimental Procedures and one figure and can be found with this article online at http://dx.doi.org/10.1016/j.celrep.2017.03.011.

## AUTHOR CONTRIBUTIONS

A.W., J.R.W., P.J.M., and F.V.M. performed the studies. M.L. and M.B.-Y. generated the transgenic lines. A.W. and D.C. conceived and designed the experiments. All authors contributed to editing of the manuscript.

## ACKNOWLEDGMENTS

This work was funded by the MRC UK. J.R.W. received an MRC/Imperial Chain-Florey Clinical PhD Fellowship. We thank Dr. Alex Sardini (MRC LMS) for help with the CLAMS studies and data analysis.

Received: August 15, 2016
Revised: February 2, 2017
Accepted: March 1, 2017
Published: March 28, 2017

## REFERENCES

Arad, M., Seidman, C.E., and Seidman, J.G. (2007). AMP-activated protein kinase in the heart: role during health and disease. Circ. Res. 100, 474–488.

Barnes, B.R., Marklund, S., Steiler, T.L., Walter, M., Hjälm, G., Amarger, V., Mahlapuu, M., Leng, Y., Johansson, C., Galuska, D., et al. (2004). The 5$^{0}$-AMP-activated protein kinase gamma3 isoform has a key role in carbohydrate and lipid metabolism in glycolytic skeletal muscle. J. Biol. Chem. 279, 38441–38447.

Barré, L., Richardson, C., Hirshman, M.F., Brozinick, J., Fiering, S., Kemp, B.E., Goodyear, L.J., and Witters, L.A. (2007). Genetic model for the chronic activation of skeletal muscle AMP-activated protein kinase leads to glycogen accumulation. Am. J. Physiol. Endocrinol. Metab. 292, E802–E811.

Benziane, B., Björnholm, M., Lantier, L., Viollet, B., Zierath, J.R., and Chibalin, A.V. (2009). AMP-activated protein kinase activator A-769662 is an inhibitor of the Na(+)-K(+)-ATPase. Am. J. Physiol. Cell Physiol. 297, C1554–C1566.

Bergeron, R., Previs, S.F., Cline, G.W., Perret, P., Russell, R.R., 3rd, Young, L.H., and Shulman, G.I. (2001). Effect of 5-aminoimidazole-4-carboxamide-1-beta-D-ribofuranoside infusion on in vivo glucose and lipid metabolism in lean and obese Zucker rats. Diabetes 50, 1076–1082.

Carling, D., Thornton, C., Woods, A., and Sanders, M.J. (2012). AMP-activated protein kinase: new regulation, new roles? Biochem. J. 445, 11–27.

Cool, B., Zinker, B., Chiou, W., Kifle, L., Cao, N., Perham, M., Dickinson, R., Adler, A., Gagne, G., Iyengar, R., et al. (2006). Identification and characterization of a small molecule AMPK activator that treats key components of type 2 diabetes and the metabolic syndrome. Cell Metab. 3, 403–416.

Crute, B.E., Seefeld, K., Gamble, J., Kemp, B.E., and Witters, L.A. (1998). Functional domains of the alpha1 catalytic subunit of the AMP-activated protein kinase. J. Biol. Chem. 273, 35347–35354.

Dandapani, M., and Hardie, D.G. (2013). AMPK: opposing the metabolic changes in both tumour cells and inflammatory cells? Biochem. Soc. Trans. 41, 687–693.

Davies, S.P., Carling, D., Munday, M.R., and Hardie, D.G. (1992). Diurnal rhythm of phosphorylation of rat liver acetyl-CoA carboxylase by the AMP-activated protein kinase, demonstrated using freeze-clamping. Effects of high fat diets. Eur. J. Biochem. 203, 615–623.

Donnelly, K.L., Smith, C.I., Schwarzenberg, S.J., Jessurun, J., Boldt, M.D., and Parks, E.J. (2005). Sources of fatty acids stored in liver and secreted via lipoproteins in patients with nonalcoholic fatty liver disease. J. Clin. Invest. 115, 1343–1351.

Duarte, J.A., Carvalho, F., Pearson, M., Horton, J.D., Browning, J.D., Jones, J.G., and Burgess, S.C. (2014). A high-fat diet suppresses de novo lipogenesis and desaturation but not elongation and triglyceride synthesis in mice. J. Lipid Res. 55, 2541–2553.

Dushay, J.R., Toschi, E., Mitten, E.K., Fisher, F.M., Herman, M.A., and Maratos-Flier, E. (2014). Fructose ingestion acutely stimulates circulating FGF21 levels in humans. Mol. Metab. 4, 51–57.

Foretz, M., Ancellin, N., Andreelli, F., Saintillan, Y., Grondin, P., Kahn, A., Thorens, B., Vaulont, S., and Viollet, B. (2005). Short-term overexpression of a constitutively active form of AMP-activated protein kinase in the liver leads to mild hypoglycemia and fatty liver. Diabetes 54, 1331–1339.

Foretz, M., Hébrard, S., Leclerc, J., Zarrinpashneh, E., Soty, M., Mithieux, G., Sakamoto, K., Andreelli, F., and Viollet, B. (2010). Metformin inhibits hepatic gluconeogenesis in mice independently of the LKB1/AMPK pathway via a decrease in hepatic energy state. J. Clin. Invest. 120, 2355–2369.

Fullerton, M.D., Galic, S., Marcinko, K., Sikkema, S., Pulinilkunnil, T., Chen, Z.P., O'Neill, H.M., Ford, R.J., Palanivel, R., O'Brien, M., et al. (2013). Single phosphorylation sites in Acc1 and Acc2 regulate lipid homeostasis and the insulin-sensitizing effects of metformin. Nat. Med. 19, 1649–1654.

Girard, J., Ferré, P., and Foufelle, F. (1997). Mechanisms by which carbohydrates regulate expression of genes for glycolytic and lipogenic enzymes. Annu. Rev. Nutr. 17, 325–352.

Hardie, D.G., and Carling, D. (1997). The AMP-activated protein kinase–fuel gauge of the mammalian cell? Eur. J. Biochem. 246, 259–273.

Hawley, S.A., Ford, R.J., Smith, B.K., Gowans, G.J., Mancini, S.J., Pitt, R.D., Day, E.A., Salt, I.P., Steinberg, G.R., and Hardie, D.G. (2016). The Na+/glucose cotransporter inhibitor canagliflozin activates AMPK by inhibiting mitochondrial function and increasing cellular AMP levels. Diabetes 65, 2784–2794.

Henriksen, B.S., Curtis, M.E., Fillmore, N., Cardon, B.R., Thomson, D.M., and Hancock, C.R. (2013). The effects of chronic AMPK activation on hepatic triglyceride accumulation and glycerol 3-phosphate acyltransferase activity with high fat feeding. Diabetol. Metab. Syndr. 5, 29.

Hudgins, L.C., Hellerstein, M.K., Seidman, C.E., Neese, R.A., Tremaroli, J.D., and Hirsch, J. (2000). Relationship between carbohydrate-induced hypertriglyceridemia and fatty acid synthesis in lean and obese subjects. J. Lipid Res. 41, 595–604.

Matteoni, C.A., Younossi, Z.M., Gramlich, T., Boparai, N., Liu, Y.C., and McCullough, A.J. (1999). Nonalcoholic fatty liver disease: a spectrum of clinical and pathological severity. Gastroenterology 116, 1413–1419.

Mayes, P.A. (1993). Intermediary metabolism of fructose. Am. J. Clin. Nutr. 58 (5, Suppl), 754S–765S.

Milan, D., Jeon, J.T., Looft, C., Amarger, V., Robic, A., Thelander, M., Rogel-Gaillard, C., Paul, S., Iannuccelli, N., Rask, L., et al. (2000). A mutation in PRKAG3 associated with excess glycogen content in pig skeletal muscle. Science 288, 1248–1251.

Postic, C., and Girard, J. (2008). Contribution of de novo fatty acid synthesis to hepatic steatosis and insulin resistance: lessons from genetically engineered mice. J. Clin. Invest. 118, 829–838.

Postic, C., Shiota, M., Niswender, K.D., Jetton, T.L., Chen, Y., Moates, J.M., Shelton, K.D., Lindner, J., Cherrington, A.D., and Magnuson, M.A. (1999). Dual roles for glucokinase in glucose homeostasis as determined by liver and pancreatic beta cell-specific gene knock-outs using Cre recombinase. J. Biol. Chem. 274, 305–315.

Rui, L. (2014). Energy metabolism in the liver. Compr. Physiol. 4, 177–197.

Schönke, M., Myers, M.G., Jr., Zierath, J.R., and Björnholm, M. (2015). Skeletal muscle AMP-activated protein kinase g1(H151R) overexpression enhances whole body energy homeostasis and insulin sensitivity. Am. J. Physiol. Endocrinol. Metab. 309, E679–E690.

She, P., Burgess, S.C., Shiota, M., Flakoll, P., Donahue, E.P., Malloy, C.R., Sherry, A.D., and Magnuson, M.A. (2003). Mechanisms by which liver-specific PEPCK knockout mice preserve euglycemia during starvation. Diabetes 52, 1649–1654.

Stein, S.C., Woods, A., Jones, N.A., Davison, M.D., and Carling, D. (2000). The regulation of AMP-activated protein kinase by phosphorylation. Biochem. J. 345, 437–443.

Steinberg, G.R., and Kemp, B.E. (2009). AMPK in health and disease. Physiol. Rev. 89, 1025–1078.

Tappy, L., and Lê, K.A. (2010). Metabolic effects of fructose and the worldwide increase in obesity. Physiol. Rev. 90, 23–46.

Viollet, B., Athea, Y., Mounier, R., Guigas, B., Zarrinpashneh, E., Horman, S., Lantier, L., Hebrard, S., Devin-Leclerc, J., Beauloye, C., et al. (2009). AMPK: Lessons from transgenic and knockout animals. Front. Biosci. (Landmark Ed.) 14, 19–44.

Woods, A., Azzout-Marniche, D., Foretz, M., Stein, S.C., Lemarchand, P., Ferré, P., Foufelle, F., and Carling, D. (2000). Characterization of the role of AMP-activated protein kinase in the regulation of glucose-activated gene expression using constitutively active and dominant negative forms of the kinase. Mol. Cell. Biol. 20, 6704–6711.

Xiao, B., Heath, R., Saiu, P., Leiper, F.C., Leone, P., Jing, C., Walker, P.A., Haire, L., Eccleston, J.F., Davis, C.T., et al. (2007). Structural basis for AMP binding to mammalian AMP-activated protein kinase. Nature 449, 496–500.

Xiao, B., Sanders, M.J., Carmena, D., Bright, N.J., Haire, L.F., Underwood, E., Patel, B.R., Heath, R.B., Walker, P.A., Hallen, S., et al. (2013). Structural basis of AMPK regulation by small molecule activators. Nat. Commun. 4, 3017.

Yavari, A., Stocker, C.J., Ghaffari, S., Wargent, E.T., Steeples, V., Czibik, G., Pinter, K., Bellahcene, M., Woods, A., Martínez de Morentin, P.B., et al. (2016). Chronic Activation of g2 AMPK Induces Obesity and Reduces b Cell Function. Cell Metab. 23, 821–836.

Younossi, Z.M., Koenig, A.B., Abdelatif, D., Fazel, Y., Henry, L., and Wymer, M. (2016). Global epidemiology of nonalcoholic fatty liver disease-Meta-analytic assessment of prevalence, incidence, and outcomes. Hepatology 64, 73–84.

Zadra, G., Photopoulos, C., Tyekucheva, S., Heidari, P., Weng, Q.P., Fedele, G., Liu, H., Scaglia, N., Priolo, C., Sicinska, E., et al. (2014). A novel direct activator of AMPK inhibits prostate cancer growth by blocking lipogenesis. EMBO Mol. Med. 6, 519–538.

Zhou, G., Myers, R., Li, Y., Chen, Y., Shen, X., Fenyk-Melody, J., Wu, M., Ventre, J., Doebber, T., Fujii, N., et al. (2001). Role of AMP-activated protein kinase in mechanism of metformin action. J. Clin. Invest. 108, 1167–1174.

Zordoky, B.N.M., Nagendran, J., Pulinilkunnil, T., Kienesberger, P.C., Masson, G., Waller, T.J., Kemp, B.E., Steinberg, G.R., and Dyck, J.R.B. (2014). AMPK-dependent inhibitory phosphorylation of ACC is not essential for maintaining myocardial fatty acid oxidation. Circ. Res. 115, 518–524.